Geomorphic process mechanisms and quantification of storm-induced intertidal boulder transport using Radio Frequency Identification (RFID) tagging technology.

by

Linley John Hastewell

The thesis is submitted in partial fulfilment of the

requirements for the award of the degree of

DOCTOR OF PHILOSOPHY

of the University of Portsmouth

April 2020

Declaration

Whilst registered as a candidate for the above degree, I have not been registered for any other research award. The results and conclusions embodied in this thesis are the work of the named candidate and have not been submitted for any other academic award.

Word Count: 55,358

"The waves broke and spread their waters swiftly over the shore. One after another they massed themselves and fell; the spray tossed itself back with the energy of their fall. The waves were steeped deep-blue save for a pattern of diamond-pointed light on their backs which rippled as the backs of great horses ripple with muscles as they move. The waves fell; withdrew and fell again, like the thud of a great beast stamping."

Virginia Woolf, The Waves, p.77.

Dedicated to my late father who never got to see the dream realised.

Contents

List of Figures

List of Tables

Acknowledgements

I am indebted to many people who have provided me with support throughout the duration of this research study. Foremost, my supervisory team have been integral to the successful completion of the thesis. Specific mention goes to Dr. Malcolm Bray, as the original first supervisor for the majority of the study he has been a great sounding board for my ideas throughout and has advised me in the meticulous way I have grown to appreciate. His knowledge and insight have been invaluable and his enthusiasm in the field, infectious. I am grateful to Dr. Rob Inkpen who took over the mantle of first supervisor and has provided me with encouragement, support and valuable advice throughout, particularly during the write up. Dr. Phil Soar has also been a valued member of the team offering his advice and support when called upon.

To the many work colleagues who have offered words of wisdom over the years, special mention must go to Dr. Mark Hardiman and Dr. Julia Brown who have been particularly supportive and encouraging throughout. I am indebted to Martin Schaefer who was always willing to accompany me in the field even when it involved early morning ferry journeys and often late evening returns. Without his input and assistance the study would not have been as successful as it was. I am also eternally grateful to those people that accompanied me in the field offering support for no other reason than to gain some field-based experience and to simply help out. Without their input the study would not have been possible.

I also wish to thank Dr. Ritienne Gauci who has also been a valuable sounding board for discussion and a friend throughout. My sincerest thanks to those colleagues and friends from the University of Trieste, Dr. Stefano Devoto, Dr. Stefano Furlani and Dr. Sara Biolchi who were so willing to include me in their research and showed me the utmost hospitality during my time in Italy.

From a personal perspective, I am indebted to my parents who were always eager to learn of the progress that had been made, even though they may not have fully understood. I only wish they could both have seen it reach its end. Above all, to my wife Emma who has supported me throughout and worked tirelessly to help me achieve this goal. None of this would have been possible without her. I am forever indebted for her love and support. To our two beautiful children Jessica and Max who have kept my feet firmly on the ground. I'll forever regret those lost moments, missing out on trips to the cinema and the park so I could complete this study. I hope you will understand and appreciate my reasons for this and I look forward to being able to spend more time together as a family.

Abstract

Coastal boulder deposits, within the inter- and supratidal zone represent sedimentary signatures of extreme storm wave and/or tsunami origin. However, owing to the infrequency of such high-magnitude events there is a limited understanding of the complex mechanisms that govern boulder transport upon rocky coasts. Existing studies frequently focus on geographically remote coastal locations which are exposed to considerable oceanic swell waves. Owing to the inhospitable nature of these sites they are typically unpopulous and lacking in associated infrastructure. By contrast, rocky coastal sites subject to moderate wave regimes that are regularly exposed to low-magnitude, high-frequency storm activity are generally more populated with increased housing provision and a greater level of municipality. Notwithstanding the reduced level of storm wave competence, such sites are rarely evaluated in terms of boulder transport response to contemporary storm events despite exhibiting sedimentary assemblages which are indicative of storm wave deposition.

Current data pertaining to boulder transport is often limited to qualitative observational assessment from isolated field sites or increasingly, via the use of remotely sensed data. Furthermore, the inability to regularly monitor sediment transport of boulder-sized clasts means displacement is rarely accurately quantified.

This thesis aims to document and accurately quantify boulder transport in response to contemporary storm waves at a coastal location subjected to low-magnitude, high-frequency storm events. Quantification was achieved by undertaking a sediment tracing field study which incorporated monitoring the displacement amongst an array of specific intertidal boulders. Using a novel field technique, Radio Frequency Identification tags (RFID's) were embedded in selected boulders. Each RFID tag is pre-programmed with a unique serial number which enabled identification of tagged boulders in the field. Coordinate data for each tagged boulder was obtained using a Differential Global Positioning Navigation Satellite System (DGNSS). Repeated field surveys following storm activity were conducted to relocate the tagged clasts; once relocated the bolder location was rerecorded. On completion of the three-year study coordinate data for each of the 104 tagged boulders provided a spatial and temporal framework within which boulder transport pathways could accurately be quantified.

Additionally, the processes and mechanisms that facilitate boulder production, transport and deposition on the shore platforms at the field site are defined. This is undertaken with a view to better understanding the interrelationship between a host of boundary conditions which modify and ultimately regulate shore platform evolution.

The chapters within this thesis present a range of the findings from the field study including an extensive review of the RFID tagging methodology (Chapter 2). This comprehensive account provides coastal researchers with the specific details required to implement a successful tagged boulder monitoring campaign.

The key findings arising from this empirical field-based study are presented in Chapter 3 which addresses the overarching aim of the thesis in terms of accurately quantifying boulder transport. The data identifies that despite the low/moderate wave climate at the field site, boulder displacement is widespread which suggests a need to reassess the perceived geomorphic docility of relatively sheltered coastal locations.

Additional noteworthy findings include: (1) the statistically significant difference between transport distances attributed to constrained and unconstrained boulders, suggesting the pre-transport morphological setting exerts considerable control over boulder transport potential; (2) boulder production is initiated by undermining which is enhanced by the presence of geological discontinuities within the boulder producing unit; (3) moderate storm waves are able to mobilise very coarse boulders above the calculated wave parameters derived from widely-cited hydrodynamic equations; (3) sediment-laden, low-energy waves facilitate platform modification with respect to the formative processes of intertidal pool development, the pools subsequently act to impede boulder transport (Chapter 4); (4) storm-induced reworking of intertidal boulders modifies wider landform morphology in terms of collective boulder displacement altering large-scale landform features (Chapter 5); (5) the processes by which boulder production, transport and deposition occur are inextricably linked and are reflected at various coastal sites across a range of scales producing similar landform features and sedimentary assemblages (Chapter 5).

Given the anticipated increase in storm frequency and intensity arising from changing climate patterns the rate at which future geomorphic modification and landform evolution occurs on intertidal shore platforms is expected to accelerate. Therefore, it is necessary to establish the responsiveness of such coastal features with an emphasis on better understanding the ability and the extent to which storm waves are able to detach, transport and deposit boulder-sized clasts within the intertidal zone.

Acronyms

BL - Bembridge Ledge

BR - Black Rock

CCO - Channel Coast Observatory

CTD - Cumulative Transport Distance

DGNSS - Differential Global Positioning Navigation Satellite System

DEM - Digital Elevation Model

EM - Electromagnetic

H_s - Significant wave height (the average height of the highest one third of waves at a location during a wave measurement period).

H_{max} - Maximum wave height (the highest wave from crest to trough, recorded during a wave measurement period).

IBTD - Individual Boulder Transport Distance

kHz - Kilohertz

MCZ - Marine Conservation Zone

(M)LW - (Mean) low water

(M)HW - (Mean) high water

MS - Morphological setting

OD - Ordnance datum

PIT - Passive Integrated Transponder

RFID - Radio Frequency Identification

RMSE - Root Mean Square Error

RTK - Real-Time Kinematic

TIP - Tag insertion point

UAV - Unmanned Aerial Vehicle

UCS - Uniaxial Compressive Strength

Chapter 1 - Thesis introduction

Thesis format and structure

The format of this thesis adopts the Continental Style which differs from that of the more traditional manuscript. Unlike the traditional thesis format the Continental Style Thesis is structured around a series of published, and/or publishable research manuscripts. For the purpose of clarity the thesis format and structure is defined at the outset of this introductory chapter. The thesis consists of six chapters as described below.

Chapter 1 - Introduction

This introductory chapter defines the thesis format and structure and presents the aims of the research along with a study preface which introduces the key concepts that define the processes associated with shore platform evolution and morphology. The study aims and rationale are clearly defined and justified in terms of existing gaps identified from the literature and the means by which the overarching aim will be determined is also presented. Furthermore, a series of research questions are posed which will be addressed through the course of the thesis. The study is also placed in a geographical context alongside previous boulder transport studies that have been conducted in the U.K. and Ireland. Furthermore, the decision to use Radio Frequency Identification (RFID) tagging to monitoring boulder displacement is advocated based on (1) stakeholder approval; (2) the success of previous RFID deployments in littoral settings; (3) the use of a novel, modified technique being used for the first time on a boulder-sized array. Finally, the selected field site location is justified on the basis of an abundant supply of boulder-sized, detached material available for transport; further detail regarding site geology is also provided.

Chapters 2, 3 and 4 comprise the manuscript submissions. Prior to each manuscript chapter, a brief summary is provided that introduces the paper and details the contributions made by the named authors.

Chapter 2 - A proposed methodology adopting Radio Frequency Identification (RFID) technology to quantify storm induced boulder mobility. (*Published manuscript*).

This manuscript has been peer-reviewed and published in Earth Surface Processes and Landforms.

The project aim is based on quantifying the extent to which moderate, contemporary storm waves are able to mobilise boulders within the intertidal zone. In order to achieve this it was necessary to adopt a suitable means of monitoring boulder displacement both spatially and temporally. The use of RFID tagged boulders allowed for a discreet yet effective means of documenting clast mobility. Chapter 2 provides comprehensive detail on the RFID methodology employed to achieve the project aim. The chapter presents a number of recommended procedures and protocols that should be adhered to in order to conduct a robust scientific assessment of boulder transport under contemporary storm conditions.

Chapter 3 - Quantification of contemporary storm-induced boulder transport on an intertidal shore platform using RFID technology. (*Accepted for publication*).

This manuscript has been peer-reviewed and accepted for publication in Earth Surface Processes and Landforms. The version paginated within this chapter is the original manuscript prior to any suggested reviewer alterations.

Addendum: the revised, published version has been inserted into the thesis appendices, Appendix 5, page 244.

This chapter documents the findings from the three-year field study with data being drawn from the RFID tagged boulder array. The empirical evidence presented indicates that moderate storm waves are capable of displacing sizeable boulders within the intertidal zone. It also highlights the significance of morphological and topographic control in restricting boulder transport.

Chapter 4 - Identification of plate-forme à vasques on a temperate shore platform? Quantitative analysis of morphology and relationships at Bembridge, Isle of Wight. (*Published manuscript*).

This manuscript has been peer-reviewed and published in Zeitschrift für Geomorphologie.

This chapter highlights the wider geomorphology of one of the study sites, with focus on a network of intertidal pools. A topographic survey and field observations from the site were used to present insight to the relationships governing form and occurrence of the pools. With respect to boulder transport the undulating terrain presented by the pools aids retention of detached boulders, impeding further landward displacement.

In terms of justifying the respective journals chosen for publication, two manuscripts relating directly to boulder transport processes (Chapters 2 and 3) were submitted to Earth Surface

Processes and Landforms. This journal was selected as it is a highly-respected, leading geomorphology journal owing to its high impact factor (3.598), thus reflecting the quality of the submitted manuscripts. Publication in such a prestigious journal was deemed necessary given these two manuscripts form the basis of the thesis submission. Furthermore, the journal has previously published a number of key boulder transport papers, therefore it was considered publication in this journal would solicit the greatest degree of dissemination amongst coastal researchers with shared interests.

Zeitschrift für Geomorphologie was selected as it is a well-respected international geomorphology journal (impact factor: 0.987) which has a traditional focus on process and form relationships. The theme and subject matter addressed in the submitted manuscript was thought to be well aligned with previous works published in the journal.

Note: references cited in the submitted and published manuscripts appear collectively within the broader bibliography, page 268.

Chapter 5 - Additional findings and future research

This chapter focuses on additional research that was conducted during the doctoral study. The empirical and theoretical work undertaken is of a preliminary nature and was deemed to be underdeveloped; therefore it was not included in the submitted manuscripts. However, the information generated provided a valuable insight to the mechanisms that facilitate the production, transport and deposition of individual boulder-sized clasts at the study sites. Additional findings presented herein provide an understanding of the impacts of contemporary storm wave activity on shore platform morphology and modification at a broader scale. The significance of the findings and their association with increased understanding of the boulder production, transport and deposition processes warranted inclusion within the thesis.

This chapter also presents a proposed theoretical model which conceptualises the processes and mechanisms that facilitate boulder production, transport and deposition. The model is applied to both tagged boulder study sites and a further two intertidal settings within the U.K.

Also included in this chapter are details of collaborative work that will form the basis of future research aimed at improving understanding of the collective boulder transport processes across a range of study sites subjected to differing wave and tidal regimes. This is current research that is being undertaken with partners at other academic institutes including the University of Malta and the University of Trieste (Italy).

Chapter 6 - Synthesis and Conclusions

This chapter concludes the thesis by identifying the key findings that arose from the study. Additionally, the contribution to boulder transport research and the limitations of the study are discussed. The thesis is summarised and the concluding remarks are presented based on the information and data drawn from the preceding chapters.

Study aims and rationale

The coastal margins lie at the intersection between land and sea. Therefore, they are exposed to a host of erosive agents that shape and modify the coastal environment. However, the management of these dynamic areas is becoming increasingly problematic with conflict arising from burgeoning coastal populations, associated infrastructure and the anticipated impacts resulting from the changing global climate.

It is reported that future storm wave heights in higher latitudes are likely to increase and become more frequent under a range of future IPCC climate scenarios (Wolf and Woolf, 2006; Young *et al*., 2011; Semedo *et al*., 2012). In order to mitigate against these anticipated climatic changes and associated impacts it is necessary to establish the responsiveness of our coastal environment to contemporary storm activity.

This study focuses on the rocky coastal fringes with an emphasis on better understanding the capability of present-day storm waves to detach, transport and deposit boulders upon intertidal shore platforms. The key aim of the research is to quantify the extent to which contemporary, low-magnitude, high-frequency storm events are able to transport detached boulders at the selected field location, (Bembridge, Isle of Wight). Owing to the complexity of the various factors influencing boulder transport, e.g. tides, wave climate, lithology and aspect, amongst others, it was considered that data derived from empirical field experimentation would be more representative than that drawn from theoretical laboratory testing which would fail to accurately reflect the complexity of the natural environment.

At the commencement of the study two prominent research gaps were identified within the existing boulder transport literature.

(1) The majority of coastal studies focus on locations and landform features that are more readily modified and responsive to contemporary storm activity, e.g. fine-grained beaches (Naylor *et al*., 2010; Trenhaile, 2016). This has led to a lack of research, and consequentially,

understanding of the responsiveness of rocky coasts to present day storm events. With respect to boulder transport studies, previous research has favoured exposed coastal locations subjected to dynamic wave climates associated with considerable fetch distances (Etienne and Paris, 2010; Goto *et al*., 2011; Cox *et al*., 2018). In such energetic coastal settings clast displacement is to be expected. However the effect of storm wave activity in fetch-limited locations subjected to moderate wave activity is unknown (Dasgupta, 2011) despite the presence of surficial boulder deposits indicative of storm-induced transport and deposition.

(2) It is reported by Paris *et al*. (2011) and Moses (2014) that our current understanding of boulder transport dynamics is lacking in empirical and quantifiable field data. Much of the current research is based on repeat qualitative observations with limited accurate data on clast displacement (Paris *et al*., 2011). With the notable exception of Naylor *et al*. (2016) there are no known published studies that accurately quantify the extent to which an array of specific boulders are displaced by contemporary storm activity.

The identified gaps raised a series of research questions that the study aims to address. These questions helped formulate the direction of the research during the initial stages of development and provided a basis for the research aims to be defined. The key research questions were;

(1) Are contemporary low-magnitude, high-frequency storm events in sheltered, fetch-limited seas capable of displacing intertidal boulders? If so, to what extent are the boulders mobilised?
(2) Can an array of boulders be tracked and repeatedly recovered within the intertidal zone as part of a long-term field study? If so, which tracing technique would be the most appropriate?
(3) What are the processes by which boulder transport occurs, in terms of the mechanisms that initiate boulder production, the wave forces that facilitate transport and the factors influencing deposition?

In order to address these research questions it was necessary to select a rocky coastal site which was considered to be, (i) fetch-limited, (ii) relatively sheltered with exposure to low/moderate wave conditions, and (iii) possess a shore platform with an adequate supply of source material in the form of detached boulder-sized clasts. Furthermore, the field methodology needed to provide a means of monitoring an identifiable set of boulders allowing for the collation of quantifiable boulder displacement both temporally and spatially.

A coastal site at Bembridge on the eastern side of the Isle of Wight was found to be suitable owing to its sheltered location, limited fetch and exposure to high-frequency, low-magnitude storm activity. The site presents extensive limestone shore platforms and evidence of contemporary boulder displacement in the form of boulder assemblages (e.g. boulder beach and boulder berm) and individually emplaced surficial deposits. Moreover, the site comprises two distinct, separate areas; these being Bembridge Ledge and Black Rock. Having two study sites in close proximity was thought to be beneficial in terms of assessing the similarity, or difference between locations subject to the same storm activity. Additionally, favourable access to both sites reduced the logistical burden and enabled a swift response when recording boulder transport following storm activity. The presence of a wave monitoring network 5 km from the study site provided an insight to the inshore and nearshore wave conditions that we infer facilitated clast displacement.

The lack of boulder producing units in the sloping cliffs to the rear of both selected field sites provided assurances regarding boulder provenance. Thus, boulder origin is assigned to the bedrock units that form the shore platforms. Furthermore, with no reported evidence of tsunamigenic activity in recent years (Long, 2017) it is possible to attribute boulder transport and deposition to storm wave activity alone.

The selection of an appropriate field methodology was agreed following discussions with stakeholders (Natural England). It was agreed the chosen method would need to be of limited aesthetic intrusion to the site and its users. Following preliminary testing in both the field and laboratory it was decided that Radio Frequency Identification (RFID) tagging would provide the most suitable means of gathering the necessary data to quantify contemporary, storm-induced boulder transport. We modified the existing RFID sediment tracing technique which has been used predominantly in gravel and cobble-sized sediments (Allan *et al*., 2006) to better suit deployment in boulder-sized clasts. In doing so a field-based methodology has been devised that uses Differential Global Positioning Navigation Satellite System (DGNSS) to accurately quantify intertidal boulder transport.

The highlighted research gaps, the suitability of the study site and the selected field-based methodology (RFID tagging) are aligned with fulfilling the overarching aim of the study; to accurately quantify the extent to which contemporary storm conditions are able to displace intertidal boulders in a low to moderate wave climate. In addressing the study aim the thesis will also present insight to the key processes that facilitate boulder production, transport and deposition.

Study Preface

This section serves to introduce a number of the key themes that are relevant to shore platform processes and the mechanisms that facilitate boulder transport and shape these coastal landforms. It also provides insight on site specifics and elaborates on the chosen method of sediment tracing whilst also placing the study in the broader context of the existing research.

Early studies relating to the formative processes of shore platform evolution were pioneered by James Dwight Dana, a geologist working under the auspices of the United States Navy. He was selected to a team of scientific observers for an expedition that departed from Norfolk, Virginia, U.S.A., on 18th August 1838 destined for the far reaches of the South Pacific (Pirsson, 1919). Throughout the expedition, Dana compiled a significant amount of information relating to the geology and formation of the many landform features he encountered. Upon reaching the Bay of Islands in New Zealand, he made a series of observations including that of islands surrounded by a shore platform lying above the low water mark (Dana, 1849). He attributed the formation of this landform to wave action; erosion occurring where the plunging wave strikes the rock surface. He referred to these features as "*The Old Hat*" islands (Figure 1.1).

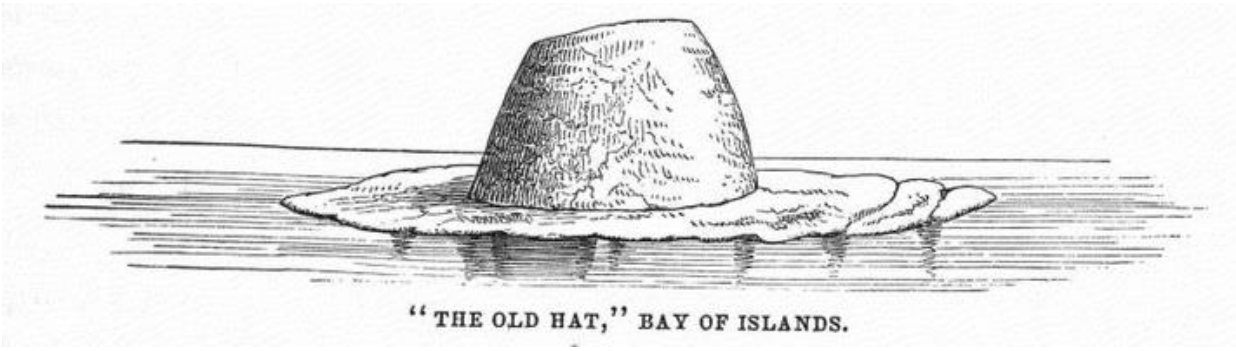

Figure 1.1. Dana's "Old Hat" islands as observed in the Bay of Islands, New Zealand, (Dana, 1849, page 442).

Dana's reference to shore platforms received little further attention until Bartrum (1916) provided further explanation for the formation of The Old Hat coastal features. He identified the significance of subaerial weathering as an agent of erosion; weathering occurring at the cliff face with removal of material by subsequent wave action. From this point forward there would be much conjecture between geomorphologists as to the primary source of erosion in the development of shore platforms; the waves versus weathering debate (Stephenson, 2000; Kennedy *et al*., 2011).

The early work of these pioneering scientists initiated a branch of geomorphological study focussing on the formative processes that dictate the evolution of rocky coasts. This field of study has since developed and is of growing interest given the challenges facing coastal communities and infrastructure resulting from global climate change; such as rising sea levels (Cabanes *et al*., 2001; Ablain *et al.,*2009) and the anticipated increase in storm frequency and intensity (Beniston *et al*., 2007; Berg *et al*., 2013). These factors are likely to have global implications on the future rates of erosion at rocky coasts by altering wave climates, tidal regimes and sediment transport patterns (Trenhaile, 2016). The significance of rocky coast erosion is put in to perspective when considering an estimated 80% of the global coastline is considered rocky coastal cliffs (Emery and Kuhn, 1982) although this figure has since been re-evaluated to a more conservative 52% (Young and Carilli, 2019). Nevertheless, the requirement to future-proof coastal zones against the anticipated impacts of climate change is profound given the shifts in population demographics towards developing coastal megacities (Small and Nicholls, 2003). Such migratory trends, driven by rapid economic growth are set to continue into the future presenting an increased socio-economic risk, particularly in low-elevation coastal zones (Neumann *et al*., 2015). Considering the consequences of exacerbated coastal erosion it is imperative that we attain a greater understanding on the impacts of contemporary hydrodynamic conditions on rocky coasts, more specifically shore platforms.

Shore platform evolution

The evolution of the shore platform is a product of a host of physical, chemical and biological processes and site-specific geological, geographical and environmental conditions (Temme *et al*., 2017). Understanding landform genesis provides insight to the aforementioned processes and conditions and affords the opportunity to determine the role they play in shaping this conspicuous coastal landform. Therefore, in addressing shore platform evolution we gain a greater understanding of landform evolution from a contemporary and future perspective. This is necessary to better understand the function that boulder production and transport mechanisms have in shaping platform modification and in terms of implementing management strategies to mitigate against the increased risk of erosion to either the platform or the hinterland to which it serves as a natural defence.

Shore platforms act as an interface between the resisting forces of the land and the erosive forces associated with wave activity. Wave energy is attenuated across shore platforms through the interaction with surface topography and roughness (Ogawa *et al*., 2011) and consequently they act as natural barriers protecting the hinterland that they front. Therefore, an increased awareness of

how these landforms respond to contemporary storm wave activity is required to determine possible rates of erosion.

Trenhaile (1980) published a paper entitled *'Shore platforms: a neglected coastal feature'*. Since then interest in shore platform processes and the mechanisms that govern their evolution has grown. Seminal works by Trenhaile (1987) and Sunamura (1992) provide a thorough account of the geomorphology of rocky coasts and offer a comprehensive insight to shore platform genesis and development. Within the texts they present three distinct shore platform types (Figure 1.2), they are:

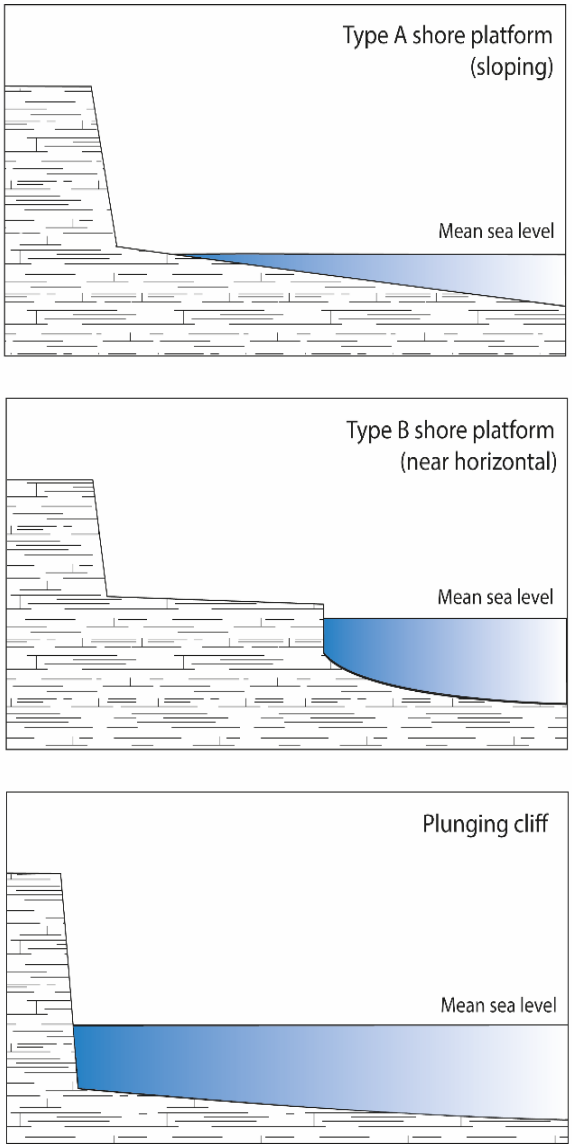

Type A - gently sloping platforms (1-5°) which extend from the cliff-platform junction to below the low-tide level with no significant break in topography, or abrupt seaward terminus. These are generally located in marcrotidal settings.

Type B - near, or sub-horizontal platforms (< 1°) which extend from the cliff-platform junction to a point of termination marked by an abrupt drop at the seaward edge. They are most common in meso, and microtidal environments.

Plunging cliff - near vertical cliff faces that plunge directly below sea level, frequently found in resistant rock types.

Figure 1.2. Shore platform types, adapted from Sunamura (1992).

The limestone shore platforms at both Bembridge sites (Bembridge Ledge and Black Rock) are categorised as 'Type B' owing to the presence of an abrupt seaward terminus and the sub to near-horizontal platform surface. As a result, the focus herein will relate to 'Type B' platforms.

Shore platforms are familiar features of rocky coasts. They are formed predominantly as a result of the erosive forces of waves and/or weathering processes (Kennedy *et al.,* 2011; Stephenson *et al*., 2013). These distinct coastal landforms vary in morphology not only because of the erosive forces attributed to waves and weathering, but also due to the geology; the material upon which the platform is formed. This can range from resistant rock types such as granite, as found on the Atlantic coast of northwest Ireland (Knight and Burningham, 2011), to the less resistant sedimentary chalk platforms of the south coast of the U.K. (Moses and Robinson, 2011). Trenhaile (1987 and 1997) also identifies tidal regime as significant in the evolution of platform morphology, whereby a linear relationship (r^2 = 0.92) exists between platform slope and tidal range. The greater the period of submersion and the broader the vertical range over which wave energy is expended results in an increased slope gradient (Trenhaile and Kanyaya, 2007).

A fundamental characteristic of shore platform evolution is that of platform width. In its simplest terms, width is defined by the distance between the landward and seaward platform limits (Kennedy, 2015). Width is controlled by a number of variables, including tidal range, wave climate, surface downwearing, subaerial erosion and wave impacts at the cliff-platform junction (Trenhaile, 1983 and 1997; Stephenson and Kirk, 2000). The rate and extent to which platform width develops is a reflection of the efficacy of these variables. Sunamura (1992, page 181) suggests that cliff recession is required for the evolution of both Type A and Type B platforms. It is also suggested that erosion at the seaward margin is negligible under current sea levels. However, this was based on laboratory experimentation with homogenous material lacking lithological structure and from observations that the platform terminus was often covered in flora and fauna, even following storm wave attack (Sunamura, 1992, page 167).

However, the premise of Sunamura (1992) that erosion is limited at the platform terminus is argued by Dickson *et al*. (2013), Trenhaile and Kanyaya (2007) and Moses (2014) who identify erosion at the seaward platform edge *and* at the cliff-platform junction as key factors driving platform width, and thus development. This is supported by the findings presented in this study (Hastewell *et al.*, 2019a; Hastewell *et al.*, 2020) whereby boulder production resulting from block detachment at the exposed platform front has been documented under moderate wave conditions. Evidently, meso-

erosion is taking place at the platform edge suggesting that such processes are occurring across a much narrower temporal scale than had previously been realised.

Platform development is presented in the form of two proposed theoretical models adapted from Sunamura (1992) with consideration afforded to erosion at the platform terminus (Figure 1.3). The model assumes a consistent sea-level and a setting where wave energy dominates over downwearing; (1) the equilibrium model, and (2) the steady state model.

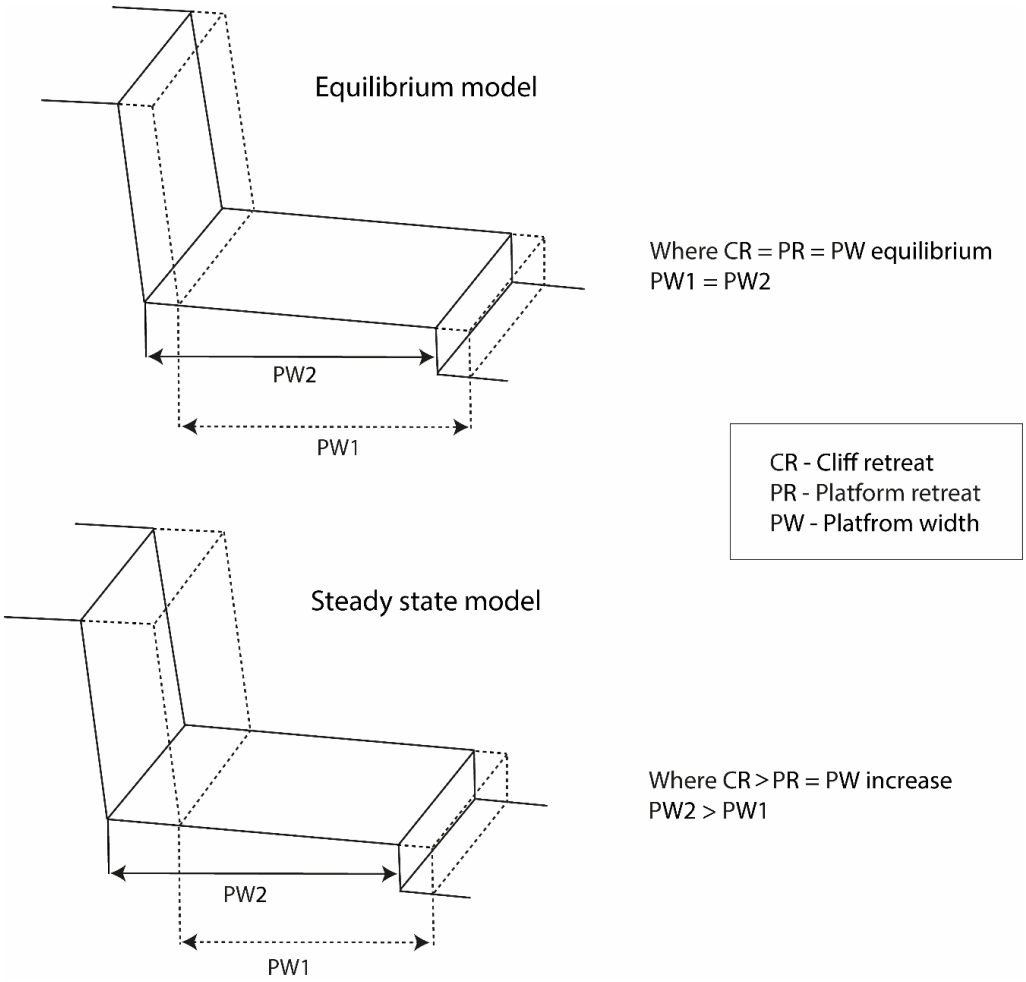

Figure 1.3. Schematic diagrams of shore platform evolutionary models, adapted from Sunamura (1992).

1 - Equilibrium model

Where the rate of retreat at the cliff-platform junction (CR) is equal to that of the seaward edge (PR), platform width (PW) remains constant and remains in equilibrium. Where erosion rates are negligible over large temporal scales, the platform adopts a static equilibrium state (Trenhaile, 1983).

2 - Steady state model

When the rate of erosion at the cliff-platform junction (CR) exceeds that of the seaward edge (PR) platform width (PW) increases to the point where wave action is no longer able to reach, and erode the cliff toe. Once this stage has been attained platform downwearing occurs reducing the slope angle (Moses, 2014). Once the slope angle has been reduced sufficiently wave action will reactivate erosion at the cliff-platform junction and platform width will increase; the process then recommences, *ad infinitum*, assuming no coastal management intervention and sea-level remains unchanged. The platform is thought to be in a steady state of development.

With the threat of sea-level rise and the likelihood of more frequent and intense periods of storm activity it is anticipated that the timescales between cessation and reactivation of erosion at the cliff toe will be reduced, resulting in accelerated retreat at the cliff-platform interface. Therefore, monitoring, and where possible quantifying changes to platform width either at the landward and/or seaward margins will provide insight on contemporary platform evolution and the degree to which geomorphic modification occurs (Trenhaile, 1987; Dornbusch and Robinson, 2011). In terms of relevance to this study, shore platform width has been identified as a factor in the displacement of intertidal boulders in terms of the available distance across which transport can occur (Hastewell *et al.*, 2020).

Shore platform inheritance

Shore platform morphology is modified by the erosive effect of wave action. Consequently, these factors are generally confined within the intertidal zone. Therefore, sea-level is fundamental to the evolution of rocky coasts and the development of shore platforms (Kennedy, 2014). Whilst this may appear evident from present-day marine processes over geological timescales sea-levels vary as a result of interglacial stages which results in the occurrence of erosion and deposition across a wider vertical frame than is signified by present-day sea-level. This means that some coastal features may be inherited from previous high-water stands (Blanco-Chao *et al*., 2003). Such fluctuating sea-levels make it difficult to determine whether shore platform development is deemed to be of contemporary or inherited origin (Trenhaile, 2002).

With respect to the Bembridge shore platforms, these are overlaid by deposits of Pleistocene origin (Insole *et al*., 1998) which are particularly prevalent at Bembridge Ledge. These deposits form a raised beach upon the shore platform which is elevated up to 7 m above Ordnance Datum. The deposit contains pollen, plant macrofossils and diatoms associated with deposition in an estuarine

environment (Holyoak and Preece, 1983). The deposit has produced material that has been dated to the Ipswichian Interglacial (115 ka), (Preece *et al*., 1990; Insole *et al*., 1998). Therefore, the underlying limestone platform has been exposed from the erosion of the overlying deposit and thus an element of platform morphology may be deemed as inherited from previously higher sea-level stands.

However, there are no consolidated platforms above the present-day exposures and erosion of the overlying raised beach deposit is considered contemporary; resulting from storm wave activity and sub-aerial processes e.g. excessive rainfall and poor drainage. The active erosion of the raised beach is identified in Figure 1.4, which depicts recent slumping in the raised beach cliff deposit. Basal deposition acts to protect the cliff at the cliff/beach interface until such time that wave energy removes the deposit exposing the cliff base to renewed wave erosion.

Figure 1.4. Bembridge Ledge raised beach deposit and WWII gun battery.

Figure 1.4 also documents what is reportedly a gun battery (foreground) of Second World War origin which was originally located on the cliff top at Bembridge Ledge (Oxford Archaeology, 2002). Field surveys conducted by Oxford Archaeology published in 2002 place the gun battery 6.4 m from the cliff. Subsequent field measurements conducted as part of this study, recorded in 2015, indicate

the distance from the gun battery to the cliff has since increased to 11.6 m; amounting to an additional 5.2 m of erosion from the cliff over the intervening thirteen years.

This suggests the exhumation of the limestone platform via the removal of the overlying raised beach is borne of contemporary processes associated with the present day sea-level stand. Additionally, it identifies that the rate of cliff retreat exceeds that of platform edge retreat and thus the platform conforms to the steady state model, as illustrated in Figure 1.3, and is currently widening.

Whilst erosion rates at the platform edge have not been quantified as the cliff has, the findings detailed within this thesis identify that the liberation of material, in the form of detached blocks, occurs sporadically during storm wave activity. This results in isolated incidents of erosion at the platform edge opposed to the more widespread cliff erosion. However, the detached boulders are of consequence to understanding the storm wave capabilities at the site and how the local platform morphology influences boulder transport processes.

Boulder transport studies (U.K.)

Research interest on coastal boulder deposits has grown in recent years, perhaps in response to the devastating impacts of the Indian Ocean tsunami of 2004, (Goto *et al*., 2007; Goto *et al*., 2010a; Etienne *et al*., 2011; Nandasena *et al*., 2011a). The geographic distribution of research sites reflects the breadth of interest from coastal researchers globally; with field locations in the Pacific Ocean (Nakata and Kawana, 1995; Noormets *et al*., 2004; Goto *et al*., 2010b; Spiske and Bahlburg, 2011; Yamada *et al*., 2014), the Caribbean (Spiske *et al*., 2008; Morton *et al*., 2008; Buckley *et al*., 2012) to numerous sites within the Mediterranean basin (Scicchitano *et al*., 2007; Maouche *et al*., 2009; Shah-Hosseini *et al*., 2013; Biolchi *et al*., 2016; Biolchi *et al*., 2019a).

Whilst the number of studies are too numerous to list from a global perspective, U.K. and Irish based studies contribute to the growing body of literature in the field of coastal boulder deposits. Figure 1.5 has been modified from Moses (2014) who identified the distribution of shore platforms throughout the U.K. and Ireland. The shore platform distribution map has been revised to identify the geographic distribution across which boulder transport studies have been conducted in the U.K. and Ireland.

A requirement of boulder transport studies is a suitable outcrop of bedrock from which boulders can be liberated and displaced by wave activity. The shore platform serves as an appropriate

landform for this process, being regularly exposed to the erosivity of storm wave activity. Thus, shore platforms are capable of providing the base material (boulders) that are detached from the seaward margin of the platform and subsequently transported and deposited by wave energy. This inextricable relationship is reflected in the locations of shore platforms and existing boulder studies.

The numbers represent key areas at which boulder transport studies have been conducted. Table 1.1 accompanies Figure 1.5 in detailing boulder transport research studies and the corresponding study locations.

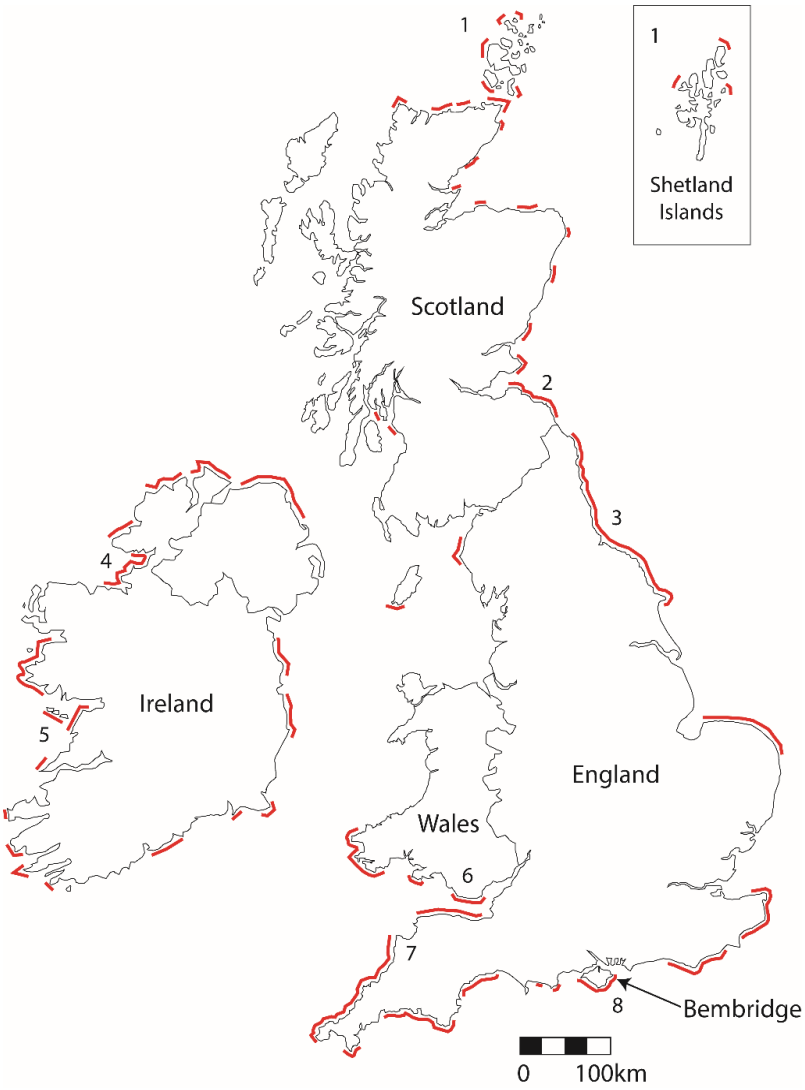

Figure 1.5. Shore platform distribution in the British Isles (red), adapted from Moses (2014). Numbered areas refer to published studies on boulder transport, see Table 1.1.

Table 1.1. Boulder transport studies undertaken in the U.K. and Ireland

Area No.	Region	References
1	Northern Scotland (Shetland & Orkney Islands)	* Hall, A. M., Hansom, J. D., Williams, D. M., & Jarvis, J. (2006). * Hansom, J. D., Barltrop, N. D. P., & Hall, A. M. (2008). * Scheffers, A., Scheffers, S., Kelletat, D., & Browne, T. (2009).
2	East Lothian, Scotland	Hall, A. M. (2011).
3	North Yorkshire, England	Kennedy, D. M., Woods, J. L., Naylor, L. A., Hansom, J. D., & Rosser, N. J. (2019).
4	Northwest Ireland	Knight, J., Burningham, H., & Barrett-Mold, C. (2009). Knight, J., & Burningham, H. (2011).
5	Western Ireland (including the Aran Islands)	Williams, D. M., & Hall, A. M. (2004). * Hall, A. M., Hansom, J. D., Williams, D. M., & Jarvis, J. (2006). * Hansom, J. D., Barltrop, N. D. P., & Hall, A. M. (2008). Cox, R., Zentner, D. B., Kirchner, B. J., & Cook, M. S. (2012). Cox, R., Jahn, K. L., Watkins, O. G., & Cox, P. (2018). Erdmann, W., Kelletat, D., & Kuckuck, M. (2017). Herterich, J. G., Cox, R., & Dias, F. (2018). Erdmann, W., Kelletat, D., & Scheffers, A. (2018). * Scheffers, A., Scheffers, S., Kelletat, D., & Browne, T. (2009). Cullen, N. D., & Bourke, M. C. (2018)
6	South Wales	Naylor, L. A., & Stephenson, W. J. (2010). Naylor, L. A., Stephenson, W. J., Smith, H. C., Way, O., Mendelssohn, J., & Cowley, A. (2016). Stephenson, W. J., & Naylor, L. A. (2011). Cruslock, E. M., Naylor, L. A., Foote, Y. L., & Swantesson, J. O. (2010).
7	North Devon, England	Naylor, L. A., Rodrigues, B. A., Tancock, D., Brady, A. (2010). Brayne R. P. (2015).
8	Isle of Wight, England	Hastewell, L. J., Schaefer, M., Bray, M., & Inkpen, R. (2019a). Hastewell, L. J., Inkpen, R., Bray, M., & Schaefer, M. (2020).

References for boulder transport studies highlighted with an asterisk (*) are repeated due to the co-location of the study sites.

The inclusion of the research presented from Bembridge provides coastal researchers with an additional U.K. location at which to monitor the displacement of coastal boulder deposits resulting from storm-induced transport.

Boulder production, transport and deposition

Prior to embarking on an overview of boulder production, transport and deposition it is necessary to address the question; what is a boulder? In sedimentary terms size classifications are based on a series of grades relative to the coarseness of individual particles based on the intermediate axis. These grades are defined by classifications between two contiguous values.

The widely used Udden-Wentworth scale resulted from the modification to Udden's original classification system (1914) by Wentworth (1922). As of April 2020, Google Scholar states the Wentworth paper has been cited 5,940 times. However, this classification fails to adequately account for boulder size sedimentary clasts defining any particle with an intermediate axis ≥256 mm (0.25 m) as a boulder. The result of no clearly defined classification above 256 mm led to researchers adopting various approaches to boulder size classification, as detailed in Blair and McPherson (1999). This led to inconsistencies throughout the literature and hindered comparative studies (Oak, 1984).

The modified Udden-Wentworth scale proposed by Blair and McPherson (1999) incorporates sub-divisions to better define boulder size as highlighted in Figure 1.6. By adopting the universal size classification system of Blair and McPherson, as recommended by Paris *et al*. (2011), inconsistencies regarding nomenclature will be reduced. Furthermore, a unified framework will be beneficial when drawing comparisons between boulder sedimentary studies. Throughout this study, we adopt the Blair and McPherson (1999) size classification system.

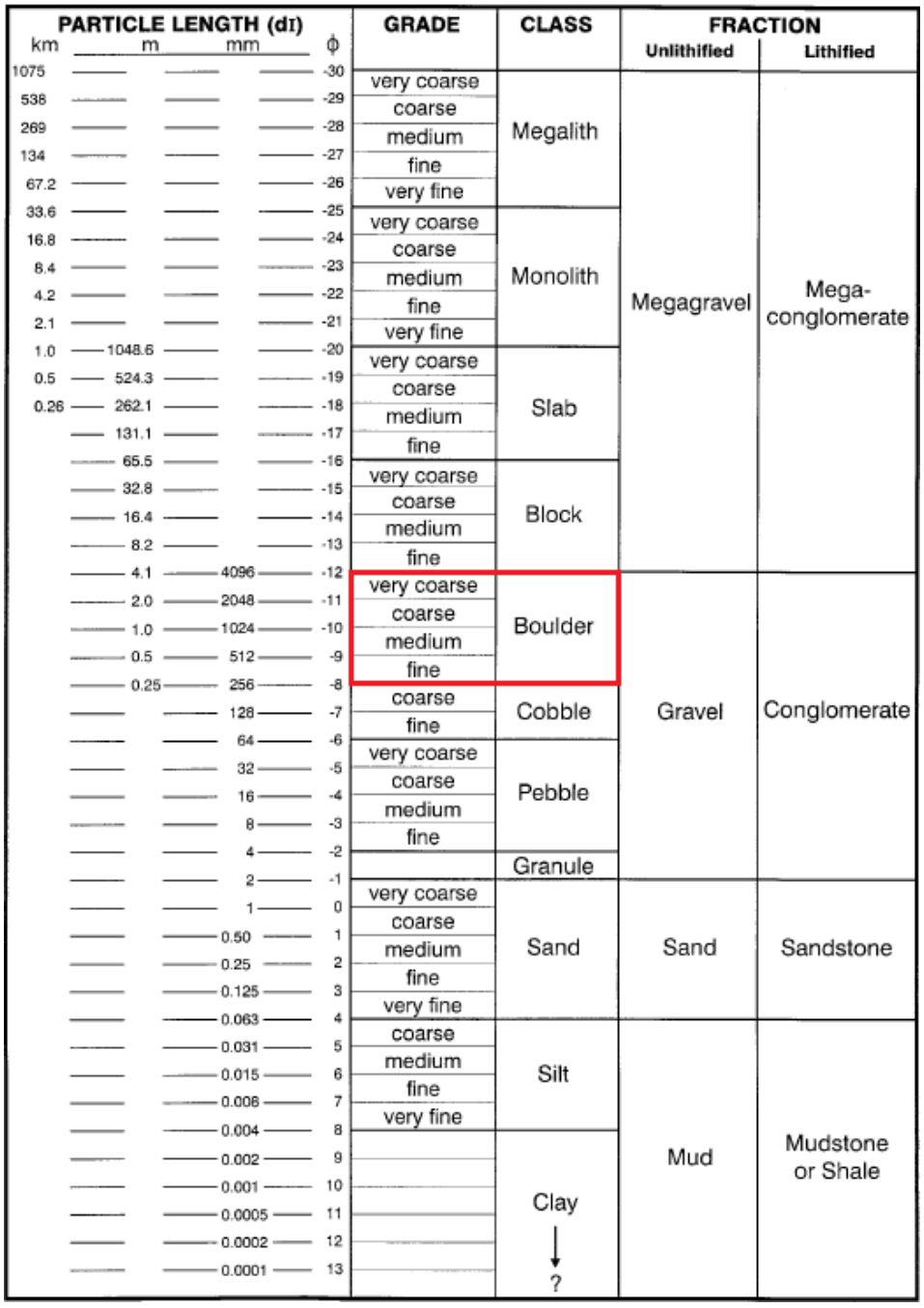

Figure 1.6. The modified Udden-Wentworth scale for defining particle size from Blair and McPherson (1999). The boulder size classification is highlighted.

The production of intertidal boulders and the subsequent transport and deposition is a key theme of this thesis; without production, there is no transport. As such, an introduction to the linked processes is necessary prior to the key boulder transport chapters (Chapters 2 and 3).

Surficial boulder deposits located upon shore platforms have long been of interest to coastal geomorphologists as indicators of historic, high energy, hydrodynamic events (Stephenson and

Abazović, 2016). Dana (1849, page 442) makes reference to the production and distribution of boulders upon shore platforms, stating, "*As the rock is not stratified, the sea does not tear off and throw large masses on the shores*". This statement highlights the significance of lithological structure in the boulder production process, in particular the role of geological discontinuities; defined by Gillespie *et al*. (2011) as interruptions or terminations in the continuity of rocks. As intimated by Dana (1849) and more recently affirmed by Naylor and Stephenson (2010), the mechanisms by which boulders are produced is strongly influenced by lithological structure, i.e. the presence of well-defined bedding and jointing within the bedrock of the shore platform.

Lithology is of increased significance in mid-latitude coastal settings that are subject to storm activity. Consequently, erosivity at these sites is dominated by mechanical wave impacts which are able to penetrate between the bedding and jointing of the platform strata (Trenhaile and Kanyaya, 2007; Stephenson and Kirk, 2000). Water ingress to the joint structure of the bedrock from breaking waves exerts a considerable increase in pressure within the air-filled cavities. As the wave recedes, the compressed air expands leading to the propagation of the cavity (Sunamura, 1992). Continued crack development eventually facilitates the liberation of the block from the bedrock, a process termed 'quarrying'. The efficacy of the quarrying process is dependent on alternating air/water filled cavities. Subsequently, the mechanisms by which quarrying occurs and boulders are produced is thought to be restricted to just below the still water level and the crest of the wave (Trenhaile, 1987).

In mid and high-latitudes wave activity is the dominant erosive force on shore platforms in terms of facilitating the detachment of boulder-sized material from the bedrock shore platform (Trenhaile, 2016). Figure 1.7 presents a schematic diagram of the erosive wave forces that promote boulder production at the platform edge. As previously identified, the ability of waves to quarry boulders within the intertidal zone is greater towards the still water level. This is magnified, as the point at which waves break during high tide is generally greater owing to the increased nearshore water depth (Trenhiale, 2007). The shaded (blue) indicator, at right in Figure 1.7, represents increased erosivity in the vertical frame towards the higher tidal level.

Whilst erosive processes related directly to wave action are generally confined vertically to the extent of the tidal range low-pressure storm fronts frequently generate larger swell waves that extend this erosive zone (red). Associated wave activity facilitates the removal of basal material that under normal circumstances protects the cliff toe. This results in exposure to erosion and subsequent retreat of the cliff and a widening of the shore platform (Sunamura, 1992).

Horizontally, the ability of breaking waves to quarry boulders from the platform edge diminishes landward as represented by the faded blue sector, at centre. Shock is absorbed at the platform front and water ingress is restricted to those directly exposed joints and bedding planes.

Abrasion to the rocky substrate occurs throughout the tidal range, and can be magnified when waves are sediment-laden leading to the platform downwearing (Robinson, 1977).

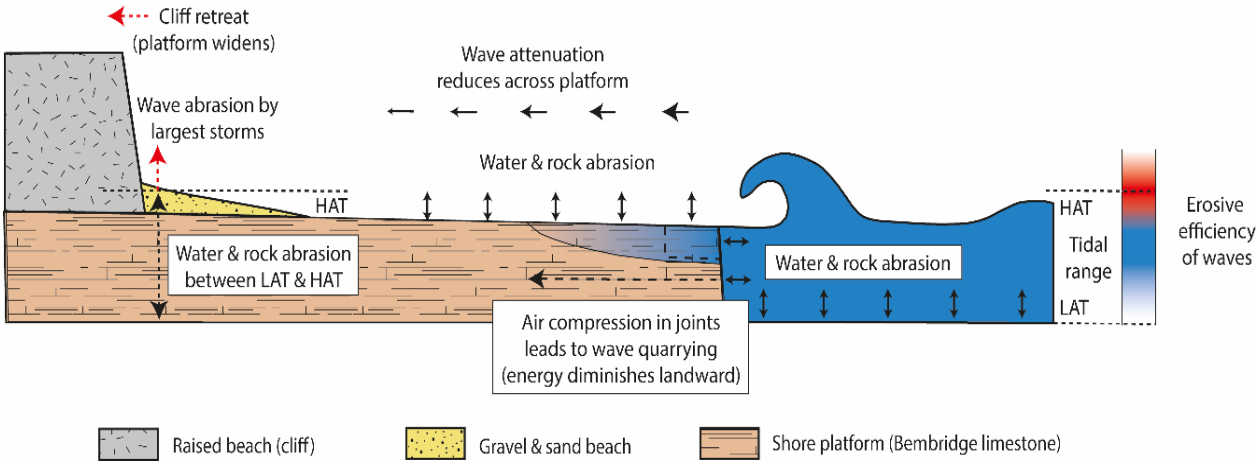

Figure 1.7. Schematic diagram identifying processes of wave erosion on a shore platform. Adapted from Sanders (1968) and Trenhaile (1997).

Whilst Figure 1.7 has been adapted from Sanders (1968) and Trenhaile (1997) it also reflects empirical examples based on findings from both Bembridge field sites. These observations have contributed to an increased understanding of the boulder production process that has informed subsequent findings relating more broadly to the processes and mechanisms associated with boulder production, transport and deposition.

Stephenson and Naylor (2011) present a conceptual model of boulder production which incorporates the subsequent transport and deposition (Figure 1.8). They suggest that boulder production, is driven by wave action, geological discontinuities and weathering processes. The transport/entrainment and deposition of detached, mobile boulders is presented collectively with boulder breakdown occurring via remobilisation.

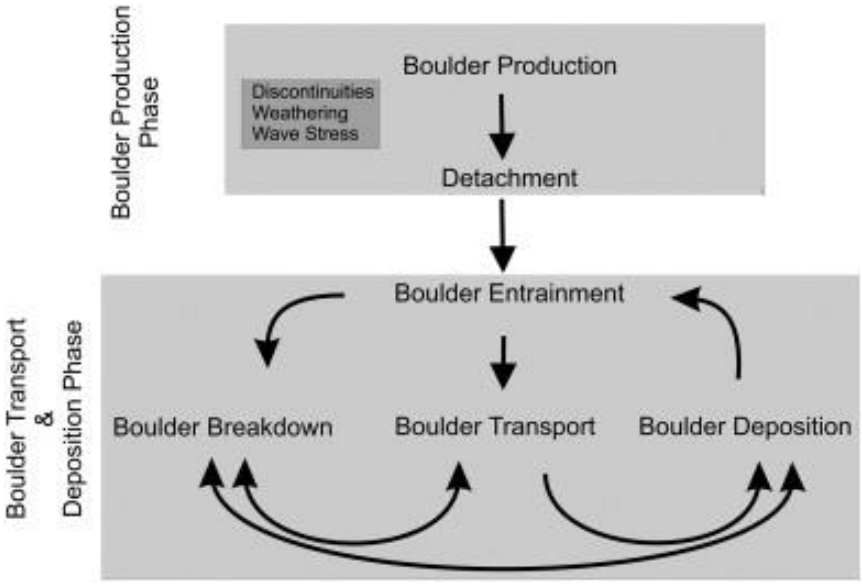

Figure 1.8. Boulder production and transport as defined by Stephenson and Naylor, (2011).

The conceptual model proposed by Stephenson and Naylor, (2011) is reflected in examples obtained from the Bembridge field study. A number of incidents of boulder production were recorded over the study period. Figure 1.9 provides an example whereby the detachment process has been initiated as a result of quarrying from the discontinuous lithology of the bedrock. The exposure and orientation of the heavily jointing strata towards the incoming wave activity at the platform edge allows for the ingress of water from the breaking wave which liberates the boulder from its setting. The removal of the boulder has resulted in a socket which exposes an unweathered rock surface suggesting recent detachment (Hall *et al*., 2008), (Figure 1.9 a and b). This quarried boulder formed part of the RFID tagged array which enabled its unequivocal identification on the shore platform. The transport pathway, from source to deposition amounted to 14.3 m as recorded using the DGNSS.

The post-detachment transport has in part been facilitated not only by the magnitude of the waves ability to physically propel the boulder but also in the lack of obstruction on the shore platform surface; a factor that is addressed in depth in Chapter 3. It is assumed that deposition has occurred at the point where the assailing force of the wave is no longer able to sustain a landward trajectory. However, it is also conceivable that transport may have occurred in smaller incremental movements with deposition resulting from intermittent rest periods between accumulated step lengths (Wheatcroft *et al*., 1990).

Figure 1.9. Boulder production, transport and deposition at Bembridge Ledge (tag ID: 1134); (a) in-situ block prior to being quarried from the surrounding bedrock; (b) exhumed boulder socket and transport pathway; (c) boulder transport from socket to deposition on the shore platform. The arrow denotes the boulder transport pathway. Note the additional displacement of the stared clast in 1.9a and 1.9b. For scale, the DGNSS pole is extended to a height of 2.0 m.

Boulder deposits located on shore platforms are not exclusively derived from block detachment at the platform terminus (Stephenson and Naylor, 2011). The evolution of shore platforms occurs as a direct result of landward cliff retreat (Sunamura, 1992). When the receding cliffs comprise consolidated beds of discontinuous strata the removal of underlying material by wave action at the cliff toe frequently undermines the overlying beds (Hoek and Bray, 1981). In time, an overhang

develops. Continued removal of basal material further enhances the overburden until such time that gravity loading exceeds material rock strength (Herterich *et al*., 2018). This results in boulders being removed from the cliff face and deposited at the cliff toe. Figure 1.10 identifies the accumulation of dolomite boulders that have been liberated from the cliff; deposition occurs at the cliff/platform interface. This example from Kimmeridge Bay, Dorset (U.K.) arises from the removal of the erodible underlying shale which is readily eroded leading to undermined outcrops of the well-jointed dolomite strata.

The deposited boulder talus provides a protective role to the cliff base (Hénaff *et al*., 2006). However, in terms of boulder transport these deposits may be limited in their ability to be further displaced. The closely packed boulders and the proximity of the cliff restrict landward transport. However, where cliff-toe deposits can be activated and reworked by wave activity such material may be drawn seaward on to the platform, thus enabling the potential for subsequent landward mobility (Paris *et al*., 2011).

Where cliff structure permits the removal of blocks from the cliff face a dual process can be attributed to the production of platform emplaced boulders. In the case of Bembridge such consolidated, cliff-bound units are not present. Therefore the principal mechanism of boulder production is attributed to detachment of material at the platform terminus.

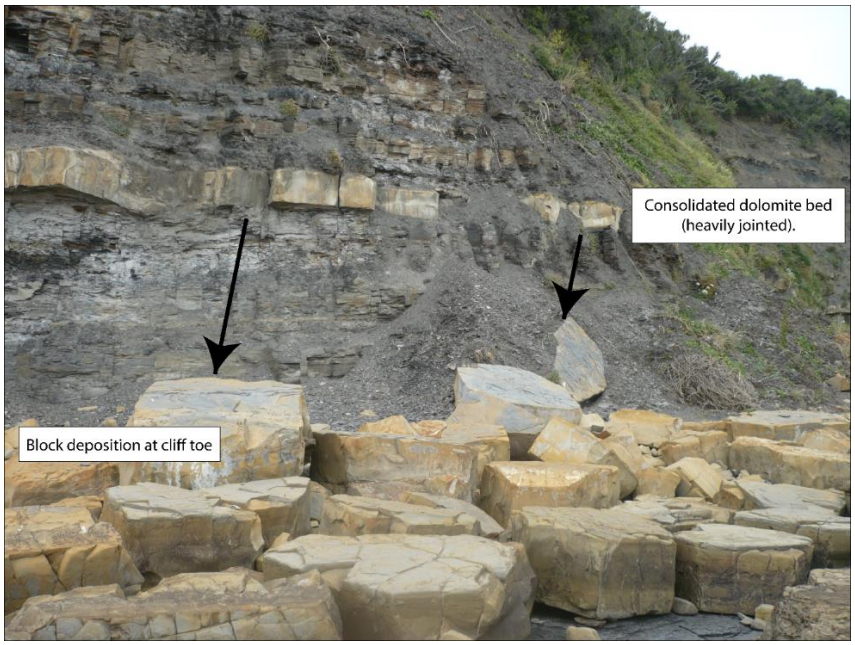

Figure 1.10. Boulder production resulting from rock falls from and eroding cliff, Kimmeridge Bay, Dorset. Removal of underlying cliff material (shale) liberates overlying blocks from the discontinuous dolomite bed.

Sediment tracing

Employing a sediment tracing technique to monitor boulder displacement was integral to the success of the research study in allowing for the unequivocal identification of the monitored boulders. To determine the most appropriate technique it was necessary to evaluate the available options in terms of addressing the methods used in previous littoral sediment transport studies. Henceforth, an overview of sediment tracing research studies is presented as a means of justifying the use of RFID tagging in the monitoring the displacement of intertidal boulders.

There are a range of available sediment tracing techniques that have been utilised historically to monitor the displacement of material in the littoral zone across a range of sediment sizes. Each method has its relative merits and selection may relate to any number of study-specific characteristics (e.g. particle size to be monitored, likely area of dispersion). Although Chapter 2 highlights the RFID technology and methodology employed as part of this study we provide a more comprehensive review of alternative sediment tracing techniques. In doing so we justify the reasoning behind the decision to select RFID tagging as the most appropriate means of tracing boulder displacement.

Knowledge regarding sedimentary transport pathways and rates of accretion and erosion at a range of scales is invaluable to policymakers who are entrusted with safeguarding coastal environments from processes of erosion. Furthermore, the ability to monitor sediment displacement provides a valuable insight to the transport mechanisms and the hydrodynamic conditions that facilitate such mobility (Lee *et al*., 2000; Sear *et al*., 2000).

The ability to monitor sediment transport is enhanced by the use of tracers. In principle, this involves marking sediment, referred to as tagging, with a distinguishing feature in order to differentiate it from the indigenous sediments it is aimed at replicating. Tracers are then deployed at a known location at a specific time providing a spatial and temporal point of reference. Over time the tracers are dispersed as a result of a given hydrodynamic force, e.g. wave action. Periodic field surveys are undertaken to relocate the tagged sediment in order to record where they have been transported from/to over a known period of time. Repeat relocation surveys provide a series of coordinates for the tagged material allowing the user to establish sediment pathways with a spatial and temporal context.

Tracers have successfully been deployed in coastal settings to monitor the displacement of a range of sediment sizes from sand (Bertin *et al*., 2007), cobbles (Dickson *et al*., 2011) and fine boulders

(Brayne, 2015). Methods of sediment tracing have developed considerably with advances in technology from the simplistic use of painted sedimentary particles to more sophisticated electronic tracer techniques. The choice of tracer technique is dependent on a host of factors including, but not limited to, environmental setting (e.g. littoral/fluvial) sediment size, site location, expected area of distribution and timescale of study.

In early sediment transport studies Richardson (1902) deployed broken brick fragments, referred to as brickbats, to observe shingle movement on Chesil Beach (Dorset, U.K.). The use of radioisotopic tracers was used throughout the 1950's. Sediment classes including silt, sand and pebbles were tagged with Scandium (Putman and Smith, 1956; McHenry and McDowell, 1962) and Barium (Kidson *et al*., 1958; Steers and Smith, 1956). The tracers emitted gamma radiation allowing tagged material to be relocated on the beach and underwater using a Geiger counter. However, the short half-life of the tracers limited the longevity of the studies and owing to growing concerns regarding public safety alternative methods soon gained favour. Pantin (1961) deployed magnetic concrete tracers to monitor sediment transport on the seabed; using a dredge to collect seabed samples which were later sieved using a bespoke magnetic flume.

The use of fluorescent painted sediment favoured for monitoring sand-sized particles was widely used during the 1960's and continues to be deployed as it provides a cost effective means of observing littoral transport (Jolliffe, 1963; Yasso, 1962; Badr and Lotfy, 1999; Ciavola *et al*., 1998; Bertin *et al*., 2007; Oliveria *et al*., 2017). The luminescence of the tagged material enables detection using UV light either in the field (during hours of darkness) or from samples taken in the field and later analysed in a darkened room. However, there are limitations regarding the amount of tracer material recovered. As the tracer cloud disperses over time the amount of material recovered diminishes reducing its effectiveness for longer-term studies. Additionally, tracer burial further reduces rates of recovery.

Wright *et al*. (1978) make reference to the poor tracer recovery rates of shingle using visual techniques, commonly less than 15%, and proposed the use of artificial aluminium pebbles as a means of addressing this. Field trials of the method proved successful with recorded recovery rates varying from 27% to 63%. A distinct advantage of this method was the ability to detect buried material at depths of 0.4 m.

Bray *et al*. (1996) deployed both aluminium and electronic tracers pebbles; the latter consisting of artificial resin formed pebbles surrounding a transmitter. The battery powered electronic pebble emitted a low-frequency electromagnetic signal that was detectable using a receiver. The range of

detection was reportedly 1.0 - 1.5 m; a considerable improvement on preceding detection ranges. Additionally, recovery rates were greatly enhanced to between 60% and 100%. Similar recovery rates (up to 99%) were recorded by Lee *et al.* (2000) using the same methodology. A considerable advantage of the electronic tracer pebbles is the ability to transmit a unique code enabling the identification of individual particles. However, despite the advances in detection range and favourable recovery rates the method was limited by the operational durability of the encased battery.

These previous studies have improved our understanding of particle mobility although various shortcomings suggest an alternative technique could provide added benefit to broaden our knowledge of the complex interactions between hydrodynamic conditions and sediment transport pathways.

The use of RFID tagged sediments has provided coastal researchers with a tool that requires no internal battery, thus presenting the opportunity for long-term studies. Furthermore, the ability to detect buried material enhances rates of tag recovery. A number of littoral studies have employed RFID tracing technology as a means of determining sediment transport rates although these have largely focused on gravel and cobble-sized sediments up to 128 mm (Allan *et al*., 2006; Nichols, 2004; Curtiss *et al*., 2009; Dickson *et al*., 2011; Miller *et al*., 2011; Dolphin *et al*., 2016).

Having achieved limited success with a variety of tracer techniques including painted and magnetised clasts Allan *et al*. (2006), encouraged by the deployment of RFID tags in fluvial studies employed the method on the highly energetic Oregon (U.S.A.) coastline. Notwithstanding the dynamic wave conditions (average winter wave heights of 3.5 m and storm waves exceeding 10 m) tag recovery remained high retrieving 90% of the 400 tagged cobbles after eight months, reducing to 18% after seventeen months.

Transport rates of very coarse pebbles were monitored by Dickson *et al*. (2011) whereby 180 RFID tagged cobbles were deployed over an eight month period. Recovery rates on completion ranged from 0 - 30% across three sites. The poor recovery rates were attributed to high-energy wave activity which dispersed tagged material beyond the confines of the study site. Curtiss *et al*. (2009) deployed RFID tagged gravel to identify seasonality in sediment transport achieving recovery rates above 80%. They reported burial of tracers due to storm activity and unfavourable tides as being responsible for reduced recovery.

Dolphin *et al.* (2016) conducted a field study spanning three years, believed by the authors to be the longest running study using RFID technology to monitor coastal gravel displacement. The study recorded consistently high detection rates, achieving 78% on completion based on 940 tagged particles.

The aforementioned studies are restricted to the intertidal zone owing to the presence of tidal water hindering accessibility. However, adaptations to the detection equipment have extended the use of RFID technology in to the subtidal zone enabling underwater detection (Benelli *et al*., 2009; Bertoni *et al*., 2010; Benelli *et al*., 2012).

Drawing upon the success of these previous studies highlighted the potential for RFID technology in tracing sediment mobility. These studies were instrumental in making an informed decision to opt for this tracing technique as part of this sediment monitoring programme. However, despite the potential for the use of RFID tagging in monitoring intertidal sediment transport previous RFID deployments have largely been limited to monitoring gravel and cobble-sized clasts. RFID tagging as a means of monitoring boulder-sized clasts is thought to be limited to one previously unpublished study. Brayne (2015) deployed RFID tagged sediments across a range of particle size classes from medium pebbles to fine boulders (intermediate axis 128 mm up to 0.5 m). Notwithstanding the Brayne study, which only encompasses the smallest boulder classification, an entire RFID tagged boulder array has not previously been deployed and monitored over the timescales involved in this study. The findings reported herein form the first known study of its kind where RFID technology has been deployed exclusively on boulder-sized clasts. The favourable recovery rates recorded have provided a wealth of information and insight suggesting the methodology has considerable potential in providing coastal researchers with a reproducible means of accurately quantifying contemporary boulder transport pathways.

Site description (Bembridge)

The published manuscripts present brief site descriptions, however, owing to the concise nature required in the manuscript format it was not feasible to elaborate further than was necessary on the site location from an ecological and geological perspective. This introductory chapter offers an opportunity to present a more in-depth description of the site, with added emphasis on the geology. This was deemed appropriate given the significant role geological characteristics play in the boulder production process (Stephenson and Naylor, 2011).

The coastal village of Bembridge lies at the easternmost point of the Isle of Wight (Figure 1.11). The foreshore is dominated by extensive limestone platforms, or ledges, that protrude into the Solent. The Forelands area sits between the two study sites, Bembridge Ledge and Black Rock which extends into Long Ledge as identified in Figure 1.11. Collectively, the platform features stretch around the coastline for 3 km from the RNLI lifeboat station in the north, (Figure 1.11b) to the edge of Whitecliff Bay in the south west (Figure 1.11c).

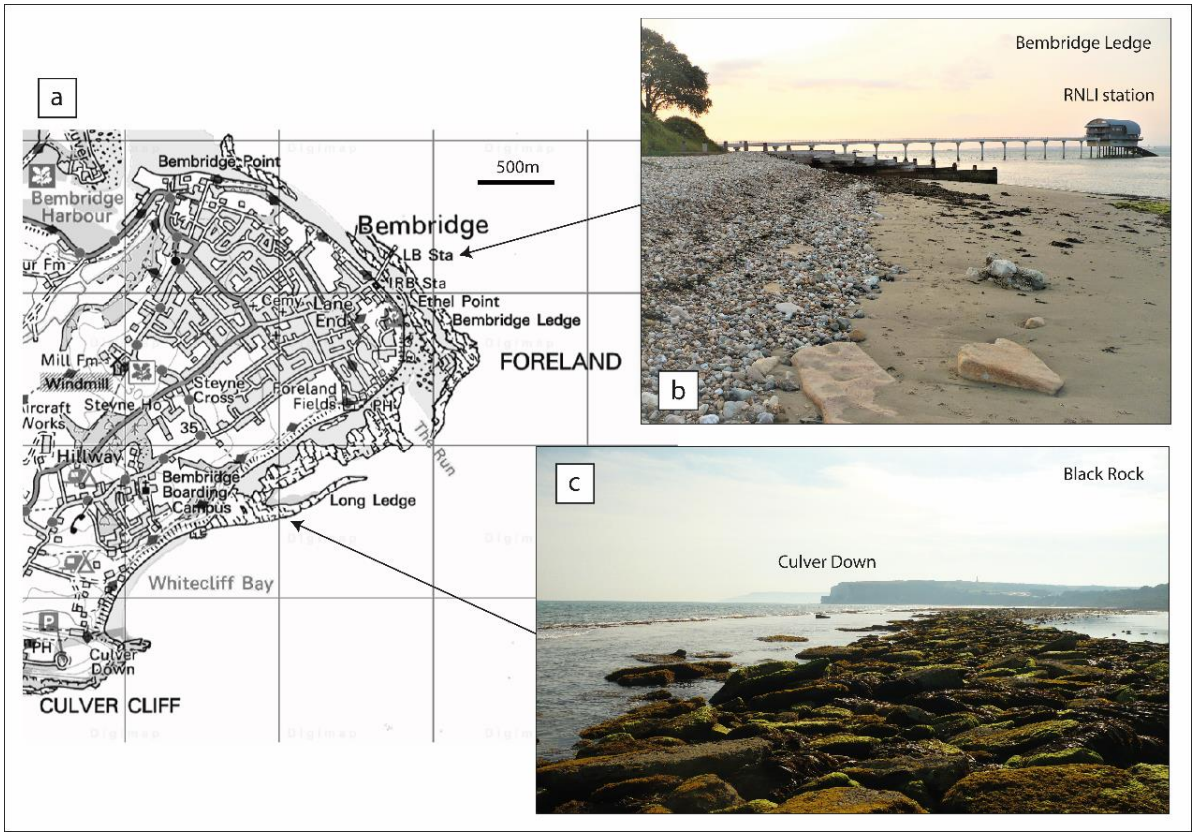

Figure 1.11. Bembridge, Isle of Wight; (a) OS map of Bembridge; (b) Bembridge Ledge, looking north, RNLI lifeboat house at right; (c) Long Ledge looking southwest towards Black Rock and Whitecliff Bay, Culver Down can be seen in the distance, at centre.

The platforms are reportedly the most easterly example of limestone shores in the English Channel (Collins *et al*., 1990) and support a vast array of intertidal and sub-tidal marine species of International importance (Collins and Mallinson, 2000). Additional site descriptions are found in Chapters 2, 3 and 4.

Bembridge is a site of great significance from an ecological, environmental and geological perspective. However, until this study, it has not been subjected to scrutiny from a geomorphological perspective. The significance of the site is reflected in the number of assigned

designations. Bembridge forms part of the Solent European Marine Site (EMS) as designated by Natural England. In addition to this, it is also a Site of Special Scientific Interest (SSSI), a Special Protected Area (SPA) and a Special Area of Conservation (SAC) under the South Wight Maritime SAC which covers both the coastline and subtidal areas (Isle of Wight Council & Royal Haskoning. 2010). The Bembridge Ledges provide valuable intertidal feeding grounds for a host of bird species; hence, it is protected under the Solent and Southampton Water Ramsar site. Much of the ecological significance of the Bembridge Ledges arises from the large, slow-draining intertidal pools found on the shore platform. These are host to a variety of species including many, more commonly found in the sublittoral zone (English Nature, 2001). These intertidal pools are subject to investigation as part of this thesis, see Chapter 4: Identification of plate-forme à vasques on a temperate shore platform? Quantitative analysis of morphology and relationships at Bembridge, Isle of Wight.

In addition to the aforementioned designations, on 31st May 2019, Bembridge, including the area covering the study sites of Bembridge Ledge and Black Rock was classified as a Marine Conservation Zone (MCZ) by the Department for Environment, Food and Rural Affairs (DEFRA, 2019). The MCZ covers a 75 km^2 inshore area of intertidal and subtidal habitats. The zone has been designated to protect the diversity of the marine species that are found in the area.

Site geology

Aside from the ecological designations Bembridge is also a Geological Conservation Review (GCR) site. The GCR site encompasses the Whitecliff Bay and Bembridge Ledges SSSI which was designated in 1955 (Munt, 2008). Bembridge sits within the Hampshire Basin which underlies Southern England and the north of the Isle of Wight (Yuangdetkla *et al*., 2011). The area has been extensively researched due to the cliff section at Whitecliff Bay where the exposed stratigraphy presents deposits from Cretaceous chalks to late Eocene, early Oligocene limestones, overlaid by Quaternary deposits. The Whitecliff Bay section (Figure 1.12, by West, 2015), documents changing depositional environments from marine through to brackish, estuarine and finally freshwater (Insole *et al*., 1998). The highlighted cliff section (Figure 1.12, at right) identifies the Bembridge Marls and Limestone units at the northeastern extremity. From this point the units extend northeasterly with the limestone bed forming the ledges that are the focus of this study.

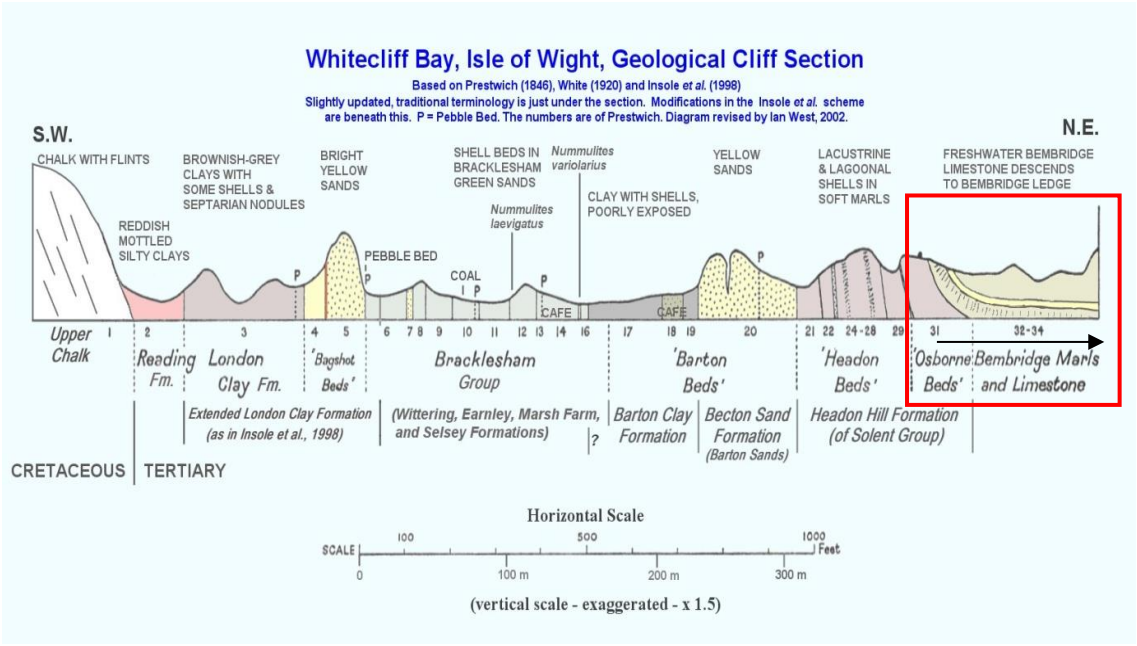

Figure 1.12. Whitecliff Bay cliff section (West, 2015). The study sites of Black Rock and Bembridge Ledge are located adjacent to the highlighted Bembridge Marls and Limestone section.

Detail of the Bembridge bedrock units obtained from Edina Digimap, Geology Roam identify the three key units of the study site which will be further described herein (Figure 1.13).

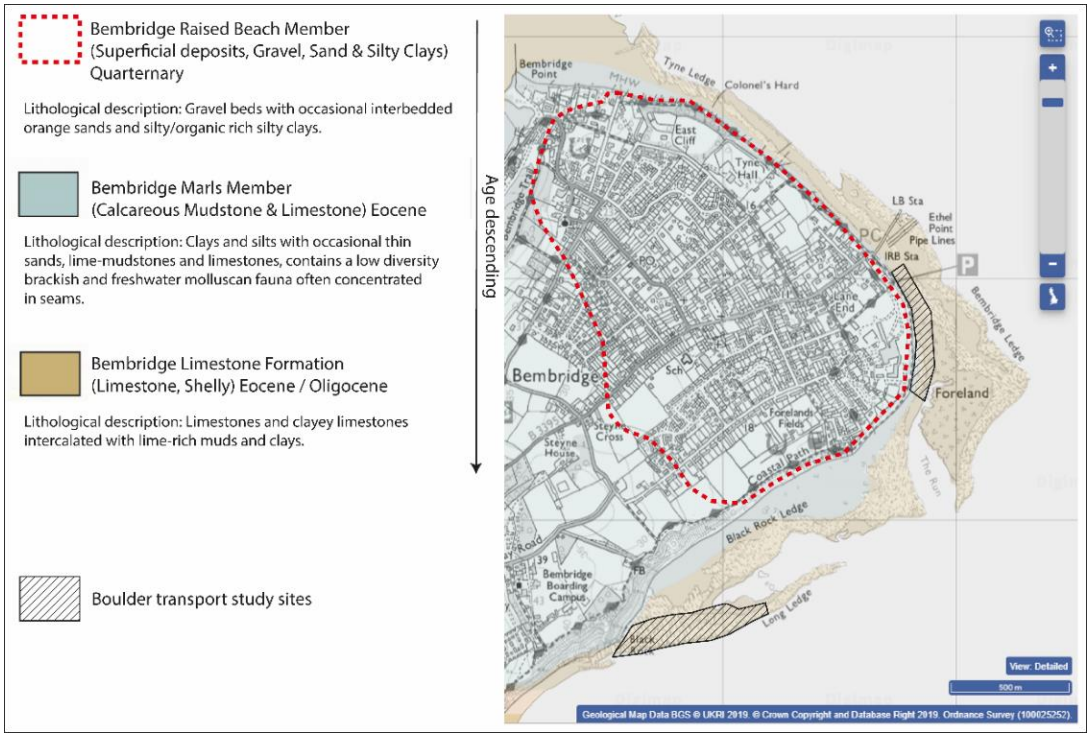

Figure 1.13. Edina Geology Roam imagery displaying the distribution of the geological units at the research sites (Scale 1:50,000).

Bembridge Limestone

The deposits that form the Bembridge Limestone are of Late Eocene / Early Oligocene age (Armenteros and Daley, 1998; Daley and Edwards, 1990; Gale *et al*., 2006) and form part of the Solent Group, Figure 1.14. It comprises beds of cream coloured limestone positioned between the Headon Hill and Bouldnor Formations (Hopson, 2011). Bembridge Limestone is unique to the Isle of Wight and can be found at locations to the west (Prospect Quarry) and north (Gurnard) of the island with additional deposits at Bembridge which form the extensive shore platforms (Insole and Daley, 1985).

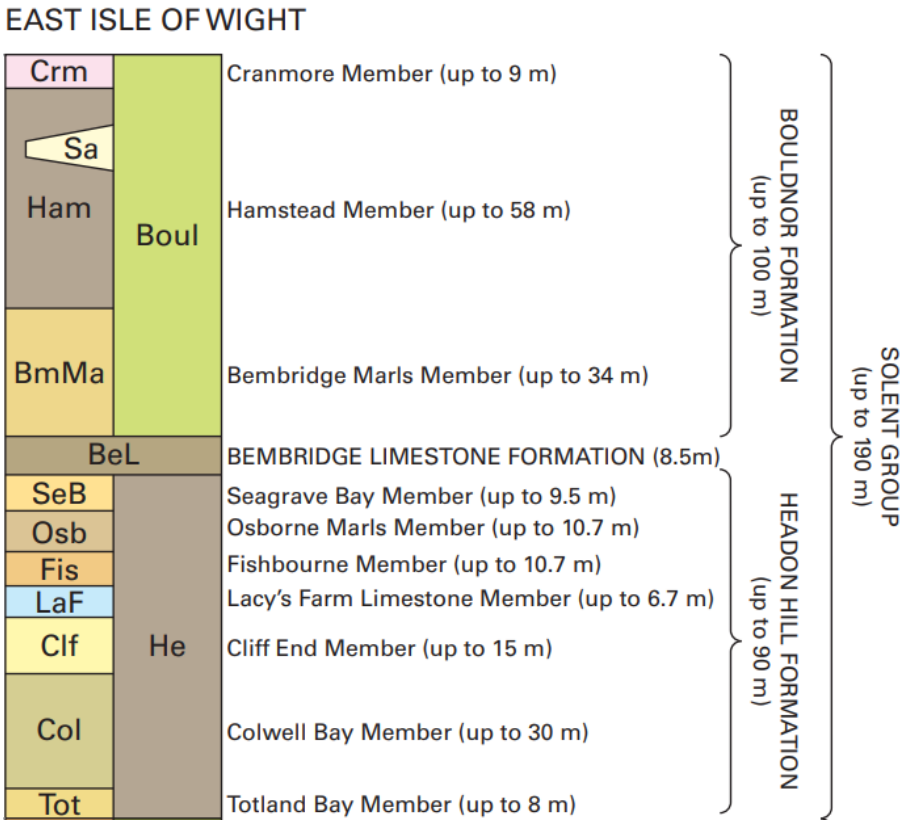

Figure 1.14. Geological formation of the Solent Group, including the Bembridge Limestone formation (taken from, Hopson, 2011, page 755).

The Bembridge limestone is of freshwater, lacustrine origin, having developed in a low-energy carbonate lake. This was established by the presence of fossilised freshwater gastropods, namely *Galba* and *Planorbina* (Armenteros *et al.*, 1997). The lacustrine facies of the Bembridge Limestone comprise two subfacies; marl/marly limestones (wackestone), and well-cemented cream-coloured limestone (Armenteros and Daley, 1998). These facies can be seen clearly at Bembridge Ledge, the upper limestone layer consisting of compact, tabulated and well-cemented, cream-coloured

limestone, overlaying grey tabulated marly limestone Figure 1.15. The expansive joint sets of the limestone units at Bembridge Ledge facilitates the detachment of material at the platform edge.

Figure 1.15. Subfacies of the Bembridge Limestone, heavily jointed limestone overlying marl-rich limestone, image from Bembridge Ledge.

The Bembridge Limestone has long been heralded for its strength and suitability as a building material. Historically, it has been extensively excavated from inland quarries since the times of Roman occupation. Additionally, the foreshore of the Bembridge Ledges were also exploited owing to the well-defined bedding and jointing which facilitated ease of extraction (Historic England, 2016). The stone was used extensively on the island and its durability resulted in its export to the mainland for construction throughout Hampshire and beyond (Colenutt, 1892). The use of the rock as a building material is a testament to its strength and durability.

Bembridge Marls

Daley (1973) analysed fossil assemblages including gastropods and bivalves found within the Bembridge Marls to establish that they accumulated during a short-lived brackish transgression. He

categorised the assemblages by way of the associated ecological conditions within which they were likely to inhabit suggesting they were formed in: (a) an estuary; (b) brackish lagoons; (c) coastal lakes, subject to occasional ingress of brackish waters; (d) flood plain lakes. Armentros and Daley (1998) proposed a conceptual palaeogeograpahic model suggesting a lacustrine origin for the limestone facies. This, they attributed to a freshwater environment analogous to the present-day Florida Everglades; a low-gradient drainage system with varying salinity levels, from freshwater to brackish.

Quaternary raised beach

The cliff to the rear of Bembridge Ledge consists of Pleistocene interglacial deposits that form the Bembridge Raised Beach. The raised beach is thought to represent deposition from the peak high sea-level during the Ipswichian Interglacial warm period (MIS 5e), (Insole *et al*., 1998 and Oxford Archaeology, 2002). Results from thermoluminesence dating of sand lenses from the basal layer confirmed this, dated at 115.1 ka (Preece *et al.*, 1990). The Pleistocene deposits define a geological unconformity as they lie upon Bembridge Limestone and Bembridge Marls thought to be late Eocene, early Oligocene, 36 - 33 Ma (Armenteros and Daley, 1998).

The base of the cliff is characterised by occasional exposures of the Bembridge Marl which transition well-rounded gravels in an occasional orange sand matrix. The abundance of gravels are interpreted as a storm beach, deposited during a period where sea levels were higher than at present (Oxford Archaeology, 2002). The deposit then gives way to matrix supported gravels within silty clays, interpreted as a solufluction deposit (Preece *et al*., 1990). This in turn becomes an organic-rich silt/clay which has produced an abundant pollen sequence (Preece and Scourse, 1987).

Site-specific geological characteristics are known to exert control on the boulder production process (Naylor and Stephenson, 2010; Stephenson and Naylor, 2011). However, the subsequent transport of detached coarse clastic material is seldom quantified due to difficulties with repeatedly tracking the same boulders spatially and temporally. Sediment tracing techniques can be deployed as a means of promoting understanding of boulder displacement within the littoral zone.

Chapter 2 - Intertidal boulder transport: a proposed methodology adopting Radio Frequency Identification (RFID) technology to quantify storm-induced boulder mobility.

Paper introduction

A number of research gaps were highlighted during the preliminary literature research. These are identified in Chapter 1 - Thesis introduction (page 4-5). Paris *et al*. (2011) and Moses (2014) both identify a lack of empirical field data that accurately quantifies the distances over which intertidal boulders are displaced during storm events. To address this oversight it was necessary to undertake a sediment tracer study. Such a study allows the user to monitor and record the displacement of a select number of tracer particles, in this case boulders, at a given location.

Regardless of sediment size, the tracers must be distinguishable from the indigenous sediments, thus facilitating the relocation and recording of the geospatial coordinates. The simplest way to identify a tracer particle is to number it and/or make it distinctive and unique from all the other surrounding particles; this often involves daubing the particle surface with a resistant paint. Stephenson and Naylor (2011) employed such a technique to observe boulder displacement on the limestone shore platforms of South Wales. However, the painted tracer technique has a number of limitations, not least the inability to relocate the tracer (boulder) in the event it becomes buried by accumulated sediments. Further limitations are highlighted within this chapter, page 40.

During the initial preparatory stages of the research study it was necessary to approach stakeholders to gain authorisation to use the Bembridge site. Representatives from Natural England advised that the use of brightly painted boulders was not permissible given the designations of the Bembridge site as detailed on page 28-29. Furthermore, it was felt that boulders with such distinctive markings would attract unwanted attention from the general public. Therefore, it was necessary to select an alternative, discreet boulder tracing technique, hence the use of Radio Frequency Identification (RFID) tagging technology.

The widespread use of RFID tagging in littoral studies revealed a technology that was capable of withstanding the inclement conditions that occur at the coastal margins. However, these studies focus on sediment sizes below that of boulders (intermediate axis ≤ 0.25 m), see Table 2.1. As a consequence it was necessary to modify the tagging methodology employed for gravels to enable efficient tagging of boulders in the field, as opposed to the laboratory. Given the extent of the

undertaking it was deemed prudent to document the procedural steps that were completed as part of the successful study. The following chapter acts as a stand-alone methodology providing fellow coastal researchers with a comprehensive guide which can be adopted when undertaking comparable boulder transport studies. The findings, based on 2 years of tagged boulder deployment, are provided merely as a means of demonstrating the capability of the method and giving insight to the data that can be generated.

Reference: Hastewell, L.J., Schaefer, M., Bray, M., & Inkpen, R. (2019a). Intertidal boulder transport: A proposed methodology adopting Radio Frequency Identification (RFID) technology to quantify storm induced boulder mobility. *Earth Surface Processes and Landforms* 44(3): 681-698. DOI:org/10.1002/esp.4523

Contribution of named authors:

> L.J. Hastewell - first author, completed all fieldwork tasks with assistance from field operatives; wrote the manuscript in full. Submitted the manuscript and undertook referee corrections and amendments.
>
> M. Schaefer - assisted in the field on numerous occasions, created the Python script that allowed for the quantification of transport distances and provided brief text input to the 'Field survey equipment' section.
>
> Dr's Bray and Inkpen acted as reviewers of the draft manuscript.

Abstract

Boulder transport is an area of growing interest to coastal scientists as a means of improving our understanding of the complex interactions between extreme wave activity and the evolution of rocky coasts. However, our knowledge of the response of intertidal boulder deposits to contemporary storm events remains limited due to a lack of quantifiable field-based evidence.

We address this by presenting a methodology incorporating Radio Frequency Identification (RFID) tagging and Differential Global Positioning Navigation Satellite System (DGNSS) technology to monitor and accurately quantify the displacement of RFID tagged boulders resulting from storm wave activity. Based on preliminary findings we highlight the suitability of the technology and methodology to better understand the spatial and temporal response of intertidal boulders to contemporary storm events.

We inserted RFID tags in 104 limestone boulders (intermediate axes from 0.27 to 2.85 m) across a range of morphogenic settings at two sites on the intertidal shore platforms at Bembridge, Isle of Wight (U.K.). Fifteen topographic surveys were conducted between July 2015 and May 2017 to relocate and record tagged boulder locations (tag recovery rate: 91%). The relocated boulder coordinate data from both sites identified 164 individual transport events in 63% of the tagged boulder array amounting to 184.6 m of transport, including the displacement of a boulder exceeding 10.0 tonnes.

Incidents of boulder quarrying and overturning during transport were also recorded, demonstrating that despite the relatively sheltered location intertidal boulders are created and regularly transported under moderate storm conditions. This suggests that contemporary storm events have a greater propensity to mobilise boulders in the intertidal range than has previously been realised.

Consequently, by documenting our methodology we provide guidance to others and promote further use of RFID technology to enable new hypotheses on boulder transport to be tested in a range of field settings and wave regimes.

Introduction

The anticipated increase in storm activity and intensity resulting from climate change (Easterling *et al*., 2000; Beniston *et al*., 2007) is expected to drive geomorphic alteration to shore platforms and increase the vulnerability of coastal zones globally (Paris *et al*., 2011). Given the irreversible erosional impact of storm waves on rocky coasts (Naylor *et al*., 2010) understanding the geomorphic response to such events is of growing significance. As a result, storm wave impacts on rocky coasts are of increasing interest in terms of understanding landform evolution and monitoring coastal change.

The presence of large boulders on shore platforms is testament to the dynamic nature of the coastal environment. However, the mechanisms that facilitate detachment, transport and deposition of boulder-sized sediment within the intertidal zone are poorly understood. We defined boulders as clasts with an intermediate (*I*) axis between 0.25 and 4.1 m (Blair and McPherson, 1999).

Sediment tracing provides a means of monitoring and quantifying displacement while offering an insight to the hydrodynamic conditions that enable episodes of mobility (Lee *et al*., 2000; Sear *et al*., 2000). The basic principle of sediment tracing is to introduce material to a study site which is distinct from, yet accurately reflects the physical properties (e.g. particle size, shape and density)

of the indigenous sediment (Sear *et al*., 2000; Lee *et al*., 2007; Black *et al*., 2007). This can be achieved using artificial tracers such as aluminium cast material (Bray *et al*., 1996) or by adapting the indigenous material found at the selected study site. Following tracer deployment, successive searches are undertaken to recover the particles and record their precise location allowing distance, direction and frequency of transport to be determined.

In littoral settings sediment tracers are monitored *in-situ* where they are subjected to a series of site-specific conditions (e.g. wave climate, tidal regime, topography and bathymetry) which are difficult, if not impossible to accurately replicate within the confines of the laboratory. This paper demonstrates the feasibility of using Radio Frequency Identification (RFID) technology in combination with periodic topographic surveys using Differential Global Positioning Navigation Satellite System (DGNSS) to accurately quantify the mobility of intertidal boulders resulting from contemporary storm activity.

Historically, tracer techniques have included painted sediment (Russell, 1960; Jolliffe, 1963; Nordstrom and Jackson, 1993); radioisotopic tracers (Steers and Smith, 1956; Kidson *et al*., 1958), magnetic tracers (Osborne, 2005), aluminium tracers (Wright *et al*., 1978), electronic radio transmitters (Bray *et al*., 1996) and RFID's (Dickson *et al*., 2011; Dolphin *et al*., 2016) as a means of monitoring littoral sediment transport across a range of particle sizes. The development of tracer techniques has been driven by the need to improve tracer recovery rates over broader timescales. Table 2.1 identifies how different tracer methods and technological advances have facilitated this. It also highlights the preponderance of research focusing on pebble and cobble-sized particles, and subsequently, the paucity of long-term tracer studies relating specifically to the mobility of boulder-sized clasts. Further reviews pertaining to the development of sediment tracing techniques have been published by Sear *et al*. (2000) and Chapuis *et al*. (2014).

Table 2.1. Littoral tracer studies of coarse sediment reporting the selected tracer technique, duration of study and rate of recovery

Authors & date	Tracer method/technique	Particle size (after Blair & McPherson, 1999)	No. of deployed tracers	Study duration	Reported recovery rate
Kidson *et al*., 1958	Radioactive	Size not specified - pebbles	2000	6 weeks	~5%
Jolliffe, 1964	Artificial (concrete) & painted	Coarse pebbles / fine cobbles	2500	4.5 days	58%
Nordstrom & Jackson, 1993	Painted	Fine / coarse pebbles	8.9 kg	29 days	6% (0.53 kg)
Ciavola & Castiglione, 2009	Painted	Cobbles (>64 mm)	35.1 kg	4 days	30% (10.5 kg)
Naylor *et al*., 2016	Painted and numbered	Coarse cobbles - fine / medium boulders	48	4 days	81%
Wright *et al.* 1978	Aluminium	Very coarse pebbles	75	17 days	61%
Bray *et al*., 1996	Aluminium & Electronic	34 - 65mm: very coarse pebbles	246 & 139 respectively	6 weeks	47-96% & 80-100% respectively
Osborne, 2005	Magnetic	Intermediate axis between 19-108 mm: coarse pebbles / fine cobbles	90	2 months	93%
Allan *et al*., 2006	RFID	Mean 6.5 ϕ (90.5 mm): fine cobbles	400	17 months	90% after 8 months, 18% after 17 months
Curtiss *et al*., 2009	RFID	23 mm: coarse pebbles	96	14 months	above 80% throughout survey
Dickson *et al*., 2011	RFID	minimum long and short axes of 60 mm and 30 mm respectively	180	8 months	0-30%
Miller & Warwick., 2012	RFID	64-128 mm: fine cobbles	54	24 hours	93-100%
Dolphin *et al*., 2016	RFID	Size not specified: gravel	940	3 years	78% on completion
Han *et al*., 2017	RFID	64mm: very coarse pebbles / fine cobbles	200	2 days	33% (75 of 200)

RFID tagging has proven to be effective in transport studies in both fluvial (Bradley & Tucker, 2012; Liébault *et al*., 2012) and littoral settings (Allan *et al*., 2006; Dickson *et al*., 2011; Dolphin *et al*., 2016). It has facilitated longer term monitoring studies yielding more favourable recovery rates when compared with alternative methods. The success of previous RFID-based studies documenting sediment transport was integral to our decision to adopt this technology for monitoring boulder displacement.

It is well documented that storm waves have the ability to detach, transport and deposit boulders on intertidal shore platforms (Stephenson and Naylor, 2011; Paris *et al*., 2011; Etienne and Paris, 2010; Barbano *et al*., 2010; Goto *et al*., 2011; Biolchi *et al*., 2016; Shah-hosseini *et al*., 2011; Cox *et al*., 2012). Boulder accumulations on shore platforms frequently develop distinctive geomorphic features such as clusters, ridges, fields and cliff top deposits (Nott, 2003a; Paris *et al*., 2011). These boulder assemblages have been used to infer the mechanisms by which detachment, transport and emplacement occur, including past tsunamigenic wave events (Engel and May, 2012; Nandasena *et al*., 2013; Mottershead *et al*., 2014; Etienne *et al*., 2011; Goto *et al*., 2012) and contemporary storm activity (Hall, 2011; Fichaut and Suanez, 2011; Autret *et al*., 2016, Cox *et al*., 2018). However, despite growing interest in the effects of extreme waves the subsequent modes and rates of boulder transport over time are poorly understood owing to a lack of accurate, reliable and quantifiable field data (Goto *et al*., 2011; Paris *et al*., 2011; Moses, 2014).

Recent studies have sought to address this by documenting boulder transport during, and resulting from, contemporary storm events. Extreme storm activity occurred in the winter of 2013-2014 which had a dramatic impact on the Atlantic coastline of Europe (Masselink *et al*., 2016a) with reports of significant wave heights exceeding 9 m (Castelle *et al*., 2015). During this period Autret *et al*. (2016) recorded the morphological and sedimentological alteration of cliff-top boulder deposits. They documented quarrying of 178 clasts, one weighing 86 tonnes, and the transport of 507 blocks some as far as 40 m inland at elevations up to 14 m above mean sea level. This was achieved using unmanned aerial vehicles (UAV's) and kite-mounted cameras which were deployed to obtain pre/post site imagery for comparative purposes. These techniques were complimented by field observations of boulder mobility and the use of pressure sensors to establish hydrodynamic conditions during the period of storm activity.

Stephenson and Naylor, (2011) and Naylor *et al*. (2016) employed marine paint as a tracer to document evidence of periodic detachment, entrainment, deposition and the breakdown of boulders. The latter study quantified the transport distance of fine and medium-sized boulders and

is thought to be the first intra-storm assessment of boulder transport. Using painted tracers an 81% recovery rate (n = 39/48) was achieved over a four day monitoring period. Despite the valuable insights gained from these studies the paint methodology has limitations, as follows: (1) the reliance on visual detection prevents relocation of buried tracers resulting in reduced rates of recovery; (2) the paint coating may arouse unwanted attention and encourage anthropogenic transport; (3) prolonged exposure leads to paint abrasion limiting the longevity of the study; (4) being visually obtrusive issues may arise with gaining authorisation for the use of painted tracers in sensitive and designated coastal locations. These factors suggest an alternative, more discreet technique is required for effectively tracing boulder displacement over monthly and annual timescales, RFID tagging provides a viable alternative. Furthermore, with a non-visual mode of detection, RFID tags allow for the relocation of buried clasts, resulting in improved rates of recovery (Bray *et al*., 1996).

Despite the potential of RFID tags for quantifying boulder transport (Paris *et al*., 2011) their use has focused predominantly on mixed gravels and cobbles (Allan *et al*., 2006; Miller *et al*., 2011; Dolphin *et al*., 2016) opposed to boulder-sized clasts (Table 2.1). The limited use of RFID's to monitor boulder displacement may be due to perceived limitations with the technique, identified by Paris *et al*. (2011) and Naylor *et al*. (2016). Specifically, the ability of the tags to remain operational, concerns with clast breakdown and the ability to recover tagged material in a short tidal window. To date, we are aware of only one study that has incorporated the use of RFID's in monitoring clast mobility that extends into the boulder size range (Brayne, 2015); where the maximum size classification used was fine boulders with an intermediate axis up to 0.51 m. We broaden the scope of this previous work and allay concerns with the use of RFID's having conducted the first known field investigation applying RFID tagging to boulder-sized clasts only, from fine through to very coarse boulders.

We embedded RFID tags in 104 limestone boulders across two sites, Bembridge Ledge and Black Rock (n = 54) at Bembridge, Isle of Wight, U.K. Boulders were selected from the indigenous sediment to reflect a range of shapes, particle sizes and morphological settings. Between July 2015 and May 2017 fifteen topographic surveys were conducted to relocate tagged boulders. Recovered boulder positions were recorded using DGNSS; the collated data providing a spatial and temporal context to boulder displacement. This coordinate data was processed using a tailored Python script (see Appendix 1) which calculates the distance and azimuth between successive points.

The focus of this paper is the RFID methodology. We describe in detail the procedures undertaken and recommend a series of considerations, highlighting best practice for successful field tag

deployment and monitoring. We draw upon incidents of mobility from the field surveys to illustrate the capability and effectiveness of the methodology for use in future boulder transport studies.

RFID Methodology

RFID operational overview

The term RFID describes the various technologies that utilise radio waves to identify objects (Aluf, 2017). It has been integrated into numerous mainstream applications, primarily as a means of asset tracking. RFID technology comprises four key components, a transponder, more commonly referred to as a tag, an antenna, a reader and a user interface (PDA), (Figure 2.1).

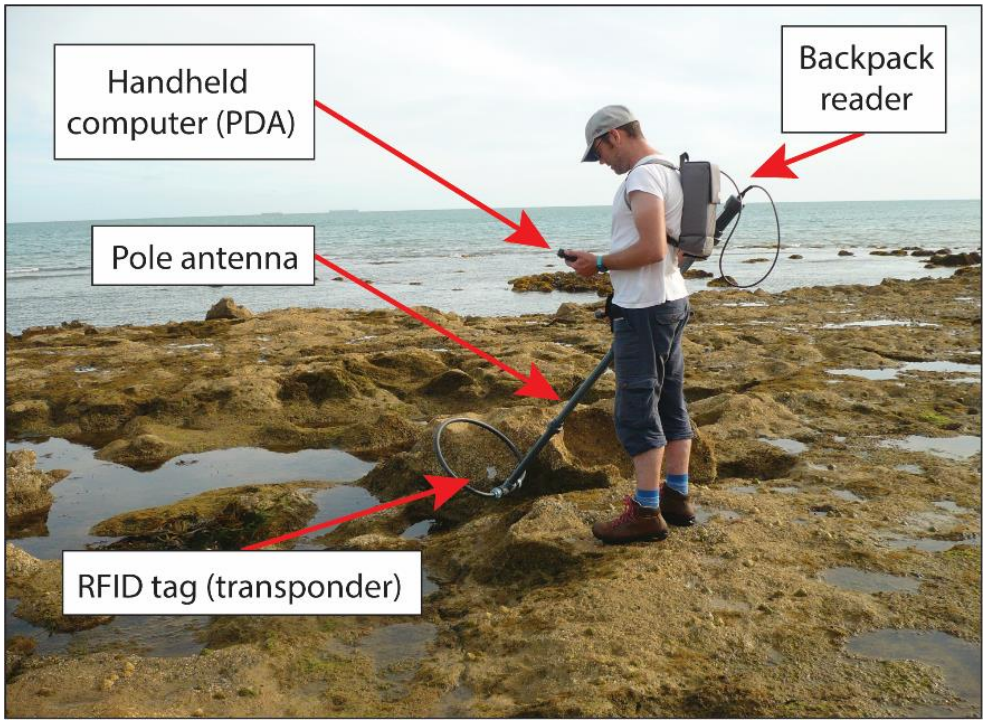

Figure 2.1. RFID detection equipment. (Photo, M. Schaefer).

1 - RFID TAGS (transponder): the tags enclosed circuitry is housed within a hermetically sealed glass casing. Each tag is pre-programmed with a unique 16-digit ID code allowing for the unequivocal identification of an individual object, in this instance a boulder.

2 - POLE ANTENNA: connected to the reader via a cable the circuitry housed within the antenna tubing emits and receives electromagnetic signals via the circular loop. The pole is operated in the field in a sweeping movement, similar to that of a conventional metal detector.

3 - BACKPACK READER: powered by a 14.8 volt lithium polymer (Li-Po) battery the reader is housed in a backpack. It produces a low frequency (134.2 kHz) electromagnetic signal which is transmitted via the pole antenna.

4 - HANDHELD COMPUTER (PDA): featuring specialist software that enables the identification of the unique tag ID number. This is wirelessly connected to the reader via a Bluetooth adapter.

Tag detection occurs when the pole antenna comes within range of a deployed tag, detection range details are documented in Table 2.2, page 46. The emitted electromagnetic signal from the loop of the pole antenna provides sufficient power to prompt tag activation. The tag becomes energised and transmits a return signal containing the unique tag ID code which is received by the antenna and relayed to the reader. An audible alarm also alerts the user to the detection of a tag. The return signal is translated by the reader and transmitted via the Bluetooth functionality to the PDA or alternative mobile device, notifying the user of the tag ID code (Figure 2.2).

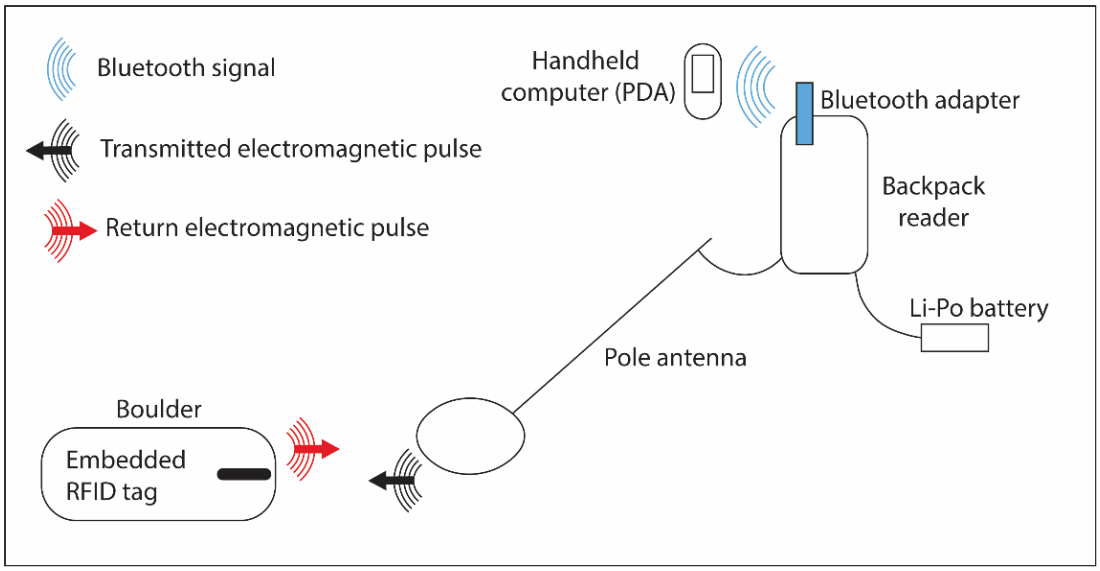

Figure 2.2. Schematic diagram of RFID operation illustrating signal transmittance to/from a boulder embedded RFID tag.

RFID tags can be described as active or passive in their operation (Nichols, 2004). Active tags require a power source (e.g. a battery) which renders them impractical for sediment tracking purposes based on size, cost and longevity of operation. Passive tags, also referred to as Passive Integrated Transponder (PIT) tags have no internal power source making them smaller (tag sizes of 12 mm, 23 mm and 32 mm in length are available). Without the need for a battery the tags have a potentially unlimited operational capacity (Want, 2006) although Allan *et al.* (2006) suggest a more conservative 50 year lifespan.

RFID systems are available from a variety of sources. We selected a field ready solution supplied by Oregon RFID as the manufacturer's specification fulfilled our criteria of tag detection ranges approaching 1.0 m.

Typically, existing tracer techniques rely on the collection and removal of sediment from a study site for tagging in the comfort of a laboratory with access to a range of specialist equipment (Dickson *et al*., 2011; Allan *et al*., 2006). Size constraints dictate boulder tagging must be conducted in the field. This generates a number of novel issues which require consideration prior to, and during tag deployment to ensure a successful monitoring campaign. These will be addressed herein.

Site selection and description

A pre-requisite of any proposed site is the presence of coarse clastic material known to be mobile during periods of increased wave activity. Accessibility is a key consideration as site visits may be required at short notice in response to storm activity. Further consideration is afforded to the locality of wave recording devices to establish hydrodynamic conditions relating to specific storm events which provides insight to the wave thresholds required to initiate transport.

Bembridge is located at the most easterly point of the Isle of Wight (50.6883°N, -1.06982°W), (Figure 2.3). It was selected as it fulfils the aforementioned criteria. We selected two field sites, Bembridge Ledge and Black Rock Ledge upon which 104 RFID tags were inserted into boulders of varying size and shape (n = 50 and n = 54 respectively). Each site covers an area of approximately 0.1 km^2. Boulders are distributed across both sites either as individual, solitary clasts, or collectively as clusters or as distinct assemblages such as boulder ridges. The nearest wave buoy, operated by the Channel Coast Observatory (CCO) is located approximately 5 km to the southwest of the study site at Sandown Bay. The buoy is positioned 1.2 km from the coast in a water depth of 10.7 m (chart datum). There is also a tidal gauge recording wave and tidal parameters located on Sandown Pier (Figure 2.3c). Wave, tidal and selected meteorological parameters are recorded every 30 minutes (CCO, 2017a).

The area is classified as meso-tidal with a spring and neap tidal range of 3.7 m and 1.8 m respectively. Current research relating to boulder transport has focused on site locations with considerable fetches (Scheffers *et al*., 2009; Switzer and Burston, 2010; Noormets *et al*., 2004). Comparably, Bembridge has a limited fetch (Figure 2.3d), its eastern aspect providing shelter from large Atlantic swell waves and the prevailing south westerly wind and wave direction. Bembridge

Ledge is east facing opposed to Black Rock with its southern aspect which is more exposed to wave activity.

Average wave direction is dominant in the southern quadrant with a mean of 164° over the 22 month study period (July 2015 - May 2017). Average significant wave height (H_s) was 0.6 m and a maximum wave height (H_{max}) of 6.8 m was recorded over the same period (CCO, 2017b).

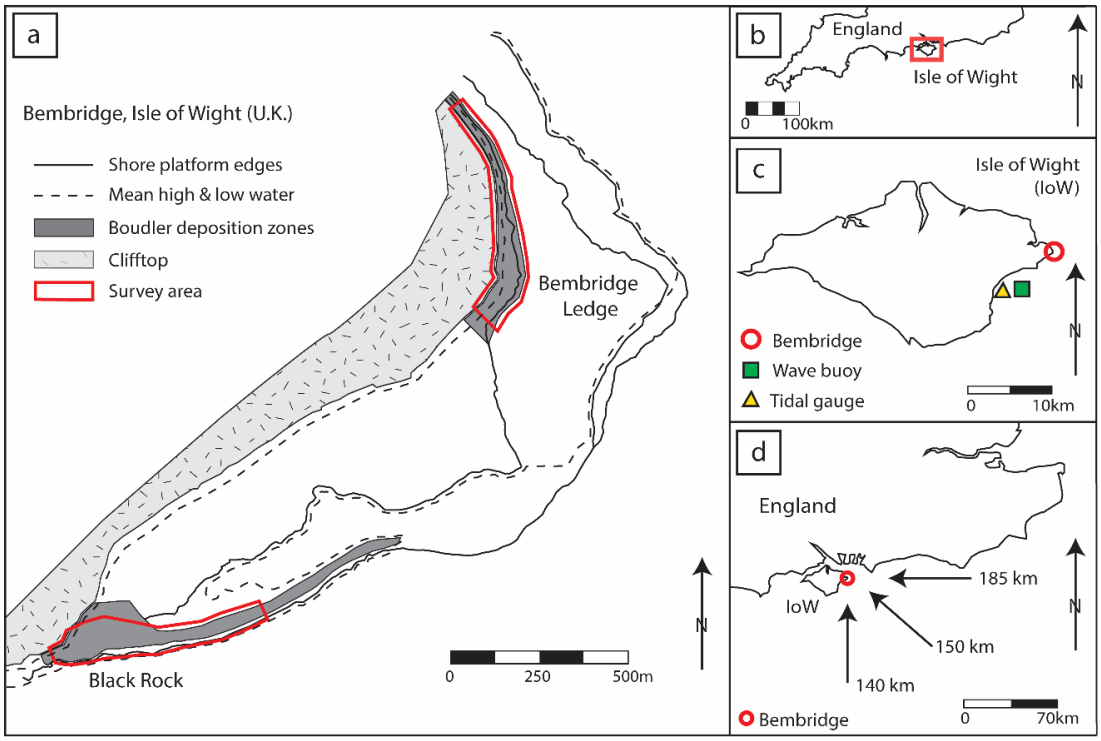

Figure 2.3. Bembridge study sites. (a) Black Rock and Bembridge Ledge - tagged boulders are located within the highlighted survey areas; (b) Isle of Wight's geographic location within the UK; (c) proximity of wave and tidal recording locations relative to the study site; (d) fetch distances to the study site.

A key feature of the Bembridge coastline is an extensive series of intertidal terraced shore platforms that extend up to 500 m seaward at its widest point. The platforms are characterised by an abrupt terminus, akin to the type-B shore platform as described by Sunamura (1992). The platforms are formed of well-jointed, near horizontally bedded Late Eocene Bembridge Limestone (Daley and Edwards, 1990; Armenteros and Daley, 1998). The limestone beds are interspersed by thin layers of Bembridge Marl which are preferentially eroded creating an overburden of the more consolidated limestone. The overburden, coupled with dense bedding and jointing facilitates the liberation of blocks from the shore platform edge (Trenhaile, 2002; Knight *et al*., 2009; Hall, 2011). Block removal, or quarrying, occurs when waves break against fractured rock structures resulting

in increased pressure within air-filled joints (Stephenson and Kirk, 2000; Knight and Burningham, 2011). Increased wave impact pressures promote crack propagation leading to boulder quarrying (Müller *et al.*, 2003). Many of the Bembridge boulders (including RFID tagged clasts) originate from the quarrying process, and are therefore, created, and subsequently transported and deposited by wave activity within the intertidal zone (Figure 2.4).

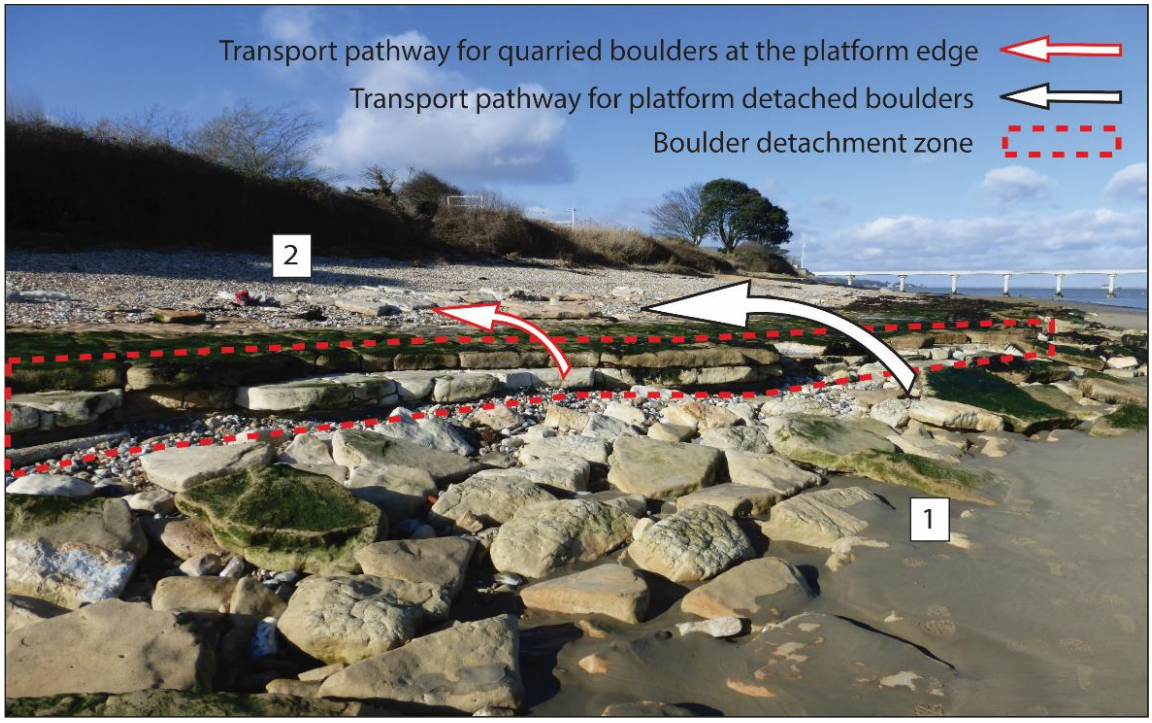

Figure 2.4. Boulder detachment, transport and deposition at Bembridge Ledge. The clearly defined bedding and jointing at the platform terminus facilitates the production of boulders via quarrying and undermining. (1) Detached boulders deposited seaward of the platform edge awaiting transport; (2) transported boulders deposited upon the gravel beach. Boulder transport pathways are highlighted.

Tag selection

RFID tags used in sediment tracing are available in three sizes, 12 mm, 22 mm and 32 mm. The choice of tag size depends on; (1) the size of clast to be tagged: the tag required needs to be smaller than the clast into which it is being inserted; (2) the likelihood of clast burial: the smaller the clast size the greater the likelihood of burial, therefore the vertical tag detection range requires consideration; (3) the required tag detection range: the distance across which a tag can be detected is contingent on a number of factors including tag size, tag orientation, proximity of noise (e.g. electrical appliances), reader battery level and antenna diameter (Oregon RFID, 2017; Allan *et al.*,

2006; Chapuis *et al*., 2014). To maximise the tag detection range we selected 32 mm tags thus increasing the likelihood of tag recovery (Chapuis *et al*., 2014; Oregon RFID, 2017).

As part of the pre-deployment testing we conducted a series of laboratory trials to establish the significance of tag orientation on the detection range. We placed the 32 mm RFID tag horizontally on the floor aligned along the north-south axis with the visible copper wire circuitry (Figure 2.5) orientated north, 0°, replicating Chapuis *et al*. (2014). We approached the tag from the north, east, south and west with the antenna elevated 0.1 - 0.2 m above the ground. When the audible detection alarm was activated we recorded the distance from the end of loop antenna to the tag. Testing was conducted on 5 different tags with 20 approaches from the aforementioned cardinal directions. The results identified that approaching the tag 'head on' from the north towards the copper coil tag end provided a greater read range than from any other direction (Table 2.2). We recorded a mean detection range of 0.77 m, within 15% of the manufacturer's published detection range of 0.89 m (Oregon RFID, 2017). Similar experimental analysis by Chapuis *et al*. (2014) suggested approaching the tag from the northeast maximises tag detection although this was based on 23 mm tags opposed to 32 mm.

Table 2.2. The effect of tag approach direction on detection range; all values expressed in metres.

	Mean detection range (m)								
Tag approach	Tag 1	Tag 2	Tag 3	Tag 4	Tag 5	Mean	Min. range	Max. range	Std deviation
North	0.78	0.78	0.78	0.78	0.76	0.77	0.72	0.84	0.03
East	0.42	0.44	0.43	0.43	0.42	0.43	0.36	0.50	0.03
South	0.61	0.62	0.62	0.63	0.62	0.62	0.56	0.69	0.03
West	0.35	0.34	0.35	0.34	0.34	0.34	0.29	0.41	0.03

Prior to insertion within the boulder, tags were checked in the laboratory to ensure operational functionality by placing them within range of the antenna. The last four digits of the transmitted tag ID were noted. Tags were placed in a protective silicone sleeve to provide additional protection from impact forces during displacement.

The ends of the sleeved tag were capped with a waterproof sealant and allowed to cure. This created a waterproof seal around the tag providing further protection and prolonging operational use. The silicon sleeve was numbered with the last 4-digits of the tag ID code and the copper coiled end was marked for identification in the field at the time of insertion (Figure 2.5).

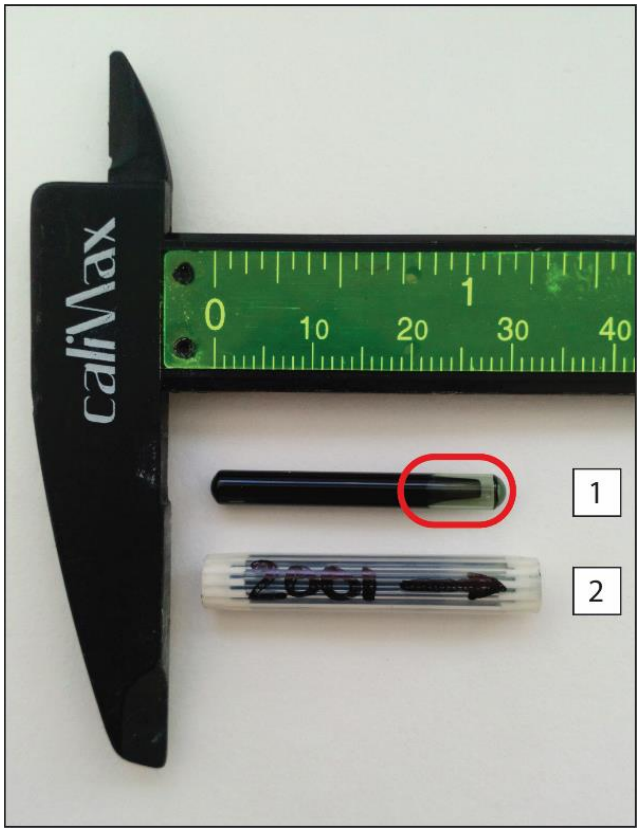

Figure 2.5. RFID tag; (1) 32 mm RFID tag, the copper coils are located in the transparent end of the tag, circled; (2) RFID tag within a numbered protective silicone sleeve.

Boulder selection

Prior to selecting boulders for tagging a number of factors should be considered as they can affect the ability to successfully relocate and record boulders within a single tidal cycle. These include site terrain, tidal regime, spatial distribution of tagged boulders, the number of RFID tag detectors, and the availability of field assistance. Additionally, wave climate requires consideration as this has the ability to disperse tracers across a wider area extending the time required to relocate tagged clasts.

A key factor in tracer studies relates to the effectiveness of the introduced material to accurately reflect the physical properties, namely size and shape of the indigenous sediment (Black *et al*., 2007). This was achieved by measuring a random selection of 100 indigenous boulders at each of the two Bembridge sites, recording the long (*L*), intermediate (*I*) and short (*S*) axial dimensions. These measurements were also used to establish boulder shape as characterised by Zingg (1935). Comparisons of size and shape between the indigenous and tagged boulders are presented in Table 2.3. The values express a degree of similarity between the two populations.

Table 2.3. Particle size and shape of indigenous and tagged boulders, mean boulder size classifications are based on the length of the intermediate axis.

		Bembridge Ledge	Black Rock
Size	Mean indigenous boulder size (m)	0.76	0.84
	Mean tagged boulder size (m)	0.78	0.82
Shape (Zingg, 1935)	Disc (% indigenous / tagged)	(65 / 66)	(49 / 46)
	Blade (% indigenous / tagged)	(32 / 30)	(19 / 15)
	Rod (% indigenous / tagged)	(1 / 2)	(13 / 11)
	Sphere (% indigenous / tagged)	(2 / 2)	(19 / 28)

Samples of the Bembridge Limestone were analysed in the laboratory to determine rock density using the displacement method. Repeated experimentation produced values of 2.4 g/cm^3. All tagged boulders were formed of the local Bembridge Limestone.

The number of boulders selected for tagging was based on the ability to recover the entire array within a single tidal window. With time allocated to setting up the survey equipment and based on a working team of two persons we estimated it would be possible to relocate between 50 - 55 boulders during each survey. Further consideration should be reserved for tagging boulders in close proximity to one another. This relates to the detection range of the RFID tags. For example, with an approximate tag detection range of 0.75 m, upon detection, any two or more tagged boulders within that range may simultaneous transmit a tag ID code. These multiple transmissions create a shadowing effect whereby both tags are activated yet only one code can be received and displayed on the PDA (Lamarre *et al*., 2005; Dolphin *et al*., 2016; Chapuis *et al*., 2014). Therefore, it is suggested the minimum distance between tagged boulders should exceed the mean detection range of the deployed tags.

In selecting boulders for tagging we aimed to represent a range of zones from both survey areas as Naylor *et al*. (2016) identify the significance of morphological setting in controlling boulder mobility. These locations also serve to establish a pre-transport setting for each tagged boulder. The

significance of the pre-transport setting is well documented when used in conjunction with hydrodynamic equations to calculate the magnitude of retrospective wave conditions responsible for boulder transport (Nott, 2003a; Spiske and Bahlburg, 2011; Nandasena *et al.,* 2011b; Switzer and Burston, 2010). The boulder zones are summarised in Table 2.4.

Table 2.4. RFID tagged boulder zones, pre-transport setting and description; Bembridge Ledge (BL) and Black Rock (BR).

Shore platform boulder zones	Pre-transport setting	Description	Number (BL / BR)	Figure
Located on the seaward side of the shore platform.	Platform edge (detached)	Boulders located at the edge of the shore platform which are fully detached and awaiting transport. The tagged clasts located here are impeded in their transport potential by the raised shore platform edge.	15 / 2	2.4 (1)
Located at the shore platform edge.	Platform edge (joint bound)	Described by Nott (2003a) as joint bound blocks. The geologically discontinuous lithology at Bembridge creates angular blocks at the platform edge. These blocks may, or may not, be fully detached from the platform edge being constrained on one or more sides by the surrounding strata.	4 / 3	2.6 & 2.9 (inset)
Located on the shore platform (limited transport potential owing to local topography and/or morphology).	Platform top (constrained)	Boulders deposited on the platform, the transport of which is considered to be restricted by local topography and/or morphological features, i.e., positioned in a depression or imbricate against a rock feature (scarp) or other boulder/s (Trenhaile 2016).	16 / 25	2.11a
Located on the shore platform (greater transport potential owing to local topography and/or morphology).	Platform top (unconstrained)	Boulders deposited on the platform, further transport is unhindered by local topography and/or morphological features (Trenhaile 2016).	15 / 24	2.7

Owing to differences in local conditions it was not possible to maintain consistency of selected boulders between sites, therefore some classifications are underrepresented. This is due to the limited availability and accessibility of suitable boulders to tag, e.g. the lower platform elevation at Black Rock restricts access to boulders located seaward of the shore platform to only the lowest spring tides.

Finally, boulder selection was limited to those boulders that were deemed too large to be moved by human intervention. All tagged boulders had an intermediate axis >0.25 m, this restricted the agent of transport to wave activity alone.

Field tag deployment

The current literature refers to the deployment of RFID tags in gravel and cobbles only. There are no published accounts relating to the specific requirements for boulder tagging. We aim to address this with a detailed review of the tagging procedure demonstrating some key refinements that are required for boulder-sized sediments.

Firstly, holes have to be drilled into boulders in the field to enable tag insertion. In preparation, drill tests were conducted within the laboratory on samples of the indigenous boulder rock type (Bembridge Limestone). These tests provided a valuable assessment on the operational capacity of the drill and the longevity of the battery and drill bits. Testing identified the necessity for a quality, industrial cordless drill and drill bits. We found the Makita 8391DWPQ 18v Ni-Cad Cordless Hammer Drill and DeWalt Extreme II 7 mm masonary drill bits performed particularly well.

Due to the number of boulders to be tagged in the field and based on the preceding laboratory tests a number of spare drill bits and a second drill battery were required together with a means of recharging drill batteries in the field. We achieved this using a 12V car battery connected to a power inverter which converts DC power to AC enabling continued recharging of the spare drill battery whilst the other is in use. The additional weight may prompt logistical considerations particularly where a study site has restricted access and/or limited field assistance is available. Due to the changeable weather conditions at coastal locations the battery recharging equipment was kept dry by securing it in a watertight receptacle.

The chosen location for tag insertion within the boulder is of great importance. To accurately quantify boulder transport it is necessary to relocate and record the same position on tagged boulders during each survey; we selected the tag insertion point (TIP) for this purpose. Tag insertion in the *L/I* plane should be avoided as in the event of transport the boulder may be overturned on to the *L/I* plane obstructing access to the TIP. To increase the likelihood of accessing the TIP the tag should be inserted in the *S*-axis parallel with the orientation of the *L*-axis, as in Figure 2.6. Knowing the location of tag insertion makes identifying the TIP easier should the boulder become colonised with algae and/or barnacles.

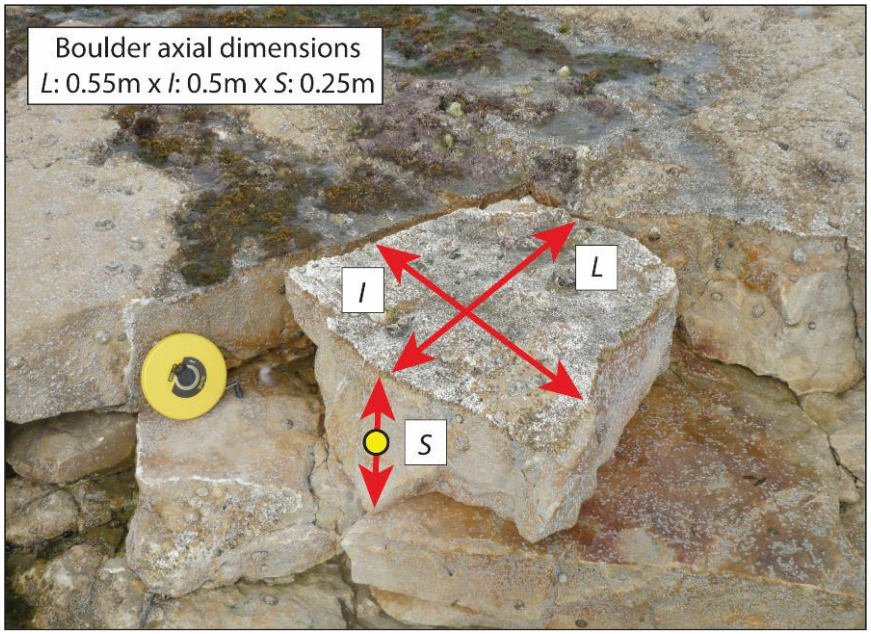

Figure 2.6. Recommended tag insertion point (TIP) within the S-axis as indicated by the circle.

Once a suitable TIP was identified a drill hole was made to the required depth (at least 40 mm) with a 7 mm drill bit (the required hole depth and width is dependent on tag size). Excess dust was expelled from the hole prior to tag insertion to create a dust-free surface. A waterproof, silicon-based sealant (Evo-Stik Wet grab) was injected into the hole, filling to approximately 75%. The pre-prepared sleeved tag was inserted with the copper coils orientated towards the drilled exit hole. This was based on the increased read range of the tags positioned in this manner, as identified in Table 2.2. Once embedded any excess sealant was removed. A further protective seal was applied using Plastic Padding Marine Epoxy creating an additional barrier to prevent the ingress of seawater (R. Brayne, 8th April 2014, pers. comm.). Prior to application the epoxy should be mixed as per the manufacturer's instruction. Curing time varies between products and depending on ambient temperature meaning incoming tides may not allow for the necessary curing times. Hence, it is important to use an epoxy resin that can, if necessary, be applied and cured underwater. Once embedded it is advisable to ensure the tag is detectable and the unique ID code can be transmitted from within the boulder prior to moving on to the next tag insertion. We suggest undertaking laboratory trials of the adhesive and protective properties of the chosen sealant and epoxy prior to full-scale field deployment.

Existing research has indicated that wave activity is capable of flipping, or overturning a range of boulder sizes (Sousa 1979; Noormets *et al*., 2004; Imamura *et al*., 2008). Such events can be inferred by algal growth on a boulders underside (Knight *et al*., 2009), by the presence of biotic indicators

(Mastronuzzi and Sansò 2004) or using comparative photographic evidence (Cox *et al*., 2018). The ability to identify overturning during entrainment provides a useful insight to the mode of transport. To establish when incidents of overturning occur we suggest drilling a secondary orientation hole, approximately 0.01 m deep above the TIP. This identifies the upward orientation of the boulder at the time of tag deployment. Any relocated boulder found with the orientation hole below the TIP can unequivocally be identified as being overturned during transport.

Recording tagged boulder characteristics

On completion of the tagging procedure a series of boulder characteristics were noted, as described in Table 2.5.

Table 2.5. Details the suggested boulder characteristics that should be recorded at the time of tag insertion.

Item	Noted characteristics	Description	Use	Figure
1	Boulder axial dimensions	The long (*L*), intermediate (*I*) and short (*S*) axis measurements are measured.	To establish boulder shape and approximate mass.	2.6 & 2.9
2	Rock type	Noted to determine rock density by conducting laboratory testing on rock samples using the displacement method.	Values used to calculate boulder mass.	N/A
3	Long (L) axis orientation	Recording the boulder orientation offers insight to the transport direction as mobilised boulders often have the *L*-axis aligned perpendicular or parallel to the direction of travel (Nott, 2003b).	Subsequent measurement of the *L*-axis orientation during relocation surveys can help establish where small rotational movements (entrainment) may have occurred between surveys.	N/A
4	Distinguishing features	Distinctive boulder shape, impact scars, abrasion markings or biological indicators such as algal growth, evidence of boring and/or the presence of organisms (e.g. limpets, barnacles).	This may suggest the direction or mode of transport and provide insight to the pre-transport setting and direction and/or mode of transport.	2.7 & 2.9
5	Morphological context	Is the boulder topographically constrained in its ability to be transported, e.g. buried, imbricate against other clasts, located within a depression or against a raised scarp? Accumulated sediment may result in boulder burial during subsequent surveys restricting mobility.	Provides detail on the morphological setting which is known to influence boulder mobility (Naylor *et al*., 2016).	2.8, 2.9 & 2.11a
6	Boulder photograph	Individual boulder images capture a broader visual account of the boulder setting.	Used to compile a boulder identification inventory for each survey. This proved useful for tag relocation and comparative purposes throughout the study.	2.1, 2.6, 2.7, 2.8, 2.9 & 2.11

7	Record the boulder location using the TIP	The DGNSS rover pole is placed next to the TIP and the coordinate recorded. The last 4-digits of the unique tag ID code are entered to the DGNSS interface for processing following survey completion.	Provides a spatial and temporal account of the boulder location.	2.7 & 2.8
8	Noting the position of the orientation hole	Noting the location of the orientation hole relative to the TIP (above the TIP at time of tag deployment). This is of relevance when conducting relocation surveys.	Identifies incidents of boulder overturning during transport if orientated differently to previous survey.	2.7

Under favourable conditions the tag insertion procedure and collation of characteristics took approximately 5 - 8 minutes per boulder.

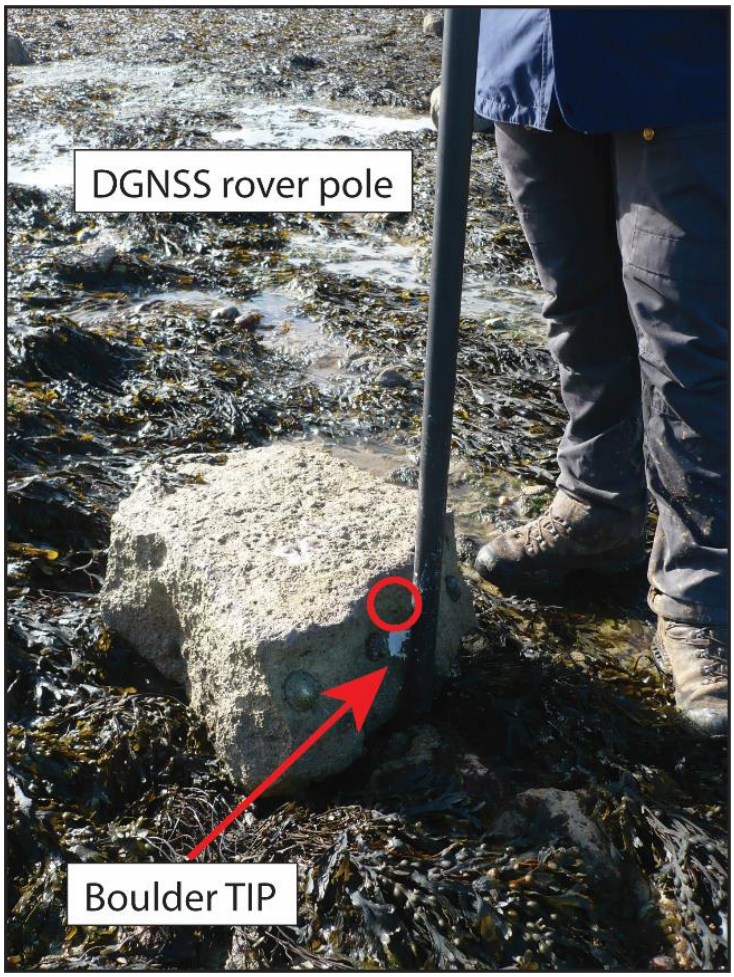

Figure 2.7. Recording of the boulder location; the DGNSS pole is positioned against the tag insertion point (TIP). The orientation hole is highlighted by the circle and the attached limpets are noted for purposes as described in Table 2.5, item 4.

Tag retrieval surveys

In order to determine boulder displacement it was necessary to relocate each boulder during periods of low water. The frequency of the retrieval surveys was dictated by a number of factors including the occurrence of storm activity, favourable tides and availability of field assistance. As part of this study fifteen surveys were undertaken between July 2015 and May 2017 (seven at Bembridge Ledge and eight at Black Rock).

To date RFID studies relocate tagged sediment by systematically scanning the survey area with the pole antenna used much like a standard metal detector (Nichols, 2004; Dolphin *et al*., 2016). To ensure a more productive use of time in the field we utilised the 'stake-out survey' functionality of the Topcon DGNSS. This allows the user to upload boulder coordinate data as recorded on the preceding survey to the DGNSS handheld interface. By accessing the uploaded data points in the field the user is directed to the previously recorded coordinate of the selected boulder as indicated on the interface display screen. If the boulder was not relocated at that location the RFID detection equipment was used to scan the surrounding area until it was found. Once relocated, boulder characteristics 3 - 8 as described in Table 2.5 were documented.

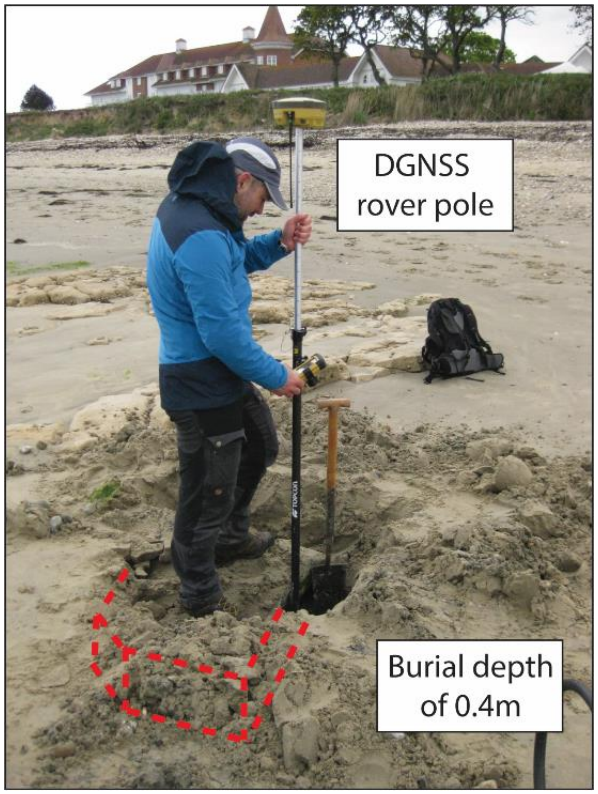

Figure 2.8. RFID tagged boulder relocated and excavated following seasonal accretion of sand. The TIP is being recorded with the DGNSS rover; the dashed line represents the remaining buried boulder.

At Bembridge Ledge we found that tagged boulders deposited towards the beach toe were subject to burial from the seasonal accretion of sediment. Despite being obscured from view we were able to relocate buried boulders using the RFID equipment to depths of 0.4 m, this was the maximum burial depth recorded during the study. Upon relocation, the overlaying sediment was removed and the TIP recorded (Figure 2.8). Once the boulder location was recorded the excavated sediment was replaced.

Field survey equipment

In order to detect boulder movement in the centimetre range a DGNSS setup was required to provide a high survey resolution. Recreational GPS receivers or mobile phones with GNSS capabilities do not offer this level of precision (Schaefer and Woodyer, 2015). DGNSS uses static base stations with known positions to correct for the biases that cause GNSS errors (van Sickle, 2008; Kaplan and Hegarty, 2005). Boulder relocation surveys were conducted using a Topcon Hiper V in Real-time Kinematic (RTK) mode. This uses a local base station that sends out a correction signal in real time to a mobile GNSS receiver (rover), providing a relative horizontal accuracy of 5 mm, +/- 0.5 ppm, (Topcon, 2017).

Defining boulder transport

In coarse sediment transport studies the distinction between entrainment and transport is frequently unclear (Naylor *et al*., 2016). By establishing a displacement threshold it was possible to discriminate between entrainment and transport, making it possible to establish when boulder transport had, or had not, occurred. Previous studies have monitored clast displacement by embedding datalogging tri-axial accelerometers within clasts (Stephenson and Abazović, 2016; Brayne, 2015). The loggers record three-dimensional tilt and acceleration of the clast allowing the user to differentiate between small incremental entrainment events, such as motion about a fixed point, and major movement in a specific direction, akin to transport (Brayne, 2015).

Alternative methods have been employed that avoid the use of loggers, the cost of which can be prohibitive. Naylor *et al*. (2016) define transport whereby the distance moved and the combined root mean squared error (RMSE) exceed half the a-axis length of a given clast, the RMSE being calculated from GPS, rover pole positioning and clast re-measurement error. This method was adopted as it was not possible to re-record the same point on individual boulders. Unlike the aforementioned study we have a fixed point (the TIP) from which the boulder location can repeatedly be re-recorded. Therefore, in defining transport we combine the error from the relative

accuracy of the DGNSS, the setup of the base station and the RMSE of re-surveying the TIP. The RMSE is based on recording four fixed points (two at each site) with the DGNSS as part of the field surveys. A total of 30 measurements were recorded giving a RMSE of +/- 0.03 m in the horizontal and vertical axis, although maximum values of 0.08 m were recorded. Consequently, based on the cumulative error values we conservatively set the horizontal and vertical error at 0.1 m. We incorporate this as an entrainment/transport threshold whereby any recorded movement calculated via the Python script exceeding 0.1 m is defined as being transported. Conversely, values below 0.1 m are deemed to be entrained only and are not incorporated into the total transport distance values presented in Table 2.6.

Results

Herein, we highlight a range of metrics derived from the RFID boulder coordinate data obtained during successive field surveys. The data is aimed to provide an insight to the feasibility of the methodology. Additionally, we demonstrate the capability of the method by presenting examples of mobility that occurred during the field study which further augment the use of RFID's in boulder transport monitoring.

Recovery rates

On completion of the 22 month study we achieved a mean tag recovery rate of 91% across the two sites; minimum / maximum tag recovery rates were 68% / 100% at Bembridge Ledge, and 81% / 100% at Black Rock (Table 2.6). Reduced tag recovery was attributed to the seasonal accretion of sediment leading to boulder burial at Bembridge Ledge and unfavourable and unsafe tidal conditions at Black Rock.

Boulder transport

A total of 15 field surveys were conducted between July 2015 and May 2017 to relocate tagged boulders across the two study sites. Once relocated, RFID tag locations were recorded using DGNSS survey equipment. Successive surveys created a series of coordinates for each of the 104 tagged boulders. A bespoke Python script (see Appendix 1) was created to automatically collate the recorded boulder coordinates and produce a series of inter-survey transport data statistics, including the total transport distance and direction of transport, Table 2.6.

The generated data identified 63% of the 104 tagged boulders as being transported at least once (n = 66/104), i.e. were mobile over distances exceeding 0.1 m. On completion of the study we recorded 164 transport events culminating in a total transport distance (TTD) of 184.9 m across the two sites; TTD is defined as the combined distance over which all tagged boulders were transported. This metric was selected to highlight the range over which the RFID tags remained operational opposed to an individual boulder specific function of transport. Boulder transport data is tabulated in Table 2.6.

At Bembridge Ledge 94 transport events were documented amounting to a TTD of 117.0 m. Of that figure, the highest percentage of mobility (42%, TTD - 49.3 m) occurred between July 2015 and 3rd February 2016. Between these survey dates increased wave activity recorded by the CCO wave buoy occurred between 30th December 2015 and 7th January 2016. Peak storm activity occurred on 3rd January 2016, when maximum significant wave heights (H_s) of 3.3 m, maximum wave height (H_{max}) of 5.4 m and a peak wave period of 7.7 seconds were recorded (CCO, 2017b). Surveys at Black Rock on 3rd December 2015 and 6th January 2016 identify a TTD of 6.9 m during this period which coincides with the increased wave activity recorded on the 3rd January 2016. Interestingly, peak storm waves occurred between low water and 2 hours thereafter. The most significant transport distances were recorded in boulders located around low water on the exposed shore platform. This suggests boulder transport is influenced not only by storm wave activity but by tidal state at the time of peak storm intensity which determines where on the profile storm energy is focused. This corresponds with comparable work on the role of tidal state in beach morphodynamics (Kroon and Masselink, 2002; Castelle *et al*., 2015; Masselink *et al*., 2016b).

At Black Rock, 70 transport events amounting to a TTD of 67.9 m were recorded over the study period. Of that figure the highest percentage of boulder mobility, (41% - 27.7 m) occurred between surveys conducted on 19th February and 31st May 2016. This coincides with increased wave energy associated with Storm Katie (28th March 2016). For a period of 6.5 hours H_s values exceeded 2.0 m, with a maximum H_s value of 4.2 m and H_{max} of 6.6 m being recorded; wave periods ranged between 6.3 - 10 seconds (CCO, 2017b). Conversely, surveys at Bembridge Ledge encompassing this period (17th February - 1st April 2016) identified 13 incidents of mobility covering a transport distance of 6.2 m, only 5% of the cumulative transport total. This disparity is thought to be the result of the southerly wind and wave direction during the storm event (mean: 170°). The southerly aspect of Black Rock being more exposed to the storm opposed to the north-easterly orientation of Bembridge Ledge which was afforded a degree of protection.

Incidents of mobility - Bembridge Ledge

At Bembridge Ledge 76% (n = 38/50) of the tagged boulders were mobile at least once. The TTD for individual tagged boulders ranged between 0.1 m and 21.5 m, mobile boulder mass ranged between an estimated 0.1 t - 1.3 t, Table 2.6.

Transport was documented in a boulder weighing approximately 1.2 t that had become detached from the platform edge yet remained *in-situ* (Figure 2.9), inset. It was surveyed on 3rd February 2016 however, the subsequent survey conducted on 17th February 2016 indicated transport of 7.2 m landward from its previous location, Figure 2.9. Whilst mobile the boulder was overturned prior to deposition at the foot of the shingle beach where the slope angle increases. Overturning was identified by algal growth on the underside of the boulder and varified by the orientation hole being located below the TIP, as opposed to above, as at the time of tag deployment. The transport event described is thought to be attributed to increased wave activity associated with Storm Imogen (8th February 2016) when H_s of 2.5 m were recorded, with a wave period of 7 seconds. Further storm induced transport totalling 2.8 m was recorded for this clast amounting to 10.0 m over the 22 month monitoring period.

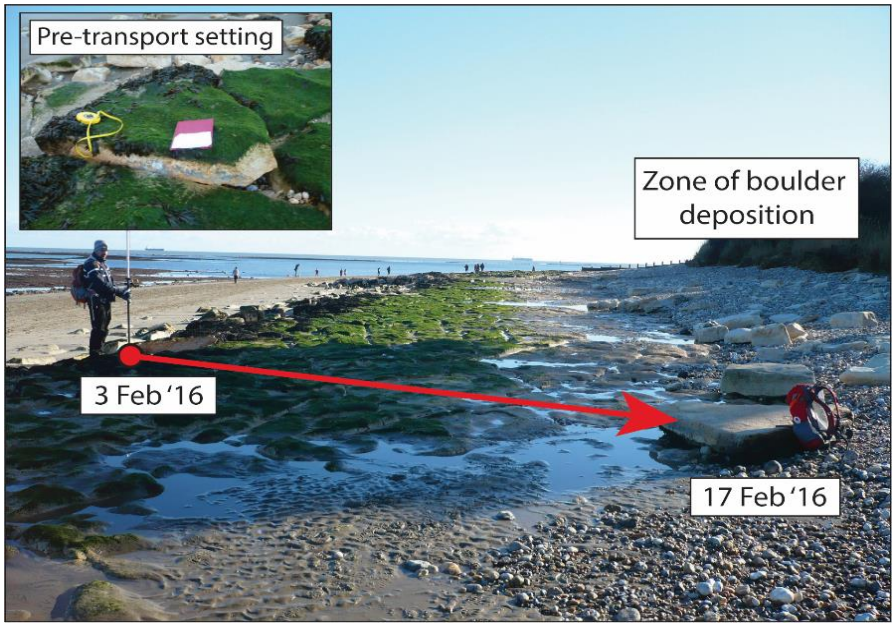

Figure 2.9. Evidence of transport, Bembridge Ledge. Boulder location recorded on 3rd February 2016, (circle), relocated 7.2 m from its initial position on 17th February 2016. The arrow indicates the direction of transport, algal growth on the boulder underside; inset, axial dimensions of the boulder in-situ at the platform edge prior to being transported (3rd February 2016), extensive algal growth on exposed upper plane. A4 pad for scale.

The coordinate data attributed to the aforementioned boulder was processed using the Python script to create a visual interpretation in ArcGIS which documents the spatial and temporal boulder displacement (Figure 2.10).

Note: The complete visual outputs created via ArcGIS from the Python script are found in Appendix 2.

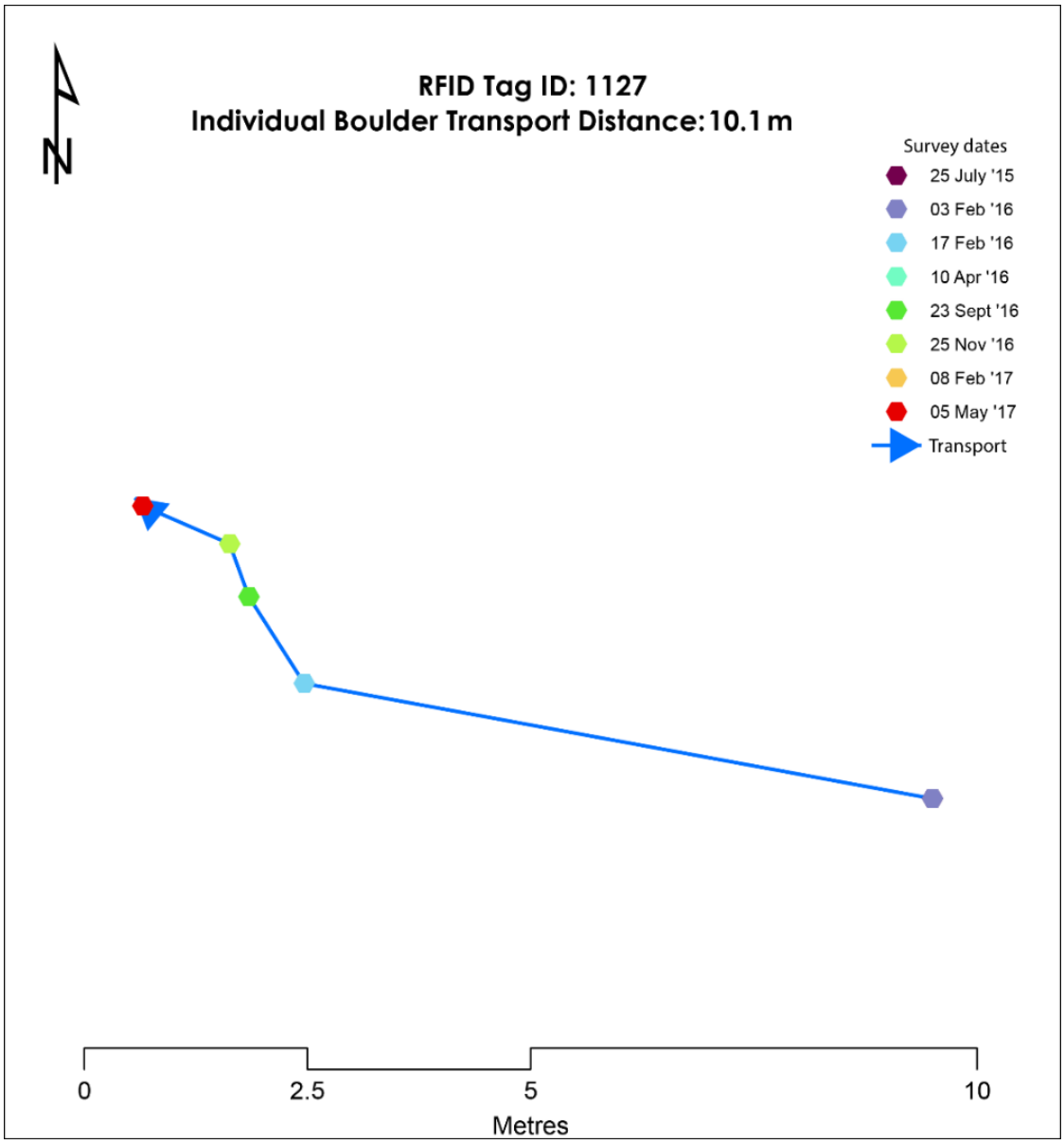

Figure 2.10. ArcGIS visual output documenting the direction of incremental step lengths and the total transport distance for the boulder pictured in Figure 2.9. The absence of colour markers associated with specific survey dates indicates that no transport was recorded on that date.

Incidents of mobility - Black Rock

At Black Rock 52% (n = 28/54) of the tagged boulders were mobile at least once. TTD for individual tagged boulders ranged between 0.1 m and 10.1 m. Mobile boulder mass ranged between an estimated 0.1 t - 11.9 t, Table 2.6.

A boulder located 20.0 m from the platform edge weighing an estimated 5.0 t was tagged at the commencement of the field campaign. It was not visible on the aerial imagery captured by the CCO in August 2013 and is thought to have been transported and deposited during the winter storms of 2013 - 2014. The boulder location was recorded on 19th February 2016 identified by the circle in Figure 2.11a.

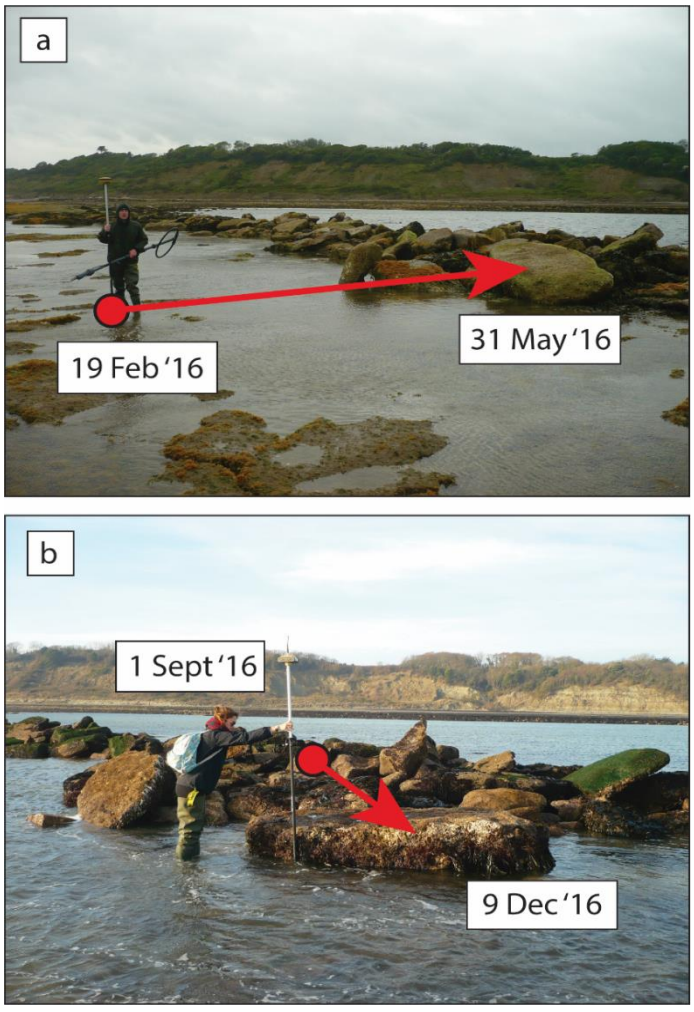

Figure 2.11. Evidence of transport, Black Rock. (a) boulder mobility recorded at Black Rock following Storm Katie, deposition against boulder ridge; (b) boulder mobility recorded at Black Rock following Storm Angus. Circles indicate the previously recorded boulder location, arrows infer the direction of transport.

It was relocated on 31st May 2016 having been transported 6.4 m landward and overturned prior to deposition, imbricate against an extensive boulder ridge. The transport event described is thought to be attributed to Storm Katie (27th March 2016) when maximum H_s was recorded as 4.2 m, with a maximum wave period of 12.5 seconds. Post Storm Katie transport was attributed to wave activity associated with Storm Angus on 20th November 2016, maximum H_s of 4.0 m and wave period of 6.8 seconds (CCO, 2017b) whereby the boulder was overturned 180° and deposited 2.5 m seawards from its previously recorded location, circle in Figure 2.11b.

In both highlighted instances boulder transport was impeded by topographic (raised shingle beach at Bembridge Ledge) and geomorphic (boulder ridge at Black Rock) features. This emphasises the significance of local geomorphology in restricting and controlling boulder transport potential affirming the findings of Pérez-Alberti and Trenhaile (2015b) and Naylor *et al*. (2016) who suggest geomorphic landforms exert a degree of control over boulder transport potential.

Table 2.6. Summary of boulder transport data from Bembridge Ledge and Black Rock from July to May 2017.

[a] - Maximum significant wave height (m) - as recorded by the Channel Coast Observatory wave buoy (Sandown Bay).

[b] - Maximum wave height (m) - as recorded by the Channel Coast Observatory wave buoy (Sandown Bay).

BEMBRIDGE LEDGE

(50 RFID tagged boulders)

Survey Period From	To	Boulders transported (% of total)	Total boulder transport dist. (m)	Daily transport dist. between survey periods (m/day)	Boulder transport dist. % of total	Mean transport dist. (m): (Max. dist.)	Mean mass of transported boulders (t): (Max. mass)	Mean direction of transport (°)	Overturning events	Max. Hs between survey period (m)[a]	Hmax between survey period (m)[b]	Date of storm activity (named where applicable).	Mean tag recovery rate
25 Jul '15	3 Feb '16	21 (42)	49.3	0.25	42	2.3 (16.1)	0.5 (1.1)	229	6	3.3	5.35	3rd January 2016	94%
3 Feb '16	17 Feb '16	12 (24)	12	0.8	10	1.0 (7.5)	0.6 (1.2)	226	1	2.45	3.98	8th March 2016 (Imogen)	74%
17 Feb '16	1 Apr '16	13 (26)	6.2	0.14	5	0.5 (1.2)	0.6 (1.2)	177	0	4.22	6.59	28th March 2016 (Katie)	78%
1 Apr '16	23 Sept '16	11 (22)	5.6	0.03	5	0.5 (1.6)	0.5 (1.3)	192	0	1.77	3.04	10th April 2016	68%
23 Sept '16	25 Nov '16	13 (26)	12.7	0.2	11	1.0 (4.6)	0.5 (1.2)	233	3	3.99	6.84	20th November 2017 (Angus)	90%
25 Nov '16	8 Feb '17	15 (30)	27.1	0.36	23	1.8 (8.9)	0.5 (1.2)	246	1	2.38	3.99	3rd February 2017	100%
8 Feb '17	5 May '17	9 (18)	4.1	0.05	4	0.5 (2.3)	0.5 (1.3)	260	0	2.46	4.32	22nd March 2017	100%
TOTAL		94	117			1.1 (st. dev 0.7)			11				86%

BLACK ROCK

(54 RFID tagged boulders)

Survey Period From	To	Boulders transported (% of total)	Total boulder transport dist. (m)	Daily transport dist. between survey periods (m/day)	Boulder transport dist. (% of total)	Mean transport dist. (m): (Max. dist.)	Mean mass of transported boulders (t): (Max. mass)	Mean direction of transport (°)	Overturning events	Max. Hs between survey period (m)[a]	Hmax between survey period (m)[b]	Date of storm activity (named where applicable).	Mean tag recovery rate
10 July '15	3 Dec '15	15 (28)	9.5	0.07	14	0.3 (2.9)	0.4 (1.8)	189	3	2.2	3.85	26th July 2015	81%
3 Dec '15	6 Jan '16	12 (22)	6.9	0.2	10	0.6 (2.8)	0.6 (1.8)	192	3	3.3	5.35	3rd January 2016	93%
6 Jan '16	19 Feb '16	12 (22)	10.5	0.24	15	0.9 (4.0)	1.0 (5.0)	181	2	2.6	4.82	7th January 2016	100%
19 Feb '16	31 May '16	12 (22)	27.7	0.27	41	2.3 (7.8)	2.0 (11.9)	240	2	4.22	6.59	28th March 2016 (Katie)	100%
31 May '16	1 Sept '16	4 (7)	1.3	0.01	2	0.3 (0.8)	0.4 (0.7)	97	0	1.51	2.42	20th August 2016	100%
1 Sept '16	9 Dec '16	6 (11)	9.6	0.1	14	1.6 (3.1)	3.4 (11.9)	194	1	3.99	6.84	20th November 2017 (Angus)	98%
9 Dec '16	22 Feb '17	7 (13)	1.3	0.02	2	0.2 (0.4)	0.7 (1.5)	143	0	2.38	3.99	3rd February 2017	91%
22 Feb '17	24 May '17	2 (4)	1.1	0.01	2	0.6 (0.8)	0.3 (0.4)	26	0	2.46	4.32	22nd March 2017	100%
TOTAL		70	67.9			0.9 (st. dev 0.7)			11				95%
TOTALS		164	184.9			1.0 (st. dev. 0.7)			22				91%

Discussion

Our proposed methodology, employing RFID tags embedded in an array of boulder-sized clasts has enabled us to identify and accurately quantify boulder mobility as a result of contemporary storm activity. Upon completion of the study we achieved a mean tracer recovery rate of 86% at Bembridge Ledge and 95% Black Rock. Field data identified periodic boulder mobility resulting from contemporary storm activity (Table 2.6) despite the locations relatively low to moderate wave exposure in comparison to previously studied boulder transport sites.

Boulder transport

By establishing an entrainment/transport threshold we can reliably identify transport events and differentiate them from entrainment. Using the TIP we are able to relocate and record a specific point on each tagged boulder. This allows us to apply a universal displacement threshold that is applicable to each tagged boulder regardless of size. This is advantageous over alternative methods applied by Naylor *et al*. (2016) as it provides greater precision, particularly for coarser sized clasts, when defining the distance over which a boulder has been transported.

The calculated transport data identified more frequent incidents of mobility at Bembridge Ledge than Black Rock. This is, in part, due to the difference in lithology between the two sites. The boulder producing limestone outcrops at the sites differ in both the extent of jointing and bed thickness. Owing to the thinner, more discontinuous lithology at Bembridge Ledge smaller, tabular boulders are produced which have a lower transport threshold than the larger boulders produced at Black Rock, corroborating the significance of localised geology on boulder production as described by Stephenson and Naylor (2011). Additionally, there are more obstructions to transport at Black Rock, including a greater number of detached clasts and an extensive boulder ridge. These features restrict landward mobility and result in a higher number of topographically constrained deposits (Trenhaile, 2016).

The close proximity of the recorded wave data to the study sites allows us to infer the likely agent of transport and identify the wave conditions under which boulder mobility occurs. Furthermore, by incorporating a boulder orientation indicator we were able to identify 22 incidents of boulders being overturned during transport, 11 at each site; 68% of these occurring between July 2015 and 19th February 2016. These constitute overturning in 13% of the recorded movements suggesting it is significant but relatively infrequent. Knowing how clasts respond to hydrodynamic conditions under which they have been transported is of considerable significance when applying numerical

models to hindcast wave characteristics such as height and/or velocity (Goto *et al*., 2009; Nandasena *et al*., 2011a; Nandasena *et al*., 2011b).

Addressing limitations and uncertainties

Prior to the commencement of the study we had reservations regarding the suitability of the RFID tagging technology to monitor boulder transport based on limitations as highlighted by Paris *et al*. (2011) and Naylor *et al*. (2016). They describe a number of potential issues with the technique which we are now able to allay.

(1) Would RFID tags withstand the harsh coastal conditions and remain operational throughout the study?

Despite the successful use of RFID tags in long term coastal sediment monitoring (Allan *et al*., 2006; Dolphin *et al*., 2016), and our pre-deployment sealant checks, concerns remained regarding how the unfavourable conditions and prolonged exposure might affect tag operation and/or retention within the boulder. However, we experienced no issues with tag functionality during the survey period. With the exception of five lost tags, which we were able to replace, the remaining 99 tags remained fully operational and detectable throughout the study. Tag loss was attributed to poor sealant adhesion, perhaps as a result of insufficient curing times. We have since trialled a vinylester chemical anchor resin (ProVenture PRO V200) opposed to the widely available silicone sealant. The resin has performed well in laboratory tests involving wetting and drying in saltwater solutions and has since been deployed in the field to replace the lost tags and to date has functioned well.

(2) How effective would the RFID equipment be in relocating tagged boulders, particularly buried clasts?

The RFID equipment performed well in the field. Throughout the survey period it was apparent that concerns over relocating tagged boulders related to environmental factors beyond our control rather than limitations with the equipment and/or methodology. At Bembridge Ledge we frequently encountered incidents of burial following the accretion of sand and shingle. However, we were able to detect buried clasts up to a depth of 0.4 m. Owing to the extent of burial and time constraints it was not always possible to excavate the overlying sediment; additional manpower may have offered increased opportunity to excavate buried clasts. Black Rock recovery rates were reduced as a result of unfavourable tidal states due to the low elevation of an area of the field site in proximity to mean low water. On occasion this created hazardous surveying conditions rendering

a number of boulders inaccessible. Hindsight and greater consideration of tagged boulder location relative to mean low water may have reduced the likelihood of such an occurrence and improved rates of tag recovery.

(3) Would clast breakdown impact on recovery rates?

We documented clast breakage in one of the 104 tagged boulders. The limited mobility of the clast (TTD - 0.65 m) suggests breakdown was not attributed to transport impact but due to the inherent weaknesses within the boulder; breakdown occurred along a number of structural joints.

There was no evidence to suggest the drilling required for tag insertion initiated boulder breakdown, as encountered by Cassel *et al*. (2017). Great care was taken to avoid drilling through any discontinuity planes which suggests clasts exhibiting structural joints should be avoided when selecting boulders to tag.

(4) Would it be possible to relocate and document the tagged boulders within a single tidal window?

The 'stake-out survey' functionality on the DGNSS hastened the boulder recovery process allowing us to maximising the time available in the field. It enabled the recovery of tagged boulders within the 0.1 km^2 survey area with greater ease than randomly searching the survey area. Had this feature not been incorporated into the methodology the ability to relocate tagged boulders would have been compromised.

The overall performance of RFID tagged boulders has been encouraging. Coupled with the proposed methodology they have provided new data on the extent to which boulders are transported in the intertidal zone by contemporary storm events. Additionally, they have provided an insight to the mode of transport when mobilised through the simple addition of an orientation indicator. The success of this deployment has enabled the study to continue into a third year. It is anticipated that with regular monitoring and maintenance of the tag array the study can continue indefinitely ensuring this will be the first known long-term study using RFID tagged boulders to quantify boulder transport resulting from storm activity.

Conclusion

Drawing upon previous RFID transport studies and the findings presented here we assert that RFID technology and the proposed methodology are an efficient and effective means of monitoring and quantifying the response of intertidal boulders to contemporary storm events. Using RFID tagged

boulders it has been possible to identify transport episodes resulting from periods of increased wave activity. The collated data has enabled the production of vector diagrams via a bespoke Python script which detail the distance and direction of boulder transport.

The existing literature relating to boulder transport focuses on coastlines subjected to considerable storm induced wave energy (Cox *et al*., 2012; Etienne and Paris, 2010; Goto *et al*., 2011; Knight and Burningham, 2011). Significantly, the RFID methodology has enabled us to identify boulder detachment, transport and overturning in a relatively sheltered, fetch-limited intertidal site subjected to moderate wave conditions. This demonstrates that contemporary storm events have a far greater ability to mobilise boulders than had previously been realised.

To further augment the methodology additional deployments are recommended in more exposed settings using larger boulders subjected to higher energy wave regimes. Additionally, the methodology and technology may be extended for use in the supratidal zone for long-term monitoring of cliff-top boulder deposits such as those identified by Autret *et al*. (2018) and Cox *et al*. (2018). This may provide greater understanding on the impact, ability and associated risk of extreme wave events to mobilise boulders which may require a reassessment of our current understanding of storm wave hydrodynamics.

The methodology can also be utilised with emerging technologies, such as UAV monitoring (Pérez-Alberti & Trenhaile, 2015a, 2015b; Biolchi *et al*., 2016) to provide greater spatial resolution on the mechanisms that facilitate the transport of intertidal boulders.

This study has highlighted the feasibility of both the RFID technology and our proposed methodology to provide coastal researchers with a new field technique to accurately assess boulder mobility. By adopting the methodology the opportunity exists for researchers to clearly define and quantify boulder transport pathways and provide clarity on the impacts and responses of contemporary storm events in shaping rocky coast landforms.

Footnote - Permissions

Under the Marine Licensing (Exempted Activities) Order 2011 the deployment of scientific equipment, including sediment tracers such as RFID's is deemed a Category 2 exemption and may not require a marine license (Marine Licensing Order, 2011). However, owing to the sensitive nature of the study site we obtained an exemption from the Marine Management Organisation (MMO) and sort approval from Natural England prior to tag deployment.

See Appendix 3 for documentation of the MMO exemption and permission from Natural England.

References

See Bibliography, page 268.

Chapter 3 - Quantification of contemporary storm-induced boulder transport on an intertidal shore platform using RFID technology.

Paper introduction

This chapter documents the transport data derived from the RFID tagged boulders following three years of field deployment. In doing so, it addresses the study aim more specifically by quantifying clast displacement under moderate storm conditions. The reader is provided with a deeper understanding of the extent to which contemporary, moderate storm events displace boulders within the intertidal zone.

Furthermore, it addresses the key mechanisms required to initiate and facilitate the transport process documenting incidents of boulder production by a range of mechanisms including wave quarrying. It also proposes that the boulder pre/post transport morphological setting exerts significant control on transport potential.

The mode by which transport occurs is also addressed with the data suggesting boulders that are overturned during displacement are transported over greater distances than those displaced by sliding. Significantly, this empirical field data confirms the findings reported by Imamura *et al*. (2008), Nandasena and Takana (2013b), Zainali and Weiss (2015) and Noormets *et al*. (2004) who used lab-based experimentation and hydrodynamic modelling to establish overturning as dominant over sliding. The findings also further demonstrate that contrary to existing research on boulder displacement extreme, low frequency, high magnitude storm events are not necessary to mobilise sizable clasts, up to and exceeding 10.0 tonnes.

Owing to the previous methodological chapter every effort has been made to limit the detail within the methodology whilst still providing the reader with an understanding of the steps required. This chapter therefore focuses moreso on the findings of the 3 year deployment and the subsequent interpretation of the RFID derived data.

Reference: Hastewell, L.J., Inkpen, R., Bray, M., & Schaefer, M. (2020). Quantification of contemporary storm-induced boulder production and transport on an intertidal shore platform using RFID technology.

The paper has since been peer-reviewed and has been accepted for publication in Earth Surface Processes and Landforms subject to reviewers amendments. The version presented here is the

original manuscript submission. The revised, corrected version that has since been published is available in Appendix 5.

The submitted manuscript lists the aforementioned authors, the contribution of the named authors is hereby noted as follows:

> *LJ Hastewell - first author, arranged, organised and completed all fieldwork tasks with assistance from field operatives; processed and interpreted the data and wrote the manuscript in full.*
>
> *Dr's Inkpen and Bray acted as reviewers of the draft manuscript.*
>
> *M. Schaefer - included for his invaluable field assistance and as creator of the Python script.*

Abstract

Extreme storm events are known to produce, entrain, transport and deposit sizable boulders along rocky coastlines. However, the extent to which these processes occur under moderate, fetch-limited wave conditions is seldom considered. In this study we quantify boulder transport at a relatively sheltered location subjected to high frequency, low magnitude storm activity. This was achieved by deploying Radio Frequency Identification (RFID) tags within 104 intertidal limestone boulders ranging in size from fine to very coarse (intermediate axis: 0.27 - 2.85 m). The study was conducted over three years (July 2015 - July 2018) and encompassed numerous storm events. Tagged boulders were relocated during 17 field surveys and their positions recorded using Differential Global Positioning Navigation Satellite System (DGNSS).

On completion, we identified boulder displacement in 69% of the tagged array. The accrued boulder transport distance amounted to 233.0 m from 195 incidents of displacement including the movement of a boulder weighing an estimated 11.9 tonnes. Transport was not confined to autumn and winter storms alone as displacement was also recorded during summer months (April - September) despite the reduction in wave magnitude.

Boulder production by wave quarrying was documented in three tagged clasts confirming observations that the shore platform is actively eroding. Incidents of overturning during transport were also recorded (n = 26) including multiple overturning of clasts weighing up to 5.0 tonnes. The data identifies a statistically significant difference (maximum *p*-value: ≤0.03) between the transport

distances attributed to constrained and unconstrained boulders suggesting the pre-transport morphological setting exerts considerable control over boulder transport potential.

The findings identify low to moderate storm waves as a key component in the evolution of the study sites. More broadly, we claim that high frequency, low magnitude storms regularly modify these overlooked rocky coastal locations suggesting the hydrodynamic wave capability at such sites may have been underestimated.

Introduction

Rocky coasts are susceptible to geomorphological change by a range of erosive agents. This is manifest most profoundly by the presence of large coastal boulder deposits which are frequently found on exposed intertidal shore platforms and supratidal cliff-tops (Stephenson and Naylor, 2011; Etienne and Paris, 2010; Hall *et al*., 2006; Cox *et al*., 2018, Biolchi *et al*., 2019a). The emplacement of such deposits act as signatures of past extreme wave events (Mastronuzzi and Sansò, 2000; Goto *et al.* 2010b; Paris *et al*., 2011; Shah-hosseini *et al*., 2011; Lau *et al*., 2016) and reflect the magnitude of the wave activity that initiated boulder production, transport and deposition (Nott, 2003a; Goto *et al*., 2009; Nandasena *et al*., 2011b; Nandasena and Tanaka, 2013a). Consequently, these boulders have been used as proxies for extreme storm events including typhoon/hurricane/cyclone generated storms (Scheffers and Scheffers, 2006; Fichaut and Suanez, 2011; Cox *et al*., 2012; Terry *et al*., 2016; Kennedy *et al*., 2017; Cox *et al*., 2018; Terry and Lau, 2018), and/or tsunami (Scicchitano *et al*., 2007; Maouche *et al*., 2009; Etienne *et al*., 2011; Engel and May, 2012; Mottershead *et al*., 2014).

Contemporary storm events have also been reported as capable of producing, entraining and transporting intertidal and supratidal clasts (Goto *et al*., 2011; Naylor *et al*., 2016; Autret *et al*., 2018). However, previous studies commonly address boulder displacement at exposed sites which are subjected to high-magnitude, low-frequency storm events (Goto *et al*., 2009; Hansom and Hall, 2009; Etienne and Paris, 2010; Autret *et al*., 2016). Coastal sites subjected to low and moderate wave climates have been widely overlooked (Dasgupta, 2011) despite the presence of boulder assemblages indicative of depositional storm activity. Furthermore, a lack of emperical, field data on the extent to which intertidal boulders respond to contemporary low magnitude, high frequency storm events remains unexplored and unknown (Paris *et al*., 2011).

This sediment tracing study aims to broaden our current understanding of boulder transport processes by quantifying boulder transport at two separate sites, (Bembridge Ledge and Black Rock)

on the relatively sheltered east coast of the Isle of Wight (U.K.). The location has a limited fetch and a low to moderate wave regime (Hastewell *et al*., 2019a). Boulder displacement has been monitored over a three year period using 104 intertidal limestone boulders, each embedded with a Radio Frequency Identification (RFID) tag. The tagged boulders were periodically relocated during field surveys and their positions recorded using Differential Global Positioning Navigation Satellite System (DGNSS).

In the course of fulfilling the study aim we further develop previous work by Naylor and Stephenson (2010); Stephenson and Naylor, (2011); Naylor *et al.* (2016) in identifying the key mechanisms that facilitate boulder production, the removal of blocks from the shore platform bedrock and highlight the significance of platform morphology on boulder transport capability.

Inshore and nearshore wave data and tidal parameters were recorded throughout the study at two wave monitoring stations approximately 5 km from the study sites. The data provides insight to the hydrodynamic conditions that we infer initiated episodes of boulder transport. We consider these data with respect to calculated wave heights derived from hydrodynamic modelling which has been employed previously to retrodict the minimum wave height required to initiate boulder detachment and subsequent transport (Lorang 2000; Nott 2003a; Mastronuzzi and Sansò, 2004; Switzer and Burston, 2010; Etienne and Paris, 2010; Barbano *et al*., 2010; Nandasena *et al*., 2011b).

The transport of intertidal boulders presented herein provides a greater understanding of the responsiveness of rocky coasts to contemporary, high-frequency, low-magnitude storm events and the underlying processes and mechanisms that influence boulder production, transport and deposition within the intertidal zone. The findings will be of increased significance given the changing climate is predicted to invoke an increase in storm frequency and intensity (Leckebusch *et al*., 2006; Beniston *et al*., 2007) which is expected to alter future wave climates, tidal regimes and sediment transport patterns and potentially increase rates of erosion at rocky coasts (Trenhaile, 2016).

Site Location

Bembridge is located on the east coast of the Isle of Wight, southern England and comprises a 3 km shoreline fronted by a wide shore platfrom (Figure 3.1). Two survey sites were selected, each covering approximately 0.1 km^2, Bembridge Ledge and Black Rock, herein referred to as BL and BR respectively.

Site selection was based on accessible intertidal boulders that were known to be mobile under low to moderate wave conditions. This was evident from the presence of sedimentary signatures and clastic assemblages, including a boulder beach and berm, which are indicative of storm-induced transport. Additionally, by using two sites with differing coastal aspects it was possible to study the effects of coastal orientation and storm exposure on boulder displacement. Furthermore, unlike many previously studied boulder transport sites Bembridge has not been subjected to any recent or paleotsunamigenic impacts (Long, 2017). The lack of a competing mechanism allows us to ascribe boulder transport and the formation of associated geomorphic features to storm-driven activity alone.

Figure 3.1. Location of study sites (a) Isle of Wight, (U.K.); (b) Bembridge, on the easterly point of the Isle of Wight, wave and tidal monitoring stations relative to site location; (c) study sites, Bembridge Ledge (sheltered) and Black Rock (moderately exposed), tagged boulders are indicated by the circular symbols.

The study site is comprised of near-horizontal beds of late Eocene Bembridge Limestone interspersed with less resistant Bembridge Marls (Armenteros and Daley, 1998; Insole *et al*., 1998).

The limestone beds form extensive intertidal shore platforms characteristic of type-B shore platforms, being near/sub-horizontal with an abrupt seaward terminus (Trenhaile, 1987; Sunamura, 1992).

The tidal regime is classified as meso-tidal with a neap and spring tidal range of 1.8 m and 3.7 m respectively. Bembridge has a limited fetch ranging from 140 km to the south and 185 km to the east (Hastewell *et al*., 2019a). Its location on the east coast of the Isle of Wight provides shelter from Atlantic swell waves and the prevailing south-westerly wind direction.

Bembridge Ledge

BL is comprised of a tiered intertidal shore platform, the lowest of which extends 500 m at its widest point. Collectively, the platforms are similar in form to those depicted and described by Hills (1972, p.87) as a *"terraced platform with several low terraces."* The landward platform edge ranges in height from 0.2 - 1.0 m and is densely jointed with discontinuities orientated predominantly to the north and east towards incoming wave energy. This lithological characteristic promotes block removal at the platform edge which provides source material for transport to occur (Figure 3.2a).

Boulders are transported landward across a near-horizontal (0° to +1°) wave scoured platform which varies in width from 5 m to 55 m. Boulders are found most frequently as solitary clasts on the upper platform surface or emplaced and occasionally buried within the mixed sand and gravel beach that fronts a low cliff formed in a Quaternary raised beach deposit (Insole *et al*., 1998). The beach dissipates wave energy, reducing transport capacity resulting in boulder deposition (Buscombe and Masselink, 2006; Almeida *et al*., 2015), (Figure 3.2b).

Platform topography is generally smooth, with the exception of the occasional raised scarp, ranging from 0.1 m and 0.5 m in height. Additionally, a series of shallow intertidal pools cover an area of the platform (0.007 km^2). The pools are encircled by raised rims, approximately 0.10 m in height. Isolated boulders are located within the pools which impede further transport, Figure 3.2c, (Hastewell *et al*., 2019b).

Figure 3.2. Bembridge Ledge (a) boulder production at the platform edge; (b) shore platform and boulder deposition on the gravel beach; (c) deposition of detached boulders in shallow, intertidal pools.

Black Rock

The limestone unit that forms the seaward shore platform is of greater bed thickness with fewer geological discontinuities when compared with BL and hence it produces boulders of greater size, generally ranging from medium (intermediate axis 0.5 m to 0.1 m) to very coarse (intermediate axis 2.0 m to 4.1 m), after Blair and McPherson (1999).

The seaward platform edge is between 1.0 - 1.5 m in height and is defined as horizontal (0°) to sub-horizontal in places with a slight landward dip (-1°) which facilitates transport across the wave scoured platform. Generally, only the largest boulders are located on the exposed platform surface as wave energies are sufficient to facilitate the complete removal of small and medium sized clasts. Where boulders are present they are found as solitary clasts located between the platform edge and a boulder beach that extends in to a boulder berm which lies between 5 m and 25 m from the platform edge (Figure 3.3a).

The boulder beach and berm hinder landward transport by trapping and accumulating displaced clasts. Both features are interpreted as distinctive sedimentary signatures of boulder transport and deposition. The seaward margin of the boulder beach and berm is characterised by imbricate, stacked clasts indicative of storm deposition (Nott, 2003b; Switzer and Burston, 2010), Figure 3.3b. The boulder beach covers an area of approximately 0.002 km^2 and is comprised of fine to coarse clasts. The berm consists of fine to very coarse clasts and extends 0.8 km from west to east, parallel with the platform edge. Berm width varies from 5 m to 20 m.

To the rear of the berm lies a tidal lagoon with scattered cobbles on its bed. Platform topography then rises to the edge of a second, more landward horizontal (0°) intertidal rocky outcrop (upper platform) from which small boulders are detached, transported and deposited sporadically on the upper platform (Figure 3.3c).

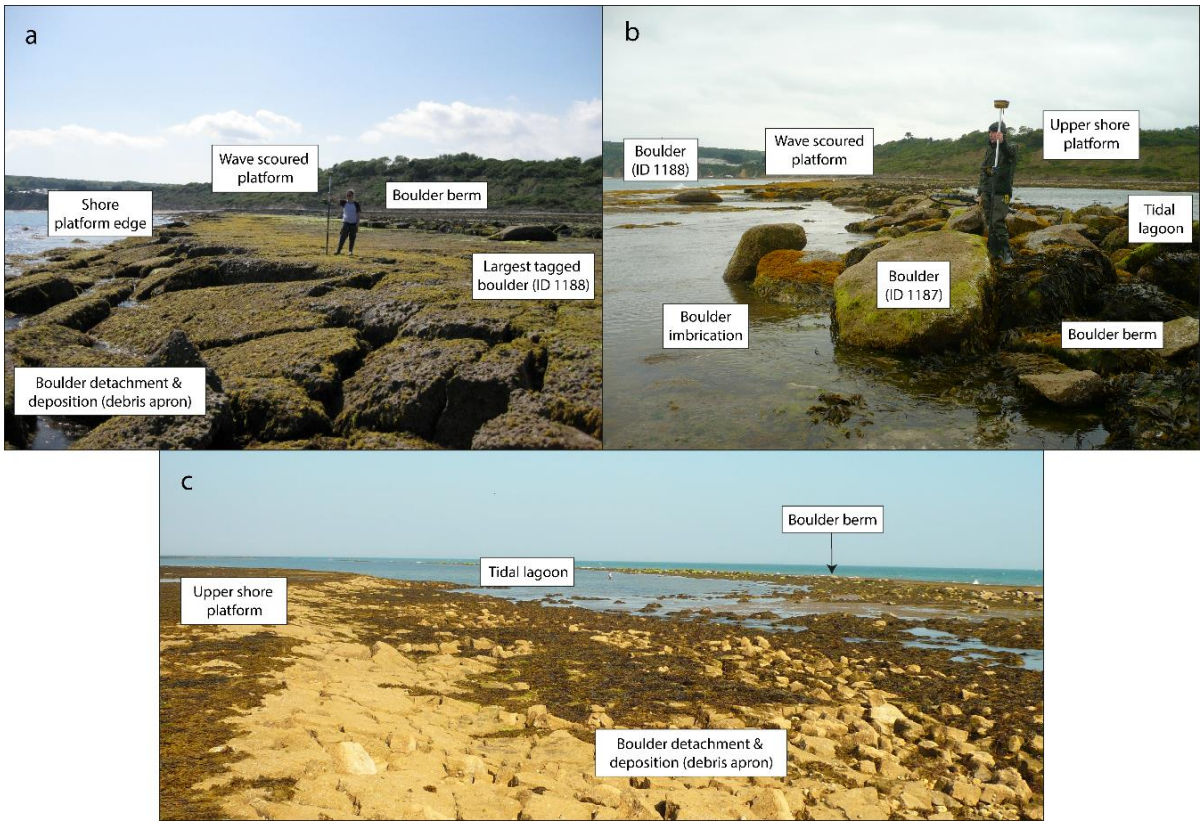

Figure 3.3. Black Rock (a) boulder production, transport and deposition; (b) boulder deposition creates an extensive boulder berm, clast tag ID: 1187 has an estimated mass of 5.0 t. The largest tagged boulder is identified in Figures a and b (tag ID: 1188; (c) boulder deposition at the front of the upper platform. The arrow indicating the boulder berm identifies the approximate location of image capture in Figures a and b. For scale, the DGNSS pole is extended to a height of 2.0 m.

Methods

Boulder selection

We employed RFID tagging technology to monitor and quantify the displacement of an array of tagged boulders. This was achieved by recording the coordinates of each tagged boulder at the time of tag deployment. Subsequent field surveys were undertaken to relocate the clasts and rerecord their coordinate locations thus providing a spatial and temporal framework within which to quantify clast displacement. However, as with all sediment tracing studies prior to tag deployment it is necessary to ensure the tagged material accurately reflects the physical properties (e.g. size, shape and density) of the indigenous sediment (Lee *et al*., 2000; Sear *et al*., 2000).

Size

Size homogeneity between indigenous and tagged boulders was achieved by conducting an assessment of the boulder populations prior to tag deployment. This data was used to inform tagged boulder selection. Measurements of the long (*L*), intermediate (*I*) and short (*S*) axial dimensions of 100 randomly selected boulders at each site allowed for the classification of boulders by size, adopting the nomenclature of Blair and McPherson (1999). A comparison between the % frequency of the assigned size classifications between the indigenous and tagged boulders demonstrates that a representative sample has been achieved in terms of size (Figure 3.4).

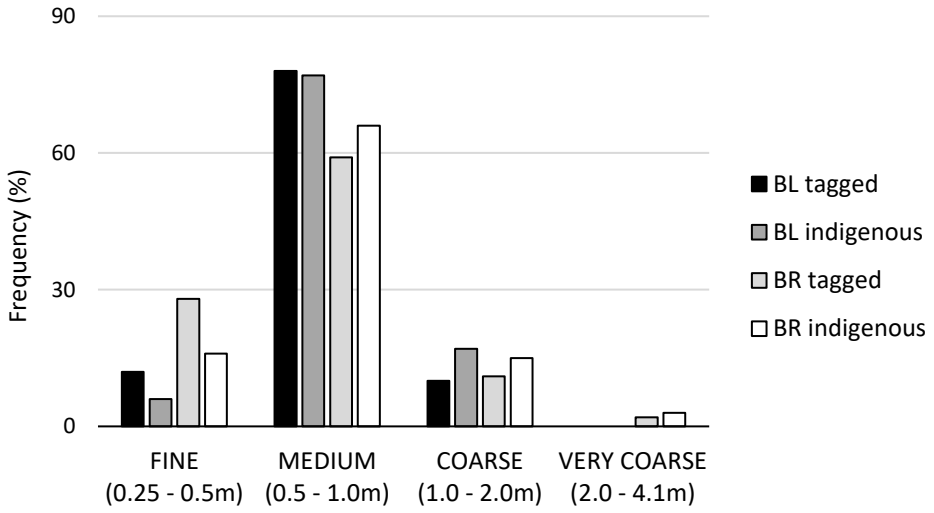

Figure 3.4. Frequency (%) of boulder size classification of indigenous and tagged boulder size for BL and BR based on intermediate (I) axial dimensions (classified in accordance with Blair and McPherson, 1999).

Shape

Axial dimensions of indigenous and tagged boulders were used to determine clast shape based on Zingg (1935). Figures 3.5a and 3.5b identify the majority of boulders at both sites as disk-shaped (BL: tagged: 65% / indigenous: 66% and BR: tagged: 46% / indigenous: 49%). The greater number of disk-shaped clasts at BL, and the limited variability in shape is attributed to the relative consistency in the short axis of the BL clasts (mean c-axis: 0.27 m) which corresponds with the mean thickness of the boulder producing limestone unit exposed at the platform edge (approximately 0.25 m). This supports boulder provenance and suggests clast size is litho-structurally controlled (Stephenson and Naylor, 2011; Salzmann and Green, 2012).

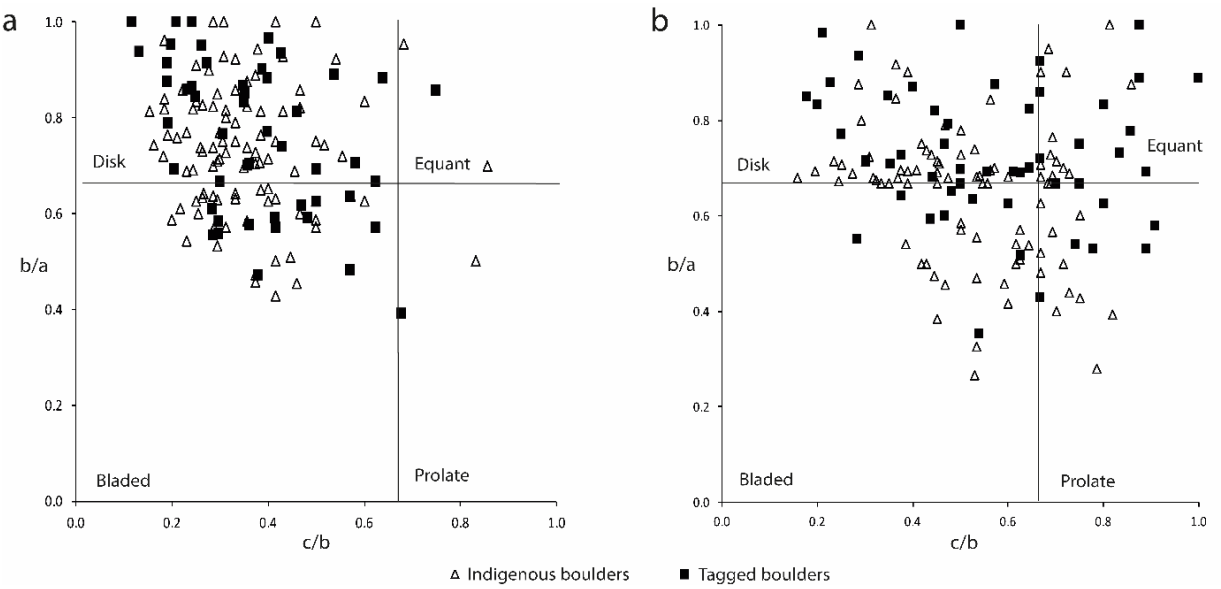

Figure 3.5. Zingg plots defining clast shape of indigenous and tagged boulder populations at (a) Bembridge Ledge and (b) Black Rock.

Density

Rock density of the Bembridge Limestone was measured using the water displacement method. Based on samples obtained from the study site a rock density of 2.4 g/cm^3 was recorded, all tagged boulders were formed of Bembridge Limestone. On the basis of our preliminary assessment we assert that the physical properties (size, shape and density) of the tagged array are representative of the indigenous boulder population.

Morphological setting

The position of a boulder prior to displacement is reported to be a key component in controlling its transport potential (Naylor *et al*., 2016; Zainali and Weiss 2015; Nott, 2003a; Spiske and Bahlburg, 2011; Nandasena *et al.*, 2011a; Switzer and Burston, 2010). Therefore, tagged boulders were selected to reflect a range of different morphological settings (MS) to establish its significance on transport distance. These settings are categorised in Table 3.1.

*Table 3.1. RFID tagged boulder morphological settings, pre-transport location, description and the respective number of tagged boulders within each category at each site, Bembridge Ledge (BL) and Black Rock (BR). * the number of assigned clasts relates to the MS prior to initial transport.*

MS No.	Morphological setting (MS)	Pre-transport location	Description	Number* (BL / BR)
1	Located seaward of the shore platform.	Platform edge (detached)	**Position:** fully detached boulders fronting the platform edge, awaiting transport.	13 / 3
			Transport potential: impeded by the shore platform edge.	
2	Located at the shore platform edge.	Platform edge (joint bound)	**Position:** Described by Nott (2003a) as joint bound blocks, the geologically discontinuous lithology at Bembridge creates angular blocks at the platform edge. They may, or may not, be fully detached from the platform edge.	4 / 2
			Transport potential: constrained on one or more sides by the surrounding strata.	
3	Located on the shore platform.	Platform top (constrained)	**Position:** located on the shore platform.	20 / 25
			Transport potential: restricted by topography and/or morphological features, i.e., deposited in a depression or imbricate against a rock feature (scarp) or other boulder/s (Trenhaile, 2016).	
4	Located on the shore platform.	Platform top (unconstrained)	**Position:** located on the shore platform.	13 / 24
			Transport potential: transport is unhindered by topography and/or morphological features (Trenhaile, 2016).	

Each morphological setting is defined by the potential for a boulder to be displaced. These boulders are referred to as being either constrained or unconstrained (Trenhaile, 2016). Of the four MS's, three are designated as constrained (MS1, MS2 and MS3) meaning boulder transport is impeded

by a range of geomorphic and/or topographic landform features such as the gravel beach, boulder beach/berm and/or imbricate boulders. Unconstrained clasts are represented in MS4; these clasts are unimpeded in their ability to be displaced. Figure 3.6 provides examples for each MS. We hypothesised the unconstrained boulders (MS4) would be mobilised more frequently and over greater distance when compared with constrained clasts represented in other MS's.

Of the 50 tagged boulders within the BL study area; 60% are located on the platform and gravel beach, the remaining 40% are positioned on the seaward side of the platform edge. At BR, 74% of the tagged boulders are located on the seaward platform, the remaining 26% on the upper platform. There are no tagged boulders located seaward of the platform terminus at BR as the low water (LW) level would restrict access to spring tides only.

Figure 3.6. Examples of the four morphological settings (MS) as identified at BL.

RFID

RFID technology has been used previously in littoral studies as a means of monitoring the incremental displacements of a range of sediment sizes. Previous studies have concentrated on

mixed sediments including gravel, cobbles and small boulders (Allan *et al*., 2006; Nichols, 2004; Dickson *et al*., 2011; Miller *et al*., 2011; Brayne, 2015; Casamayor *et al*., 2015; Dolphin *et al*., 2016; Han *et al*., 2017) as opposed to focusing purely on boulder-sized clasts. As such, this research forms the first long-term, monitoring study to quantify intertidal boulder transport using RFID tagging.

RFID technology was favoured over alternative methods of boulder tracing such as marine paint (Stephenson and Naylor, 2011; Naylor *et al*., 2016) as the sensitive environmental designations at the sites required a discreet and unobtrusive means of detection. Furthermore, unlike painted clasts RFID technology enables the detection of buried material which results in improved rates of tag recovery (Bray *et al*., 1996).

RFID equipment consists of a transponder, referred to as a tag, an antenna, a backpack reader and a handheld user interface (PDA), (Figure 3.7).

Figure 3.7. RFID tagged boulder relocation at BR using tag detection equipment (at left) and recording of boulder location using DGNSS (at right). For scale, the DGNSS pole is extended to a height of 2.0 m.

With no internal power source, the RFID tag is small enough to be embedded within a boulder, we used tags measuring 32 x 4 mm. Each tag is pre-programmed with a unique 16-digit reference number that enables the unequivocal identification of tagged material in the field. The antenna, powered by the backpack reader, emits a low frequency electromagnetic signal (135 kHz). When in range of a deployed tag the emitted signal activates the embedded tag to transmit its unique reference number. This is received via the antenna and relayed to the handheld PDA which displays the numerical code enabling the identification of the embedded tag and associated boulder. RFID detection equipment manufactured by Oregon RFID was chosen on the basis of the tag detection range of approximately 1.0 m (Oregon RFID, 2017) although during pre-deployment checks we recorded a mean detection range of 0.77 m (Hastewell *et al*., 2019a).

RFID tagging protocol

The application of RFID technology to monitor boulder transport is comprehensively explained within Hastewell *et al*. (2019a), (Chapter 2) and is summarised below. RFID tags were inserted in a drilled hole within selected boulders and sealed with a waterproof sealant and marine epoxy resin. We refer to this as the tag insertion point (TIP). The TIP was used as a fixed point from which the boulder coordinates were repeatedly recorded during tagged boulder relocation surveys. An additional hole was drilled above the TIP to indicate the upward orientation of the boulder at the time of deployment, referred to as the orientation hole. The was used as an indicator of the transport mode; any boulder relocated during subsequent field surveys with the orientation hole below the tag was identified as being overturned during transport. Once deployed a number of boulder characteristics were recorded including the axial dimensions, a-axis orientation and boulder positional coordinate data. This was recorded using a Topcon Hiper V in real-time kinematic (RTK) mode (referred to as the DGNSS) which provided a relative horizontal accuracy of 5 mm, +/- 0.5 ppm. (Topcon, 2018).

Boulder production and transport

These data presented herein are based on findings from a three year study (July 2015 - July 2018) whereby boulder transport pathways were quantified using RFID tags embedded in 104 intertidal limestone boulders; 50 at Bembridge Ledge and 54 at Black Rock. The tagged boulders were relocated during low water using the RFID detection equipment; 17 relocation surveys were conducted (8 at BL and 9 at BR), Table 3.2.

Table 3.2. Tag deployment, boulder relocation survey dates and time elapsed (days) between surveys at Bembridge Ledge and Black Rock.

BEMBRIDGE LEDGE	Survey no.	Survey date (from)	Survey date (to)	Interval between surveys (no. of days)
Year 1	**S1**	25 July 2015*	03 February 2016	193
	S2	03 February 2016	17 February 2016	14
	S3	17 February 2016	01 April 2016	44
	S4	01 April 2016	23 September 2016	175
Year 2	**S5**	23 September 2016	25 November 2016	63
	S6	25 November 2016	08 February 2017	75
	S7	08 February 2017	05 May 2017	86
Year 3	**S8**	05 May 2017	10 May 2018	370

BLACK ROCK	Survey no.	Survey date (from)	Survey date (to)	Interval between surveys (no. of days)
Year 1	**S1**	10 July 2015*	03 December 2015	146
	S2	03 December 2015	06 January 2016	34
	S3	06 January 2016	19 February 2016	44
	S4	19 February 2016	31 May 2016	102
	S5	31 May 2016	01 September 2016	93
Year 2	**S6**	01 September 2016	09 December 2016	99
	S7	09 December 2016	22 February 2017	75
	S8	22 February 2017	24 May 2017	91
Year 3	**S9**	24 May 2017	11 July 2018	352

* - tag deployment date.

Once relocated, the boulder coordinates were rerecorded using the DGNSS. The data was stored with the unique tag ID code for processing. By conducting repeat surveys, we generated a series of coordinate points (x, y, z) for each tagged boulder. The coordinate data was processed in ArcGIS using a Python script which calculated the distance and azimuth between successive points providing a spatial and temporal frame within which individual boulder transport pathways could be determined and accurately quantified; the Python script is included in Appendix 1.

Geomorphological surveys were conducted concurrently with the relocation surveys. General site observations including evidence of block detachment and transport were recorded using a digital camera. This empirical data complimented the quantitative transport data allowing us to theorise mechanisms of boulder production and transport.

As part of the study, it was necessary to define boulder transport in order to differentiate it from entrainment. To accomplish this an entrainment/transport threshold value was established. This

was based on the combined errors associated with the relative accuracy of the DGNSS, the setup of the base station and the RMSE of resurveying the TIP. Being able to repeatedly rerecord a specific point (the TIP) on each boulder during each survey ensured a greater level of precision in defining the boulders coordinate location. As a result, this method was chosen over potential alternatives discussed in Hastewell *et al*. (2019a). To determine the RMSE value four fixed points were recorded in the same manner as the TIP during field surveys. Thirty fixed point measurements resulted in a RMSE of +/- 0.03 m in the horizontal and vertical axis, although maximum values of 0.08 m were recorded. Based on the cumulative values we conservatively set the horizontal and vertical error at 0.1 m. Therefore, the entrainment/transport threshold value was set at 0.1 m. Transport values calculated via the Python script exceeding 0.1 m were defined as transported; values below 0.1 m were classified as static and/or entrained only. Subsequently, those values <0.1 m were not incorporated into any transport distance values.

Wave climate and tidal regime

Wave induced erosion is considered significant in modulating geomorphic change on rocky coasts (Trenhaile, 1987; Ogawa *et al*., 2011). Therefore, an understanding of the wave conditions relative to periods of mobility is necessary to better understand wave/transport processes. We utilise wave and tidal data obtained from two wave-monitoring stations managed by the Channel Coast Observatory (CCO). A WaveRider REX system located on Sandown Pier approximately 6 km southwest of the study site provided inshore wave conditions including wave period (seconds), significant wave height in metres (H_s) and maximum wave height (H_{max}). Tidal water levels were also recorded. In addition, a waverider buoy located 5 km to the southwest of the study site, (Figure 3.1b) 1.2 km from the coast in a water depth of approximately 8.0 m (OD) provided data on the nearshore wave direction, wave period, H_s and H_{max} values. Wave data was recorded every 30 minutes, tidal every 10 minutes.

To define storm activity we apply the CCO storm threshold value of 1.6 m for the Sandown Pier monitoring station. This figure is based on extreme value analysis of wave data which identifies the 0.25 year return period for significant wave height (H_s), i.e. the wave value exceeded on average 4 times per year (CCO, 2018). When referring to the nearshore wave buoy we adopt the storm threshold of 2.5 m (CCO, 2015).

Wave data from the inshore pier monitoring station was used to infer the storm conditions that occured at the field sites, thus providing estimates of the wave conditions that facilitated block detachment and displacement. Field observations indicated that the inshore wave data better

reflected the wave conditions encountered at the study site therefore it was favoured over the nearshore alternative. Furthermore, Héquette and Cartier (2016) recommend the use of wave parameters recorded closer to shore opposed to data derived offshore as a greater degree of interaction with seafloor bathymetry alters wave characteristics.

Hydrodynamic modelling

Hydrodynamic equations have previously been applied as a means of distinguishing between storm and/or tsunami boulder deposition (Williams and Hall, 2004; Scheffers *et al*., 2009; Goto *et al.* 2010c; Furlani *et al*., 2011a; Weiss, 2012; Mottershead *et al*., 2014; Biolchi *et al*., 2019a). Equations proposed by Nott (2003a) have been widely used to infer the estimated minimum wave height required to mobilise clasts based on the pre-transport setting, submerged, sub-aerial or joint-bound (Scicchitano *et al*., 2007; Maouche *et al*., 2009; Barbano *et al*., 2010; Switzer and Burston, 2010; Etienne and Paris, 2010; Roig-Munar *et al*., 2019). These equations have subsequently been modified by a number of authors including Noormets *et al*. (2004), Imamura *et al*. (2008), Pignatelli *et al*. (2009), Benner *et al*. (2010) and most notably, Nandasena *et al*. (2011b). We apply the equations of Nandasena *et al*. (2011b) to the known axial dimensions of the three largest displaced boulders located at BR (RFID tag ID 1187, 1188 and 1189), (Table 3.3). These clasts were selected to reflect the upper range of displaced boulders and being located within 60 m of each other they would have been subjected to the same/similar wave activity. The calculated wave heights were then considered with respect to the known wave data recorded at the local wave monitoring stations.

Table 3.3. Hydrodynamic equations proposed by Nandasena *et al*. (2011b).

Nandasena et al. (2011)	Input values
Subaerial / submerged boulder $Hs \geq \frac{2c\left(\frac{\rho_b}{\rho_w} - 1\right)(cos\theta + \mu s\, sin\theta)}{C_l}$	ρb = boulder density (2.4g/cm^{-3}) ρ_w = seawater density (1.025g/cm^{-3}) μs = coefficient of static friction (0.7) C_l = coefficient of lift (0.178) a = a-axis (boulders longest axis) b = b-axis (boulders intermediate axis) c = c-axis (boulders shortest axis) θ = platform gradient (0.0 zero)
Joint bound boulder $Hs \geq \frac{2c\left(\frac{\rho_b}{\rho_w} - 1\right)cos\theta}{C_l}$	

Results

RFID recovery rates

On completion of the study we achieved a mean RFID tag recovery rate of 92%, (88% at BL and 96% at BR). The high rate of recovery is unprecedented in previously reported littoral tracer studies over similar timescales (Chapuis *et al*., 2014; Hastewell *et al*., 2019a). Tag recovery rates at BL were impacted by burial of tagged boulders within the beach following the seasonal accretion of sands and gravel. Unfavourable tidal and wave conditions during three BR surveys prevented access to a number of boulders located near the LW mark that affected our ability to relocate all tagged boulders. The RFID tags performed well in the field and remained functional throughout and beyond the study period enabling the monitoring programme to continue indefinitely.

Boulder production

Findings from geomorphological surveys undertaken at both sites provided a basis upon which we propose the mechanisms of boulder production. At BL block removal is controlled by the litho-structural characteristics of the shore platform bedrock. The heavily jointed and well-bedded unit is exploited by breaking waves promoting detachment by wave quarrying of angular blocks (Naylor and Stephenson, 2010). Quarrying occurs where the ingress of water from breaking waves penetrates into the joints and bedding planes that separate individual blocks. Air pressure within the joints and planes increases leading to crack propagation that eventually liberates the block from its adjacent neighbours (Stephenson and Kirk, 2000; Trenhaile and Kanyaya, 2007, Trenhaile, 2019), (Figure 3.8, inset a). Boulder production is also initiated by undermining, whereby a consolidated

limestone unit lies above a thin bed of clay-rich marl. The preferential erosion of the subjacent marl layer creates an overhang. As the overhang increases the overlaying blocks fracture along existing discontinuities (Switzer and Burston, 2010; Herterich *et al*., 2018), (Figure 3.8, inset b). Liberated blocks are deposited immediately seaward of the platform edge where repeated block detachment generates an accumulation of boulders which act as source material for landward transport (Figure 3.8).

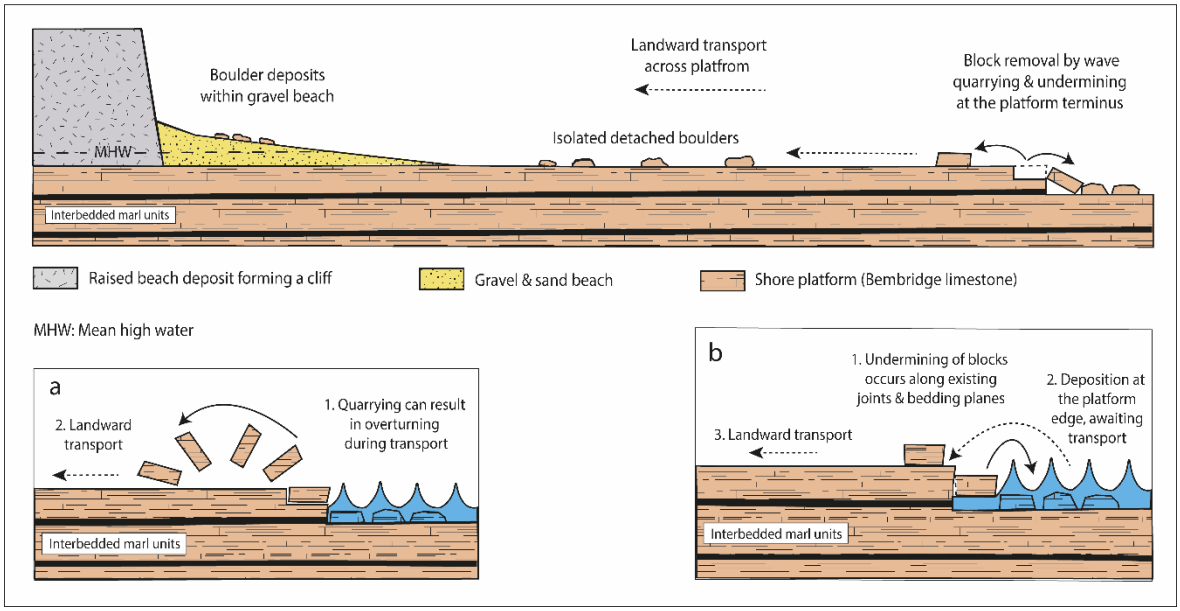

Figure 3.8. Bembridge Ledge - schematic diagram identifying modes of production, transport and deposition; inset, (a) the removal of blocks by quarrying; inset, (b) block removal by undermining.

At BR the lithology of the unit facilitates a mode of detachment that is dominated by an alternate undermining process occurring around the mean low water mark. Abrasive material (sands and gravels) mobilised by wave-driven currents have created a notch within the limestone unit beneath the shore platform edge (Trenhaile, 2015). Gravity loading of the overburden eventually overcomes material rock strength causing platform surface fracturing which leads to block failure and detachment (Kogure *et al*., 2006), (Figure 3.9, inset a).

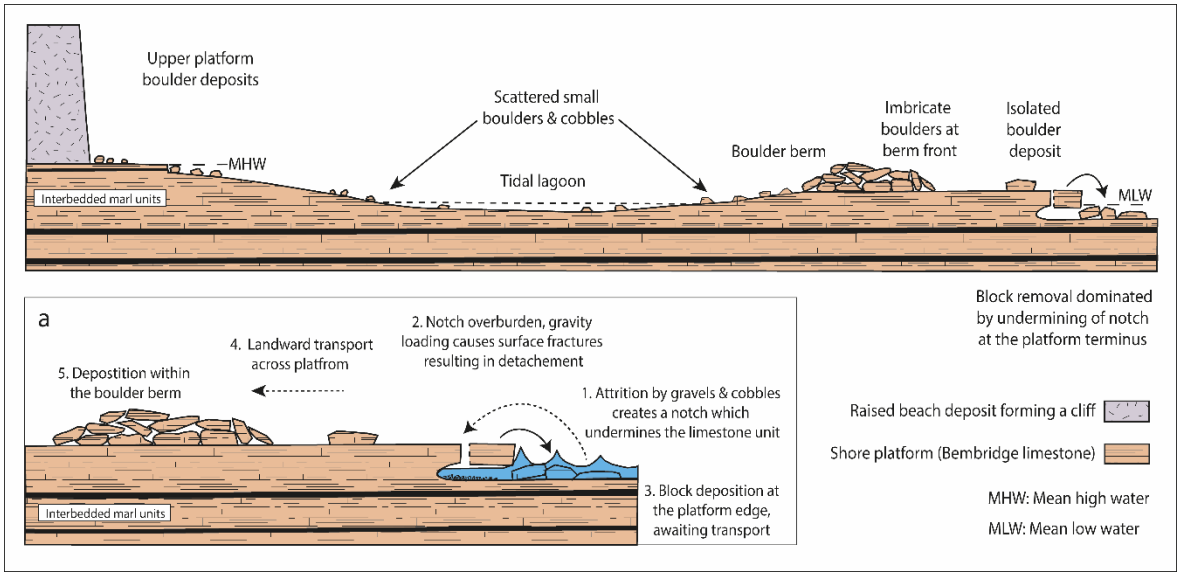

Figure 3.9. Black Rock - schematic diagram identifying modes of boulder production, transport and deposition; inset, (a) the removal of blocks by undermining at the shore platform terminus.

As with BL, the detached material accumulates at the front of the platform producing a debris apron which allows for individual boulders to be lifted/rolled on to the platform surface (Figure 3.9).

Boulder transport

The relocated tagged boulder coordinate data was utilised to quantify clast displacement. This was achieved by processing the coordinate data in ArcGIS via a Python script, (Appendix 1). The geospatial data output provided values for the distance and direction of transport between previously recorded coordinate points (Appendix 2). The data identified the individual boulder transport distance (IBTD) for each tagged clast between surveys. The IBTD's were added for each survey to identify the cumulative transport distance (CTD). The transport values and analysis thereof are presented in a series of tables (Tables 3.4 to 3.7).

Tables 3.4 and 3.5 present data for each mobile tagged boulder and include the axial dimensions, morphological setting (MS) and mass, amongst others. Python outputs for distance (m) and direction (°) of displacement of individual transport events are also reported relative to the specific survey periods, as dated. Incidents of overturning are highlighted by the shaded cells. Transport events resulting in boulder transfer between MS's are identified in bold and italicised text along with the associated transport distance and direction that was recorded. Those boulders identified by the MS prefix/suffix nomenclature e.g. MS4/3 were originally located in MS4 then subsequently transferred to MS3. Immobile boulder details are not included in these tables.

Table 3.4. Bembridge Ledge - summary of individual boulder characteristics, distance (m) and direction (°) of transported boulders between specified survey periods.

*boulder mass (axial dimensions x density)

Shape is defined by Zingg (1935), D - disk, E - equant, B - bladed, P - prolate

RFID No	A axis (m)	B axis (m)	C axis (m)	MS	Shape	Mass (t) #	Times trans	S1 - S2 (25 July 15 - 3 Feb 16)	S2 - S3 (3 - 17 Feb 16)	S3 - S4 (17 Feb - 1 Apr 16)	S4 - S5 (1 Apr 16 - 23 Sept 16)	S5 - S6 (23 Sept - 25 Nov 16)	S6 - S7 (25 Nov 16 - 8 Feb 17)	S7 - S8 (8 Feb - 5 May 17)	S8 - S9 (5 May 17 - 10 May 18)	Total IBTD (m)
1102	1.10	0.70	0.40	4	B	0.7	2	0.0	0.0	0.2 (289°)	0.0	0.5 (178°)	0.0	0.0	0.0	0.7
1104	1.10	0.68	0.32	3	B	0.6	1	0.0	0.0	0.0	0.0	0.0	1.5 (336°)	0.0	0.0	1.5
1105	1.57	0.87	0.25	3	B	0.8	4	0.0	0.2 (267°)	0.5 (94°)	0.2 (178°)	0.0	0.0	0.0	0.4 (297°)	1.3
1107	0.80	0.73	0.20	4	D	0.3	7	0.8 (107°)	0.0	0.2 (91°)	0.2 (169°)	0.1 (5°)	0.5 (193°)	0.3 (286°)	0.6 (346°)	2.7
1108	1.05	0.62	0.30	4	B	0.5	3	0.0	0.0	0.0	0.0	0.2 (86°)	0.5 (282°)	0.0	9.0 (154°)	9.7
1109	0.98	0.69	0.25	4	D	0.4	2	0.0	0.0	0.0	1.6 (71°)	0.0	0.0	0.0	1.6 (256°)	3.2
1111	1.05	0.60	0.25	4	B	0.4	6	2.7 (304°)	0.9 (44°)	0.9 (356°)	0.3 (187°)	0.0	0.7 (1°)	0.0	0.3 (57°)	5.8
1112	0.75	0.70	0.30	1	D	0.4	3	0.8 (159°)	0.0	0.0	0.3 (48°)	0.0	0.1 (285°)	0.0	0.0	1.2
1113	1.00	0.85	0.30	1	D	0.6	1	0.1 (301°)	0.0	0.0	0.0	0.0	0.0	0.0	0.0	0.1
1115	1.50	1.00	0.30	3	D	1.1	2	0.2 (344°)	0.0	0.3 (24°)	0.0	0.0	0.0	0.0	0.0	0.5
1116	0.85	0.75	0.30	3	B	0.5	1	0.0	0.0	0.0	0.0	0.0	0.0	0.0	0.8 (123°)	0.8
1117	0.90	0.87	0.35	3	D	0.7	4	0.2 (42°)	0.3 (4°)	0.1 (337°)	0.0	0.0	0.0	0.0	0.1 (146°)	0.7
1118	1.20	1.05	0.20	3	D	0.6	2	0.4 (341°)	0.0	0.0	0.0	0.0	0.0	0.0	0.2 (263°)	0.6
1120	1.15	1.05	0.20	3	D	0.6	4	0.1 (108°)	0.0	0.0	0.0	1.4 (274°)	0.1 (348°)	0.5 (280°)	0.0	2.1
1123	1.15	0.67	0.20	4***/3***	B	0.4	3	0.9 (283°)	***0.0***	***0.0***	***0.0***	***0.0***	***0.3 (1°)***	***0.1 (222°)***	***0.0***	1.3
1124	0.65	0.50	0.20	3	D	0.2	1	0.4 (350°)	0.0	0.0	0.0	0.0	0.0	0.0	0.0	0.4
1125	1.00	0.86	0.20	3	D	0.4	2	0.0	0.0	0.0	0.0	0.0	0.0	0.2 (138°)	0.2 (118°)	0.4
1127	1.60	1.50	0.20	2***/3***	D	1.2	5	0.0	7.2 (280°)	***1.2 (327°)***	***0.0***	***0.6 (340°)***	***1.1 (294°)***	***0.0***	***0.1 (315°)***	10.2
1128	0.80	0.50	0.25	4	B	0.2	6	4.9 (128°)	0.4 (210°)	0.7 (246°)	1.3 (116°)	1.6 (296°)	0.0	0.0	0.5 (208°)	9.4
1129	0.70	0.40	0.25	4	B	0.2	4	0.7 (22°)	0.0	0.0	0.8 (182°)	0.1 (334°)	0.0	0.0	1.1 (349°)	2.7
1130	1.05	0.60	0.25	4	B	0.4	4	0.0	0.2 (257°)	0.0	0.4 (341°)	0.2 (273°)	0.0	0.0	0.4 (265°)	1.2
1131	0.85	0.60	0.35	1	D	0.4	2	0.4 (256°)	0.0	0.0	0.1 (273°)	0.0	0.0	0.0	0.0	0.5
1133	0.60	0.40	0.25	1	D	0.1	1	0.9 (72°)	0.0	0.0	0.0	0.0	0.0	0.0	0.0	0.9
1134	0.80	0.65	0.30	2	D	0.4	2	0.0	0.0	0.0	0.0	0.0	0.3 (332°)	0.0	14.3 (282°)	14.6
1135	1.00	0.90	0.35	1	D	0.8	1	0.1 (344°)	0.0	0.0	0.0	0.0	0.0	0.0	0.0	0.1
1136	1.10	0.95	0.23	3	D	0.6	2	0.0	0.1 (311°)	0.0	0.0	0.0	0.0	0.0	0.1 (52°)	0.2
1137	1.00	0.70	0.25	3	D	0.4	2	0.0	0.0	0.1 (203°)	0.2 (316°)	0.0	0.0	0.0	0.0	0.3
1138	1.40	0.97	0.20	1	D	0.7	1	0.0	0.0	0.0	0.0	0.0	0.0	0.3 (344°)	0.0	0.3
1140	0.95	0.95	0.20	1***/4***	D	0.4	7	0.5 (311°)	0.8 (343°)	0.2 (169°)	0.0	0.2 (174°)	8.9 (265°)	***2.3 (334°)***	***0.3 (7°)***	13.2
1141	1.15	0.45	0.30	1	D	0.4	1	0.0	0.0	0.0	0.0	0.0	0.0	0.1 (106°)	0.0	0.1
1142	1.30	0.90	0.45	1	D	1.3	2	0.0	0.0	0.0	0.1 (263°)	0.0	0.0	0.1 (240°)	0.0	0.2
1143	0.85	0.65	0.20	4	D	0.3	2	16.1 (317°)	0.0	0.0	0.0	0.0	5.4 (335°)	0.0	0.0	21.5
1144	0.95	0.80	0.20	4	D	0.4	3	0.0	0.0	0.0	0.0	4.6 (313°)	6.3 (282°)	0.0	5.5 (356°)	16.4
1145	1.20	0.67	0.20	3	B	0.4	1	0.0	0.4 (13°)	0.0	0.0	0.0	0.0	0.0	0.0	0.4
1146	1.05	1.00	0.20	3	D	0.5	3	0.0	0.1 (350°)	0.0	0.0	0.0	0.0	0.1 (335°)	0.3 (335°)	0.5
1147	0.70	0.60	0.45	3	E	0.5	3	0.3 (288°)	0.0	0.3 (102°)	0.0	0.0	0.3 (281°)	0.0	0.0	0.9
1148	0.85	0.75	0.48	2***/3***	D	0.7	5	15.0 (315°)	***0.1 (346°)***	***1.2 (39°)***	***0.0***	***0.1 (217°)***	***0.1 (279°)***	***0.0***	***0.0***	16.5
1150	0.70	0.70	0.17	4	D	0.2	3	1.7 (359°)	0.0	0.4 (21°)	0.0	2.1 (343°)	0.0	0.0	0.0	4.2
1151	1.10	0.65	0.27	4	B	0.5	4	2.0 (273°)	1.4 (246°)	0.0	0.0	1.0 (200°)	1.1 (234°)	0.0	0.0	5.5

Table 3.5. Black Rock - summary of individual boulder characteristics, distance (m) and direction (°) of transported boulders between specified survey periods.

RFID No	A axis (m)	B axis (m)	C axis (m)	MS	Shape	Mass (t)#	Times trans	S1 - S2 (10 July 15 - 3 Dec 15)	S2 - S3 (3 Dec'15 - 6 Jan 16)	S3 - S4 (6 Jan 16 - 19 Feb 16)	S4 - S5 (19 Feb 16 - 31 May 16)	S5 - S6 (31 May 16 - 1 Sept 16)	S6 - S7 (1 Sept 16 - 9 Dec 16)	S7 - S8 (9 Dec 16 - 22 Feb 17)	S8 - S9 (22 Feb 17 - 24 May 17)	S9 - S10 (24 May 17 - 11 July 18)	Total IBTD (m)
1152	1.50	1.00	0.50	3	D	1.8	3	0.1 (229°)	0.1 (25°)	0.0	0.0	0.0	0.0	0.0	0.0	0.1 (224°)	0.3
1154	0.90	0.80	0.70	3	E	1.2	1	0.0	0.0	0.0	0.1 (262°)	0.0	0.0	0.0	0.0	0.0	0.1
1158	1.35	0.80	0.35	3	B	0.9	1	0.0	0.0	0.0	0.0	0.0	0.0	0.0	0.0	0.3 (103°)	0.3
1160	1.30	1.00	0.25	3	D	0.8	4	0.2 (239°)	0.1 (346°)	0.0	0.1 (161°)	0.0	0.0	0.2 (64°)	0.0	0.0	0.6
1162	1.25	1.10	0.25	3	D	0.8	1	0.0	0.0	0.0	0.0	0.0	0.0	0.1 (264°)	0.0	0.0	0.1
1163	0.75	0.70	0.20	4***/3***	D	0.3	5	2.9 (147°)	2.8 (337°)	4.0 (343°)	***0.1 (327°)***	***0.0***	***0.2 (145°)***	***0.0***	***0.0***	***0.0***	10.0
1164	0.75	0.50	0.35	3	E	0.3	5	1.5 (244°)	0.7 (54°)	0.2 (43°)	0.0	0.0	0.0	0.2 (359°)	0.0	1.3 (12°)	3.9
1165	1.00	0.75	0.35	3	D	0.6	1	0.0	0.0	0.0	0.0	0.0	0.0	0.0	0.0	0.4 (199°)	0.4
1166	1.35	1.15	0.40	4	D	1.5	2	0.0	0.1 (243°)	0.0	0.0	0.0	0.0	0.1 (86°)	0.0	0.0	0.2
1168	0.65	0.60	0.40	4	E	0.4	6	0.4 (46°)	0.6 (318°)	1.4 (351°)	2.1 (23°)	0.0	0.9 (179°)	0.0	0.0	1.0 (28°)	6.4
1175	0.80	0.52	0.25	3	B	0.2	4	0.2 (294°)	0.0	0.0	0.0	0.1 (280°)	0.0	0.0	0.8 (14°)	0.2 (305°)	1.3
1177	0.45	0.40	0.40	1	E	0.2	1	0.2 (179°)	0.0	0.0	0.0	0.0	0.0	0.0	0.0	0.0	0.2
1178	0.60	0.50	0.40	3	E	0.3	2	0.1 (229°)	0.0	0.1 (58°)	0.0	0.0	0.0	0.0	0.0	0.0	0.2
1179	0.50	0.50	0.25	3	D	0.2	2	0.5 (164°)	0.2 (78°)	0.0	0.0	0.0	0.0	0.0	0.0	0.0	0.7
1180	1.25	0.80	0.30	3	B	0.7	1	0.0	0.0	0.0	0.0	0.1 (22°)	0.0	0.0	0.0	0.0	0.1
1181	0.80	0.50	0.30	4***/3***	B	0.3	2	1.2 (141°)	***0.2 (200°)***	***0.0***	***0.0***	***0.0***	***0.0***	***0.0***	***0.0***	***0.0***	1.4
1182	0.70	0.60	0.40	4	E	0.4	2	0.2 (93°)	0.1 (87°)	0.0	0.0	0.0	0.0	0.0	0.0	0.0	0.3
1183	0.60	0.50	0.40	4	E	0.3	5	0.8 (232°)	0.1 (352°)	0.1 (73°)	0.2 (313°)	0.3 (61°)	0.0	0.0	0.0	0.0	1.5
1184	0.85	0.45	0.35	3	P	0.3	1	0.0	0.0	0.0	0.0	0.0	0.0	0.0	0.0	0.5 (331°)	0.5
1185	0.65	0.60	0.40	4	E	0.4	7	0.0	0.0	0.6 (317°)	2.5 (16°)	0.8 (23°)	2.1 (69°)	0.4 (32°)	0.3 (37°)	4.8 (31°)	11.5
1186	0.65	0.45	0.40	3	E	0.3	1	0.1 (26°)	0.0	0.0	0.0	0.0	0.0	0.0	0.0	0.0	0.1
1187	2.90	1.60	0.45	4***/3***	B	5.0	3	0.0	0.0	0.9 (4°)	6.4 (335°)	***0.0***	***2.5 (110°)***	***0.0***	***0.0***	***0.0***	9.8
1188	2.90	2.85	0.60	4	D	11.9	2	0.0	0.0	0.0	0.5 (60°)	0.0	3.1 (308°)	0.0	0.0	0.0	3.6
1189	2.00	1.70	0.30	4	D	2.4	3	0.0	0.0	0.2 (110°)	1.6 (351°)	0.0	0.8 (354°)	0.0	0.0	0.0	2.6
1190	1.40	0.60	0.40	2	P	0.8	1	0.0	0.0	0.1 (290°)	0.0	0.0	0.0	0.0	0.0	0.0	0.1
1192	1.25	0.75	0.35	4***/3***	B	0.8	4	0.0	1.1 (15°)	1.8 (334°)	5.4 (354°)	***0.0***	***0.0***	***0.1 (87°)***	***0.0***	***0.0***	8.4
1195	0.85	0.45	0.40	4	P	0.4	1	0.0	0.0	0.0	0.9 (324°)	0.0	0.0	0.0	0.0	0.0	0.9
1197	0.95	0.55	0.50	4	P	0.6	4	0.2 (283°)	0.8 (253°)	0.9 (82°)	7.8 (348°)	0.0	0.0	0.0	0.0	0.0	9.7
1199	0.80	0.50	0.40	1	P	0.4	2	0.0	0.0	0.2 (216°)	0.0	0.0	0.0	0.0	0.0	0.2 (228°)	0.4
7352	0.50	0.27	0.20	4	P	0.1	2	0.7 (295°)	0.0	0.0	0.0	0.0	0.0	0.0	0.0	0.4 (228°)	1.1
7353	1.20	0.85	0.30	3	D	0.7	1	0.0	0.0	0.0	0.0	0.0	0.0	0.0	0.0	2.7 (20°)	2.7
7354	0.58	0.40	0.25	4	D	0.1	1	0.0	0.0	0.0	0.0	0.0	0.0	0.0	0.0	0.6 (135°)	0.6
7356	0.45	0.35	0.30	4	E	0.1	2	0.0	0.0	0.0	0.0	0.0	0.0	0.1 (109°)	0.0	0.1 (262°)	0.2

Tables 3.6 and 3.7 summarise a range of site-specific transport data for BL and BR covering the three year study period.

Table 3.6. Bembridge Ledge - summary of transport values and wave conditions relative to each survey. Wave data is taken from the inshore wave monitoring station at Sandown Pier.

BEMBRIDGE LEDGE (n = 50)	25-Jul-15	03-Feb-16	17-Feb-16	01-Apr-16	23-Sep-16	25-Nov-16	08-Feb-17	05-May-17	STUDY TOTAL
	03-Feb-16	17-Feb-16	01-Apr-16	23-Sep-16	25-Nov-16	08-Feb-17	05-May-17	10-May-18	
Transport events (≥0.1 m)	21	12	13	11	13	15	9	18	112
CTD (m)	49.2	12.1	6.3	5.5	12.7	27.2	4.0	35.8	152.8
Mean IBTD (m)	2.3	1.0	0.5	0.5	1.0	1.8	0.4	2.0	1.4
CTD as % of study total	32%	8%	4%	4%	8%	18%	3%	23%	
Daily transport (CTD/no. of days)	49.2/193=0.25	12.1/14=0.86	6.3/44=0.14	5.5/175=0.03	12.7/63=0.20	27.2 /75=0.36	4.0/86=0.04	35.8/370=0.10	152.8/1026=0.15
Overturning events	6	1	0	0	3	1	0	1	12
Max H_s (m)	1.7	1.6	1.9	1.5	2.3	1.6	1.5	1.9	2.3
Max H_{max} (m)	3.3	2.2	2.3	2.2	2.9	2.3	2.4	2.8	3.3
Date of max. wave height	1 Jan ‘16	6 Feb ‘16	28 Mar ‘16	10 Apr ‘16	20 Nov ‘16	27 Jan ‘17	30 Apr ‘17	13 Feb ‘18	
Max. wave period (s)	6.4	7.1	8	No data	8	No data	4.9	7.1	
Wave direction (°)	140	169	170	130	154	115	115	159	

Table 3.7. Black Rock - summary of transport values and wave conditions relative to each survey. Wave data is taken from the inshore wave monitoring station at Sandown Pier.

BLACK ROCK (n = 54)	10-Jul-15 03-Dec-15	03-Dec-15 06-Jan-16	06-Jan-16 19-Feb-16	19-Feb-16 31-May-16	31-May-16 01-Sep-16	01-Sep-16 09-Dec-16	09-Dec-16 22-Feb-17	22-Feb-17 24-May-17	24-May-17 11-Jul-18	STUDY TOTAL
Transport events (≥0.1 m)	15	12	12	12	4	6	7	2	13	83
CTD (m)	9.3	6.9	10.5	27.7	1.3	9.6	1.2	1.1	12.6	80.2
Mean IBTD (m)	0.6	0.6	0.9	2.3	0.3	1.6	0.2	0.6	1.0	1.0
CTD as % of study total	12%	9%	13%	35%	2%	12%	1%	1%	16%	
Daily transport (CTD/no. of days)	9.3/146=0.06	6.9/34=0.20	10.5/44=0.24	27.7/102=0.27	1.3/93=0.01	9.6/99=0.10	1.2/75=0.01	1.1/91=0.01	12.6/352=0.03	80.2/1036=0.08
Overturning events	3	3	2	2	0	1	0	0	3	14
Max Hs (m)	1.5	1.7	1.6	1.9	1.0	2.3	1.6	1.1	1.9	2.3
Max Hmax (m)	2.4	3.3	2.3	2.3	1.6	2.9	2.3	2.4	2.8	3.3
Date of max. wave height	5 Oct '15	1 Jan '16	6 Feb '16	28 Mar '16	01 Aug '16	20 Nov '16	27 Jan '17	30 Apr '17	13 Feb '18	
Max. wave period (s)	No data	6.4	7.1	8	No data	8	No data	4.9	7.1	
Wave direction (°)	145	140	169	170	175	154	115	115	159	

The mass of displaced boulders at BL ranged from 0.1 t to 1.3 t. At BR, mobile boulder mass ranged from 0.1 t to 11.9 t. At both sites the a-axis orientation of tagged boulders was generally aligned perpendicular to the direction of transport (Nott, 2003b), (Figures 3.10, BL and 3.11, BR). Transport occurred relative to the prevailing wave direction from within the south-eastern quadrant. The easterly aspect of BL affords a greater level of shelter from the dominant south-south-westerly (SSW) wind and southerly wave approach when compared with BR.

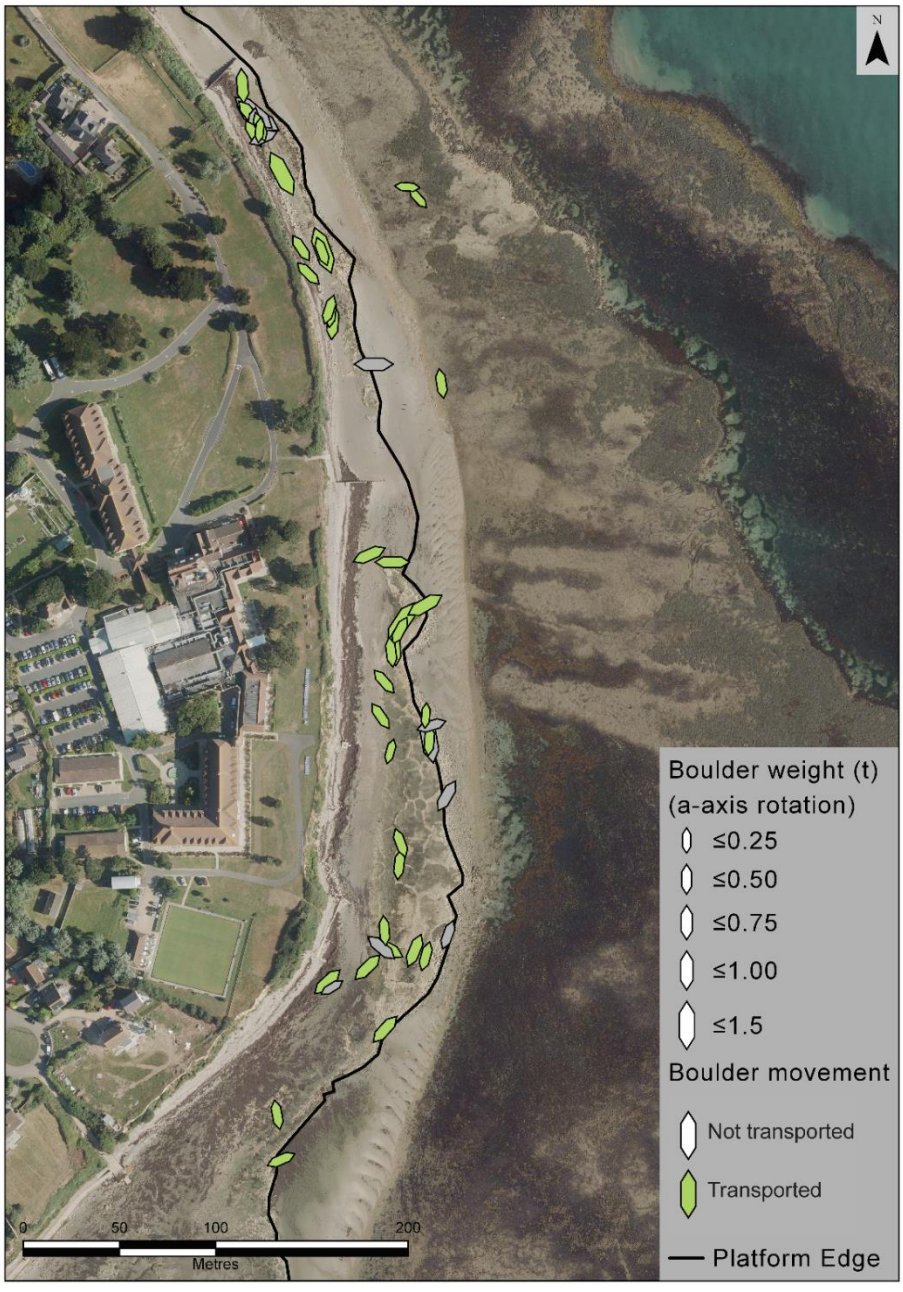

Figure 3.10. Bembridge Ledge site map identifying tagged boulder location, mass range, a-axis orientation and transport capacity.

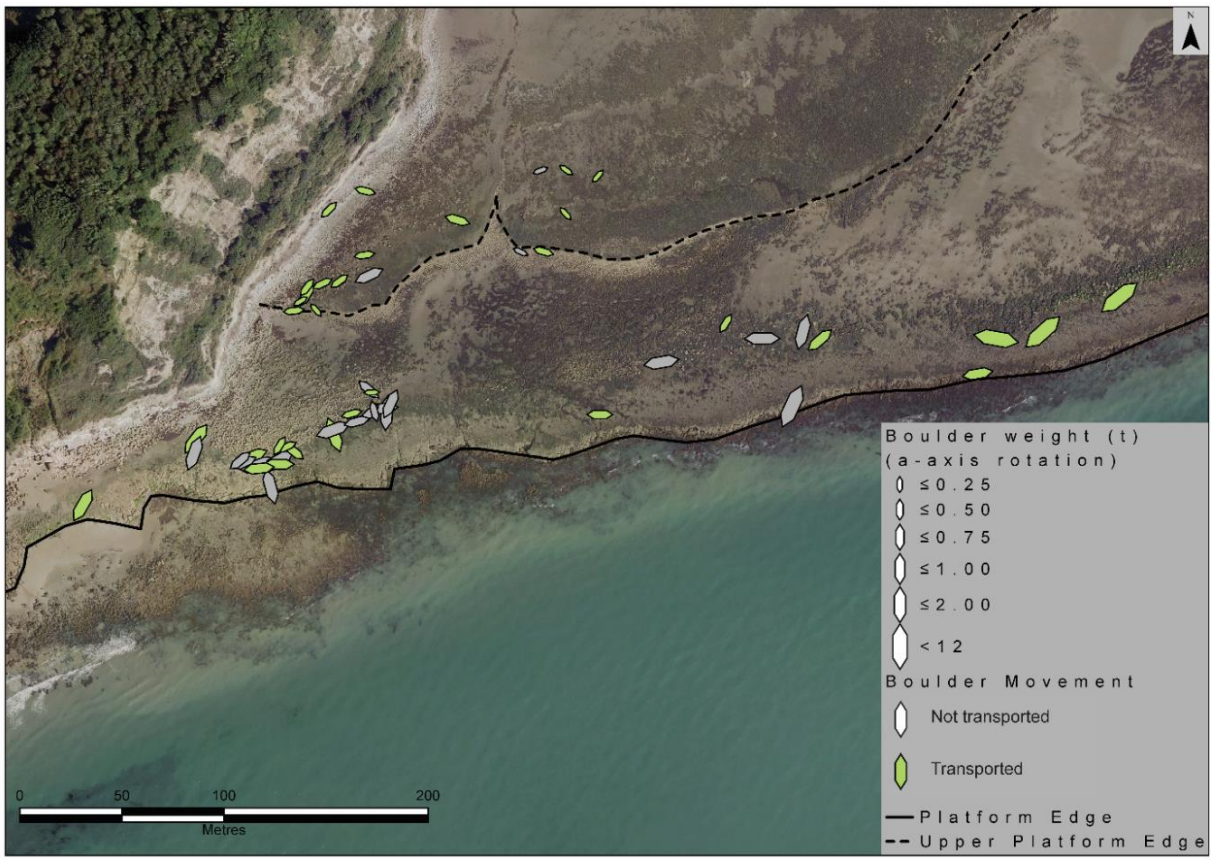

Figure 3.11. Black Rock site map identifying tagged boulder location, mass range, a-axis orientation and transport capacity.

Morphological classification

Each boulder was classified within a specific MS in accordance with the categories detailed in Table 3.1 and Figure 3.6. This enabled each transport event to be designated to a specific MS. The collated data is presented in Table 3.8.

MS 1 - constrained in its ability to be transported, located seaward of the shore platform;

MS 2 - constrained in its ability to be transported, joint-bound at the platform edge;

MS 3 - constrained in its ability to be transported, located on the shore platform surface;

MS 4 - unconstrained in its ability to be transported, located on the shore platform surface;

Table 3.8. Summary of boulder transport values by morphological setting at Bembridge Ledge and Black Rock.

	Morphological setting (MS)	Transport total (m) (% of total)	No. of times transported (% of total)	No. of boulders (movers/non-movers)	Mean transport distance per event (m)
Bembridge Ledge	1	14.0 (9%)	17 (15%)	13 (9/4)	0.8
	2	36.8 (24%)	4 (3%)	4 (3/1)	9.2
	3	15.5 (10%)	42 (38%)	20 (14/6)	0.4
	4	86.5 (57%)	49 (44%)	13 (13/0)	1.8
	TOTAL	**152.8**	**112**	**50 (39/11)**	**1.4**
Black Rock	1	0.6 (1%)	3 (4%)	3 (2/1)	0.2
	2	0.1 (0%)	1 (1%)	2 (1/1)	0.1
	3	14.3 (18%)	32 (38%)	25 (14/11)	0.4
	4	65.2 (81%)	47 (57%)	24 (8/16)	1.4
	TOTAL	**80.2**	**83**	**54 (25/29)**	**1.0**
TOTAL (BL & BR)	1	14.6 (6%)	20 (10%)	16 (11/5)	0.7
	2	36.9 (16%)	5 (3%)	6 (4/2)	7.4
	3	29.8 (13%)	74 (38%)	45 (28/17)	0.4
	4	151.7 (65%)	96 (49%)	37 (21/16)	1.6
	TOTAL	**233.0**	**195**	**104 (64/40)**	**1.2**

IBTD values for mobile clasts were plotted relative to the MS within which transport occurred, (Figures 3.12a and 3.12b). Each incremental transport event ≥0.1 m is represented by the respective symbol identified in the legend. The figures demonstrate graphically the apparent significance of the morphological setting on the recorded boulder tranport distances.

- Those boulders identified by the MS prefix/suffix nomenclature e.g. MS4/3 were originally located in MS4 then subsequently transferred to MS3;
- Immobile boulder details are not included in these tables;
- Enlarged symbols indicate an incident of overturning;

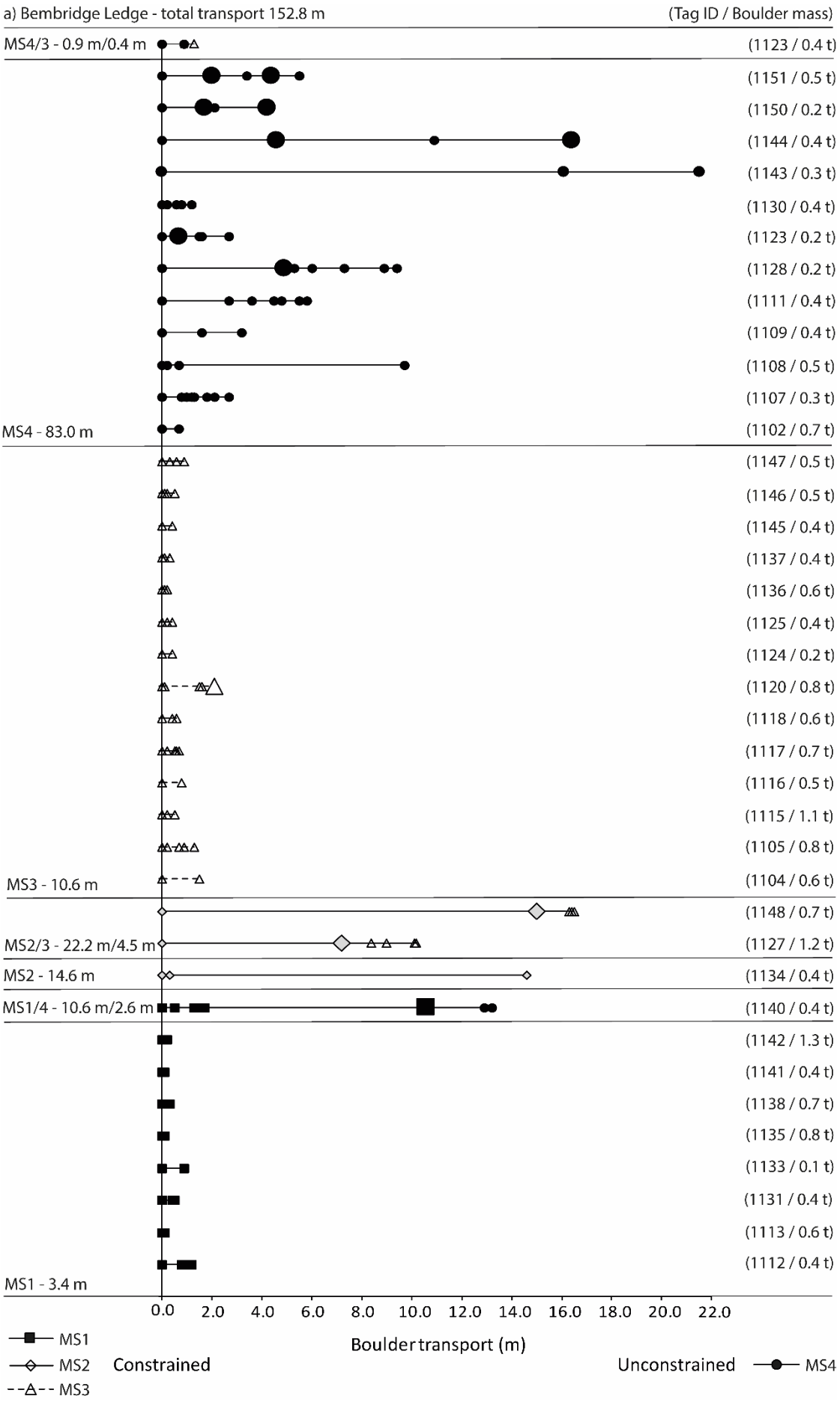
a) Bembridge Ledge - total transport 152.8 m
(Tag ID / Boulder mass)
MS4/3 - 0.9 m/0.4 m
(1123 / 0.4 t)
(1151 / 0.5 t)
(1150 / 0.2 t)
(1144 / 0.4 t)
(1143 / 0.3 t)
(1130 / 0.4 t)
(1123 / 0.2 t)
(1128 / 0.2 t)
(1111 / 0.4 t)
(1109 / 0.4 t)
(1108 / 0.5 t)
(1107 / 0.3 t)
MS4 - 83.0 m
(1102 / 0.7 t)
(1147 / 0.5 t)
(1146 / 0.5 t)
(1145 / 0.4 t)
(1137 / 0.4 t)
(1136 / 0.6 t)
(1125 / 0.4 t)
(1124 / 0.2 t)
(1120 / 0.8 t)
(1118 / 0.6 t)
(1117 / 0.7 t)
(1116 / 0.5 t)
(1115 / 1.1 t)
(1105 / 0.8 t)
MS3 - 10.6 m
(1104 / 0.6 t)
(1148 / 0.7 t)
MS2/3 - 22.2 m/4.5 m
(1127 / 1.2 t)
MS2 - 14.6 m
(1134 / 0.4 t)
MS1/4 - 10.6 m/2.6 m
(1140 / 0.4 t)
(1142 / 1.3 t)
(1141 / 0.4 t)
(1138 / 0.7 t)
(1135 / 0.8 t)
(1133 / 0.1 t)
(1131 / 0.4 t)
(1113 / 0.6 t)
(1112 / 0.4 t)
MS1 - 3.4 m
0.0
2.0
4.0
6.0
8.0
10.0
12.0
14.0
16.0
18.0
20.0
22.0
Boulder transport (m)
MS1
MS2
MS3
Constrained
Unconstrained
MS4

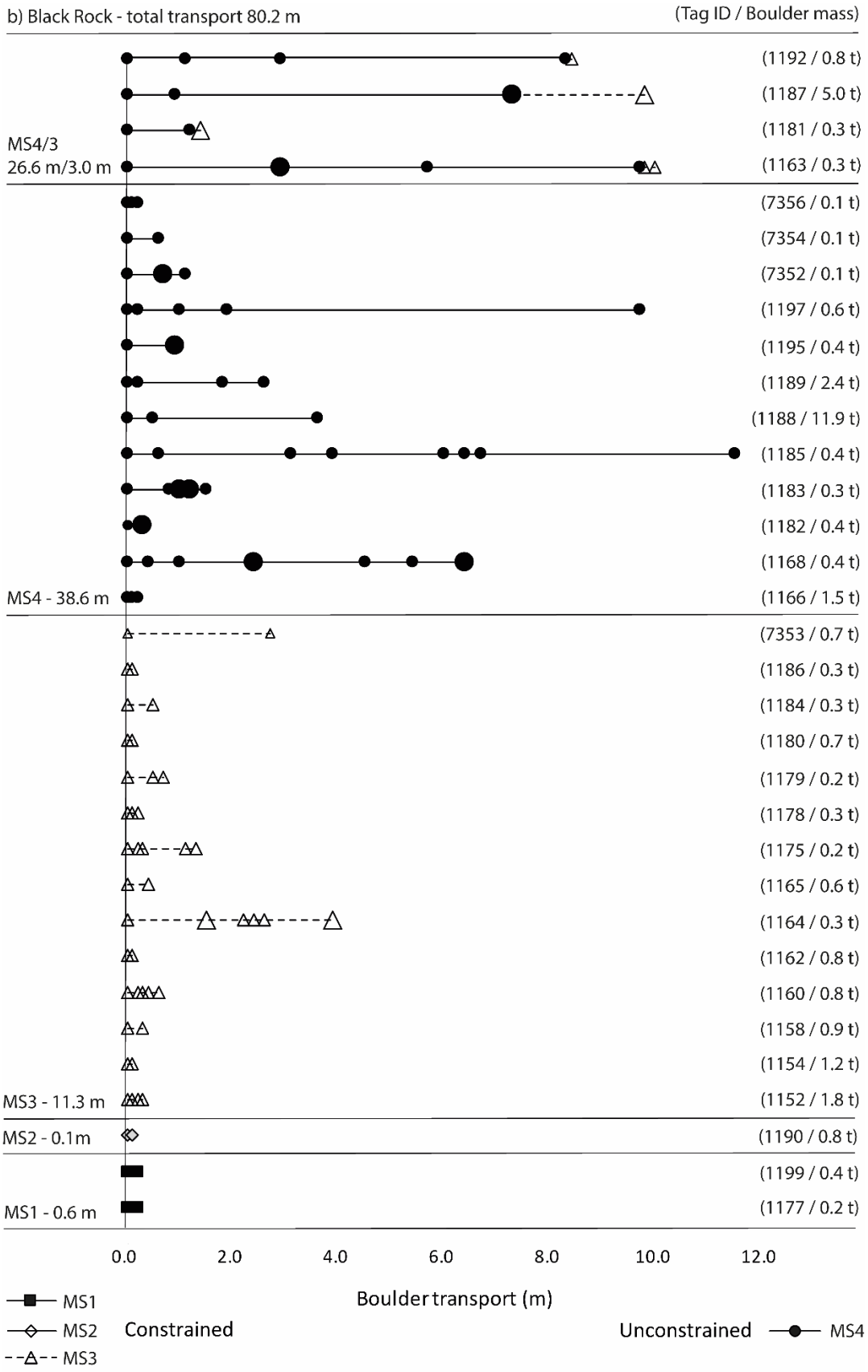

Figure 3.12. Individual boulder transport events identified by MS at (a) Bembridge Ledge and (b) Black Rock.

Wave climate and tidal regime

Analysis of the CCO wave data over the three year study identified maximum inshore H_s and H_{max} values of 2.3 m and 3.3 m respectively (CCO, 2018). Inshore H_s exceeded the CCO storm threshold of 1.6 m on 42 occasions representing 0.07% of the total number of recorded H_s wave values (n = 63,741); H_{max} values exceeded the threshold 817 times representing 1.28% of the total number of recorded wave values (n = 63,741). Inshore wave heights (H_s and H_{max}) recorded during the study period are presented relative to the relocation surveys and the CCO storm threshold (Figure 3.13).

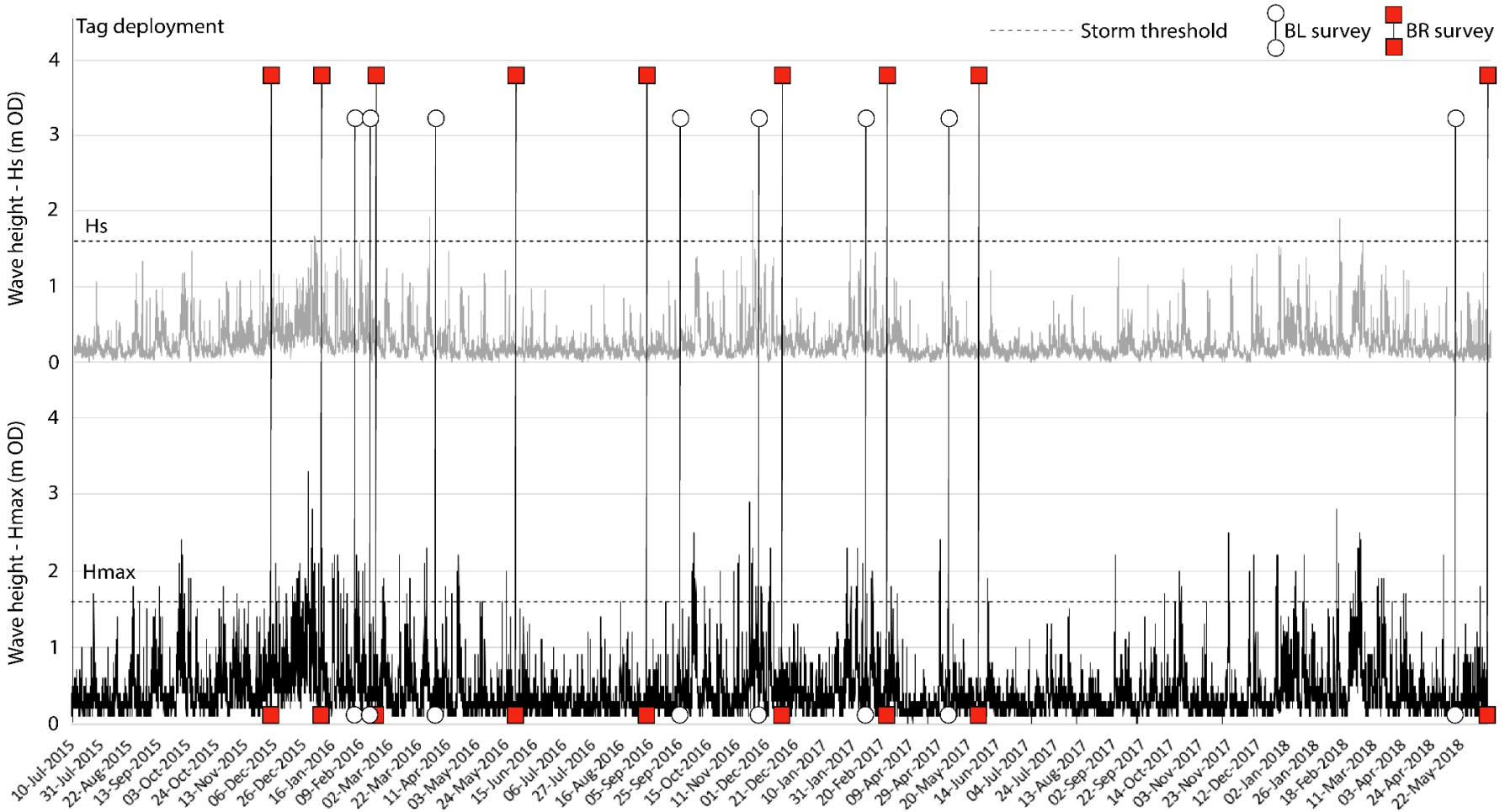

Figure 3.13. Inshore wave data from Sandown Pier (Hs and Hmax) and CCO storm threshold value (1.6 m). Boulder relocation surveys are identified as indicated relative to wave activity.

Data from the nearshore wave buoy identified that H_s values exceeded the storm threshold of 2.5 m on 85 occasions representing 0.16% of the total number of recorded H_s wave values (n = 51,695). H_{max} waves exceeded the threshold 1022 times representing 1.97% of the total number of recorded wave values (n = 50,743). H_s and H_{max} wave heights exceeding the 2.5 m threshold are presented in Figures 3.14a and 3.14b. The data identifies storm wave activity and intensity as dominant from a SSE direction, mean wave orientation was 164°, +/- 30°. This aligns with the southerly aspect of the shore platfrom edge at BR but would strike BL at an oblique angle. Notably, a smaller proportion of the H_{max} waves originate from an ESE direction, which could directly impact BL.

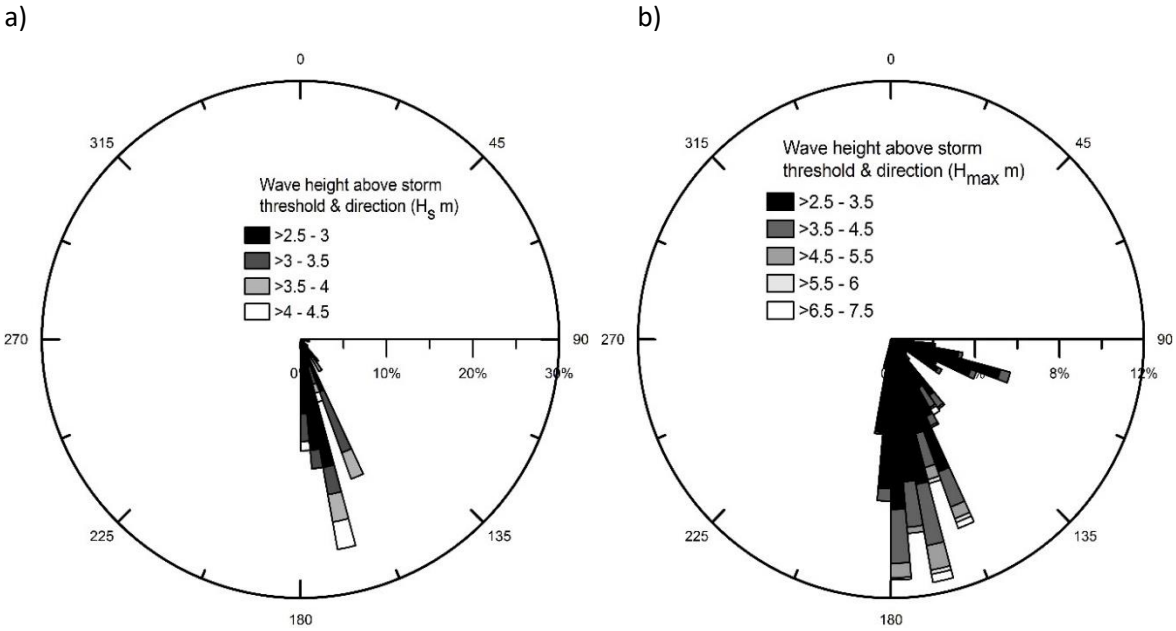

Figure 3.14. Wave height, frequency (%) and direction(°). (a) significant wave height: Hs (m); (b) maximum wave height: Hmax (m). This data was recorded from the nearshore CCO wave buoy located in Sandown Bay.

Hydrodynamic modelling

The hydrodynamic equations of Nandasena *et al*. (2011b) were utilised to determine the minimum wave height required to initiate displacement of the three boulders of greatest mass which were all located at BR. Each pre-transport scenario was addressed, the results are presented in Table 3.9.

Table 3.9. Summary details of boulder characteristics and calculated minimum wave heights (m). JB: joint-bound; SM/SA: submerged/sub-aerial.

RFID No.	A axis (m)	B axis (m)	C axis (m)	Volume (m^3)	MS	Mass (t) #	Times trans-ported	IBTD (m)	Nandasena (JB) wave height (m)	Nandasena (SM/SA) wave height (m)
1187	2.90	1.60	0.45	2.09	4/3	5.0	3	9.8	10.4	6.8
1188	2.90	2.85	0.60	4.96	4	11.9	2	3.6	12.7	9.0
1189	2.00	1.70	0.30	1.02	4	2.4	3	2.6	8.2	4.5

Discussion

RFID

This study represents the first long-term intertidal boulder transport monitoring programme of its kind. By documenting the findings from the RFID derived data we present coastal researchers with a new and effective tool to assess boulder transport dynamics resulting from contemporary storm impacts. The favourable tag recovery rate (92%) has provided a wealth of valuable data which demonstrates the suitability of the methodology and dispels concerns regarding RFID use in harsh coastal environments (Paris *et al*., 2011; Naylor *et al*., 2016). The longevity of the tags operational capacity (4 years and continuing at present) allows for longer-term assessments of storm occurrences and the associated boulder transport responses to be determined.

Boulder production

The production of boulders by the removal of tagged clasts at the platform edge was recorded three times at BL, conversely, there were no incidents documented at BR. We propose the increased occurrence of block removal by quarrying at BL was directly related to the denser jointing and thinner, well bedded limestone units suggesting boulder production is determined by site-specific geological controls (Kennedy, 2010; Naylor and Stephenson, 2010).

We present an example of boulder production by quarrying at BL (tag ID: 1148), Figure 3.15. The pre-transport tagged boulder was integrated as part of the shore platform edge prior to detachment, as recorded on 25 July 2015. The dotted line represents the well-defined joints that enable water ingress from breaking waves (Figure 3.15a). During a relocation survey on 3 February 2016 the tagged block had been removed. The remnants of block removal presented a socket which

clearly displayed differing colouration from the surrounding bedrock unit indicating recent exhumation (Hall *et al*., 2008), (Figure 3.15b). The detached boulder was relocated 15.0 m from the socket having been overturned during transport as indicated by the downward position of the orientation hole. The boulders landward trajectory was impeded by a raised scarp (0.2 m) suggesting local morphological features exert influence on boulder transport (Figure 3.15c and 3.15d).

Figure 3.15. Bembridge Ledge - block removal by quarrying from the platform edge, tag ID: 1148. (a) pre-transport tagged boulder; (b) post-transport boulder socket; (c) post-transport deposition; (d) transport pathway as indicated by the arrow, pre-transport detach detachment setting (at left) to deposition (at right). For scale, the DGNSS pole is extended to a height of 2.0 m.

Boulder transport

Despite the moderate storm wave climate compared with previous boulder transport study sites (Goto *et al*., 2009; Knight and Burningham, 2011; Cox *et al*., 2012; Autret *et al*., 2016) these data demonstrate that extreme storm conditions are not necessary to mobilise boulder-sized clasts.

The total distance of boulder transport measured over the three year study amounted to 233.0 m, 66% (152.8 m) occurring at BL and 34% (80.2 m) at BR. This resulted from 195 individual transport events each ≥0.1 m, 57% (n = 112) occurred at BL, 43% (n = 83) at BR. Of the 104 boulders in the array, 69% (n = 72) were mobile at least once over distances ranging from 0.1 m to 21.5 m with a greater number of mobile clasts at BL: 39/50 (78%) than BR: 33/54 (61%). Of the 72 displaced boulders, 11% were mobilised on five or more separate occasions. Transported boulders were represented in each of the boulder size categories (Blair and McPherson, 1999) including a very coarse clast (estimated mass: 11.9 t) that was transported twice accumulating an IBTD of 3.6 m. Daily transport distances derived from the CTD (m) / no. of days between surveys were 53% greater at BL than BR, 0.15 m/per day compared with 0.08 m/per day. Furthermore, the study total for transport distance at BL was 90% higher than at BR. We attribute this, in part, to litho-structural differences in the boulder producing bedrock units at the sites (Cruslock et al., 2010; Stephenson and Naylor, 2011; Naylor and Stephenson, 2010). The more densely jointed bedrock at BL produces a greater number of smaller, mobile clasts compared to BR (BL: mean tagged boulder mass = 0.5 t / max. 1.3 t and BR: mean = 1.1 t / max. 11.9 t).

Seasonality of boulder displacement was evident with increased transport occurring between September and February, corresponding with greater wave magnitudes associated with autumn and winter storm events (Tables 3.6 and 3.7). However, the longevity of the study demonstrated that boulder transport also occurred during periods of quiescence, e.g. spring and summer months (April - September). The transport data identified boulder displacement occurred even under low-energy wave conditions when the inshore H_s failed to breach the CCO storm threshold of 1.6 m. At BL between 1 April and 23 September 2016, 11 transport events occurred amounting to displacement of 5.5 m, 4% of the BL study total of 152.8 m, (mean transported boulder mass, 0.5 t). At BR between 31 May and 1 September 2016 transport of 1.3 m, 2% of the BR study total of 80.2 m was recorded from four transport events, (mean transported boulder mass, 0.4 t). The maximum recorded inshore H_s during these periods were 1.5 m and 1.0 m respectively.

The output from the Python script detailed transport distance (m) and the direction of displacement between points (°). This provided insight to the boulder transport pathways and clast deposition.

Notably, the dominant direction of transport at BL occurred between 270° and 0°, at BR this occurred in a northerly direction, between 315° and 45°. Transport at both sites appears to be closely aligned with the prevailing southerly wave approach. The directional transport data was applied to the shoreline orientation at each site to establish the onshore/offshore sediment flux. At BL the general orientation of the platform edge runs from north to south, thus transport orientated between 0° and 180° was regarded as transported offshore. Transport between 180° and 360° was deemed to be transported onshore. The data identified 80% (123.0 m) of the 152.8 m study total at BL was transported onshore, the remaining 20% (29.8 m) offshore (Figure 3.16a). At BR the platform edge is orientated east to west. Therefore, transport orientated between 90° and 270° was considered offshore transport, instances orientated between 270° and 90° were classed as onshore transport. Of the 80.2 m study total, 81% (64.9 m) was orientated onshore, 19% (15.3 m) offshore (Figure 3.16b).

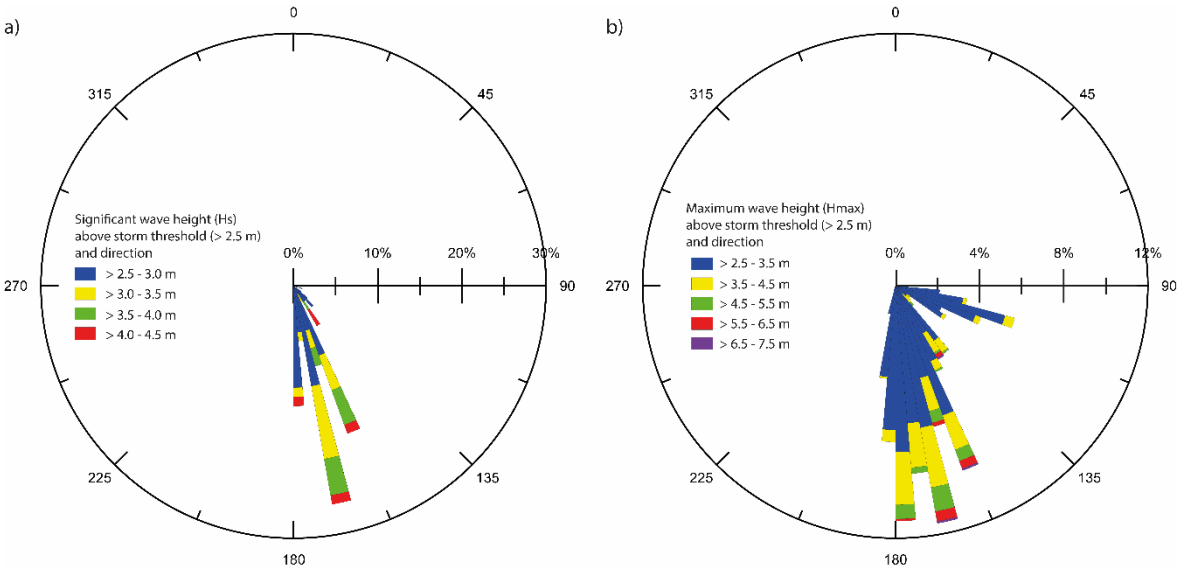

Figure 3.16. Frequency and orientation of boulder transport categorised by IBTD (m) as specified in the figure legends. Shore platform orientation is indicated by the centrally located dashed line. (a) Bembridge Ledge; (b) Black Rock.

At both sites the majority (~80%) of boulder transport resulted in onshore deposition as dictated by the dominant storm wave approach at, and across the shore platform surface. The higher percentage values for onshore transport suggest both sites are depositional with regard to boulder-sized sediments. This may be beneficial with continued deposition reducing wave attenuation across the shore platform minimising the wave energy delivered to the cliff/platform interface (Trenhaile, 2016). The orientation of the platform edge at BL relative to the prevailing wave activity produces more cross-shore boulder transport than at BR. Furthermore, the offshore transport at

both sites indicates that wave backwash is capable of mobilising boulder-sized clasts (Knight *et al*., 2009; Knight and Burningham, 2011).

Boulder deposition by storm waves was apparent from the recorded a-axis orientation of each tagged boulder. The a-axis is reported to be aligned parallel to the shore platform and/or perpendicular to the direction of storm wave approach (Nott, 2003b; Salzmann and Green, 2012). At BL, 74% of a-axis orientations were aligned between 315° and 45°. At BR, 70% were aligned between 45° and 135°. Figures 3.10 (BL) and 3.11 (BR) highlight the general trend of tagged boulders aligned parallel with the shore platform edge, indicative of transport under storm wave conditions. McKenna (2005) suggests, not only is a-axis orientation a reflection of storm wave approach but also the lack of an orientational trend may result from boulder collision. The field evidence and presence of widely scattered individual clasts on the platforms suggests boulder-boulder interactions are likely to be infrequent and do not significantly impact on boulder transport potential.

Although the field data affirms that low to moderate storm waves facilitate boulder transport the complexity of the mechanisms and processes that enable such transport require further investigation. Previous research has indicated a range of parameters exert influence on boulder displacement including geological discontinuities (Naylor and Stephenson, 2011; McKenna *et al*., 2011), boulder mass (Goto *et al*., 2011), shape (Imamura *et al*., 2008), pre-transport setting (Nandasena *et al*., 2011a; Nott, 2003a), surface roughness (Weiss, 2012) morphological setting (Naylor *et al*., 2016) and boulder interactions/collisions (Knight and Burningham, 2011; Nandasena and Tanaka, 2013b).

Naylor *et al*. (2016) identified a limited relationshsip between transport distance and boulder mass. Our data supports these findings whereby Figures 3.17a and 3.17b identify no significant relationship between boulder transport and mass (r^2 values of 0.01 and 0.02 at BL and BR respectively). This implies that boulder transport is not a direct function of mass suggesting an alternative factor governs the extent to which transport occurs.

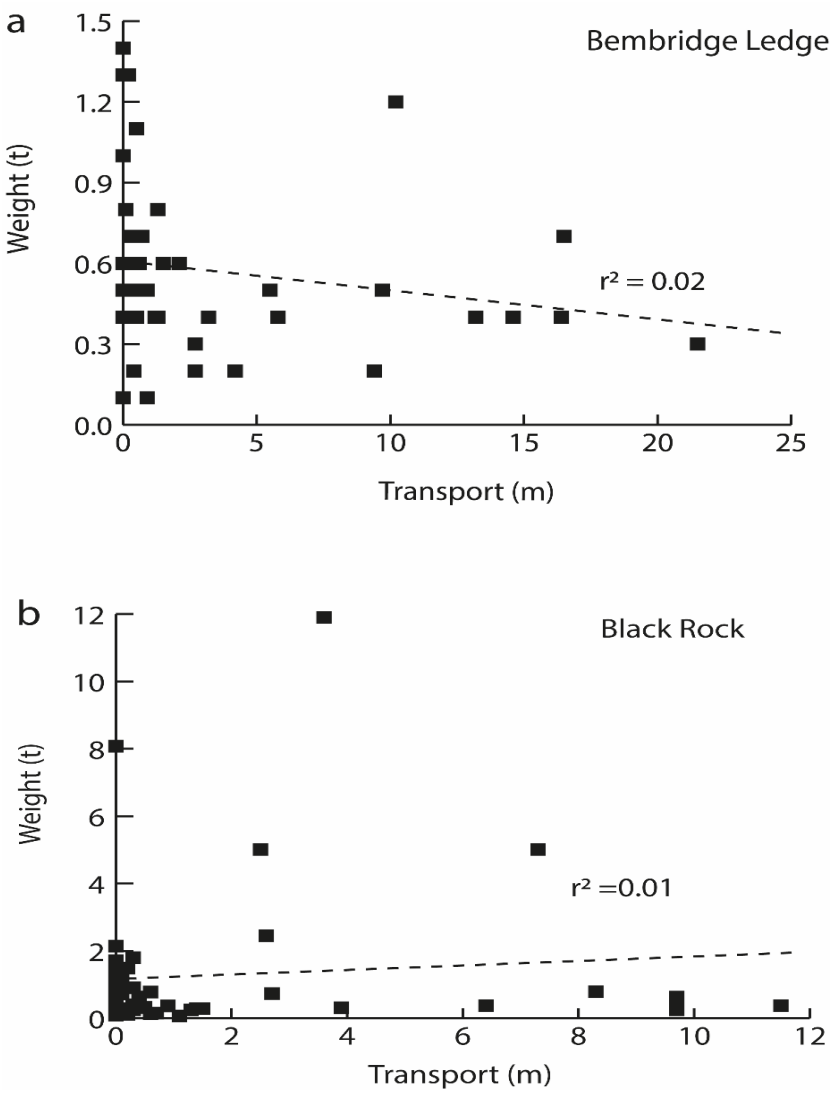

Figure 3.17. Graphical representation of recorded transport distance against boulder mass (a) Bembridge Ledge; (b) Black Rock.

The role of morphological setting

Given the aforementioned limited relationship between boulder mass and transport we considered the morphological pre-transport boulder setting as a factor in controlling clast displacement. Data presented in Table 3.8 and Figures 3.12a and 3.12b suggests a clearer relationship between clast displacement and the morphological setting of the tagged boulders.

Morphological setting 1 (MS1): incorporating MS1/4.

Boulders assigned to MS1 were generally moved only short distances owing to the impediment of the platform edge. Only one boulder (tag ID: 1140) at BL was translocated from a constrained

setting (MS1) to an unconstrained setting (MS4) on the platform surface. Although originally constrained by the platform edge, wave activity initiated incremental movements prior to storm conditions emplacing the clast on to and across the platform amounting to 10.6 m of transport, the boulder was known to have been overturned during transport. Subsequent wave activity when in an unconstrained setting (MS4) amounted to a further 2.6 m of transport. Collectively, MS1 clasts amounted to just 6% (14.6 m) of study total transport (233.0 m), the lowest of all MS's.

Morphological setting 2 (MS2): incorporating MS2/3.

Transport of boulders classified as MS2 related to incidents of block removal from the platform edge. We recorded three incidents of wave quarrying at BL, an example is provided (Figure 3.15). Once block removal occurred, subsequent wave action provided sufficient lift force to elevate the boulders on to the shore platform. Quarried boulders (tag ID 1127*, ID 1134 and ID 1148*) were displaced 7.2 m*, 14.3 m and 15.0 m* respectively. Highlighted boulders (*) were identified as being overturned during transport.

Despite the limited number of quarried boulders the data indicates that following clast removal from a joint-bound setting transport distances were considerable when compared with displacement from other MS's, 7.4 m per transport event compared with 0.7 m (MS1), 0.4 m (MS3) and 1.6 m (MS4). The total transport distance attributed to quarried boulders equates to 36.9 m, 16% of the study total from just 3% of the recorded transport events. Although the number of quarrying events is insignificant, the associated displacement is considerable. It also suggests the platform edge at BL is actively eroding. By contrast, quarrying was not recorded at BR.

Morphological setting 3 (MS3).

Although recorded transport events were frequent, clast mobility was impeded by morphological features including raised scarps, intertidal pools and the gravel beach at BL and the boulder beach and berm at BR. This resulted in small incremental displacements, only 12% of MS3 transport incidents exceeded 0.5 m. By comparison, 60% of MS4 transport events were ≥0.5 m. The restricted displacement of MS3 boulders is further reflected in the transport values; 13% of the study transport total from 38% of the transport events producing the lowest mean distance per transport event, 0.4 m. Notably, 53% of the boulders that failed to move during the study were assigned to MS3.

Morphological setting 4 (MS4): incorporating MS4/3.

MS4 boulders constitute 65% (57% at BL, 81% at BR) of the study total transport from 49% of the transport events, producing a mean distance per event of 1.6 m. Figures 3.12a and 3.12b indicate a preponderance of displaced MS4 and MS4/3 boulders. Significantly, they also highlight that subsequent to periods of mobility, those MS4 clasts translocated to a constrained setting (MS4/3) were limited in their ability to be further displaced, as evidenced by the respective suffix values. This supports the work of Naylor *et al*. (2016) who suggest the post-transport morphological setting also exerts limitations on boulder displacement.

The findings indicate, and support our hypothesis, that collectively unconstrained boulders (MS4) were transported further and more frequently than those in constrained settings (MS1, MS2 and MS3). However, individual constrained clasts liberated from a joint bound setting (MS2) were transported further during the initial detachment phase.

A series of Mann-Whitney tests were conducted to determine whether a statistically significant difference existed between boulder transport distances and the morphological setting, (constrained/unconstrained). This was carried out for BL, BR and BL and BR collectively ($\alpha = 0.05$). The test was conducted with and without non-mobile boulders (exc. non-movers), Table 3.10.

Table 3.10. Mann-Whitney tests results; boulder transport distances summarised by morphological setting (MS1 / MS2 / MS3 - constrained; MS4 - unconstrained).

Bembridge Ledge (n = 50)	***p*-value**	**Median (m) Constrained / Unconstrained**
Constrained (n =37) vs. Unconstrained (n = 13)	0.0001	0.4 / 4.2
Constrained (n = 26) vs. Unconstrained (n = 13) (exc. non-movers)	0.0010	0.6 / 4.2

Black Rock (n = 54)	***p*-value**	**Median (m) Constrained / Unconstrained**
Constrained (n = 30) vs. Unconstrained (n = 24)	0.0323	0.1 / 0.8
Constrained (n = 17) vs. Unconstrained (n = 16) (exc. non-movers)	0.0017	0.3 / 2.0

Bembridge Ledge & Black Rock (n = 104)	***p*-value**	**Median (m) Constrained / Unconstrained**
Constrained (n = 67) vs. Unconstrained (n = 37)	0.0002	0.2 / 1.5
Constrained (n = 43) vs. Unconstrained (n = 29) (exc. non-movers)	0.0000	0.5 / 3.2

Statistical analysis highlights the significance of the morphological setting in facilitating boulder transport. The distance over which constrained and unconstrained boulders are mobilised is significantly different at both sites, all *p*-value's ≤0.05. The median values also highlight the difference in transport distances attributed to unconstrained/constrained boulders. We therefore assert that the extent to which a boulder is displaced is significantly affected by the pre, and post morphological setting.

Aside from the aforementioned factors affecting transport there is a spatial component that requires consideration. At BL the beach is the main geomorphic obstacle impeding boulder transport. Platform width, measured from the platform terminus to the beach ranges from approximately 5 m to 55 m. At BR landward transport is impeded by the boulder beach and berm; platform width from the seaward terminus to these features ranges from 15 m to 40 m. While both landforms restrict mobility, the available distance across which transport can occur prior to encountering such an obstacle is greater at BL than at BR. Hence, the larger recorded transport distances.

The emperical data presented herein and previous boulder transport studies clearly demonstrate the occurrence of boulder mobility under moderate storm wave activity. However, there is limited quantitative evidence regarding transport modes during entrainment and displacement (Paris *et al.*, 2011; Goto *et al*., 2011, Naylor *et al*., 2016). Incorporating the orientation hole to each tagged boulder provided insight to transport mechanisms during episodes of mobility. Those clasts found with the orientation hole below the embedded RFID tag were known to have been overturned at least once during entrainment and/or transport. Of the 195 transport events recorded, 13% (n = 26, BL: 12 and BR: 14) resulted in overturning. Such incidents at BL accounted for 46% (69.7 m) of the total transport, the mean overturning transport distance was 5.8 m; the maximum overturning transport distance was 16.1 m. At BR overturning accounted for 24% (19.6 m) of the total transport at the site, producing a mean overturning transport distance 1.4 m. The maximum overturning transport distance was 6.4 m. Collectively, 38% (89.3 m) of the study transport total was attributed to overturning, consequently, 62% to displacement by sliding. The data demonstrates, with field-based evidence, that overturning of boulders weighing up to 5.0 t is possible during high-frequency, low-magnitude storm events. Furthermore, it affirms the assertion that overturning results in greater transport distances than sliding (Imamura *et al*., 2008) and confirms the findings of Nandasena and Takana (2013b), Zainali and Weiss (2015) and Noormets *et al*. (2004) who applied numerical modelling to establish sliding as the more dominant mode of transport.

Wave climate and tidal regime

Transport and wave data presented in Tables 3.6 and 3.7 indicate that increased wave magnitude does not always correspond with greater transport distance. To demonstrate this Table 3.11 presents a summary of transport and wave parameters relating to two consecutive surveys at BL. The transport distances associated with the period between 23 September and 25 November 2016 coincided with Storm Angus (20 November 2016) when the largest H_s value of the study was recorded, H_s = 2.3 m at Sandown Pier.

Table 3.11. Summary details of transport at BL and associated maximum inshore wave conditions recorded at Sandown Pier.

	Duration between surveys (days)	Daily transport distance (m)	Total mass of transported boulders (t)	No. of transport events	Transport distance (m)	Mean IBTD (m)	Max. H_s (m)	Max. H_{max} (m)	Wave direction (°)	Wave period (s)
23 Sept - 25 Nov '16	63	0.2	6.3	13	12.7	1.0	2.3	2.9	154	8.0
25 Nov '16 - 8 Feb '17	75	0.4	7.6	15	27.2	1.8	1.6	2.3	115	8.0

The data identifies the greater transport distance is attributed to the latter survey period despite the reduced storm wave activity. The key difference between the two event periods is the direction of storm wave approach relative to the aspect of the shore platform. Wave activity associated with Storm Angus occurred from a SSE direction (154°) opposed to the ESE (115°) as was the case with the weaker storm event. It is proposed that the ESE wave direction had a greater transport potential on the east-facing platform of BL than the more southerly wave activity. This suggests that wave magnitude alone is not a reliable or accurate indicator of boulder transport potential (Kennedy *et al.*, 2019) and other factors including storm wave direction relative to the coastal aspect require consideration.

The extent to which transport of coarse and very coarse clasts occurred under low to moderate storm wave activity was unexpected. The transport data identified the three largest mobile clasts, (as defined by mass), were all located at BR, (estimated mass, 2.4 t - tag ID: 1189; 5.0 t - tag ID: 1187 and 11.9 t - tag ID: 1188). During the study these three boulders were displaced 2.6 m, 9.8 m and 3.6 m respectively, totalling 16.0 m. The majority of transport (93%) occurred between 19 February

- 31 May 2016 which coincided with Storm Katie, and 1 September - 9 December 2016 which coincided with Storm Angus. The inshore wave and tidal data were consulted to better understand the hydrodynamic conditions that we assert facilitated displacement of these clasts. Wave parameters (H_s and H_{max}) and the corresponding tidal state at the peak of Storms Katie and Angus are presented in Figures 3.18a and 3.18b. The CCO storm threshold (1.6 m) was included to indicate the extent to which the threshold was exceeded.

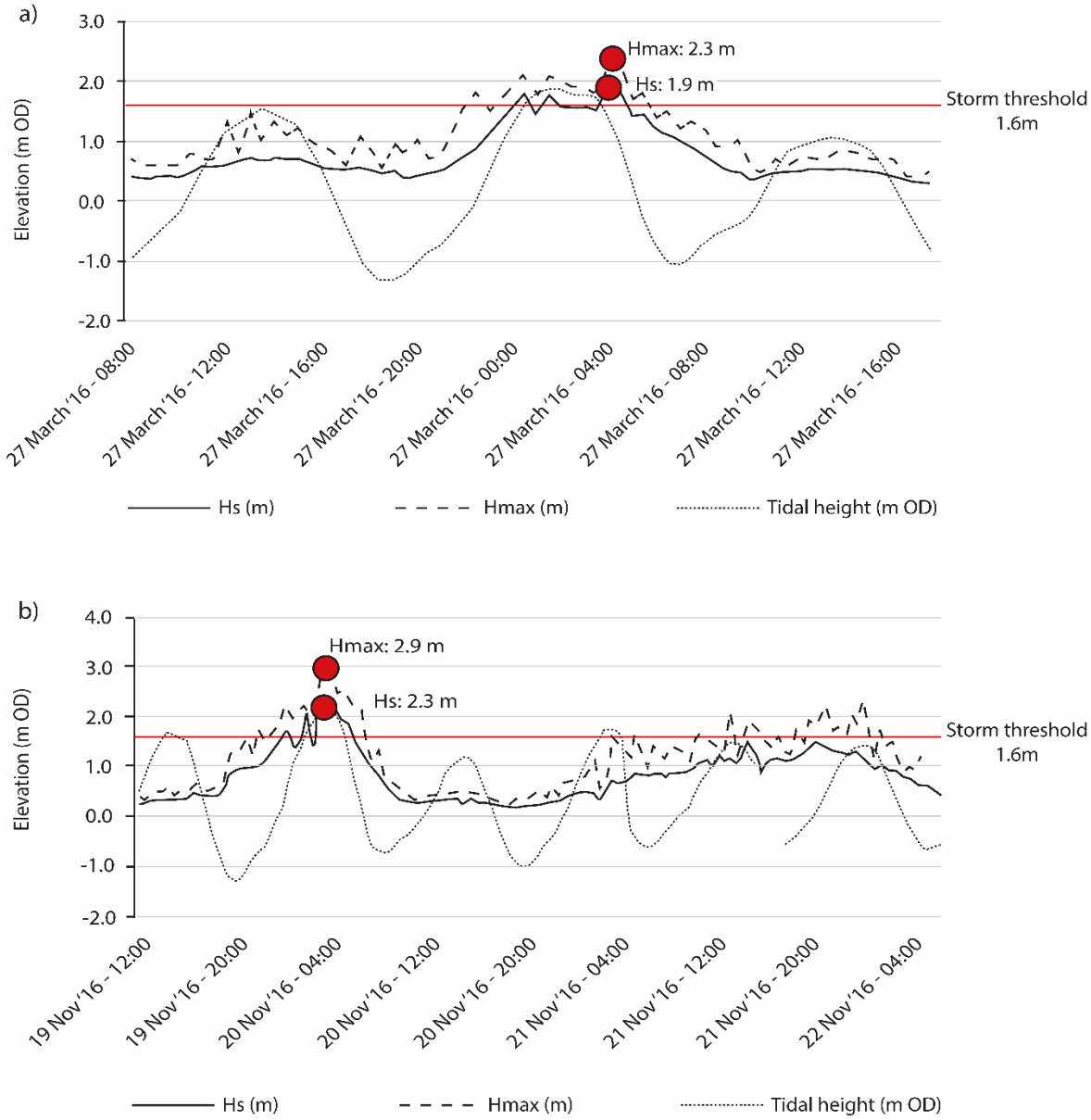

Figure 3.18. Peak wave activity (Hs and Hmax) and tidal height relative to the CCO storm threshold. The vertical bar represents peak wave activity, wave heights associated with (a) Storm Katie (27 - 28 March 2016) and (b) Storm Angus (19 - 22 November 2016). Note: due to the difference in tidal elevation between Sandown Pier (OD -2.44 m) and Bembridge (OD -2.74 m) an adjustment of +0.3 m was applied to the tidal data to better reflect water levels at the study sites.

The inshore H_s wave values peaked during Storm Katie and Angus at 1.9 m and 2.3 m respectively, whilst peak H_{max} values were 2.3 m and 2.9 m. The data further supports our assertion that moderate storm waves are capable of mobilising large boulders.

Hydrodynamic modelling

We applied the measured boulder characteristics for the three largest mobile clasts to the widely cited equations of Nandasena *et al*. (2011b). The predicted values provide a value for the estimated minimum wave height required to initiate displacement, Table 3.9. The calculated wave heights overestimate the maximum recorded wave heights associated with Storms Katie and Angus. The predicted wave height for the submerged/subaerial scenario of the 5.0 t boulder (tag ID: 1187) exceeds the highest recorded H_{max} value of 2.9 m by 3.9 m. The disparity in wave values further highlights shortcomings in the use of hydrodynamic equations which fail to adequately address the complexity and interaction between a range of geomorphic and hydrodynamic factors effecting boulder transport capacity (Zainali and Weiss, 2015; Biolchi *et al*., 2019a).

It was initially considered that the close proximity of the two study sites would enable comparisons to be drawn between locations. However, despite geological and climatic similarities there are a host of additional factors that differ such as lithology, topography, morphological features, shore platform exposure and aspect. Such fundamental differences make direct comparisons between sites problematic, as demonstrated by the disparity between transport distances and the varying response to the same storm events. Whilst similarities exist between what may be considered 'comparable settings' the range and complexity of the underlying transport processes and mechanisms and the degree to which they apply at any given location means universal theories governing boulder transport should be applied with caution.

Conclusion

The quantitative transport data derived from the novel application of RFID tagged boulders augments the feasibility of the methodology in determining the extent to which intertidal boulder transport occurs as a result of contemporary storm activity. Based on the RFID derived data the study identifies several key findings that explicate the phenomena of intertidal boulder transport. Firstly, the substantive field data and observations provide compelling evidence that incidents of boulder production, transport, overturning and emplacement are not confined to extreme, infrequent, high-magnitude storm events. On the contrary, low-magnitude, high-frequency storm waves at this relatively sheltered location are capable of transporting and reworking intertidal clasts

exceeding 10.0 t. Furthermore, it identifies contemporary storm activity as an effective agent of erosion and geomorphic modification on intertidal rocky coasts.

Secondly, the data demonstrates the significance of the pre-, and post-transport morphological setting in the ability to impede and facilitate boulder transport. The limited transport recorded by clasts in constrained morphological settings supports the notion that morphological features represent significant barriers to clast mobility (Trenhaile, 2016; Naylor *et al*., 2016; Hastewell *et al*., 2019a).

Finally, we affirm that boulder transport is governed by a host of complex interactions including, but not limited to:

(a) site-specific characteristics: platform morphology, boulder location relative to morphological features, litho-structure of the boulder producing units, aspect relative to storm wave approach, and;

(b) hydrodynamic conditions: storm wave magnitude and direction.

We recommend further application of the RFID methodology across a range of coastal settings from areas subjected to low/moderate wave climates to those exposed to extreme cyclone/hurricane generated storms. The resulting data will improve insight to the impacts of storm activity of differing magnitudes allowing for a greater understanding and interpretation of the mechanisms that facilitate such displacements.

Furthermore, the findings can be adopted to develop and refine deficiencies in the existing hydrodynamic equations, many of which are based on theoretical assumptions and laboratory experimentation with limited input from empirical field data (Imamura *et al*., 2008; Nandasena and Tanaka, 2013a & 2013b).

The unexpected size of the largest mobile boulders and the extent to which transport occurred suggests the capabilities of moderate contemporary storm events are vastly underestimated and rocky coastal landscapes are more susceptible to erosion than previously realised. The anticipated increase in storm frequency and intensity could have irreversible consequences for the future of rocky coasts globally.

References

See Bibliography, page 268.

Chapter 4 - Identification of plate-forme à vasques on a temperate shore platform? Quantitative analysis of morphology and relationships at Bembridge, Isle of Wight.

Chapter introduction

This chapter focuses on the wider geomorphology of the shore platform at Bembridge Ledge. More specifically, it relates to the discovery of a network of shallow, rimmed, intertidal pools which are analogous with a landform termed 'plate-forme à vasques'. The chapter draws upon findings from a series of field surveys which were conducted to quantify and describe the intertidal pool network.

The presence of these pools presented an opportunity to document a landform feature that has historically only been described in warmer tropical and Mediterranean climates (Trenhaile, 1987). Not only is this of significance from a geomorphological perspective but also in the context of this study. The ridges that surrounded each of the pools varies in height between 0.05 - 0.15 m presenting an undulating terrain across a small area of the shore platform at Bembridge Ledge. These topographic features act as traps, retaining boulders that are deposited within them. Therefore, the presence of the pools and their resulting morphology impede boulder transport.

Reference: Hastewell, L.J., Inkpen, R., & Bray, M. (2019). Identification of plate-forme à vasques on a temperate shore platform? Quantitative analysis of morphology and relationships at Bembridge, Isle of Wight. *Zeitschrift für Geomorphologie,* (2): 145-162. DOI: .org/10.1127/zfg/2019/0600

The submitted manuscript lists the aforementioned authors, the contribution of the named authors is hereby noted as follows:

> *LJ Hastewell - first author, arranged, organised and completed all fieldwork tasks with assistance from field operatives; processed and interpreted the data and wrote the manuscript in full.*
>
> *Dr's Inkpen and Bray acted as reviewers of the draft manuscript.*

Abstract

Enigmatic shallow vasques-type pools are identified for the first time on a temperate limestone shore platform. Like their counterparts found in tropical and Mediterranean climatic regions the pools occupy the intertidal zone and are separated from each other by raised ridges that facilitate the retention of tidal water. Ebb tidal water drains via low points in the ridges flowing through an interconnected network of pools towards the platform edge. The formative processes associated with ridge formation are generally attributed to bioconstruction or bioerosion. We assert that the adopted ridge forming processes differ between geographic locations based primarily on regional climate which restricts the presence of bioconstructing organisms. Additionally, the direction of water flow through the pool network is predetermined by the shore platform gradient which in turn shapes pool morphology via the process of coalescence.

Further interpretation and relationships are drawn from field observations and the analysis of a comprehensive set of morphometric measurements of 24 pools derived from field surveys using Differential Global Positioning Navigation Satellite System (DGNSS) and aerial image analysis. The paper quantifies the morphology, geometry and distribution of the pools providing a baseline protocol to inter-compare similar landforms. We attempt to define the relationships governing form and occurrence and identify surface topography and water flow as key components in defining the geomorphology at the site. We propose a theory for pool network evolution which highlights the respective recession rates of the landward cliff and platform edge as significant in maintaining this unique and valuable intertidal habitat with national and European conservation designations.

Introduction

It is reported that rocky, cliffed coasts cover as much as 52% of global shorelines (Young and Carilli, 2019). With such a wide geographic distribution it is reasonable to expect a broad range of coastal landforms derived from processes of erosion. Such features are particularly pronounced in coastal limestone and arise from a range of biological, chemical and physical regimes and the complex interactions between them. The efficacy of these processes is dependent on factors including, but not limited to, geology, lithology, wave and meteorological climate, tidal regime, sediment flux and ecological zonation (De Waele and Furlani, 2013).

We have identified distinctive intertidal pools on a near-horizontal shore platform at Bembridge on the Isle of Wight (U.K.), which have hitherto been unexplained in both form and process. The pools

create an interconnected network of shallow bowl-shaped depressions that are separated from each other by lobed ridges formed of the local Bembridge limestone (Figure 4.1). The ridges facilitate the retention of tidal water within the pools, although on the receding tide water flows from pools at the rear of the platform into adjoining pools of lower elevation towards the platform front. Inter-pool flow is achieved by water drainage via low points in the ridges; over time, repeated flow progressively widens the ridge breaks, herein referred to as breaches, leading to the development of an extensive pool drainage network.

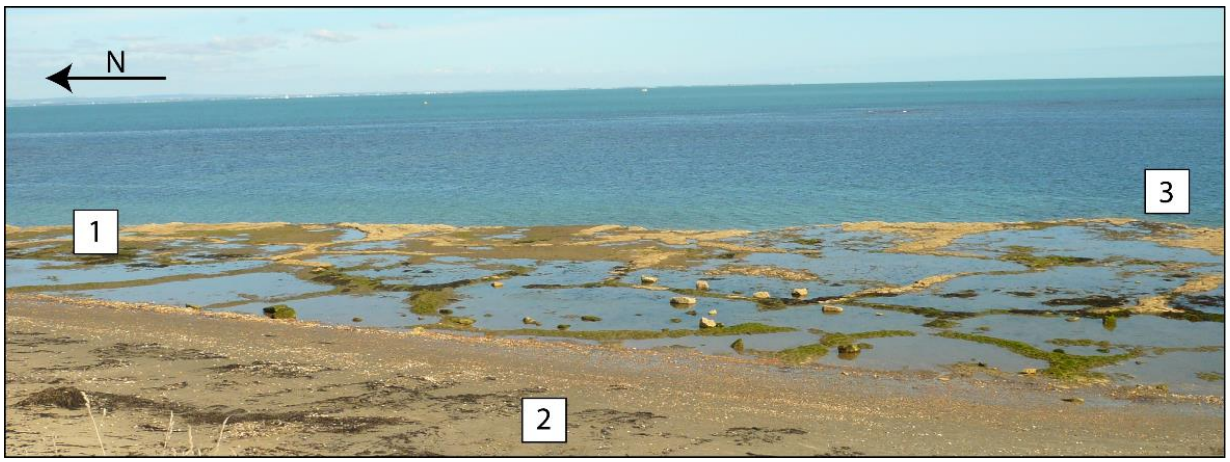

Figure 4.1. Bembridge pool features. (1) intertidal pool network exposed by the receding tide; (2) toe of migratory beach, the accretion of sand is covering parts of the most landward pools; (3) shore platform terminus.

The morphology and interaction between the Bembridge pools draws many comparisons with previously identified coastal features termed 'plate-forme à vasques' which have been identified by Guilcher (1953, 1954) Dalongeville (1977) and Battistini (1981) amongst others. The vasques pools are reportedly formed on limestone and aeolianite shore platforms within the intertidal zone (Guilcher, 1953; De Waele and Furlani, 2013). Trenhaile (1987, page 245) provides a concise description of plate-forme à vasques, describing them as "*wide (several decimetres), shallow pools with flat bottoms, which form a network of tiered, terrace-like steps. The pools are separated by sinuous, narrow lobed ridges between 1 and 20 cm in height, running continuously for dozens of metres. They develop between high and low tidal levels and are submerged at high water but are fed by breaking waves at low tidal levels, with the return flow cascading into lower pools*"**.**

Trenhaile (1987) also states that plate-forme à vasques have only been documented in intertropical and Mediterranean climatic zones, including Madagascar (Battistini, 1980, 1981), Lebanon (Dalongeville, 1977), Morocco (Guilcher, 1953; El Akhdar *et al*., 1990), South Africa (Miller and

Mason, 1994), Puerto Rico (Kaye, 1959), Algeria (Guilcher, 1954, Peres and Picard, 1952), Sicily (De Waele and Furlani, 2013), Israel (Safriel, 1966), Guam (Taboroši and Kázmér, 2013) and Curaçao (Focke, 1978; Trenhaile, 2015). Significantly, the features identified at Bembridge and described herein are the first reported vasques-like landforms to be identified and described in a temperate climate. This suggests the processes governing pool formation may not be limited to the previously identified climatic zones, potentially extending the geographic range over which these features may be observed.

Researchers from a range of scientific disciplines have identified coastal pool features that bear morphological similarity with plate-forme à vasques. This has resulted in a number of alternative terms being applied to similar landforms (Finkl, 2004; De Waele and Furlani, 2013). Plate-forme à vasques have also been referred to as terraced pools (Safriel, 1966; Miller and Mason, 1994), tidal terraces (Kaye, 1959) rimmed terraces (Emery, 1962), rimmed pools (Taboroši and Kázmér, 2013), surf platforms (Focke, 1978) and surf benches (Woodroofe, 2014). Whilst landform nomenclature differs photographic evidence in the aforementioned papers indicates the features are morphologically analogous with plate-forme à vasques. Therefore, we include details obtained from these sources in respect to detailing the vasques landforms.

Plate-forme à vasques morphology

A key feature of vasques pools are the ridges that surround the inner depression. Photographic images in Battistini (1980, 1981) and Taboroši and Kázmér (2013) identify vasques pools in tropical latitudes as having narrow, sinuous partitioning ridges, a few centimetres wide with near vertical sides. Those pools identified in the eastern Mediterranean have ridges that are broader and more lobed by comparison with their tropical counterparts (Safriel, 1966; Dalongeville, 1977). This morphotype is also reflected in vasques pools documented in Algeria, in the western Mediterranean (Peres and Picard, 1952; Guilcher, 1954), on the Atlantic coasts of Morocco (Guilcher, 1953; El Akhdar *et al*., 1990) and Spain (Stevčić *et al*., 2017). In all locations the flat bottomed pools collectively present a terraced profile which facilitates the drainage of water across pool ridges from the upper, more elevated pools to the lower ones located towards, or at the water's edge. They are located in the intertidal range and are either filled by breaking waves at the seaward margin or covered, and later exposed by cyclical tidal inundation and retreat (Trenhaile, 1987).

Plate-forme à vasques formation

The processes governing pool formation and evolution are not fully understood although they are generally attributed to bioconstruction, bioprotection and/or corrosion. The formative stage of vasques genesis commences with ridge development. Pool ridges can be categorised as constructed or non-constructed (Trenhaile, 1987). The former is generally attributed to bioconstruction, the latter, bioprotection (Guilcher, 1958). Bioconstruction (constructed ridge margins) facilitates ridge formation by the build-up of encrusting, calcareous algae and/or vermetids (Viles and Spencer, 2014). These organisms favour conditions found at the pool edges where water flow is greatest. This stimulates further colonisation creating ridges of uneven heights which leads to the terraced pool profile (Taboroši and Kázmér, 2013). Bioprotection (non-constructed ridge margins) is defined as protection provided to a surface by the colonisation of organisms (Naylor and Viles, 2002). In this instance protection is afforded to the residual rock ridges that encircle pools by the presence of epilithic algal growth (Guilcher, 1953; Trenhaile, 1987). The algae create a barrier reducing the exposure to erosion of the elevated rock ridges which is not afforded to the inner pool. This facilitates preferential erosion within the pool opposed to the ridges that encompasses them (Abbott and Pottratz 1969). Corrosion, by dissolution of calcium carbonate in seawater has been purported as a factor in the development of intertidal pools (Emery, 1946; Taboroši and Kázmér, 2013) and plate-forme à vasques (Guilcher, 1953). This process is particularly effective during the night as reported by Miller and Mason (1994) who documented diurnal fluctuations with lower pool water pH values being recorded at night. This was attributed to the uptake of carbon dioxide by algal photosynthesis during hours of daylight followed by the subsequent emission during the night. The resulting dissolution removes calcium carbonate in the pool depressions more so than the surrounding ridges (Guilcher, 1958).

Existing research on plate-forme à vasques has adopted a descriptive approach addressing morphological setting and making inferences as to the developmental processes facilitating pool formation (Guilcher, 1953; Dalongeville, 1977; Battistini, 1980 and 1981; El Akhdar *et al.*, 1990). Therefore this study is unique and novel, not only in researching plate-forme à vasques in a temperate climate but also in undertaking a detailed quantification of these landforms. In doing so we aim to:

(1) present qualitative and quantitative descriptions of the landform features based on empirical field data and aerial imagery relating to individual pool morphology;

(2) assess the processes governing pool formation and development;

(3) develop an evolutionary model applicable to pool formation in a temperate climate.

It is hoped that our quantitative methods of morphological description and analysis will form an important baseline approach for future comparative studies of these landforms enabling researchers to inter-compare similar vasques features at other locations more consistently and objectively.

Having conducted topographic field surveys using Differential Global Positioning Navigation Satellite System (DGNSS) and utilised aerial imagery we detail the morphology of 24 vasques-type pools and present a summary of morphological data and an interpretation of the pool network based on field investigations and analysis of the topographic data. We consider the influence of topography on pool development and propose theories of pool evolution.

Site description

Bembridge is located at the most easterly point of the Isle of Wight, off the south coast of the United Kingdom (Figure 4.2). The coastline features a near horizontal limestone shore platform known as Bembridge Ledge which dips gradually to the northest (0 - 2°). The rocky promontory extends up to 500 m at its widest point and presents a series of three terraced shore platforms formed of well jointed late Eocene Bembridge Limestone (Armenteros and Daley, 1998; Insole *et al.,* 1998; Daley and Edwards, 1990). The discontinuous upper limestone bed that forms the platform on which the pools are located sits above a thin (0.1 - 0.2 m) malleable marl layer. The preferential erosion of the marl bed results in undermining of the more consolidated overlying limestone. This leads to the removal of tabular blocks from the platform terminus which enables the progressive landward migration of the platform edge. The detached blocks are transported landward by storm wave activity (Hastewell *et al*., 2019a; Hastewell *et al*., 2020) frequently becoming deposited in the intertidal pools (Figure 4.3).

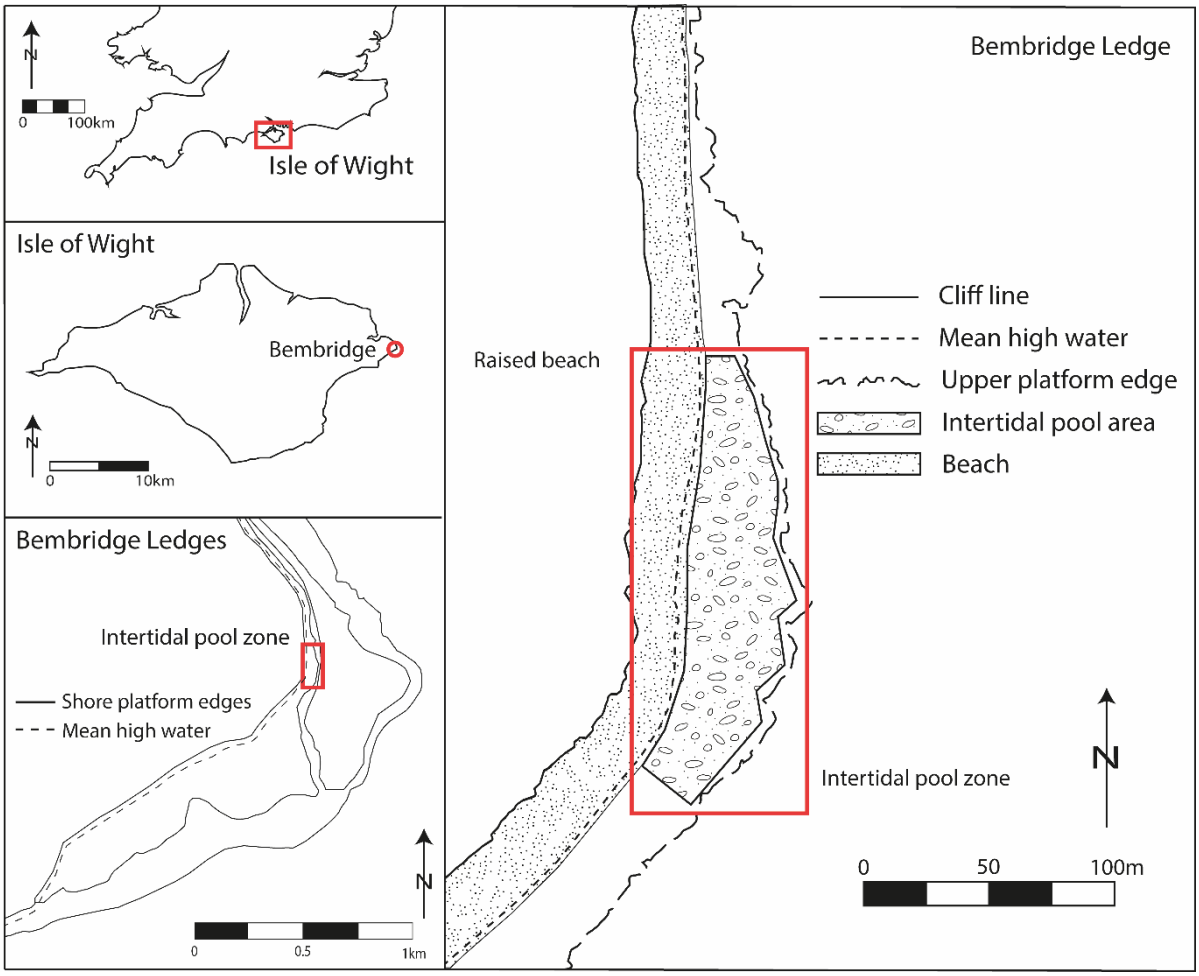

Figure 4.2. Site location, Bembridge on the most easterly point of the Isle of Wight, U.K.

A Quaternary raised beach forms a 4 - 6 m cliff at the rear of the platform. The cliff is comprised of coarse sands and gravels (Insole *et al*., 1998) and is occasionally subjected to episodes of erosion from storm activity which liberates material depositing gravels and sand at the cliff toe. Deposition at the cliff toe/platform interface creates a variable mixed gravel and sand beach. The maximum beach width extends approximately 30 m from the cliff. Beneath the cliff and beach is the uppermost limestone platform which stretches approximately 80 m at its widest point coming to an abrupt terminus akin to the type-B shore platform described by Sunamura (1992). It is on the surface of the upper platform that the shallow vasques-type pools are located (Figure 4.3). This platform is located within the mid-high intertidal range ensuring all the pools are inundated during each tidal cycle (spring and neap tidal range is 3.7 m and 1.8 m respectively). The incoming and retreating tide takes less than an hour to cover and uncover all the pools meaning there is little difference in duration of exposure/immersion from the pools at the rear of the platform and those at the front.

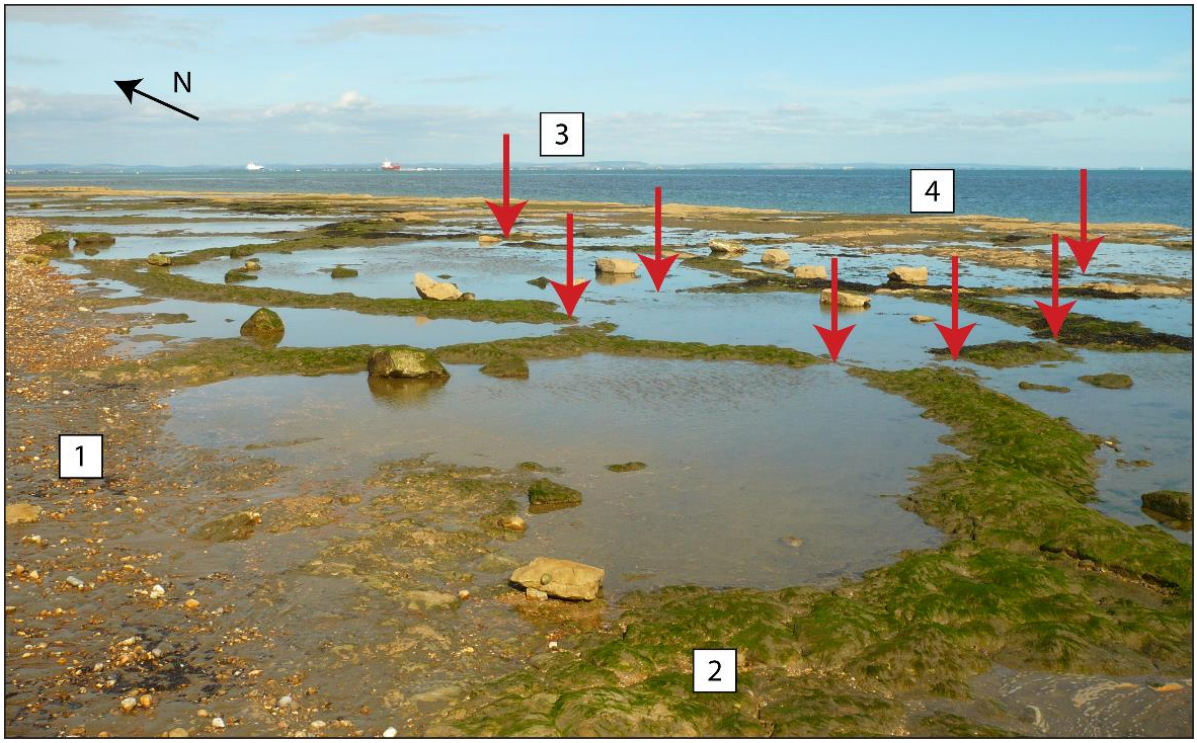

Figure 4.3. Bembridge pool features. (1) migratory beach toe; (2) lobed pool ridges colonised by algal growth which aids the retention of sand; (3) arrows identify breaches in the lobed ridges which facilitate the flow of water between pools; (4) upper platform terminus.

Climatically, Bembridge has a minimum and maximum yearly average temperature of 7.9°C and 13.9°C respectively. Annual average rainfall amounts to 870.8 mm and average annual hours of sunshine are 1923.0 with 21.8 annual average frost days. Meteorological data was obtained from the U.K. Met Office weather station at Ventnor, 13 km south west of the study site (Met Office, 2018). Wind conditions are dominant from a southwesterly direction, average wind direction in 2017 was 221°, average wind speed was 4.9 m/s (CCO, 2018).

The Bembridge pools are confined to an area of the shore platform covering approximately 7,000 m^2. They are formed entirely of the local Bembridge limestone and are therefore, considered as residual, non-constructed ridges. By comparison with pools found in tropical and Mediterranean climates the Bembridge pool ridges are broader, generally measuring between 0.5 - 0.8 m with a flatter lobed profile. Rather than being sinuous, the ridges meander for tens of metres with those located in the upper intertidal zone being covered with algal growth. In terms of pool and ridge morphology the Bembridge pool type is analogous with the plate-forme à vasques depicted in the diagrammatic representation by Trenhaile (1987), (Figure 4.4).

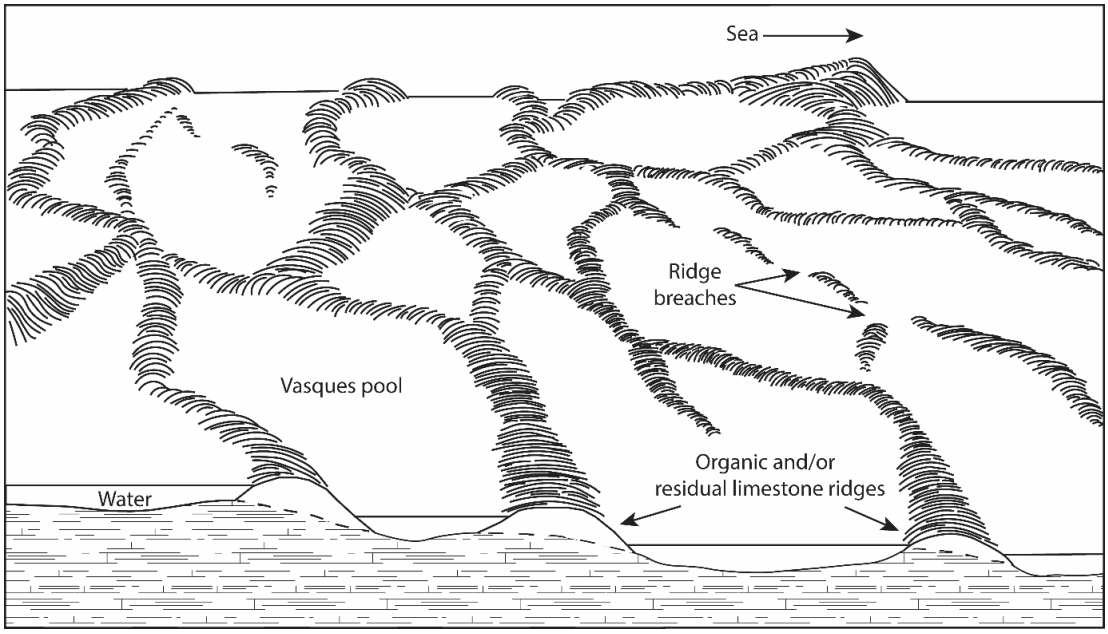

Figure 4.4. Diagrammatic representation of a plate-forme à vasques adapted from Trenhaile, 1987. (page 245). By permission of Oxford University Press.

Each pool is separated by the raised, lobed ridges that encircle a depression which retains water as the tide recedes. Algal growth including *Ulva lactuca, Enteromorpha intestinalis* and *Fucus serratus* pervade many of the pool ridges particularly those found towards the rear of the platform. The pool ridges are intersected by breaches that allow the drainage of water from the more elevated pools at the rear of the platform to the adjoining pools towards the front of the platform. Ecologically, the pools and surrounding platforms provide a valuable habitat for a range of intertidal species, some of which are found at the most southerly extent of their range (Collins *et al*., 1990). The niche habitat and ecological diversity that the pools support are reflected in the sites assigned environmental designations; Site of Special Scientific Interest (SSSI), Area of Outstanding Natural Beauty (AONB), Special Area of Conservation (SAC) *Special Protection Areas* (*SPAs*) and Ramsar status (Isle of Wight Council & Royal Haskoning, 2010). Such designations emphasise the significance of the pool network and the importance of increased understanding of the evolutionary processes that facilitate pool genesis and denudation.

Methodology

Data collection was obtained from two sources, topographic field surveys using DGNSS and ortho-rectified aerial imagery captured in August 2013 and published by the Channel Coast Observatory (CCO) in 2014, resolution X and Y-axis 0.001 m (Figures 4.5 and 4.6). The aerial imagery was incorporated into a GIS for interpretation using ArcMap 10.5.1. We conducted a series of

topographic surveys in July 2017 on 24 pools to determine a series of geometric characteristics using a Topcon Hiper V in RTK mode providing a horizontal accuracy of 5 mm, +/-0.5 ppm (Topcon, 2017).

During the DGNSS surveys we collected 413 topographic data points from 24 pools. This data comprised coordinates obtained from the pool ridges (n = 180), the inner ridge (n = 148) and the pool bottom (n = 85). The difference between mean values for pool ridges and pool bottom were used to determine pool depth (m). Aerial imagery of the site, captured in August 2013 by the CCO was utilised in combination with the measurement tool in ArcMap 10.5.1 to determine a range of morphometric pool parameters as displayed in Figure 4.5. These include, (1) pool length (m), measured as a straight line along the longest axis; (2) pool width (m), recorded as the widest point perpendicular to the long axis; (3) distance from the pool to the platform terminus and the beach toe (m), measured from a central point in each pool; (4) pool circumference and area (m/m^2), measured around the pool perimeter. The pool area value was multiplied by pool depth to provide an estimation of pool volume (m^3). Pool orientation (°) was recorded along the long axis in the field; results were recorded as deviations (+/-) from 0°.

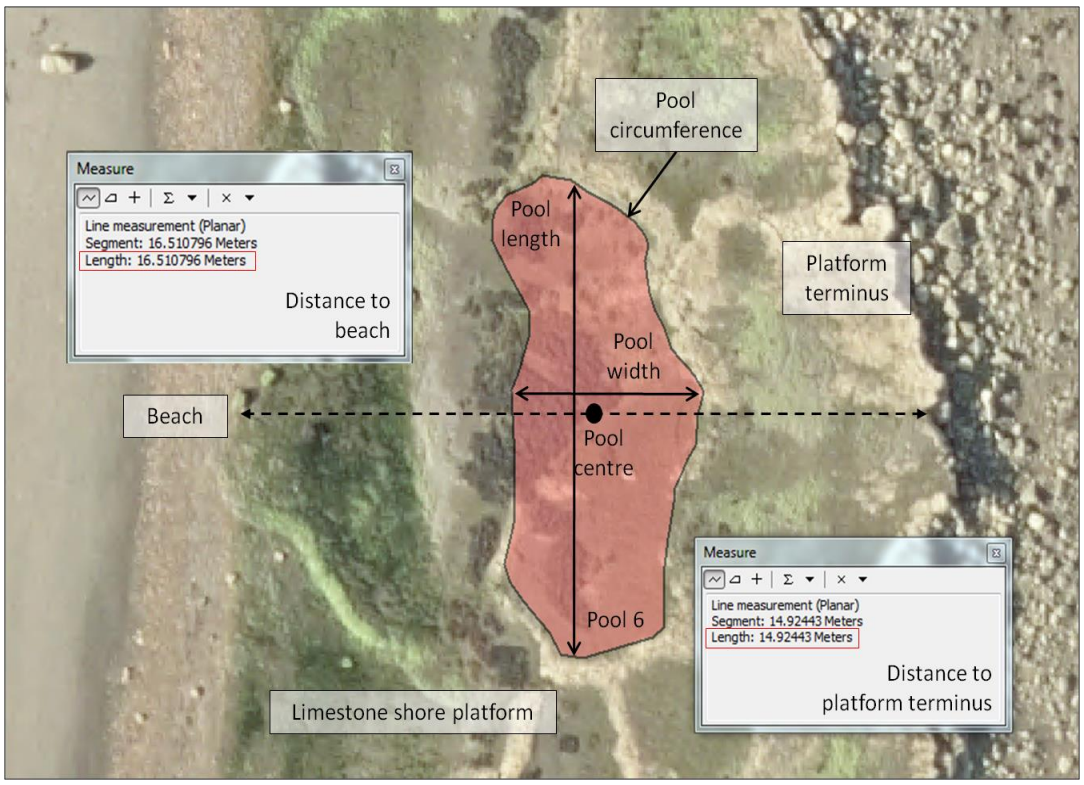

Figure 4.5. Identifies the definition and quantification undertaken to determine pool dimensions and distance values to the beach and platform terminus. Image courtesy of Channel Coastal Observatory (CCO, 2017b).

Results

By means of a qualitative comparison we document a range of morphological features and environmental factors relating to plate-forme à vasques from the tropics, the Mediterranean, the Atlantic coasts of Morocco and Spain and Bembridge. The aim being to establish where similarities and differences exist between landform types (Table 4.1).

Table 4.1. Comparative assessment of pool morphology and local factors associated with plate-forme à vasques from differing geographic locations.

		Plate-forme à vasques (Tropics)	**Plate-forme à vasques (Mediterranean)**	**Plate-forme à vasques (Atlantic coast)^**	**Bembridge pools (Temperate)**	**Recommended reference/s**
Climate	Tropical	✓	X	X	X	Taboroši & Kázmér (2013)
	Mediterranean	X	✓	✓	X	Safriel (1966), El Akhdar *et al*. (1990)
	Temperate	X	X	X	✓	None to date
Ridge / pool morphology	Narrow, sinuous & steep	✓	✓	X	X	Battistini (1981)
	Broad, curved & lobed	X	✓	✓	✓	Trenhaile (1987); Stevčić *et al*. (2017)
	Elongated pool shape parallel and/or perpendicular to shore	✓	✓	✓	✓	Kaye (1959); Focke (1978); Battistini (1981)
Ridge formation	Constructed (e.g. vermetids & calcareous algae)	✓	✓	X	X	De Waele and Furlani (2013)
	Non-constructed (e.g. residual rock)	X	✓	✓	✓	Guilcher (1954); Trenhaile (1987)
Pool size (depth)	≤0.3 m	✓	✓	✓	✓	Guilcher (1953); Kaye (1959)
Pool size (longest axis)	<10 m	✓	✓	✓	✓	Battistini (1980)
	>10 m	✓	✓	✓	✓	Miller and Mason (1994); Battistini (1980 and 1981)
Pool zonation	At waters/platform edge, pools fed by breaking waves	✓	✓	✓	X	Safriel (1966); Focke (1978)
	Distanced from waters/platform edge	X	X	✓	✓	Stevčić *et al*., (2017)
	Lower intertidal	✓*	✓*	X	X	Guilcher (1953)

	Mid intertidal	✓*	✓*	✓	✓	Focke (1978); Dalongeville (1977)
	High intertidal	✓*	✓*	✓	✓	Stevčić *et al*., (2017)
Tidal regime#	Micro (tidal range 0 – 2 m)	✓	✓	X	X	Guilcher (1954); Safriel (1966)
	Meso (tidal range 2 – 4 m)	X	X	✓	✓	El Akhdar *et al*., (1990)
	Macro (tidal range >4 m)	X	X	X	X	Not Applicable
Water flow	Flowing over ridges	✓	✓	X	X	Trenhaile (1987); Taboroši and Kázmér (2013)

* - Whilst zonation of the tropical and Mediterranean pools extends across the entire intertidal zone the reader is reminded that the vertical range of these micro tidal zones (0 - 2 m) is less than those sites located in mesotidal (2 - 4 m) areas.

- Tidal definitions taken from Short, (1991).

^ - Whilst not being located on the Mediterranean Sea the Atlantic coasts of Morocco and Spain are considered to be subject to a Mediterranean climate (Aschmann, 1984).

Information populating Table 4.1 has been drawn from the literature with some detail being obtained from photographic images where accompanying texts fail to adequately describe or quantify the features.

The topographic data derived from the DGNSS field surveys were overlaid on an aerial image (CCO, 2017b) of the site (Figure 4.6) with each numbered pool corresponding with the measurement data presented in Table 4.2.

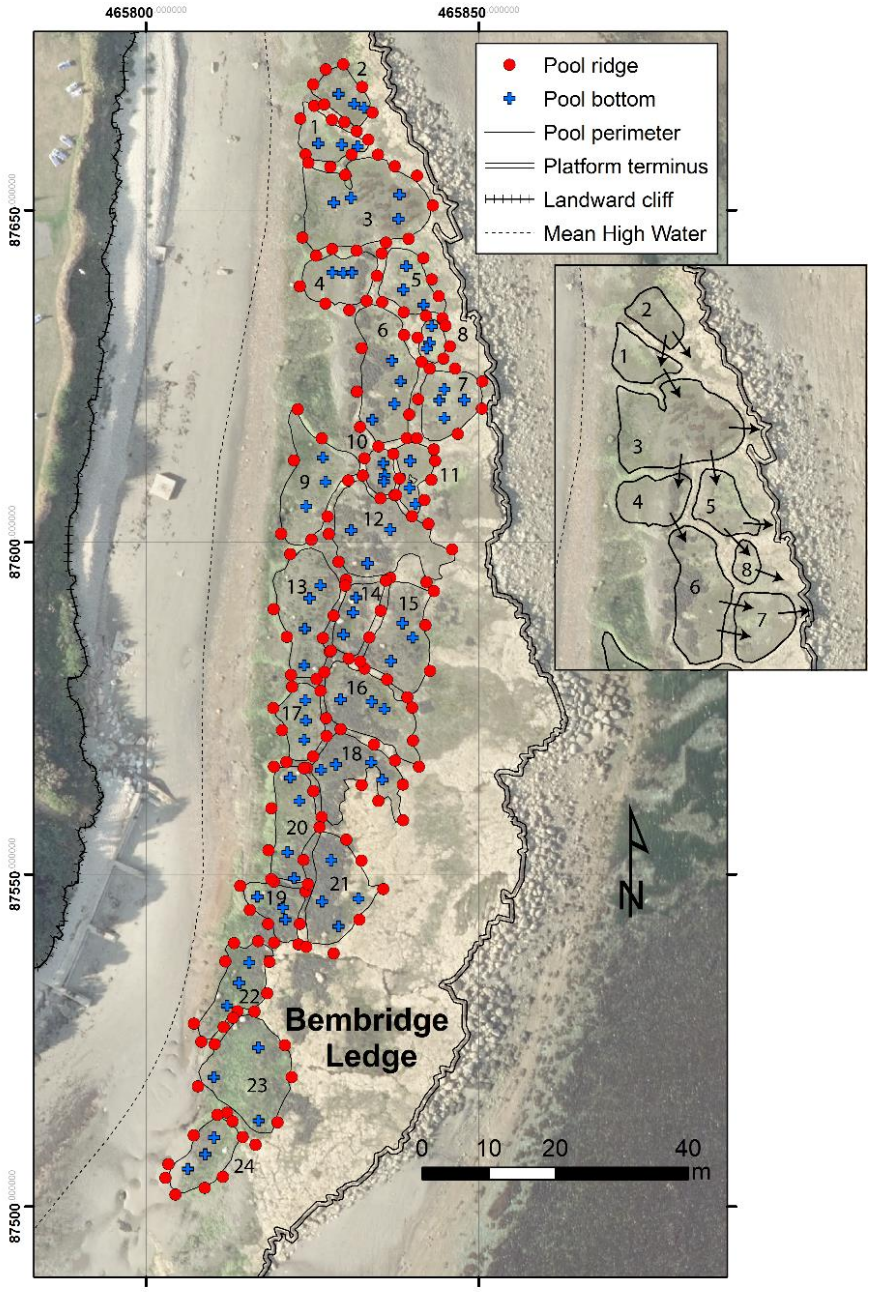

Figure 4.6. Surveyed pool boundaries including topographic data points for pool ridge height and pool bottom; inset, pool water drainage, the arrows indicate the flow of water via ridge breaches between selected pools. Aerial imagery courtesy of Channel Coast Observatory (CCO, 2017b).

Table 4.2. Summary of pool characteristics collated from DGNSS field surveys and aerial imagery. Pool numbers correspond with those displayed in Figure 4.6; (#) pool depth is calculated as the difference between the mean ridge height and the mean pool bottom value; (*) 'distance from' values were established as clarified in Figure 4.5; (+) pool volume is calculated by multiplying the pool area by the mean pool depth, this figure is an estimate as it assumes a uniform pool depth; (^) pool orientation is given as deviation from North, 0°.

Pool no.	Pool length (m)	Pool width (m)	Pool depth (m)#	Ratio (length: width)	Ratio (length: depth)	Distance from platform edge* (m)	Distance from beach* (m)	Pool circumference (m)	Pool area (m^2)	Pool volume+ (m^3)	Length axis orientation ^ (°)
1	11.8	5.9	0.15	2.0 : 1	79 : 1	12.4	7.0	31.1	51.4	7.7	-60
2	9.2	5.4	0.10	1.7 : 1	92 : 1	8.2	8.8	27.0	45.9	4.6	-40
3	19.0	13.0	0.17	1.5 : 1	112 : 1	14.0	11.5	63.7	200.3	34.1	-90
4	11.2	7.5	0.13	1.5 : 1	86 : 1	18.7	8.3	32.9	69.6	9.1	-90
5	12.3	7.8	0.12	1.6 : 1	103 : 1	8.7	18.0	33.0	62.0	7.4	-40
6	20.7	8.8	0.14	2.4 : 1	148 : 1	14.9	16.5	52.0	138.6	19.4	0
7	11.8	9.5	0.13	1.2 : 1	91 : 1	6.7	26.3	32.9	76.5	10.0	+45
8	6.8	4.3	0.07	1.6 : 1	97 : 1	7.4	22.4	17.3	20.6	1.4	0
9	20.2	11.7	0.18	1.7 : 1	112 : 1	27.4	6.5	52.9	120.4	21.7	-20
10	6.9	4.6	0.13	1.5 : 1	53 : 1	17.3	16.3	19.0	25.5	3.3	0
11	11.1	5.6	0.13	2.0 : 1	85 : 1	12.4	21.1	29.4	39.5	5.1	0
12	19.8	13.1	0.21	1.5 : 1	94 : 1	17.5	17.4	60.6	156.2	32.8	-50
13	19.4	9.9	0.18	2.0 : 1	108 : 1	31.9	6.8	49.2	128.9	23.2	0
14	11.9	5.4	0.15	2.2 : 1	79 : 1	24.2	14.1	30.6	55.1	8.3	+30
15	17.0	9.8	0.15	1.7 : 1	113 : 1	19.2	21.0	45.1	110.9	16.6	0
16	19.5	8.8	0.19	2.2 : 1	103 : 1	29.5	18.3	48.6	119.5	22.7	-50
17	11.8	7.0	0.19	1.7 : 1	62 : 1	39.2	8.8	30.9	58.7	11.2	0
18	14.0	13.9	0.18	1.0 : 1	78 : 1	22.9	14.1	63.5	95.6	17.2	+10
19	11.3	6.6	0.20	1.7 : 1	57 : 1	30.0	6.7	30.4	51.4	10.3	-50
20	17.5	6.6	0.22	2.7 : 1	80 : 1	33.1	7.4	44.9	89.5	19.7	0
21	17.0	9.7	0.23	1.8 : 1	74 : 1	26.5	14.2	46.2	117.0	26.9	0
22	17.1	7.0	0.19	2.4 : 1	90 : 1	33.1	3.4	44.2	76.6	14.6	+40
23	18.0	13.8	0.26	1.3 : 1	69 : 1	29.2	7.8	48.6	157.1	40.8	0
24	13.1	6.3	0.15	2.1 : 1	87 : 1	17.0	3.0	33.2	68.2	10.2	+40
Mean	**14.5**	**8.4**	**0.16**	**1.8 : 1**	**90 : 1**	**20.9**	**12.7**	**40.3**	**89.0**	**15.8**	**-14**
Std. dev.	**4.3**	**3.0**	**0.04**	**0.4 : 1**	**21 : 1**	**9.4**	**6.5**	**13.12**	**45.9**	**10.4**	
Coef. of Vari	**30%**	**36%**	**25%**	**23%**	**23%**	**45%**	**51%**	**33%**	**52%**	**66%**	
Minimum	**6.8**	**4.3**	**0.07**	**1.0 : 1**	**53 : 1**	**6.7**	**3.0**	**17.3**	**20.6**	**1.44**	
Maximum	**20.7**	**13.9**	**0.26**	**2.7 : 1**	**148 : 1**	**39.2**	**26.3**	**63.7**	**200.3**	**40.8**	

Variation in pool size is reflected in the axial dimensions with minimum and maximum pool size ranging from 6.8 to 20.7 m in length and 4.3 to 13.9 m in width. The mean pool length : width ratio of 1.8 : 1 suggests the pools are approximately twice as long as they are wide. This corresponds with Figure 4.6 which identifies a general trend towards an elongated pool shape. Pool depth ranges from 0.07 to 0.26 m resulting in a mean pool length : depth ratio of 90 : 1 highlighting the significant difference between the rates of lateral and vertical erosion. Pool area values range from 20.6 m^2 to 200.3 m^2 with smaller pools generally located closer to the platform edge (Figure 4.6). Pool dimension data from Table 4.2 was analysed to identify relationships between key characteristics that may provide insight to pool formation and evolution (Figures 4.7a and 4.7b).

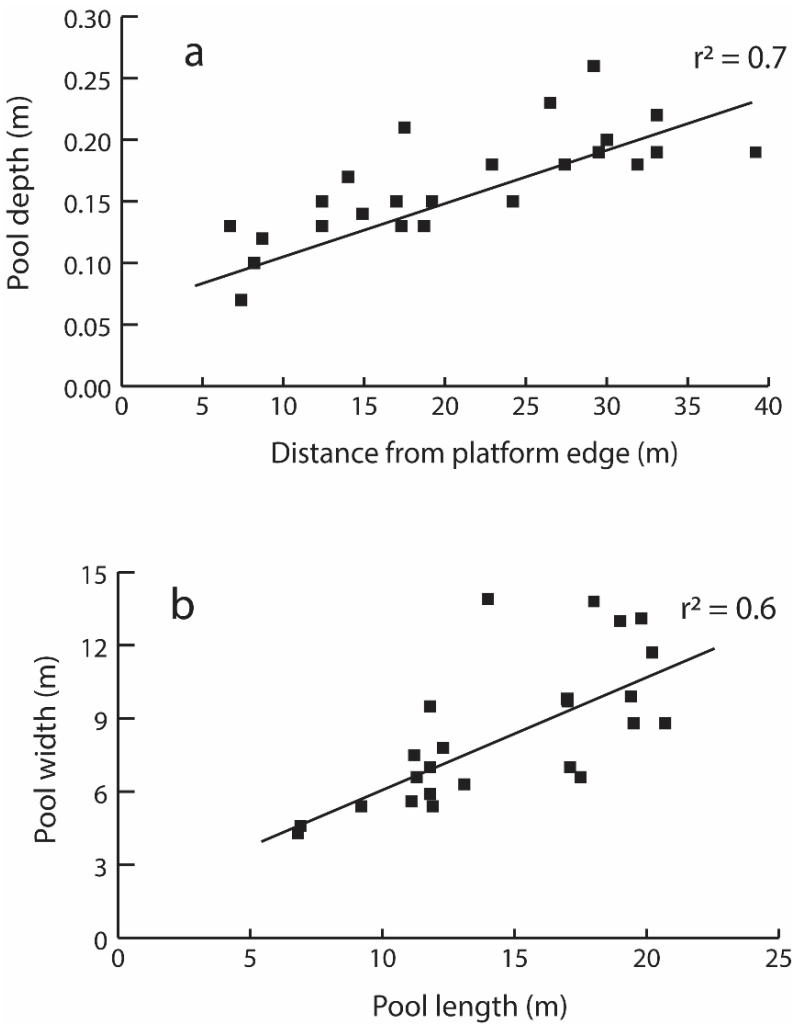

Figure 4.7. Relationship between pool and platform morphology with respective r^2 values. (a) pool depth and distance from the platform edge; (b) pool width and pool length.

The DGNSS data obtained in the field is presented in Surfer (Version 15) to determine the spatial variation in surface topography (Figures 4.8a, b and c). The data identifies spatial variation in platform topography as defined in the contour and profile graphics.

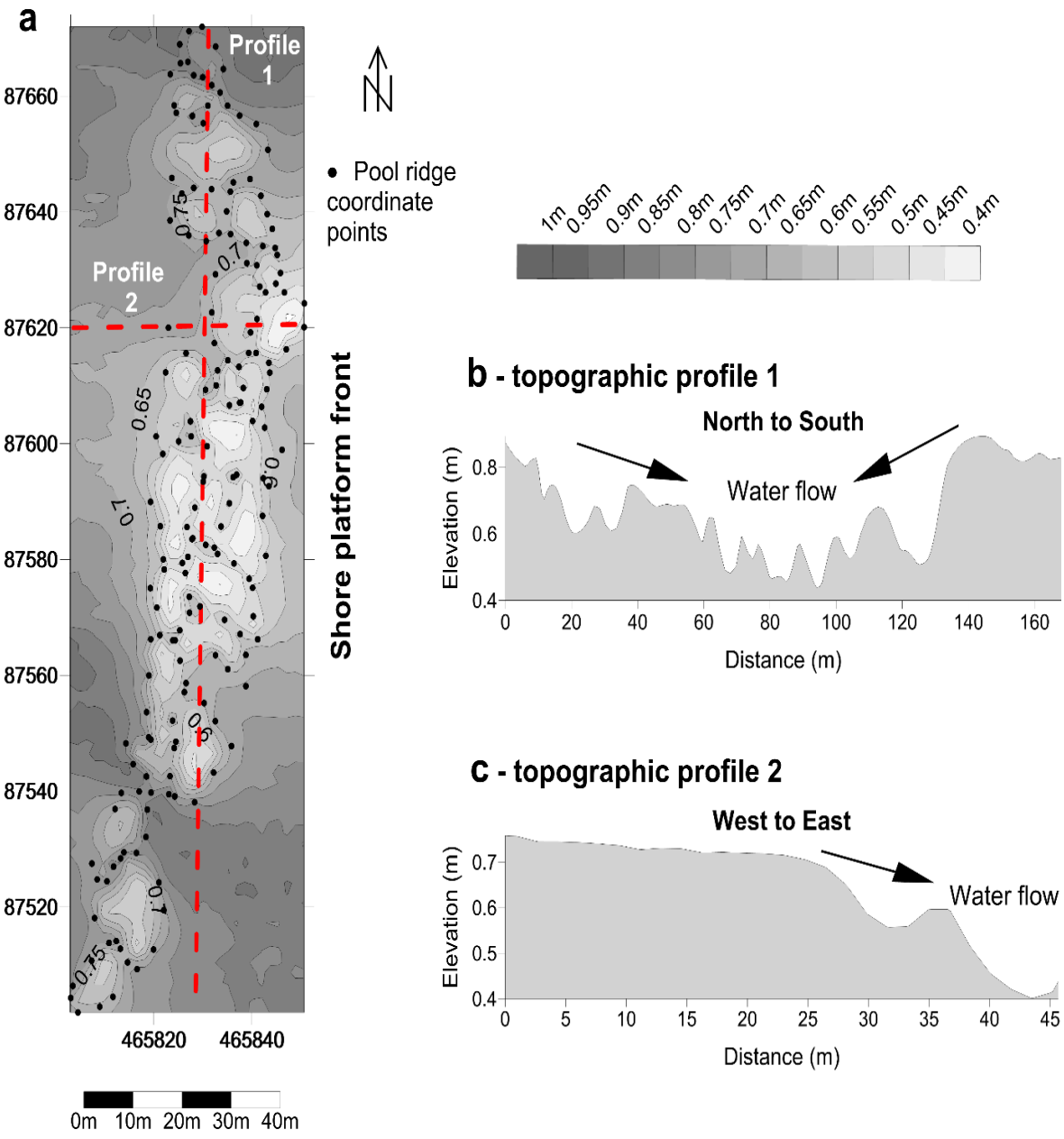

Figure 4.8. Shore platform topography. (a) DGNSS pool coordinate data points presented in Surfer; the black dots signify the pool ridges, contoured intervals are set at 0.05 m increments; (b) topographic profile 1 identifies variation across the pool network, from north to south; (c) topographic profile 2 identifies variation across the pool network, from west to east (platform back to front); water flow direction is indicated by the arrows. Topographic profiles are vertically exaggerated; elevation is based on metres above Ordnance Datum (Newlyn, U.K.).

Discussion

Formative processes

The qualitative comparative assessment (Table 4.1) suggests distinct morphological similarities, most notably, in size and shape, between the Bembridge landforms and previously reported plate-forme à vasques despite being located in different climatic regions. The key differences between pools from differing climatic zones appears to be in the morphology of the pool ridges and the relative pool position on the platform. Pool ridge morphology is determined by the presence/absence of bioconstructing organisms. The bioconstructive process of formation for tropical and some Mediterranean plate-forme à vasques is widely attributed to vermitids which inhabit the intertidal zone in warm temperate and tropical seas (Keen, 1961; Milazzo *et al*., 2015; Breves and Junqueira 2017). This is supported by Safriel (1966) who reports on the limited role of vermetids in the formation of intertidal pools in the more temperate northern and western Mediterranean in contrast to the sub-tropical waters of the eastern Mediterranean (Israel) and along the North African coast where abundant vermetid populations exist. Further evidence is provided by Peres and Picard (1952) who identified vermetids as bioconstructors of the ridges on vasques pools located on the coast of Algeria. Significantly, Guilcher (1954) notes that in the same area plate-forme à vasques are also found with residual rock ridges. This dual process form is also reflected in the vasques pools on the more temperate Atlantic coast of Morocco (Guilcher, 1953; El Akhdar *et al*., 1990). This suggests that the limited spatial distribution of vermetids, which is dictated by water temperature and regional climate, influences ridge formation of plate-forme à vasques. Consequently, this restricts the vermetid contribution to pool formation in cooler temperate zones such as Bembridge. Owing to the fact the Bembridge pool ridges are formed of residual limestone and the absence of vermetids we discount the role of bioconstruction in pool formation. Unlike the tropical and Mediterranean pools algal growth coverage of the Bembridge ridges suggests bioprotection as a key contributing factor in process form development. The shielding effect of the algae on the ridges (Figures 4.3 and 4.9b) conserves the substrate by promoting the retention of sand and reducing the efficiency of the wetting and drying process and the associated thermal oscillations which facilitate substrate removal (Moura *et al*., 2012; Coombes *et al*., 2013; Gowell *et al*., 2015).

The algal layer also acts as a protective barrier against abrasion by mobile sand. This could imply a limited significance with regards to the constructed/non-constructed distinction for these landforms (Trenhaile, 1987). In both cases it is the protective function of the biological activity

(vermetids in the tropics, algal growth at Bembridge) that creates and maintains the ridges between pools which is central to the development of the linked forms. Whether the ridges are the result of bioconstruction or bioprotection is extraneous once established as both sets of ridges have the same functional impact on the pools and their development.

We propose that the location of plate-forme à vasques in the intertidal zone differs geographically as a result of region-specific tidal range. The microtidal regime of both the tropics and Mediterranean restricts the supply of tidal water to a limited vertical range. Therefore, these pools and the ridge-forming vermetids that rely on water flow to survive can only exist in the area that are subject to tidal inundation. Comparatively, in mesotidal areas such as the Atlantic coastline of Morocco and Bembridge the greater tidal range ensures the supply of water extends across a broader vertical range. This results in the pools being distributed over a larger area than in more restrictive mircotidal seas and therefore the pools extend a greater distance from the platform edge.

The occurrence of similar pool features in different climatic settings can be considered an example of equifinality. The concept of equifinality has been widely applied within physical geography (e.g. Bevan and Freer, 2001; Luo *et al*., 2009; Nicholas and Quine, 2010) and seems to be relevant to the features identified in this paper. While the processes that dictate the formation and development of the pools appears to differ between climatic regions the end form presents striking morphological similarities. The differences in the processes that produce these forms, biotic in one climate and abiotic in another, suggest the forms themselves may represent a stable end-point for erosion within the context of these shore platforms. The process of producing the forms is secondary to the relationships between the processes, the characteristics of the rock and the erosional environment which combine to produce an analogous set of forms. The forms are the outcome of a set of relationships rather than being the singular result of a specific set of processes in a particular environment. This is similar to the identification of the relationships between erosion, rock strength and environmental conditions for tafoni formation and development identified by Burridge and Inkpen (2015) in their generalised mathematical model.

Pool and surface morphology

Field observations identified a reduction in ridge prominence between pools at the rear and mid-platform and those located in proximity to the platform terminus (Figures 4.9a and 4.9b). This suggests a greater efficacy of the erosive agents influencing surface morphology at the platform front. We ascribe this to a combination of factors; (1) sediments entrained in breaking waves at the

platform edge abrade the platform surface reducing topographic relief (Blanco-Chao *et al*., 2007; Feal-Pérez and Blanco-Chao, 2013); (2) increased wave exposure at the platform edge inhibits algal growth (Figure 4.9a) which is known to provide a degree of protection against wave action (Pinsky *et al*., 2013; Gowell *et al*., 2015); (3) reduced algal coverage presents an ecological opportunity for intertidal grazing organisms, such as limpets which are known to erode shore platform surfaces through downwearing (Donn and Boardman, 1988; Naylor *et al*., 2012). The impacts of the aforementioned factors diminish towards the rear of the platform reducing the rate at which the ridges erode. The observed pool ridge differences are reflected in the data analysis. A statistically significant distance dependent relationship exists (r^2 = 0.7, *p*-value <0.01, α 0.05) between pool depth, which is a function of ridge height, and the distance from the platform edge. Therefore, the greater the distance from the edge of the platform the deeper the pools are likely to be (Figure 4.7a). In addition, the migratory beach serves both a protective and erosive role. Firstly, in providing protective coverage to the most landward pools during periods of sediment accretion which limits pool exposure to erosion, maintaining ridge features (Figure 4.9b); secondly, by increasing the supply of sand which acts as an abrasive agent to the unprotected pools.

The encircling pool ridges are significant in the development of the individual form and the wider pool network. Water retained in the pools by the receding tide drains from each pool into an adjoining one at a lower elevation. The platform slope gradient (Figure 4.8b and 4.8c) channels pool water flow towards, and eventually over the platform edge (Figure 4.6, inset). At Bembridge, pool drainage occurs by the passage of water via low points in the ridges (breaches); a characteristic shared with plate-forme à vasques which occurs across all climatic zones. Over time the flow of water denudes the ridge, further expanding the breach facilitating increased water flow. Breaches may also arise where small patches of the otherwise algae-covered ridges become exposed to erosion when algal coverage is lost. This provides an opportunity for colonisation by grazing organisms (e.g. limpets) which may downwear the ridge creating a breach enabling pool water drainage (Figure 4.9b (2)). The presence of detached, boulder-sized clasts in the pools proffered the suggestion that they may influence pool morphology (Figures 4.3 and 4.9b). Repeated monitoring of boulder transport across the shore platform indicates that the elevated pool rims impede landward clast mobility (Hastewell *et al*., 2019a; Hastewell *et al*., 2020). However, boulder transport appears to be limited to small incremental episodes of mobility, generally tens of centimetres. Furthermore, we were unable to identify any impact marks on the surrounding pool rims that may have resulted from boulder/pool ridge impacts during transport. This suggests there is little evidence to indicate that the boulders influence pool formation and/or evolution.

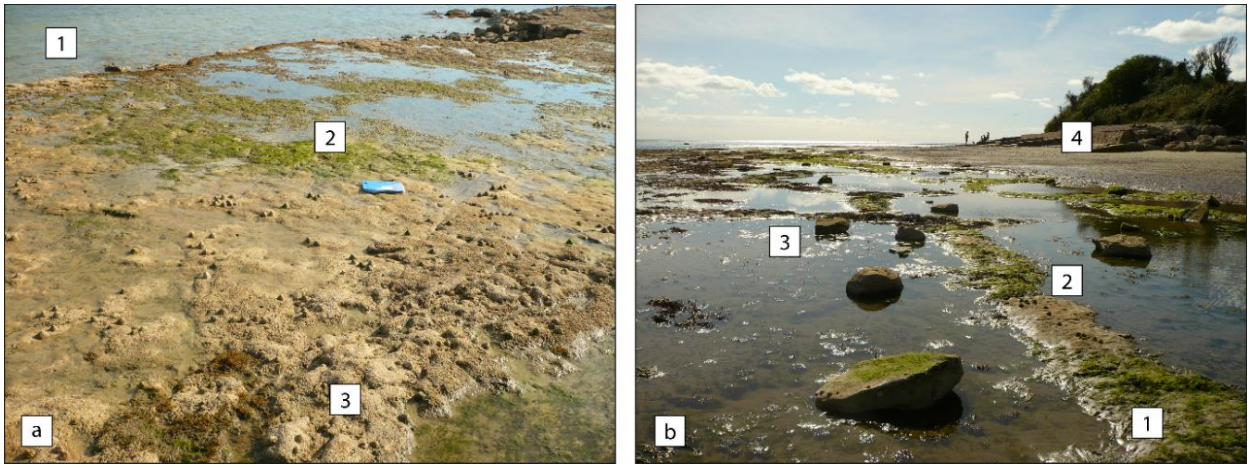

Figure 4.9. Pool features on shore platform. (a) Platform front, file for scale (0.25 x 0.3 m). (1) platform terminus; (2) denuded pool ridges are less pronounced than the lobed ridges found at the rear of the platform, note the lack of algal coverage and the presence of limpets; (3) mid-platform raised rim edge; (b). Rear platform pool features. (1) prominent pool ridge formed of residual rock partially covered in sand and colonised by algal growth (Ulva lactuca, Enteromorpha intestinalis); (2) exposed pool ridge devoid of algae subsequently colonised by limpets; (3) deposition of detached boulders from the platform terminus; (4) migratory beach toe partially covering landward pool ridges.

The functional relationship between ridges and pools signifies the importance of the similarities in water flow between differing climatic regions. The position of the pools within the intertidal range is of less significance to form development than the supply and flow of water between pools. Pool development is governed by the retention of water within the pools and the breaching of ridges. This occurs whether the pools are located at the edge, middle or rear of the shore platform. The essential factor in form development is a supply of water and a slope gradient between pools to enable ridge breaching.

We identify the significance of these factors in defining the wider morphology of the site as highlighted by the aerial imagery (Figure 4.6) and morphometric analysis (Table 4.2). These datasets indicate a dominant pool orientation aligned parallel with the shore platform edge and an elongated pool shape, both morphological features shared with previously reported plate-forme à vasques. Pool orientation, measured along the longest axis of each pool indicates that 75% (18/24) of the pools surveyed are orientated in a northerly direction, 0° (+/- 45°). We attribute pool orientation and shape to the flow of water via ridge breaches. The direction of water flow is governed by the shore platform slope gradient. At Bembridge this is dominant along a north to south bearing and to a lesser extent west to east as depicted in Figures 4.8b and 4.8c. This ensures

water flow occurs towards the middle and the seaward margin of the platform as evidenced by the occurrence of ridge breaches both laterally and seaward across the platform (Figure 4.6, inset). Water is channelled via the breaches along the dominant axis (north/south) with repeated flow progressively widening the breaches allowing for the amalgamation of pools, thus pool size increases in length over width, elongation. This suggests the relationship between length and width is independent of size and reflects a process driven relationship.

Pool coalescence

As alluded to, we ascribe the morphological distinction between pool length and width to the process of coalescence with adjacent pools. Emery (1946) identified coalescence of coastal basins in California, U.S.A. Gómez-Pujol and Fornós (2010) refer to the coalescence of elliptical, adjoining pools creating larger features on the limestone coasts of the Balearic Islands. Similarly, Taboroši and Kázmér (2013) highlight coalescence of what they refer to as pits on a limestone tidal bench in Bali. Whilst these features differ morphologically from plate-forme à vasques, being measured in the tens of centimetres opposed to metres, they each demonstrate the role of coalescence in the evolution of coastal pool landforms.

Field observations identified evidence of pool coalescence in progress at Bembridge. Figure 4.10 identifies pool no. 11 (Figure 4.6) in a transitional stage, an amalgamation of what was previously two individual pools. Originally separated by a pool ridge, the slope gradient between pools, (the higher pool, at right, is elevated 0.06 m above the lower pool) facilitates the flow of retained water from the higher, to the lower elevation. Over time two ridge breaches have been created further enhancing water flow between the now interconnected pools. The progressive widening of these breaches has created an isolated residual rock island, at centre, a vestige of the original ridge.

We suggest coalescence is initiated by the changing topography of the platform whereby the slope gradient directs the flow of water from higher surface elevations at the northern and southern margins of the pool network towards the platform centre (Figure 4.8b). Water flow focused along a central axis on the platform enhances directional erosion resulting in pool elongation and to a lesser extent pool widening. This is supported by the quantitative analysis whereby we have established a statistically significant relationship between pool length and width ($r^2 = 0.6$, *p*-value <0.01, α 0.05) and the mean pool length : width ratio (1.8 : 1), in Table 4.2, which indicates that length increases at approximately double the rate of the width.

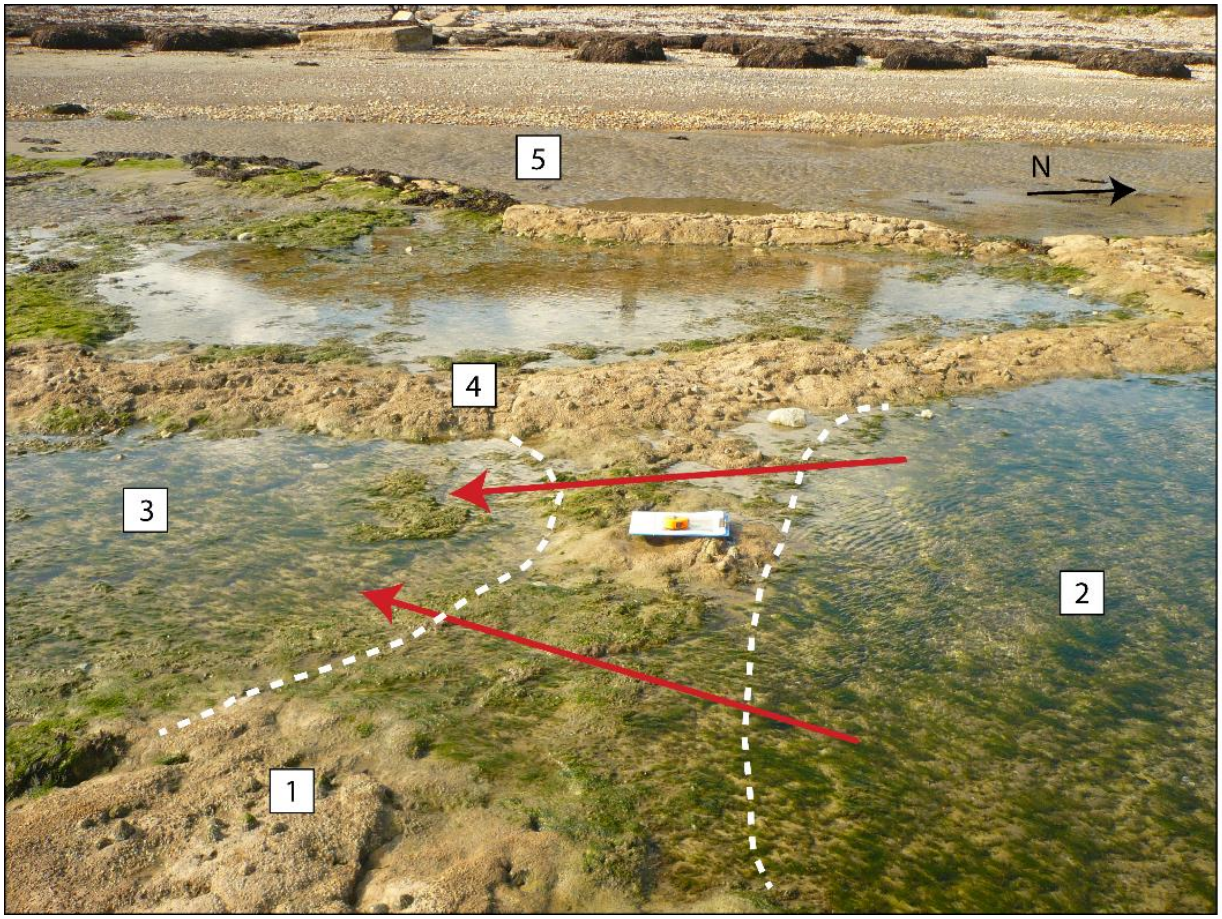

Figure 4.10. Coalescence in progress. (1) the existing pool ridge (2) the upper, elevated pool (3) the lower pool into which water flows between the ridge breaches (arrows) (4) adjacent pool ridge (5) toe of migratory beach. Note the isolated island, at centre, pad for scale: 0.25 x 0.3 m. The dashed lines highlight the suggested original pool ridge.

The frequency of the length : width ratios (Figure 4.11) identifies a positively skewed distribution with a greater number of pools presenting an elongated shape suggesting when initially formed, pool shape is more equally proportioned between length and width. Elongation by coalescence indicates that over time the pools develop in size with pool length increasing over pool width. The process of coalescence would be expected to produce an increase in the frequency of larger length : width ratios particularly for lengthier pools.

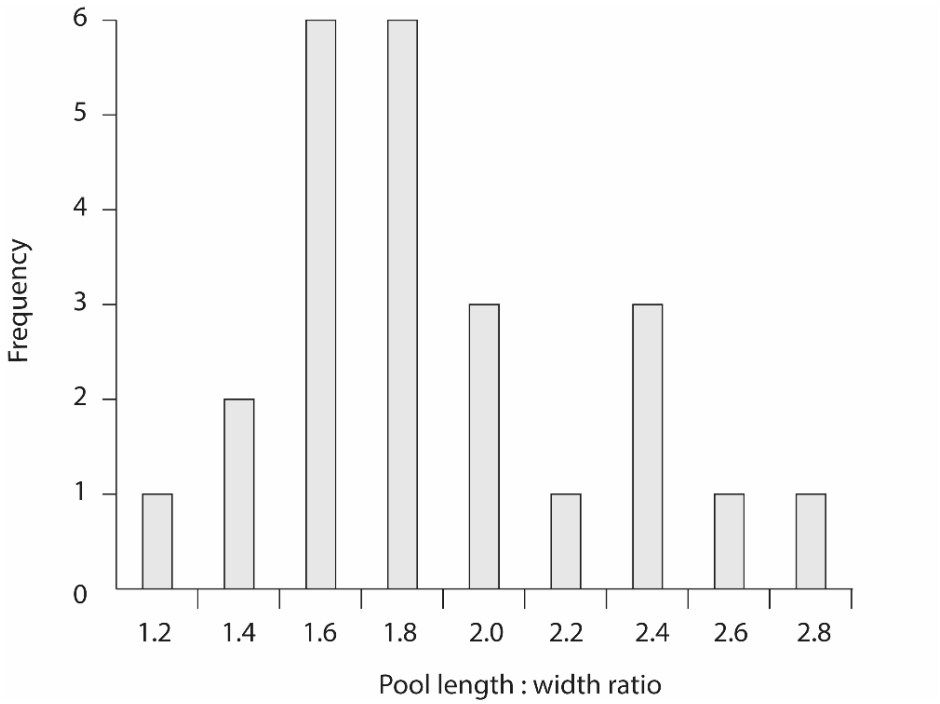

Figure 4.11. Frequency of pool length : width ratio, based on measurements derived from CCO aerial imagery.

Proposed pool evolutionary model

The processes that enable pool development are regulated by landward migration of the shore platform and the adjoining hinterland (Figure 4.12). Currently, the beach and cliff retreat more rapidly than at the platform edge resulting in a widening of the platform. The subsequent exposure of the limestone surface at the beach toe presents the opportunity for pool development. Variations in microtopography on the exhumed platform surface facilitate the pooling of water at low points. This allows for algal colonisation on high points (proto-ridges) providing bioprotection which is not afforded to the submerged concavity (proto-pools).

The pool drainage network develops as a result of the sloping platform terrain. The slope gradient from north to south, south to north ensures water flow along this bearing via ridge breaches once the tide recedes. This repeated process driven by tidal inundation and retreat reinforces the drainage breaches which gradually widen facilitating the process of pool coalescence. New pools develop landward of the original pools as the beach and cliff migrate, hence the landward pool ridges are most prominent as they are most recently formed. Furthermore, they are distanced from the erosive forces as described previously that are magnified towards the platform terminus.

Removal of material by block detachment from the platform terminus facilitates the landward encroachment of the platform edge. The progressive migration of the platform edge towards the most seaward pools brings with it increased exposure to wave influence resulting in greater abrasion and reduced bioprotection. The zonation of algal species migrates landward with the retreating shore platform and the proximity to the associated wave activity at the platform terminus. Thus, algal coverage decreases seaward, reducing the protective function that was previously provided to the pools at the platform front. This leads to the progressive denudation of the ridges so that the mid-platform pools become shallower and the most seaward pools are eventually erased.

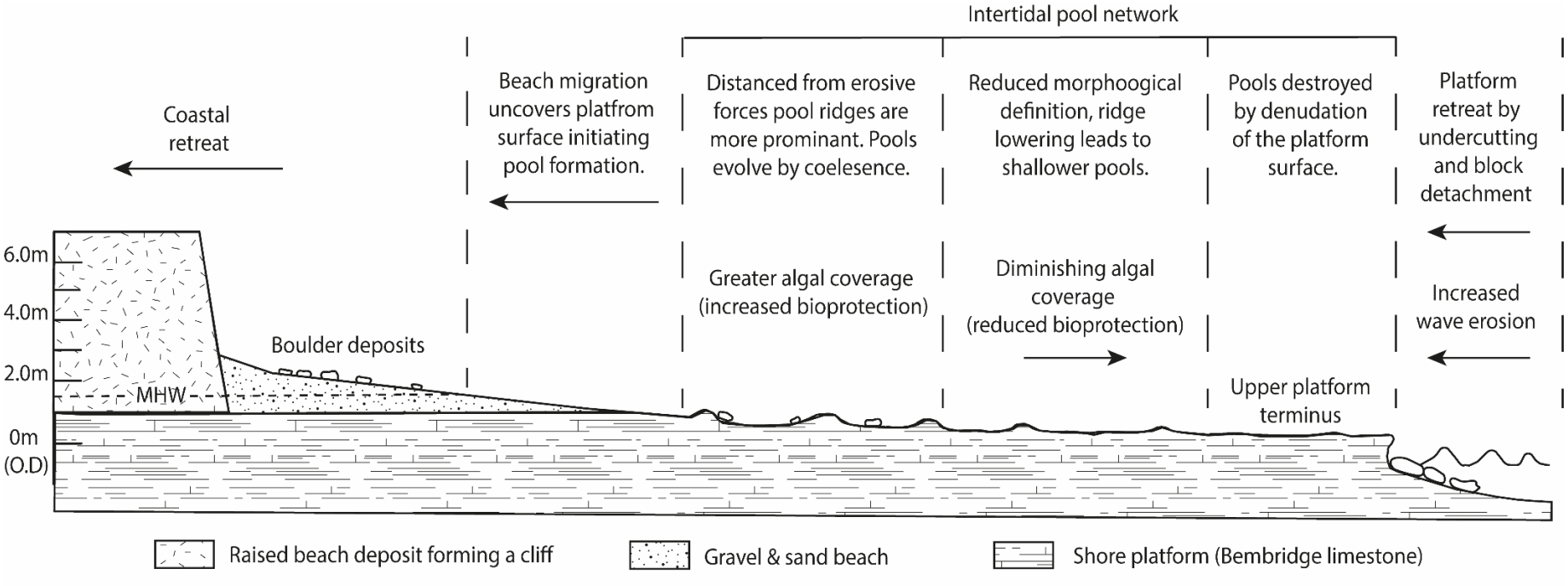

Figure 4.12. Proposed evolutionary model, profile view (not to scale).

Conclusions

We have identified and documented a network of intertidal pools that bear strong morphological similarity with plate-forme à vasques. Previous reporting of such features has been restricted to tropical and Mediterranean climates. Therefore, the discovery of these landforms in temperate waters presents a significant finding and extends the geographical range across which these features are to be found and subsequently researched.

Morphological pool characteristics differ between geographic locations, most notably in the distinction between the roles of bioconstruction and bioprotection in ridge formation which we attribute to climatic variation. Tropical pool ridges of bioconstructive origin are formed by vermetids and calcareous, encrusting algae. The influence of these organisms is limited to warm tropical and Mediterranean waters which provide a favourable habitat for growth. As water temperatures decrease so does the abundance of vermitids (Safriel, 1966) and as such pool ridge morphology alters exhibiting both the constructed and the residual rock form. Given the absence of vermetids and a cooler temperate climate the Bembridge pool ridges are formed of the local limestone and are therefore attributed primarily to bioprotection.

Previous research on plate-forme à vasques has lacked detailed quantitative data acquisition. By adopting a more empirical approach our data presents new insights to the processes that govern the morphology and evolution of these intertidal pools. Our findings indicate that Bembridge pool morphology is hydrodynamically controlled by the flow of water between adjoined pools. As with previously identified plate-forme à vasques, on the receding tide the Bembridge pools drain via low points in the ridges (breaches). The flow of water is predetermined by the slope gradient of the shore platform. The dominant slope angle directs water via the breaches from the northern and southern margins to the centre of the pool network. Continued water flow along this bearing erodes the ridges between adjoining pools eventually leading to coalescence which produces the characteristically elongated pool shape. In quantifying platform topography we assert its significance in shaping the pools, both individually and from a wider geomorphological context.

The proposed evolutionary model highlights the significance of the rate of landward retreat for both the cliff and beach and the shore platform edge. The current steady state of equilibrium between the two facilitates the development of the ridges and the pool network. Therefore, maintaining the pools and the valuable intertidal habitat they provide is reliant on recession rates of the beach and cliff exceeding that of the platform edge. Any alteration, in terms of coastal

defence that interferes with the rates of recession could jeopardise the continued development of the pool network leading to loss of habitat and the species that are reliant upon them.

We suggest future studies of similar sites where intertidal pools are found consider the acquisition of topographic survey data and calculation of quantitative descriptors. This will allow for inter-comparison across a range of different climatic coastal zones which will facilitate an increased understanding of how the wider site geomorphology affects intra-site morphology allowing for additional evolutionary landform models to be proposed.

References

See Bibliography, page 268.

Chapter 5 - Additional findings and future research

This chapter presents additional findings, both empirical and theoretical, that were established during the course of this research study. The findings reported were deemed to be exploratory in nature and therefore were not included in the submitted manuscripts. However, despite additional research being required to develop the work further, the preliminary findings have been instrumental in formulating an increased understanding of the key processes that facilitate boulder production, transport and deposition and subsequent landform modification. This has helped develop the thesis as well as inform, and improve the submitted manuscripts. It was therefore deemed relevant and worthy of inclusion within the thesis submission. Each of the sub-headings below are addressed within this chapter and relate to specific phases in the transport process as indicated:

- Geophysical assessment - Ground Penetrating Radar (*Boulder production*)
- Hydrodynamic factors enabling boulder transport (*Boulder transport*)
- Broader-scale geomorphic change (*Boulder transport and deposition*)
- A proposed conceptual model for the production, transport and deposition of intertidal boulders (*Boulder production, transport and deposition*)

Additionally, during the course of this study a number of opportunities arose to forge collaborative partnerships with fellow coastal researchers. This resulted in further RFID tagged boulder deployments at a number of alternative coastal locations subjected to varying degrees of hydrodynamic activity. Successful deployments at these additional sites will further inform on the capabilities of contemporary storm waves to displace coastal boulders. Detail of the existing work undertaken with these research partners is presented within this chapter.

Geophysical assessment - Ground Penetrating Radar (GPR)

An insight to the boulder production phase at Bembridge was obtained from a geophysical assessment of the shore platform at Black Rock; this was undertaken using Ground Penetrating Radar (GPR). The generated data and subsequent interpretation provided a significant insight to the process that facilitates boulder detachment at the site. Additionally, the findings suggest the presence of a landform feature, in the form of a network of cavities beneath the shore platform, which may not have been previously described.

The rationale for deploying a Ground Penetrating Radar (GPR) was based on field observations made at Black Rock which suggested the presence of air pockets beneath the shore platform. During a field visit, bubbles were seen emanating from small cracks (2 - 5 cm in length) located approximately 10 m from the shore platform edge, this area is highlighted by a black star in Figure 5.3. The bubbles appeared 2 - 3 seconds after waves broke at the platform terminus. It was hypothesised that the breaking waves were forcing water in to a cavity beneath the platform surface. As the water entered the cavity, air was expelled via the surface cracks.

The potential discovery of cavities beneath the shore platform was considered significant with regards to the detachment process at the Black Rock site. It suggested the extent to which the platform edge was undermined, a primary mechanism in detachment at the site, may have been greater than originally realised. This also presented an alternative detachment mechanism to that of undermining along existing geological discontinuities as is the case at Bembridge Ledge. This detail was used to differentiate the two schematic diagrams of detachment, transport and deposition at the two Bembridge sites (Figures 3.8 and 3.9).

In order to confirm initial suspicions of a subsurface cavity feature it was necessary to conduct a preliminary assessment of the seaward edge of the platform. However, this was problematic given that access was restricted to low water during spring tides. A subsequent field survey was arranged when tidal conditions were suitable to grant safe access to the seaward edge of the platform.

Upon observing the seaward platform edge it was evident that such a cavity existed; a number of other features were noted as illustrated in Figure 5.1. An abraded notch had been worn into the limestone walls of the cavity. The presence of rounded gravels suggested notch development may have been accelerated through a process of attrition. Using a laser measurement device it was possible to determine the depth of the cavity. The laser was pointed into the void and focused on the most landward rock wall, identified by the white circle; at centre of Figure 5.1, the distance was recorded as 13.1 m. This initial assessment of the cavity and its distance to/from the point at which the surface bubbles were observed suggested the presence of further cavities beneath the platform surface.

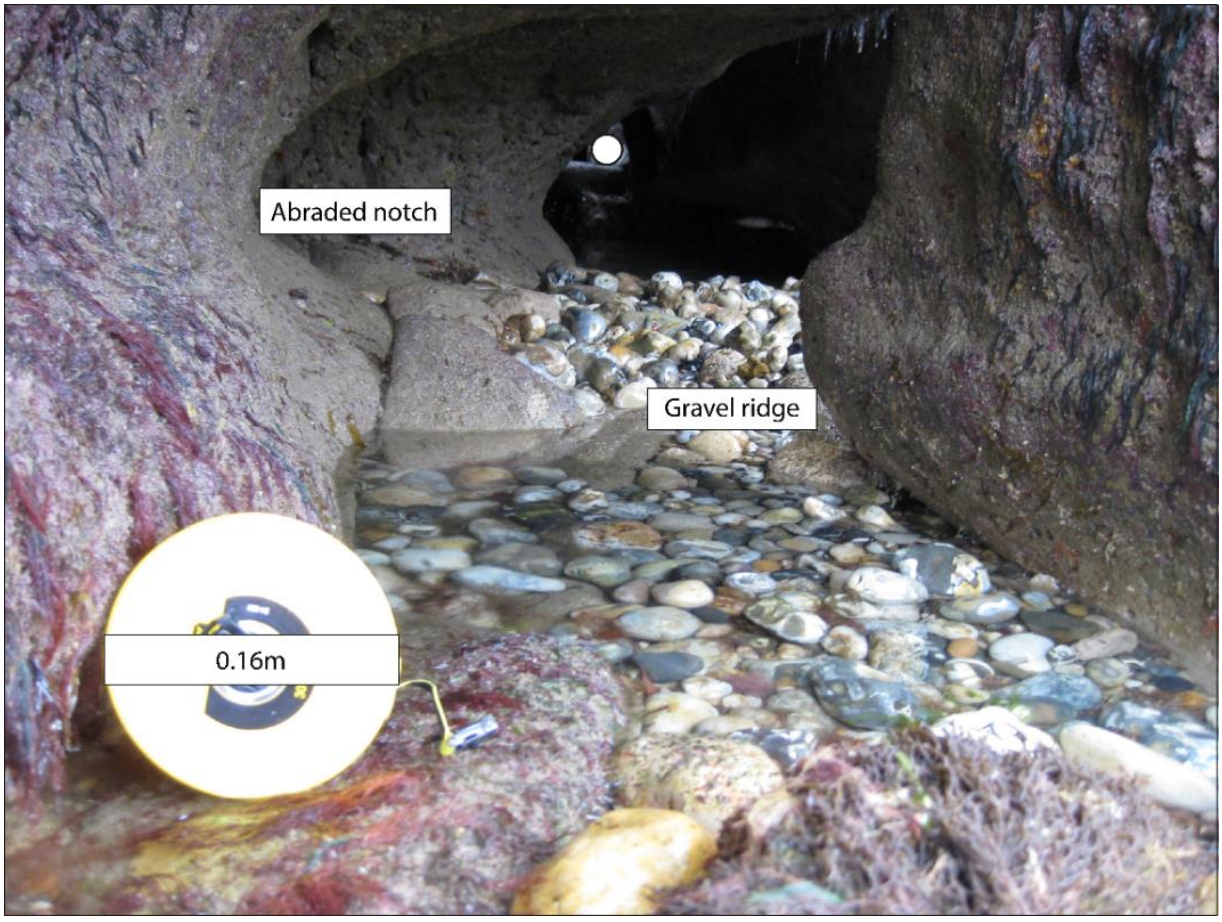

Figure 5.1. View from the platform edge looking into a subsurface cavity, (this viewpoint is highlighted in Figure 5.3). Note the heavily abraded walls and rounded gravels. The raised gravel ridge in the centre of the image can be seen on the GPR profile in Figure 5.4.

Further to observing the subsurface cavities, a geophysical assessment was considered using GPR. The intention was to establish the extent to which the subterranean cavity network extended with a view to improving insight to the boulder production process at Black Rock. The GPR technique is used as a non-invasive method for recording subsurface features and changes in subsurface materials. The principle involves the emission of an electromagnetic (EM) signal in the form of a radar wave transmitted from an antenna. The signal penetrates the underlying ground and is reflected by changes in material dielectric constants; this being a materials ability to store electrical energy when an electric field is emitted (Jeffery *et al*., 2020). This reflected energy can arise from differing subsurface lithologies, (e.g. changes in sediment size or facies), mineralogy, rock density and water content (Jol *et al*., 1996).

The technique has been used in coastal environments to document the internal structure of beach ridges (Clemmensen and Nielsen, 2010; Tamura, 2012; Hesp 2013), paleo shorelines (Mauz *et al*.,

2013) and to quantify sedimentary deposition, beach thickness and volume (Gunn *et al*., 2006; Hampson *et al.,* 2008; Dickson *et al*., 2009). Despite these previous coastal applications, use of the technology directly on shore platforms is believed to be limited to a single study. Calder and Kennedy (2013) used GPR to determine shore platform surface morphology lying beneath a mixed sediment cover using a 250 MHz antenna. The scant use of GPR on intertidal rocky substrates may be due to a limitation of the technology which relates to signal interference from the GPR when encountering saline water. The high conductivity of the salt water attenuates all propagating radar waves interfering with the signal preventing effective data acquisition.

Notwithstanding the known operational limitations, a field survey was undertaken to gather subsurface data from the shore platform at Black Rock. The survey was conducted using a Mala ProEx system with a 500 MHz shielded antenna (Figure 5.2). This was pulled across the shore platform along a series of transect lines, with positional data being collected using a Topcon Hiper V in Real-time Kinematic (RTK) mode. The collected GPR data was post-processed using Mala Groundvision software.

Figure 5.2. Mala GPR ProEx system with shielded 500 MHz antenna.

The GPR survey area covered approximately 40 x 30 m of the Black Rock shore platform. The survey was conducted during low water to limit the amount of salt water present on the platform surface and within the suspected cavity network beneath. GPR data was amassed from 24 transect lines. The transects were intended to be of equidistant spacing running parallel and perpendicular to the shoreline. However, in order to avoid small surface depressions filled with salt water and large clumps of damp algal growth it was necessary to deviate from the planned survey lines (Figure 5.3).

Two transect lines have been selected to provide insight to the subterranean cavity features. Line 1, appears as the red vertical transect in Figure 5.3. This corresponds with the cavity pictured in Figure 5.1. This transect served as a valuable means of ground-truthing the collected data as the depth of the cavity, as highlighted in the GPR profile (Figure 5.4) was comparable with the distance value recorded with the laser measuring device, 13.1 m.

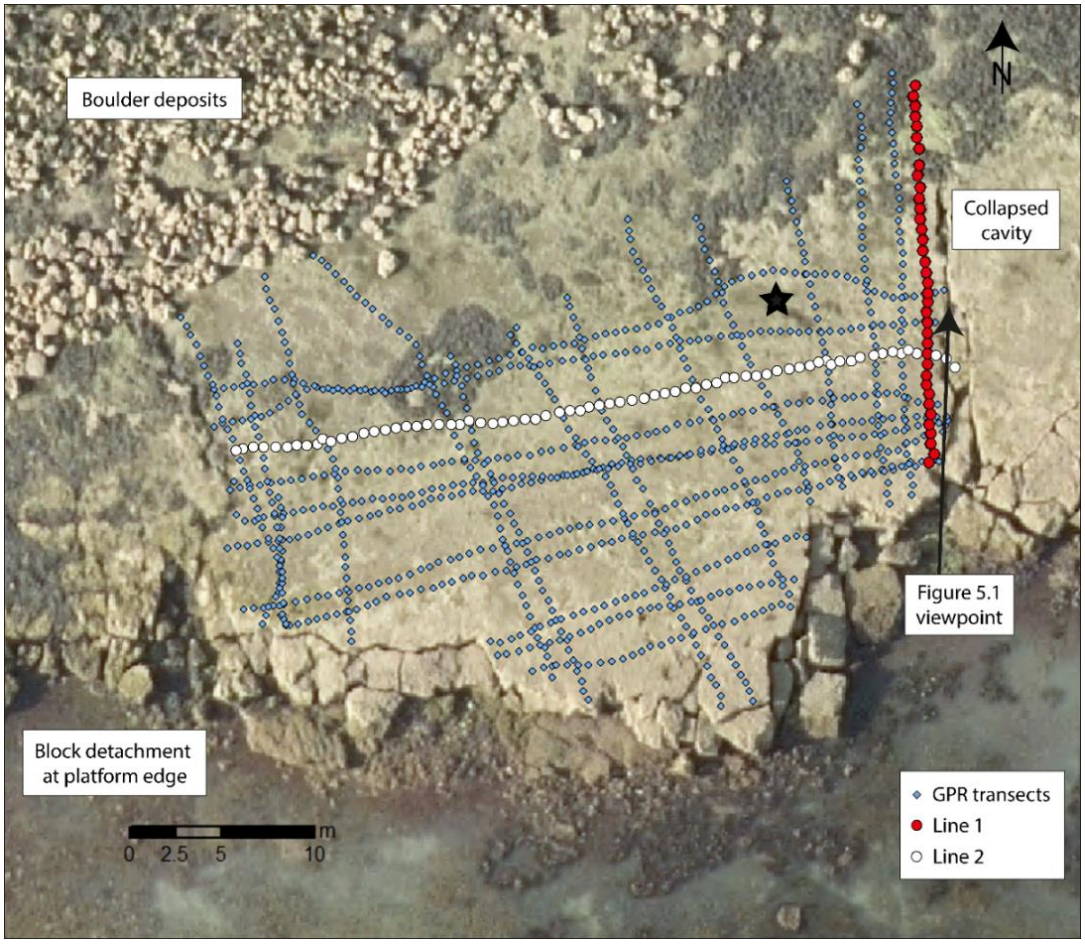

Figure 5.3. Aerial image of the GPR survey area. GPR transect lines (blue); Line 1 (red) transect line refers to the cavity depicted in Figure 5.1 and the GPR profile in Figure 5.4; Line 2 (white) transect line refers to the GPR profile in Figure 5.5. The black star identifies the area that surface bubbles were initially observed. Aerial image courtesy of the Channel Coast Observatory (CCO).

The gravel ridge identifiable in Figure 5.1 is also evident in the GPR profile (Figure 5.4). Notably, the distance from the cavity opening to the gravel ridge corresponded with the hand-measured value. Finally, the width of the limestone unit at the platform edge also matched the hand-measured value. The GPR profiles display a strong signal as it passes through the consolidated limestone unit of the upper platform (Figures 5.4 and 5.5). This is evident from the clearly defined signal return in the upper 1.0 m of the profile images. As the EM signal passes towards the low water mark, signal attenuation deteriorates preventing further data acquisition. The black area in Figure 5.4 matches the void space within the observed cavity (Figure 5.1). Being able to link the GPR data to recorded field observations was invaluable when interpreting the remaining profiles. Where similar void-like spaces were identified from GPR profiles, they were interpreted as subterranean cavities, (e.g. Figure 5.5).

The preliminary GPR data indicates that a network of subterranean cavities are present beneath the Black Rock shore platform. Those cavities that are accessible from the platform front appear to be eroded by continued wave abrasion and attrition by gravels acting as tools. It may not be possible for gravels to be transported into the more landward cavities as the level of interconnectivity between cavities is, as yet uncharted. Therefore, whether they are eroded in the same manner is currently unknown.

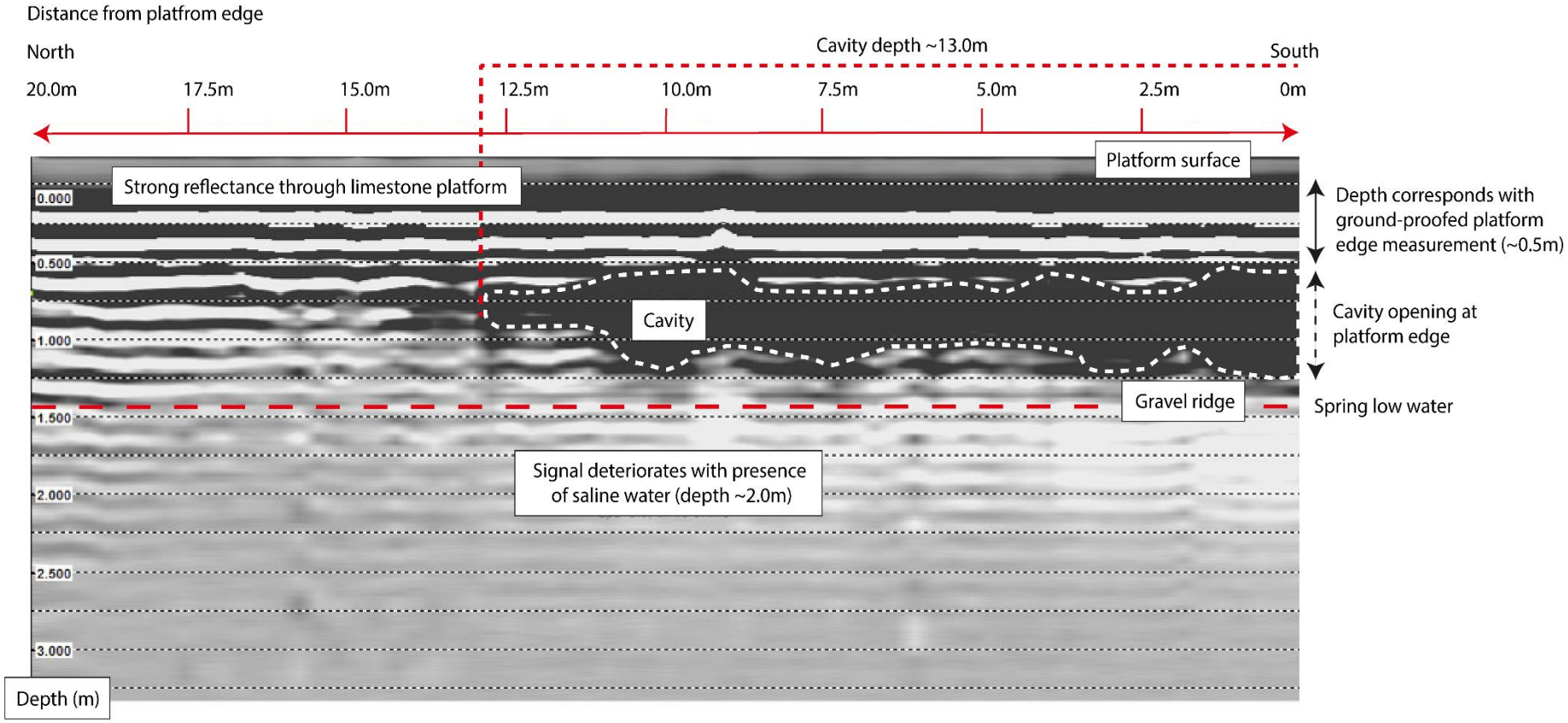

Figure 5.4. Annotated GPR profile, Line 1.

Line 2, (Figure 5.3) is highlighted as the white horizontal transect. Despite the distance from the platform edge (between 10 - 20 m), the corresponding GPR profile (Figure 5.5) identifies a series of black void spaces identical to those confirmed as void spaces from profile line 1. We interpret these as cavities beneath the shore platform, the cavities being supported, and possibly separated from each other by what are assumed to be limestone pillars.

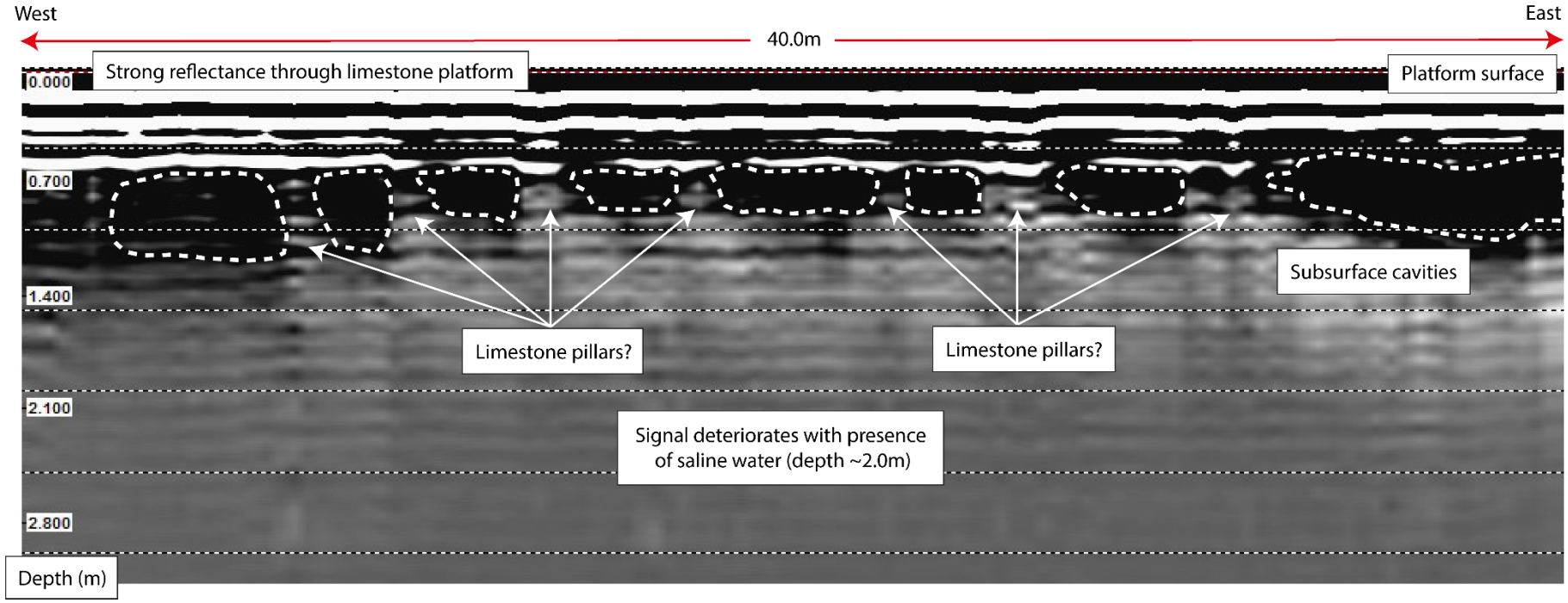

Figure 5.5. Annotated GPR profile, Line 2.

The significance of the cavity network in the boulder detachment process should not be underestimated. The GPR profile (Figure 5.4) indicates that the platform edge is approximately 0.5 m thick at this location and the lithological unit is known to have few geological discontinuities. Undermining of the substrate is known to occur, as evidenced by the eroding tidal notch, and the subsurface cavities described herein. The lack of jointing means that when undermining occurs, cracks form in the substrate of the overburden which propagate and ultimately lead to the fracture of the bedrock (Herterich *et al*., 2018) producing detached blocks at the front of the platform. This is in contrast to detachment along pre-existing joints as occurs at Bembridge Ledge. Thus, the fractures form the initial stage in the boulder life-cycle, that of production. Evidence of these fractures are found across the shore platform surface at Black Rock with some extending up to 15 m inland (Figure 5.6). The landward extent of the surface fractures can result in the undermining of multiple blocks as evidenced by the collapse of subsurface cavities highlighted in Figures 5.3 and 5.6.

This observation coupled with the GPR profile data suggests the cavity network may extend, in places, up to 15 - 20 m landward of the platform edge. Considering Figures 5.3 and 5.6 are located approximately 250 m from each other the area across which the subterranean cavity network extends may be considerable.

The discovery of the subterranean cavities warrants further field investigation as the evidence suggests they play a significant role in controlling the boulder production process at Black Rock. It is proposed that a repeat GPR survey be conducted on the same limited area when the tidal state is higher, ensuring that the cavities are filled with seawater. It is anticipated that the operational restrictions of the GPR technology, (signal attenuation in salt water) will prove beneficial in confirming the presence and position of the void spaces. The small-scale survey area was deemed suitable for an exploratory assessment of the underlying platform structure but the limited spatial coverage was insufficient for inclusion in the published manuscripts. Future publication of the cavity network will require a more extensive GPR survey. Where surface terrain permits, the GPR survey will be extended to provide wider platform coverage. The acquired GPR profiles will then be post-processed and combined with the accompanying positional data to create fence diagrams providing a greater spatial awareness of the degree to which the cavity network extends beneath the platform.

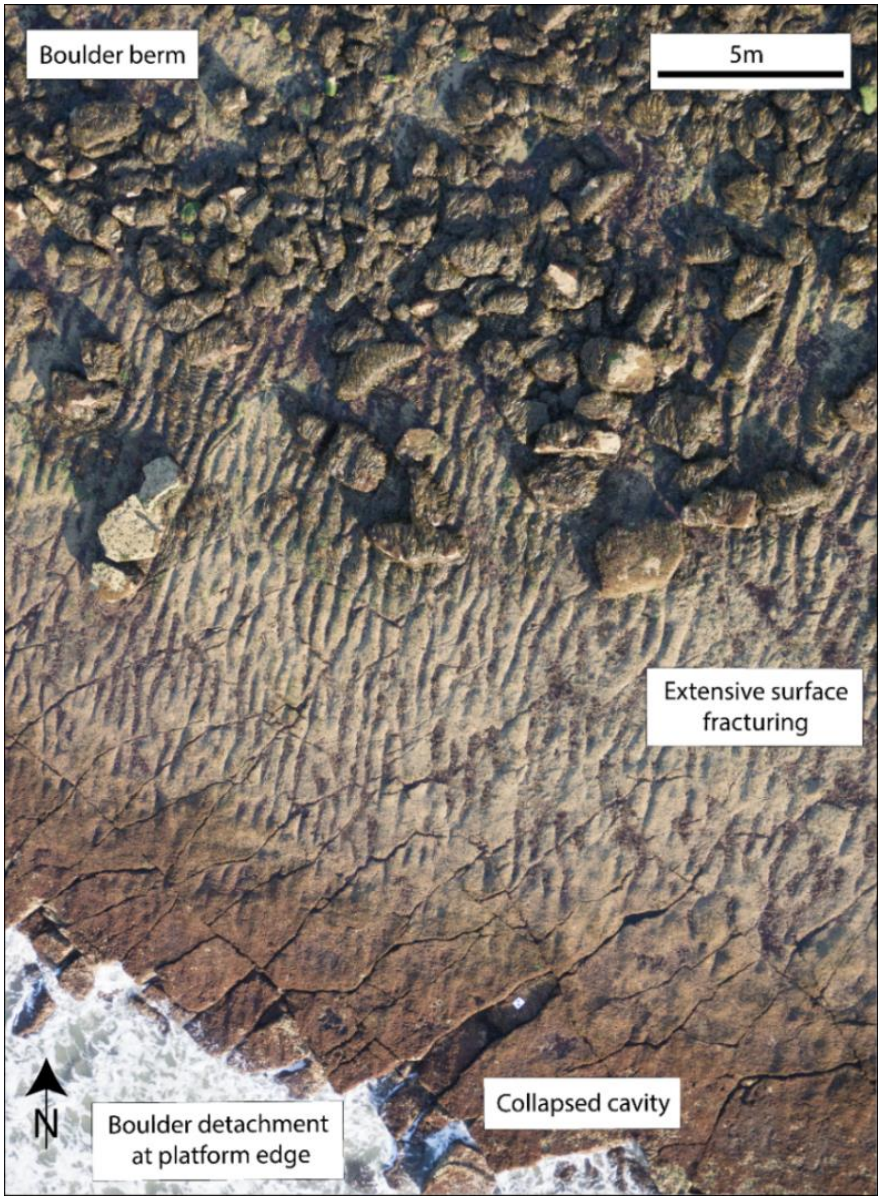

Figure 5.6. Shore platform surface at Black Rock. The landward extent of the surface fractures suggests the undermining of the bedrock strata extends some distance landward of the platform terminus. Image captured using a DroneX X8-M UAV.

The GPR data has provided a valuable insight to further developing and enhancing our existing understanding of shore platform processes at Bembridge and potentially other coastal locations. The unique capability of the GPR has proffered detail on shore platform features that have hitherto been unexplored and unexplained. The findings have been used to draw awareness to an alternate boulder production process; one where the lack of geological discontinuities results in fracturing of the overlying bedrock. The processes and mechanisms addressed in the preceding chapters focus on the resulting morphological alterations occurring at the platform terminus (production) and on the shore platform surface (transport and deposition). However, by documenting the subsurface

morphology of the shore platform and identifying its wider role in the boulder transport process, (boulder production) a more thorough understanding of the detachment mechanisms at the site has been obtained. It also identifies large-scale platform morphology as a controlling factor in a wider evolutionary context. Additionally, by using the GPR we have identified a subsurface shore platform feature that is yet to be recognised within the boulder transport literature and perhaps even the wider coastal geomorphological literature.

Hydrodynamic factors enabling boulder transport

A hydrodynamic experiment is proposed to test a hypothesis relating specifically to boulder transport. The use of hydrodynamic equations to estimate wave heights required to move boulders of a known size are widespread in the boulder transport literature. The equations of Nandasena *et al*. (2011b) are applied in Chapter 3, table 3.9 with wave heights calculated for the three largest tagged boulders. However, whilst the equations are often used as a means of distinguishing between transport mechanisms (storm of tsunami), their effectiveness and accuracy has been questioned (Hastewell *et al*., 2020; Cox *et al*., 2020). In the case of this study, the calculated wave heights required to displace the three tagged boulders considerably exceeds the known wave conditions. This implies that there are other factors involved in the transport process that the equations are unable to accurately represent. Field observations suggests this may relate to platform topography. By using a wave flume with a replica shore platform which can be modified to reflect undulations in the platform terrain an improved awareness of differing boulder transport processes can be established.

The findings presented in Chapters 2 and 3 demonstrate that sizeable boulders are frequently mobilised under moderate storm conditions. The use of numerical modelling as presented in Chapter 3 suggests that the equations proposed by Nandasena (2011b) overestimate the wave height required to initiate boulder displacement when compared with the CCO recorded wave values. Percentage differences between the calculated wave heights (Chapter 3, Table 3.9), and the highest inshore H_s value recorded during the study (Chapter 3, Table 3.7) ranged from 65% to 118%. This suggests failings in the equations that need to be addressed in order to improve our understanding of the mechanisms by which boulders are displaced under moderate storm conditions. The disparity between the calculated and recorded wave heights requires further explanation as discussed in Chapter 3, page 112.

With a view to developing and improved understanding of the discrepancy between the recorded and calculated wave values a controlled experimental study is to be conducted using a wave tank

with a constructed 3 m shore platform model (Figure 5.7). Replica boulders formed of Bembridge Limestone will be placed in the flume channel and subjected to repeated water flow. Similar experimental models have been conducted by Nandasena and Tanaka (2013a & 2013b) and Imamura *et al*. (2008) who used wave flumes of a comparable size to model boulder transport by tsunami waves. Similarly, Hansom *et al*. (2008) and Watanabe *et al*. (2019) modelled displacement of supra-tidal cliff deposits using a wave tank.

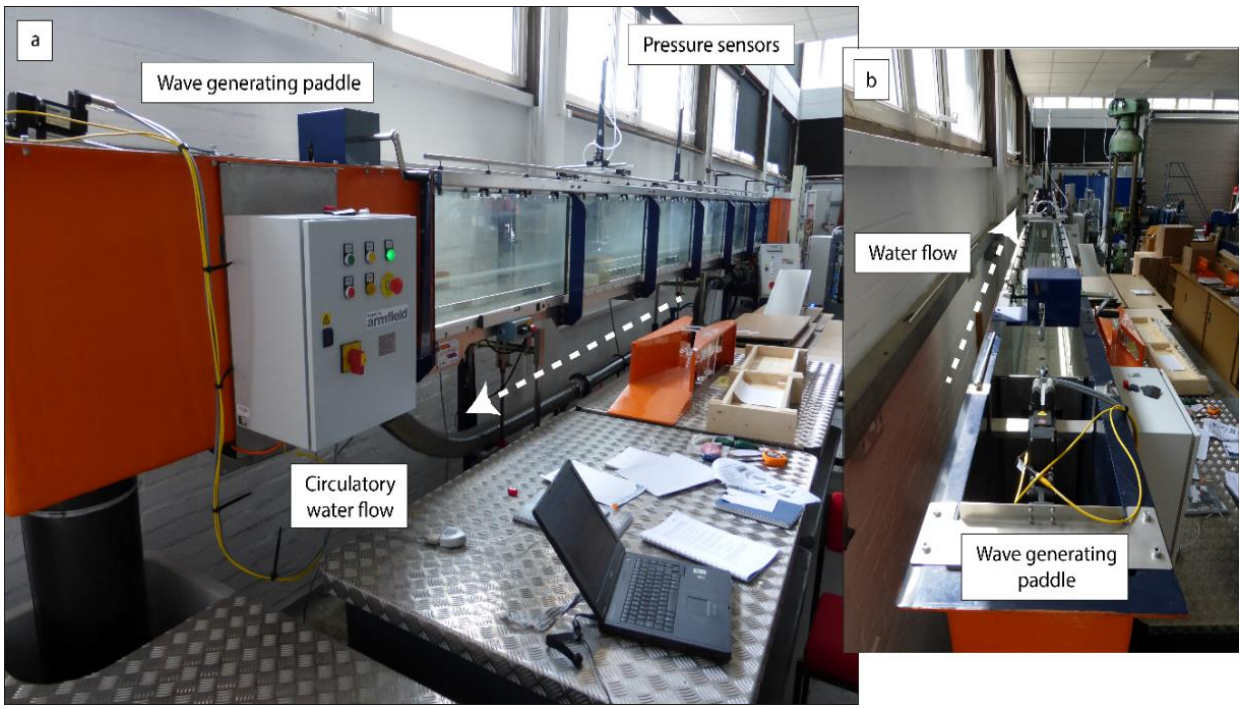

Figure 5.7. (a) Annotated image of the Armfield S6 MKII flume; (b) view along the flume channel.

The constructed shore platform surface has been covered in plasticine allowing for topographic features to be incorporated. The significance of these features on the processes of transport and deposition can then be modelled experimentally. Key topographic features will include vasques-like intertidal pools as described in detail in Chapter 4 and planar morphological features, as found at the Black Rock research site.

These features are located where the shore platform adopts a sub-horizontal slope angle (-1°) a series of parallel overflow runnels are carved into the platform surface, perpendicular to the platform edge (Figure 5.8). Similar bedform runnels have been identified in the chalk platforms of the south east coast of the U.K. (Dornbusch *et al*., 2008). The runnels deepen to landward as a result of tidal overflow across the negative slope angle. As the tide rises, waves break against the platform edge and water is channelled downslope. The overflow increases with the flood tide until the

features are fully submerged. Over time, continued flow has abraded the runnels which can reach a depth of 0.2 m. The development of the runnel network can be exacerbated by sediment laden water flow leading to increased incision (Moses and Robinson, 2011; Fagherazzi and Mariotti, 2012). However, the role of these features in the wider context of platform evolution is unknown (Moses, 2014).

Using the RFID transport data and via field observations we suggest these runnel bedforms play a role in the boulder transport process which may in part explain how moderate storm waves are capable of displacing sizeable boulders thought to be beyond the known wave competence of the study site. It is reported that surface roughness impedes boulder displacement (Weiss, 2012; Hastewell *et al*., 2020), however, we hypothesis that roughness, in the form of the ridges and runnels may also promote transport.

The runnels at Black Rock are present on a small area of the platform (approximately 0.003 km^2). Within this area the largest coarse boulders are detached, transported and deposited amongst the boulder berm; incidentally, the largest RFID tagged boulder (tag ID 1188) is located in this zone (Figure 5.8b). At Black Rock the boulders positioned on the ridges that separate the runnels have fewer points of contact than those blocks sat upon a flat platform surface. Additionally, a greater surface area is exposed on the underside of the boulder. Furthermore, Fagherazzi and Mariotti (2012) identified increased flow velocities and bottom shear stresses higher than the critical shear stress in a mudflat runnel network. These factors suggest that water flow beneath the boulders is channelled through the runnels under increased pressure. It is hypothesised that water flow through the runnels provides an enhanced lift force to the underside of the boulder facilitating displacement. By replicating the runnel/ridge bedforms in the experimental flume this hypothesis can be tested.

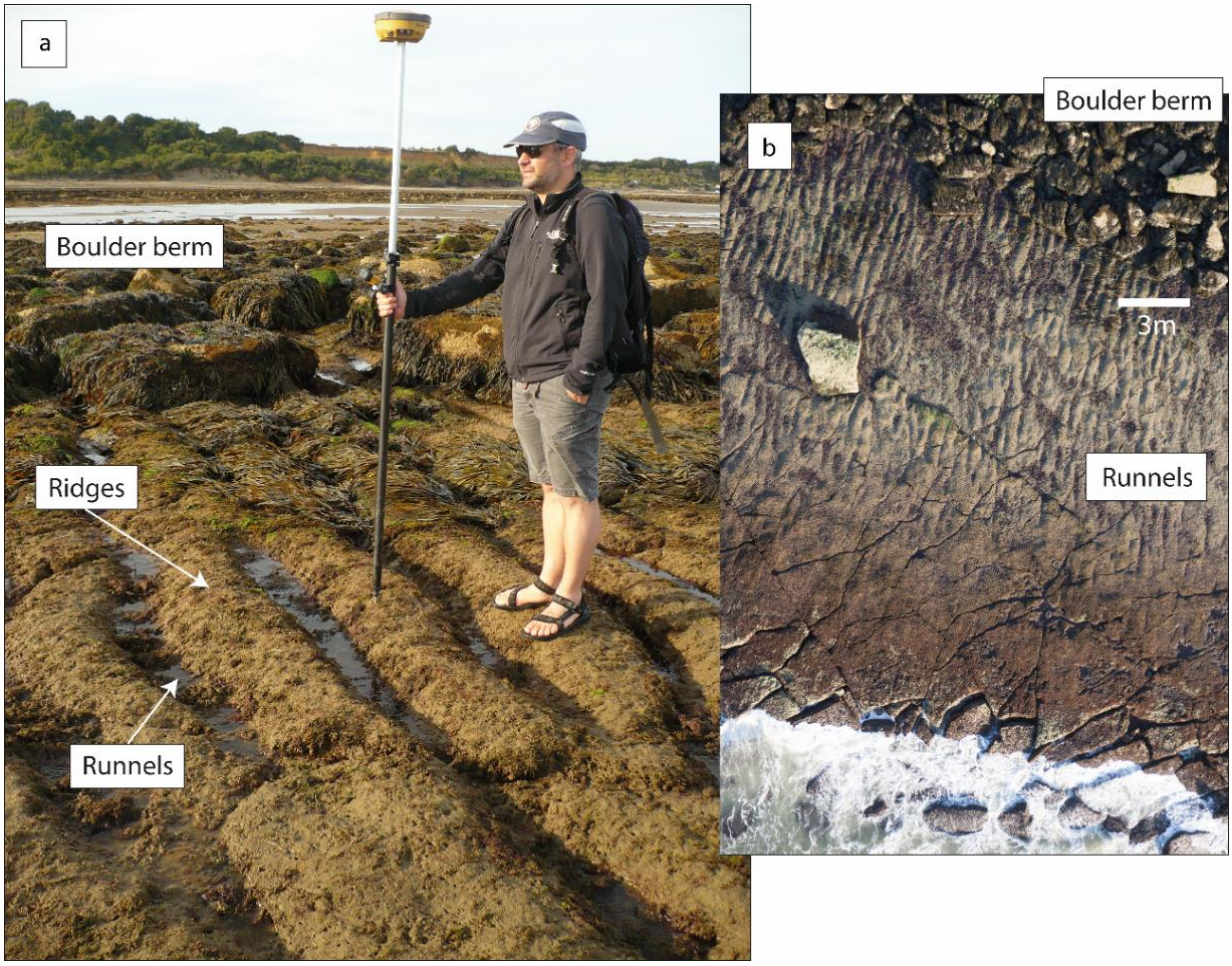

Figure 5.8. (a) surface runnels on the shore platform at Black Rock, deposition of large boulders can be seen in the boulder berm, the DGNSS pole is extended to 2.0 m; (b) aerial imagery captured from a DroneX X8-M UAV (October 2015) showing the largest tagged boulder (tag ID: 1188), left of centre, positioned on the surface runnels/ridges.

Whilst the experimental model cannot fully replicate all the boundary conditions of the field site it can simulate a host of controlling factors which may improve understanding of boulder transport mechanisms that occur on shore platforms. Furthermore, it may provide insight to how hydrodynamic forces are able to displace boulders far larger than would be anticipated under moderate storm wave conditions. With respect to the key processes of production, transport and deposition the findings will elucidate how surface forms either facilitate boulder displacement and/or promote deposition, in turn highlighting the significance of platform surface morphology which is the focus of the chapter describing the vasques-like intertidal pools (Chapter 4). In addition to determining the role of surface topography in clast displacement it is anticipated that the findings will also inform on the mode of transport (sliding/overturning) and clarify how and/or when overturning occurs. Furthermore, it may afford explanation as to why boulders overturned

during displacement appear to be mobilised over greater distances as identified by the RFID tagged array (Chapter 3, pages 96 and 97).

Broader-scale geomorphic change

The key aim of this thesis, identified in Chapter 1, is to determine the extent to which contemporary low-magnitude, high-frequency storm events are able to displace boulders in the intertidal zone. To this end, the findings presented in the preceding chapters (Chapters 2 and 3) have addressed this. However, whilst providing valuable insight to boulder transport processes at an individual scale, little is known about the displacement of boulders at a broader, more widespread scale, i.e., landform modification. Post-storm, field-based observations at Black Rock indicated that minor alteration occurred at the seaward edge of the boulder berm (Figure 5.9).

Figure 5.9. Boulder displacement at the seaward front of the boulder berm.

In order to determine evidence of large-scale geomorphic, landform modification it was necessary to draw upon historic aerial imagery. The use of aerial imagery is extensive as a means of monitoring geomorphic change at varying scales across many different environments, including the coastal

zone (Maiti and Bhattacharya, 2009; Kumar *et al*., 2010; Ford, 2011). More traditional methods of aerial image capture can be obtained via orbiting satellites and/or low flying aircraft (Figure 5.10). Satellite data covers a large surface area with regular revisit times. However, the spatial resolution of the images produced often limits their use when monitoring small-scale (centimetre to metre) morphological change (Klemas, 2015). Manned aircraft flights provide an improved resolution as demonstrated in Figure 5.10b, although such flights are costly and therefore data capture is often infrequent (Klemas, 2011).

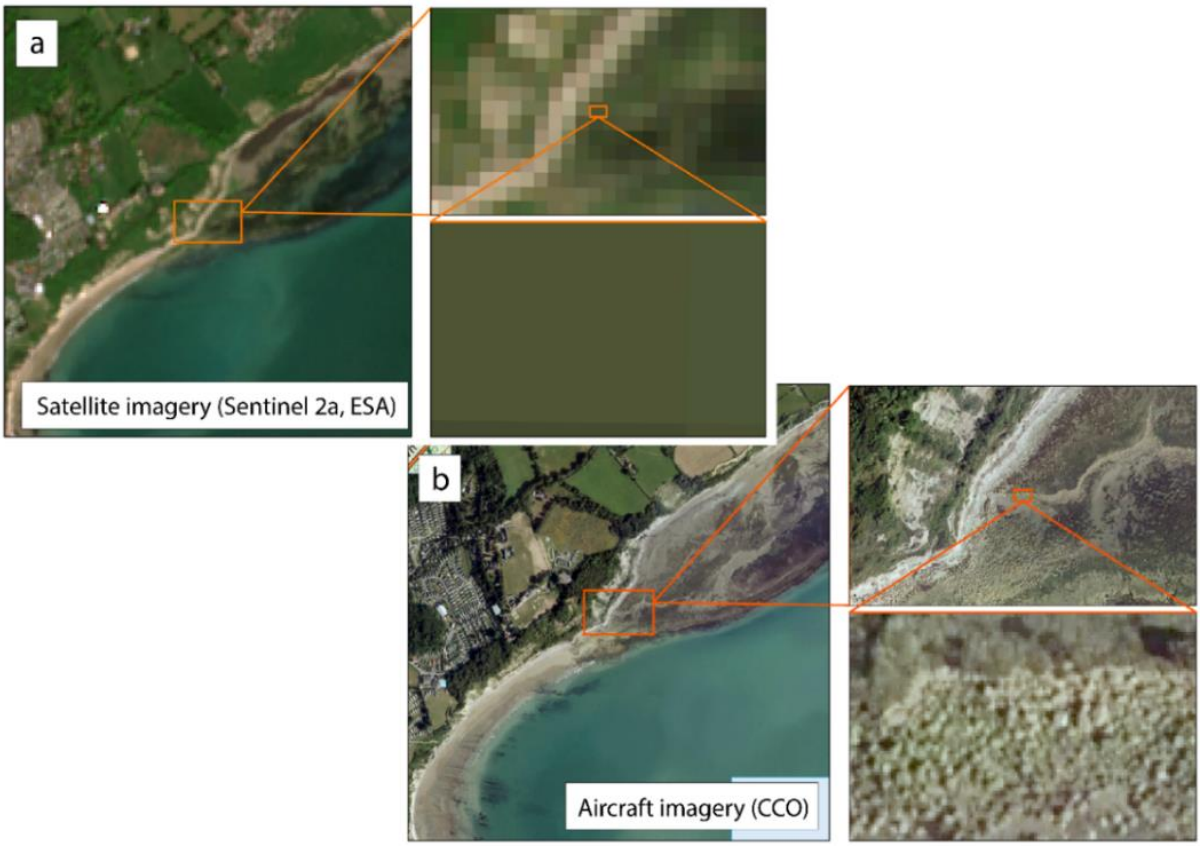

Figure 5.10. Comparison of image capture at Bembridge. (a) satellite imagery from Sentinel 2a, European Space Agency; (b) image captured from a low-flying aircraft, Channel Coast Observatory.

The CCO use manned aircraft flying at low altitude to capture aerial imagery around the U.K. coastline, including the Isle of Wight. This imagery was utilised to observe the possible occurrence of more widespread geomorphic change at Bembridge. The availability of historic imagery enabled a comparative analysis of displacement between episodes of data collection thus allowing for a much broader temporal perspective than is afforded within the relatively short timescale of a standard doctoral study.

Aerial imagery from the CCO covering an 11 year period (2005 - 2016) was consulted to observe whether large-scale geomorphic change had, or had not, occurred to the boulder berm at Black Rock. The berm, as pictured in Figure 5.11, is comprised of many thousands of detached and transported boulders ranging in size from fine (intermediate axis between 0.25 - 0.5 m) to very coarse (intermediate axis between 2.0 - 4.1 m). The berm extends for approximately 800 m from west to east, running parallel with the shore platform edge.

Aerial images captured in 2005, 2008, 2013 and 2016 were processed in ArcGIS (vers. 10.5.1). The seaward edge of the berm was mapped using the line tool option. This allowed for comparison of the historic demarcated seaward berm edge (Figure 5.11). The resulting data identified that between 2005 and 2013 movement of the berm edge was limited to minor shifts most likely arising from the supplanting of individual boulders.

However, during the period 2013 to 2016 the edge of the boulder berm moved over 7 m landward in some areas. The 2013 image was captured in August, prior to the winter period of 2013 - 2014 which was dominated by a series of low-pressure storm fronts that reportedly made this the stormiest winter on record (Matthews *et al*., 2014; Masselink *et al*., 2016a; Masselink *et al*., 2016b). Wave heights at the Sandown Bay wave monitoring station recorded a maximum H_s of 3.5 m and a H_{max} of 5.9 m over the winter period. The highest values recorded since wave monitoring commenced at the location in 2006.

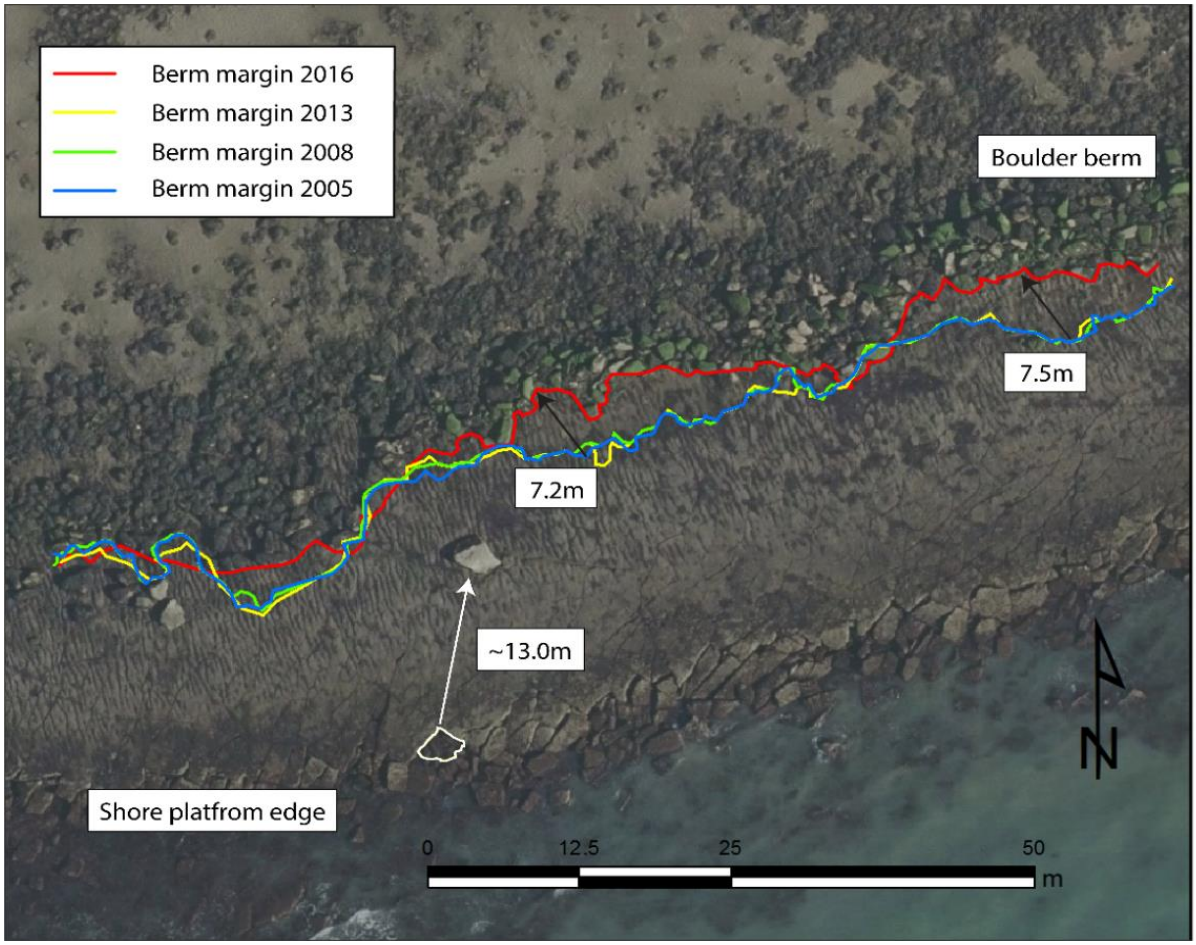

Figure 5.11. Landform modification by storm waves at Black Rock. Collective displacement of boulders resulting in the landward migration of the boudler berm. The white line highlights the socket that remains following the exhumation of the largest RFID tagged boulder (tag ID: 1188), the arrow depicts the transport pathway and distance.

These data establish moderate contemporary storm waves as agents of mass boulder displacement resulting in the modification of sizable geomorphic features. Thus, storm activity at Bembridge initiates geomorphic change on a larger-scale than had previously been realised. This reinforces the findings of Pérez-Alberti and Trenhaile, (2015a), Gómez-Pazo *et al*. (2019) and Nagle-McNaughton and Cox, (2020) who documented widespread, collective mass boulder movement using Unmanned Aerial Vehicles (UAV's).

Unmanned Aerial Vehicles (UAV's) in observing coastal geomorphic change

Recent technological advances in the manufacture and production of UAV's has led to a proliferation of their use in the geoscience arena, particularly in the coastal zone (Mancini *et al*., 2013; Gonçalves and Henriques, 2015; Turner *et al*., 2016; Casella *et al*., 2016, Albuquerque *et al*.,

2018; Jeong *et al*., 2018; Laporte-Fauret *et al*., 2019). UAV's provide a unique perspective on geomorphic features via the capture of centimetre resolution geo-referenced imagery and topographic data (Murfitt *et al*., 2017). The acquired data is subsequently processed using specialist software to create Digital Elevation Models (DEM's) of the area surveyed.

UAV's offer a viable alternative to image capture by satellite and/or manned aircraft in that they provide higher resolution imagery at a lower cost (Gómez-Pazo *et al*., 2019). This is beneficial when monitoring centimetre-scale geomorphic modification in the coastal zone. Figure 5.12 illustrates the comparative image resolution and clarity between UAV and manned aerial image capture from Black Rock, Bembridge. Image resolution from the UAV imagery allows for individual blocks to be highlighted and examined in detail (Figure 5.12, inset).

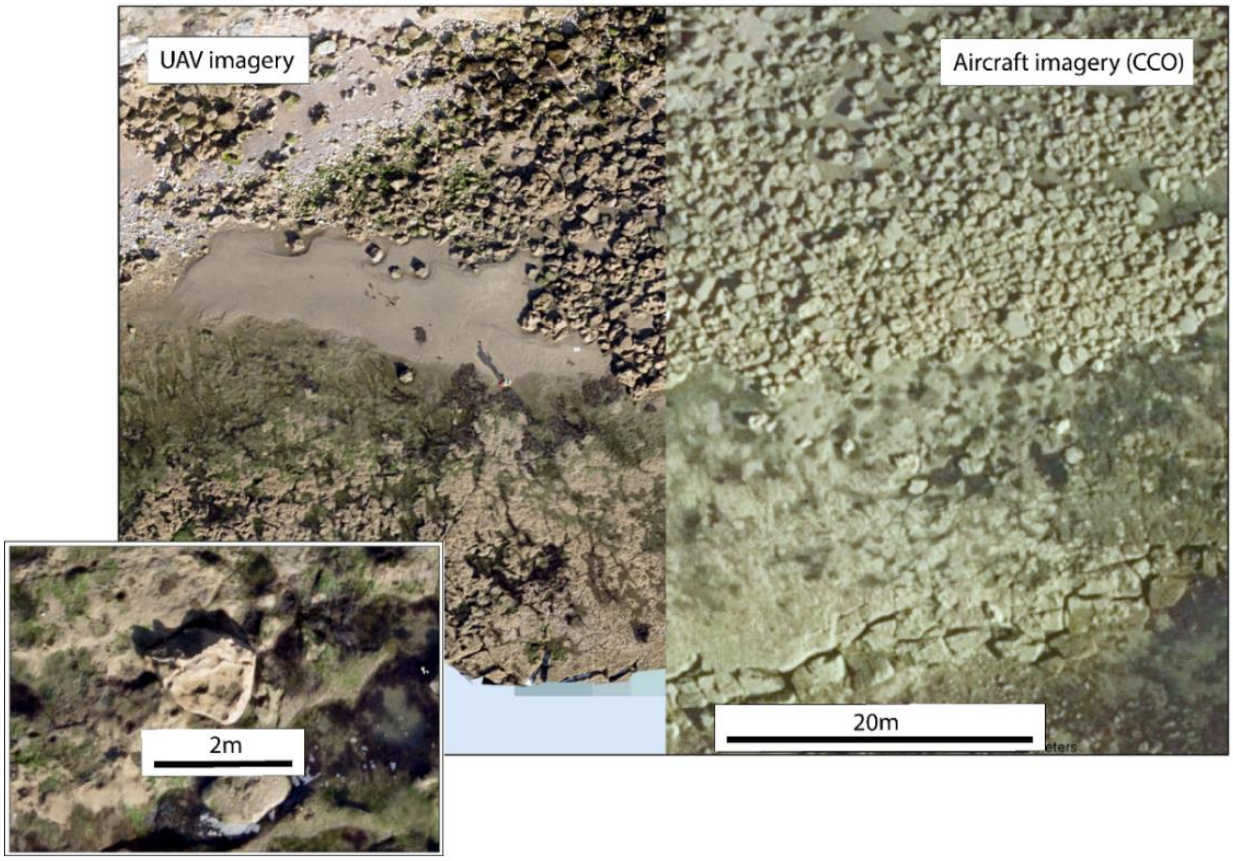

Figure 5.12. Comparison between aerial imagery captured by UAV (left) and aircraft (right); inset, boulder close-up from UAV captured imagery.

A key advantage of using UAV's is the increased operational flexibility. This allows for surveys to be scheduled in accordance with appropriate tidal states and deployment can be achieved swiftly in response to specific events. Furthermore, they allow for data capture from inaccessible areas that

may be deemed beyond the reasonable safety limits imposed on field operatives. Consequently, the use of UAV's in coastal studies has increased in recent years including the monitoring of coastal boulder assemblages (Pérez-Alberti and Trenhaile, 2015a, 2015b; Autret *et al*., 2016; Gómez-Pazo *et al*., 2019).

A UAV was deployed at Black Rock in October 2015.0 to collect aerial imagery of the site. Owing to flight restrictions, it was not possible to capture imagery from Bembridge Ledge. The UAV, a DroneX X8-M, was fitted with a Sony a6000 digital camera allowing for a ground resolution of <1 cm (Figure 5.13).

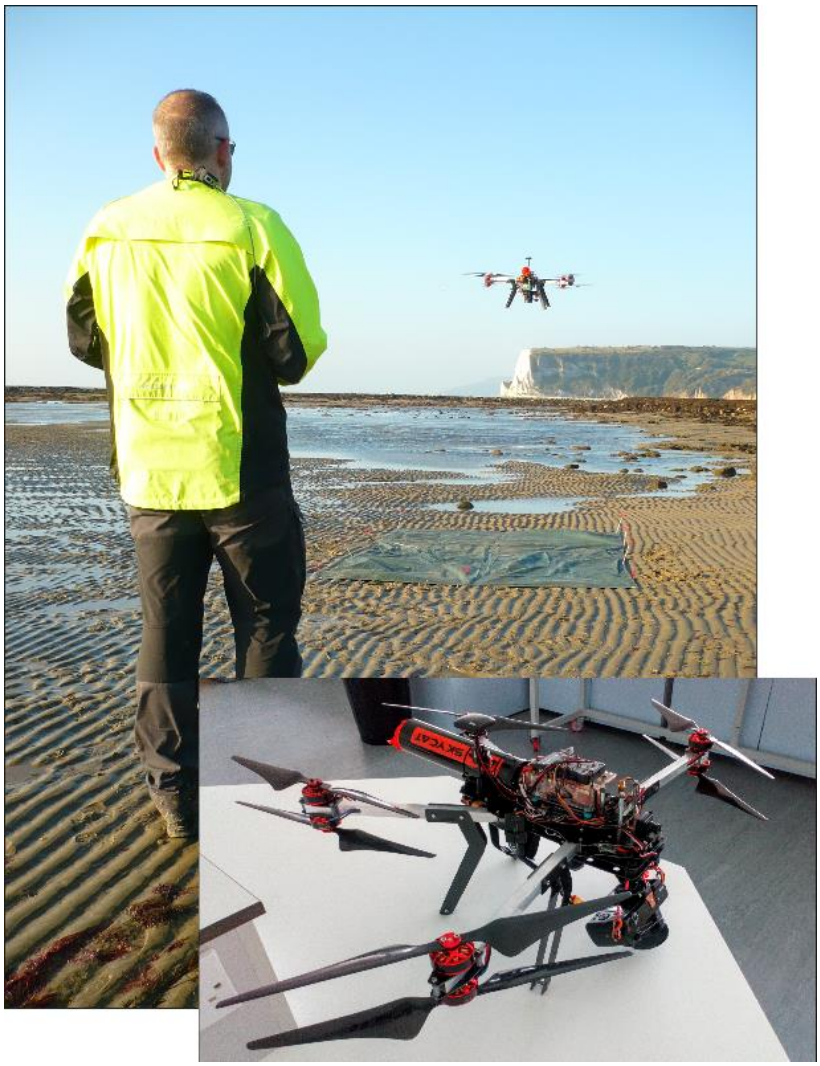

Figure 5.13. DroneX X8-M in flight at Black Rock; inset, DroneX X8-M.

Flight preparation involved pre-programming a flight plan to maximise area coverage. Mission Planner software was used to designate a number of waypoints and programme the image capture detail based on flight altitude and image overlap (Figure 5.14).

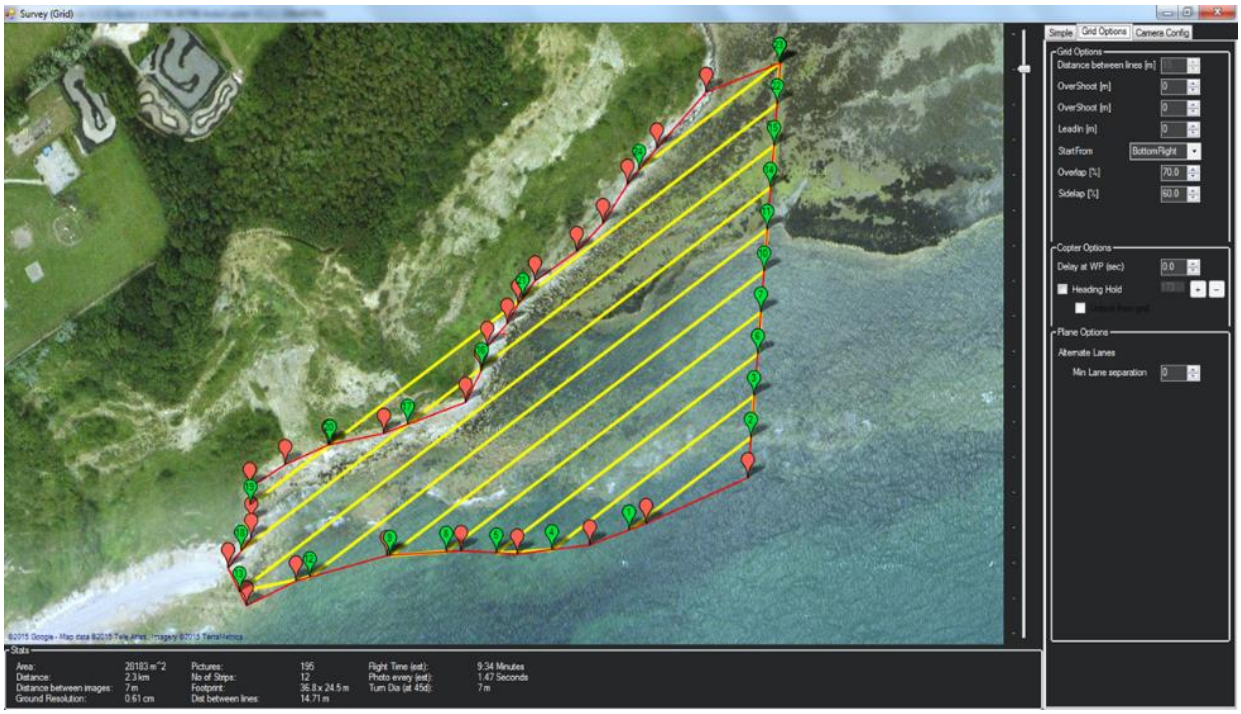

Figure 5.14. Mission Planner software - mission preparation for a section of the Black Rock shore platform. The waypoints create a gridded flight plan over which the UAV flies.

For the mission depicted in Figure 5.14 flight altitude was set at 30 m, 195 images were captured with a ground resolution of 0.6 cm, image overlap was 70%, sidelap, 60%. The software calculated the mission time based on in-flight speed and area coverage; in this instance it was 9.34 minutes, well within the recommended safe flight time of the UAV battery.

The UAV captured imagery has been used throughout this thesis as a means of illustrating landform features and processes (e.g. figures 5.6, 5.8b, 5.11, 5.12, 5.16, 5.17, and 5.18). In addition, the resulting UAV imagery was processed using Agisoft Metashape software to create a DEM of the Black Rock site. The data was also used to create a 3-dimensional fly-through animation in ArcGIS Pro which has been used as a digital tool in research presentations (Figure 5.15). The intention is to conduct additional UAV flights at the site in order to compare subsequent changes in boulder positioning and investigate further larger-scale geomorphic modification at the site.

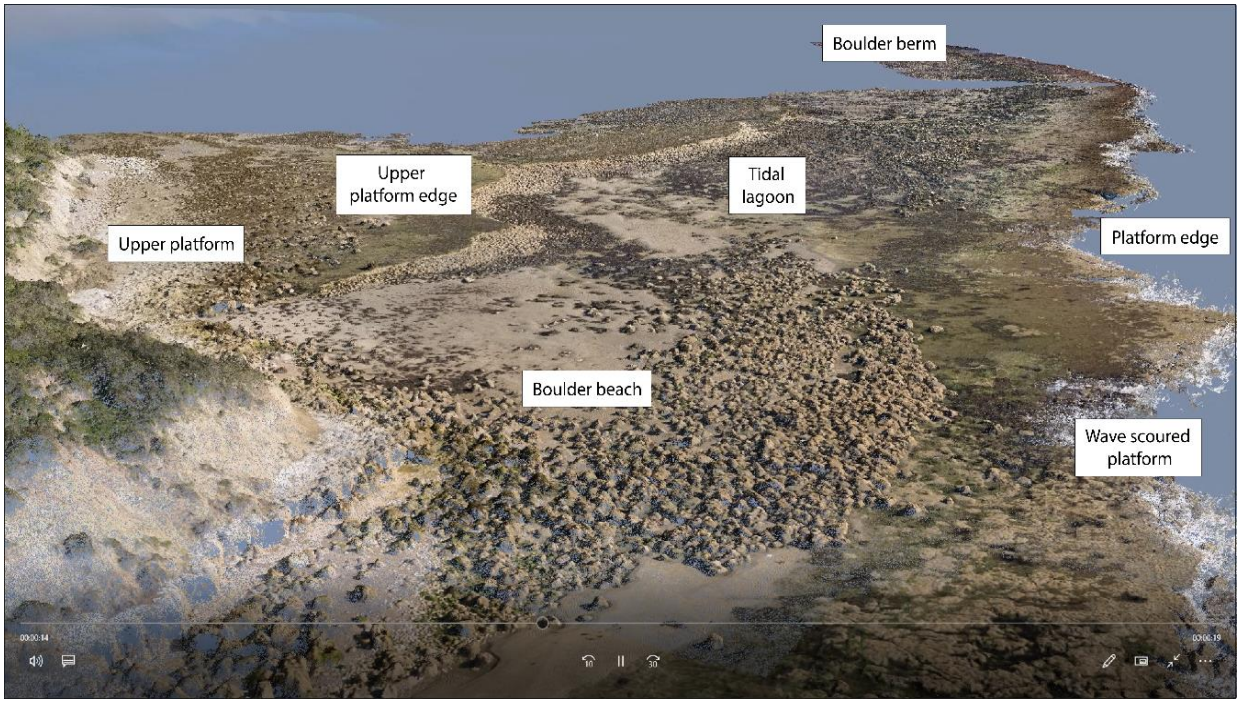

Figure 5.15. Image capture from the 3-dimensional fly-through animation created from UAV images, (credit, Martin Schaefer).

A proposed conceptual model for the production, transport and deposition of intertidal boulders

One of the key research questions stipulated in the introductory chapter was: *what are the processes by which boulder transport occurs, in terms of the mechanisms that initiate boulder production, the wave forces that facilitate transport, and the factors influencing deposition?* The data presented in the previous chapters (Chapters 2, 3 and 4), and within this chapter endeavour to address this question in terms of the individual components (production, transport and deposition). However, whilst these areas are well represented in the geomorphic literature there appears to be no single study that clearly and comprehensively documents the evolutionary life-cycle of displaced intertidal clasts; from source to sink.

Stephenson and Naylor (2011) provide insight to the processes and mechanisms that facilitate boulder transport using a two-phase conceptual model (see Chapter 1, figure 1.8). They identify boulder production as the initial phase followed by the collective representation of transport/entrainment and deposition. The model proposed by Stephenson and Naylor (2011) appears to be based on theoretical constructs without thorough interpretation and/or direct supporting field evidence. Using observations gained during this study and via the interpretation of

Unmanned Aerial Vehicle (UAV) and aerial imagery from Bembridge and other locations the conceptual model of Stephenson and Naylor (2011) has been modified. The revised model demonstrates a three-phase process consisting of individual components; boulder production, entrainment/transport and deposition. This is presented in the context of a worked example from Black Rock, (Figure 5.16), and is later applied to additional sites (Kimmeridge Bay and Lyme Regis, Figures 5.20 and 5.21 respectively) by means of validating the proposed model.

Platform undermining has been incorporated within the model as this is a primary mechanism in the boulder production phase at both Bembridge sites. This has also been observed at other sites to be described herein. A distinction has been made by defining the revised model with three individual process phases, opposed to two, as each process occurs within discrete zones with limited evidence of interaction between detached clasts in phase 2 (transport) and phase 3 (deposition). Each phase is presented as being inextricably linked to a particular zone on the shore platform. These zones are defined as follows and described herein:

(1) Boulder production zone;

(2) Boulder transport/entrainment zone;

(3) Boulder deposition zone;

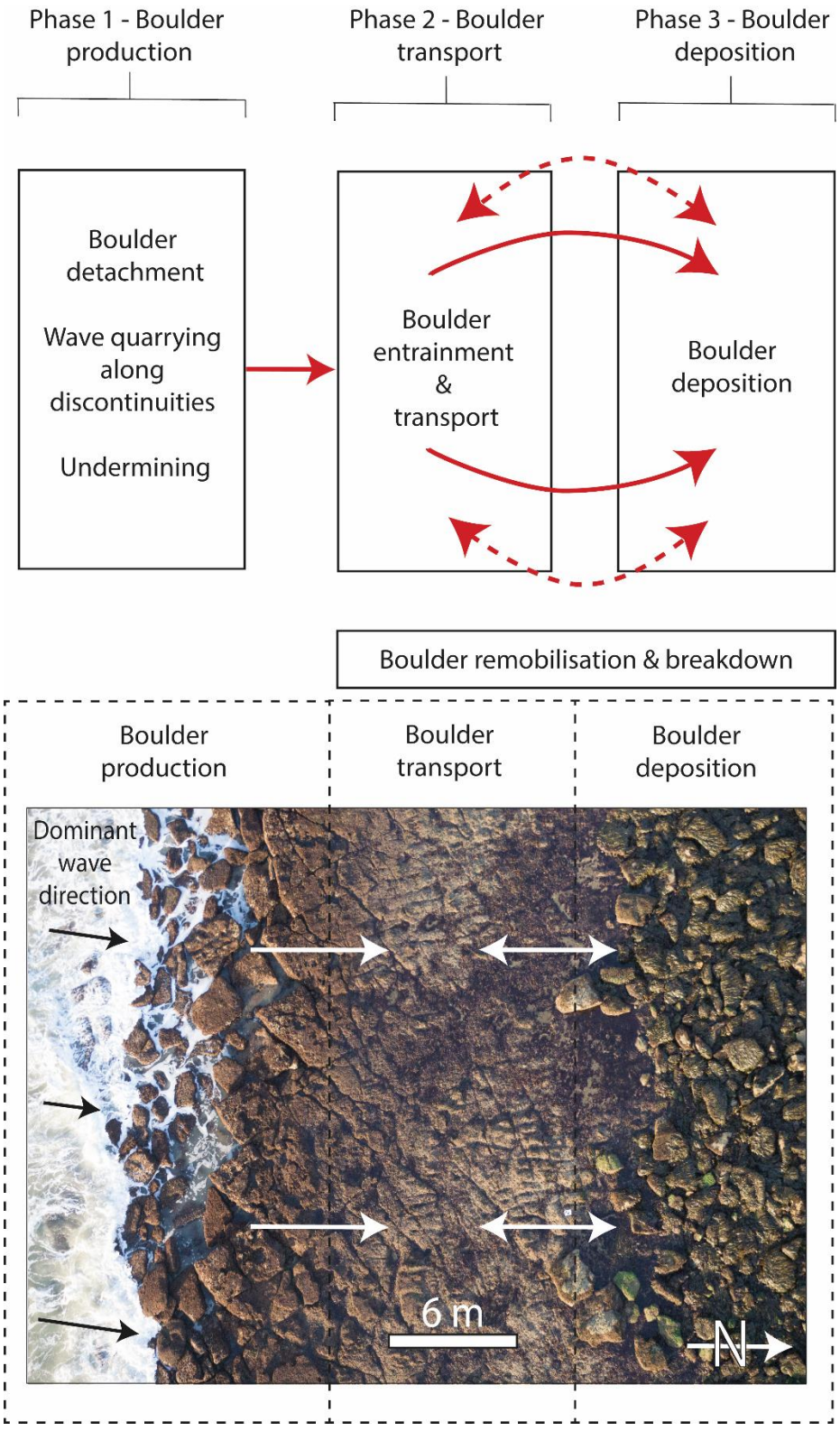

Figure 5.16. Boulder 'life-cycle' conceptual model identifying the three-phase process of boulder production, transport and deposition, modified from Stephenson and Naylor (2011). A UAV image from Black Rock, Bembridge presents a worked example of the revised conceptual model. Repeated boulder deposition has produced the boulder berm, at right.

The model is based on findings from field surveys that suggest the initial phase of boulder production is strongly controlled by the litho-structural component of the boulder producing unit which facilitates detachment along pre-existing geological discontinuities and/or fractures. This is evident from the Bembridge sites where a more readily erodible unit is positioned below a more resistant rock bed; this initiates block detachment by undermining. The process is enhanced at Bembridge Ledge where an increased number of discontinuities are present. This promotes the exhumation of smaller, more mobile clasts either by undermining and/or wave quarrying (Hastewell *et al*., 2020; Naylor and Stephenson, 2010). The lack of joint sets in the shore platform at Black Rock ensures liberation by wave quarrying is infrequent, subsequently undermining dominates. However, a divergent undermining process occurs to that of Bembridge Ledge. The detachment of material appears to result from undermining via notch development and the existence of a cavity network that extends beneath the shore platform. The degree to which the network extends is currently unknown and therefore its influence on the wider geomorphology at the site is currently indeterminable. However, as highlighted in Chapter 5, pages 141 - 151, the existence of the notch and associated cavities undermines the overlaying material and in the absence of discontinuities the rock mass fractures under gravity loading producing larger-sized clasts when compared with the discontinuous strata at Bembridge Ledge. Those boulders that are not transported landward at the time of liberation accumulate at the seaward edge of the shore platform. Pre-transported blocks remain located in this deposition zone until such time that wave energy is sufficient to elevate the boulder on to the platform, thus enabling the transport phase.

Boulder transport occurs when the hydrodynamic forces inherent in breaking waves (drag, lift, inertia, buoyancy, and gravity) exceed the resisting forces applied to the static boulder (Nandasena *et al*., 2011b). The ensuing transport is reliant on adequate wave energy to elevate the detached boulder from the platform edge, on to, and across the shore platform. The extent to which transport occurs is governed by the physical force of momentum from wave energy coupled with a favourable platform surface devoid of obstruction and topographic discrepancies. At both Bembridge sites, the shore platform lies immediately adjacent to the deposition zone (platform edge), thus providing a ready supply of boulders available for transport. The shore platform provides a satisfactory surface for displacement as it is generally free of smaller, surficial deposits as wave energy is sufficient to remove all but the largest clasts (Kennedy and Beban, 2005; Morton *et al*., 2008). Transport can be curtailed by insufficient hydrodynamic energy or by boulder interaction with small-scale features measuring tens of centimetres (e.g. static individual boulders), topographic anomalies measuring tens of metres (e.g. plate-forme à vasques, raised scarps) or large-scale geomorphic assemblages measuring hundreds of metres (e.g. boulder beach or boulder

berm). The transport zone is considered transient, acting as a conduit between boulder production and deposition. Clasts located here can be reworked transitioning from deposition to transport and/or entrainment. This reoccurring process can facilitate block breakdown although limited evidence of this was observed during the study.

The same factors that limit boulder transport, promote deposition. This occurs when the resisting forces acting upon the mobile boulder exceed the assailing wave force that initiated entrainment and transport. Deposition can be expedited by boulder interaction with morphological obstructions (e.g. a beach, cliff or individual/collective boulder deposits) or when wave energy is attenuated which may be hastened by changing platform topography. This can occur where slope angle increases and raised scarps or intertidal pools (plate-forme à vasques) are present. In the example provided in the conceptual model (Figure 5.16), the boulder berm is considered a vestige of the production, transport and deposition process. The existence of the berm curtails landward transport leading to deposition. Over time the berm develops in size exerting a greater influence in the deposition zone. As a repository of potentially mobile material the boulders may be reworked and broken down via remobilisation (Stephenson and Naylor, 2011).

This three-phase process of boulder production, transport and deposition is integral to better understanding the mechanisms that enable clast displacement and the subsequent landform modification that occurs as a result. In order to support and substantiate the modified conceptual model examples are presented that offer an insight to the production, entrainment/transport and deposition processes at varying scales at both Bembridge sites (Figures 5.17 - 5.19), and a further two field locations (Figures 5.20 - 5.24).

Boulder production at the seaward edge of the Black Rock platform dislodges very coarse boulders often measuring many metres in width (Figures 5.17). Transport then occurs across the platform prior to deposition at the point where mobility is impeded or wave energy is no longer sufficient to further displace the boulder. The wave scoured platform surface suggests the key factor influencing deposition is boulder interaction when encountering previously deposited clasts which form an assemblage which forms the fringes of the boulder beach.

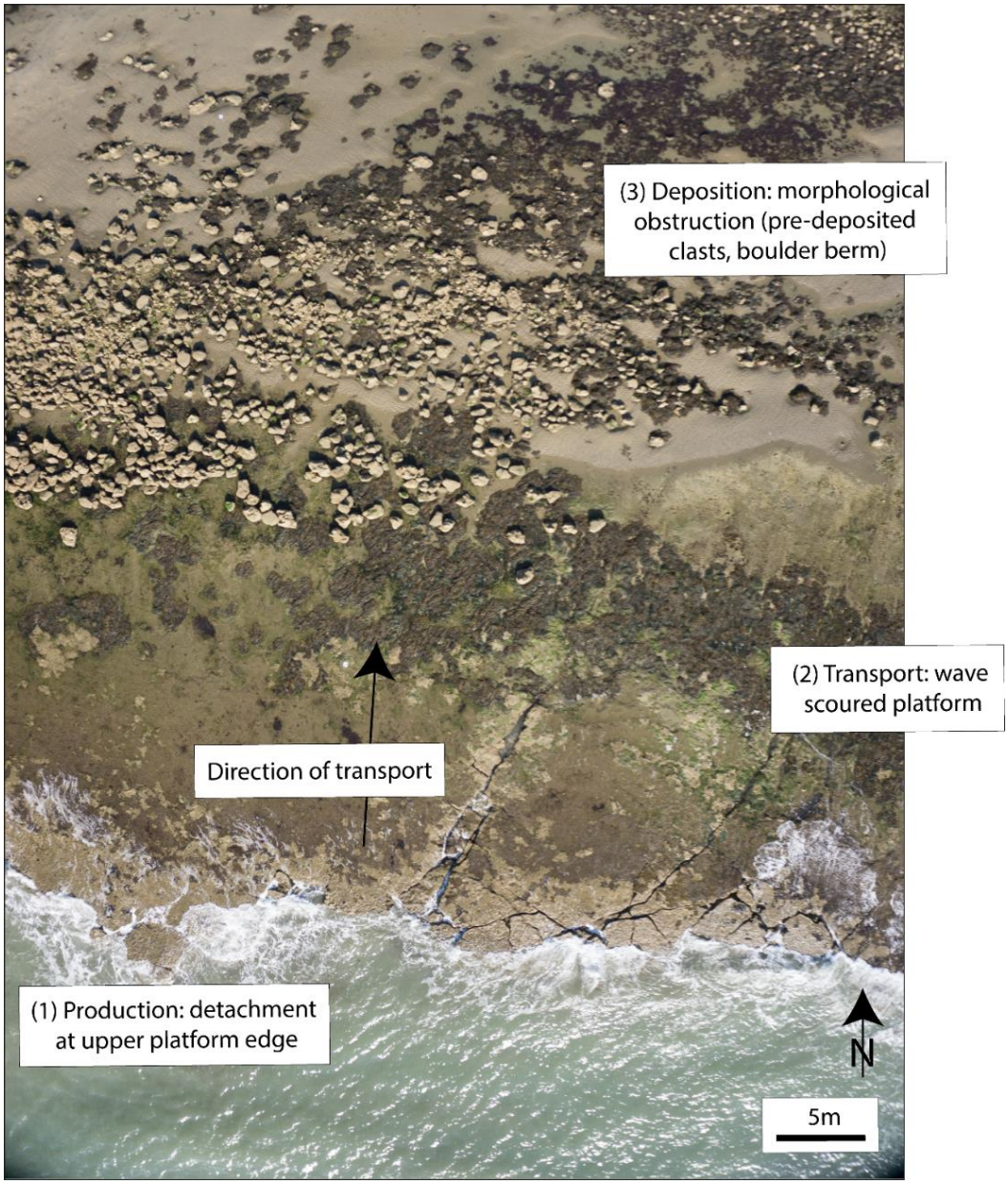

Figure 5.17. Seaward platform edge at Black Rock - boulder production, transport and deposition.

Whilst larger-sized clasts are generated at the seaward platform edge at Black Rock, smaller boulders are also produced from the upper platform which is identified in Figure 5.18. This size difference is a reflection of the litho-structural properties of the boulder-producing units, namely the more discontinuous strata that forms the upper platform and the presence of a thin, less consolidated underlying marl unit which promotes undermining and the production of finer, more mobile boulders measuring tens of centimetres.

Transport is expedited across the wave scoured platform; a rocky outcrop (right of centre) presents a stepped terrain which acts to impede transport. Deposition occurs with boulders becoming trapped at the raised edge leading to an accumulation of clastic material.

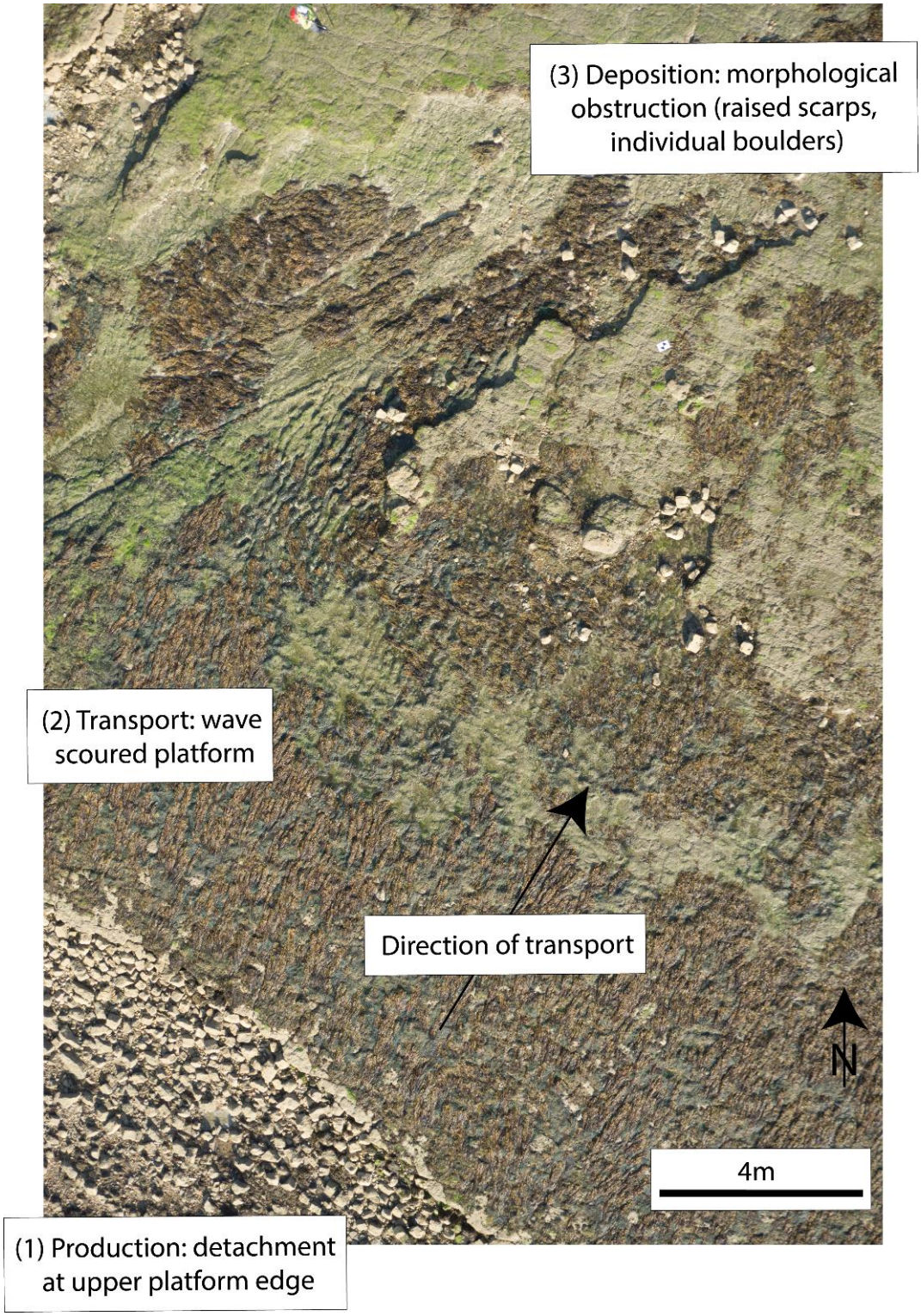

Figure 5.18. Landward upper platform edge at Black Rock - boulder production, transport and deposition.

The same three-phase process occurs at Bembridge Ledge (Figure 5.19).

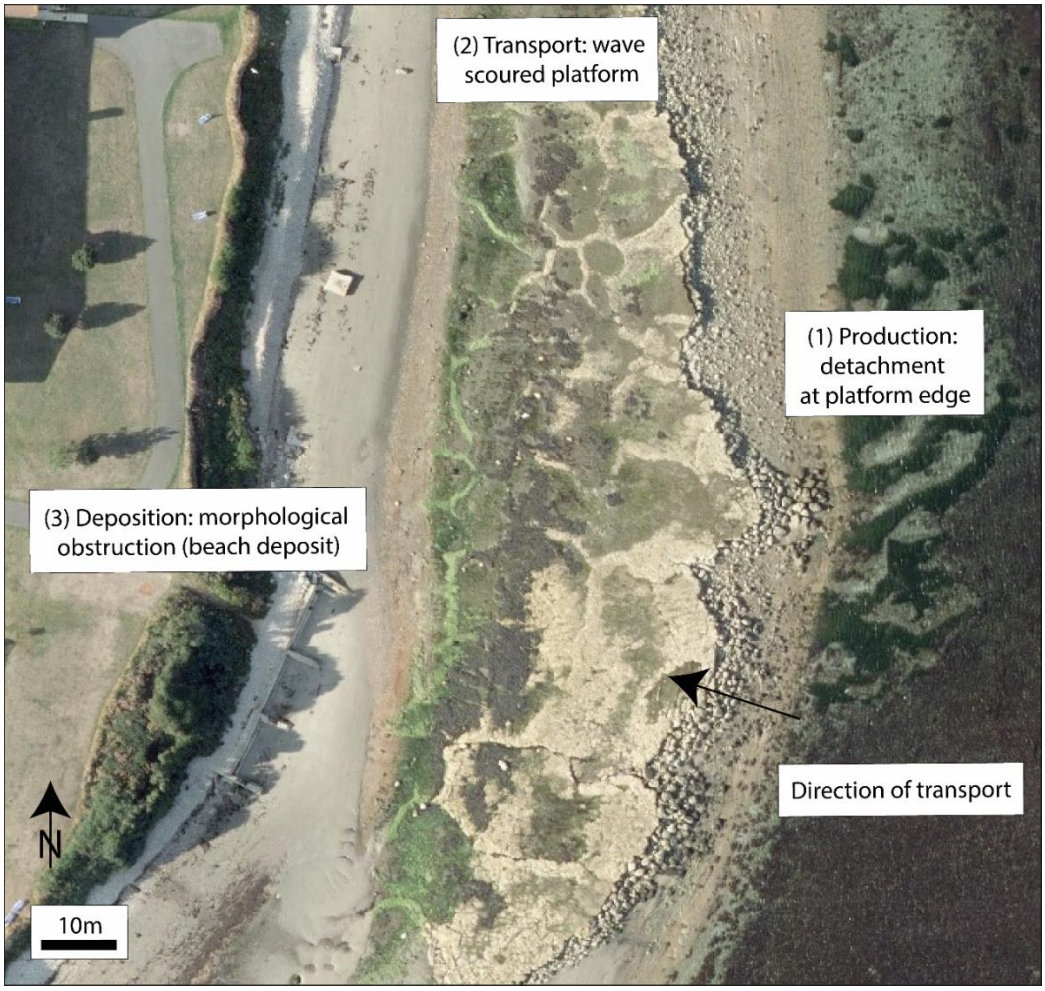

Figure 5.19. Shore platform edge at Bembridge Ledge - boulder production, transport and deposition. (Aerial image, Channel Coast Observatory, 2017b).

As the examples at both Bembridge sites demonstrate, boulder production occurs at the platform edge as a result of wave quarrying and/or undermining associated with the structural integrity of overlying geological units or via notch development and detachment under gravity loading. Transport is facilitated via displacement across the wave-scoured platform surface which is generally devoid of obstruction. Deposition results from interaction with a form of morphological impediment (e.g. individual/collective boulder deposits, scarps or the beach which presents an increase slope angle).

To broaden the scope of the findings detailed it was necessary to determine whether the same processes and mechanisms occurred at alternative coastal locations. Additional sites displaying evidence of boulder production, transport and deposition were identified on the south coast of the U.K. at Kimmeridge Bay and Lyme Regis (Dorset). Having identified suitable sites the opportunity arose to apply the modified conceptual model at different locations subject to a range of controlling

factors. This enabled us to establish whether the same processes and mechanisms were reflected at other locations thus helping to affirm and further validate the conceptualised model.

Observations from Kimmeridge Bay demonstrate that despite differences in the factors that govern boulder production, transport and deposition including geology, lithology, wave exposure and coastal aspect the same outcomes ensue (Figure 5.20). Storm waves quarry blocks from the well-jointed dolomite bed and are subsequently transported across the wave scoured platform prior to deposition which results from the interaction with other boulders amassed at the cliff toe.

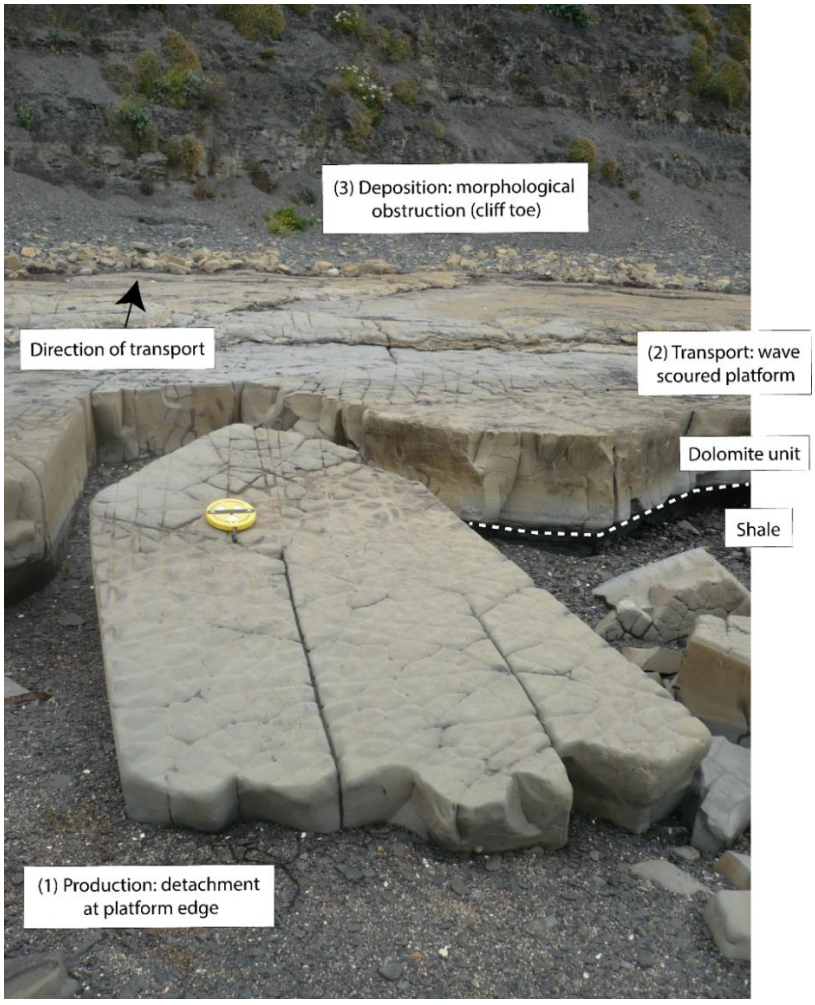

Figure 5.20. Shore platform edge at Kimmeridge Bay - boulder production, transport and deposition.

Significantly, the process of boulder production is initiated by undermining whereby an erodible bed of Eudoxus shale is located below the consolidated dolomite bed (West, 2009). This presents an analogous litho-structural sequence to Bembridge Ledge, in that a more consolidated upper unit lies upon a more readily erodible one, fragments of shale can readily be dislodged by hand. The erodible material is removed leading to undermining and block removal, as at Bembridge Ledge.

The same production, transport and deposition process has also been observed at Lyme Regis, 60 km west of Kimmeridge Bay (Figure 5.21). As with the previously identified sites boulder production occurs by undermining. This results from the preferential erosion of the shales that underlay the more resistant argillaceous limestone of the Blue Lias formation (West, 2018). Blocks are detached from the rock ledges along existing geological discontinuities. Detached material is deposited at the seaward edge of the ledges where it is available for transport. Wave energy, where sufficient, elevates the detached blocks above the raised ledge and across the transport surface; the smooth topography facilitates landward displacement. Transport continues until such time that mobilised boulders are impeded by interaction with pre-deposited boulders or become obstructed by the concrete coastal defence. The concrete defence works were completed in June 2015, it is therefore conjectured that transport and deposition of these clasts occurred between then and the time of the picture being taken (31st August 2019).

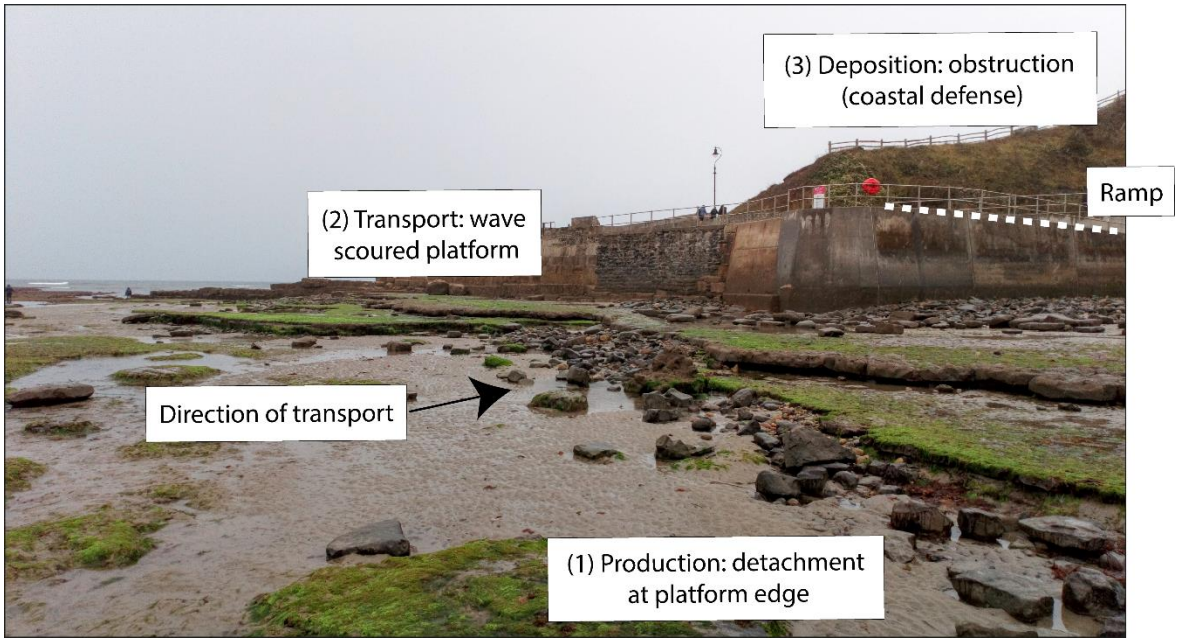

Figure 5.21. Platform edge at Lyme Regis - boulder production, transport and deposition.

The findings presented indicate that the processes of production, transport and deposition occur across a range of scales, from centimetres to many metres. Furthermore, they add to, and appear to corroborate the work of Cruslock *et al*. (2010) regarding equifinality, whereby different controlling mechanisms and erosive agents produce comparable erosion products and landform features. This has been demonstrated at two sites from the same location (Bembridge) and is supported by additional examples from two further contrasting field sites, Kimmeridge Bay and Lyme Regis. The field evidence identifies the three-phase process as consequential, with any one phase being the direct result of the preceding process. The findings suggest that production is

contingent on geological discontinuities of the boulder producing unit affirming the work of (Naylor and Stephenson, 2010; Stephenson and Naylor, 2011) whilst transport and deposition are likely controlled by topography and the presence of morphological obstructions (Hastewell *et al*., 2020).

However, despite the similarities between the aforementioned sites additional images taken at Kimmeridge Bay and Lyme Regis present further insight to the mechanisms that govern the boulder production, transport and deposition processes. The additional images were taken a short distance from the locations identified in Figure 5.20 (Kimmeridge Bay) and Figure 5.21 (Lyme Regis), see Figure 5.22.

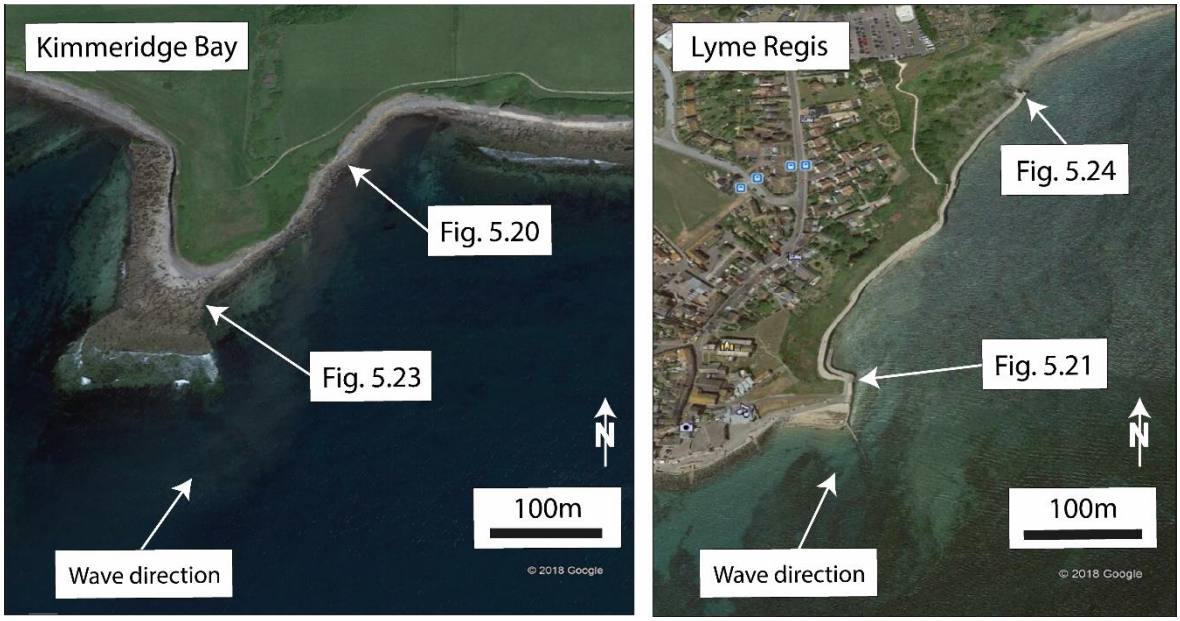

Figure 5.22. Field locations of images captured at Kimmeridge Bay and Lyme Regis. Mean annual wave direction based on CCO data from 2006 to 2019, at Kimmeridge Bay 216°, (as recorded by the CCO wave buoy at Chesil Beach) and Lyme Regis 206°, (as recorded by the CCO wave buoy at West Bay).

At Kimmeridge Bay approximately 200 m separates the two sites depicted in Figures 5.20 and 5.23, yet is was noted that despite the presence of detached boulders deposited at the edge of the platform the transport surface was devoid of surficial deposits that would be expected to accumulate at the cliff toe (Figure 5.23).

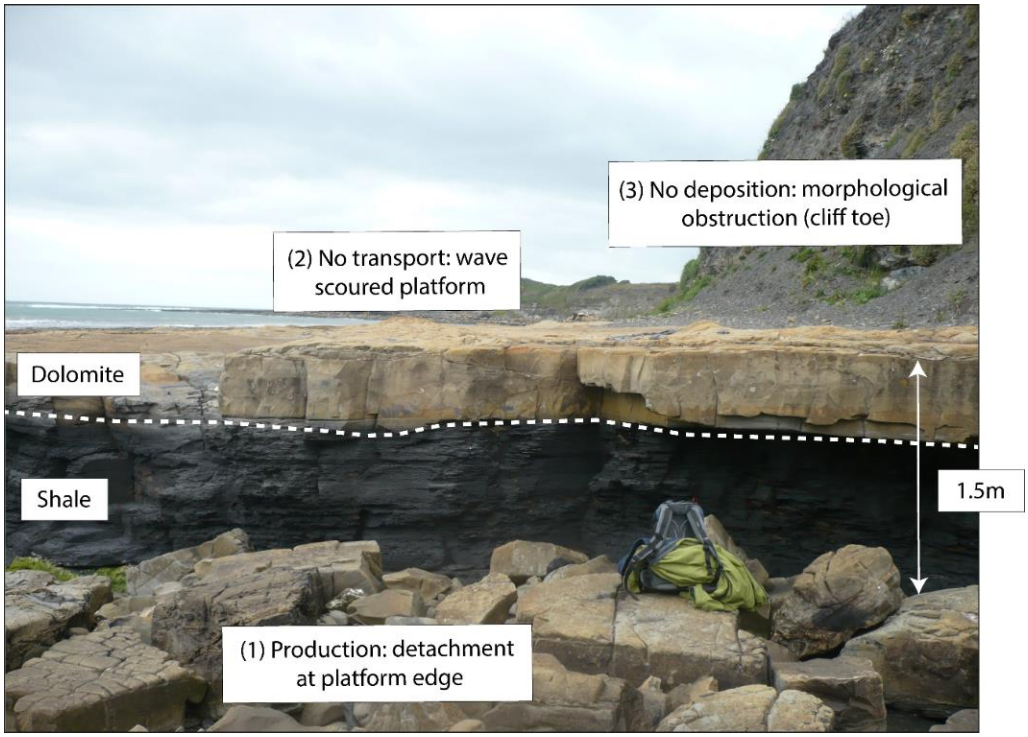

Figure 5.23. Shore platform edge at Kimmeridge Bay - boulder production, detached blocks available for transport yet no evidence of displacement and/or post-transport deposition.

At Lyme Regis, the two sites identified in Figure 5.22 are separated by approximately 350 m yet there is no evidence of boulder transport and subsequent deposition at the location in Figure 5.24, note the same ramp is highlighted in both Figures 5.21 and 5.24.

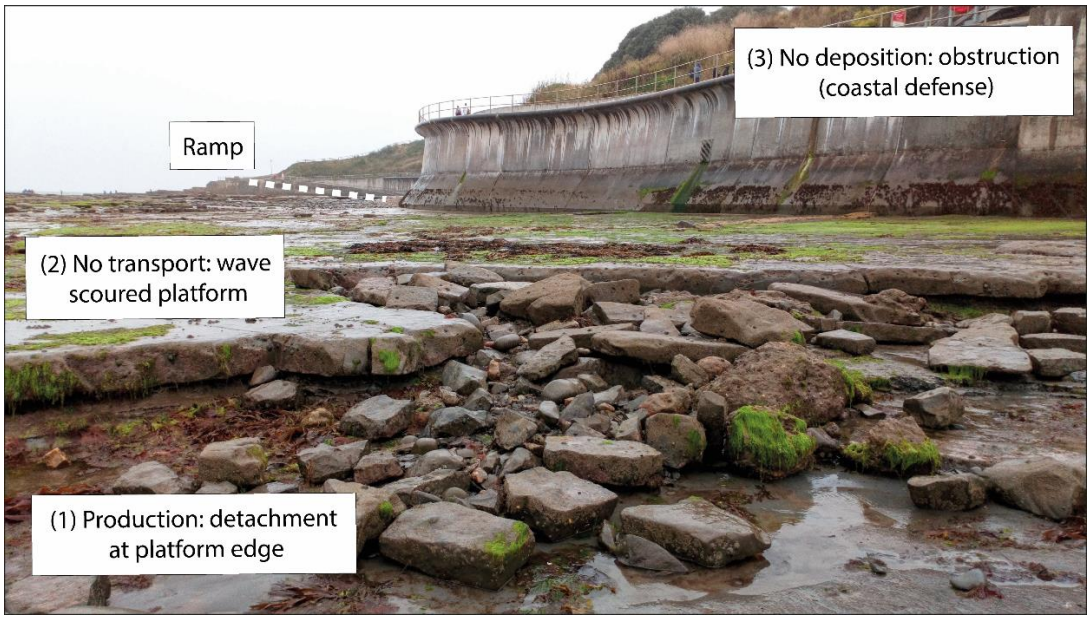

Figure 5.24. Shore platform edge at Lyme Regis - boulder production, detached blocks available for transport yet no evidence of displacement and/or post-transport deposition.

The figures from Kimmeridge Bay (5.20 & 5.23) and Lyme Regis (5.21 & 5.24) demonstrate that despite a shared geology, lithology, morphological setting, wave climate and tidal regime certain site-specific controls influence where boulder transport does, or does not occur. In the case of Kimmeridge Bay the notable difference between the two locations is the height of the transport surface above which the detached pre-transported boulders are deposited. Although Figure 5.20 is located in the more sheltered setting of Kimmeridge Bay wave energy need only elevate the detached material approximately 0.5 m on to the transport surface. By contrast, Figure 5.23 is more exposed to storm wave energy, being located at the seaward opening of the bay, yet the transport surface is elevated 1.5 m above the detached boulders. This therefore requires a greater hydrodynamic force to raise the detached boulders to a point where they are capable of being displaced. Evidently, the storm wave energy at this location is not sufficient to accomplish this.

The two Lyme Regis sites are comparable in ridge height above which material must be elevated to enable transport to occur. However, the level of exposure to storm wave activity differs. The dominant wave direction ensures that waves propagate over the platform surface and thus energy at the more landward site in Figure 5.24 is reduced, limiting the wave capacity to transport detached boulders.

Clastic material deposited seaward of a discontinuous platform edge acts as an indicator of boulder liberation by wave quarrying and/or undermining. Provenance can usually be confirmed by comparing rock types and block size with joint density (Knight and Burningham, 2011). If evidence of transport is absent, such as a paucity of individual surficial clasts on the platform surface and depositional signatures are absent then the limiting factor is considered to be one that influences transport.

Therefore, intra-site differences in any one aspect of the controlling mechanisms governing boulder production, transport and deposition can lead to the breakdown of the process resulting in no transport, and thus no depositional signatures. This intimates that in order to better understand boulder transport future studies should address individual process phases in isolation rather than collectively. In doing so, this will provide a more robust understanding of site-specific transport processes and the broader geomorphological response to contemporary storm activity.

By way of summary, the proposed conceptual model and the findings arising identify two salient outcomes.

(1) Despite inter-site differences in any number of controlling factors (e.g. geology, lithology, wave regime and tidal range), the same processes of production, transport

and deposition are reflected at various sites at a range of scales producing similar resulting landform features and sedimentary assemblages. However, site-specific differences can dictate if, and where, boulder production, transport and deposition occurs.

(2) The conceptual model presented in Figure 5.16 appears to be applicable across a range of contrasting field settings suggesting a degree of universality in the processes that dictate intertidal boulder production, transport and deposition. Further observations at alternative coastal sites subjected to different boundary conditions will be undertaken to further develop and assert the validity of the model. Furthermore, the model can be applied remotely using aerial imagery of a suitable resolution, or in the field in the absence of quantifiable RFID derived boulder transport data.

As previously stated, the data and findings arising from the research presented in this chapter are currently underdeveloped; hence, they were not included in the manuscript submissions that form the basis of the thesis. However, not only have they provided additional understanding on the processes that govern boulder production, transport and deposition they will also form the basis of further enhancing our understanding of the complex mechanisms and interactions that affect how shore platforms respond to forces of storm wave erosion across a range of scales.

Research collaboration

During this research study, a number of collaborative partnerships have been fostered both within the home institution (University of Portsmouth) and at institutions within Europe. These partnerships are presented here as joint-research currently being undertaken which will form the basis of future research outputs. The collaborations have centred on two key themes; (1) using geomorphic field evidence to improve awareness of the potential hazards that have befallen coastal zones as a result of historic, extreme wave activity and; (2) providing opportunities to deploy the RFID tagging technology described in Chapters 2 and 3 in coastal settings subjected to a host of different controlling factors.

The additional RFID tag deployments are aimed at developing a network of sites across which the responsiveness of individual boulders can be monitored and quantified. This will improve awareness of the capability and effects of storm waves on coarse clastic sediment under a range of varying site-specific conditions and across different scales. Using alternative locations also provides the opportunity to determine the applicability of the conceptualised model of production, transport

and deposition; can this be applied as a universal model? Furthermore, in conceiving a network of RFID tagged boulder sites we endeavour to augment the methodology and present RFID tagging as a standardised technique in monitoring the displacement of coastal boulder deposits.

University of Portsmouth (U.K.)

As part of the University of Portsmouth coastal research team I was heavily involved in collecting field data for publications relating to boulder deposits found within the Maltese archipelago. This culminated in the following papers within which my contribution was acknowledged.

> Mottershead, D., Bray, M., Soar, P., & Farres, P. J. (2014). Extreme wave events in the central Mediterranean: Geomorphic evidence of tsunami on the Maltese Islands. *Zeitschrift für Geomorphologie*, 58(3): 385-411.
>
> Mottershead, D. N., Bray, M. J., Soar, P. J., & Farres, P. J. (2015). Characterisation of erosional features associated with tsunami terrains on rocky coasts of the Maltese islands. *Earth Surface Processes and Landforms*, 40(15): 2093-2111.
>
> Mottershead, D., Bray, M., & Deguara, J. C. (2019). Tsunamigenic landscapes in the Maltese Islands: the Comino channel coasts. In *Landscapes and Landforms of the Maltese Islands* (pp. 273-288). Springer, Cham.

I was also a named author on the oral presentation, 'Storm or tsunami? Or Storm and tsunami? Boulder transport histories on the shoreline of Malta', (Mottershead *et al*., 2017) which was delivered at the 5th International Tsunami Field Symposium, Lisbon, Portugal, (3rd - 7th September 2017).

Following the publication of the RFID tagging methodology (Hastewell *et al*., 2019a) further opportunities for collaboration arose with research institutes within Europe, namely, the University of Malta and the University of Trieste (Italy).

University of Malta

The Maltese islands, formed of Malta, Gozo and Comino, are located centrally within the Mediterranean. The islands are occasionally subjected to storm wave conditions exceeding 9.0 m (Mottershead *et al*., 2015) and the favourable lithology produces extensive boulder deposits (Figure 5.25). The islands have attracted much interest from coastal geomorphoogists with a number of

boulder transport studies emanating from the area in recent years (Furlani *et al*., 2011c; Mottershead *et al*., 2014; Mottershead *et al*., 2015; Mottershead *et al*., 2019; Biolchi *et al*., 2016a; Biolchi *et al*., 2016b; Deguara and Gauci, 2017; Deguara and Scerri, 2019).

Additionally, being located in a tectonically active region of the Mediterranean means the area has been affected by past tsunamagenic wave events (Scicchitano *et al*., 2007, Mottershead *et al*., 2019). The exposure to these two competing mechanisms, storm and tsunami, has fuelled debate regarding the assailing force under which boulders have been produced, transported and deposited.

Figure 5.25. Boulder deposition on the shore platform at Zonqor, Malta.

Subsequent to the highlighted research on wave capabilities in the Maltese archipelago opportunites arose with Dr. Ritienne Gauci (University of Malta) to undertake a pilot study monitoring the contemporary displacement of coastal boulder deposits at various sites on the Maltese islands. Twenty-five RFID tags have been supplied for deployment at shore platform locations within the archipelago. It is hoped that by establishing an array of RFID tagged boulders throughout the Maltese islands it will be possible to improve understanding of storm wave capabilities with a view to determining the mechanisms by which these boulders are displaced,

storm, or tsunami. The findings may suggest storm wave competence on the islands is greater than previously realised which could result in improved risk mitigation for the many Maltese coastal communities. Additionally, RFID tag deployment in Malta provides an opportunity to establish how efficiently the RFID methodology performs when subjected to a more dynamic wave regime, as suggested in Chapter 2, page 66.

University of Trieste (Italy)

Interest from coastal researchers at the University of Trieste (Italy) was aroused following the publication of the RFID methodology, Hastewell *et al.* (2019a). Biolchi *et al.* (2019) recently identified boulder deposits at Premantura on the Istrian Peninsula of Croatia. Significantly, the boulder deposits are found in a semi-enclosed, fetch-limited shallow basin, akin to that of the Bembridge sites. Biolchi *et al.* (2019) used a range of field, numerical and analytical techniques including geological, geomorphological and UAV surveys, hydrodynamic modelling and ^{14}C Accelerator Mass Spectrometry (AMS) dating. The aim being to determine the means by which boulder detachment and displacement occurred, storm or tsunami? The findings indicate that the boulder elevation above current sea-level and the distance inland of some documented clasts were within the competence of contemporary storm-induced transport, therefore discounting a tsunamagenic origin for deposition.

Having established storm waves as the agent of geomorphic modification it was considered that further research at the site would benefit from the deployment of the RFID technology as a means of determining the frequency and extent to which the boulders were being displaced by contemporary storm waves. Following discussions with the authors of the aforementioned publication a research visit to the Univeristy of Trieste was completed in May 2019. During the visit a number of project ideas were identified following field visits to two separate sites.

Site 1 - Premantura, Istrian Peninsula, Croatia.

The favourable performance of the RFID tagged boulders and the data generated (Hastewell *et al*., 2019a & 2020) suggested the methodology was a robust and reliable means of determining boulder transport capability. Discussions prior to the Trieste visit centred on the deployment of a small number of RFID tags at the field site in Premantura, Croatia. On visiting the site 8 RFID tags were embedded in selected boulders with known coordinate locations (Figure 5.26). The tagged array consisted of detached (n = 7) and joint-bound (n = 1) boulders. The Premantura site shares similarities with Bembridge in regard to the moderate wave climate and the shallow, fetch-limited

location. Tag deployment was undertaken in readiness for the winter storm period, 2019 - 2020. A further 20 RFID tags have been supplied to the University of Trieste to be deployed across other sites within the Premantura area. The results generated will form the basis of future research publications and provide an increased understanding of the wave impacts at this location.

The RFID tag deployment in Premantura offers an opportunity to establish the feasibility of the the tagging technology and methodology in the identification and quantification of boulder displacement in the supratidal zone, as suggested in Chapter 2, page 66.

Figure 5.26. Tagged boulder on sloping shore platform; inset, tagged boulder, RFID tag circled. (Premantura, Croatia).

Site 2 - Punta Grossa (*Italian*), Debeli rtič (*Slovenian*), Slovenia.

An additional coastal site was identified and visited on the Adriatic coast of Slovenia. The site has been studied previously by Furlani *et al*. (2011b) and Furlani *et al*. (2011c) who assessed coastal retreat at the site using repeat photogrammetry and rock geomechanical properties. The detachment of blocks from the cliff face has resulted in extensive deposition of coarse clastic

material at the cliff toe (Figure 5.27). Due to the regular joint spacing many of the liberated blocks share similar axial dimensions. The methodology employed in Hastewell *et al*. (2019a & 2020) lends itself to the relocation of such clasts as it allows for the unequivocal identification of tagged boulders. The use of RFID tagging will provide an opportunity to determine the rate of displacement for blocks located at the cliff/platform interface. These blocks serve a protective function to the cliff and the land, property and infrastructure which it supports therefore an understanding of the boulder transport pathways is required in order to better manage the site and mitigate against future erosive events.

Figure 5.27. Accumulated block deposition at the cliff/platform interface resulting from discontinuous sandstone strata susceptible to block detachment (Punta Grossa, Slovenia). Note the distinct consolidated sandstone strata within the Flysch cliff.

In addition to documenting those clasts already detached (as above) RFID use is being considered to better understand the rates at which block liberation occurs from the Flysch cliff. This will present an alternative application for the RFID tags. It is anticipated that the tags will be embedded in a number of sandstone blocks exposed within the cliff face, (Figure 5.27); their initial location will be documented using DGNSS. Subsequent field visits will be conducted to relocate the tagged blocks to establish whether they remain in-situ or have been removed from the cliff face. This will provide a means of establishing how susceptible the cliff is to processes of erosion. It may also grant insight to the 'life-cycle' of the liberated material, from source to sink and present an opportunity to

expand further the conceptual model of boulder production, transport and deposition by proposing an alternative mechanism for boulder production.

Further to the visit the collaborative research undertaken with the University of Trieste has been presented at the International Association of Geomorphologists Regional Conference held in Athens, Greece, (19th - 21st September 2019).

Title: A multidisciplinary approach for the investigation of the dynamics of a boulder deposit on a low-lying rocky promontory in the Northern Adriatic Sea.

Dr. Stefano Devoto delivered the presentation, see Appendix 4, page 227.

By conducting similar boulder transport studies at various coastal locations we aim to further augment the suitability of the RFID methodology and broaden the scope of this research by establishing similarities with regards to geomorphic response to a range of storm wave processes and magnitudes.

Funding sources including the British Society for Geomorphology (BSG), Royal Geographical society (RGS) and the Erasmus programme are being sought along with internal institutional funding streams to facilitate future field visits to the deployment sites.

Chapter 6 - Synthesis and Conclusions

Synthesis

The research conducted and the reported findings within the thesis are intended to offer a more comprehensive understanding of the responsiveness of boulder-sized clasts to contemporary storm wave activity. The study aim and associated research questions stipulated at the outset were presented in the context of better understanding the complex interrelationship between a myriad of site-specific conditions and their influence on the boulder transport dynamics at the chosen field location.

The synthesis draws upon the published results and additional findings in the preceding chapters to highlight the following:

- Key findings and contributions to boulder transport research;
- Study limitations;

Key findings and contributions to boulder transport research

The key findings arsing are based upon the empirical field-based study which accurately quantified the extent to which contemporary, low-magnitude, high-frequency storm events were able to transport detached boulders at the selected field location. This was achieved by conducting a sediment tracer monitoring programme using RFID tagged boulders. The selected tagged boulders were periodically recovered and their locations recorded over a three year period, thus providing a spatial and temporal framework within which boulder transport pathways could clearly and accurately be defined. Furthermore, observational data collection and interpretation were utilised to improve awareness of the multiplicity of factors initiating and affecting the boulder transport process.

(1) Contemporary low-magnitude, high-frequency storm waves are capable of displacing boulder-sized clasts.

Existing boulder transport research focuses on coastal areas exposed to considerable fetch distances that are subjected to infrequent, dynamic, often extreme storm wave conditions where transport is to be expected. In targeting such high-energy sites coastal researchers have overlooked fetch-limited locations exposed to low/moderate storm wave activity. This study was intended to

provide a more complete understanding of the level of response on rocky coasts in terms of boulder transport at a field site location which reflects characteristics that have hitherto been neglected.

The transport data presented in Chapters 2 and 3, clearly identifies that extreme storm waves are not necessary to mobilise sizable boulders. Evidence of displacement of clasts up to and exceeding an estimated 10.0 t are presented, despite the perceived, less hydrodynamic conditions. It is anticipated that this research will act as a locus from which future studies can be undertaken in more sheltered, fetch-limited coastal locations.

Notably, since the conclusion of this field study additional boulder transport research has been conducted in the semi-enclosed, shallow basin of the Northern Adriatic Sea; a setting exposed to low/moderate storm waves with limited fetch (Biolchi *et al*., 2019a; Biolchi *et al*., 2019b). It was found that despite the limited wave exposure the displacement of supratidal coastal boulder deposits occurs during contemporary storm activity. Collectively, these studies present compelling evidence that questions the geomorphic docility of relatively sheltered coastal sites. Additional studies in similar areas exposed to limited hydrodynamic forcing will broaden the scope of the existing research and provide a greater appreciation and understanding of how these coastal zones respond to present-day storm activity.

The aim of the reseach was focused on the transport of individual boulders. To broaden the scope and scale of the study from individual clasts to the modification of larger-scale boulder assemblages aerial imagery was interpreted. The results helped gain a more complete understanding of the extent to which the wider platform morphology was modified by contemporary storm wave activity. Historic aerial imagery of the Bembridge area identified displacement of entire landform features, namely the boulder berm at Black Rock. Many hundreds, if not thousands of intertidal boulders were seen to have been moved over 7.5 m in some areas across the platform surface during/following the storm events of 2013 - 2014. This casts further doubt on the perceived geomorphic quiescence of such sheltered coastal locations and suggests that contemporary storm waves present a much greater threat in terms of larger-scale broader geomorphic modification.

(2) RFID tagging as a mean of quantifying boulder transport.

This study, and the subsequent findings are unique in terms of being able to quantify boulder transport in the intertidal zone. This has been achieved via the successful deployment and recovery of the RFID tagged boulders. Based on previous RFID sediment tracing research, as highlighted in Chapter 2, table 2.1, this study is thought to be the longest-running RFID boulder transport field survey to date, currently 56 months. The longevity of the study, and subsequently the continuing

operation of the tags may reflect the limited displacement of the boulders when compared to RFID tracer studies on gravels and cobbles (Allan *et al*., 2006; Dolphin *et al*., 2016). These two studies ran for a period of 17 and 36 months respectively with Dolphin *et al*. (2016) recording maximum transport distances exceeding 1000 m. The restrictive boulder transport distribution is likely to prove favourable in terms of promoting longer-term studies. The limited rate of dispersal will limit the likelihood of damage to the tag and aid swift relocation, thus improving tag recovery rates.

The modified field methodology presents coastal researchers with an alternative technique which presents an opportunity for the long-term assessment of boulder displacement in a range of coastal settings. Future studies will assist in elucidating the boulder transport process and providing further insight to the role of storm wave activity on geomorphic modification to rocky coasts.

(3) Platform topography/morphology plays significant role in facilitating and hindering transport.

A principal outcome from the findings was the influence of surface topography and morphology on enabling boulder transport. By classifying tagged boulders as either constrained, or unconstrained in their ability to be displaced it was possible to determine the relationship between the pre-transport setting and the distance over which displacement occurred. As hypothesised, the data analysis suggested a statistically significant difference between transport distances amongst those boulders categorised as constrained versus unconstrained (maximum p-value ≤ 0.03) which corroborates the findings of Naylor *et al*. (2016). Observational insight from the plate-forme à vasques study (Chapter 4) also identified the significant role of platform topography in the boulder displacement process. The research identifies a host of physical, chemical and biological erosive agents which act to create distinctive landform features that directly contribute to platform evolution and influence the boulder transport process. Notably, each of the five RFID tagged boulders located in the vasques pools were transported during the study although they remained within the confines of the ridged pools which hindered landward mobility. This suggests the undulating topography created by the vasques pools impedes boulder displacement and promotes deposition.

A morphological factor which is seldom considered in transport studies is platform width. This imposes considerable influence on transport potential in terms of the exposed, wave-swept platform acting as a transport corridor which facilitates displacement. Therefore, the greater the width of the platform, the greater the transport potential. This was reflected in the study as the maximum platform width at Bembridge Ledge and Black Rock were 55 m and 40 m respectively; the documented transport distances for the sites were 152.8 m and 80.2 m. Whilst a host of

additional factors are necessary in facilaiting the displacement of intertidal boulders, transport potential should be considered when considering appropriate management practices aimed at mitigating against landform modification and the risks posed by future storm wave hazards and the associated inundation events.

(4) Improved understanding of the mode of transport.

As part of the modified RFID tagging methodology a transport mode indicator was included to distinguish the mode of boulder transport, either sliding, or overturning. This was achieved by using a rudimentary technique in which a hole was drilled above the embedded tag at the time of deployment. This identified the upward orientation of the boulder at the commencement of the field study. Any relocated boulder found to have been displaced and displaying the orientation hole below the tag could unequivocally be established as having been overturned during transport.

A lack of empirical field-based data relating to the transport mode means that much of the current research is based on assumptions draw from field observations (Mastronuzzi and Sansò, 2004; Knight *et al*., 2009) and/or hydrodynamic modelling (Nandasena and Tanaka, 2013b). By employing the orientation hole it was possible to determine that 13% of all transport events across both Bembridge sites (n = 195) resulted from overturning. Significantly, the data identifies that despite the relatively small proportion of transport events the distances attributed to overturning accounted for 38% of the transport total (233.0 m) suggesting that although overturning events are less frequent, the resulting transport is significant.

The significance of understanding how boulders respond to hydrodynamic conditions under which they have been displaced is of considerable value when employing numerical models to hindcast wave characteristics such as height and/or velocity (Goto *et al*., 2009). Conceivably, the simple addition of the orientation hole could assist in generating valuable data which can be applied to help refine existing hydrodynamic equations.

(5) Insight to the boulder production process

An integral aspect in the boulder transport process is the production phase. The study highlights the key mechanisms which enable detachment to occur. Fundamental to boulder production are the processes of quarrying and undermining both of which occur at the shore platform edge. These processes are influenced by two factors (i) geology/lithostructure at Bembridge Ledge; (ii) morphology at Black Rock.

The denser, more widespread geological discontinuities of the shore platform at Bembridge Ledge present a lithostructure that is receptive to block removal by wave quarrying. Furthermore, a readily erodible sub-platform layer of marl presents the opportunity for undermining of the boulder-producing limestone unit; this further aids the production process. Conversely, the more consolidated bedrock unit of the Black Rock platform is deficient in geological discontinuities. However, through a process of attrition a low-tide notch has been created below the platform which creates an overburden at the platform edge. In addition, a recently discovered subterranean network of cavities beneath the platform unit presents a supplementary structural component that promotes further undermining. These dual factors result in an ever-increasing overburden which undermines the platform and enhances gravity loading. Bedrock fractures occur at the platform edge when the resisting force of the rock is exceeded which produces blocks that are then available for transport.

(6) A proposed, modified conceptual model for boulder production, transport and deposition.

Based on the collated data and observational findings in the field an improved understanding of the mechanisms affecting boulder transport processes has been derived. Existing research focuses on the transport mode and frequently overlooks the pre-and post transport phases of production and deposition. The findings herein identify the three key phases as being interlinked and fundamental in shaping the wider geomorphology and evolution of the site. This is theorised in the conceptual model depicted in Figure 5.16.

The conceptual model, modified from Stephenson and Naylor (2011) presents insight to the boulder 'life-cycle', from source (production), through transport, to sink (deposition). The linked processes occur in the same manner irrespective of site location. This is further demonstrated having applied the model to sites at Kimmeridge Bay and Lyme Regis. Despite differences in boundary conditions at all sites the same outcomes identified in the model are replicated, suggesting an element of equifinality. Production is reliant on a suitable lithostructural component; transport is facilitated by unobstructed passage across the wave-swept platform; and deposition results from the dissipation of wave energy and/or due to interference with platform features (e.g. scarps) or other surficial deposits.

In producing the conceptual model it is conceivable that it may present coastal managers and researchers alike with a visual assessment tool to qualitatively appraise the extent to which boulder transport occurs at any given coastal location.

Study limitations

The study was conducted to document and quantify boulder transport arising from contemporary storm conditions and more broadly to improve understanding of the processes that regulate such displacement in a fetch-limited coastal location. This was achieved by conceiving and implementing a novel, field-based methodology involving sediment tracing. The deployment of RFID tags, whilst widespread in finer-graded sediments such as pebbles and cobbles, has not previously been employed for such a long-term study on boulder-sized clasts. The data obtained from the RFID tagged boulders assisted in achieving the study aims and research objectives. However, being the first research study of its kind presented a number of fundamental limitations that are addressed further.

Measurement accuracy

The level of accuracy in recording the boulder coordinates during relocation surveys is discussed at length in the 'Defining boulder transport' section (Chapter 2, page 55 - 56). The measurement accuracy was based on the cumulative error associated with the relative accuracy of the DGNSS, the setup of the base station and the re-surveying of the RFID tagged boulders. With an added contingency the figure was set at 0.1 m. This value served a dual purpose in that it was also used to establish a boulder entrainment/transport threshold. The recorded boulder coordinate data allowed for a distance measurement (m) to be attributed to the displacement of each boulder between field surveys. Distance values between coordinate points that fell below the entrainment/transport threshold of 0.1 m were considered to be entrained opposed to transported and were not included in the transport distance totals. The application of this threshold value results in entrainment values (those recorded measurements < 0.1 m) being omitted from the published transport data. Thus, the cumulative distance of both entrainment and transport would mean the recorded values presented herein would have been marginally higher. It is suggested that future studies make reference to the distinction between these two separate values.

RFID relocation surveys

Over the three-year study a total of 17 field surveys were completed. These surveys were undertaken principally to relocate RFID tagged boulders. Despite the relatively close proximity of the study sites to the University of Portsmouth campus (approximately 12 km) it was necessary to travel by car and ferry to reach the destination. In addition, the tidal state at Bembridge had to be conducive to allow the field survey to be completed in a safe and suitable time-window; surveying

commenced on the falling tide and was completed on the rising tide. Furthermore, it was impossible to conduct a field survey with any fewer than two operatives, one to carry out the RFID detection equipment and document relevant details, another to record the boulder locations using the DGNSS. Availability of the required field equipment and accompanying operatives was often irregular. These factors each presented a financial and logistical burden that frequently hampered response rates to storm activity. Had these factors been more manageable an increasaed number of field surveys could have been completed. This would have provided a greater temporal frequency and granted further insight to boulder transport response to contemporary storm conditions.

Boulder selection

The boulders selected for tagging were all located within the intertidal zone. As a result boulder relocation field surveys had to be conducted during low water in a short tidal window of approximate 4 - 6 hours. In order to achieve this it was necessary to restrict the number of boulders that needed to be relocated. It was found that two field operatives were able to undertake the relocation of approximately 50 - 55 boulders in the allocated time available across the survey area. This meant that all findings presented are based on a limited number of boulders from each site. With an increased number of tagged boulders it would have been possible to gather additional transport data which may have provided further insight to the complex mechanisms governing boulder transport processes. However, in order to relocate those additional boulders more field equipment would be required (i.e. additional RFID detection kit and DGNSS). This would require additional manpower resource of at least a further 2 operatives which was not feasible. However, despite the limited number of tagged boulders the data arising provided a wealth of valuable data that revealed the capability of low-magnitude, high-frequency storm activity to displace boulders within the intertidal zone which was hitherto undocumented.

Conclusion

Transported coastal boulders located in the supra- and intertidal zone have been used extensively as a diagnostic tool to infer wave magnitude as an agent of transport (Barbano *et al*., 2010; Switzer and Burston, 2010; Vacchi *et al*., 2012; Cox *et al*., 2012; Shah-Hosseini *et al*., 2013 Autret, *et al*., 2016). However, to date, research in this area focuses on coastal zones which are regularly exposed to extreme wave conditions where clast displacement is to be expected. As a result boulder transport in lower energy coastal settings has hitherto been widely neglected (Dasgupta, 2011). Consequently, there is limited understanding of the extent to which boulder transport occurs in such settings under moderate, contemporary storm conditions, moreover, what are the

fundamental morphological, lithological and hydrological mechanisms that facilitate such displacement?

The aims of this research were based on addressing these omissions and developing an increased awareness and understanding of boulder transport dynamics at a field site subjected to a low/moderate wave climate. Primarily, the intention was to accurately quantify the degree to which intertidal boulders were displaced as a result of contemporary storm waves. This was achieved by creating an array of 104 RFID tagged boulders using indigenous limestone clasts located at Bembridge, a relatively sheltered intertidal location on the eastern side of the Isle of Wight. The coordinate position of each boulder was recorded at the time of RFID deployment, and displacement was periodically monitored over a three year period. The relocation and rerecording of the RFID tagged boulder locations provided a series of consecutive coordinate waypoints. The amassed boulder coordinate data was processed using a bespoke Python script (Appendix 1) which produced a numerical output via an Excel spreadsheet which quantified a range of geospatial statistics including boulder transport distance (m) and azimuth (°). An additional output was generated via ArcGIS which generated a vector plot depicting the transport pathways for each transported boulder (Appendix 2).

The resulting data from this field-based research has helped achieve the assigned aim of quantifying the extent to which contemporary storm waves displace intertidal boulders. On completion of the study the total transport distance attributed to the tagged boulder array was 233.0 m. This clearly demonstrates that boulder transport occurs under moderate storm conditions confirming that displacement is not the exclusive preserve of coastal settings subject to extreme wave activity. Significantly, it was established that even the largest tagged boulders weighing in excess of 5.0 t and 10.0 t were periodically mobilised and in some cases overturned. Additionally, evidence of landform modification has been recorded via the exhumation and reworking of sizable clasts within the intertidal zone. The dynamism of the selected field sites is also manifest in macro-scale modification to extensive morphological features (boulder berm).

Despite storm waves being sufficient to mobilise very coarse sized boulders it was noted that much smaller clasts failed to be displaced throughout the duration of the study. This was attributed to the morphological setting of each tagged boulder. Displacement was found to be obstructed by a range of morphological features ranging in size from tens of centimetres (e.g. previously displaced boulders) to tens, even hundreds of metres (e.g. plate-forme à vasques, boulder berm). The findings

identified that transport distances were significantly greater in those boulders that were unconstrained in their ability to be displaced when compared with constrained boulders.

The litho-structural component of the boulder-producing units was also deemed to be of consequence. The greater transport distances were recorded at Bembridge Ledge (152.8 m) when compared with Black Rock (80.2 m). This is in part attributed to the difference in the discontinuities of the boulder-producing units at each site. The heavily jointed boulder-producing unit at Bembridge Ledge has clearly defined bedding and jointing as opposed to Black Rock which is devoid of such geological characteristics. This leads to the quarrying of smaller, more readily transportable boulders at Bembridge Ledge.

Storm wave data obtained from the nearby wave monitoring station recorded hydrodynamic conditions throughout the study. They recorded a maximum inshore H_s of 2.3 m. Comparison was drawn from the recorded wave heights and the calculated minimum wave heights required to initiate displacement in the three largest RFID tagged boulders. This was based on the calculated values derived from the widely cited Nandasena equation (Nandasena *et al*., 2011b). A significant disparity was established between the recorded and calculated wave heights which overestimated wave magnitude by as much as 118%. The findings support the recommendation of Zainali and Weiss (2015) that simplified hydrodynamic equations be modified to account for findings from three-dimensional simulations. We also suggest the inclusion of a parameter that accounts for the presence/absence of morphological obstructions that are identified herein as exerting significant impediment to boulder displacement.

Using field-based quantifiable and observational evidence a modified conceptual model has been presented that highlights the universality of the boulder production, transport and deposition process. Despite the multiplicity of different interrelated controlling factors at contrasting field locations the same processes and mechanisms and resulting landform signatures are apparent across a range of scales. Furthermore, variance in the factors influencing intra-site boulder production, transport and deposition can result in disruption to the process, meaning transport can occur at one site location but not another. It is proposed that the conceptual model may act as a beneficial management tool for the identification of boulder transport sites providing users with an immediate qualitative assessment of coastal vulnerability based on the extent to which boulder displacement occurs.

This research advances the current understanding of boulder transport by accurately quantifying displacement in response to contemporary storm wave activity and presenting additional insight to

the key processes and mechanisms that are required to initiate clast mobility and subsequent deposition. The successful quantification of boulder displacement using the novel RFID tracing technique is testament to the applicability of the methodology. This provides coastal researchers with a 'tried and tested' technique that can be deployed at any coastal location to accurately quantify boulder transport and landform modification resulting from contemporary and extreme storm wave events. Furthermore, the unequivocal data produced suggests its use would be of benefit in coastal areas where debate exists over whether boulders have, or have not been displaced (Cox, 2019), or where the transport mode is contested (Morton *et al*., 2008; Lorang, 2011). Such deployments could provide an opportunity to better understand wave competence and conceivably, may elucidate the storm and/or tsunami wave conundrum.

The more widespread use of the RFID methodology in a range of coastal settings will act to further enhance our understanding of the responsiveness of rocky coasts in a changing global climate. Improved understanding of the response mechanisms will be critical in accurately assessing coastal vulnerability and risk and mitigating against future storm wave hazards. It is anticipated that this data will better inform policymakers tasked with adaptive planning to improve resilience and safeguard coastal populations, infrastructure and natural capital on a global scale.

Appendices

Appendix 1 - Python Script

```
Creator: M.Schaefer, GIS Manager, University of Portsmouth
Title: Point to point comparison over time.
Purpose: Monitor change over time for uniquely identified points.
Data Requirements: A list of identified points that have been measured over multiple surveys.
This program will work out the distance, azimuth and change in height between every instance of
a point with the same ID.
   Input is a csv file with no heading:
      year (or survey ID), id, x, y, z
         e.g. 2008,FEAT01,449850.6,75308.663,19.9
Required modules: sys, os, csv, pandas, numpy, arcpy
Python version: 2, 3
ESRI: ArcGIS Desktop, ArcGIS Pro
Data output: Two shapefiles, point and line. Two csv files, one with movement between surveys
and one with total movement between first and last survey.

"""
import sys
import os
import arcpy
import csv
import pandas as pd
import numpy as np
import itertools

def proc_main():
   """
   Main try-except-finally block with error handling
   """
   arcpy.AddMessage('Starting...')
   try:
      #Run actual functionality
      proc_run()
   except Exception as e:
      arcpy.AddMessage  ('Error: {}'.format(str(e)))
   finally:
      arcpy.AddMessage ('Completed')

def proc_run():
   """
   Main program functionality
   """
   # Overwrite pre-existing files
   arcpy.env.overwriteOutput = True
   in_file = arcpy.GetParameterAsText(0)
   proj = arcpy.GetParameterAsText(1)
```

```
    #
    arcpy.AddMessage('Processing: {}'.format(in_file))
    #file management
    fsplit = func_pathsplit(in_file)
    survey_comp = os.path.join(fsplit[0], fsplit[2] + '_InterSurveyData.csv')
    total_comp = os.path.join(fsplit[0], fsplit[2] + '_TotalSurveyData.csv')
    shpoutput = os.path.join(fsplit[0], fsplit[2] + '_MovementLine.shp')
    #create line shp
    arcpy.AddMessage('Creating: {}'.format(shpoutput))
    arcpy.CreateFeatureclass_management(fsplit[0],
                                fsplit[2] + '_MovementLine.shp', 'POLYLINE', '',
                                'DISABLED', 'ENABLED', proj)
    #create point shapefile from input
    proc_point(in_file, proj)
    #process movement
    header = ('timestamp', 'id', 'x', 'y', 'z')
    df = pd.read_csv(in_file, names = header, index_col = False)
    #process data
    c_o_time, c_total = func_change(df)
    #write output file
    #arcpy.AddMessage('Writing: {}'.format(survey_comp))
    c_o_time.to_csv(survey_comp, index_label = 'index')
    c_total.to_csv(total_comp, index_label = 'index')
    #create line shp
    lines = proc_create_lines(df, shpoutput)
    arcpy.AddField_management(shpoutput, 'Length', 'FLOAT', 8,2)
    arcpy.CalculateField_management(shpoutput, 'Length', '!shape.length!', 'PYTHON')

def func_pathsplit(in_file):
    """
    Helper function, splits full paths into components
     Output: [dir,full filename, filename no ext, ext]
            0       1            2        3
    """
    dir = os.path.dirname(in_file)
    fullfile = os.path.basename(in_file)
    noext = os.path.splitext(fullfile)[0]
    ext = os.path.splitext(fullfile)[1]
    return [dir, fullfile, noext, ext]

def proc_point(in_file, proj):
    """
    Take a csv file with no header and XYZ in fields 3,4,5
    """
    fsplit = func_pathsplit(in_file)
    outShp = os.path.join(fsplit[0], fsplit[2] + '_MovementPoints.shp')
    arcpy.MakeXYEventLayer_management(in_file,'FIELD3','FIELD4','Lyr',proj,'FIELD5')
    #create point shp
    arcpy.AddMessage('Creating: {}'.format(outShp))
    arcpy.CopyFeatures_management('Lyr',outShp)
```

```
def proc_create_lines(in_df, shpoutput):
    """
    input [key: [year, id, x, y, z]]
              0   1  2  3  4
    """
    #Check ID Datatype
    if in_df['id'].dtype.kind in 'i':
        arcpy.AddField_management(shpoutput, 'Point_ID', 'SHORT', 8)
    elif in_df['id'].dtype.kind in 'f':
        arcpy.AddField_management(shpoutput, 'Point_ID', 'DOUBLE', 8,2)
    else:
        arcpy.AddField_management(shpoutput, 'Point_ID', 'TEXT', 12)
    #loop through df
    exclude = []
    for values in in_df.itertuples():
        #process every point id only once
        if values[2] not in exclude:
            #for each point find all instances of that point --> df of all matching points
            df1 = (in_df[in_df['id'] == values[2]]).sort_values('timestamp')
            proc_write_line(df1, shpoutput)
            #
            exclude.append(values[2])
def proc_write_line(df_coords, shpoutput):
    """
    input coordinates of movement of one point over x years
    Input: df('timestamp', 'id', 'x', 'y', 'z')
    """
    point = arcpy.Point()
    array = arcpy.Array()
    cursor = arcpy.da.InsertCursor(shpoutput, ['Point_ID', 'SHAPE@'])
    for i in df_coords.itertuples():
        point.X = i[3]
        point.Y = i[4]
        point.Z = i[5]
        array.add(point)
    polyline = arcpy.Polyline(array)
    array.removeAll()
    cursor.insertRow([df_coords.iloc[0][1], polyline])
    del cursor

def func_change(df):
    """
    Run through df of points and calc distance between same points in different surveys
    Input: df('timestamp', 'id', 'x', 'y', 'z')
    Output: df change over surveys
            df change first to last survey
    """
    l = []
    l2 = []
    exclude = []
    #iterate through point data set
```

```
    for values in df.itertuples():
        #process every point id only once
        if values[2] not in exclude:
            #for each point find all instances of that point --> df of all matching points
            df1 = (df[df['id'] == values[2]]).sort_values('timestamp')
            length = len(df1)
            index = 0
            #compare every point to the subsequent timestamp
            while index < length - 1:
                l.append(itertools.chain(df1.iloc[index].values.tolist(), df1.iloc[index + 1].values.tolist()))
                index += 1
            #compare the first to the last timestamp for total change
            l2.append(itertools.chain(df1.iloc[0].values.tolist(), df1.iloc[length - 1].values.tolist()))
            #
            exclude.append(values[2])
    #convert to df
    cols = ('from_year', 'from_id', 'x1' ,'y1', 'z1', 'to_year', 'to_id', 'x2', 'y2', 'z2')
    df_yr_on_yr =  pd.DataFrame(l, columns = cols)
    df_final =  pd.DataFrame(l2, columns = cols)
    #calculate change through broadcasting
    df_yr_on_yr = calc_dist(df_yr_on_yr)
    df_final = calc_dist(df_final)
    return df_yr_on_yr.sort_values(['from_id', 'from_year']), df_final.sort_values(['from_id',
'from_year'])

   def calc_dist(df_out):
    """
    Calculates columns for dist, delta_z and azimuth
    input df('from_year', 'from_id', 'x1' ,'y1', 'z1', 'to_year', 'to_id', 'x2', 'y2', 'z2')
    output: df('from_year', 'from_id', 'x1' ,'y1', 'z1', 'to_year', 'to_id', 'x2', 'y2', 'z2', 'dist', 'delta_z',
'azimuth')
    """
    df_out['dist'] = np.round(np.sqrt((df_out['x1'] - df_out['x2'])**2 + (df_out['y1'] -
df_out['y2'])**2),3)
    df_out['delta_z'] = np.round(df_out['z2'] - df_out['z1'],3)
    df_out['azimuth'] = np.round(np.degrees((np.arctan2((df_out['x2']-df_out['x1']), (df_out['y2']-
df_out['y1'])))),0)
    #if azimuth is negative add it to 360
    df_out['azimuth'] = df_out['azimuth'].map(lambda x: 360 + x if x < 0 else x)
    return df_out

if __name__ == '__main__':
    #run main program
    proc_main()
```

Appendix 2 - Python ArcGIS transport vector plots.

The transport data output from the Python script (Appendix 1) calculates the Individual Boulder Transport Distance (IBTD) based on the accumulated values from all survey measurements. This includes calculated values that fall below 0.1 m.

As described in Chapter 2, pages 55 - 56, we incorporated a threshold value which allowed us to make the distinction between entrainment and transport. Boulder displacement values calculated via the Python script that fell below the threshold of 0.1 m were deemed as being entrained and were not included in the boulder transport data presented herein.

The vector plots act as a visual interpretation of the Python generated data with the Individual Boulder Transport Distance (IBTD) being based on the sum of the entrained and transported values. The small incremental episodes of entrainment (<0.1 m) have been omitted and the IBTD values displayed within this appendices have been amended to reflect transport values >0.1 m only.

RFID tag ID numbers from 1102 to 1151 were embedded in boulders located at Bembridge Ledge. The following vector plots from pages 197 - 209 represent transport vector plots from the Bembridge Ledge tagged boulders.

Appendices.

RFID tag ID: 1102
Individual Boulder Transport Distance: 0.7m

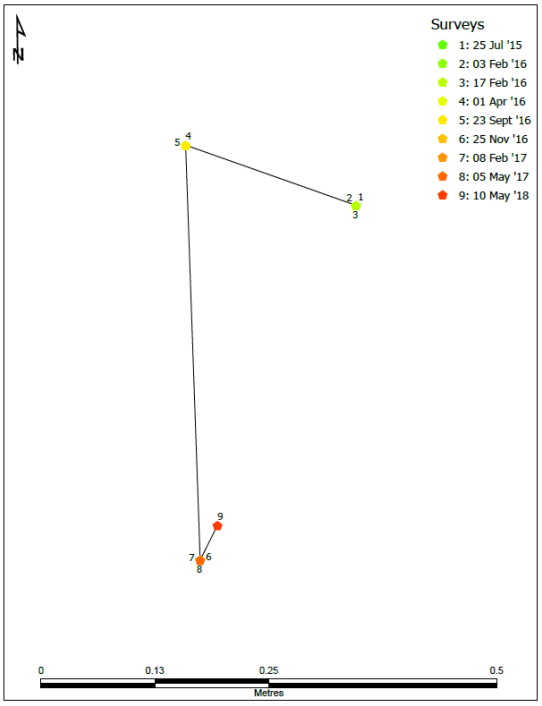

RFID tag ID: 1103
Individual Boulder Transport Distance: 0m

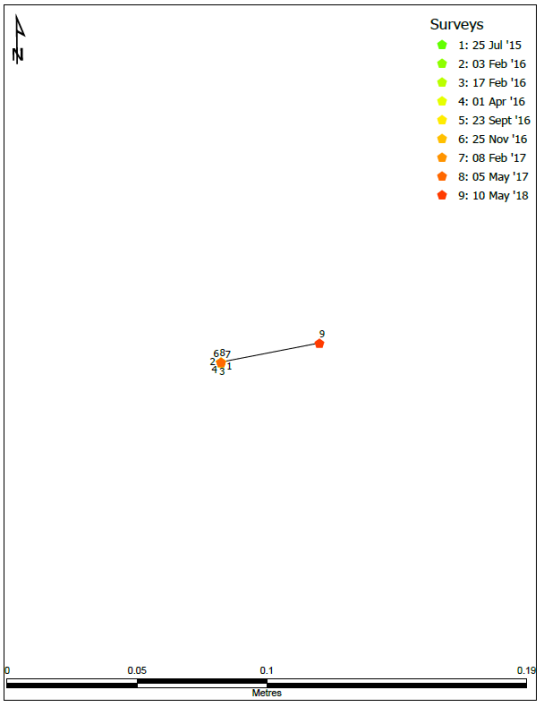

RFID tag ID: 1104
Individual Boulder Transport Distance: 1.5m

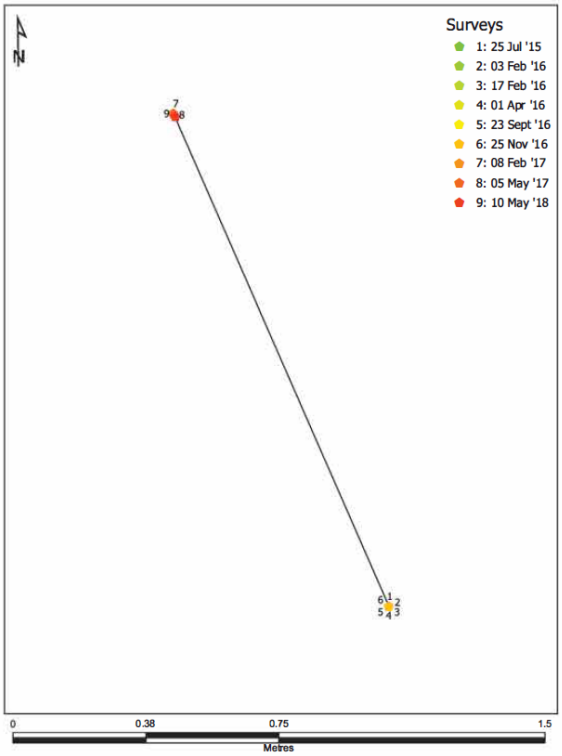

RFID tag ID: 1105
Individual Boulder Transport Distance: 1.3m

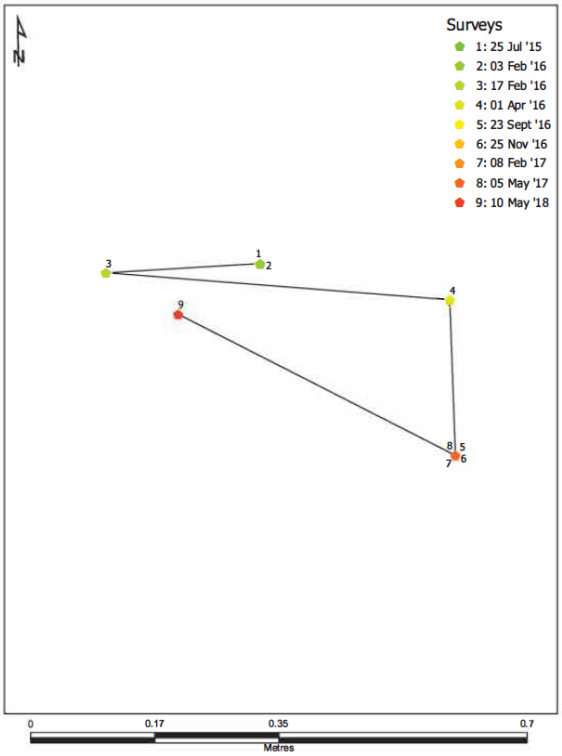

Appendices.

RFID tag ID: 1106
Individual Boulder Transport Distance: 0m

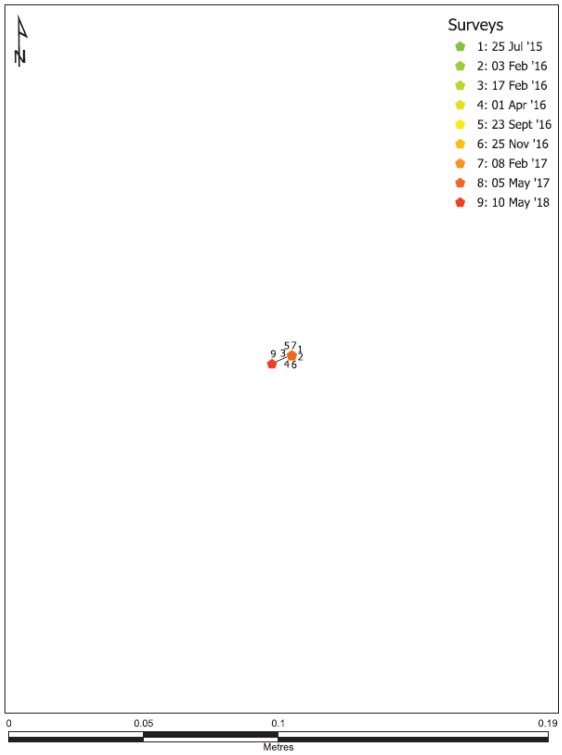

RFID tag ID: 1107
Individual Boulder Transport Distance: 2.7m

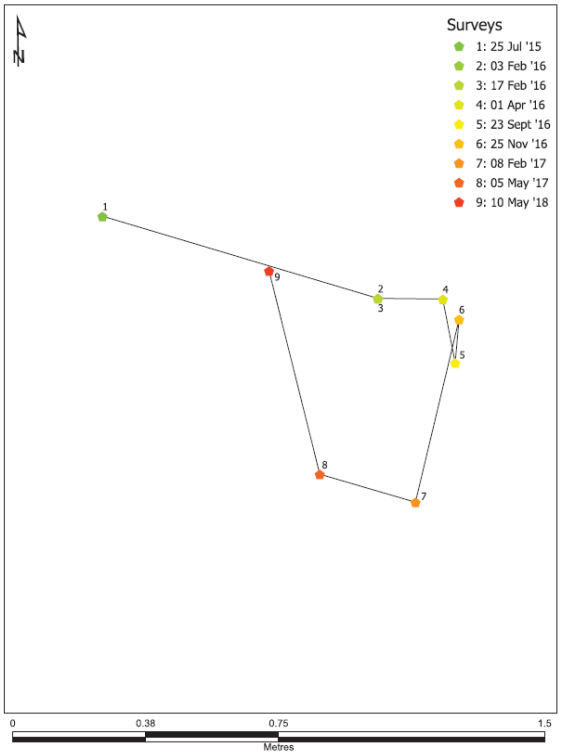

RFID tag ID: 1108
Individual Boulder Transport Distance: 9.7m

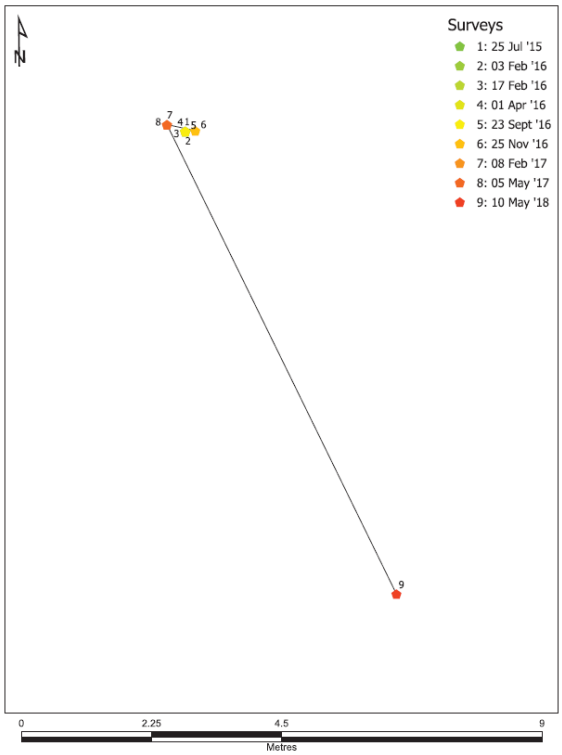

RFID tag ID: 1109
Individual Boulder Transport Distance: 3.2m

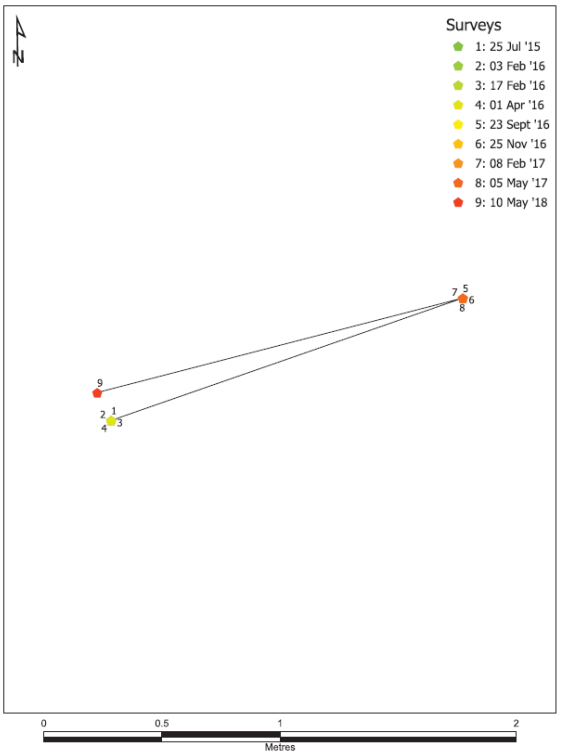

Appendices.

RFID tag ID: 1110
Individual Boulder Transport Distance: 0m

RFID tag ID: 1111
Individual Boulder Transport Distance: 5.8m

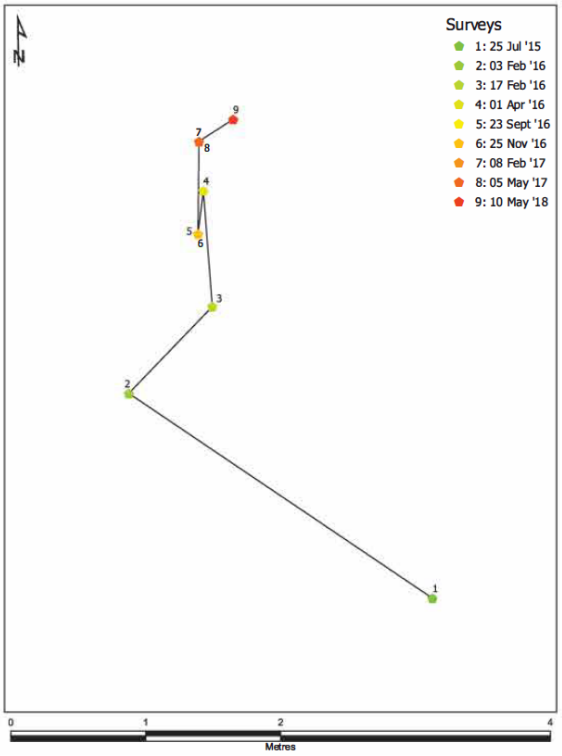

RFID tag ID: 1112
Individual Boulder Transport Distance: 1.2m

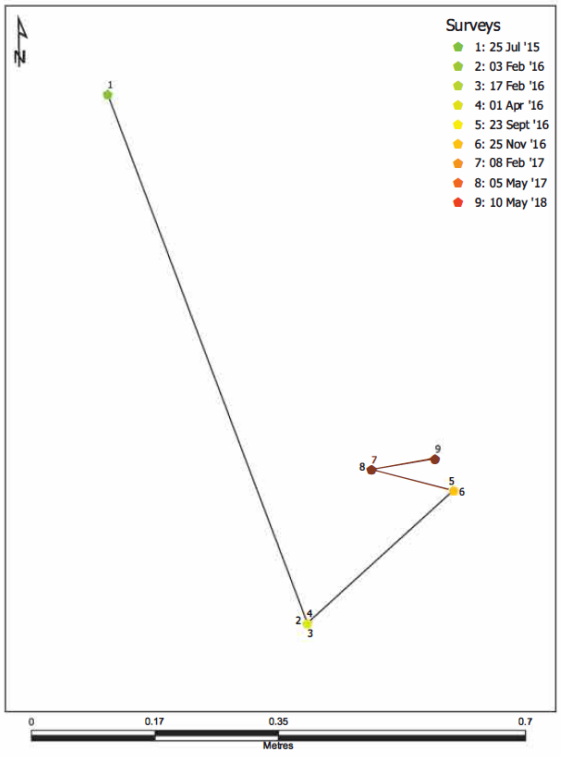

RFID tag ID: 1113
Individual Boulder Transport Distance: 0.1m

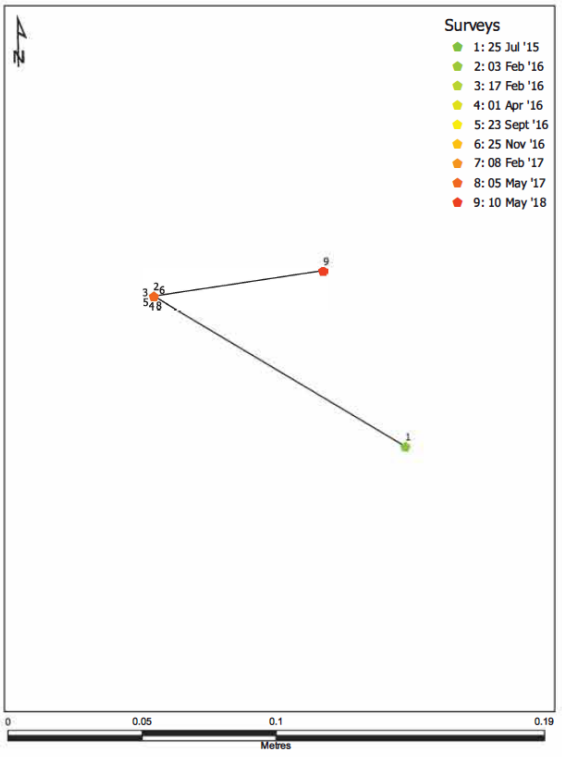

Appendices.

RFID tag ID: 1114
Individual Boulder Transport Distance: 0m

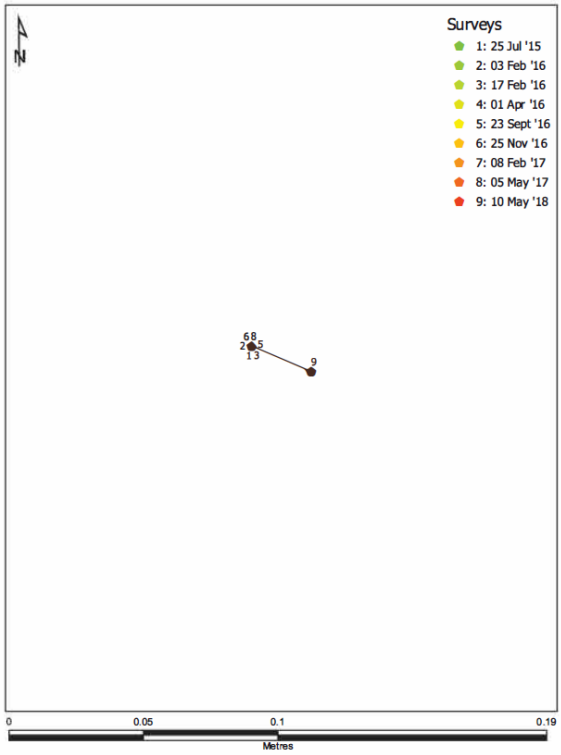

RFID tag ID: 1115
Individual Boulder Transport Distance: 0.5m

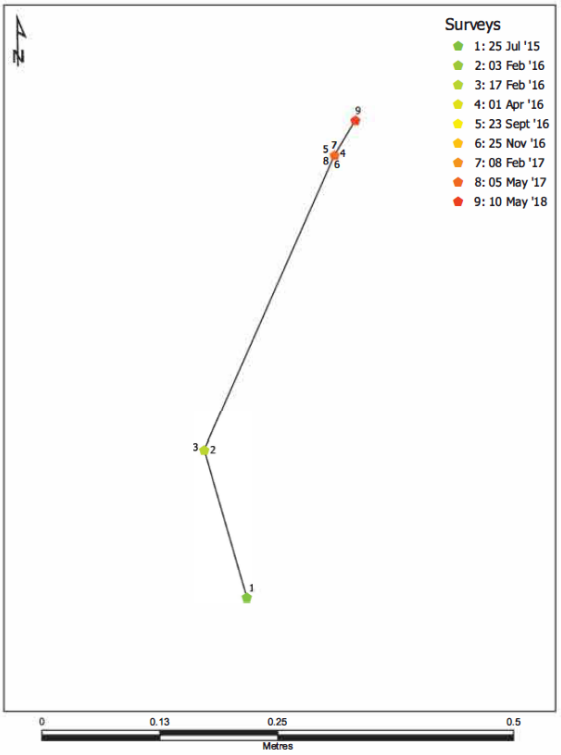

RFID tag ID: 1116
Individual Boulder Transport Distance: 0.8m

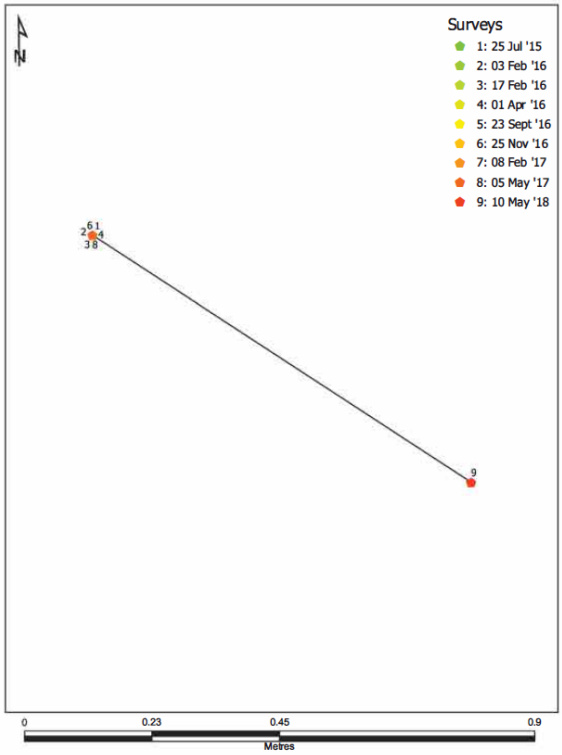

RFID tag ID: 1117
Individual Boulder Transport Distance: 0.7m

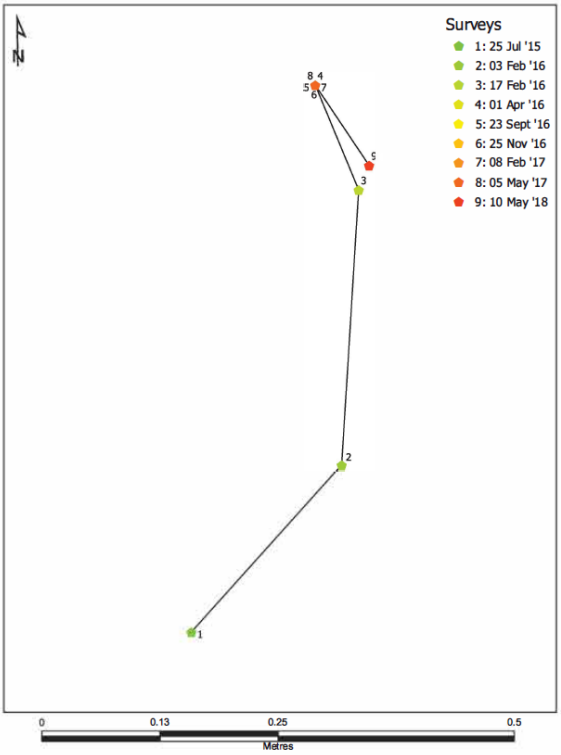

Appendices.

RFID tag ID: 1118
Individual Boulder Transport Distance: 0.6m

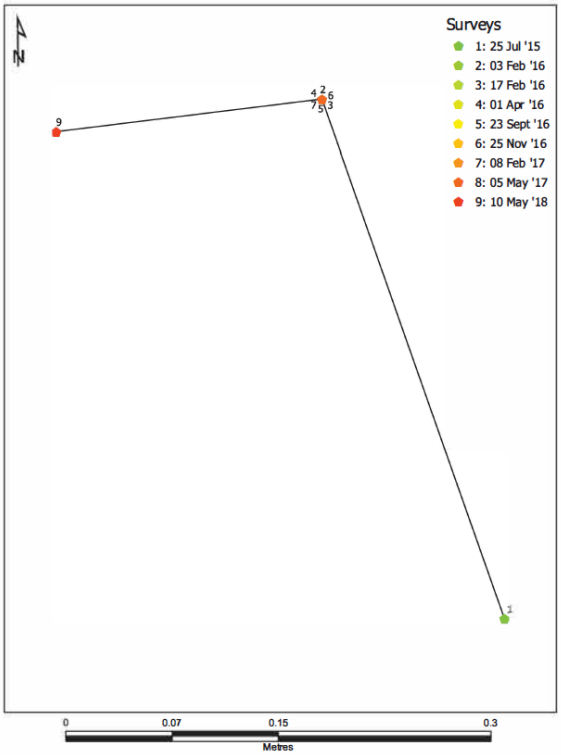

RFID tag ID: 1119
Individual Boulder Transport Distance: 0m

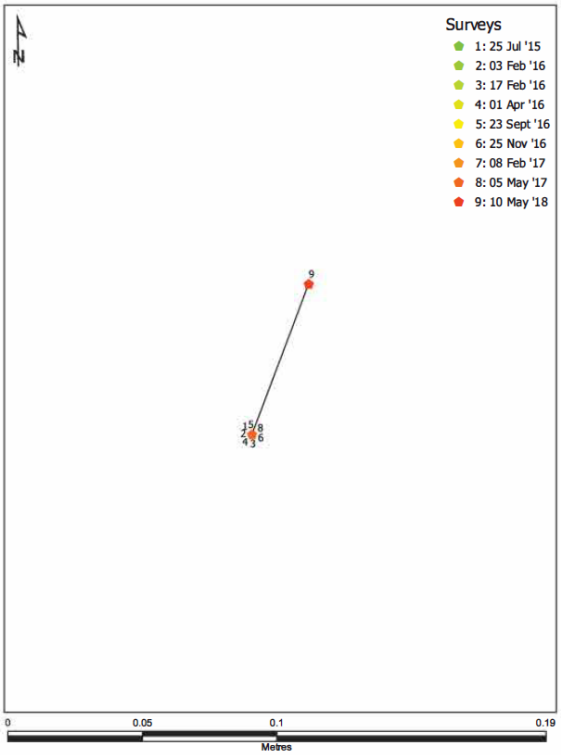

RFID tag ID: 1120
Individual Boulder Transport Distance: 2.1m

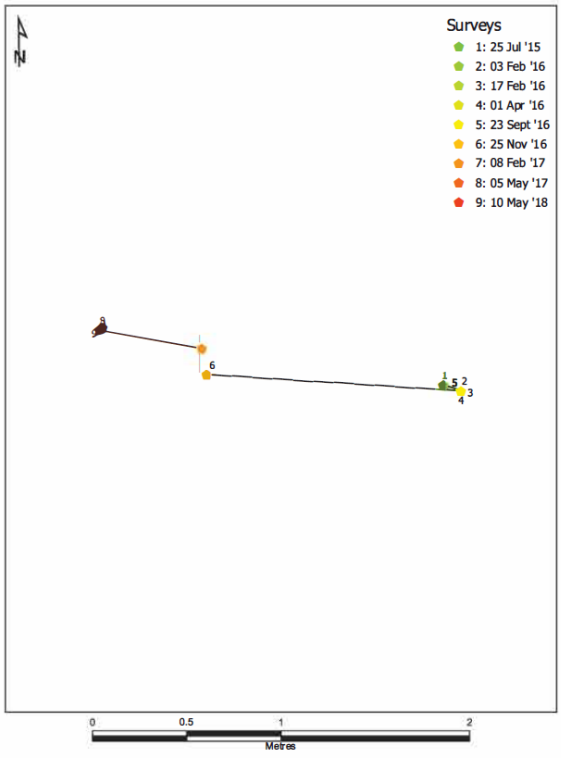

RFID tag ID: 1121
Individual Boulder Transport Distance: 0m

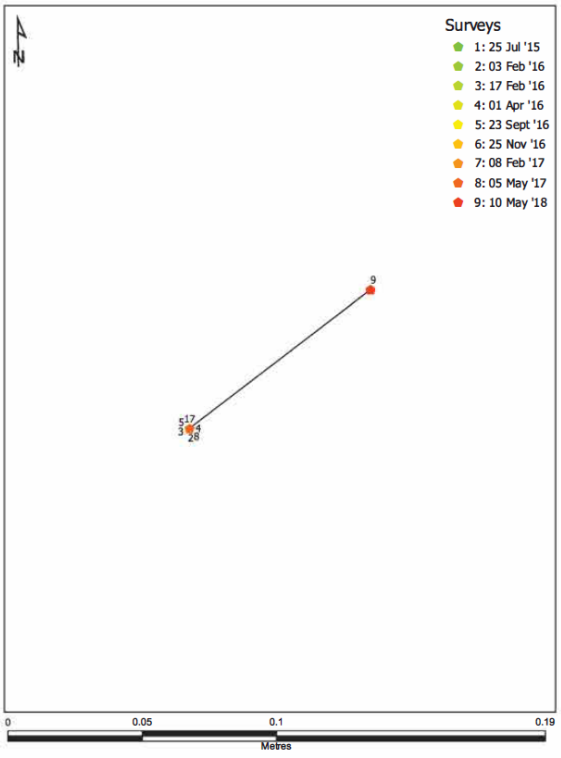

Appendices.

RFID tag ID: 1122
Individual Boulder Transport Distance: 0m

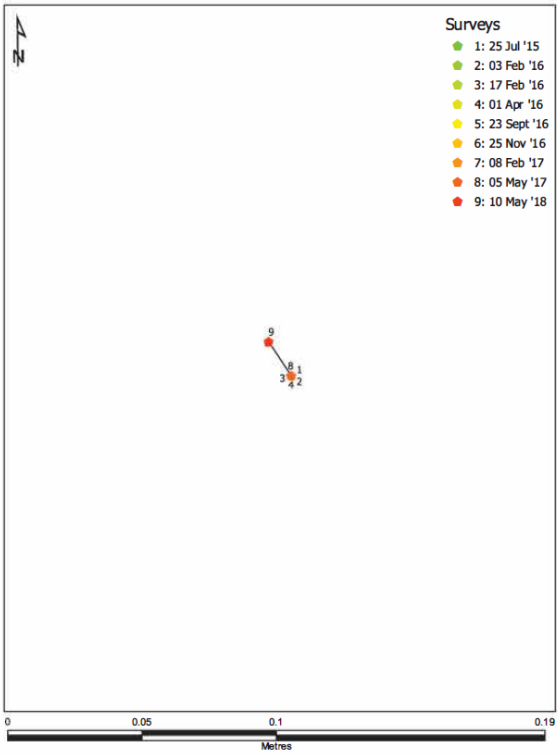

RFID tag ID: 1123
Individual Boulder Transport Distance: 1.3m

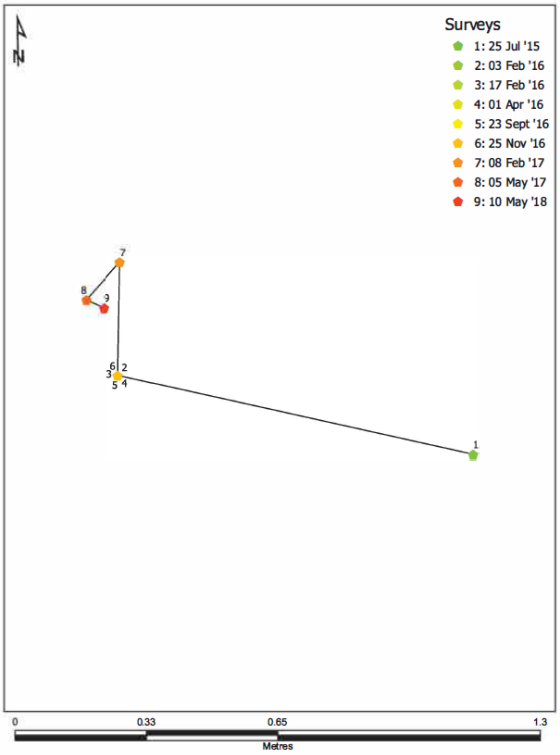

RFID tag ID: 1124
Individual Boulder Transport Distance: 0.4m

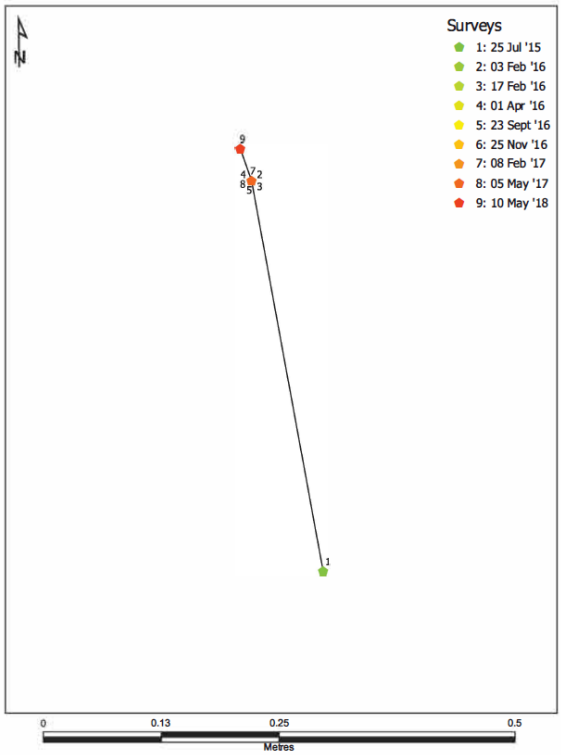

RFID tag ID: 1125
Individual Boulder Transport Distance: 0.4m

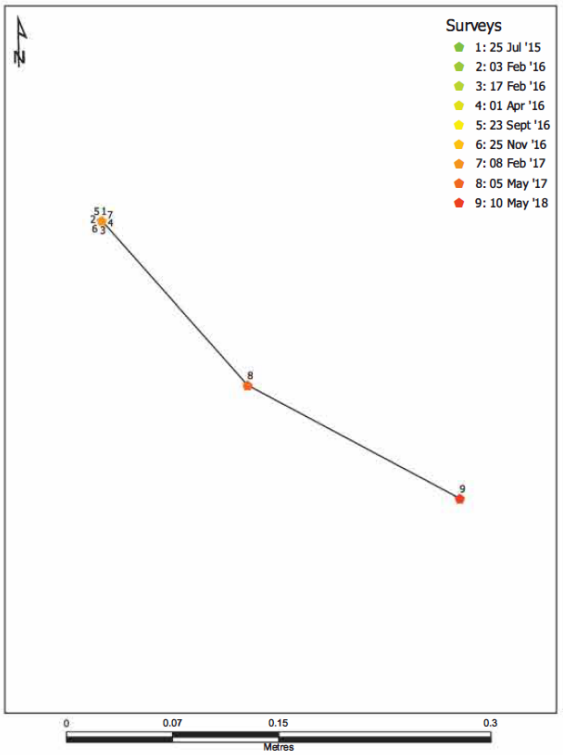

Appendices.

RFID tag ID: 1126
Individual Boulder Transport Distance: 0m

RFID tag ID: 1127
Individual Boulder Transport Distance: 10.2m

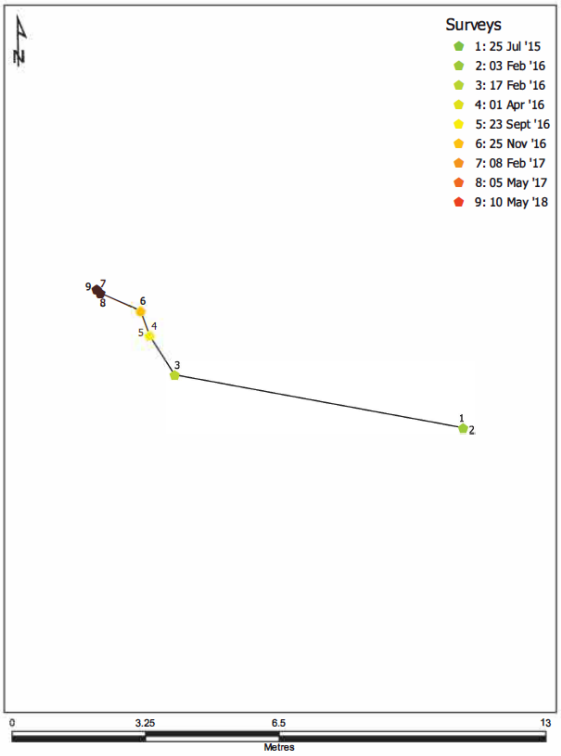

RFID tag ID: 1128
Individual Boulder Transport Distance: 9.4m

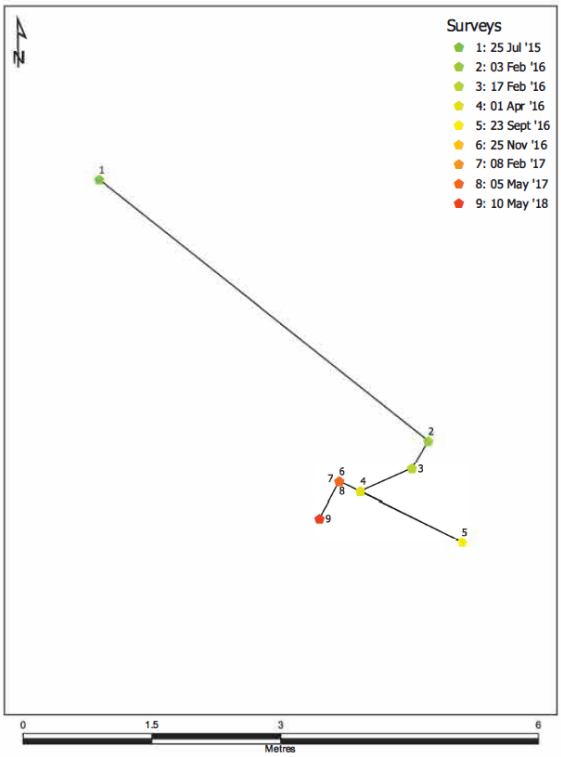

RFID tag ID: 1129
Individual Boulder Transport Distance: 2.7m

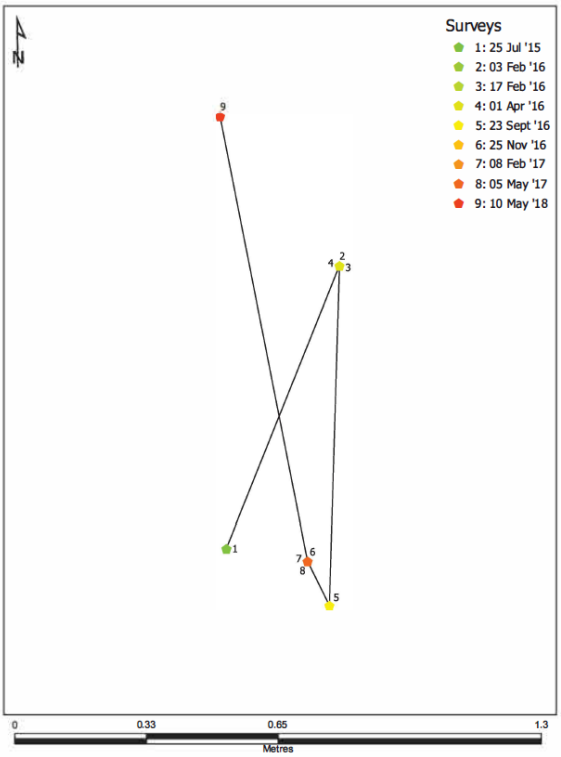

Appendices.

RFID tag ID: 1130
Individual Boulder Transport Distance: 1.2m

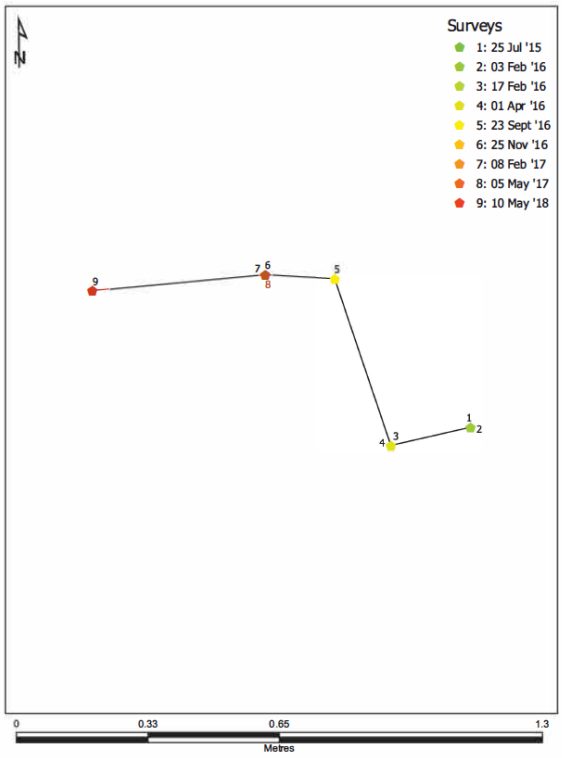

RFID tag ID: 1131
Individual Boulder Transport Distance: 0.5m

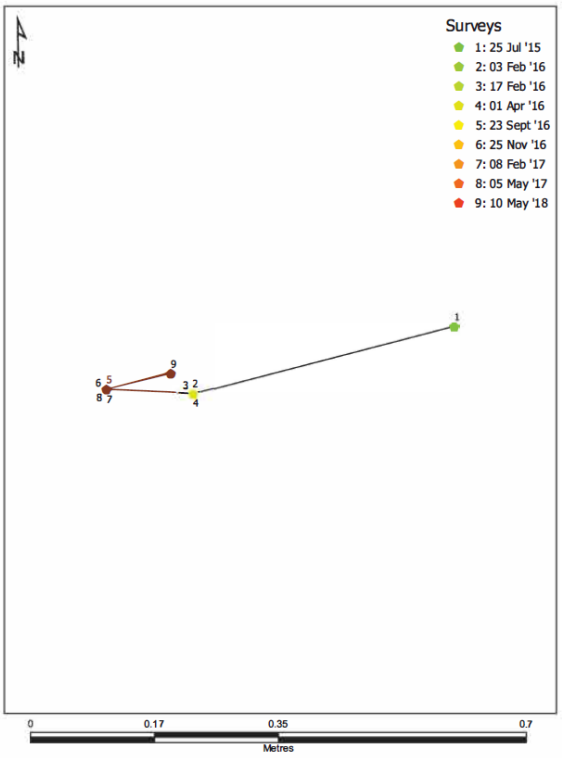

RFID tag ID: 1132
Individual Boulder Transport Distance: 0m

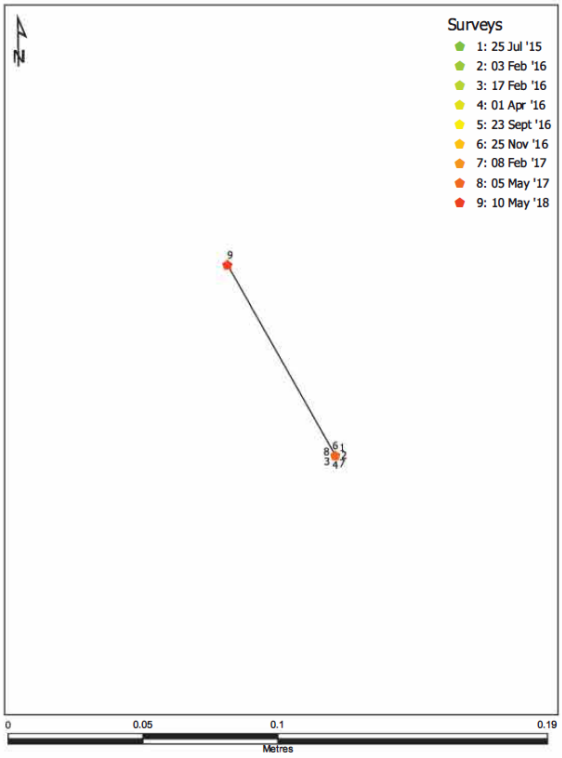

RFID tag ID: 1133
Individual Boulder Transport Distance: 0.9m

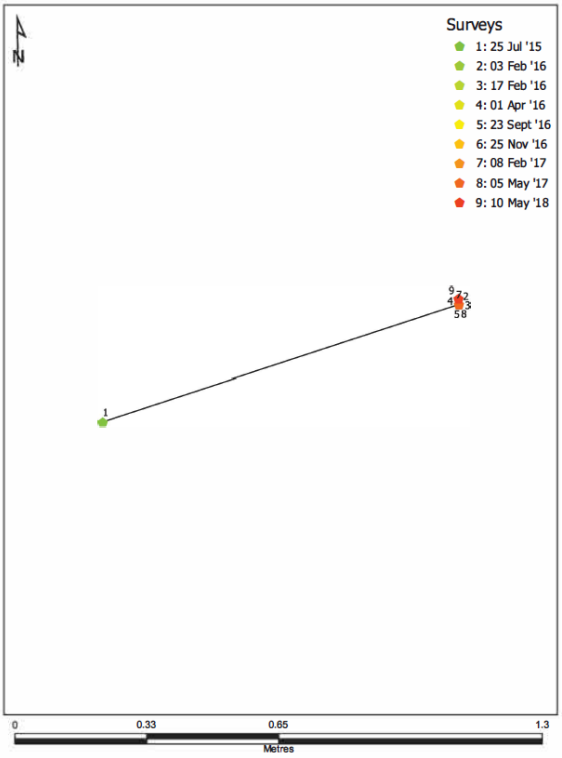

Appendices.

RFID tag ID: 1134
Individual Boulder Transport Distance: 14.6m

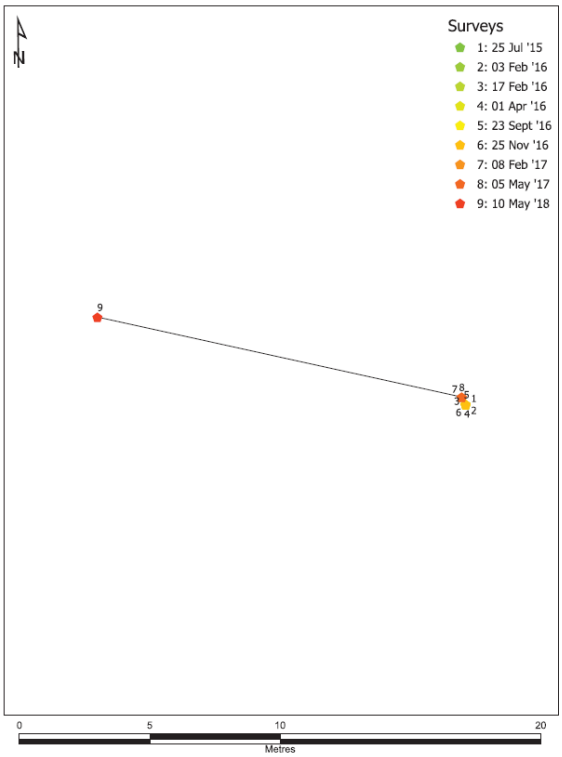

RFID tag ID: 1135
Individual Boulder Transport Distance: 0.1m

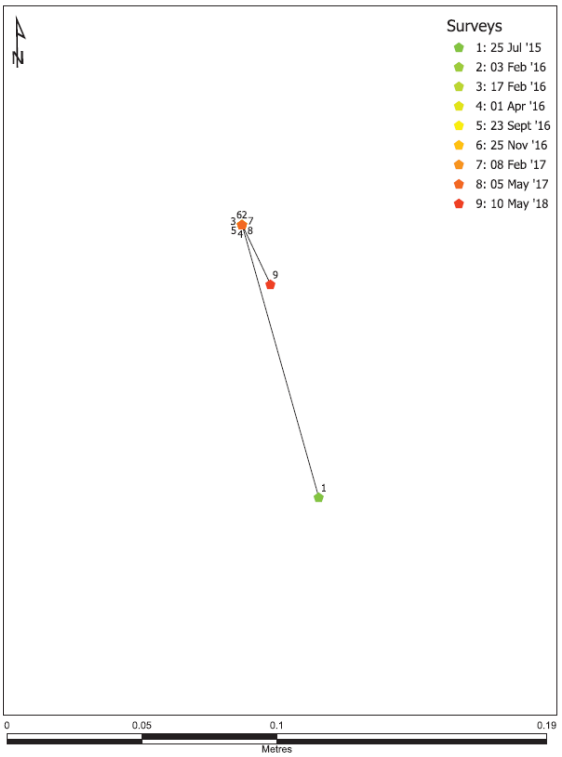

RFID tag ID: 1136
Individual Boulder Transport Distance: 0.2m

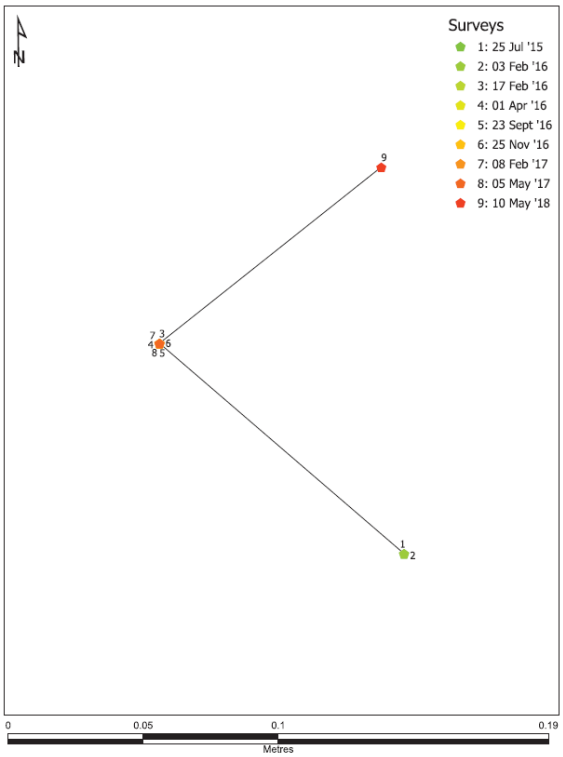

RFID tag ID: 1137
Individual Boulder Transport Distance: 0.3m

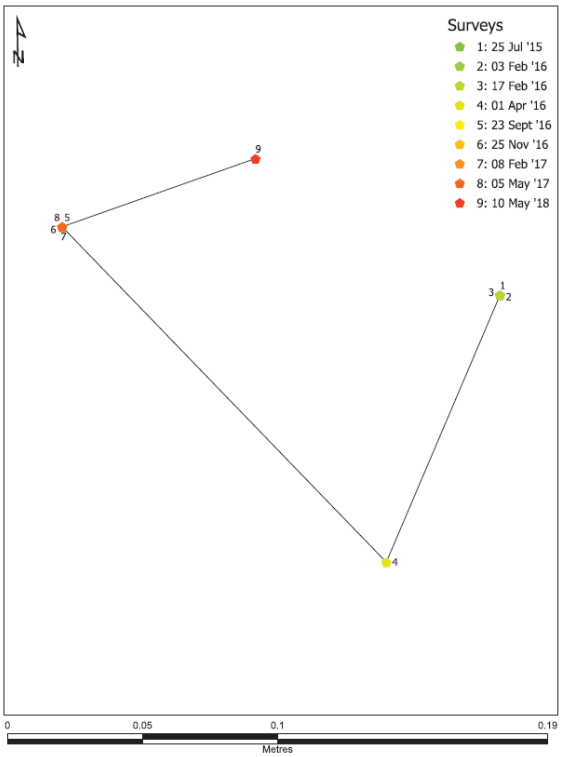

Appendices.

RFID tag ID: 1138
Individual Boulder Transport Distance: 0.3m

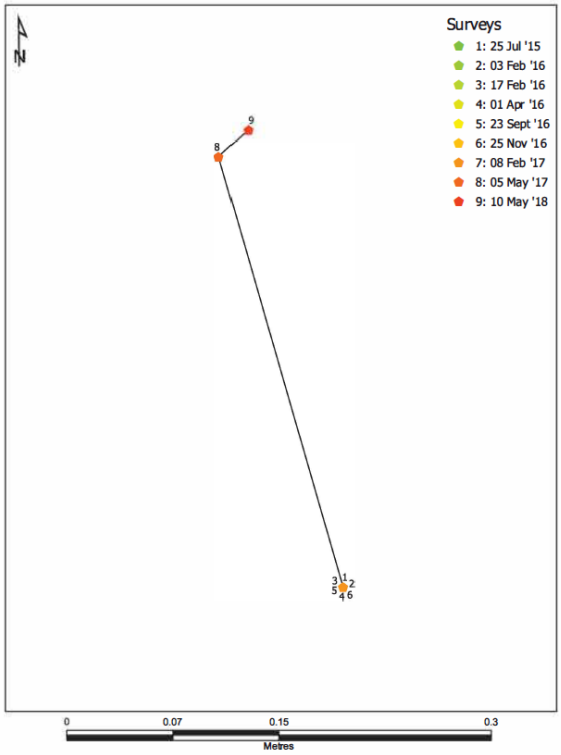

RFID tag ID: 1139
Individual Boulder Transport Distance: 0m

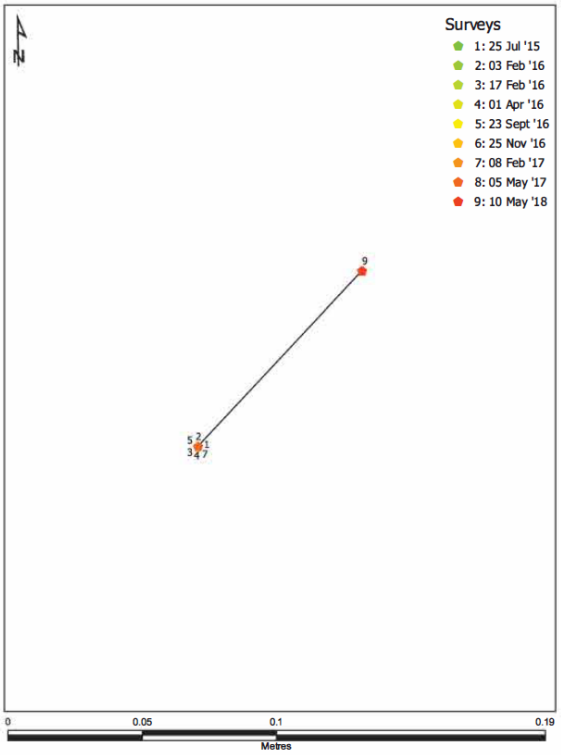

RFID tag ID: 1140
Individual Boulder Transport Distance: 13.2m

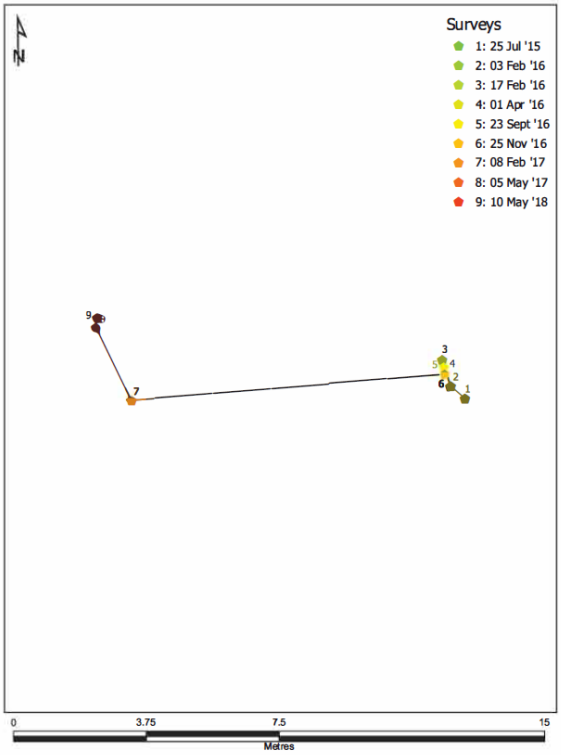

RFID tag ID: 1141
Individual Boulder Transport Distance: 0.1m

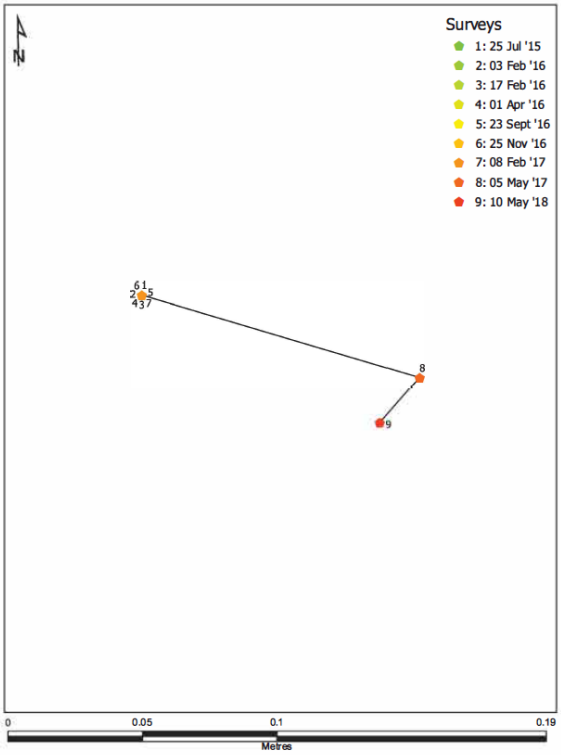

Appendices.

RFID tag ID: 1142
Individual Boulder Transport Distance: 0.2m

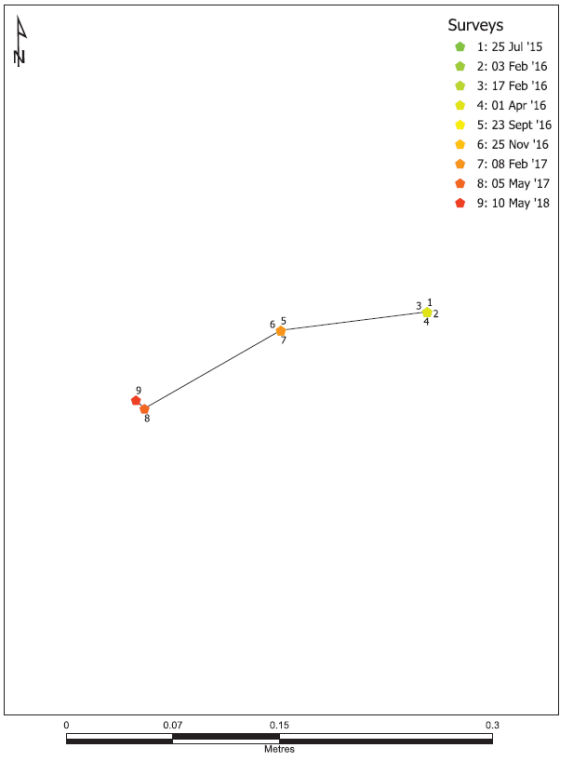

RFID tag ID: 1143
Individual Boulder Transport Distance: 21.5m

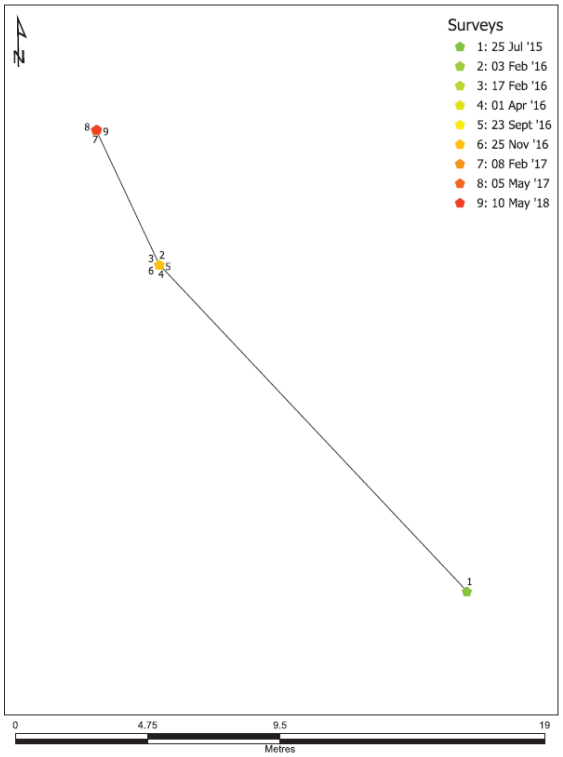

RFID tag ID: 1144
Individual Boulder Transport Distance: 16.4m

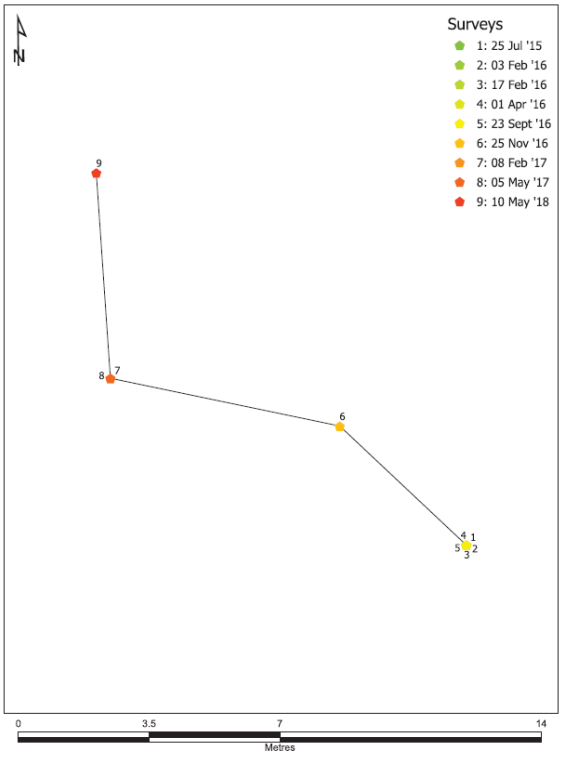

RFID tag ID: 1145
Individual Boulder Transport Distance: 0.4m

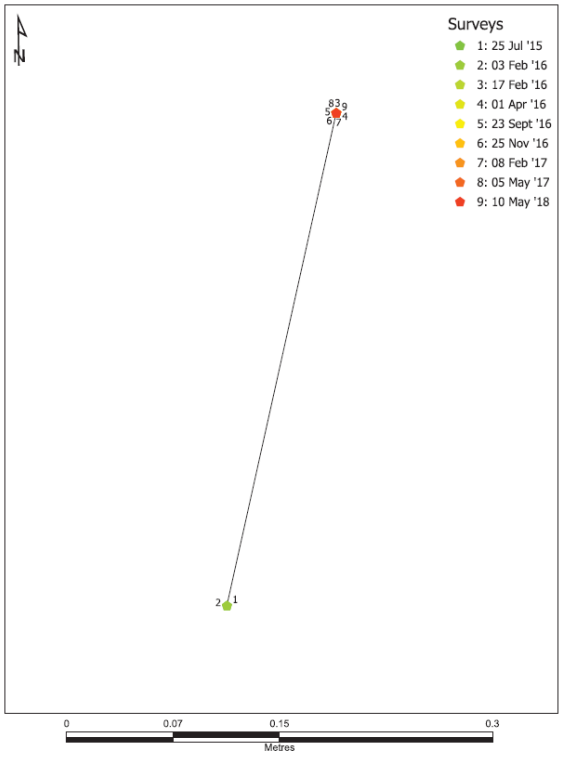

Appendices.

RFID tag ID: 1146
Individual Boulder Transport Distance: 0.5m

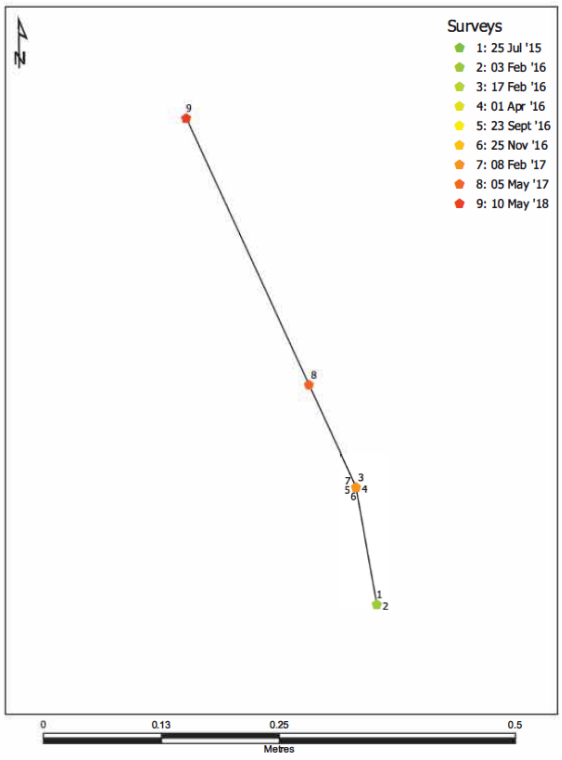

RFID tag ID: 1147
Individual Boulder Transport Distance: 0.9m

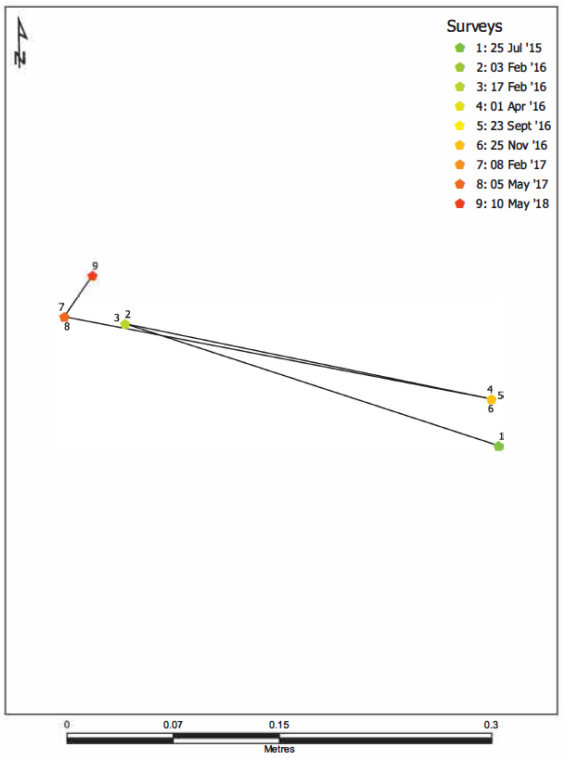

RFID tag ID: 1148
Individual Boulder Transport Distance: 16.5m

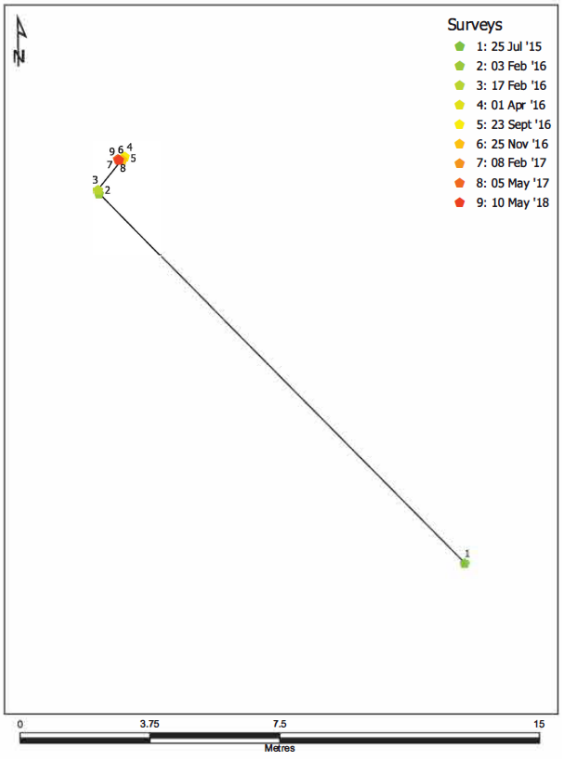

RFID tag ID: 1149
Individual Boulder Transport Distance: 0m

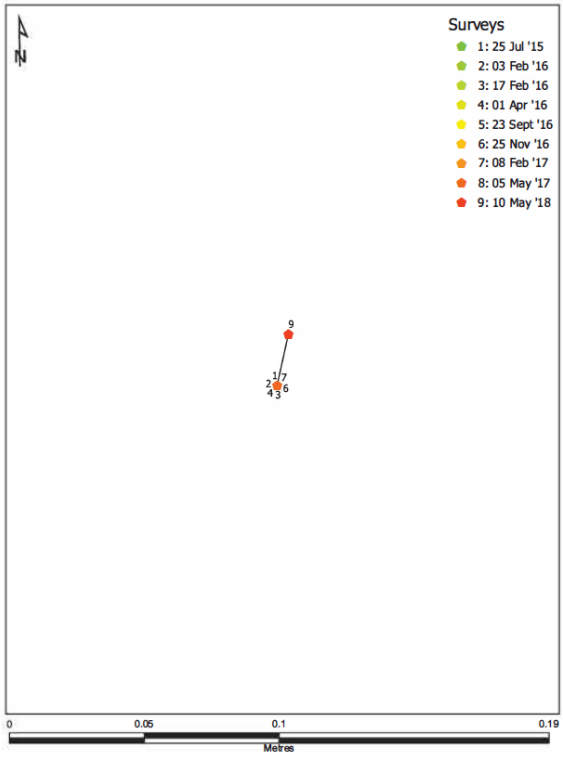

Appendices.

RFID tag ID: 1150
Individual Boulder Transport Distance: 4.2m

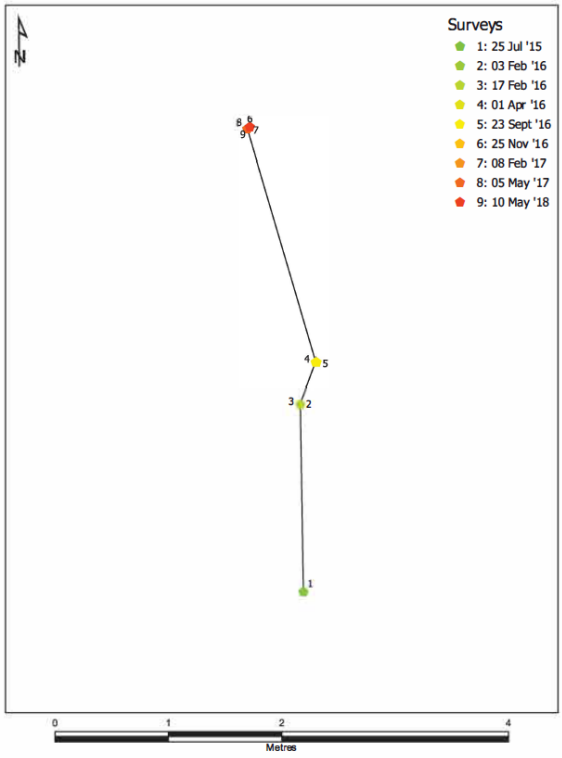

RFID tag ID: 1151
Individual Boulder Transport Distance: 5.5m

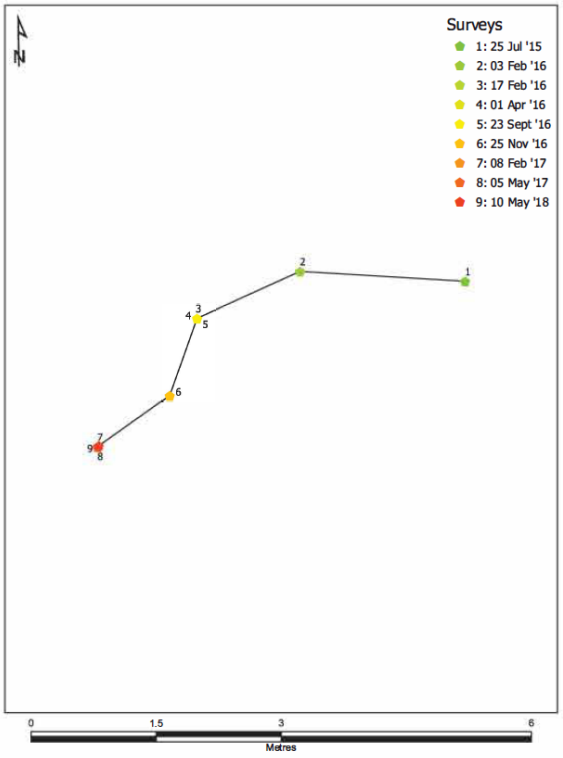

RFID tag ID numbers from 1152 to 7356 were embedded in boulders located at Black Rock. The following vector plots from pages 210 to 223 represent transport vector plots from the Black Rock tagged boulders.

RFID tag ID: 1152
Individual Boulder Transport Distance: 0.5m

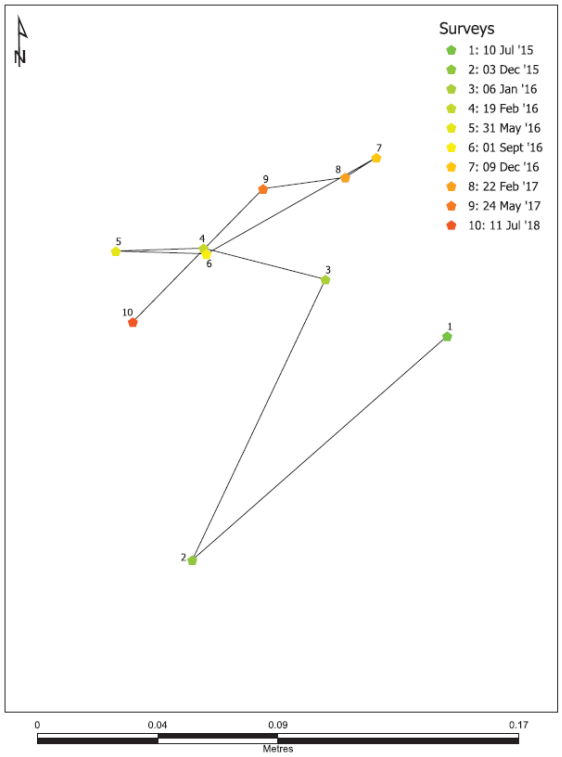

RFID tag ID: 1153
Individual Boulder Transport Distance: 0.2m

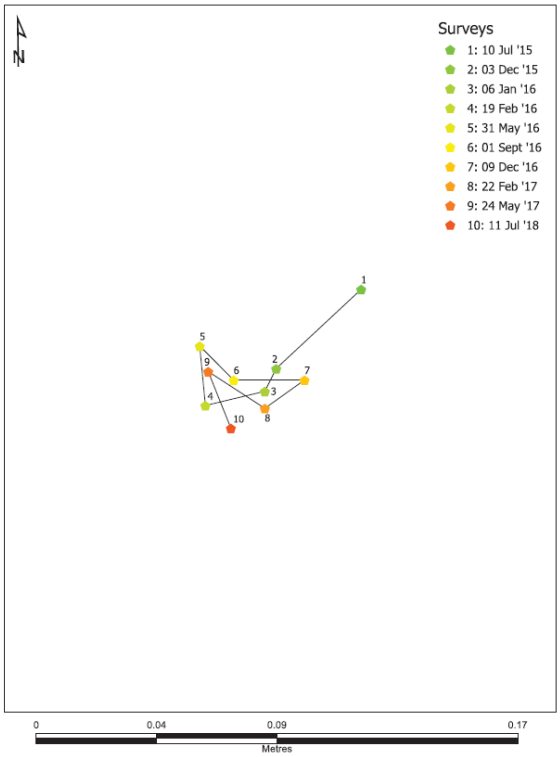

RFID tag ID: 1154
Individual Boulder Transport Distance: 0.3m

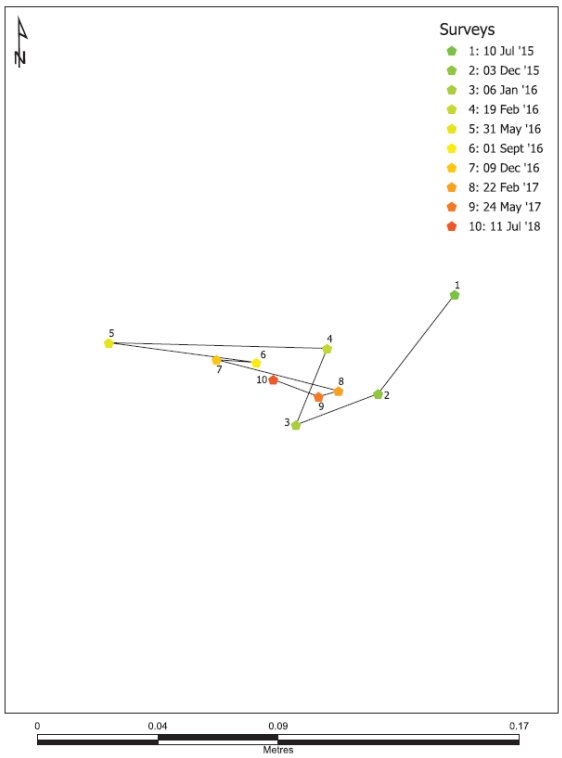

RFID tag ID: 1155
Individual Boulder Transport Distance: 0.2m

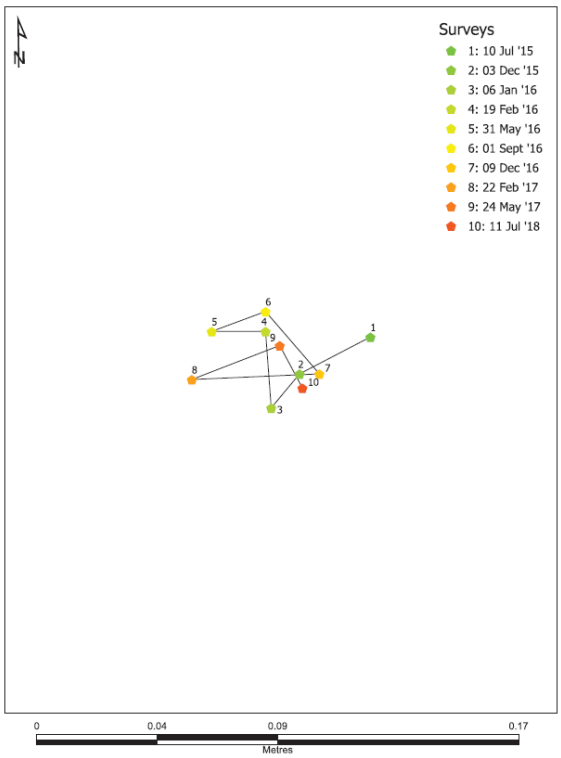

Appendices.

RFID tag ID: 1156
Individual Boulder Transport Distance: 0.2m

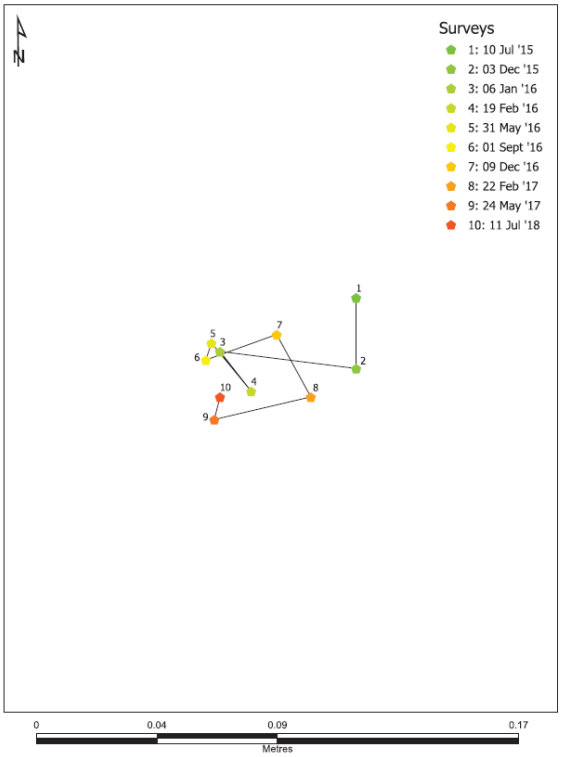

RFID tag ID: 1157
Individual Boulder Transport Distance: 0.3m

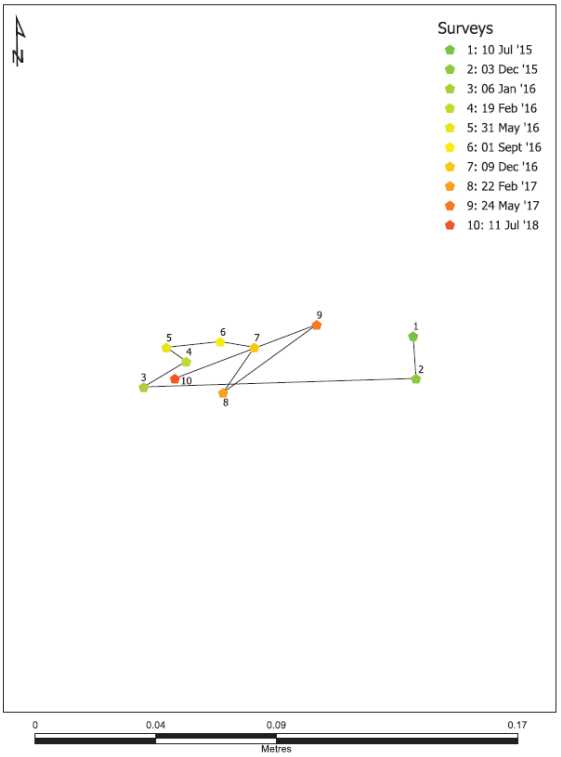

RFID tag ID: 1158
Individual Boulder Transport Distance: 0.5m

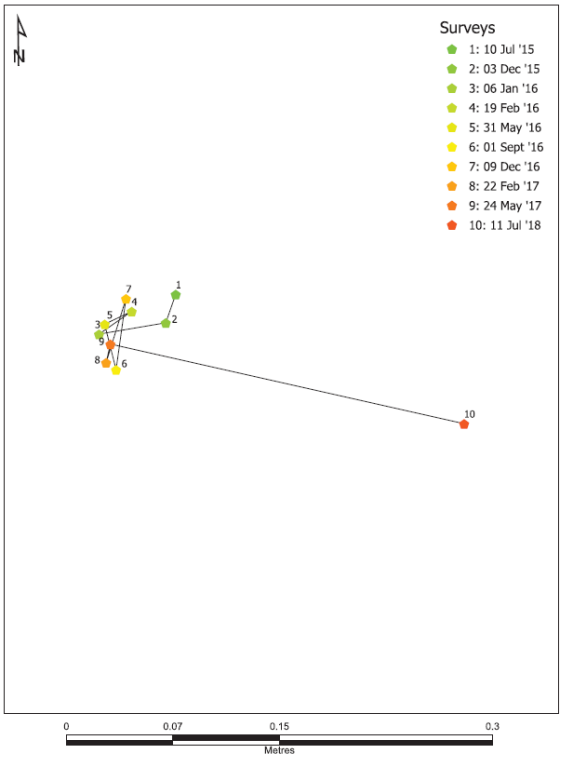

RFID tag ID: 1159
Individual Boulder Transport Distance: 0.2m

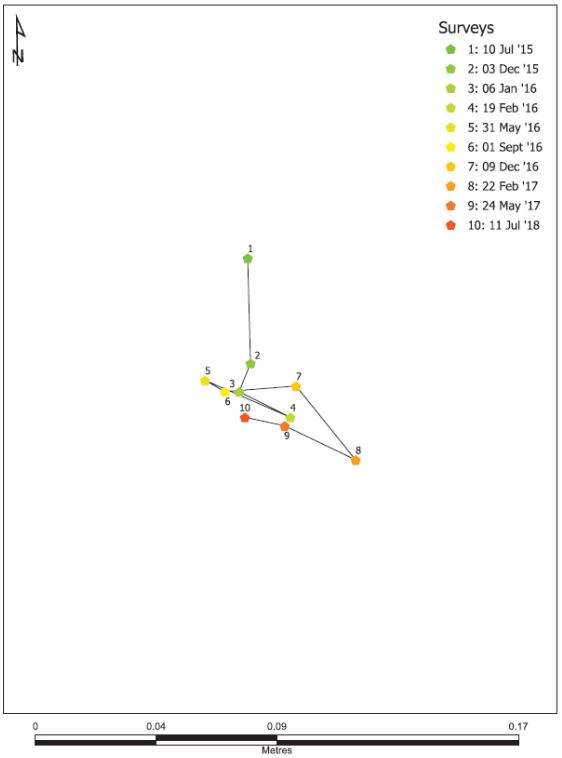

Appendices.

RFID tag ID: 1160
Individual Boulder Transport Distance: 0.7m

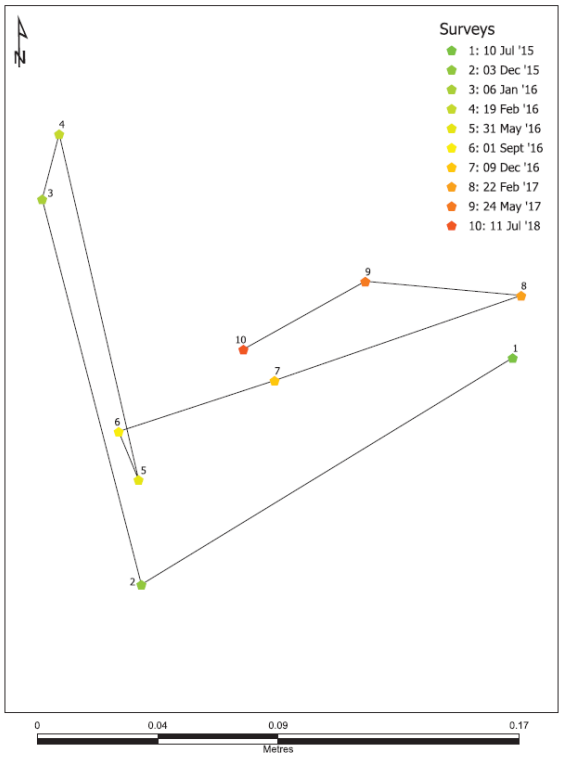

RFID tag ID: 1161
Individual Boulder Transport Distance: 0.2m

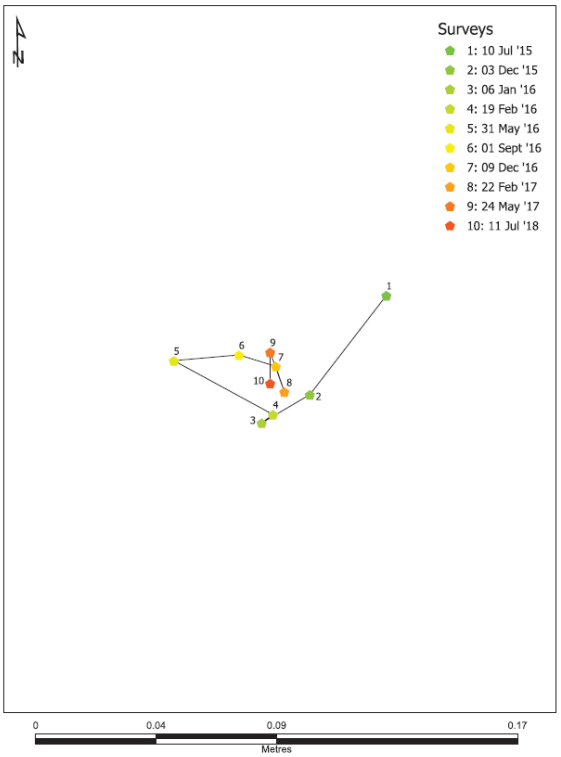

RFID tag ID: 1162
Individual Boulder Transport Distance: 0.4m

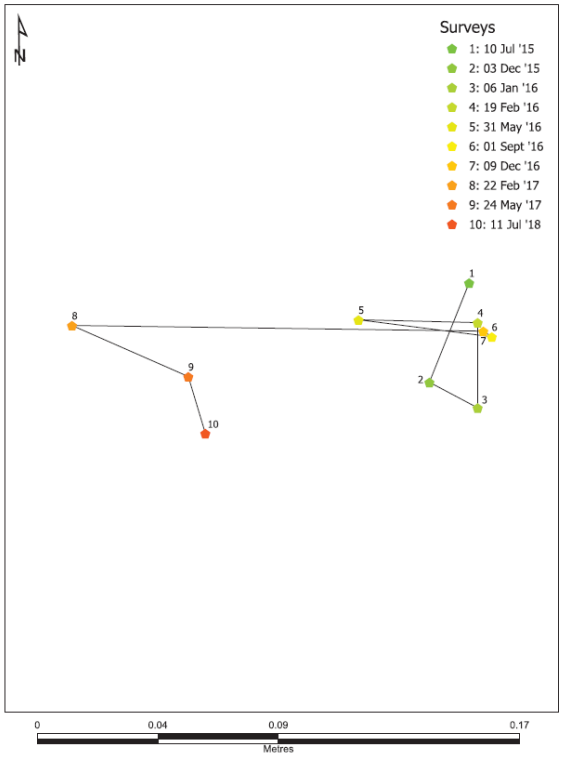

RFID tag ID: 1163
Individual Boulder Transport Distance: 10.2m

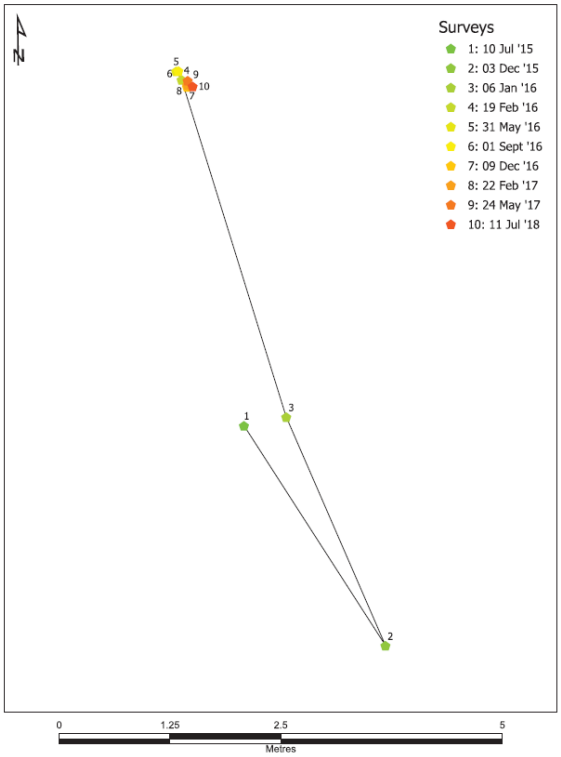

Appendices.

RFID tag ID: 1164
Individual Boulder Transport Distance: 4.3m

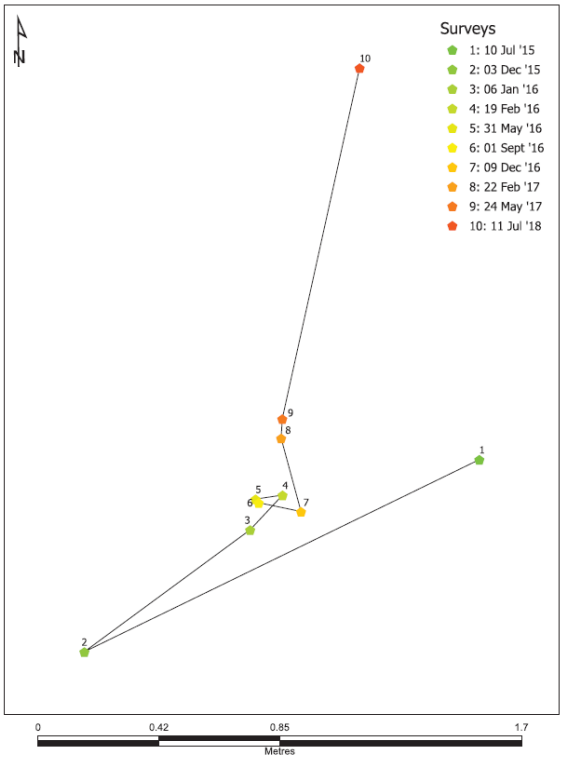

RFID tag ID: 1165
Individual Boulder Transport Distance: 0.6m

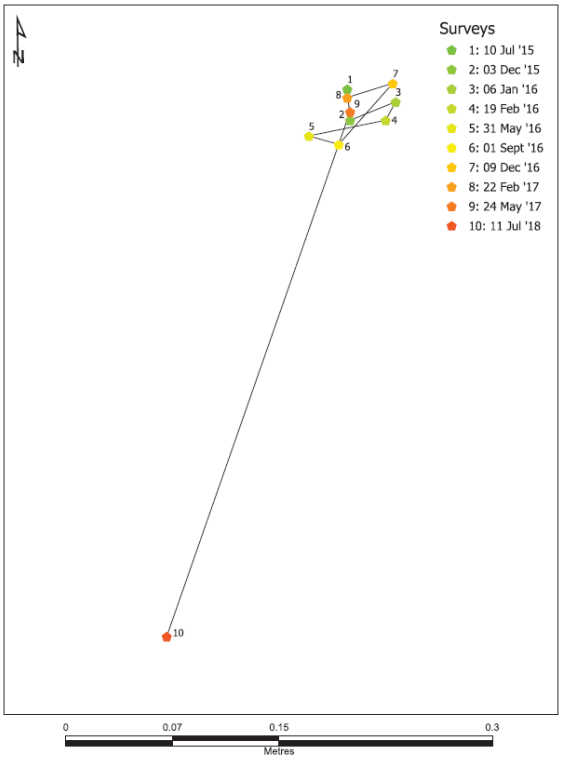

RFID tag ID: 1166
Individual Boulder Transport Distance: 0.3m

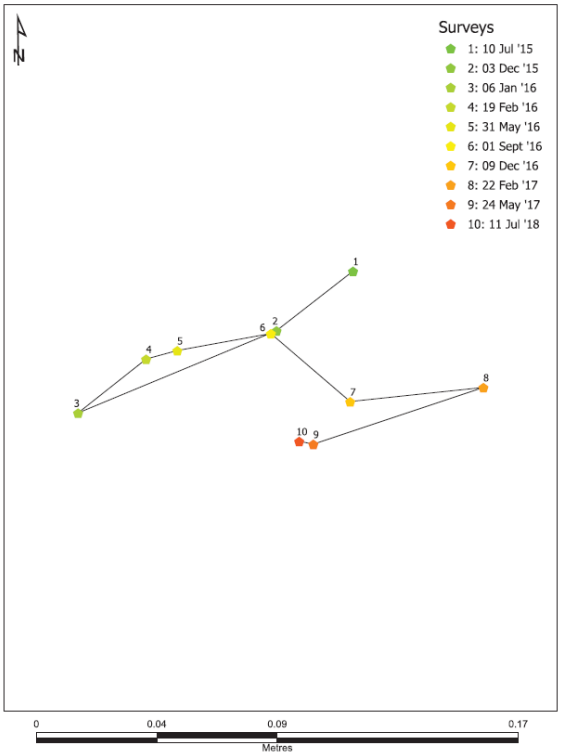

RFID tag ID: 1167
Individual Boulder Transport Distance: 0.3m

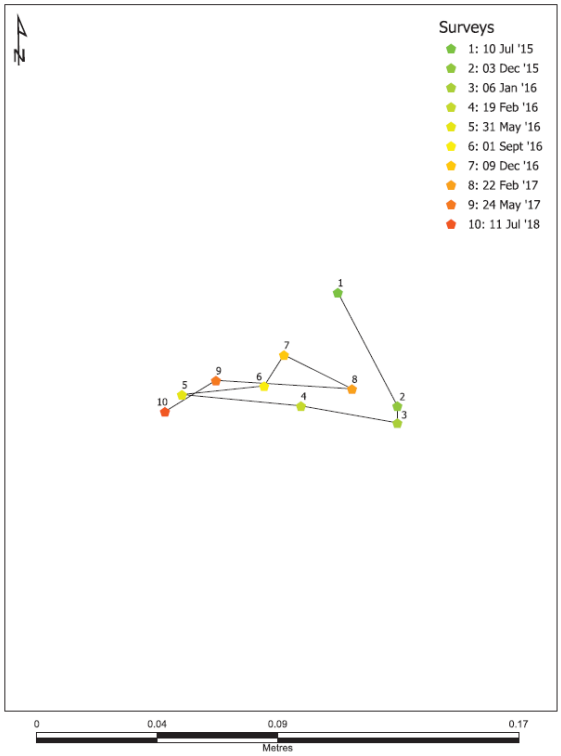

Appendices.

RFID tag ID: 1168
Individual Boulder Transport Distance: 6.4m

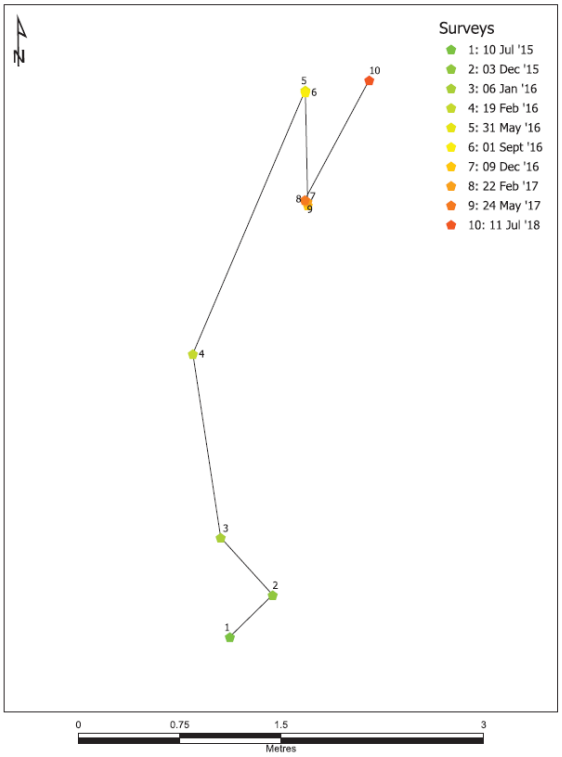

RFID tag ID: 1169
Individual Boulder Transport Distance: 0.2m

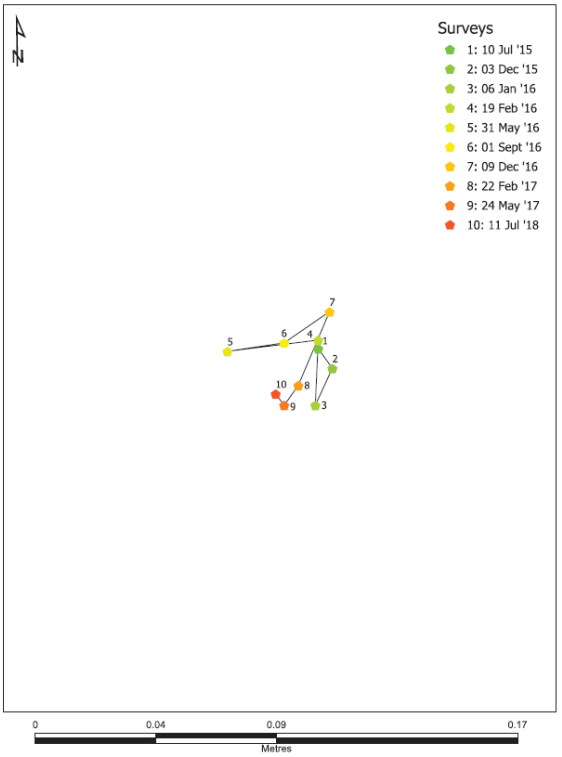

RFID tag ID: 1170
Individual Boulder Transport Distance: 0.3m

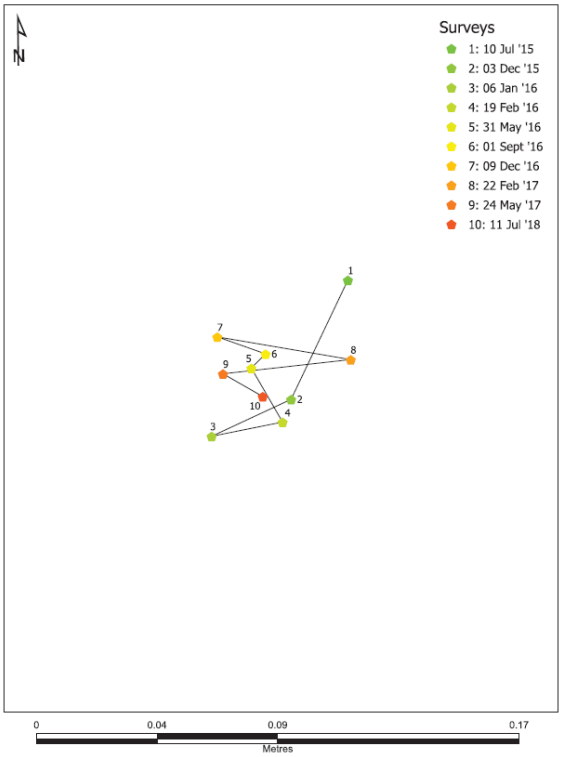

RFID tag ID: 1171
Individual Boulder Transport Distance: 0.2m

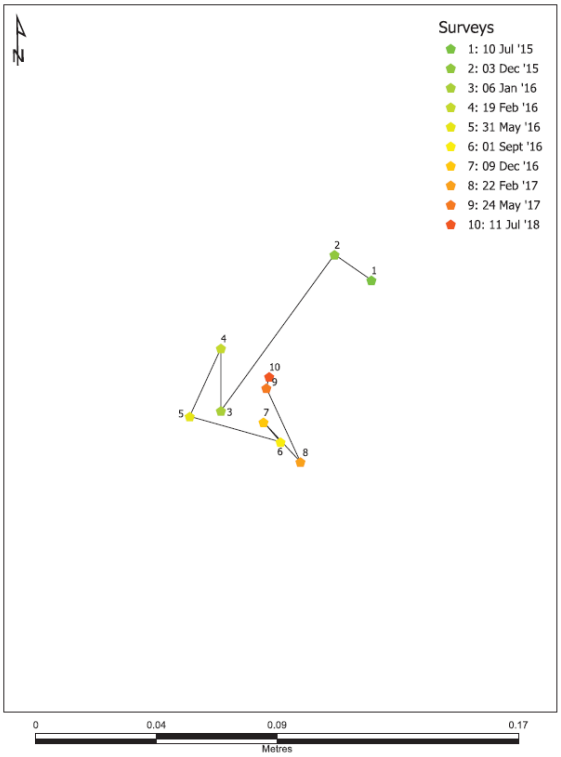

Appendices.

RFID tag ID: 1172
Individual Boulder Transport Distance: 0.2m

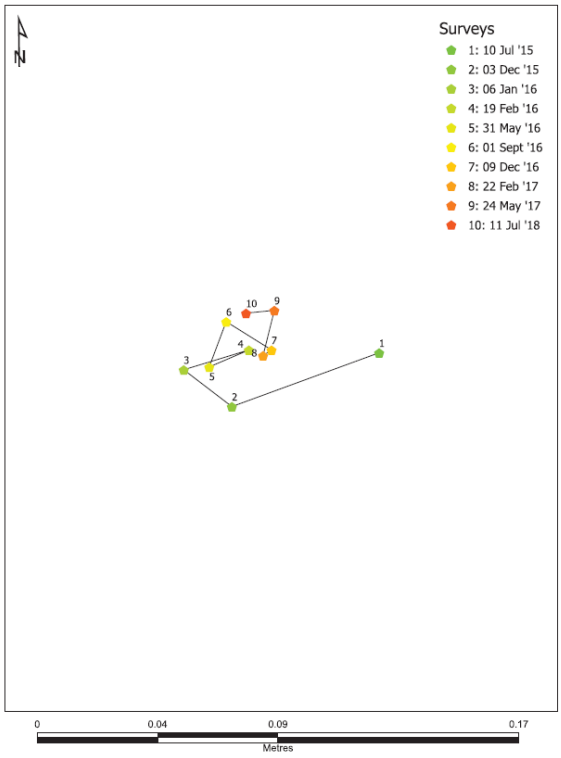

RFID tag ID: 1173
Individual Boulder Transport Distance: 0.2m

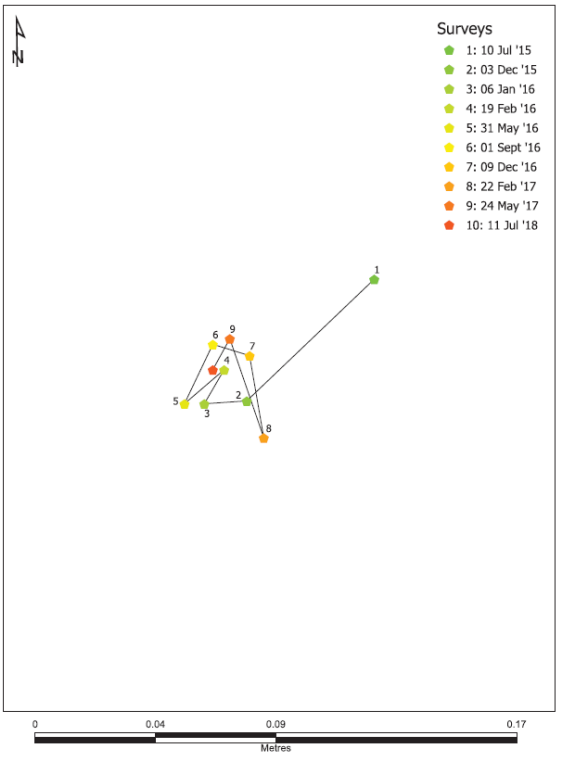

RFID tag ID: 1174
Individual Boulder Transport Distance: 0.2m

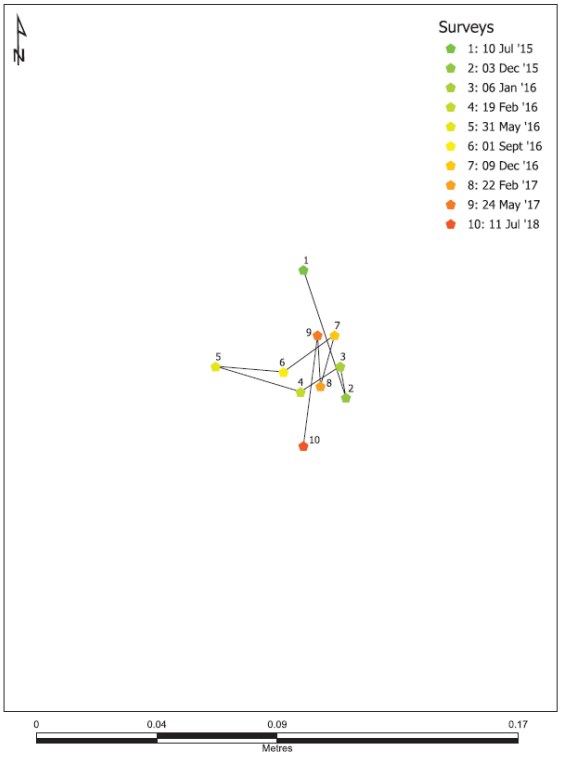

RFID tag ID: 1175
Individual Boulder Transport Distance: 1.3m

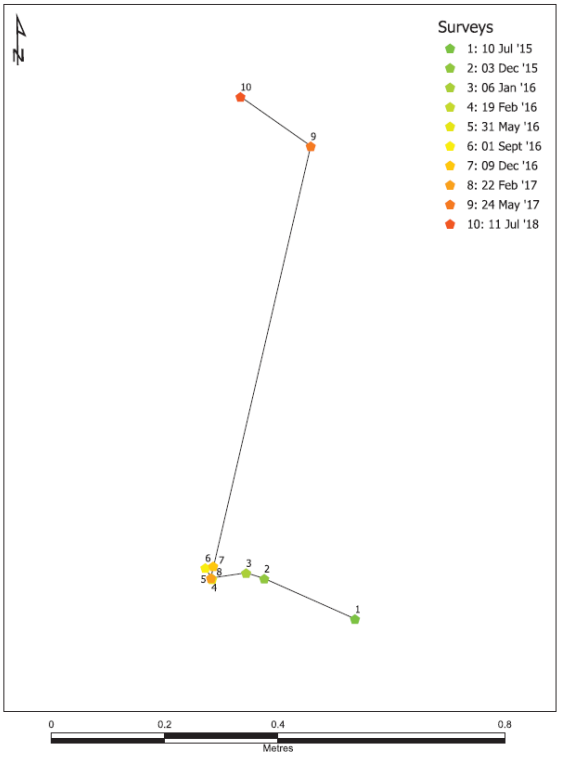

Appendices.

RFID tag ID: 1176
Individual Boulder Transport Distance: 0.2m

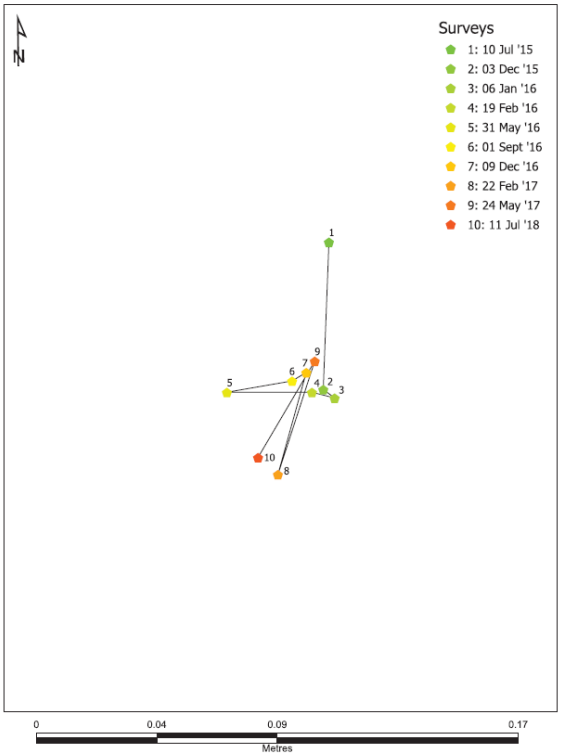

RFID tag ID: 1177
Individual Boulder Transport Distance: 0.5m

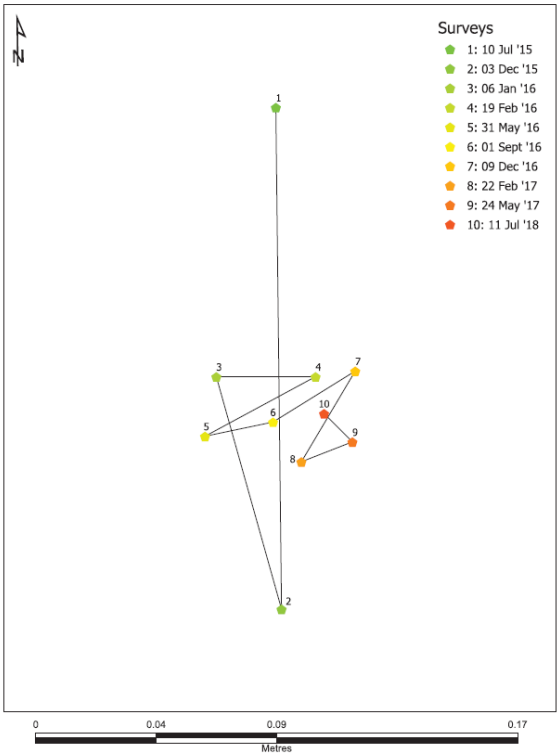

RFID tag ID: 1178
Individual Boulder Transport Distance: 0.5m

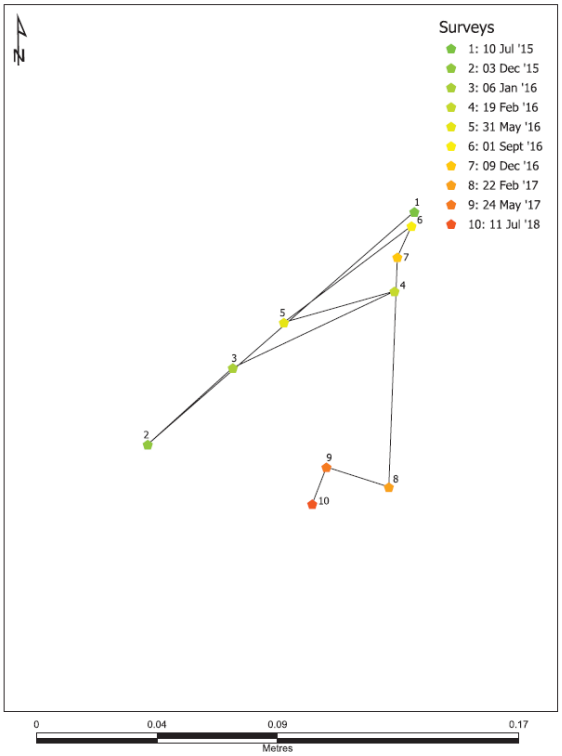

RFID tag ID: 1179
Individual Boulder Transport Distance: 1m

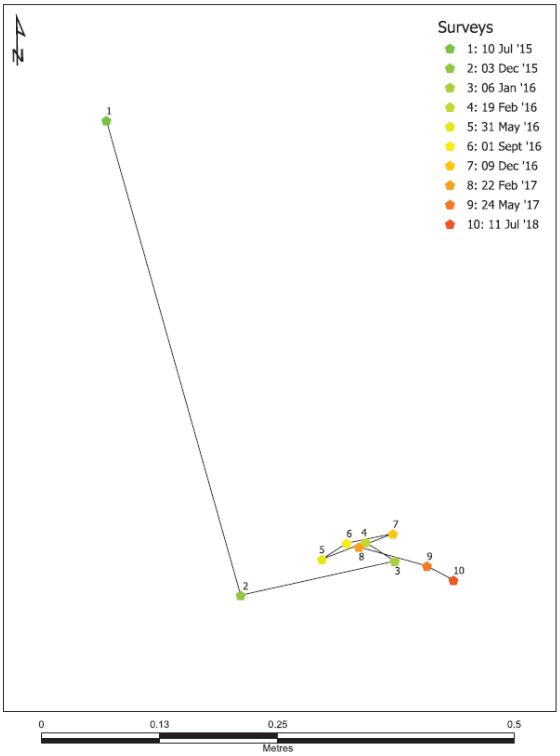

Appendices.

RFID tag ID: 1180
Individual Boulder Transport Distance: 0.4m

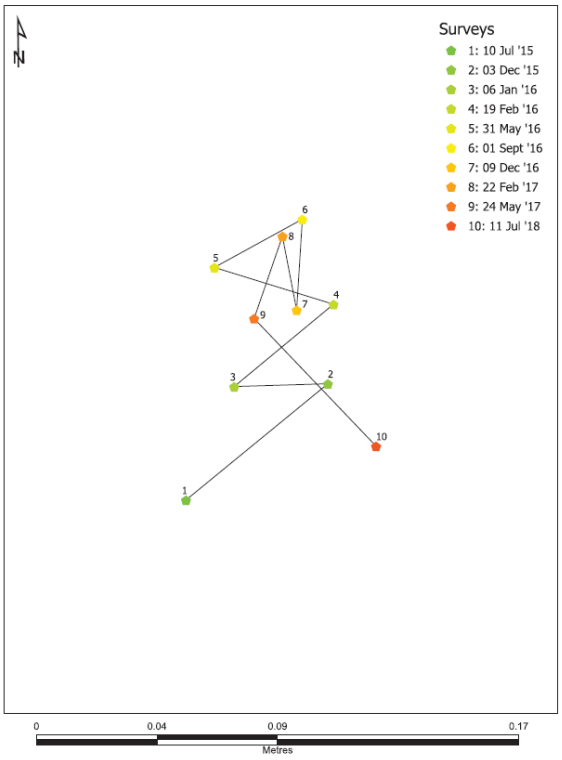

RFID tag ID: 1181
Individual Boulder Transport Distance: 1.6m

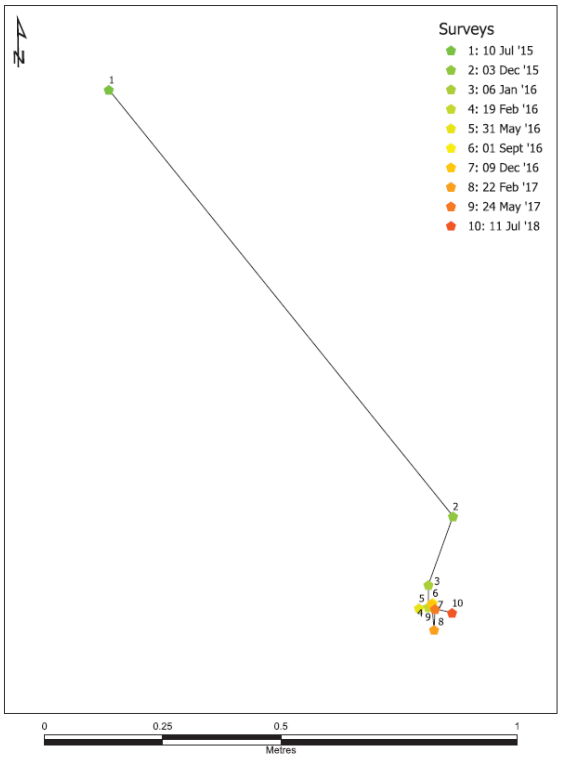

RFID tag ID: 1182
Individual Boulder Transport Distance: 0.6m

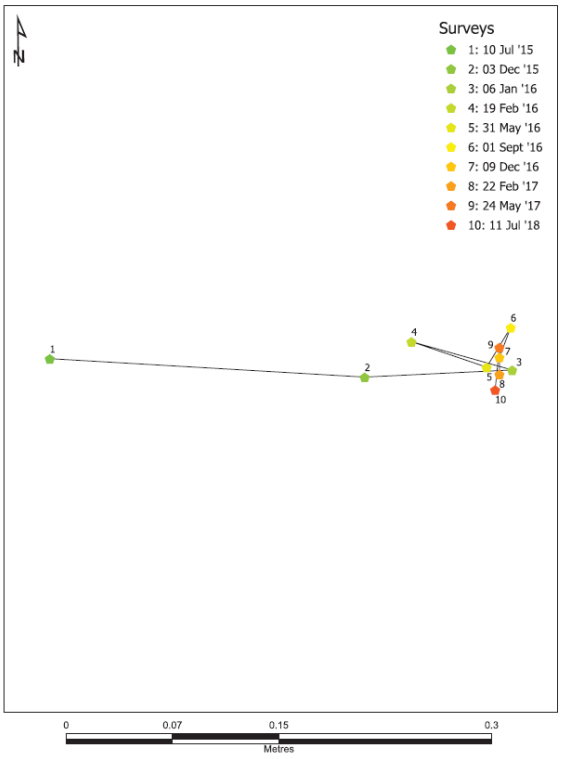

RFID tag ID: 1183
Individual Boulder Transport Distance: 1.7m

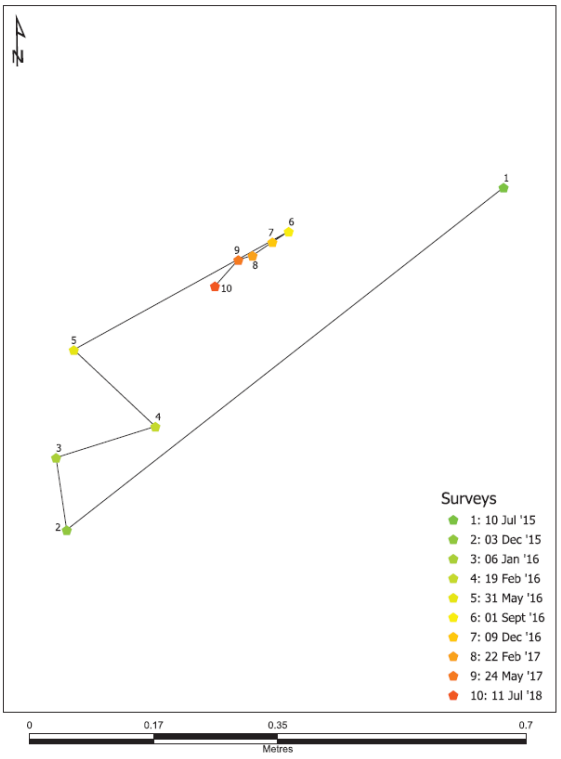

Appendices.

RFID tag ID: 1184
Individual Boulder Transport Distance: 0.8m

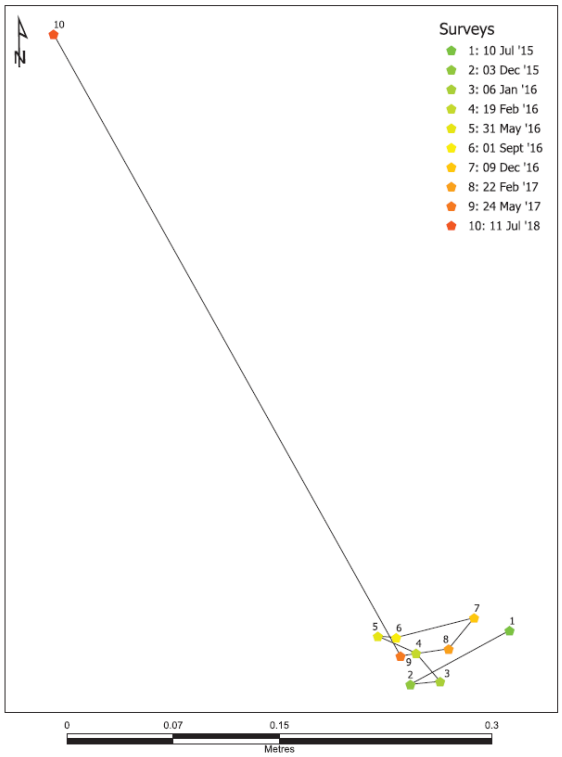

RFID tag ID: 1185
Individual Boulder Transport Distance: 11.6m

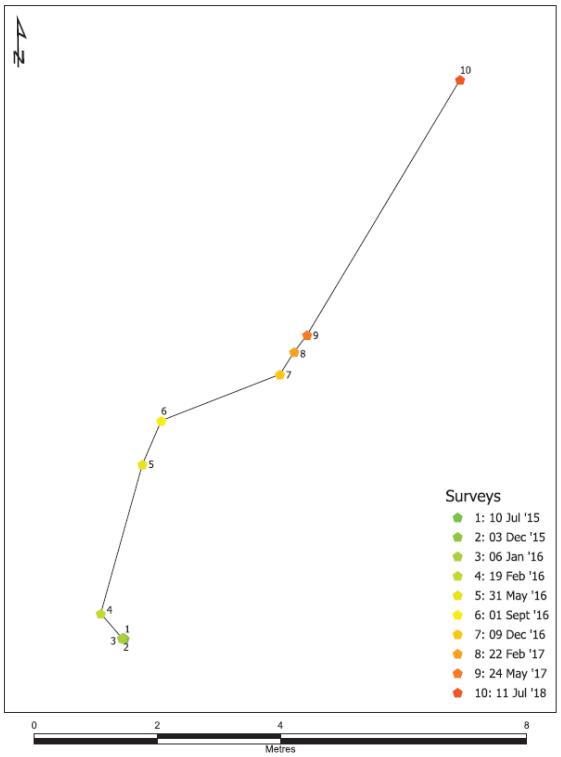

RFID tag ID: 1186
Individual Boulder Transport Distance: 0.4m

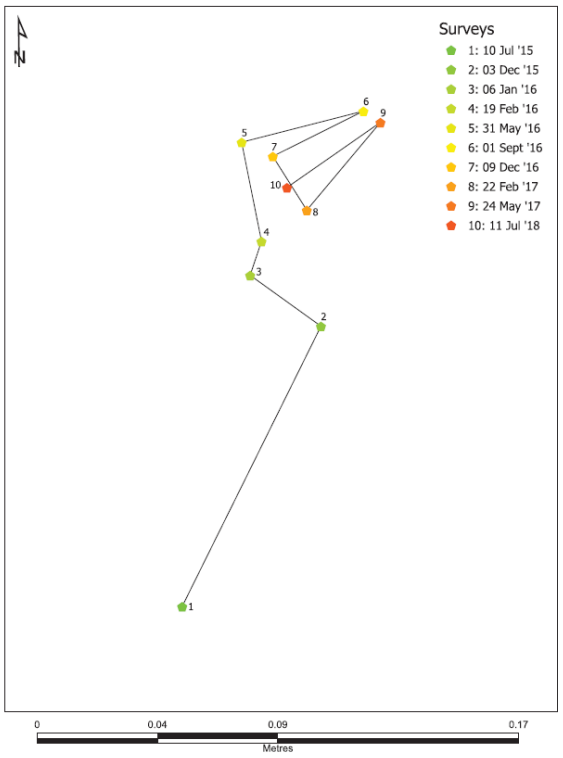

RFID tag ID: 1187
Individual Boulder Transport Distance: 9.9m

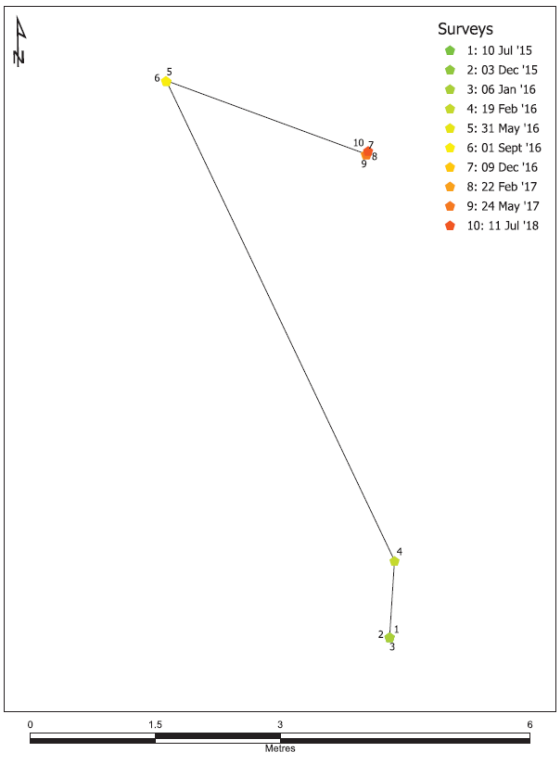

Appendices.

RFID tag ID: 1188
Individual Boulder Transport Distance: 3.9m

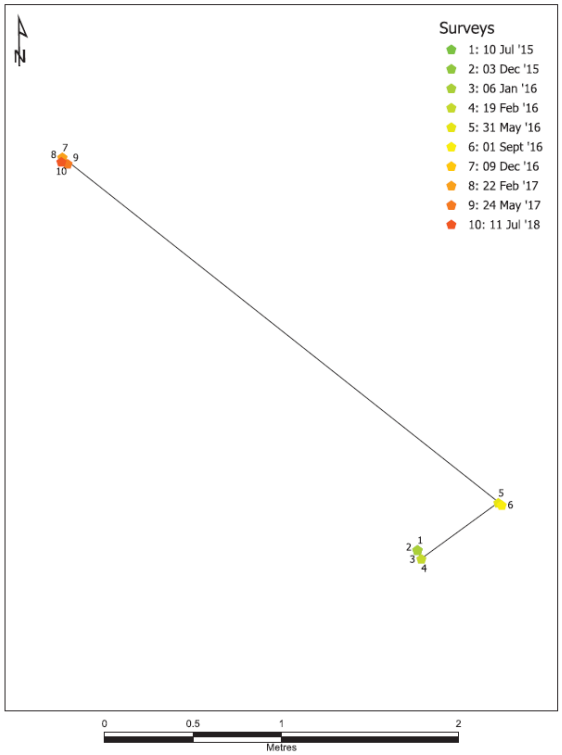

RFID tag ID: 1189
Individual Boulder Transport Distance: 2.7m

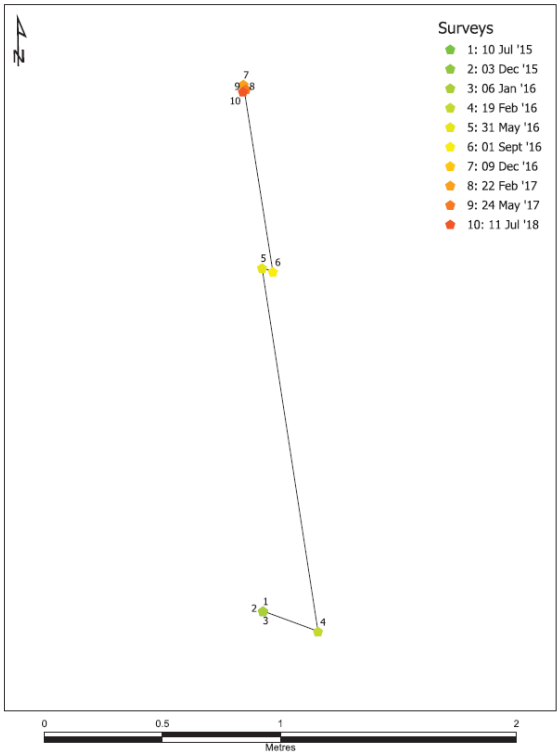

RFID tag ID: 1190
Individual Boulder Transport Distance: 0.3m

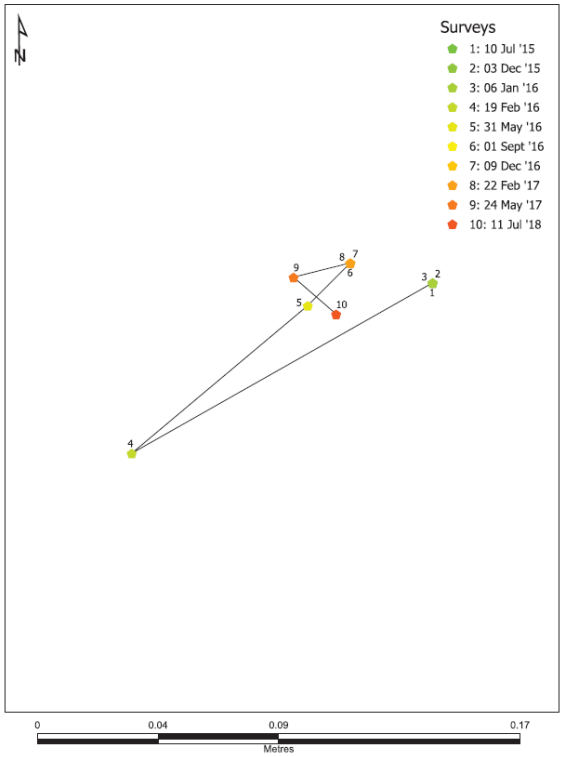

RFID tag ID: 1191
Individual Boulder Transport Distance: 0.2m

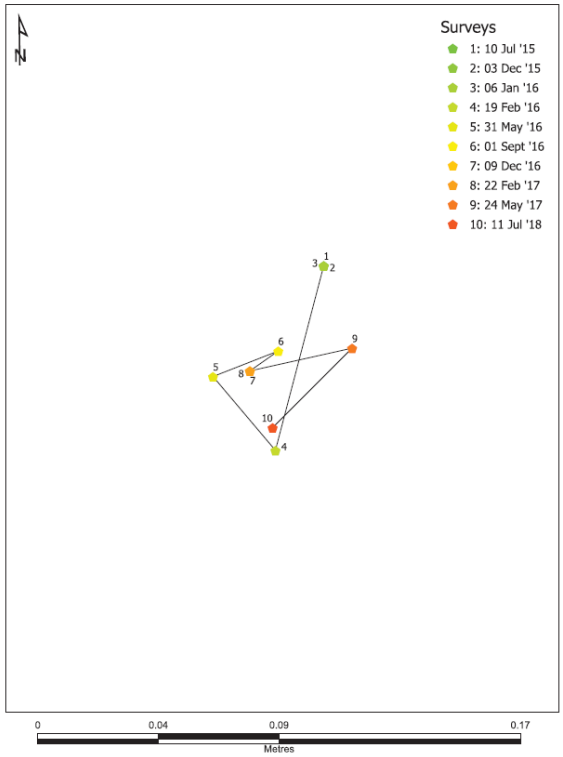

Appendices.

RFID tag ID: 1192
Individual Boulder Transport Distance: 8.6m

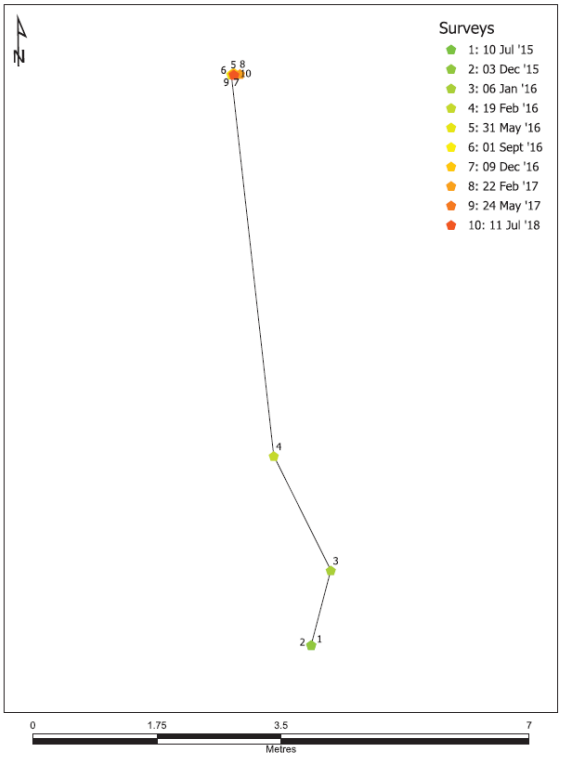

RFID tag ID: 1193
Individual Boulder Transport Distance: 0.2m

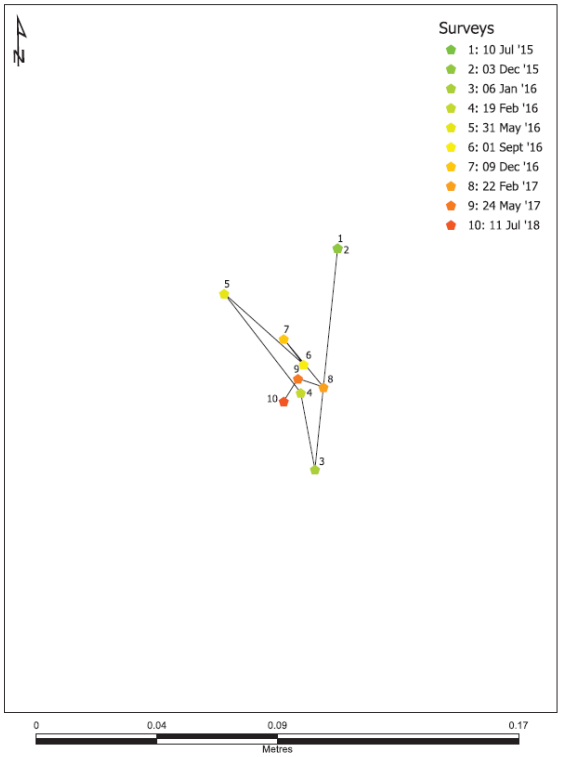

RFID tag ID: 1194
Individual Boulder Transport Distance: 0.3m

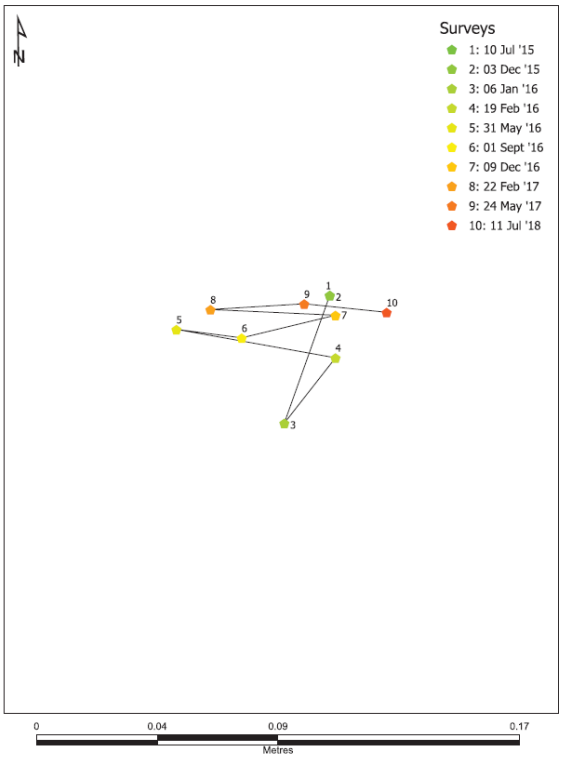

RFID tag ID: 1195
Individual Boulder Transport Distance: 1.1m

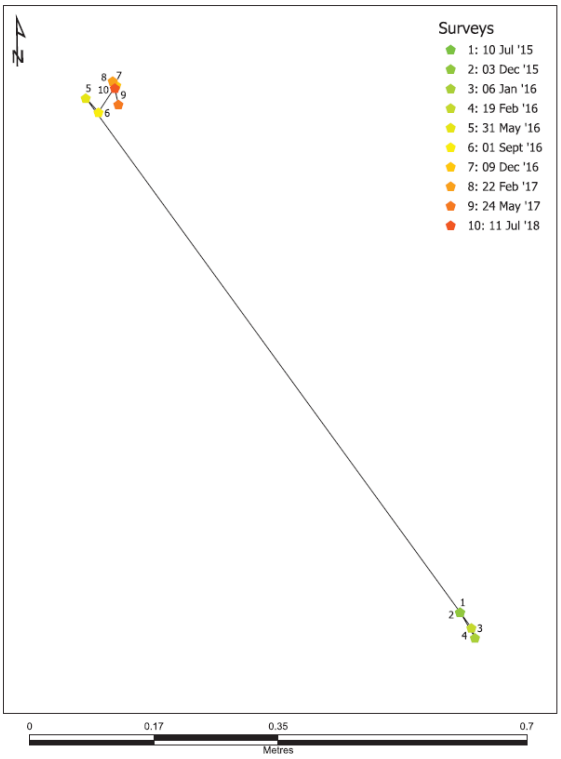

Appendices.

RFID tag ID: 1196
Individual Boulder Transport Distance: 0.3m

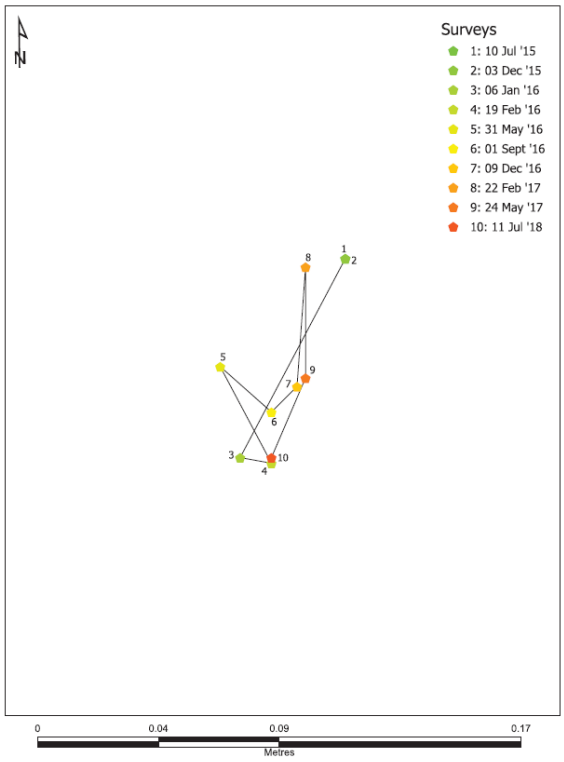

RFID tag ID: 1197
Individual Boulder Transport Distance: 10m

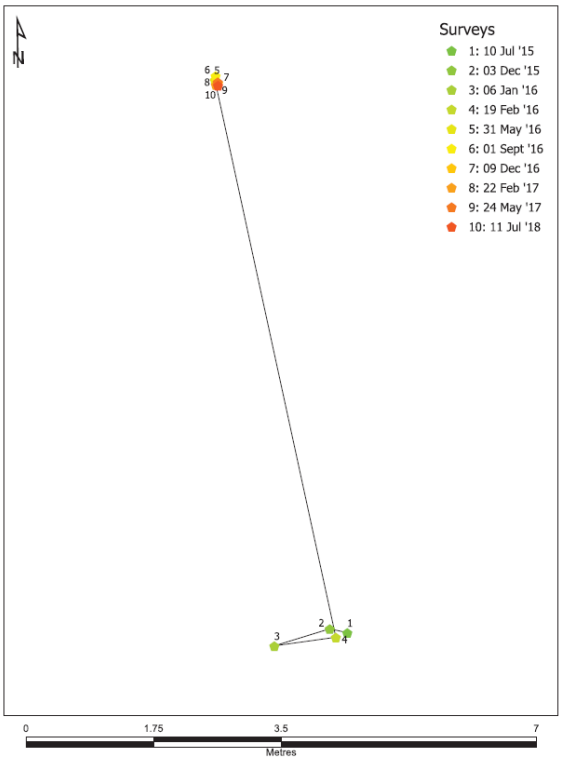

RFID tag ID: 1198
Individual Boulder Transport Distance: 0.4m

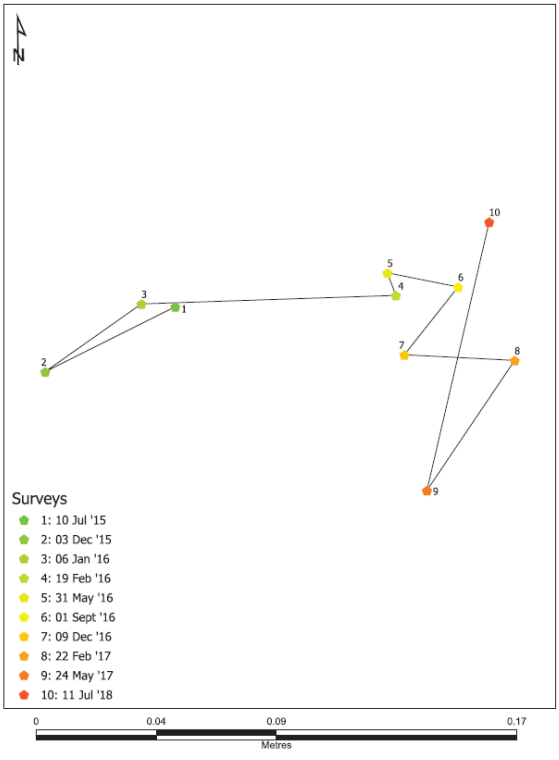

RFID tag ID: 1199
Individual Boulder Transport Distance: 0.6m

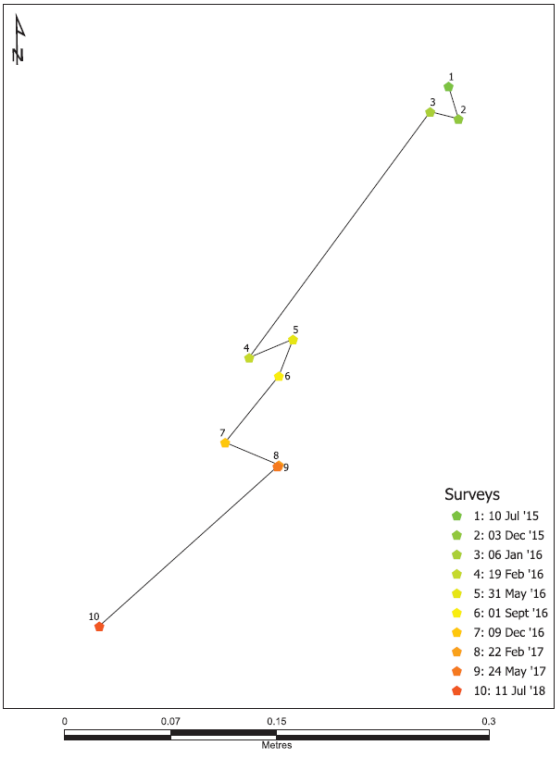

Appendices.

RFID tag ID: 7350
Individual Boulder Transport Distance: 0.2m

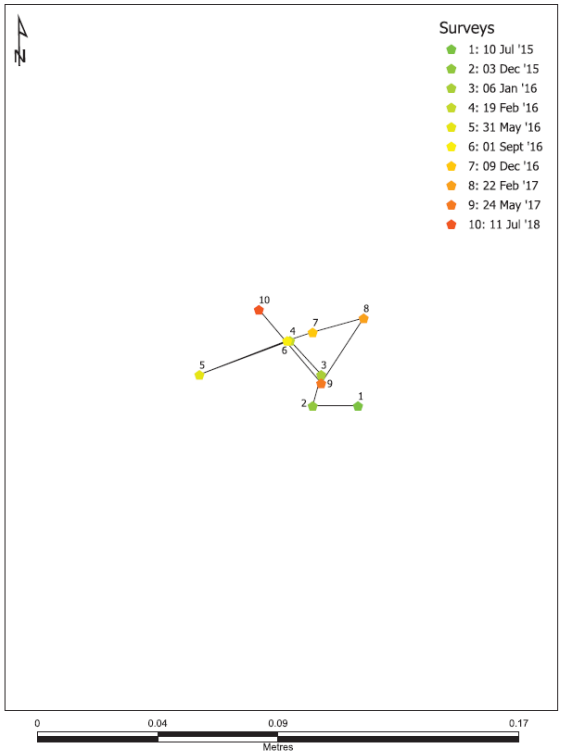

RFID tag ID: 7352
Individual Boulder Transport Distance: 0.9m

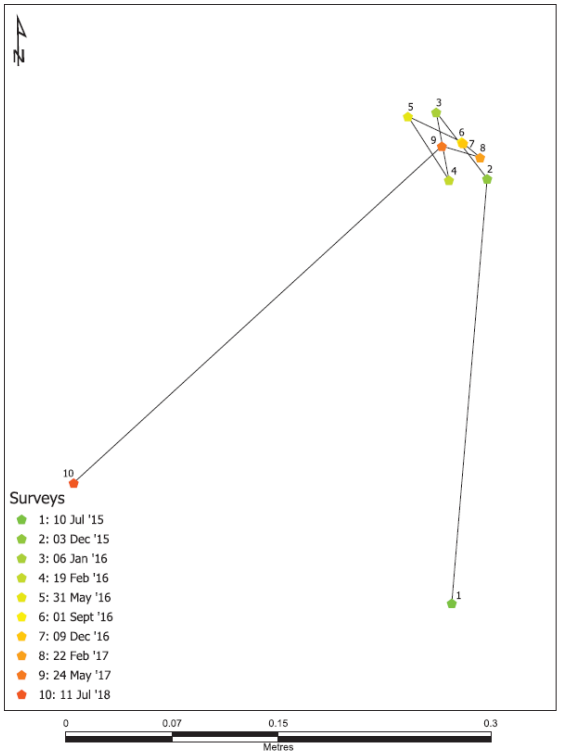

RFID tag ID: 7353
Individual Boulder Transport Distance: 2.9m

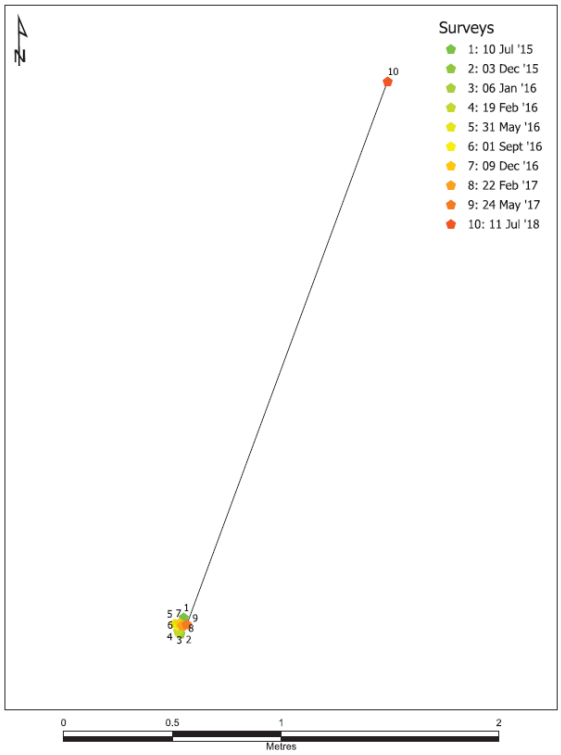

RFID tag ID: 7354
Individual Boulder Transport Distance: 0.8m

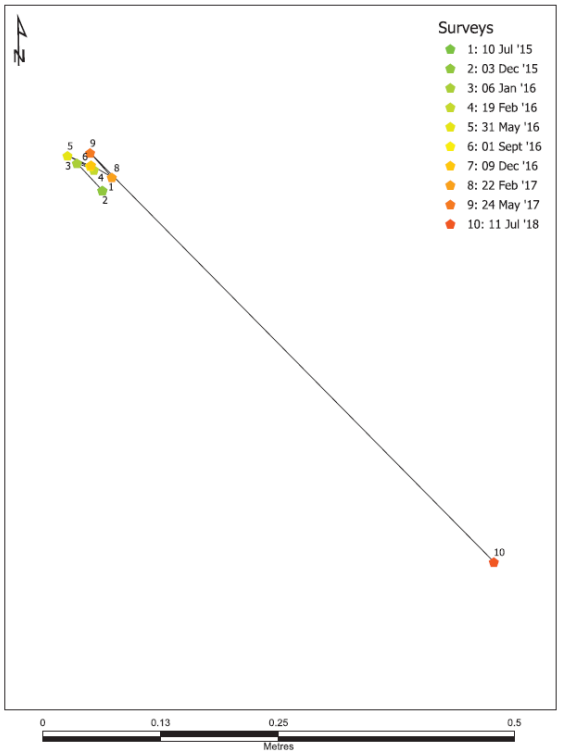

Appendices.

RFID tag ID: 7355
Individual Boulder Transport Distance: 0.2m

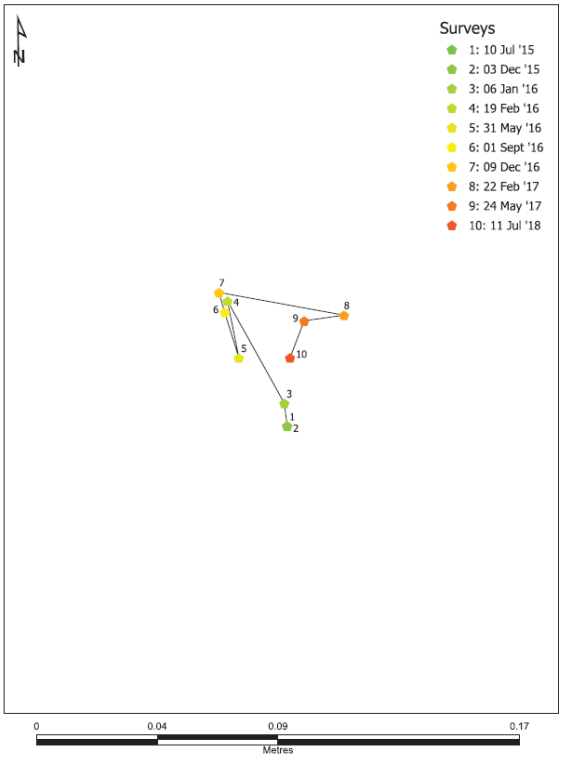

RFID tag ID: 7356
Individual Boulder Transport Distance: 0.3m

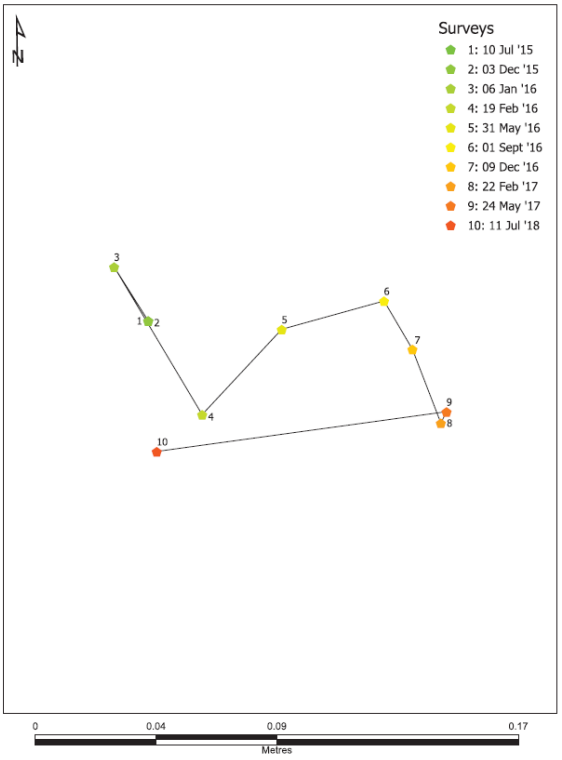

Appendix 3 - Permissions

MMO (Marine Management Organisation) Marine License Exemption

Personal details (email and postal addresses) have been obscured for the purpose of privacy.

Marine Management Organisation

Inshore Marine Licensing
Lancaster House
Hampshire Court
Newcastle upon Tyne
NE3 1RY

T +44 (0)191 376 2716
F +44 (0)191 376 2681
www.marinemanagement.org.uk

Mr Linley Hastwell
[redacted]

Your reference:
Our reference:
MLP/2013/00276

BY EMAIL ONLY

12 December 2013

Dear Mr Hastewell,

MLP/2013/00276 – Shore platform study at Bembridge
Thank you for your enquiry dated the 06 Dec 2013, regarding the above matter.

Having considered the information provided I can advise you that your proposed works fall within the Scientific Instruments section of the Marine Licensing (Exempted Activities) Order and therefore do not require a marine licence.

As part of this exemption you are required to notify the Marine Management Organisation via the link below:

http://www.marinemanagement.org.uk/licensing/marine/activities/forms/exemptionnotification.pdf

Please don't hesitate to contact me directly should you wish to discuss this matter further, quoting the following reference: Ref MLP/2013/00276.

Yours sincerely,

Siobhan Sherry
Marine Licensing Case Officer

D [redacted]
E [redacted]

Natural England permission

University of Portsmouth

Linley H [redacted]

PhD field research

Morgan, Richard (NE) [redacted] 27 May 2014 10:47
To: Linley H [redacted]
Cc: "Larter, Mark (NE)" [redacted]

Dear Linley,

Many thanks for your email which adequately addresses our request for additional information. I have now reviewed the details of your proposal in full and can confirm that the research site lies within habitats which form part of the Whitecliff Bay & Bembridge Ledges Site of Special Scientific Interest (SSSI). This SSSI is also part of the South Wight Maritime Special Area of Conservation (SAC), the Solent and Southampton Water Special Protection Area (SPA) and the Solent and Southampton Water Wetland of International Importance under the Ramsar Convention (Ramsar Site). These designations are in place to legally protect the nationally and internationally important habitats, and the species which they support, which are present in this area.

As previously discussed, proposals (such as this one) which receive licensing exemption from the Marine Management Organisation (MMO) may still require SSSI consent from Natural England if the activity has the potential to damage the special interest of the site. I have discussed your proposal with my colleague Mark Larter and we have concluded that SSSI consent is not required. On this basis, I can confirm that Natural England has no objection to this research taking place – based on the methodology provided. However, please note that this does confer or imply permission from the site landowner to undertake this research. At the time of writing we have been unable to ascertain who the landowner is at this location.

Given that you will be accessing the site on foot and using low-noise methods for tagging and monitoring, we do not object to this research taking place during the bird overwintering period. I agree though that it would be beneficial if you could inform Mark and myself prior to conducting a site visit in case we receive enquiries from members of the public.

I hope that this response is sufficient. Please don't hesitate to contact me should you have any further queries.

Kind regards,

Richard

Dr Richard Morgan

Marine Lead Adviser

Natural England

[redacted]

landline no. [redacted]

www.naturalengland.org.uk

Appendix 4 - Research dissemination

Academic outputs

Published papers

Hastewell, L. J., Schaefer, M., Bray, M., & Inkpen, R. (2019). Intertidal boulder transport: A proposed methodology adopting Radio Frequency Identification (RFID) technology to quantify storm induced boulder mobility. *Earth Surface Processes and Landforms*, 44(3): 681-698.

Hastewell, L., Inkpen, R., & Bray, M. (2019). Identification of plate-forme à vasques on a temperate shore platform? Quantitative analysis of morphology and relationships at Bembridge, Isle of Wight. *Zeitschrift für Geomorphologie*, 62(2): 145-162.

Hastewell, L., Inkpen, R., Bray, M., & Schaefer, M. (2020). Quantification of contemporary storm-induced boulder transport on an intertidal shore platform using Radio Frequency Identification (RFID) technology. *Earth Surface Processes and Landforms*.

Conference Presentations

Science Together Conference, University of Portsmouth. 6th July, 2016. The effect of storm events on boulder transport and shore platform evolution at Bembridge, Isle of Wight.

International Association of Geomorphologists Regional Conference on Geomorphology, Athens, Greece. 19th September, 2019. A multidisciplinary approach for the investigations of the dynamics of a boulder deposit on a low-lying rocky promontory in the Northern Adriatic Sea.

Devoto, S., Biolchi, S., Hastewell, L., Mantovani, M., Scicchitano, G., Korbar, T. (2019).

Oral presentation delivered by Dr. Stefano Devoto (presentation slides included, page 227).

The inclusion of the presentation slides offers insight to the current and future collaborative work that is being undertaken with colleagues at the University of Trieste as is discussed in Chapter 5.

Stefano Devoto, Sara Biolchi, Linley Hastewell, Matteo Mantovani, Giovanni Scicchitano, Tvrtko Korbar, Ivica Vilibić, Clea Denamiel, Stefano Furlani

A multidisciplinary approach for investigations of the dynamics of a boulder deposit on a low-lying rocky promontory in the Northern Adriatic Sea

INTRODUCTION

- This oral presentation shows the analysis of a coastal boulder deposit located in the N Adriatic Sea. The importance of this presentation is that this deposit is the first detected in the N Adriatic Sea, which from a hydrodynamical point of view is considered as a lake.
- We applied a multidisciplinary approach, which integrated geological and geomorphological surveys (both inland and underwater), aerial and terrestrial photogrammetry, hydrodynamics models and assessment of regional waves.
- The geomorphological investigations have been carried out since 2012 by the University of Trieste (Italy) and Croatian research institutes such as Croatian Geological Survey and the Institute of Oceanography and Fisheries.
- Recently a monitoring network has been installed by means of the collaboration with other universities and institutes such as CNR-Irpi of Padua (Italy) and University of Portsmouth (UK).
- This presentation illustrates the results of boulder mapping and monitoring. The latter has been carried out in the western side of boulder deposit, where there was a clear evidence of recent transport process.

INTRODUCTION

The most important coastal geohazard in N and Central Adriatic Sea is related to land sliding. Landslides affect only Italian coasts such as Ancona, Conero promontory (Furlani et al 2018) and Vasto (Della Seta et al 2013). Triggering factors mostly related to structural and geological features.

Conversely, there is no field evidence of coastal boulder deposits evidence of wave impacts in N and Central Adriatic Sea.

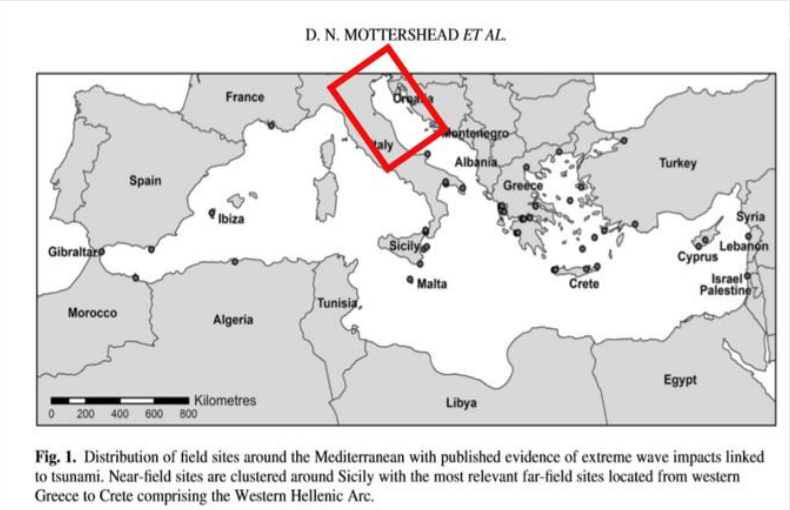

Fig. 1. Distribution of field sites around the Mediterranean with published evidence of extreme wave impacts linked to tsunami. Near-field sites are clustered around Sicily with the most relevant far-field sites located from western Greece to Crete comprising the Western Hellenic Arc.

GEOHAZARD

Severe storms can hit N Adriatic Sea and can generate impressive waves

GEOHAZARD

In particular three extremely strong events occurred in recent years; January 2014, February 2016 and October 2018.

STUDY AREA

We recognised a wide coastal boulder deposit in the South Istrian peninsula, Croatia. Other boulder sites are located in the neighbouring bays, inlets and isles.

STUDY AREA

We focussed our attention on the most spectacular deposit. It lies in a pristine area in the southernmost sector of the Istrian peninsula.

GEOMORPHOLOGY OF THE STUDY AREA

The Premantura boulder accumulation is located in the Kamenjak Nature Park and is located in the southern part of a peninsula characterized by gentle slopes which follow the orientation of dip strata. The low values of layer roughness joined with high persistent values of strata layers favour the transport along the karst pavement

BOULDER K8

- Traditional field activities were carried out aiming to mapping boulders between 2016 and 2018.
- To determine the location and distance from the shoreline, UAV-DP assisted inland field work.

- According the recent methodology developed by Terry and Goff (2014), the entire accumulation can be classified as boulders (clasts between 0.25 and 4.1 m)
- A total of 950 boulders were mapped. 44 of these were selected for analysis and measurement. In particular we measured sizes, shapes and we applied hydrodynamic equations.

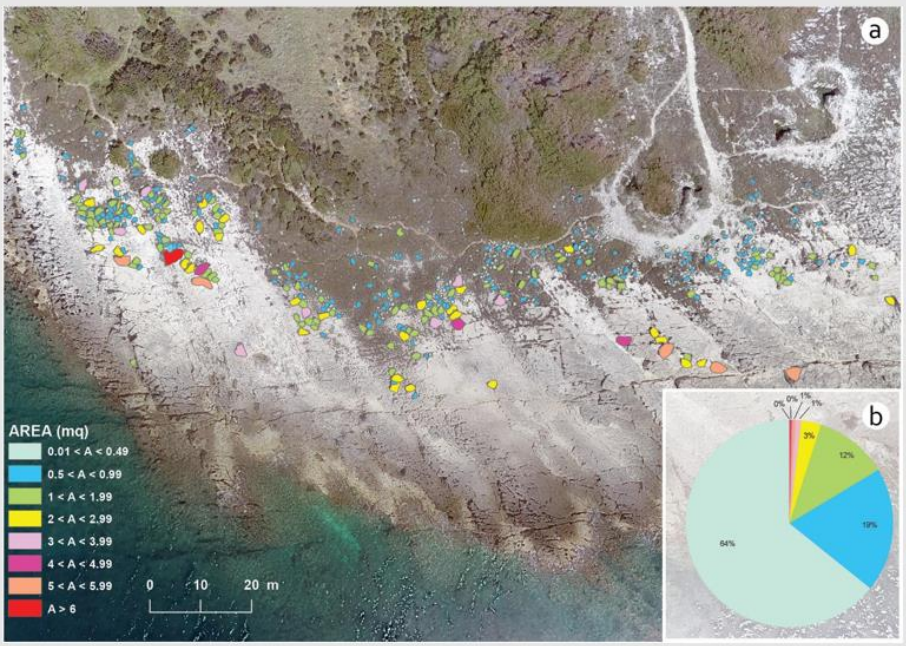

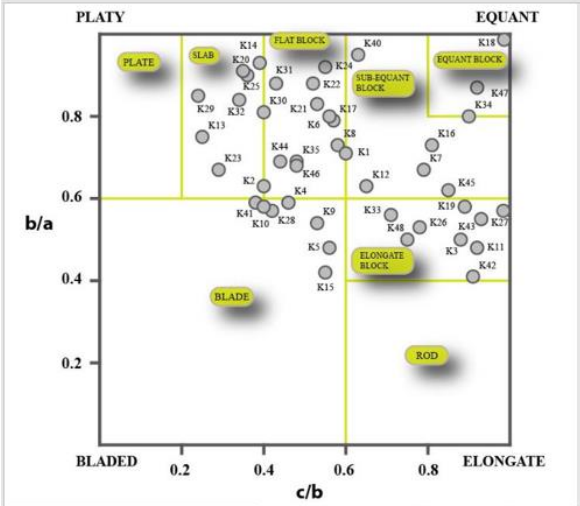

- Mass and distance from the coast were plotted on the graph below.
- The figure below show **a clear relationship** between mass and distance: boulders exceeding 10t stop at a maximum distance of 50m.
- No correlation were found between Distance and Shape.

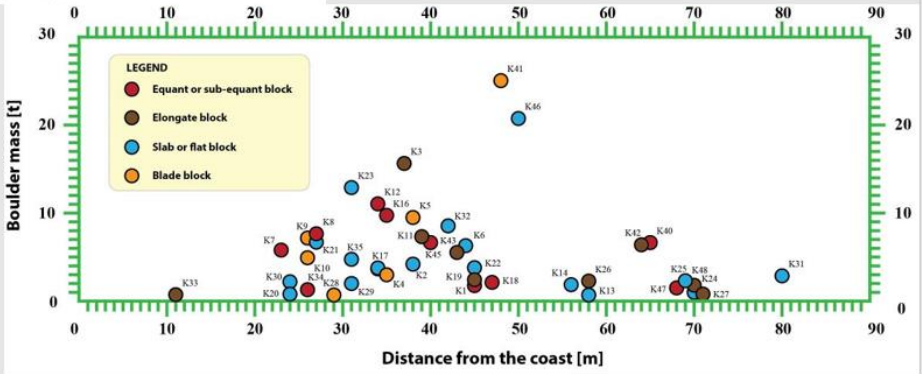

BOULDER K8

Distance from the coast: **27 m**
Elevation **2m**
Mass **7.6 t**

- Boulder K8 is clear visible because it is isolated respect to other boulders. Moreover it is located in a position near the sea (27m) in a limestone ramp.
- Other peculiar feature is an orange colour related to weathering processes and a clear pothole located some meters south. The latter was essential for calibrating distance in 3D UAV-derived model.
- K8 boulder is characterised by recent biogenic encrustations (marine origin).

HISTORICAL RECOSTRUCTION OF EXTREME WAVE EVENT

We examined photos collected by Geoswim project (Furlani et al 2014) and by Google Earth 2007, 2009, 2012, 2013, 2016)

2013 03 11

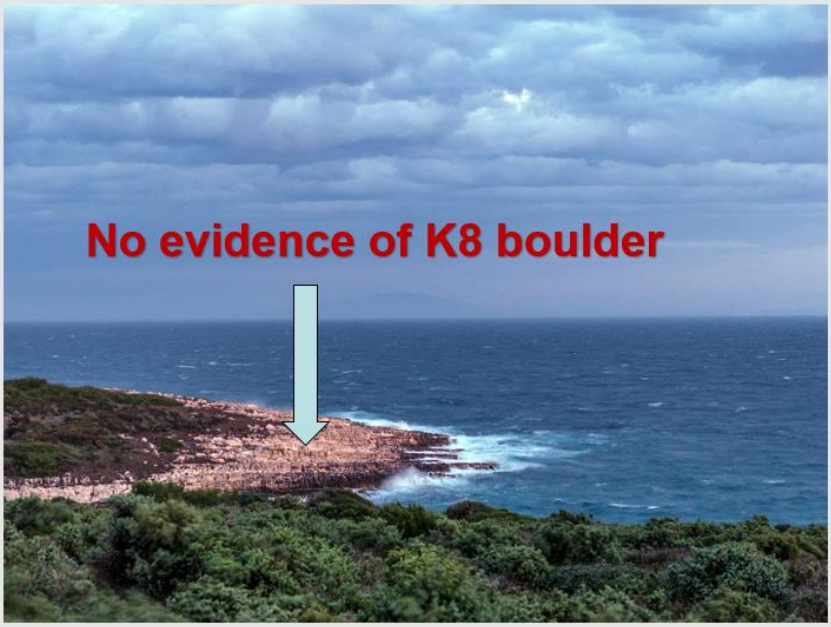

The detachment of K8 boulder was between late 2013 and early 2014 as you can see in the next slide.

HISTORICAL RECOSTRUCTION OF EXTREME WAVE EVENT

2014 06 29

ASSESSEMENT OF DATE OF DETACHEMNT OF K8 BOULDER

- The detachment of K8 boulder required a storm weight of about 13 m according to Nandasena model.
- The ECMWF data reveals that during the approximate period of K8's appearance on the shore (sometime during late 2013 – early 2014) the highest sirocco-generated waves at Premantura promontory occurred during the storm of 30th January – 2nd February 2014.
- This storm and related waves peaked on 31st January 2014, when a sirocco wind blew across the entire Adriatic Sea.
- According to Wiegel 1961 which define real wave height up to 75 % higher than SWH, waves can reach 10.6 m at location of the Premantura promontory.
- The waves could have been even higher due to the amplification caused by the bathymetry, that is particular favourable to amplify wave height.

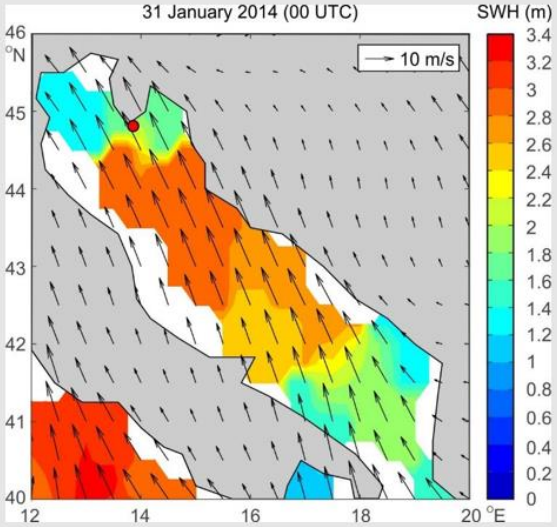

MONITORING NETWORK

- For these reasons, we have started to perform UAV surveys since 2017
- We performed three drone campaigns in 2018 (November 2018) and 2019 (April and June 2019), assisted by GCPs and FS GNNS technique, as you can see in the table below (article under review)

Table 1. Main characteristics of UAV flights carried out in 2018 and 2019.

Survey	Date	Altitude [m]	Number of pictures	Sector investigated	GSD [cm/pixel]
1	15/11/2018	30	165	W	1.039
2	15/11/2018	30	266	W	1.039
1	14/06/2019	28	294	W	0.935
2	30/04/2019	30	235	W and central	1.039
3	30/04/2019	20	229	W and central	0.693
4	30/04/2019	30	314	E	1.039
5	30/04/2019	61	253	Entire	2.078
6	30/04/2019	35	338	Central and E	1.212

MONITORING NETWORK

- According to Francioni et al (2018), UAV-DP can be considered a monitoring network and it is very useful to identify boulder dynamics

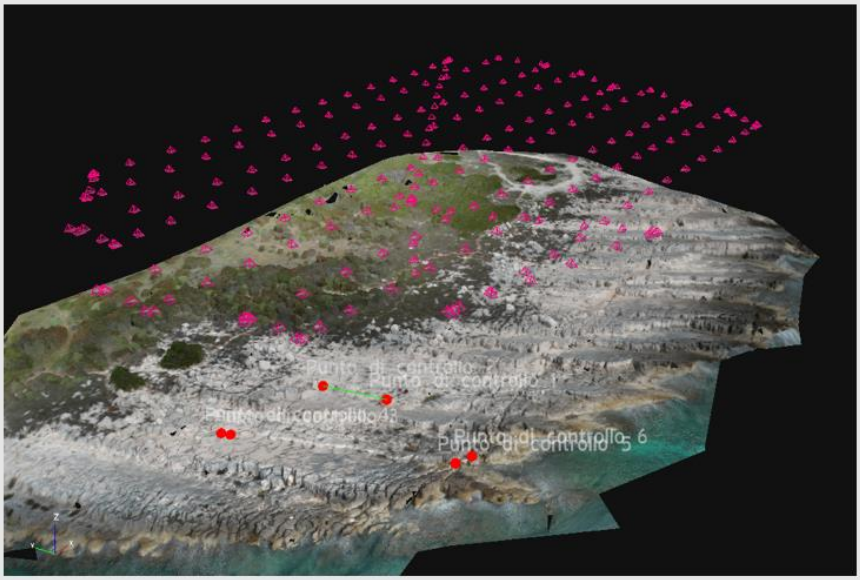

- November drone campaign was carried out two weeks after Vaia storm
- Our wave models (paper under review) for 29 October storm calculated wave heights that exceed 13 m, much more than wave heights calculated for most of 44 boulders above mentioned

Appendices.

MONITORING NETWORK

UAV-derived orthophotomosaic comparison between **2017 and 2018 surveys** validated by field activities permitted to recognise and quantify the transport or rotation motion of 14 boulders located in the western part of coastal boulder deposit. These movements are originated by VAIA severe storm which occurred on 29 October 2019.

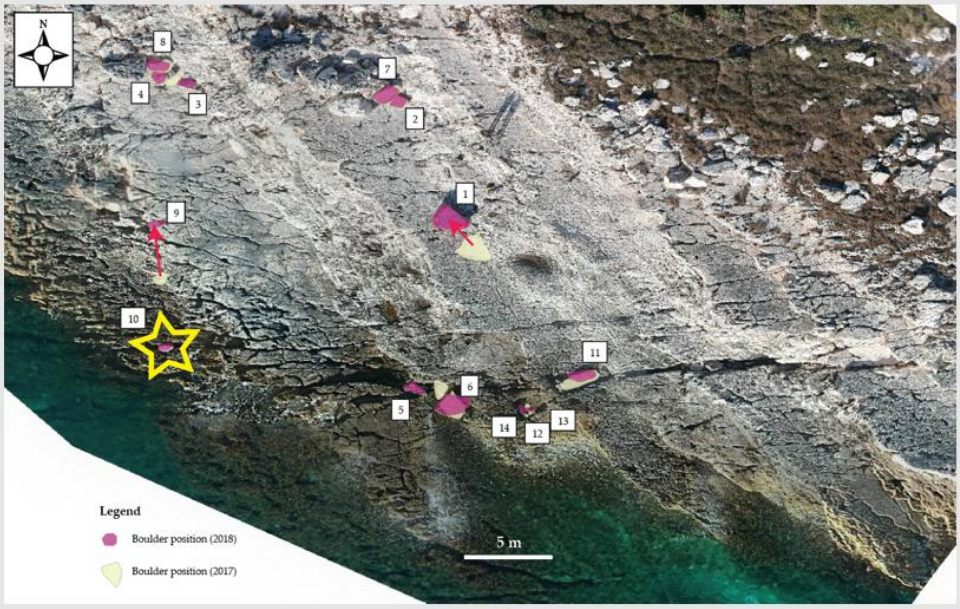

MONITORING NETWORK

2017 – 15 November 2018

Table inserted in an article under review

332

Table 2. List of boulders moved or rotated by the storm.

Boulder [#]	Axis a; b; c [m]	Displacements [m]	Direction of movement	Rotation	Nandasena wave height [m]	Notes
1	2.25; 1.65; 0.95	3	NW	Affirmative	14,22	Isolated
2	0.9; 0.9; 0.7	No transport	-	Toppled	10,48	Cluster
3	1.2; 0.6; 0.6	1	E	Affirmative	8,98	Cluster
4	1.4; 0.8; 0.7	No transport	-	Affirmative	10,48	Cluster
5	1.7; 0.9; 0.7	2	W	Affirmative	10,48	Trapped
6	2.1; 1.9; 0.7	No transport	-	Affirmative	10,48	Trapped
7	2.0; 1.4; 1.3	No transport	E	Affirmative	19,46	Cluster
8	2.0; 1.1; 0.9	No transport	-	Affirmative	13,47	Cluster
9	1.6; 0.7; 0.5	5	N	Negative	7,48	Trapped
10	1.3; 0.6; 0.6	>5	Probably N	Affirmative	8,98	New; isolated block
11	2.4; 0.9; 0.8	No transport	-	Affirmative	11,98	Isolated
12	0.8; 0.5; 0.4	0.5	SW	Affirmative	5,99	Trapped
13	0.6; 0.4; 0.3	No transport	-	Affirmative	4,49	Trapped
14	0.6; 0.4; 0.3	No transport	-	Affirmative	4,49	Trapped

Boulder movement originated by Vaia was influenced by position and possible presence of a E-W oriented joint, which trapped boulder 6, 7 12, 13, and 14

- 3D models produced using Zephyr 3D aerial software are crucial also for geomorphological observations.

- Conversely, UAV outputs did not detect any transport motion between 15 November 2018 and 30 April 2019 when we carried out the GNNS survey.

MONITORING NETWORK

- We installed a GNNS network and carried out surveys using the same procedures we have used for monitoring coastal landslides of NW Malta (Devoto et al 2012, Mantovani et al 2013, Soldati et al 2019). We are using FS techniques (Data every 2s for 20 minutes for each point (accuracy of mm).
- A master benchmark was installed just outside the area affected by possible transport processes whereas other 6 bolts were installed on 6 boulders moved by waves generated by Vaia storm.
- In order to avoid vandalism, we inserted topographic bolts. Their visual impact is much lower.

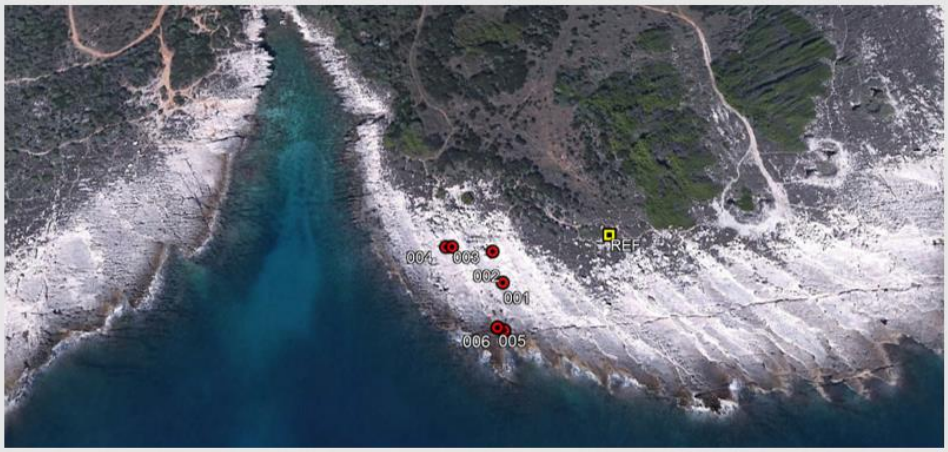

MONITORING NETWORK

APRIL 2019 – SEPTEMBER 2019

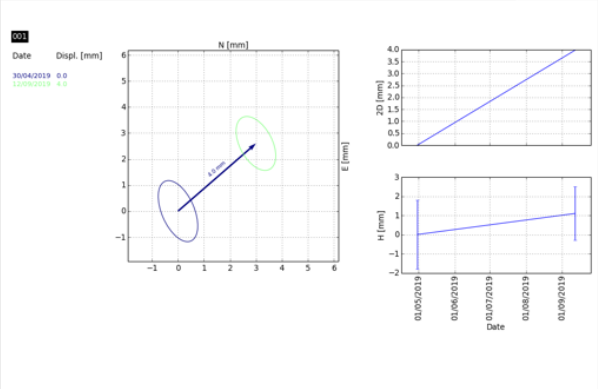

- Dr Mantovani operated GNNS survey 1 last Thursday.
- K8 boulder moved of 4.5 mm. It is not a real movement but is related to the bolts.
- Its extremely low rate of displacement is related to the fact we have inserted bolts and not benchmarks. The precarious position of the GPS antenna reduces the accuracy of the Fast Static from millimeter to centimeter.
- Any boulder monitored by GNNS show a subaerial transport process during the period investigated.

FUTURE RESEARCH ACTIVITIES

- 15th May 2019 Linley Hastewell (University of Portsmouth) joined us and we installed RFID tags on tens of boulders included 6 monitored (see Hastewell et al 2019 about boulder deposit in Isle of Wight).

Appendices.

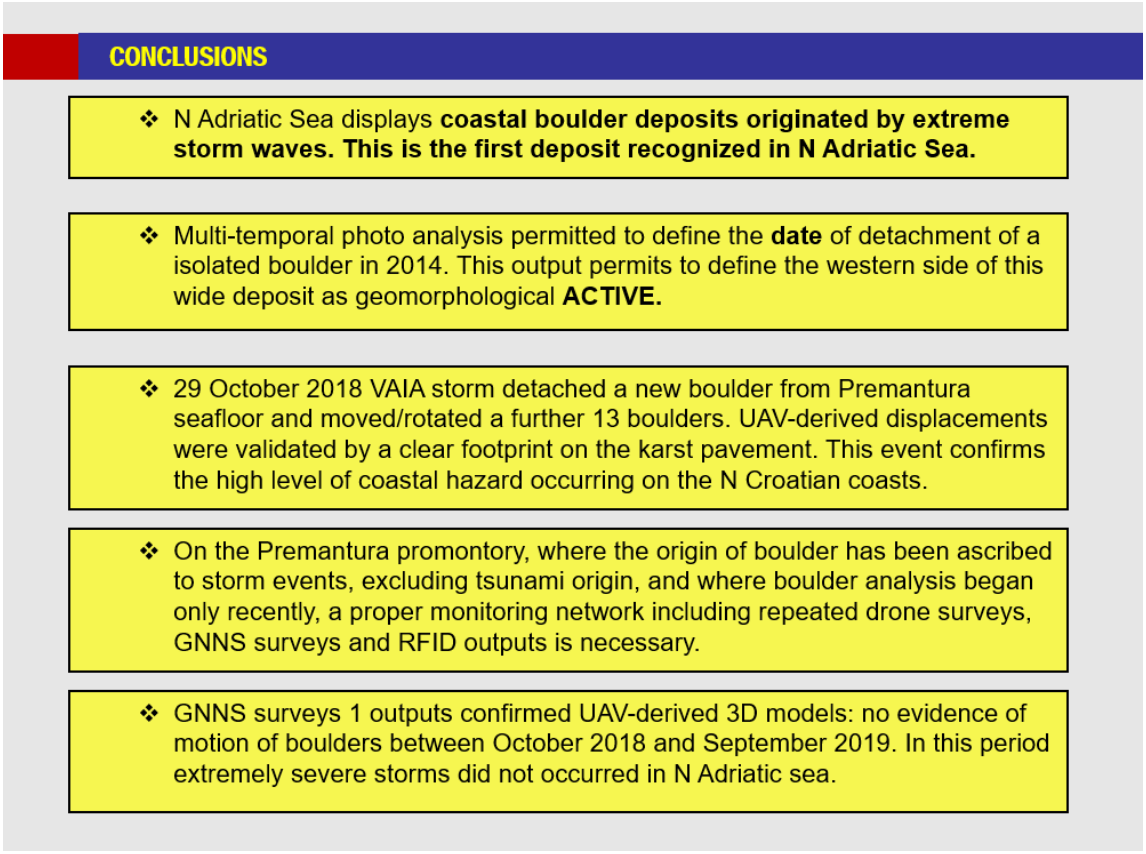

Lectures

University of Malta, Department of Geography. 20th March, 2017.

The effect of storm waves on boulder transport and shore platform evolution at Bembridge, Isle of Wight.

University of Trieste, Italy, Department of Mathematics and Geosciences. 15th May 2019.

The quantification of storm-induced boulder transport using Radio Frequency Identification (RFID) tagging on an intertidal rocky shore, Bembridge, Isle of Wight.

Conference Posters

University of Portsmouth Environment Network (UPEN) Conference, Portsmouth. 26th June, 2015.

Coastal erosion: shore platform processes and evolution at Bembridge, Isle of Wight.

British Society for Geomorphology (BSG) Annual Conference, Southampton. 7th - 9th September, 2015.

Coastal erosion: shore platform processes and evolution at Bembridge, Isle of Wight

Media exposure

Reuters UK Online - Rock 'n' roll: Storm waves can move car-sized boulders - study

Monthly Visitors: 4,016,429 (United Kingdom)

Video footage of PhD researcher Linley Hastewell's research into moderate storm waves having the power to move boulders the size of cars (Geography)

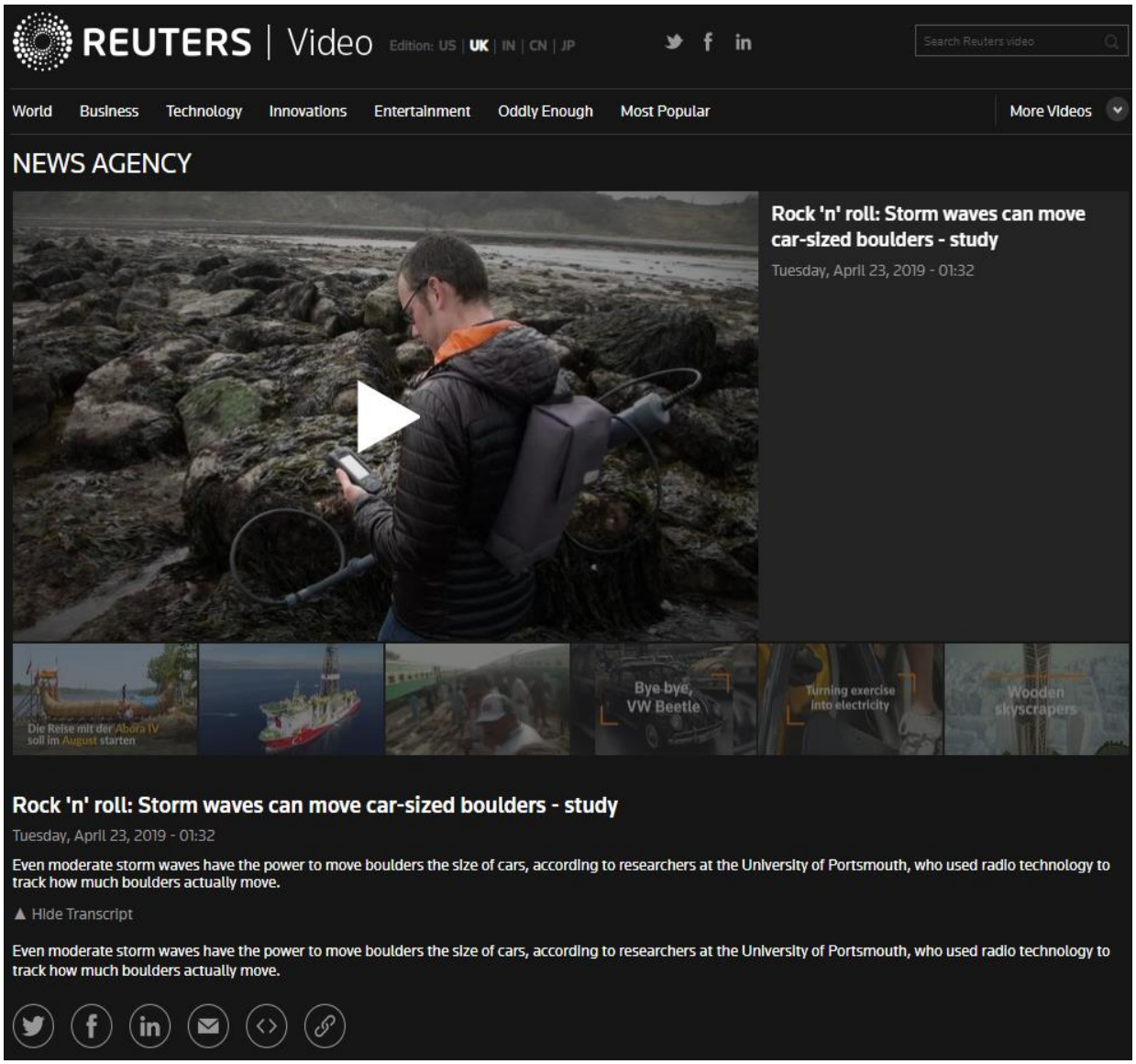

Appendices.

Interview on regional radio - BBC Radio Solent & Wave 105

Portsmouth Research Portal

UNIVERSITY OF PORTSMOUTH

Search the portal...

Home > Media > Research into storm power shows the strength of waves

Research into storm power shows the strength of waves

Press/Media: Research

Mr Linley John Hastewell

Description

University of Portsmouth researcher makes huge breakthrough in storm power study.

Period	4 Feb 2019 → 5 Feb 2019

References

Title	University of Portsmouth researcher makes huge breakthrough in storm power study.
Degree of recognition	Local
Media name/outlet	The News
Media type	Web
Country	United Kingdom
Date	5/02/19
Description	BOULDERS heavier than cars have been overturned and moved tens of metres by storms battering the Solent's sheltered bays.
URL	https://www.portsmouth.co.uk/our-region/portsmouth/university-of-portsmouth-researcher-makes-huge-breakthrough-in-storm-power-study-1-8797271
Persons	Linley Hastewell

Title	University of Portsmouth researcher makes huge breakthrough in storm power study
Degree of recognition	Regional
Media name/outlet	BBC Solent
Media type	Web
Country	United Kingdom
Date	4/02/19
Description	Coverage of research into storm power.
URL	mms.tveyes.com/mediaview/?U3RhdGlvbj01NjM1JlN0YXJ0RGF0ZVRpbWU9MiUyRjQlMkYyMDE5JTIwMTclM0EyMCU
Persons	Linley Hastewell

Appendices.

28/06/2019 Research into storm power shows the strength of waves - Portsmouth Research Portal

Title	University of Portsmouth researcher makes huge breakthrough in storm power study
Degree of recognition	Regional
Media name/outlet	Wave 105.2
Media type	Web
Country	United Kingdom
Date	4/02/19
Description	Coverage of research into storm power.
URL	mms.tveyes.com/mediaview/?U3RhdGlvbj01ODAwJlN0YXJ0RGF0ZVRpbWU9MiUyRjQlMkYyMDE5JTIwMTMlM0EwNC
Persons	Linley Hastewell

Related information

Outputs

Intertidal boulder transport: a proposed methodology adopting Radio Frequency Identification (RFID) technology to quantify storm induced boulder mobility

Local newspaper coverage (Portsmouth News).

The News

OUR REGION | PORTSMOUTH | FAREHAM | GOSPORT | HAVANT | WATERLOOVILLE | EAST HAMPSHIRE | WEST | More

University of Portsmouth researcher makes huge breakthrough in storm power study

Linley Hastewell carrying out his research at Bembridge, Isle of Wight

By TOM COTTERILL
Email

Published: 06:00
Tuesday 05 February 2019

Share this article

TRANSCRIPT: Boulders heavier than cars have been overturned and moved tens of metres by storms battering the Solent's sheltered bays, a Portsmouth researcher has found. The research, by Linley Hastewell, in the University of Portsmouth's department of geography, found rocks - some as heavy as 10.0 tonnes, were being shifted in 'mild storms' by the Isle of Wight. It is the first time evidence has been found that moderate storm waves can move very large boulders even in relatively calm waters.

He said: 'I was surprised. Everyone I've talked to about it is surprised. The Solent is a relatively sheltered location which adds to the remarkable nature of what we are seeing here. Large boulders, some weighing between 5.0 - 10.0 tonnes, are being shifted in mild storms on the sheltered eastern side of the Isle of Wight. It's a testament to the dynamic nature of our coasts and demonstrates that storm-driven waves have a far greater ability to erode and reshape the coastline than we previously realised. The research suggests we may need to reassess our current understanding of storm wave hydrodynamics.'

Although the research was carried out on the Isle of Wight, the same results are likely to be reflected on rocky coasts globally, he said. 'These coastal locations, where land meets the ocean, are our first line of defence against the erosive forces associated with storm events. How these areas respond is important for the future management of rocky coasts. The data tells us that boulders are frequently moved some distance and often overturned even in relatively small storms, which until now had never been documented in such detail.'

The research team tracked 104 limestone boulders over three years by inserting radio frequency identification (RFID) tags inside them. The boulders were located near Bembridge, on the Isle of Wight, a site protected from large Atlantic waves and the prevailing winds.

Portsmouth News website - https://www.portsmouth.co.uk/our-region/portsmouth/university-of-portsmouth-researcher-makes-huge-breakthrough-in-storm-power-study-1-8797271

Appendix 5 - Earth Surface Proceses and Landforms published article (Chapter 4, post peer-review corrections).

EARTH SURFACE PROCESSES AND LANDFORMS
Earth Surf. Process. Landforms (2020)

Published online in Wiley Online Library
(wileyonlinelibrary.com) DOI: 10.1002/esp.4834

Quantification of contemporary storm-induced boulder transport on an intertidal shore platform using radio frequency identification technology

Linley Hastewell,* Robert Inkpen, Malcolm Bray and Martin Schaefer
University of Portsmouth, School of the Environment, Geography & Geosciences, Buckingham Building, Lion Terrace, Portsmouth PO1 3HE, UK

Received 20 June 2019; Revised 31 January 2020; Accepted 3 February 2020

*Correspondence to: Linley Hastewell, University of Portsmouth, School of the Environment, Geography & Geosciences, Buckingham Building, Lion Terrace, Portsmouth PO1 3HE, UK. E-mail: linley.hastewell@port.ac.uk

ESPL
Earth Surface Processes and Landforms

ABSTRACT: Extreme storm events are known to produce, entrain, transport and deposit sizable boulders along rocky coastlines. However, the extent to which these processes occur under moderate, fetch-limited wave conditions is seldom considered. In this study we quantify boulder transport at a relatively sheltered location subject to high-frequency, low-magnitude storm activity. This was achieved by deploying radio frequency identification (RFID) tags within 104 intertidal limestone boulders ranging in size from fine to very coarse (intermediate axis: 0.27–2.85 m). The study was conducted over 3 years (July 2015–July 2018) and encompassed numerous storm events. Tagged boulders were relocated during 17 field surveys and their positions recorded using a differential global positioning navigation satellite system (DGNSS).

On completion, we identified boulder displacement in 69% of the tagged array. The accrued boulder transport distance amounted to 233.0 m from 195 incidents of displacement, including the movement of a boulder weighing an estimated 11.9 t. Transport was not confined to autumn and winter storms alone, as displacement was also recorded during summer months (April–September), despite the seasonally reduced wave magnitude.

Boulder production by wave quarrying was documented in three tagged clasts, confirming observations that the shore platform is actively eroding. Incidents of overturning during transport were also recorded, including multiple overturning of clasts weighing up to 5 t. We further identify a statistically significant difference (maximum p-value ≤ 0.03) between the transport distances attributed to constrained and unconstrained boulders, suggesting that the pre-transport morphological setting exerts considerable control over boulder transport potential.

The findings establish low to moderate storm waves as a key component in the evolution of the study site. More broadly, we claim that high-frequency, low-magnitude storms regularly modify these overlooked rocky coastal locations, suggesting that the hydrodynamic capability at such sites may previously have been underestimated.© 2020 John Wiley & Sons, Ltd.

KEYWORDS: boulder transport; storm response; RFID tagging; storm events; rocky coasts

Introduction

Rocky coasts are susceptible to geomorphological change by a range of erosive agents. This is manifest most profoundly by the presence of large coastal boulder deposits which are frequently found on exposed intertidal shore platforms and supratidal cliff tops (Hall *et al.*, 2006; Etienne and Paris, 2010; Stephenson and Naylor, 2011; Cox *et al.*, 2018, Biolchi *et al.*, 2019a, b). The emplacement of such deposits acts as a signature of past extreme wave events (Mastronuzzi and Sansò, 2000; Williams and Hall, 2004; Scheffers *et al.*, 2009; Barbano *et al.*, 2010; Goto *et al.*, 2010a, b; Paris *et al.*, 2011; Shah-hosseini *et al.*, 2011; Lau *et al.*, 2016) and reflects the magnitude of the wave activity that initiated boulder production, transport and deposition (Nott, 2003; Goto *et al.*, 2009; Nandasena *et al.*, 2011; Nandasena and Tanaka, 2013a; Roig-Munar *et al.*, 2019). Consequently, these boulders have been used as proxies for extreme storm events, including typhoon/hurricane/cyclone-generated storms (Scheffers and Scheffers, 2006; Fichaut and Suanez, 2011; Cox *et al.*, 2012; Terry *et al.*, 2016; Kennedy *et al.*, 2017; Cox *et al.*, 2018; Terry and Lau, 2018) and/or tsunami (Scicchitano *et al.*, 2007; Maouche *et al.*, 2009; Etienne *et al.*, 2011; Engel and May, 2012; Mottershead *et al.*, 2014).

Contemporary storm events have also been reported as capable of producing, entraining and transporting intertidal and supratidal clasts (Goto *et al.*, 2011; Naylor *et al.*, 2016; Autret *et al.*, 2018; Biolchi *et al.*, 2019a, b). However, previous studies commonly addressed boulder displacement at exposed sites which are subject to high-magnitude, low-frequency storm events (Goto *et al.*, 2009; Hansom and Hall, 2009; Etienne and Paris, 2010; Autret *et al.*, 2016). Coastal sites subject to low and moderate wave climates have been widely overlooked (Dasgupta, 2011), despite the presence of boulder assemblages

Appendices.

indicative of storm wave deposition. Furthermore, a lack of empirical field data on the extent to which intertidal boulders respond to contemporary low-magnitude, high-frequency storm events remains unexplored and unknown (Paris *et al.*, 2011).

This sediment tracing study aims to broaden our current understanding of boulder transport processes by quantifying boulder transport at two separate sites (Bembridge Ledge and Black Rock) on the relatively sheltered east coast of the Isle of Wight (UK). The location has a limited fetch and low to moderate wave regime (Hastewell *et al.*, 2019a). Boulder displacement has been monitored over a 3-year period using 104 intertidal limestone boulders, each embedded with a radio frequency identification (RFID) tag. The tagged boulders were periodically relocated during field surveys and their positions recorded using a differential global positioning navigation satellite system (DGNSS).

In the course of fulfilling the study aim, we further develop previous work by Naylor and Stephenson (2010), Stephenson and Naylor (2011) and Naylor *et al.* (2016) in identifying the key mechanisms that facilitate boulder production and the removal of blocks from the shore platform bedrock, and highlight the significance of platform morphology on boulder transport capability.

Inshore and nearshore wave data and tidal parameters were recorded throughout the study at two wave monitoring stations approximately 5 km from the study sites. The data provide insight to the hydrodynamic conditions that we infer initiated episodes of boulder displacement.

The transport of intertidal boulders presented herein provides a greater understanding of the responsiveness of rocky coasts to contemporary, high-frequency, low-magnitude storm events and the underlying processes and mechanisms that influence boulder production, transport and deposition within the intertidal zone. The findings will be of increased significance given that the changing climate is predicted to invoke an increase in storm frequency and intensity (Leckebusch *et al.*, 2006; Beniston *et al.*, 2007) which is expected to alter future wave climates, tidal regimes and sediment transport patterns and potentially increase rates of erosion at rocky coasts (Trenhaile, 2016).

Site Location

Bembridge is located on the east coast of the Isle of Wight, southern England and comprises a 4-km shoreline fronted by a wide shore platform (Figure 1). The study site is comprised of near-horizontal beds of late Eocene Bembridge Limestone interspersed with less resistant Bembridge Marls (Armenteros and Daley, 1998; Insole *et al.*, 1998). The limestone beds form extensive intertidal shore platforms characteristic of type-B shore platforms, being near/sub-horizontal with an abrupt seaward terminus (Trenhaile, 1987; Sunamura, 1992).

The tidal regime is classified as meso-tidal with a neap and spring tidal range of 1.8 and 3.7 m, respectively. Bembridge has a limited fetch, ranging from 140 km in the south to 185 km in the east (Hastewell *et al.*, 2019a). Its location on the east coast of the Isle of Wight provides shelter from Atlantic swell waves and the prevailing south-westerly wind direction.

Two survey sites were selected, each covering approximately 0.1 km^2 – Bembridge Ledge and Black Rock, herein referred to as BL and BR, respectively. Site selection was based on accessible intertidal boulders that were known to be mobile under low to moderate wave conditions. This was evident from the presence of sedimentary signatures and assemblages, including the deposition of individual clasts and a boulder berm, which are indicative of storm-induced transport (Figures 2 and 3). Surface striations and abrasion trails were also visible on the platform surface suggesting frequent block displacement (Hall *et al.*, 2008; Cullen and Bourke, 2018). By using two sites with differing coastal aspects it was possible to study the effects of coastal orientation and storm exposure on boulder displacement. Furthermore, unlike many previously studied boulder transport sites, Bembridge has not been subject to any recent paleotsunamigenic impacts (Long, 2017). The lack of a competing transport mechanism allows us to ascribe boulder displacement and the formation of associated geomorphic features to storm-driven activity alone.

Bembridge Ledge

Comprised of a tiered intertidal easterly oriented shore platform, the lowest part extends 500 m at its widest point. Collectively, the platforms are similar in form to those depicted and described by Hills (1972, p. 87) as a 'terraced platform with several low terraces'. The landward platform edge ranges in height from 0.2 to 1.0 m and is densely jointed with discontinuities orientated predominantly to the north and east, towards incoming wave energy. This lithological characteristic promotes block removal at the platform edge, which provides source material for transport to occur (Figure 2a).

Boulders are transported landward across the near-horizontal (0 to +1°) wave-scoured platform, which varies in width from 5 to 55 m. Boulders are found most frequently as solitary clasts on the upper platform surface or emplaced and occasionally buried within the mixed sand and gravel beach that fronts a low cliff formed in a Quaternary raised beach deposit (Insole *et al.*, 1998). The beach dissipates wave energy, reducing transport capacity and resulting in boulder deposition (Buscombe and Masselink, 2006; Almeida *et al.*, 2015) (Figure 2b).

Platform topography is generally smooth, with the exception of the occasional raised scarp, ranging from 0.1 to 0.5 m in height. Additionally, a series of shallow intertidal pools cover an area of the platform (0.007 km^2). The pools are encircled by raised rims, approximately 0.10 m in height. Isolated boulders are located within the pools, which impede further transport (Hastewell *et al.*, 2019b) (Figure 2c).

Black Rock

The southerly oriented limestone unit that forms the seaward shore platform is of greater bed thickness with fewer geological discontinuities when compared with BL and hence it produces boulders of greater size, generally ranging from medium (intermediate axis 0.5–1.0 m) to very coarse (intermediate axis 2.0–4.1 m) (after Blair and McPherson, 1999).

The seaward platform edge is between 1.0 and 1.5 m in height and is defined as horizontal (0°) to sub-horizontal in places with a slight landward dip (−1°). The wave-scoured platform is devoid of structural impediments, which facilitates transport across the platform surface (Pérez-Alberti and Trenhaile, 2015). Generally, only the largest boulders are located on the exposed platform surface, as wave energies are sufficient to facilitate the removal of small and medium-sized clasts. Where boulders are present, they are found as solitary clasts located between the platform edge and a boulder beach that extends into a boulder berm which lies between 5 and 25 m from the platform edge (Figure 3a).

The boulder beach and berm hinder landward transport by trapping and accumulating displaced clasts. Both features are

Appendices.

Figure 1. Location of study sites: (a) Isle of Wight, UK; (b) Bembridge, on the easterly point of the Isle of Wight, wave and tidal monitoring stations relative to site location; (c) study sites, Bembridge Ledge (sheltered) and Black Rock (moderately exposed), tagged boulders are indicated by the circular symbols. [Colour figure can be viewed at wileyonlinelibrary.com]

Figure 2. Bembridge Ledge: (a) boulder production at the platform edge; (b) shore platform and boulder deposition on the gravel beach; (c) deposition of detached boulders in shallow, intertidal pools. [Colour figure can be viewed at wileyonlinelibrary.com]

interpreted as distinctive sedimentary signatures of boulder transport and deposition. The seaward margin of the boulder beach and berm is characterized by imbricate, stacked clasts indicative of storm deposition (Nott, 2003; Switzer and Burston, 2010) (Figure 3b). The boulder beach covers an area of approximately 0.002 km^2 and is comprised of fine to coarse clasts. The berm consists of fine to very coarse clasts and extends 0.8 km from west to east, parallel with the platform edge. Berm width varies from 5 to 20 m.

To the rear of the berm lies a tidal lagoon with scattered cobbles on its bed. Platform topography then rises to the edge of a second, more landward horizontal (0°) intertidal rocky outcrop (upper platform) from which small boulders are detached, transported and deposited sporadically on the upper platform (Figure 3c).

Methods

RFID tagging technology was employed to monitor and quantify the displacement of an array of tagged boulders. This was achieved by recording the coordinates of each tagged boulder at the commencement of the study. Subsequent field surveys were undertaken to relocate the clasts

Appendices.

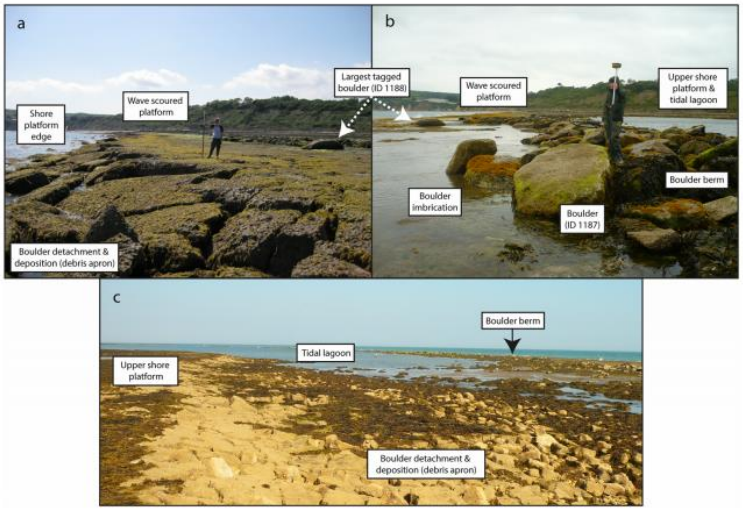

Figure 3. Black Rock: (a) boulder production, transport and deposition; (b) boulder deposition creates an extensive boulder berm, the measured clast (tag ID: 1187) has an estimated mass of 5 t – the largest tagged boulder is identified in (a) and (b) (tag ID: 1188 weighing an estimated 11.9 t); (c) boulder deposition at the front of the upper platform. The arrow indicating the boulder berm identifies the approximate location of image capture in (a) and (b). For scale, the DGNSS pole is extended to a height of 2.0 m. [Colour figure can be viewed at wileyonlinelibrary.com]

and re-record their coordinate locations, thus providing a spatial and temporal framework within which to quantify clast displacement. However, as with all sediment tracing studies, prior to tag deployment it is necessary to ensure the tagged material accurately reflects the physical properties (e.g. size and shape) of the indigenous sediments (Lee *et al.*, 2000; Sear *et al.*, 2000).

Boulder selection

Size

Size homogeneity between indigenous and tagged boulders was achieved by conducting an assessment of the boulder populations prior to tag deployment. The data were used to inform tagged boulder selection. Measurements of the long (*L*), intermediate (*I*) and short (*S*) axial dimensions of 100 randomly selected boulders at each site allowed for the classification of boulders by size, adopting the nomenclature of Blair and McPherson (1999). A comparison between the percentage frequency of the assigned size classifications between the indigenous and tagged boulders demonstrates that a representative sample has been achieved in terms of size (Figure 4).

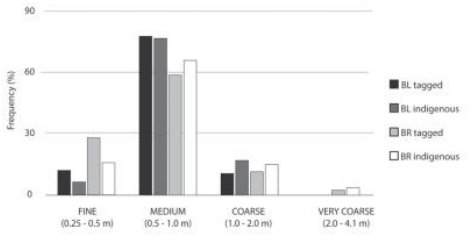

Figure 4. Frequency (%) of boulder size classification of indigenous and tagged boulders at BL and BR based on intermediate (*I*) axial dimensions (classified in accordance with Blair and McPherson, 1999).

Shape

Axial dimensions of indigenous and tagged boulders were used to determine clast shape based on Zingg (1935). Figures 5a and b identify the majority of boulders at both sites as disk-shaped (BL: tagged, 65%/indigenous, 66% and BR: tagged, 46%/indigenous, 49%). The greater number of disk-shaped clasts at BL, and the limited variability in shape, is attributed to the relative consistency in the short axis of the BL clasts (mean *c*-axis: 0.27 m), which corresponds to the mean thickness of the boulder-producing limestone unit exposed at the platform edge (approximately 0.25 m). This supports boulder provenance and suggests that clast size is litho-structurally controlled (Stephenson and Naylor, 2011; Salzmann and Green, 2012).

On the basis of our preliminary assessment, we assert that the physical properties (size and shape) of the tagged boulders are comparable with the indigenous boulder population.

Morphological setting

The position of a boulder prior to displacement is reported to be a key component in controlling its transport potential (Nott, 2003; Switzer and Burston, 2010; Nandasena *et al.*, 2011; Spiske and Bahlburg, 2011; Zainali and Weiss, 2015; Naylor *et al.*, 2016). Therefore, tagged boulders were selected to reflect a range of different morphological settings (MS's), as defined in Hastewell *et al.* (2019a), to establish their significance in terms of transport distance. Figure 6 provides examples for each MS using a field example from Bembridge Ledge.

Each morphological setting is defined by the potential for a boulder to be displaced. These boulders are referred to as being either constrained or unconstrained (Trenhaile, 2016). Of the four MSs, three are designated as constrained (MS1, MS2 and MS3), meaning that boulder transport is impeded by a range of geomorphic and/or topographic landform features such as the gravel beach, boulder beach/berm and/or imbricate boulders. Unconstrained clasts are represented in MS4; these clasts are unimpeded in their ability to be displaced. It was hypothesized that unconstrained boulders (MS4) would be mobilized

Appendices.

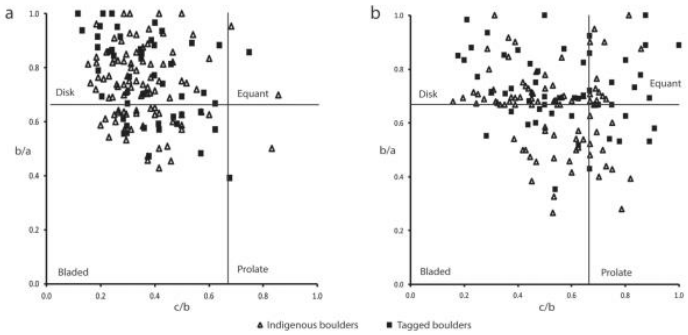

Figure 5. Zingg plots defining clast shape of indigenous and tagged boulder populations at (a) BL and (b) BR.

Figure 6. Examples of the four morphological settings (MS) as identified at BL. [Colour figure can be viewed at wileyonlinelibrary.com]

more frequently and over greater distance when compared with constrained clasts represented in other MS's.

Of the 50 tagged boulders within the BL study area, 60% were located on the platform and gravel beach, the remaining 40% were positioned on the seaward side of the platform edge. At BR, 74% of the tagged boulders were located on the seaward platform, the remaining 26% on the upper platform. There were no tagged boulders located seaward of the platform terminus at BR as the low water (LW) level would restrict access to spring tides only.

RFID

RFID technology has been used previously in littoral studies as a means of monitoring the incremental displacements of a range of sediment sizes. Previous studies have concentrated on mixed sediments including gravel, cobbles and small boulders (Nichols, 2004; Allan *et al.*, 2006; Dickson *et al.*, 2011; Miller *et al.*, 2011; Brayne, 2015; Casamayor *et al.*, 2015; Dolphin *et al.*, 2016; Han *et al.*, 2017), as opposed to focusing purely on boulder-sized clasts. As such, this research forms the first long-term monitoring study to quantify intertidal boulder transport using RFID tagging.

RFID technology was favoured over alternative methods of boulder tracing such as marine paint (Stephenson and Naylor, 2011; Naylor *et al.*, 2016), as the sensitive environmental designations at the Bembridge sites required a discrete and unobtrusive means of clast identification. Furthermore, unlike painted clasts, RFID technology enables the detection of buried material, which results in improved rates of tag recovery (Bray *et al.*, 1996).

RFID equipment consists of a transponder, referred to as a tag, an antenna, powered by the backpack reader and a handheld user interface (PDA) (Figure 7). With no internal power source, the RFID tag is small enough to be embedded within

Figure 7. RFID tagged boulder relocation at BR using tag detection equipment (left) and recording of boulder location using DGNSS (right). For scale, the DGNSS pole is extended to a height of 2.0 m. [Colour figure can be viewed at wileyonlinelibrary.com]

Appendices.

a boulder (deployed tag size 32 × 4 mm). Each tag has a pre-programmed 16-digit reference number that enables the unequivocal identification of tagged material in the field.

Tagged boulders were (re)located using the antenna. When in range, the tag transmits its unique reference number, which is displayed on the handheld interface, enabling the identification of the embedded tag and associated boulder.

Tagging protocol

The application of RFID technology to monitor boulder transport is comprehensively described in Hastewell *et al.* (2019a) and briefly summarized below. RFID tags were securely embedded within a drilled hole in each of the selected boulders, referred to as the tag insertion point (TIP). The tag was secured using a waterproof sealant and marine epoxy resin. The TIP was used as a fixed point from which the boulder coordinates were recorded during tagged boulder relocation surveys. Coordinate data were recorded using a Topcon Hiper V in real-time kinematic (RTK) mode (referred to as the DGNSS), which provided a relative horizontal accuracy of 5 mm ± 0.5 ppm (Topcon, 2018). An additional hole was drilled above the TIP to indicate the upward orientation of the boulder at the time of deployment, referred to as the orientation hole. This was used as an indicator of the transport mode; any relocated boulder found with the orientation hole below the TIP was identified as being overturned during transport.

Boulder transport

The boulder transport data are based on findings from a 3-year study (July 2015–July 2018). Transport pathways were quantified using RFID tags embedded in 104 intertidal limestone boulders; 50 at BL and 54 at BR. The tagged boulders were relocated during low water using the RFID detection equipment; 17 relocation surveys were conducted (8 at BL and 9 at BR) (Table I).

Once relocated, the boulder coordinates were re-recorded using the DGNSS. The data were stored with the unique tag ID code for processing. By conducting repeat surveys, a series of coordinate points (x, y, z) for each tagged boulder was generated. The coordinate data were processed in ArcGIS (version 10.5) using a Python script which calculated the distance and azimuth between successive points, providing a spatial and temporal frame within which individual boulder transport pathways could be determined and accurately quantified. The Python script is included in the Supporting Information Data S1.

Geomorphological surveys were conducted concurrently during relocation surveys. General site observations – including evidence of block detachment and transport – were recorded using a digital camera. Such empirical data complemented the quantitative transport data, allowing us to theorize mechanisms of boulder production and transport.

A threshold value was established to differentiate entrainment from transport. This was based on the combined errors associated with the relative accuracy of the DGNSS, the setup of the base station and the RMSE of re-surveying the TIP. Based on the cumulative values, we conservatively set the horizontal and vertical error at 0.1 m. Therefore, the entrainment/transport threshold value was set to 0.1 m. Transport values calculated via the Python script exceeding 0.1 m were defined as transported; values below 0.1 m were classified as static and/or entrained only. Subsequently, those values <0.1 m were not incorporated into any transport distance values. Additional detail on the entrainment/transport threshold is addressed in Hastewell *et al.* (2019a).

Wave climate and tidal regime

Wave-induced erosion is considered significant in modulating geomorphic change on rocky coasts (Trenhaile, 1987; Ogawa *et al.*, 2011). Therefore, an understanding of the wave conditions relative to periods of mobility is necessary to better understand wave transport processes. Wave and tidal data were obtained from two wave-monitoring stations managed by the Channel Coast Observatory (CCO). A WaveRider REX system located on Sandown Pier approximately 6 km south-west of the study site provided inshore wave conditions including wave period (s), significant wave height (H_s, m) and maximum wave height (H_{max}, m). Tidal levels were also recorded. In addition, a WaveRider buoy located 5 km to the south-west of the

Table I. Tag deployment, boulder relocation survey dates and time elapsed (days) between surveys at BL and BR

Bembridge Ledge	Survey no.	Survey date (from)	Survey date (to)	Interval between surveys (no. days)
	S1	25 July 2015[a]	03 February 2016	193
	S2	03 February 2016	17 February 2016	14
	S3	17 February 2016	01 April 2016	44
Year 1	S4	01 April 2016	23 September 2016	175
	S5	23 September 2016	25 November 2016	63
	S6	25 November 2016	08 February 2017	75
Year 2	S7	08 February 2017	05 May 2017	86
Year 3	S8	05 May 2017	10 May 2018	370
Black Rock	**Survey no.**	**Survey date (from)**	**Survey date (to)**	**Interval between surveys (no. days)**
	S1	10 July 2015[a]	03 December 2015	146
	S2	03 December 2015	06 January 2016	34
	S3	06 January 2016	19 February 2016	44
	S4	19 February 2016	31 May 2016	102
Year 1	S5	31 May 2016	01 September 2016	93
	S6	01 September 2016	09 December 2016	99
	S7	09 December 2016	22 February 2017	75
Year 2	S8	22 February 2017	24 May 2017	91
Year 3	S9	24 May 2017	11 July 2018	352

[a]Tag deployment date.

Appendices.

study site, 1.2 km from the coast in a water depth of approximately 8.0 m (OD) provided data on the nearshore wave direction, wave period, H_s and H_{max} values (Figure 1b). Wave data were recorded every 30 min, tidal every 10 min.

To define storm activity, we apply the CCO storm threshold value of 1.6 m for the Sandown Pier monitoring station. This figure is based on extreme value analysis of wave data which identifies the 0.25-year return period for significant wave height (H_s) (i.e. the wave value exceeded on average four times per year; (Channel Coast Observatory, 2018). When referring to the nearshore wave buoy we adopt the storm threshold of 2.5 m (Channel Coast Observatory, 2015).

Wave data from the inshore pier monitoring station were used to infer the storm conditions that occured at Bembridge, thus providing estimates of the wave conditions that facilitated block detachment and displacement. Field observations indicated that the inshore wave data better reflected the wave conditions encountered at the study site, therefore were favoured over the nearshore alternative. Furthermore, Héquette and Cartier (2016) recommend the use of wave parameters recorded closer to shore opposed to data derived offshore as a greater degree of interaction with seafloor bathymetry alters wave characteristics.

Results

RFID recovery rates

On completion of the 3-year study, a mean RFID tag recovery rate of 92% was achieved (88% at BL and 96% at BR). The high rate of recovery is unprecedented in previously reported littoral tracer studies over similar timescales (Chapuis *et al.*, 2014; Hastewell *et al.*, 2019a). Tag recovery rates at BL were affected by burial of tagged boulders within the beach matrix following the seasonal accretion of sands and gravel. Unfavourable tidal and wave conditions during three BR surveys prevented safe access to a number of boulders located near the LW mark, which affected the relocation of some tagged clasts.

Boulder production

Findings from geomorphological surveys undertaken at both sites provided a basis upon which we propose the mechanisms by which boulder production occurred. At BL block removal is controlled by the litho-structural characteristics of the shore platform bedrock. The heavily jointed and clearly defined bedding is exploited by breaking waves promoting detachment by wave quarrying of fracture-bound angular blocks (Naylor and Stephenson, 2010). Quarrying occurs where the ingress of water from breaking waves penetrates into the joints and bedding planes that separate individual blocks. Air pressure within the joints and planes increases, leading to crack propagation that eventually liberates the block from its adjacent neighbours (Stephenson and Kirk, 2000; Trenhaile and Kanyaya, 2007, Trenhaile, 2019) (Figure 8, inset (a)). Boulder production is also initiated by undermining, whereby a consolidated limestone unit lies above a thin bed of clay-rich marl. The preferential erosion of the subjacent marl layer creates an overhang. As the overhang increases, the overlying blocks fracture along existing discontinuities (Switzer and Burston, 2010; Herterich *et al.*, 2018) (Figure 8, inset (b)). Liberated blocks are deposited immediately seaward of the platform edge, where repeated block detachment generates an accumulation of boulders which act as source material for landward transport (Figure 8).

At BR the lithology of the unit facilitates a mode of detachment that is dominated by undermining around the mean low water mark. Abrasive material (gravels and cobbles) mobilized by wave-driven currents have created a notch within the limestone unit beneath the shore platform edge (Trenhaile, 2015). Gravity loading of the overburden eventually overcomes material rock strength, causing tension cracks resulting in block failure and detachment (Kogure *et al.*, 2006) (Figure 9a). As with BL, the detached material accumulates at the front of the platform, producing a debris apron which allows for individual boulders to be elevated onto the platform surface (Figure 9).

Boulder transport

The relocated tagged boulder coordinate data were utilized to quantify clast displacement. This was achieved by processing the coordinate data in ArcGIS (version 10.5) via a Python script. The geospatial data output provided values for the distance and direction of transport between previously recorded coordinate points. The data identified the individual boulder transport distance (IBTD) for each tagged clast between surveys. Tables II and III present data for each mobile tagged boulder and include characteristics such as the axial dimensions, MS and mass, amongst others. Python outputs for distance (m) and direction (°) of displacement for individual transport events are also reported relative to the specific survey periods, as dated. Incidents of overturning are highlighted by the shaded cells. Transport events resulting in boulder transfer between MS's are identified in bold and italicized text, along with the associated transport distance and direction that was recorded. Those boulders identified by the MS prefix/suffix nomenclature (e.g. MS4/3 were originally located in MS4 then subsequently transferred to MS3). Immobile boulder details are not included in these tables.

Additional site-specific transport data for BL and BR, and inshore wave conditions relative to each survey period, are available in the Supporting Information Table SI and SII respectively.

The mass of displaced boulders at BL ranged from 0.1 to 1.3 t. At BR, mobile boulder mass ranged from 0.1 to 11.9 t. At both sites the *a*-axis orientation of tagged boulders was generally aligned perpendicular to the direction of transport (Nott, 2003) (Figures 10 (BL) and 11 (BR)). Transport occurred relative to the prevailing wave direction from within the south-eastern quadrant. The easterly aspect of BL affords a greater level of shelter from the dominant south–south-westerly (SSW) wind and southerly wave approach when compared with BR.

Morphological classification

Each boulder was classified within a specific MS in accordance with the categories identified in Figure 6. This enabled each transport event to be assigned to a specific MS. The collated data are presented in Table IV.

IBTD values for mobile clasts were plotted relative to the MS within which transport occurred (Figures 12a and b). Each incremental transport event ≥0.1 m is represented by the respective symbol identified in the legend. Enlarged symbols indicate an incident of overturning. Boulders identified by the MS prefix/suffix nomenclature were moved (e.g. MS4/3 were originally located in MS4 (unconstrained) then subsequently transferred to MS3 (constrained)). The figures demonstrate graphically the apparent significance of the morphological setting (constrained vs. unconstrained) on the recorded boulder tranport values.

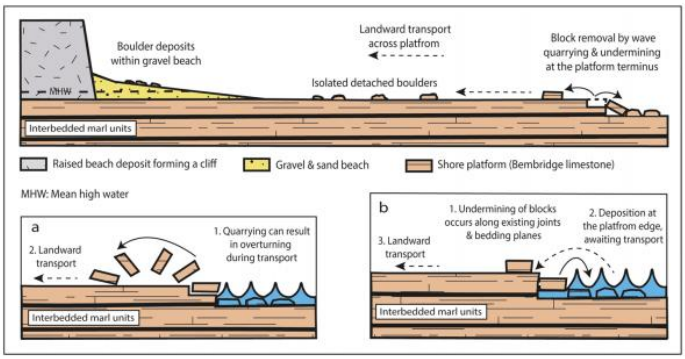

Figure 8. Bembridge Ledge – schematic diagram identifying modes of boulder production and transport; inset (a) the removal of blocks by quarrying; inset (b) block removal by undermining. [Colour figure can be viewed at wileyonlinelibrary.com]

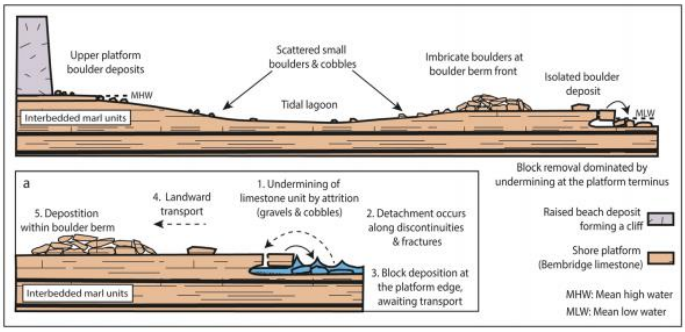

Figure 9. Black Rock – schematic diagram identifying modes of boulder production and transport; inset (a) the removal of blocks by undermining at the shore platform terminus. [Colour figure can be viewed at wileyonlinelibrary.com]

Wave climate and tidal regime

Analysis of the CCO wave data over the study period identified maximum inshore H_s and H_{max} values of 2.3 and 3.3 m, respectively (Channel Coast Observatory, 2018). Inshore H_s exceeded the CCO storm threshold of 1.6 m on 42 occasions, representing 0.07% of the total number of recorded H_s wave values (n = 63,741); H_{max} values exceeded the threshold 817 times, representing 1.28% of the total number of recorded wave values (n = 63,741). Inshore wave heights (H_s and H_{max}) recorded during the study period are presented relative to the tagged boulder relocation surveys and the CCO storm threshold (Figure 13). Inshore directional wave data are not available.

Data from the nearshore wave buoy identified that H_s values exceeded the storm threshold of 2.5 m on 85 occasions, representing 0.16% of the total number of recorded H_s wave values (n = 51,695). H_{max} waves exceeded the threshold 1022 times, representing 1.97% of the total number of recorded wave values (n = 50,743). H_s and H_{max} wave heights exceeding the 2.5 m threshold are presented in Figures 14a and b. The data identify storm wave activity and intensity as dominant from a south–south-easterly (SSE) direction; mean wave orientation was 164 ± 30°. This aligns with the southerly aspect of the shore platfrom at BR but would strike BL at an oblique angle. Notably, Figure 14b identifies a smaller proportion of H_{max} waves originate from an east-south-easterly (ESE) direction, which could directly impact BL.

Discussion

Boulder production

The deployment of RFID tagged boulders aided the identification of boulder production. Incidents of detachment amongst the tagged boulder array were recorded on three occasions at BL; detachment was not directly observed at BR. We propose that the increased occurrence of block removal by quarrying at BL was associated with the denser structural jointing and reduced bed thickness of the limestone units when compared with BR. This draws comparison with Kennedy (2010), Naylor and Stephenson (2010), Naylor *et al.* (2016) and Buchanan *et al.* (2020), who suggest that boulder production is influenced by site-specific litho-structural controls.

We present an example of boulder production by quarrying at BL (tag ID: 1148) (Figure 15). The pre-transport tagged boulder was integrated as part of the shore platform edge prior to detachment, as recorded on 25 July 2015. The dotted line represents the well-defined joints that enable water ingress from breaking waves (Figure 15a). During a relocation survey on 3

Appendices.

Table II. Bembridge Ledge – summary of individual boulder characteristics, distance (m) and direction (°) of transported boulders between specified survey periods. Cumulative survey transport totals are also provided

RFID No.	*a*-Axis (m)	*b*-Axis (m)	*c*-Axis (m)	MS	Shape	Mass (t)[a]	Times trans	S1–S2 (25 July 15–3 Feb 16)	S2–S3 (3–17 Feb 16)	S3–S4 (17 Feb–1 Apr 16)	S4–S5 (1 Apr–23 Sept 16)	S5–S6 (23 Sept–25 Nov 16)	S6–S7 (25 Nov 16–8 Feb 17)	S7–S8 (8 Feb–5 May 17)	S8–S9 (5 May 17–10 May 18)	Total IBTD (m)
1102	1.10	0.70	0.40	4	B	0.7	2	0.0	0.0	0.2 (289°)	0.0	0.5 (178°)	0.0	0.0	0.0	0.7
1104	1.10	0.68	0.32	3	B	0.6	1	0.0	0.0	0.0	0.0	0.0	1.5 (336°)	0.0	0.0	1.5
1105	1.57	0.87	0.25	3	B	0.8	4	0.0	0.2 (267°)	0.5 (94°)	0.2 (178°)	0.0	0.0	0.0	0.4 (297°)	1.3
1107	0.80	0.73	0.20	4	D	0.3	7	0.8 (107°)	0.0	0.2 (91°)	0.2 (169°)	0.1 (5°)	0.5 (193°)	0.3 (286°)	0.6 (346°)	2.7
1108	1.05	0.62	0.30	4	B	0.5	3	0.0	0.0	0.0	0.0	0.2 (86°)	0.5 (282°)	0.0	9.0 (154°)	9.7
1109	0.98	0.69	0.25	4	D	0.4	2	0.0	0.0	0.0	1.6 (71°)	0.0	0.0	0.0	1.6 (256°)	3.2
1111	1.05	0.60	0.25	4	B	0.4	6	2.7 (304°)	0.9 (44°)	0.9 (356°)	0.3 (187°)	0.0	0.7 (1°)	0.0	0.3 (57°)	5.8
1112	0.75	0.70	0.30	1	D	0.4	3	0.8 (159°)	0.0	0.0	0.3 (48°)	0.0	0.1 (285°)	0.0	0.0	1.2
1113	1.00	0.85	0.30	1	D	0.6	1	0.1 (301°)	0.0	0.0	0.0	0.0	0.0	0.0	0.0	0.1
1115	1.50	1.00	0.30	3	D	1.1	2	0.2 (344°)	0.0	0.3 (24°)	0.0	0.0	0.0	0.0	0.0	0.5
1116	0.85	0.75	0.30	3	B	0.5	1	0.0	0.0	0.0	0.0	0.0	0.0	0.0	0.8 (123°)	0.8
1117	0.90	0.87	0.35	3	D	0.7	4	0.2 (42°)	0.3 (4°)	0.1 (337°)	0.0	0.0	0.0	0.0	0.1 (146°)	0.7
1118	1.20	1.05	0.20	3	D	0.6	2	0.4 (341°)	0.0	0.0	0.0	0.0	0.0	0.0	0.2 (263°)	0.6
1120	1.15	1.05	0.20	3	D	0.6	4	0.1 (108°)	0.0	0.0	0.0	1.4 (274°)	0.1 (348°)	0.5 (280°)	0.0	2.1
1123	1.15	0.67	0.20	**4/3**	B	0.4	3	0.9 (283°)	***0.0***	***0.0***	***0.0***	***0.0***	***0.3 (1°)***	***0.1 (222°)***	***0.0***	1.3
1124	0.65	0.50	0.20	3	D	0.2	1	0.4 (350°)	0.0	0.0	0.0	0.0	0.0	0.0	0.0	0.4
1125	1.00	0.86	0.20	3	D	0.4	2	0.0	0.0	0.0	0.0	0.0	0.2 (138°)	0.0	0.2 (118°)	0.4
1127	1.60	1.50	0.20	**2/3**	D	1.2	5	0.0	7.2 (280°)	***1.2 (327°)***	***0.0***	***0.6 (340°)***	***1.1 (294°)***	***0.0***	***0.1 (315°)***	10.2
1128	0.80	0.50	0.25	4	B	0.2	6	4.9 (128°)	0.4 (210°)	0.7 (246°)	1.3 (116°)	1.6 (296°)	0.0	0.0	0.5 (208°)	9.4
1129	0.70	0.40	0.25	4	B	0.2	4	0.7 (22°)	0.0	0.0	0.8 (182°)	0.1 (334°)	0.0	0.0	1.1 (349°)	2.7
1130	1.05	0.60	0.25	4	B	0.4	4	0.0	0.2 (257°)	0.0	0.4 (341°)	0.2 (273°)	0.0	0.0	0.4 (265°)	1.2
1131	0.85	0.60	0.35	1	D	0.4	2	0.4 (256°)	0.0	0.0	0.1 (273°)	0.0	0.0	0.0	0.0	0.5
1133	0.60	0.40	0.25	1	D	0.1	1	0.9 (72°)	0.0	0.0	0.0	0.0	0.0	0.0	0.0	0.9
1134	0.80	0.65	0.30	2	D	0.4	2	0.0	0.0	0.0	0.0	0.0	0.3 (332°)	0.0	14.3 (282°)	14.6
1135	1.00	0.90	0.35	1	D	0.8	1	0.1 (344°)	0.0	0.0	0.0	0.0	0.0	0.0	0.0	0.1
1136	1.10	0.95	0.23	3	D	0.6	2	0.0	0.1 (311°)	0.0	0.0	0.0	0.0	0.0	0.1 (52°)	0.2
1137	1.00	0.70	0.25	3	D	0.4	2	0.0	0.0	0.1 (203°)	0.2 (316°)	0.0	0.0	0.0	0.0	0.3
1138	1.40	0.97	0.20	1	D	0.7	1	0.0	0.0	0.0	0.0	0.0	0.0	0.3 (344°)	0.0	0.3
1140	0.95	0.95	0.20	**1/4**	D	0.4	7	0.5 (311°)	0.8 (343°)	0.2 (169°)	0.0	0.2 (174°)	8.9 (265°)	***2.3 (334°)***	***0.3 (7°)***	13.2
1141	1.15	0.45	0.30	1	D	0.4	1	0.0	0.0	0.0	0.0	0.0	0.0	0.1 (106°)	0.0	0.1
1142	1.30	0.90	0.45	1	D	1.3	2	0.0	0.0	0.0	0.1 (263°)	0.0	0.0	0.1 (240°)	0.0	0.2
1143	0.85	0.65	0.20	4	D	0.3	2	16.1 (317°)	0.0	0.0	0.0	0.0	5.4 (335°)	0.0	0.0	21.5
1144	0.95	0.80	0.20	4	D	0.4	3	0.0	0.0	0.0	0.0	4.6 (313°)	6.3 (282°)	0.0	5.5 (356°)	16.4
1145	1.20	0.67	0.20	3	B	0.4	1	0.0	0.4 (13°)	0.0	0.0	0.0	0.0	0.0	0.0	0.4
1146	1.05	1.00	0.20	3	D	0.5	3	0.0	0.1 (350°)	0.0	0.0	0.0	0.0	0.1 (335°)	0.3 (335°)	0.5
1147	0.70	0.60	0.45	3	E	0.5	3	0.3 (288°)	0.0	0.3 (102°)	0.0	0.0	0.3 (281°)	0.0	0.0	0.9
1148	0.85	0.75	0.48	**2/3**	D	0.7	5	15.0 (315°)	***0.1 (346°)***	***1.2 (39°)***	***0.0***	***0.1 (217°)***	***0.1 (279°)***	***0.0***	***0.0***	16.5
1150	0.70	0.70	0.17	4	D	0.2	3	1.7 (359°)	0.0	0.4 (21°)	0.0	2.1 (343°)	0.0	0.0	0.0	4.2
1151	1.10	0.65	0.27	4	B	0.5	4	2.0 (273°)	1.4 (246°)	0.0	0.0	1.0 (200°)	1.1 (234°)	0.0	0.0	5.5
CUMULATIVE TRANSPORT – EVENTS (*n*)/DISTANCE (m)								21/49.2	12/12.1	13/6.3	11/5.5	13/12.7	15/27.2	9/4.0	18/35.8	112/152.8

[a]Boulder mass (axial dimensions × rock density). Density was derived via the water displacement method. Based on samples of Bembridge Limestone obtained from the study site, a rock density of 2.4 g cm^{-3} was recorded; all tagged boulders were formed of Bembridge Limestone.
Shape is defined by Zingg (1935), D = disk, E = equant, B = bladed, P = prolate.

Appendices.

Table III. Black Rock – summary of individual boulder characteristics, distance (m) and direction (°) of transported boulders between specified survey periods. Cumulative survey transport totals are also provided

RFID No.	*a*-Axis (m)	*b*-Axis (m)	*c*-Axis (m)	MS	Shape	Mass (t)[#]	Times trans	S1–S2 (10 July–3 Dec 15)	S2–S3 (3 Dec 15–6 Jan 16)	S3–S4 (6 Jan–19 Feb 16)	S4–S5 (19 Feb–31 May 16)	S5–S6 (31 May–1 Sept 16)	S6–S7 (1 Sept–9 Dec 16)	S7–S8 (9 Dec 16–22 Feb 17)	S8–S9 (22 Feb–24 May 17)	S9–S10 (24 May 17–11 July 18)	Total IBTD (m)
1152	1.50	1.00	0.50	3	D	1.8	3	0.1 (229°)	0.1 (25°)	0.0	0.0	0.0	0.0	0.0	0.0	0.1 (224°)	0.3
1154	0.90	0.80	0.70	3	E	1.2	1	0.0	0.0	0.0	0.1 (262°)	0.0	0.0	0.0	0.0	0.0	0.1
1158	1.35	0.80	0.35	3	B	0.9	1	0.0	0.0	0.0	0.0	0.0	0.0	0.0	0.0	0.3 (103°)	0.3
1160	1.30	1.00	0.25	3	D	0.8	4	0.2 (239°)	0.1 (346°)	0.0	0.1 (161°)	0.0	0.0	0.2 (64°)	0.0	0.0	0.6
1162	1.25	1.10	0.25	3	D	0.8	1	0.0	0.0	0.0	0.0	0.0	0.0	0.1 (264°)	0.0	0.0	0.1
1163	0.75	0.70	0.20	***4/3***	D	0.3	5	2.9 (147°)	2.8 (337°)	4.0 (343°)	***0.1 (327°)***	***0.0***	***0.2 (145°)***	***0.0***	***0.0***	***0.0***	10.0
1164	0.75	0.50	0.35	3	E	0.3	5	1.5 (244°)	0.7 (54°)	0.2 (43°)	0.0	0.0	0.0	0.2 (359°)	0.0	1.3 (12°)	3.9
1165	1.00	0.75	0.35	3	D	0.6	1	0.0	0.0	0.0	0.0	0.0	0.0	0.0	0.0	0.4 (199°)	0.4
1166	1.35	1.15	0.40	4	D	1.5	2	0.0	0.1 (243°)	0.0	0.0	0.0	0.0	0.1 (86°)	0.0	0.0	0.2
1168	0.65	0.60	0.40	4	E	0.4	6	0.4 (46°)	0.6 (318°)	1.4 (351°)	2.1 (23°)	0.0	0.9 (179°)	0.0	0.0	1.0 (28°)	6.4
1175	0.80	0.52	0.25	3	B	0.2	4	0.2 (294°)	0.0	0.0	0.0	0.1 (280°)	0.0	0.0	0.8 (14°)	0.2 (305°)	1.3
1177	0.45	0.40	0.40	1	E	0.2	1	0.2 (179°)	0.0	0.0	0.0	0.0	0.0	0.0	0.0	0.0	0.2
1178	0.60	0.50	0.40	3	E	0.3	2	0.1 (229°)	0.0	0.1 (58°)	0.0	0.0	0.0	0.0	0.0	0.0	0.2
1179	0.50	0.50	0.25	3	D	0.2	2	0.5 (164°)	0.2 (78°)	0.0	0.0	0.0	0.0	0.0	0.0	0.0	0.7
1180	1.25	0.80	0.30	3	B	0.7	1	0.0	0.0	0.0	0.0	0.1 (22°)	0.0	0.0	0.0	0.0	0.1
1181	0.80	0.50	0.30	***4/3***	B	0.3	2	1.2 (141°)	***0.2 (200°)***	***0.0***	***0.0***	***0.0***	***0.0***	***0.0***	***0.0***	***0.0***	1.4
1182	0.70	0.60	0.40	4	E	0.4	2	0.2 (93°)	0.1 (87°)	0.0	0.0	0.0	0.0	0.0	0.0	0.0	0.3
1183	0.60	0.50	0.40	4	E	0.3	5	0.8 (232°)	0.1 (352°)	0.1 (73°)	0.2 (313°)	0.3 (61°)	0.0	0.0	0.0	0.0	1.5
1184	0.85	0.45	0.35	3	P	0.3	1	0.0	0.0	0.0	0.0	0.0	0.0	0.0	0.0	0.5 (331°)	0.5
1185	0.65	0.60	0.40	4	E	0.4	7	0.0	0.0	0.6 (317°)	2.5 (16°)	0.8 (23°)	2.1 (69°)	0.4 (32°)	0.3 (37°)	4.8 (31°)	11.5
1186	0.65	0.45	0.40	3	E	0.3	1	0.1 (26°)	0.0	0.0	0.0	0.0	0.0	0.0	0.0	0.0	0.1
1187	2.90	1.60	0.45	***4/3***	B	5.0	3	0.0	0.0	0.9 (4°)	6.4 (335°)	***0.0***	***2.5 (110°)***	***0.0***	***0.0***	***0.0***	9.8
1188	2.90	2.85	0.60	4	D	11.9	2	0.0	0.0	0.0	0.5 (60°)	0.0	3.1 (308°)	0.0	0.0	0.0	3.6
1189	2.00	1.70	0.30	4	D	2.4	3	0.0	0.0	0.2 (110°)	1.6 (351°)	0.0	0.8 (354°)	0.0	0.0	0.0	2.6
1190	1.40	0.60	0.40	2	P	0.8	1	0.0	0.0	0.1 (290°)	0.0	0.0	0.0	0.0	0.0	0.0	0.1
1192	1.25	0.75	0.35	***4/3***	B	0.8	4	0.0	1.1 (15°)	1.8 (334°)	5.4 (354°)	***0.0***	***0.0***	***0.1 (87°)***	***0.0***	***0.0***	8.4
1195	0.85	0.45	0.40	4	P	0.4	1	0.0	0.0	0.0	0.9 (324°)	0.0	0.0	0.0	0.0	0.0	0.9
1197	0.95	0.55	0.50	4	P	0.6	4	0.2 (283°)	0.8 (253°)	0.9 (82°)	7.8 (348°)	0.0	0.0	0.0	0.0	0.0	9.7
1199	0.80	0.50	0.40	1	P	0.4	2	0.0	0.0	0.2 (216°)	0.0	0.0	0.0	0.0	0.0	0.2 (228°)	0.4
7352	0.50	0.27	0.20	4	P	0.1	2	0.7 (295°)	0.0	0.0	0.0	0.0	0.0	0.0	0.0	0.4 (228°)	1.1
7353	1.20	0.85	0.30	3	D	0.7	1	0.0	0.0	0.0	0.0	0.0	0.0	0.0	0.0	2.7 (20°)	2.7
7354	0.58	0.40	0.25	4	D	0.1	1	0.0	0.0	0.0	0.0	0.0	0.0	0.0	0.0	0.6 (135°)	0.6
7356	0.45	0.35	0.30	4	E	0.1	2	0.0	0.0	0.0	0.0	0.0	0.0	0.1 (109°)	0.0	0.1 (262°)	0.2
CUMULATIVE TRANSPORT – EVENTS (*n*)/DISTANCE (m)								15/9.3	12/6.9	12/10.5	12/27.7	4/1.3	6/9.6	7/1.2	2/1.1	13/12.6	83/80.2

Appendices.

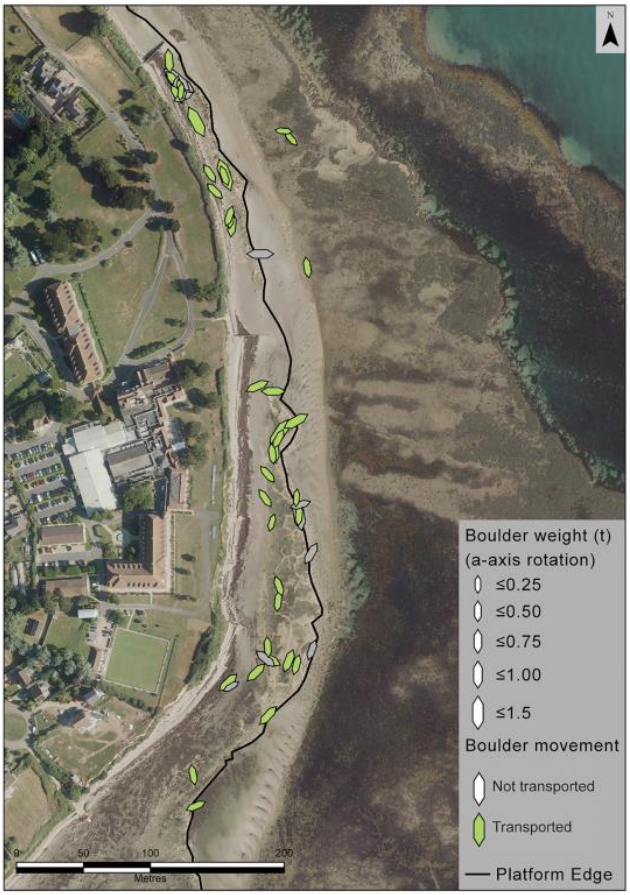

Figure 10. Bembridge Ledge site map identifying tagged boulder location, mass range, *a*-axis orientation and transport capacity. [Colour figure can be viewed at wileyonlinelibrary.com]

February 2016, the tagged block had become detached from the bedrock strata. The remnants of block removal are illustrated by a socket which clearly displays differing colouration from the surrounding bedrock unit, indicating recent exhumation (Figure 15b). The same quarrying signature was observed by Hall *et al.* (2008) on the coast of Shetland (Scotland) and by Knight and Burningham (2011) on the north-west coast of Ireland. The detached boulder was relocated 15.0 m from the socket, having been overturned during transport, as indicated by the downward position of the orientation hole. The boulder's landward trajectory was impeded by a raised scarp (0.2 m), suggesting that local morphological features exert influence on boulder transport (Figures 15c and d).

Whilst quantifying volumetric meso-erosion at the platform edge was not in the scope of this study, recorded block removal signifies that erosion readily occurs at the platform terminus. Given the protective role of shore platforms in dissipating wave energy (Stephenson and Kirk, 2000), any erosion to the platform presents the increased prospect of denudation at the cliff/platform interface. This is of significance when considering the susceptibility to erosive forces of the weakly consolidated raised beach deposit at BL. Such active erosion presents societal implications with regard to loss of natural capital and risk associated with damage to businesses, housing and associated infrastructure (Figure 15d).

Boulder transport

Despite the moderate storm wave climate compared with previous boulder transport study sites (Hall *et al.*, 2008; Goto *et al.*, 2009; Knight and Burningham, 2011; Cox *et al.*, 2012; Autret *et al.*, 2016; Naylor *et al.*, 2016), the data demonstrates that extreme storm conditions are not necessary to mobilize boulder-sized clasts.

The total distance of boulder transport measured over the 3-year study amounted to 233.0 m, 66% (152.8 m) occurring at BL and 34% (80.2 m) at BR. This resulted from 195 individual transport events each ≥0.1 m, 57% (n = 112) occurring at BL and 43% (n = 83) at BR. Of the 104 boulders in the array, 69% (n = 72) were mobile at least once over distances ranging from 0.1 to 21.5 m, with a greater number of mobile clasts at

Appendices.

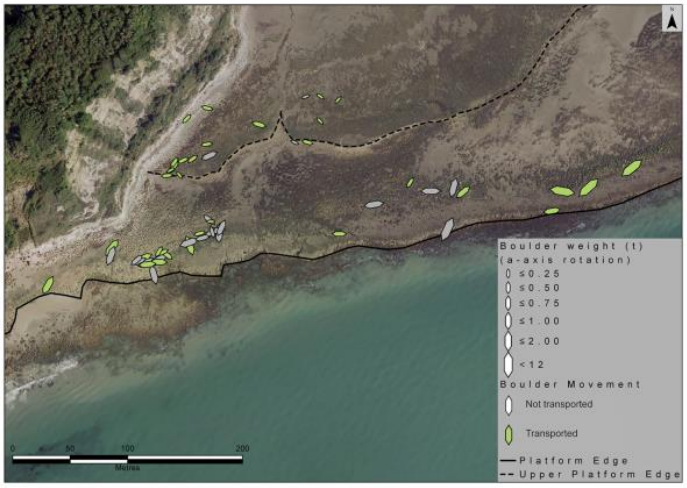

Figure 11. Black Rock site map identifying tagged boulder location, mass range, *a*-axis orientation and transport capacity. [Colour figure can be viewed at wileyonlinelibrary.com]

Table IV. Summary of boulder transport values by morphological setting at Bembridge Ledge and Black Rock

	Morphological setting (MS)	Transport total (m) (% of total)	No. of times transported (% of total)	No. of boulders (movers/non-movers)	Mean transport distance per event (m)
	1	14.0 (9%)	17 (15%)	13 (9/4)	0.8
	2	36.8 (24%)	4 (3%)	4 (3/1)	9.2
	3	15.5 (10%)	42 (38%)	20 (14/6)	0.4
	4	86.5 (57%)	49 (44%)	13 (13/0)	1.8
Bembridge Ledge	**TOTAL**	**152.8**	**112**	**50 (39/11)**	**1.4**
	1	0.6 (1%)	3 (4%)	3 (2/1)	0.2
	2	0.1 (0%)	1 (1%)	2 (1/1)	0.1
	3	14.3 (18%)	32 (38%)	25 (14/11)	0.4
	4	65.2 (81%)	47 (57%)	24 (8/16)	1.4
Black Rock	**TOTAL**	**80.2**	**83**	**54 (25/29)**	**1.0**
	1	14.6 (6%)	20 (10%)	16 (11/5)	0.7
	2	36.9 (16%)	5 (3%)	6 (4/2)	7.4
	3	29.8 (13%)	74 (38%)	45 (28/17)	0.4
	4	151.7 (65%)	96 (49%)	37 (21/16)	1.6
TOTAL (BL & BR)	**TOTAL**	**233.0**	**195**	**104 (64/40)**	**1.2**

BL: 39/50 (78%) than BR: 33/54 (61%). Of the 72 displaced boulders, 11% were mobilized on five or more separate occasions. Transported boulders were represented in each of the boulder size categories (Blair and McPherson, 1999), including a very coarse clast (estimated mass: 11.9 t, tag ID: 1188) that was transported twice, accumulating an IBTD of 3.6 m. Furthermore, the study total for transport distance at BL was 90% higher than at BR. We attribute this, in part, to litho-structural differences in the boulder-producing bedrock units at the sites (Cruslock *et al.*, 2010; Naylor and Stephenson, 2010; Stephenson and Naylor, 2011). The more densely jointed bedrock at BL produces a greater number of smaller mobile clasts compared to BR (BL: mean tagged boulder mass = 0.5 t/max. = 1.3 t and BR: mean tagged boulder mass = 1.1 t/max. = 11.9 t).

By comparison, Naylor *et al.* (2016) conducted a 4-day boulder transport study documenting the displacement of 46 painted clasts (coarse cobbles to medium boulders) during an extra-tropical cyclonic storm in 2008. Recorded transport distances were generally higher than those reported herein, with a number of clasts being displaced over several tens of metres; maximum net transport distance of a single boulder, 91.2 m. However, wave conditions were reportedly greater (H_{max} = 5.96 m) and boulder mass was generally lower (ranging from 0.014 to 0.73 t) than the Bembridge tagged clasts.

Seasonality of boulder displacement was evident, with increased transport occurring between September and February, corresponding with greater wave magnitudes associated with autumn and winter storm events. However, the longevity of the study demonstrated that transport also occurred during periods of perceived quiescence (e.g. spring and summer months; April–September). The transport data identified boulder displacement occurred even under low-energy wave conditions, when the inshore H_s failed to breach the CCO storm threshold of 1.6 m. At BL between 1 April and 23 September 2016, 11 transport events occurred, amounting to displacement of 5.5 m, 4% of the BL study total of 152.8 m (mean transported boulder mass = 0.5 t). At BR between 31 May and 1 September 2016, transport of 1.3 m, 2% of the BR study total of 80.2 m was

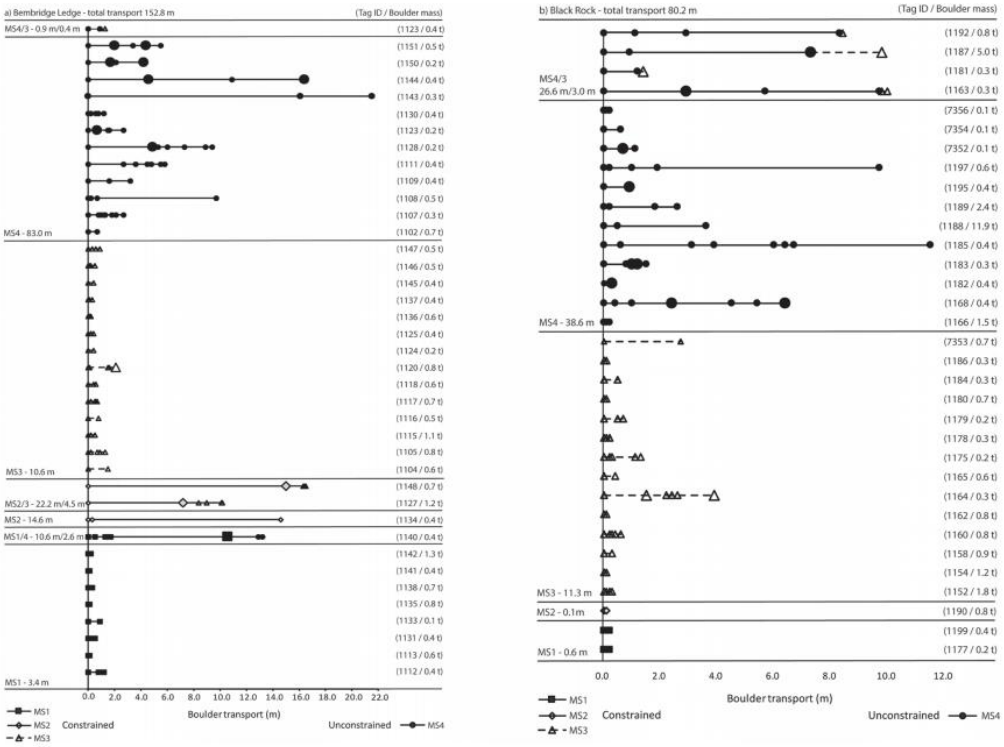

Figure 12. Individual boulder transport events identified by MS at (a) Bembridge Ledge and (b) Black Rock.

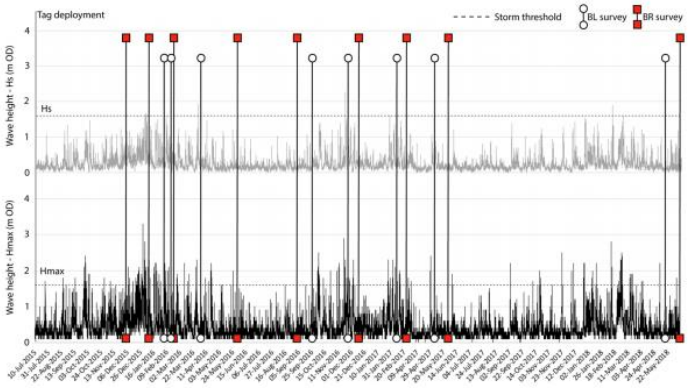

Figure 13. Inshore wave data from Sandown Pier (H_s and H_{max}) and CCO storm threshold value (1.6 m). Boulder relocation surveys are identified as indicated relative to wave activity. [Colour figure can be viewed at wileyonlinelibrary.com]

recorded from four transport events (mean transported boulder mass = 0.4 t). The maximum recorded inshore wave height (H_s) during these periods was 1.5 and 1.0 m, respectively.

The output from the Python script detailed transport distance (m) and direction of displacement between points (°). This provided insight to the boulder transport pathways and clast deposition. Notably, the dominant direction of transport at BL occurred between 270 and 0°; at BR this occurred in a northerly direction, between 315 and 45°. Transport at both sites appears to be closely aligned with the prevailing southerly wave approach. The directional transport data were applied to the shoreline orientation at each site to establish the onshore/offshore sediment flux. The general orientation of the platform edge at BL runs from north to south, thus transport

Appendices.

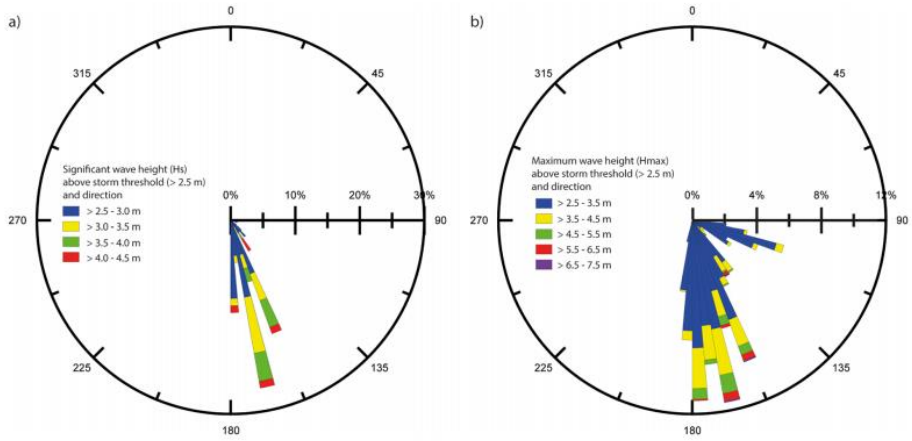

Figure 14. Nearshore wave height (Sandown Bay), frequency (%) and direction (°): (a) significant wave height, H_s (m); (b) maximum wave height, H_{max} (m). [Colour figure can be viewed at wileyonlinelibrary.com]

Figure 15. Bembridge Ledge – block removal by quarrying from the platform edge (tag ID: 1148): (a) pre-transport tagged boulder; (b) post-transport boulder socket; (c) post-transport deposition; (d) transport pathway, as indicated by the arrow, pre-transport detachment setting (left) to deposition (right). Note the active rotational sliding of raised beach cliff (right). For scale, the DGNSS pole is extended to a height of 2.0 m. [Colour figure can be viewed at wileyonlinelibrary.com]

orientated between 0 and 180° was regarded as transported offshore. Transport between 180 and 360° was deemed to be transported onshore. The data identified that 80% (123.0 m) of the 152.8 m study total at BL was transported onshore, the remaining 20% (29.8 m) offshore (Figure 16a). Conversely, the platform edge at BR is orientated east to west. Therefore, transport orientated between 90 and 270° was considered offshore transport, instances orientated between 270 and 90° were classed as onshore transport. Of the 80.2 m study total, 81% (64.9 m) was orientated onshore, 19% (15.3 m) offshore (Figure 16b).

At both sites the majority (~80%) of boulder transport resulted in onshore deposition, as dictated by the dominant storm wave approach at and across the shore platform surface. The higher percentage values for onshore transport suggest that both sites are depositional with regard to boulder-sized sediments. This may be beneficial, with continued clast deposition reducing wave attenuation across the shore platform and

Appendices.

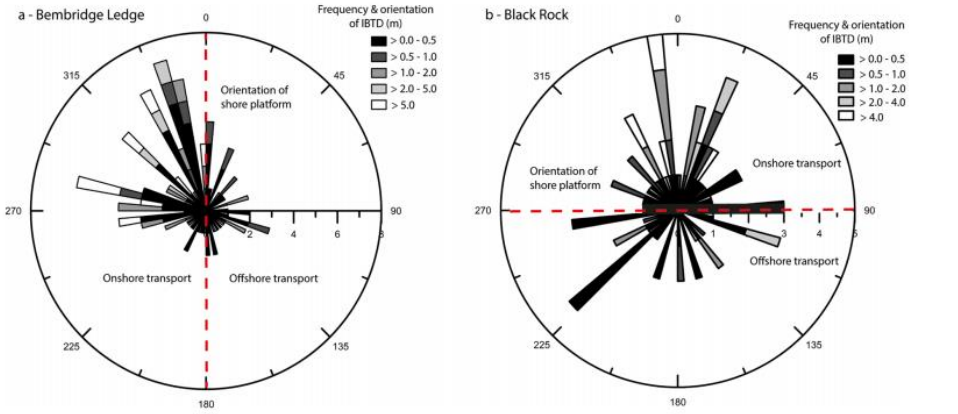

Figure 16. Frequency and orientation of boulder transport categorized by IBTD (m) as specified in the figure legends. Shore platform orientation is indicated by the centrally located dashed line: (a) Bembridge Ledge; (b) Black Rock. [Colour figure can be viewed at wileyonlinelibrary.com]

minimizing the wave energy delivered to the cliff/platform interface (Trenhaile, 2016). The orientation of the platform edge at BL relative to the prevailing wave activity produces more cross-shore boulder transport than at BR. Furthermore, the offshore transport at both sites indicates that wave backwash is capable of mobilizing boulder-sized clasts (Knight *et al.*, 2009; Knight and Burningham, 2011).

Boulder deposition by storm waves was apparent from the recorded *a*-axis orientation of each tagged boulder. The *a*-axis is reported to be aligned parallel to the shore platform and/or perpendicular to the direction of storm wave approach (Nott, 2003; Salzmann and Green, 2012). At BL, 74% of *a*-axis orientations were aligned between 315 and 45°. At BR, 70% were aligned between 45 and 135°. Figures 10 (BL) and 11 (BR) highlight the general trend of tagged boulder alignment parallel with the shore platform edge, indicative of transport under storm wave conditions. McKenna (2005) suggests not only that *a*-axis orientation is a reflection of storm wave approach, but also that the lack of an orientational trend may result from boulder collision. The field evidence and presence of widely scattered individual clasts on the platforms suggests boulder–boulder interactions are likely to be infrequent and do not impact boulder transport potential significantly.

Although the field data affirm that low to moderate storm waves facilitate boulder transport, the complexity of the mechanisms and processes that enable such transport require further investigation. Previous research has indicated that a range of parameters exert influence on boulder displacement, including geological discontinuities (McKenna *et al.*, 2011; Stephenson and Naylor, 2011), boulder mass (Goto *et al.*, 2011), shape (Imamura *et al.*, 2008), pre-transport setting (Nott, 2003; Nandasena *et al.*, 2011), surface roughness (Weiss, 2012), morphological setting (Naylor *et al.*, 2016) and boulder interactions/collisions (Knight and Burningham, 2011; Nandasena and Tanaka, 2013b).

Naylor *et al.* (2016) identified a limited relationship between transport distance and boulder mass and shape. Our data support these findings, whereby Figures 17a and b identify no significant relationship between boulder transport and mass (r^2 values of 0.01 and 0.03 at BL and BR, respectively) or shape. This implies that boulder transport is not a direct function of these properties, suggesting an alternative factor governs the extent to which transport occurs.

Role of morphological setting

Given the aforementioned limited relationship between boulder mass, shape and transport, we considered the morphological pre-transport boulder setting as a factor in controlling clast displacement. Data presented in Table IV and Figures 12a and b suggest a clearer relationship between clast displacement and the morphological setting of the tagged boulders.

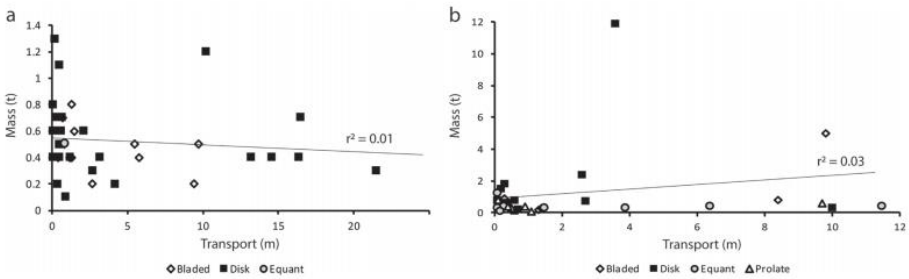

Figure 17. Recorded transport distance against boulder mass: (a) Bembridge Ledge; (b) Black Rock.

Appendices.

MS1: incorporating MS1/4

Boulders assigned to MS1 were generally moved only short distances, owing to the impediment of the platform edge. Only one boulder (tag ID: 1140) at BL was translocated from a constrained setting (MS1) to an unconstrained setting (MS4) on the platform surface. Although originally constrained by the platform edge, wave activity initiated incremental movements prior to storm conditions emplacing the clast onto and across the platform amounting to 10.6 m of transport; the boulder was known to have been overturned during transport. Subsequent wave activity when in an unconstrained setting (MS4) amounted to a further 2.6 m of transport. Collectively, MS1 clasts amounted to just 6% (14.6 m) of study total transport (233.0 m), the lowest of all MS's.

MS2: incorporating MS2/3

Transport of boulders classified within MS2 related to incidents of block detachment from the platform edge. Three incidents of wave quarrying were recorded at BL (Figure 15). Once detachment occurred, subsequent wave action provided a sufficient lift force to elevate the boulders onto the shore platform. Quarried boulders (tag ID: 1127*, 1134 and 1148*) were displaced 7.2*, 14.3 and 15.0 m*, respectively (* identifies boulders as being overturned during transport).

Despite the limited number of quarried boulders ($n = 3$), the examples provided indicate that following clast detachment from a joint-bound setting, transport distances were considerable when compared with displacement from other MS's: 7.4 m per transport event compared with 0.7 m (MS1), 0.4 m (MS3) and 1.6 m (MS4). The total transport distance attributed to quarried boulders equates to 36.9 m, 16% of the study total from just 3% of the recorded transport events. Although the number of quarrying events is insignificant, the associated displacement is considerable. It also suggests that the platform edge at BL is actively eroding. By contrast, quarrying was not recorded at BR.

MS3

Although recorded transport events were frequent, clast mobility was impeded by morphological features including raised scarps, intertidal pools, the gravel beach at BL and the boulder beach and berm at BR. This resulted in small incremental displacements, only 12% of MS3 transport incidents exceeded 0.5 m. By comparison, 60% of MS4 transport events were ≥0.5 m. The restricted displacement of MS3 boulders is further reflected in the transport values; 13% of the study transport total from 38% of the transport events producing the lowest mean distance per transport event, 0.4 m. Such was the restrictive transport potential of MS3 boulders there were no incidents of translocation to other MS's. Notably, 53% of the boulders that failed to move during the study were assigned to MS3.

MS4: incorporating MS4/3

MS4 boulders constitute 65% (57% at BL, 81% at BR) of the study total transport from 49% of the transport events, producing a mean distance per event of 1.6 m. Figures 12a and b indicate a preponderance of displaced MS4 and MS4/3 boulders. Significantly, they also highlight that subsequent to episodes of mobility, those MS4 clasts translocated to a constrained setting (MS4/3) were limited in their ability to be further displaced, as evidenced by the respective suffix values. This supports the findings of Naylor *et al.* (2016), who suggest the post-transport morphological setting also exerts limitations on boulder displacement.

The findings indicate, and support our hypothesis, that collectively unconstrained boulders (MS4) were transported further and more frequently than those in constrained settings (MS1, MS2 and MS3). However, individual constrained clasts liberated from a joint-bound setting (MS2) were transported further during the initial detachment phase.

A series of Mann–Whitney tests were conducted to determine whether a statistically significant difference existed between boulder transport distances and the morphological setting (constrained/unconstrained). This was carried out for BL, BR and BL/BR collectively ($\alpha = 0.05$). The test was conducted with and without non-mobile boulders (excluding non-movers) (Table V).

Statistical analysis highlights the significance of the morphological setting in facilitating boulder transport. The distance over which constrained and unconstrained boulders are mobilized is significantly different at both sites, $p \leq 0.05$. The median values also highlight the difference in transport distances attributed to unconstrained/constrained boulders. We therefore assert that the extent to which a boulder is displaced is significantly affected by the pre- and post-morphological

Table V. Mann–Whitney test results; boulder transport distances summarized by morphological setting (MS1/MS2/MS3 – constrained; MS4 – unconstrained)

Bembridge Ledge ($n = 50$)	*p*-Value	Median transport distance (m) constrained/unconstrained
Constrained ($n = 37$) vs. unconstrained ($n = 13$)	0.0001	0.4/4.2
Constrained ($n = 26$) vs. unconstrained ($n = 13$)(exc. Non-movers)	0.0010	0.6/4.2
Black Rock ($n = 54$)	***p*-Value**	**Median transport distance (m) constrained/unconstrained**
Constrained ($n = 30$) vs. unconstrained ($n = 24$)	0.0323	0.1/0.8
Constrained ($n = 17$) vs. unconstrained ($n = 16$) (exc. Non-movers)	0.0017	0.3/2.0
Bembridge Ledge & Black Rock ($n = 104$)	***p*-Value**	**Median transport distance (m) constrained/unconstrained**
Constrained ($n = 67$) vs. unconstrained ($n = 37$)	0.0002	0.2/1.5
Constrained ($n = 43$) vs. unconstrained ($n = 29$) (exc. Non-movers)	0.0000	0.5/3.2

Appendices.

setting. This data also validates the findings of Naylor *et al.* (2016), who identified geomorphic platform features including mass boulder assemblages and topographic irregularities as impediments to transport.

Aside from the aforementioned factors affecting transport, there is an additional spatial component that requires consideration. At BL, the mixed sand and gravel beach at the rear of the platform is the main geomorphic obstacle impeding boulder transport. Platform width, measured from the platform terminus to the beach, ranges from 5 to 55 m. At BR, landward transport is impeded by the boulder beach and berm; platform width from the seaward terminus to these features ranges from 15 to 40 m. While both landforms restrict displacement, the available distance across which transport can occur prior to encountering such an obstacle is greater at BL than at BR. Hence the larger recorded transport distances.

Mode of transport

Despite the growing interest in boulder transport studies, there remains limited quantitative evidence regarding transport modes during entrainment and displacement (Goto *et al.*, 2011; Paris *et al.*, 2011; Naylor *et al.*, 2016). Incorporating the orientation hole into each tagged boulder provides insight to transport mechanisms during episodes of mobility. Those clasts found with the orientation hole below the embedded RFID tag were known to have been overturned at least once during entrainment and/or transport. Of the 195 transport events recorded, 13% (n = 26, BL: 12 and BR: 14) resulted in overturning. Such incidents at BL accounted for 46% (69.7 m) of the total transport; the mean overturning transport distance was 5.8 m, the maximum was 16.1 m. At BR, overturning accounted for 24% (19.6 m) of the total transport at the site, producing a mean overturning transport distance of 1.4 m; the maximum was 6.4 m. Collectively, 38% (89.3 m) of the transport total was attributed to overturning, consequently 62% to displacement by sliding. The data demonstrates, with field-based evidence, that overturning of boulders weighing up to 5 t is possible during high-frequency, low-magnitude storm events. Furthermore, it affirms the assertion that overturning results in greater transport distances than sliding (Imamura *et al.*, 2008) and confirms the findings of Noormets *et al.* (2004), Nandasena and Tanaka (2013b) and Zainali and Weiss (2015), who applied numerical modelling to establish sliding as the more dominant mode of boulder transport.

Wave climate and tidal regime

Transport and wave data indicate that increased wave magnitude does not always correspond to greater transport distance. To illustrate this, Table VI presents a summary of transport and wave parameters relating to two consecutive survey periods at BL. The transport distances associated with the period between 23 September and 25 November 2016 coincided with Storm Angus (20 November 2016), when the largest wave height (H_s) of the study was recorded (H_s = 2.3 m at Sandown Pier).

The data identify that the greater transport distance is attributed to the latter survey period, despite the reduced storm wave activity. The key difference between the two event periods is the direction of storm wave approach relative to the aspect of the shore platform. Wave activity associated with Storm Angus occurred from a SSE direction (154°) opposed to ESE (115°), as was the case with the weaker storm event. It is proposed that the ESE wave direction had a greater transport potential on the east-facing platform of BL than the more southerly wave activity. This suggests that wave magnitude alone is not a reliable or accurate indicator of boulder transport potential (Kennedy *et al.*, 2019), and other factors including storm wave direction relative to the coastal aspect require consideration.

The extent to which transport of coarse and very coarse clasts occurred under low to moderate storm wave activity was unexpected. The transport data identified that the three largest mobile clasts, as defined by mass, were all located at BR – estimated mass 2.4 t, tag ID: 1189; estimated mass 5.0 t, tag ID: 1187*; estimated mass 11.9 t, tag ID: 1188 (*overturned twice). During the study, the three boulders were displaced 2.6, 9.8 and 3.6 m, respectively, totalling 16.0 m. The majority of transport (93%) occurred between 19 February and 31 May 2016, which coincided with Storm Katie (27–28 March 2016), and between 1 September and 9 December 2016, which coincided with Storm Angus (19–22 November 2016). The inshore wave and tidal data were consulted to better understand the hydrodynamic conditions that we assert facilitated displacement of these clasts. Wave parameters (H_s and H_{max}) and the corresponding tidal state at the peak of Storms Katie and Angus are presented in Figures 18a and b. The CCO storm threshold (1.6 m) is included to indicate the extent to which the threshold was exceeded.

The inshore H_s wave values peaked during Storms Katie and Angus at 1.9 and 2.3 m, respectively, whilst peak H_{max} values were 2.3 and 2.9 m. Notably, peak storm wave activity occurred at, or shortly after high water, suggesting that storm and tidal state relative to boulder elevation may be significant in mobilizing the largest boulders (Stephenson *et al.*, 2018).

Broader geomorphic modification

The RFID transport data presented herein demonstrate the occurrence of individual boulder mobility under low to moderate storm wave activity. However, further field evidence of geomorphic alteration was observed which suggested that storm waves were capable of mass boulder movement. This was manifest in the displacement of multiple clasts within the boulder berm at BR following storm activity; the boulder berm is identified in Figures 3 and 9. Aerial imagery from the CCO

Table VI. Summary of transport at BL and associated maximum inshore wave conditions recorded at Sandown Pier

	Duration between surveys (days)	Daily transport distance (m)	Total mass of transported boulders (t)	No. transport events	Transport distance (m)	Mean IBTD (m)	Max. H_s (m)	Max. H_{max} (m)	Wave direction (°)	Wave period (s)
S4–S5 (23 Sept–25 Nov 16)	63	0.2	6.3	13	12.7	1.0	2.3	2.9	154	8.0
S5–S6 (25 Nov 16–8 Feb 17)	75	0.4	7.6	15	27.2	1.8	1.6	2.3	115	8.0

Appendices.

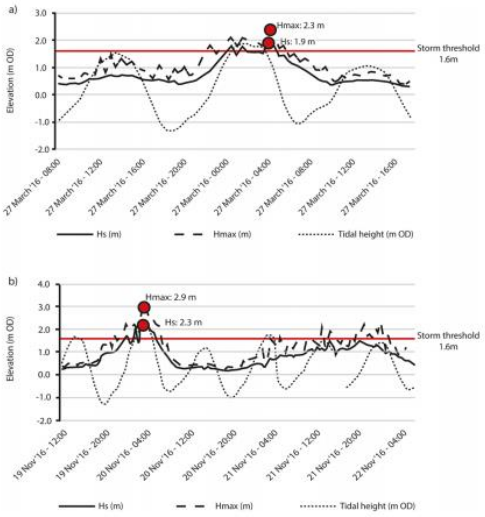

Figure 18. Peak wave activity (H_s and H_{max}) and tidal height relative to the CCO storm threshold of 1.6 m. The circles represent peak wave values as indicated. Wave and tidal conditions associated with (a) Storm Katie and (b) Storm Angus. [Colour figure can be viewed at wileyonlinelibrary.com]

was used to confirm whether mass movement of the berm had occurred under contemporary storm conditions.

Periodic images were processed in ArcGIS (version 10.5) and the seaward extent of the berm was highlighted on the available image data; this was subsequently overlaid for comparative purposes (Figure 19).

The findings identified that between 2005 and 2013, movement of the berm edge was limited to minor shifts, most likely arising from the supplanting of individual boulders. However, during the period 2013 to 2016, the seaward margin of the boulder berm moved over 7 m landward in some areas. The 2013 aerial imagery were obtained in August, prior to the winter period of 2013–2014, which was dominated by a series of low-pressure storm fronts that reportedly made this the stormiest winter on record (Matthews *et al.*, 2014; Masselink *et al.*, 2016). Nearshore wave heights at the Sandown Bay wave monitoring station registered a maximum H_s of 3.5 m and a H_{max} of 5.9 m over the 2013–2014 winter period. The highest values recorded since wave monitoring commenced at the location in 2006.

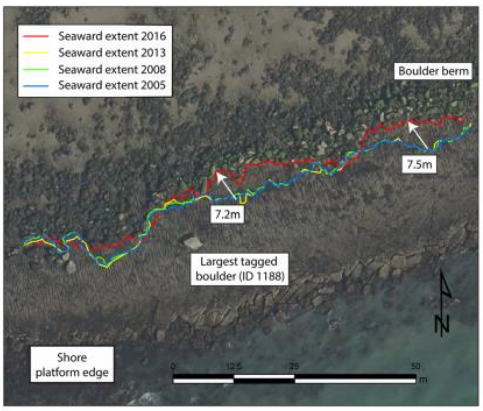

Figure 19. Large-scale geomorphic modification to the boulder berm at Black Rock. [Colour figure can be viewed at wileyonlinelibrary.com]

This establishes moderate contemporary storm waves as an agent of mass boulder displacement, resulting in the modification of sizable geomorphic features. Thus, storm activity at Bembridge initiates geomorphic change on a larger scale than had previously been realized. This reinforces the findings of Pérez-Alberti and Trenhaile (2015), Gómez-Pazo *et al.* (2019) and Nagle-McNaughton and Cox (2020), who documented widespread, collective mass movement of detached clasts using unmanned aerial vehicles (UAVs).

It was initially considered that the close proximity of the two study sites would enable comparisons to be drawn between locations. However, despite geological and climatic similarities, there are a host of additional factors that differ, such as lithology, topography, morphological features, shore platform exposure and aspect. Such fundamental differences make direct comparisons between sites problematic, as demonstrated by the disparity between transport distances and the varying responses to the same storm events. Whilst similarities exist between what may be considered 'comparable settings', the range and complexity of the underlying transport processes and mechanisms, and the degree to which they apply at any given location, means that universal theories governing boulder transport should be applied with caution.

Conclusion

This study represents the first long-term intertidal boulder transport monitoring programme of its kind. Favourable tag recovery rates (92% on completion) identified that 69% of the RFID tagged boulders were transported 233.0 m, predominantly by means of sliding, although incidents of overturning were also identified. The findings provide a wealth of quantifiable transport data which present compelling evidence that incidents of boulder detachment, overturning and displacement are not confined to extreme, infrequent, high-magnitude storm events. On the contrary, low-magnitude, high-frequency storm waves are shown to be effective agents of erosion, transport and macro-scale geomorphic modification on this relatively sheltered intertidal rocky coast.

The data identifies the pre- and post-transport morphological setting as a significant factor in facilitating and impeding boulder transport. The limited displacement of clasts in constrained morphological settings supports the notion that geomorphic platform features represent significant barriers to clast mobility (Naylor *et al.*, 2016; Trenhaile, 2016; Hastewell *et al.*, 2019a).

We affirm that boulder transport is governed by a host of complex interactions including, but not limited to:

a site-specific characteristics – platform morphology and topography, boulder location relative to morphological features, litho-structure of the boulder-producing units, aspect relative to storm wave approach and;
b hydrodynamic conditions – tidal state, storm wave magnitude and direction.

The longevity of the tags operational capacity (4 years to date) allows for the prolonged assessment of storm activity and the associated boulder transport responses to be determined. We therefore suggest further deployments of RFID tagged boulders across a range of coastal settings from low/moderate wave climates to those exposed to extreme cyclone/hurricane-

Appendices.

generated storms. Furthermore, the method may prove advantageous in coastal areas where debate exists over whether boulders have, or have not been displaced (Cox, 2019), or where the transport mode is contested (Morton *et al.*, 2008; Barbano *et al.*, 2010; Furlani *et al.*, 2011; Dewey and Ryan, 2017). Such deployments will provide an opportunity to better understand wave competence in terms of boulder transport and conceivably, elucidate the enduring storm and/or tsunami wave conundrum.

An improved awareness of the capabilities of contemporary storm events will further enhance our understanding of the responsiveness of rocky coasts in a changing global climate. Improved understanding of the response mechanisms will be critical in accurately assessing coastal vulnerability and risk, and mitigating against future storm wave hazards. It is anticipated that this data will better inform policymakers tasked with adaptive planning aimed at improving resilience and safeguarding coastal populations, infrastructure and natural capital.

Acknowledgements—The fieldwork component of this research study was financially supported by the British Society for Geomorphology and the Royal Geographical Society. The authors wish to thank the reviewers for their constructive comments, which greatly improved the manuscript. Finally, we extend our gratitude to those who willingly provided assistance in the field.

Data Availability Statement

Research data are not shared.

Conflict of Interest Statement

The authors declare that there are no conflicts of interest with regard to this research.

References

Allan JC, Hart R, Tranquili JV. 2006. The use of Passive Integrated Transponder (PIT) tags to trace cobble transport in a mixed sand-and-gravel beach on the high-energy Oregon coast, USA. *Marine Geology* **232**: 63–86.

Almeida LP, Masselink G, Russell PE, Davidson MA. 2015. Observations of gravel beach dynamics during high energy wave conditions using a laser scanner. *Geomorphology* **228**: 15–27.

Armenteros I, Daley B. 1998. Pedogenic modification and structure evolution in palustrine facies as exemplified by the Bembridge Limestone (Late Eocene) of the Isle of Wight, southern England. *Sedimentary Geology* **119**(3): 275–295.

Autret R, Dodet G, Fichaut B, Suanez S, David L, Leckler F, Ardhuin F, Ammann J, Grandjean P, Allemand P, Filipot JF. 2016. A comprehensive hydro-geomorphic study of cliff-top storm deposits on Banneg Island during winter 2013–2014. *Marine Geology* **382**: 37–55.

Autret R, Dodet G, Suanez S, Roudaut G, Fichaut B. 2018. Long-term variability of supratidal coastal boulder activation in Brittany (France). *Geomorphology* **304**: 184–200.

Barbano MS, Pirrotta C, Gerardi F. 2010. Large boulders along the south-eastern Ionian coast of Sicily: storm or tsunami deposits? *Marine Geology* **275**(1): 140–154.

Beniston M, Stephenson DB, Christensen OB, Ferro CA, Frei C, Goyette S, Halsnaes K, Holt T, Jylhä K, Koffi B, Palutikof J. 2007. Future extreme events in European climate: an exploration of regional climate model projections. *Climatic Change* **81**(1): 71–95.

Biolchi S, Furlani S, Devoto S, Scicchitano G, Korbar T, Vilibić I, Šepić J. 2019a. The origin and dynamics of coastal boulders in a semi-enclosed shallow basin: a northern Adriatic case study. *Marine Geology* **411**: 62–77.

Biolchi S, Denamiel C, Devoto S, Korbar T, Macovaz V, Scicchitano G, Vilibić I, Furlani S. 2019b. Impact of the October 2018 Storm Vaia on coastal boulders in the Northern Adriatic Sea. *Water* **11**(11): 2229. https://doi.org/10.3390/w11112229.

Blair TC, McPherson JG. 1999. Grain-size and textural classification of coarse sedimentary particles. *Journal of Sedimentary Research* **69**(1): 6–19.

Bray MJ, Workman M, Smith J, Pope D. 1996. Field measurements of shingle transport using electronic tracers. In *Proceedings of the 31st MAFF Conference of River and Coastal Engineers*, Vol. 1996; 10–14.

Brayne RP. 2015. The relationship between nearshore wave conditions and coarse clastic beach dynamics. Unpublished PhD thesis, Exeter University.

Buchanan DH, Naylor LA, Hurst MD, Stephenson WJ. 2020. Erosion of rocky shore platforms by block detachment from layered stratigraphy. *Earth Surface Processes and Landforms*. https://doi.org/10.1002/esp.4797.

Buscombe D, Masselink G. 2006. Concepts in gravel beach dynamics. *Earth-Science Reviews* **79**(1–2): 33–52.

Casamayor M, Alonso I, Cabrera J, Rodríguez S, Sánchez-García MJ. 2015. Long term recovery rates obtained using RFID technology at a mixed beach. *Geologica Acta* **13**(2): 85–96.

Channel Coast Observatory. 2015. Annual Wave Report 2015 Sandown Bay. Available at www.channelcoast.org/reports/ (accessed 30 August 2018).

Channel Coast Observatory. 2018. Wave data Sandown Pier. Available at www.channelcoast.org/data_management/online_data_catalogue/ (accessed 2 October 2018).

Chapuis M, Bright CJ, Hufnagel J, MacVicar B. 2014. Detection ranges and uncertainty of passive Radio Frequency Identification (RFID) transponders for sediment tracking in gravel rivers and coastal environments. *Earth Surface Processes and Landforms* **39**(15): 2109–2120.

Cox R, Zentner DB, Kirchner BJ, Cook MS. 2012. Boulder ridges on the Aran Islands (Ireland): recent movements caused by storm waves, not tsunamis. *The Journal of Geology* **120**(3): 249–272.

Cox R, Jahn KL, Watkins OG, Cox P. 2018. Extraordinary boulder transport by storm waves (West of Ireland, winter 2013–2014), and criteria for analysing coastal boulder deposits. *Earth-Science Reviews* **177**: 623–636.

Cox R. 2019. Very large boulders were moved by storm waves on the west coast of Ireland in winter 2013–2014. *Marine Geology*, **412**: 217–219.

Cruslock EM, Naylor LA, Foote YL, Swantesson JO. 2010. Geomorphologic equifinality. A comparison between shore platforms in Höga Kusten and Fårö, Sweden and the Vale of Glamorgan, South Wales, UK. *Geomorphology* **114**(1–2): 78–88.

Cullen ND, Bourke MC. 2018. Clast abrasion of a rock shore platform on the Atlantic coast of Ireland. *Earth Surface Processes and Landforms* **43**(12): 2627–2641.

Dasgupta R. 2011. Whither shore platforms? *Progress in Physical Geography* **35**(2): 183–209.

Dewey JF, Ryan PD. 2017. Storm, rogue wave, or tsunami origin for megaclast deposits in western Ireland and North Island, New Zealand? *Proceedings of the National Academy of Sciences* **114**(50): E10639–E10647.

Dickson ME, Kench PS, Kantor MS. 2011. Longshore transport of cobbles on a mixed sand and gravel beach, southern Hawke Bay, New Zealand. *Marine Geology* **287**(1): 31–42.

Dolphin T, Lee J, Phillips R, Taylor CJ, Dyer KR. 2016. Velocity of RFID tagged gravel in a non-uniform longshore transport system. *Journal of Coastal Research* **75**(sp1): 363–367.

Engel M, May SM. 2012. Bonaire's boulder fields revisited: evidence for Holocene tsunami impact on the Leeward Antilles. *Quaternary Science Reviews* **54**: 126–141.

Etienne S, Paris R. 2010. Boulder accumulations related to storms on the south coast of the Reykjanes Peninsula (Iceland). *Geomorphology* **114**(1–2): 55–70.

Etienne S, Buckley M, Paris R, Nandasena AK, Clark K, Strotz L, Chagué-Goff C, Goff J, Richmond B. 2011. The use of boulders for characterising past tsunamis: lessons from the 2004 Indian Ocean and 2009 South Pacific tsunamis. *Earth-Science Reviews* **107**(1–2): 76–90.

Fichaut B, Suanez S. 2011. Quarrying, transport and deposition of cliftop storm deposits during extreme events: Banneg Island, Brittany. *Marine Geology* **283**(1): 36–55.

Appendices.

Furlani S, Biolchi S, Devoto S, Saliba D, Scicchitano G. 2011. Large boulder along the NE Maltese coast: tsunami or storm wave deposits? *Journal of Coastal Research* **61**: 470. https://doi.org/10.2112/SI61-001.60.

Gómez-Pazo A, Pérez-Alberti A, Trenhaile A. 2019. Recording inter-annual changes on a boulder beach in Galicia, NW Spain using an unmanned aerial vehicle. *Earth Surface Processes and Landforms* **44**(5): 1004–1014.

Goto K, Okada K, Imamura F. 2009. Characteristics and hydrodynamics of boulders transported by storm waves at Kudaka Island, Japan. *Marine Geology* **262**(1–4): 14–24.

Goto K, Kawana T, Imamura F. 2010a. Historical and geological evidence of boulders deposited by tsunamis, southern Ryukyu Islands, Japan. *Earth-Science Reviews* **102**(1–2): 77–99.

Goto K, Miyagi K, Kawamata H, Imamura F. 2010b. Discrimination of boulders deposited by tsunamis and storm waves at Ishigaki Island, Japan. *Marine Geology* **269**(1–2): 34–45.

Goto K, Miyagi K, Kawana T, Takahashi J, Imamura F. 2011. Emplacement and movement of boulders by known storm waves – field evidence from the Okinawa Islands, Japan. *Marine Geology* **283**(1–4): 66–78.

Hall AM, Hansom JD, Williams DM, Jarvis J. 2006. Distribution, geomorphology and lithofacies of cliff-top storm deposits: examples from the high-energy coasts of Scotland and Ireland. *Marine Geology* **232**(3–4): 131–155.

Hall AM, Hansom JD, Jarvis J. 2008. Patterns and rates of erosion produced by high energy wave processes on hard rock headlands: The Grind of the Navir, Shetland, Scotland. *Marine Geology* **248**(1–2): 28–46.

Han M, Yang DY, Yu J, Kim JW. 2017. Typhoon impact on a pure gravel beach as assessed through gravel movement and topographic change at Yeocha beach, South Coast of Korea. *Journal of Coastal Research* **33**(4): 889–906.

Hansom JD, Hall AM. 2009. Magnitude and frequency of extra-tropical North Atlantic cyclones: a chronology from cliff-top storm deposits. *Quaternary International* **195**(1–2): 42–52.

Hastewell LJ, Schaefer M, Bray M, Inkpen R. 2019a. Intertidal boulder transport: a proposed methodology adopting Radio Frequency Identification (RFID) technology to quantify storm induced boulder mobility. *Earth Surface Processes and Landforms* **44**(3): 681–698.

Hastewell L, Inkpen R, Bray M. 2019b. Identification of plate-forme à vasques on a temperate shore platform? Quantitative analysis of morphology and relationships at Bembridge, Isle of Wight. *Zeitschrift für Geomorphologie* **62**(2): 145–162.

Héquette A, Cartier A. 2016. Theoretical and observed breaking wave height on a barred macrotidal beach: implications for the estimation of breaker index on beaches with large tidal range. *Journal of Coastal Research* **75**(1): 861–866.

Herterich JG, Cox R, Dias F. 2018. How does wave impact generate large boulders? Modelling hydraulic fracture of cliffs and shore platforms. *Marine Geology* **399**: 34–46.

Hills ES. 1972. Shore platforms and wave ramps. *Geological Magazine* **109**(2): 81–88.

Imamura F, Goto K, Ohkubo S. 2008. A numerical model for the transport of a boulder by tsunami. *Journal of Geophysical Research, Oceans* **113**(C1). https://doi.org/10.1029/2007JC004170.

Insole AN, Daley B, Gale A. 1998. The Isle of Wight (No. 60). Geologists' Association: London.

Kennedy AB, Mori N, Yasuda T, Shimozono T, Tomiczek T, Donahue A, Shimura T, Imai Y. 2017. Extreme block and boulder transport along a cliffed coastline (Calicoan Island, Philippines) during Super Typhoon Haiyan. *Marine Geology* **383**: 65–77.

Kennedy DM. 2010. Geological control on the morphology of estuarine shore platforms: Middle Harbour, Sydney, Australia. *Geomorphology* **114**(1–2): 71–77.

Kennedy DM, Woods JL, Naylor LA, Hansom JD, Rosser NJ. 2019. Intertidal boulder-based wave hindcasting can underestimate wave size: evidence from Yorkshire, UK. *Marine Geology* **411**: 98–106.

Knight J, Burningham H. 2011. Boulder dynamics on an Atlantic-facing rock coastline, northwest Ireland. *Marine Geology* **283**(1–4): 56–65.

Knight J, Burningham H, Barrett-Mold C. 2009. The geomorphology and controls on development of a boulder-strewn rock platform, NW Ireland. *Journal of Coastal Research* **56**: 1646–1650.

Kogure T, Aoki H, Maekado A, Hirose T, Matsukura Y. 2006. Effect of the development of notches and tension cracks on instability of limestone coastal cliffs in the Ryukyus, Japan. *Geomorphology* **80**(3–4): 236–244.

Lau AA, Terry JP, Ziegler AD, Switzer AD, Lee Y, Etienne S. 2016. Understanding the history of extreme wave events in the Tuamotu Archipelago of French Polynesia from large carbonate boulders on Makemo Atoll, with implications for future threats in the central South Pacific. *Marine Geology* **380**: 174–190.

Leckebusch GC, Koffi B, Ulbrich U, Pinto JG, Spangehl T, Zacharias S. 2006. Analysis of frequency and intensity of European winter storm events from a multi-model perspective, at synoptic and regional scales. *Climate Research* **31**(1): 59–74.

Lee MW, Bray M, Workman M, Collins MB, Pope D. 2000. Coastal shingle tracing: a case study using the 'Electronic Tracer System' (ETS). In *Tracers in Geomorphology*, Watson IDL (ed). Wiley: Chichester; 413–435.

Long D. 2017. Cataloguing tsunami events in the UK. *Geological Society, London, Special Publications* **456**(1): 143–165.

Maouche S, Morhange C, Meghraoui M. 2009. Large boulder accumulation on the Algerian coast evidence tsunami events in the western Mediterranean. *Marine Geology* **262**(1–4): 96–104.

Masselink G, Castelle B, Scott T, Dodet G, Suanez S, Jackson D, Floc'h F. 2016. Extreme wave activity during 2013/2014 winter and morphological impacts along the Atlantic coast of Europe. *Geophysical Research Letters* **43**(5): 2135–2143.

Mastronuzzi G, Sansò P. 2000. Boulders transport by catastrophic waves along the Ionian coast of Apulia (southern Italy). *Marine Geology* **170**(1–2): 93–103.

Matthews T, Murphy C, Wilby RL, Harrigan S. 2014. Stormiest winter on record for Ireland and UK. *Nature Climate Change* **4**(9): 738.

McKenna J. 2005. Boulder beaches. In *Encyclopaedia of Coastal Science*, Schwartz M (ed). Springer Science & Business Media: Kluwer; 206–208.

McKenna J, Jackson DW, Cooper JAG. 2011. In situ exhumation from bedrock of large rounded boulders at the Giant's Causeway, Northern Ireland: an alternative genesis for large shore boulders (megaclasts). *Marine Geology* **283**(1–4): 25–35.

Miller IM, Warrick JA, Morgan C. 2011. Observations of coarse sediment movements on the mixed beach of the Elwha Delta, Washington. *Marine Geology* **282**(3): 201–214.

Morton RA, Richmond BM, Jaffe BE, Gelfenbaum G. 2008. Coarse-clast ridge complexes of the Caribbean: a preliminary basis for distinguishing tsunami and storm-wave origins. *Journal of Sedimentary Research* **78**(9): 624–637.

Mottershead D, Bray M, Soar P, Farres PJ. 2014. Extreme wave events in the central Mediterranean: geomorphic evidence of tsunami on the Maltese Islands. *Zeitschrift für Geomorphologie* **58**(3): 385–411.

Nagle-McNaughton T, Cox R. 2020. Measuring change using quantitative differencing of repeat structure-from-motion photogrammetry: the effect of storms on coastal boulder deposits. *Remote Sensing* **12**(1): 42.

Nandasena NAK, Paris R, Tanaka N. 2011. Reassessment of hydrodynamic equations: minimum flow velocity to initiate boulder transport by high energy events (storms, tsunamis). *Marine Geology* **281**(1): 70–84.

Nandasena NAK, Tanaka N. 2013a. Boulder transport by high-energy (tsunamis): model development for threshold entrainment and transport. *Research Report of Department of Civil and Environmental Engineering, Saitama University* **39**(1): 1–12.

Nandasena NAK, Tanaka N. 2013b. Boulder transport by high energy: numerical model-fitting experimental observations. *Ocean Engineering* **57**: 163–179.

Naylor LA, Stephenson WJ. 2010. On the role of discontinuities in mediating shore platform erosion. *Geomorphology* **114**(1–2): 89–100.

Naylor LA, Stephenson WJ, Smith HC, Way O, Mendelssohn J, Cowley A. 2016. Geomorphological control on boulder transport and coastal erosion before, during and after an extreme extra-tropical cyclone. *Earth Surface Processes and Landforms* **41**(5): 685–700.

Nichols MH. 2004. A radio frequency identification system for monitoring coarse sediment particle displacement. *Applied Engineering in Agriculture* **20**(6): 783–787.

Appendices.

Noormets R, Crook KA, Felton EA. 2004. Sedimentology of rocky shorelines: 3. Hydrodynamics of megaclast emplacement and transport on a shore platform, Oahu. *Hawaii. Sedimentary Geology* **172**(1–2): 41–65.

Nott J. 2003. Waves, coastal boulder deposits and the importance of the pre-transport setting. *Earth and Planetary Science Letters* **210**(1–2): 269–276.

Ogawa H, Dickson ME, Kench PS. 2011. Wave transformation on a sub-horizontal shore platform, Tatapouri, North Island, New Zealand. *Continental Shelf Research* **31**(14): 1409–1419.

Paris R, Naylor LA, Stephenson WJ. 2011. Boulders as a signature of storms on rock coasts. *Marine Geology* **283**(1–4): 1–11.

Pérez-Alberti A, Trenhaile AS. 2015. Clast mobility within boulder beaches over two winters in Galicia, northwestern Spain. *Geomorphology* **248**: 411–426.

Roig-Munar FX, Rodríguez-Perea A, Vilaplana JM, Martín-Prieto JA, Gelabert B. 2019. Tsunami boulders in Majorca Island (Balearic Islands, Spain). *Geomorphology* **334**: 76–90.

Salzmann L, Green A. 2012. Boulder emplacement on a tectonically stable, wave-dominated coastline, Mission Rocks, northern KwaZulu-Natal, South Africa. *Marine Geology* **323**: 95–106.

Scheffers A, Scheffers S. 2006. Documentation of the impact of Hurricane Ivan on the coastline of Bonaire (Netherlands Antilles). *Journal of Coastal Research* **22**(6): 1437–1450.

Scheffers A, Scheffers S, Kelletat D, Browne T. 2009. Wave-emplaced coarse debris and megaclasts in Ireland and Scotland: boulder transport in a high-energy littoral environment. *The Journal of Geology* **117**(5): 553–573.

Scicchitano G, Monaco C, Tortorici L. 2007. Large boulder deposits by tsunami waves along the Ionian coast of south-eastern Sicily (Italy). *Marine Geology* **238**(1–4): 75–91.

Sear DA, Lee MW, Oakley RJ, Carling PA, Collins MB. 2000. Coarse sediment tracing technology in littoral and fluvial environments: a review. In *Tracers in Geomorphology*, Watson IDL (ed). Wiley: Chichester; 21–55.

Shah-hosseini M, Morhange C, Beni AN, Marriner N, Lahijani H, Hamzeh M, Sabatier F. 2011. Coastal boulders as evidence for high-energy waves on the Iranian coast of Makran. *Marine Geology* **290**(1): 17–28.

Spiske M, Bahlburg H. 2011. A quasi-experimental setting of coarse clast transport by the 2010 Chile tsunami (Bucalemu, Central Chile). *Marine Geology* **289**(1–4): 72–85.

Stephenson WJ, Kirk RM. 2000. Development of shore platforms on Kaikoura Peninsula, South Island, New Zealand. *Part one: the role of waves. Geomorphology* **32**(1–2): 21–41.

Stephenson WJ, Naylor LA. 2011. Geological controls on boulder production in a rock coast setting: insights from South Wales, UK. *Marine Geology* **283**(1): 12–24.

Stephenson WJ, Naylor LA, Smith H, Chen B, Brayne RP. 2018. Wave transformation across a macrotidal shore platform under low to moderate energy conditions. *Earth Surface Processes and Landforms* **43**(1): 298–311.

Sunamura T. 1992. *Geomorphology of Rocky Coasts*, Vol. **3**. Wiley: Chichester.

Switzer AD, Burston JM. 2010. Competing mechanisms for boulder deposition on the southeast Australian coast. *Geomorphology* **114**(1–2): 42–54.

Terry JP, Lau AA. 2018. Magnitudes of nearshore waves generated by tropical cyclone Winston, the strongest landfalling cyclone in South Pacific records. Unprecedented or unremarkable? *Sedimentary Geology* **364**: 276–285.

Terry JP, Dunne K, Jankaew K. 2016. Prehistorical frequency of high-energy marine inundation events driven by typhoons in the Bay of Bangkok (Thailand), interpreted from coastal carbonate boulders. *Earth Surface Processes and Landforms* **41**(4): 553–562.

Topcon. 2018. HiPer V – Topcon Positioning Systems, Inc. Available at www.topconpositioning.com/sites/default/files/product_files/hiper_v_broch_7010_2121_reve_sm.pdf (accessed 14 December 2018).

Trenhaile AS. 1987. *The Geomorphology of Rock Coasts*. Oxford University Press: New York.

Trenhaile AS. 2015. Coastal notches: their morphology, formation, and function. *Earth-Science Reviews* **150**: 285–304.

Trenhaile AS. 2016. Rocky coasts – their role as depositional environments. *Earth-Science Reviews* **159**: 1–13.

Trenhaile AS. 2019. Hard-rock coastal modelling: past practice and future prospects in a changing world. *Journal of Marine Science and Engineering* **7**(2): 34. https://doi.org/10.3390/jmse7020034.

Trenhaile AS, Kanyaya JI. 2007. The role of wave erosion on sloping and horizontal shore platforms in macro- and mesotidal environments. *Journal of Coastal Research* **23**(2): 298–309.

Weiss R. 2012. The mystery of boulders moved by tsunamis and storms. *Marine Geology* **295**: 28–33.

Williams DM, Hall AM. 2004. Cliff-top megaclast deposits of Ireland, a record of extreme waves in the North Atlantic-storms or tsunamis? *Marine Geology* **206**(1–4): 101–117.

Zainali A, Weiss R. 2015. Boulder dislodgement and transport by solitary waves: insights from three-dimensional numerical simulations. *Geophysical Research Letters* **42**(11): 4490–4497.

Zingg T. 1935. Beitrag zur Schotteranalyse. *Schweizerische Mineralogische und Petrographische Mitteilungen* **15**: 39–140.

Supporting Information

Additional supporting information may be found online in the Supporting Information section at the end of the article.

Data S1. Supporting Information

Table SI. Bembridge Ledge - summary of transport values and wave conditions relative to each survey. Wave data obtained from the inshore wave CCO monitoring station at Sandown Pier.

Table SII. Black Rock - summary of transport values and wave conditions relative to each survey. Wave data obtained from the inshore wave CCO monitoring station at Sandown Pier.

Appendix 6 - Research Ethics Review Checklist

FORM UPR16

Research Ethics Review Checklist

UNIVERSITY OF PORTSMOUTH

Please include this completed form as an appendix to your thesis (see the Research Degrees Operational Handbook for more information

Postgraduate Research Student (PGRS) Information				Student ID:	328238
PGRS Name:	Linley Hastewell				
Department:	SEGG	First Supervisor:	Dr. Robert Inkpen		
Start Date: (or progression date for Prof Doc students)	1 September 2014				
Study Mode and Route:	Part-time ☒	MPhil ☐	MD ☐		
	Full-time ☐	PhD ☒	Professional Doctorate ☐		

Title of Thesis:	The identification and quantification of storm-induced boulder transport using Radio Frequency Identification (RFID) tagging on an intertidal rocky shore, Bembridge, Isle of Wight.
Thesis Word Count: (excluding ancillary data)	44,278

If you are unsure about any of the following, please contact the local representative on your Faculty Ethics Committee for advice. Please note that it is your responsibility to follow the University's Ethics Policy and any relevant University, academic or professional guidelines in the conduct of your study

Although the Ethics Committee may have given your study a favourable opinion, the final responsibility for the ethical conduct of this work lies with the researcher(s).

UKRIO Finished Research Checklist:
(If you would like to know more about the checklist, please see your Faculty or Departmental Ethics Committee rep or see the online version of the full checklist at: http://www.ukrio.org/what-we-do/code-of-practice-for-research/)

a) Have all of your research and findings been reported accurately, honestly and within a reasonable time frame?	YES ☒ NO ☐
b) Have all contributions to knowledge been acknowledged?	YES ☒ NO ☐
c) Have you complied with all agreements relating to intellectual property, publication and authorship?	YES ☒ NO ☐
d) Has your research data been retained in a secure and accessible form and will it remain so for the required duration?	YES ☒ NO ☐
e) Does your research comply with all legal, ethical, and contractual requirements?	YES ☒ NO ☐

Candidate Statement:

I have considered the ethical dimensions of the above named research project, and have successfully obtained the necessary ethical approval(s)

Ethical review number(s) from Faculty Ethics Committee (or from NRES/SCREC):	

If you have *not* submitted your work for ethical review, and/or you have answered 'No' to one or more of questions a) to e), please explain below why this is so:

The ethics aspect of the research was addressed at the time by a departmental ethics review which was subsequently reported to the Faculty Ethics Committee as detailed below, this is taken from an email dated 16 July, 2014 (available on request).

UPR16 – April 2018

Re: Linley Hastewell's ethics proposal
PhD 2/Ethics x

Malcolm Bray <malcolm.bray@port.ac.uk>
16 Jul 2014, 18:35

to Richard, me

Richard,

Thank you very much for your favourable opinion review of Linley's proposal. I'm printing your message and attaching it to a copy I have of Linley's completed form which I then keep safely as evidence of the review (with a copy provided to Linley also).

I have reported to the Faculty Ethics Committee that a review has been completed, but they have no mechanism yet for recording the details of such reviews that fall outside of the formal reviewing procedure - it was intended that this would be covered by the online self-certification system but that is not live yet. In fact the review conducted here was considerably more rigorous than the online version would be so we can all be happy with the outcome.

I hope that you are happy for Linley to see your comments - its important for him to be assured that his application has been reviewed independently.

Many thanks

On 15 July 2014 14:08, Richard Tyler <richard.tyler@port.ac.uk> wrote:
Dear Malcolm,

Please find below my comments on Linley Hastewell's department level ethics proposal. I hope this helps but if you want me to write a formal review for the moodle site I am happy to do so.

There are no human participants for this study however the project does conduct research on a site that is subject to several special designations that protect the environment from damage or alteration. The project involves marking boulders in some way and measuring their movement over time.

The researcher has identified that hand painting a unique marker onto each boulder may be semi-permanent but aesthetically displeasing for users of the protected site. The researcher proposes to use Radio Frequency Identification (RFID) to mark boulders which will be less visible but involves drilling and inserting the RFID tag into the rock and covering with a waterproof sealant.

I understand that the researcher has sought advice and permission from two organisations (Marine Management Organisation and Natural England) to conduct this research using the proposed method. Having clarified with the researcher, I have received the communication between Linley and the organisation and I am satisfied that he has taken appropriate steps to ensure minimal disruption to the site.

I am happy to support a favourable opinion on this proposal and wish Linley the best of luck with the study.

Best wishes,
Rich

Richard Tyler
PhD Candidate
Postgraduate representative (Geography of Health Research Group - GHRG RGS-IBG)
Department of Geography
Buckingham Building
02392 846347
University of Portsmouth

Staff profile - http://www.port.ac.uk/department-of-geography/staff/richard-tyler.html -- Dr Malcolm Bray Department of Geography, University of Portsmouth, PO1 3HE 02392 842481 (direct) 02392 842507 (Departmental Office) ReplyReply to allForward		
Signed *(PGRS)*:	Linley Hastewell	**Date:** 30/09/2019

Bibliography

Abbott, A. T., & Pottratz, S. W. (1969). Marine pothole erosion, Oahu, Hawaii. *Pacific Science,* 23 (3): 276-290.

Ablain, M., Cazenave, A., Valladeau, G., & Guinehut, S. (2009). A new assessment of the error budget of global mean sea level rate estimated by satellite altimetry over 1993-2008. Ocean Science, European Geosciences Union, 2009, 5 (2): pp.193-201. Accessed on 24th July 2018, from: https://hal.archives-ouvertes.fr/hal-00990932/file/os-5-193-2009.pdf

Albuquerque, M. D. G., Leal Alves, D. C., Espinoza, J. M. D. A., Oliveira, U. R., & Simões, R. S. (2018). Determining Shoreline Response to Meteo-oceanographic Events Using Remote Sensing and Unmanned Aerial Vehicle (UAV): Case Study in Southern Brazil. *Journal of Coastal Research*, 85(sp1): 766-770.

Allan, J.C., Hart, R., & Tranquili, J.V. (2006). The use of Passive Integrated Transponder (PIT) tags to trace cobble transport in a mixed sand-and-gravel beach on the high-energy Oregon coast, USA. *Marine Geology,* 232: 63-86. DOI:10.1016/j.margeo.2006.07.005

Almeida, L.P., Masselink, G., Russell, P.E., & Davidson, M.A. (2015). Observations of gravel beach dynamics during high energy wave conditions using a laser scanner. *Geomorphology,* 228: 15-27. DOI:org/10.1016/j.geomorph.2014.08.019

Aluf, O. (2017). RFID Antennas Systems Descriptions and Analysis. In *Microwave RF Antennas and Circuits 2017*: 1-15. Springer International Publishing. DOI:10.1007/978-3-319-45427-6_1

Armenteros, I., & Daley, B. (1998). Pedogenic modification and structure evolution in palustrine facies as exemplified by the Bembridge Limestone (Late Eocene) of the Isle of Wight, southern England. *Sedimentary Geology,* 119(3): 275-295. DOI:10.1016/S0037-0738(98)00067-0

Aschmann, H. (1984). A restrictive definition of Mediterranean climates. - Bulletin de La Société Botanique de France. *Actualités Botaniques*, 131(2-4): 21-30. DOI:org/10.1080/01811789.1984.10826643

Autret, R., Dodet, G., Fichaut, B., Suanez, S., David, L., Leckler, F., Ardhuin, F., Ammann, J., Grandjean, P., Allemand, P., & Filipot, J.F. (2016). A comprehensive hydro-geomorphic study of cliff-

top storm deposits on Banneg Island during winter 2013–2014. *Marine Geology,* 382: 37-55. DOI: 10.1016/j.margeo.2016.09.014

Autret, R., Dodet, G., Suanez, S., Roudaut, G. & Fichaut, B. (2018). Long–term variability of supratidal coastal boulder activation in Brittany (France). *Geomorphology,* 304: 184-200. DOI:org/10.1016/j.geomorph.2017.12.028

Aydin, A., & Basu, A. (2005). The Schmidt hammer in rock material characterization. *Engineering Geology*, 81(1): 1-14.

Badr, A. A., & Lotfy, M. F. (1999). Tracing beach sand movement using fluorescent quartz along the Nile Delta promontories, Egypt. *Journal of Coastal Research*, 15(1): 261-265.

Barbano, M. S., Pirrotta, C., & Gerardi, F. (2010). Large boulders along the south-eastern Ionian coast of Sicily: storm or tsunami deposits? *Marine Geology*, 275(1): 140-154. DOI: 10.1016/j.margeo.2010.05.005

Bartrum, J. A. (1916). High-water rock platforms: a phase of shoreline erosion. In *Trans. Proc. New Zealand Inst,* 16: 132-134.

Battistini, R. (1980). Les vasques etagees, formes curieuses des estrans greso-calcaires au Sud de Madagascar. - *Madagascar: revue de geographie (Tananarive),* 37: 63-86.

Battistini, R. (1981). Le morphogenese des plateformes de corrosion littorale dans les gres calcaires (plateforme superieure et plateforme a vasques) et le probleme des vasques, d'apres des observations faites a Madagascar. *Revue de Geomorphologie Dynamique,* 30: 81-94.

Benelli, G., Pozzebon, A., Raguseo, G., Bertoni, D., & Sarti, G. (2009). An RFID based system for the underwater tracking of pebbles on artificial coarse beaches. In *2009 Third International Conference on Sensor Technologies and Applications,* (pp. 294-299).

Benelli, G., Pozzebon, A., Bertoni, D., & Sarti, G. (2012). An RFID-based toolbox for the study of under-and outside-water movement of pebbles on coarse-grained beaches. *IEEE Journal of Selected Topics in Applied Earth Observations and Remote Sensing*, 5(5): 1474-1482.

Beniston, M., Stephenson, D.B., Christensen, O.B., Ferro, C.A., Frei, C., Goyette, S., Halsnaes, K., Holt, T., Jylhä, K., Koffi, B., & Palutikof, J. (2007). Future extreme events in European climate: an

exploration of regional climate model projections. *Climatic Change,* 81(1): 71-95. DOI: 10.1007/s10584-006-9226-z

Benner, R., Browne, T., Brückner, H., Kelletat, D., & Scheffers. A. (2010). Boulder transport by waves: progress in physical modelling. *Zeitschrift für Geomorphologie, Supplementary Issues* 54(3): 127-146. DOI:org/10.1127/0372-8854/2010/0054S3-0022

Berg, P., Moseley, C., & Haerter, J. O. (2013). Strong increase in convective precipitation in response to higher temperatures. *Nature Geoscience*, 6(3): 181.

Bertin, X., Deshouilieres, A., Allard, J., & Chaumillon, E. (2007). A new fluorescent tracers experiment improves understanding of sediment dynamics along the Arcay Sandspit (France). *Geo-Marine Letters*, 27(1): 63-69.

Bertoni, D., Sarti, G., Benelli, G., Pozzebon, A., & Raguseo, G. (2010). Radio Frequency Identification (RFID) technology applied to the definition of underwater and subaerial coarse sediment movement. *Sedimentary Geology*, 228(3-4): 140-150.

Bevan, K. J., & Freer, J. (2001). Equifinality, data assimilation, and uncertainty estimation in mechanistic modelling of complex environmental systems. *Journal of Hydrology*, 249: 11-29.

Biolchi, S., Furlani, S., Antonioli, F., Baldassini, N., Deguara, J,C., Devoto, S., Di Stefano, A., Evans, J., Gambin, T., Gauci, R., & Mastronuzzi, G. (2016a). Boulder accumulations related to extreme wave events on the eastern coast of Malta. *Natural Hazards and Earth System Sciences,* 16: 737-756. DOI:org/10.5194/nhess-16-737-2016

Biolchi, S., Furlani, S., Devoto, S., Gauci, R., Castaldini, D., & Soldati, M. (2016b). Geomorphological identification, classification and spatial distribution of coastal landforms of Malta (Mediterranean Sea). *Journal of Maps*, 12(1): 87-99.

Biolchi, S., Furlani, S., Devoto, S., Scicchitano, G., Korbar, T., Vilibić, I., & Šepić, J. (2019a). The origin and dynamics of coastal boulders in a semi-enclosed shallow basin: A northern Adriatic case study. *Marine Geology*, 411: 62-77. DOI:org/10.1016/j.margeo.2019.01.008

Biolchi, S., Denamiel, C., Devoto, S., Korbar, T., Macovaz, V., Scicchitano, G., Vilibić, I., & Furlani, S. (2019b). Impact of the October 2018 Storm Vaia on Coastal Boulders in the Northern Adriatic Sea. *Water*, *11*(11): 2229.

Black, K.S., Athey, S., Wilson, P., Evans, D. (2007). The use of particle tracking in sediment transport studies: a review. *Geological Society, London, Special Publications,* 274(1): 73-91. DOI: 10.1144/GSL.SP.2007.274.01.09

Blair, T.C., & McPherson, J.G. (1999). Grain-size and textural classification of coarse sedimentary particles. *Journal of Sedimentary Research*, 69(1): 6-19.

Blanco-Chao, R., Costa Casais, M., Martínez Cortizas, A., Pérez Alberti, A., & Trenhaile, A. S. (2003). Evolution and inheritance of a rock coast: western Galicia, northwestern Spain. *Earth Surface Processes and Landforms*, 28(7): 757-775.

Blanco-Chao, R., Pérez-Alberti, A., Trenhaile, A. S., Costa-Casais, M., & Valcárcel-Díaz, M. (2007). Shore platform abrasion in a para-periglacial environment, Galicia, northwestern Spain. *Geomorphology*, 83(1-2): 136-151. DOI:10.1016/j.geomorph.2006.06.028.

Bray, M.J., Workman, M., Smith, J., & Pope, D. (1996). Field measurements of shingle transport using electronic tracers. In *Proceedings of the 31st MAFF Conference River and Coastal Engineers*, Vol. 1996; 10-14.

Brayne, R.P. (2015). The Relationship between Nearshore Wave Conditions and Coarse Clastic Beach Dynamics. Unpublished PhD Thesis, Exeter University.

Breves, A., & Junqueira, A. O. R. (2017). Intertidal vermetid reef as a shelter for invasive bivalves in a tropical bay. *Aquatic Ecosystem Health & Management*, 20 (4): 384-392. DOI:org/10.1080/14634988 .2017.1401416

British Standard Institution (BSI), (1986). BS 1881-202 Testing concrete - Recommendations for surface hardness testing by rebound hammer, *London, UK*.

Buckley, M. L., Wei, Y., Jaffe, B. E., & Watt, S. G. (2012). Inverse modeling of velocities and inferred cause of overwash that emplaced inland fields of boulders at Anegada, British Virgin Islands. *Natural Hazards*, *63*(1): 133-149.

Burridge, J., & Inkpen, R. (2015). Formation and arrangement of pits by a corrosive gas. *Physical Review E*, 19, p.022403

Buscombe, D. & Masselink, G. (2006). Concepts in gravel beach dynamics. *Earth-Science Reviews,* 79(1-2): 33-52. DOI:org/10.1016/j.earscirev.2006.06.003

Cabanes, C., Cazenave, A., & Le Provost, C. (2001). Sea level rise during past 40 years determined from satellite and in situ observations. *Science*, 294(5543): 840-842.

Calder, M., & Kennedy, D. M. (2013). The Application of Ground Penetrating Radar in Delineating Shore Platform Morphology: A Case Study from Wellington, New Zealand. *Journal of Coastal Research*, 29(6a): 226-234.

Casamayor, M., Alonso, I., Cabrera, J., Rodríguez, S., & Sánchez-García, M.J. (2015). Long term recovery rates obtained using RFID technology at a mixed beach. *Geologica Acta,* 13(2): 85-96.

Casella, E., Rovere, A., Pedroncini, A., Stark, C. P., Casella, M., Ferrari, M., & Firpo, M. (2016). Drones as tools for monitoring beach topography changes in the Ligurian Sea (NW Mediterranean). *Geo-Marine Letters*, 36(2): 151-163.

Cassel, M., Piégay, H., & Lavé, J. (2017). Effects of transport and insertion of radio frequency identification (RFID) transponders on resistance and shape of natural and synthetic pebbles: applications for riverine and coastal bedload tracking. *Earth Surface Processes and Landforms,* 42(3): 399-413. DOI: 10.1002/esp.3989

Castelle, B., Marieu, V., Bujan, S., Splinter, K.D., Robinet, A., Sénéchal, N., & Ferreira, S. (2015). Impact of the winter 2013–2014 series of severe Western Europe storms on a double-barred sandy coast: Beach and dune erosion and megacusp embayments. *Geomorphology*, 238: 135-148. DOI: 10.1016/j.geomorph.2015.03.006

Channel Coast Observatory (CCO). (2015). Annual Wave Report 2015 Sandown Bay. Accessed on 30th August 2018, from: http://www.channelcoast.org/reports/

Channel Coast Observatory, CCO. (2017a). Regional Coastal Monitoring Programmes Sandown Bay. [Online]. Accessed on 20th May 2017, from: https://www.channelcoast.org/data_management/real_time_data/charts/?chart=80&tab=info&disp_option=

Channel Coast Observatory, CCO. (2017b). Data management catalogue. [Online]. Accessed on 28th July 2017, from: http://www.channelcoast.org/data_management/online_data_catalogue/metadata/search/index2.php

Channel Coast Observatory (CCO). (2018). Wave data Sandown Pier. Accessed on 2nd October 2018, from: http://www.channelcoast.org/data_management/online_data_catalogue/

Chapuis, M., Bright, C.J., Hufnagel, J., & MacVicar, B. (2014). Detection ranges and uncertainty of passive Radio Frequency Identification (RFID) transponders for sediment tracking in gravel rivers and coastal environments. *Earth Surface Processes and Landforms,* 39(15): 2109-2120. DOI:org/10.1002/esp.3620

Choudhury, K., & Saha, D. K. (2004). Integrated geophysical and chemical study of saline water intrusion. *Groundwater*, 42(5): 671-677.

Ciavola, P., & Castiglione, E. (2009). Sediment dynamics of mixed sand and gravel beaches at short time-scales. Journal of Coastal Research. Special Issue No. 56. *Proceedings of the 10th International Coastal Symposium 2009*, Vol. II: 1751-1755.

Ciavola, P., Dias, N., Ferreira, O., Taborda, R., & Dias, J. M. A. (1998). Fluorescent sands for measurements of longshore transport rates: a case study from Praia de Faro in southern Portugal. *Geo-Marine Letters*, 18(1): 49-57.

Clemmensen, L. B., & Nielsen, L. (2010). Internal architecture of a raised beach ridge system (Anholt, Denmark) resolved by ground-penetrating radar investigations. *Sedimentary Geology*, 223(3-4): 281-290

Colenutt, G W. (1892). Proceedings of the Hampshire Field Club & Archaeological Society, Volume 2, Part 2 (167-180). Accessed on 26th April 2019, from: http://www.hantsfieldclub.org.uk/publications/hampshirestudies/digital/1885-99/Vol_2/Colenutt_pt2.pdf

Collins, K.J., Herbert, R.J.H. & Mallinson, J.J. (1990). The Marine Fauna and Flora of Bembridge and St. Helens, Isle of Wight. *Proceedings of the Isle of Wight Natural History & Archaeological Society* 9: 41-85.

Collins, K. J., & Mallinson, J. J. (2000). Marine habitats and communities. In *Proceedings in Marine Science* 1, Solent Science - A review (eds. Collins, M and Ansell, K). Elsevier.

Coombes, M. A., Naylor, L. A., Viles, H. A., & Thompson, R. C. (2013). Bioprotection and disturbance: seaweed, microclimatic stability and conditions for mechanical weathering in the intertidal zone. *Geomorphology*, 202: 4-14.

Cox, R. (2019). Very large boulders were moved by storm waves on the west coast of Ireland in winter 2013-2014. *Marine Geology*, 412: 217-219.

Cox, R., Zentner, D. B., Kirchner, B. J., & Cook, M. S. (2012). Boulder ridges on the Aran Islands (Ireland): recent movements caused by storm waves, not tsunamis. *The Journal of Geology,* 120(3): 249-272. DOI:org/10.1086/664787

Cox, R., Jahn, K. L., Watkins, O. G., & Cox, P. (2018). Extraordinary boulder transport by storm waves (West of Ireland, winter 2013–2014), and criteria for analysing coastal boulder deposits. *Earth-Science Reviews,* 177: 623-636. DOI:org/10.1016/j.earscirev.2017.12.014

Cox, R., Ardhuin, F., Dias, F., Autret, R., Beisiegel, N., Earlie, C.S., Herterich, J.G., Kennedy, A., Paris, R., Raby, A. & Schmitt, P. (2020). Systematic Review Shows That Work Done by Storm Waves Can Be Misinterpreted as Tsunami-Related Because Commonly Used Hydrodynamic Equations Are Flawed. *Frontiers in Marine Science*. DOI:10.3389/fmars.2020.00004.

Cruslock, E. M., Naylor, L. A., Foote, Y. L., & Swantesson, J. O. (2010). A comparison between shore platforms in Höga Kusten and Fårö, Sweden and the Vale of Glamorgan, South Wales, UK. *Geomorphology,* 114(1-2): 78-88. DOI:org/10.1016/j.geomorph.2009.02.019

Cullen, N. D., & Bourke, M. C. (2018). Clast abrasion of a rock shore platform on the Atlantic coast of Ireland. *Earth Surface Processes and Landforms*, 43(12): 2627-2641.

Curtiss, G.M., Osborne, P,D., & Horner-Devine, A.R. (2009). Seasonal patterns of coarse sediment transport on a mixed sand and gravel beach due to vessel wakes, wind waves, and tidal currents. *Marine Geology,* 259(1): 73-85. DOI: 10.1016/j.margeo.2008.12.009

Daley, B. (1973). The palaeoenvironment of the Bembridge Marls (Oligocene) of the Isle of Wight, Hampshire. *Proceedings of the Geologists' Association*, *84*(1): 83-IN4.

Daley, B., & Edwards, N. (1990). The Bembridge Limestone (Late Eocene), Isle of Wight, southern England: a stratigraphical revision. *Tertiary Research, 12*(2): 51-64.

Dalongeville, M. (1977). Formes littorales de corrosion dans les roches carbonatées du Liban. - *Etude morphologique, Méditerranée,* 30(3): 21-33.

Dana, J.D., (1849). Geology, in Wilkes, C., United States Exploring Expedition, 10: Philadelphia (C. Sherman), with Atlas: New York, Putnam. Accessed on 26th April 2016, from: https://archive.org/details/geology101849dana/page/442

Dasgupta, R. (2011). Whither shore platforms?. *Progress in Physical Geography,* 35(2): 183-209. DOI:org/10.1177/0309133310375730

De Waele, J., & Furlani, S. (2013). Seawater and biokarst effects on coastal limestones. In: Shroder, J., Frumkin, A. (Eds.), *Treatise on Geomorphology, Karst Geomorphology*, vol. 6. Academic Press, San Diego, CA. 341-350.

Deguara, J. C., & Gauci, R. (2017). Evidence of extreme wave events from boulder deposits on the south-east coast of Malta (Central Mediterranean). *Natural Hazards*, 86(2): 543-568.

Deguara, J. C., & Scerri, S. (2019). Ras il-Ġebel: An Extreme Wave-Generated Bouldered Coast at Xgħajra (Malta). In *Landscapes and Landforms of the Maltese Islands* (pp. 229-243). Springer, Cham.

Department for Environment, Food and Rural Affairs, DEFRA. (2019). Bembridge Marine Conservation Zone. Crown Copyright. Accessed on 2nd May 2019, from: https://assets.publishing.service.gov.uk/government/uploads/system/uploads/attachment_data/file/805397/mcz-bembridge-2019.pdf

Dickson, M. E., Bristow, C. S., Hicks, D. M., Jol, H., Stapleton, J., Todd, D. (2009). Beach volume on an eroding sand–gravel coast determined using ground penetrating radar. *Journal of Coastal Research*, 25 (5): 1149-1159.

Dickson, M.E., Kench, P.S., & Kantor, M.S. (2011). Longshore transport of cobbles on a mixed sand and gravel beach, southern Hawke Bay, New Zealand. *Marine Geology,* 287(1): 31-42. DOI:org/10.1016/j.margeo.2011.06.009.

Dolphin, T., Lee, J., Phillips, R., Taylor, C.J., & Dyer, K.R. (2016). Velocity of RFID tagged gravel in a non-uniform longshore transport system. *Journal of Coastal Research,* 75(sp1): 363-367. DOI:org/10.2112/SI75-073.1.

Donn, T. F., & Boardman, M. R. (1988). Bioerosion of rocky carbonate coastlines on Andros Island, Bahamas. - *Journal of Coastal Research,* 4(3): 381-394.

Dornbusch, U., Moses, C., Robinson, D. A., & Williams, R. (2008). Soft copy photogrammetry to measure shore platform erosion on decadal timescales. *Journal of Coastal Conservation*, 11(4): 193-200.

Dornbusch, U., & Robinson, D. A. (2011). Block removal and step backwearing as erosion processes on rock shore platforms: a preliminary case study of the chalk shore platforms of south-east England. *Earth Surface Processes and Landforms*, 36(5): 661-671

Easterling, D.R., Meehl, G.A., Parmesan, C., Changnon, S.A., Karl, T.R., & Mearns, L.O. (2000). Climate extremes: observations, modeling, and impacts. *Science*, 289 (5487): 2068-2074. DOI: 10.1126/science.289.5487.2068

El Akhdar, M., Guilcher, A., Moufak, F., & Rouiha, A. (1990). Processus d'érosion littorale dans les calcaires au Maroc atlantique. *Norois*, 146(1): 163-173.

Emery, K. O. (1946). Marine solution basins. *The Journal of Geology,* 54: 209-228.

Emery, K. O. (1962). Marine geology of Guam. US Geological Survey Professional Paper 403: B1-76.

Emery, K. O., & Kuhn, G. G. (1982). Sea cliffs: their processes, profiles, and classification. *Geological Society of America Bulletin,* 93(7): 644-654. DOI:org/10.1130/0016-7606(1982)93<644:SCTPPA> 2.0.CO;2

Engel, M., & May, S.M. (2012). Bonaire's boulder fields revisited: evidence for Holocene tsunami impact on the Leeward Antilles. *Quaternary Science Reviews,* 54: 126-141. DOI:org/10.1016/j.quascirev.2011.12.011.

English Nature, (2001). SOLENT EUROPEAN MARINE SITE: English Nature's advice given under Regulation 33(2) of the Conservation (Natural Habitats &c.) Regulations 1994.

Erdmann, W., Kelletat, D., & Kuckuck, M. (2017). Boulder ridges and washover features in Galway Bay, western Ireland. *Journal of Coastal Research*, 33(5): 997-1021.

Erdmann, W., Kelletat, D., & Scheffers, A. (2018). Boulder transport by storms–Extreme-waves in the coastal zone of the Irish west coast. *Marine Geology*, 399: 1-13.

Etienne, S., Buckley, M., Paris, R., Nandasena, A.K., Clark, K., Strotz, L., Chagué-Goff, C., Goff, J., & Richmond, B. (2011).The use of boulders for characterising past tsunamis: lessons from the 2004 Indian Ocean and 2009 South Pacific tsunamis. *Earth-Science Reviews*, 107(1-2): 76-90. DOI:org/10.1016/j.earscirev.2010.12.006

Etienne, S., & Paris, R. (2010). Boulder accumulations related to storms on the south coast of the Reykjanes Peninsula (Iceland). *Geomorphology*, 114(1-2): 55-70. DOI:org/10.1016/j.geomorph.2009.02.008

Fagherazzi, S., & Mariotti, G. (2012). Mudflat runnels: Evidence and importance of very shallow flows in intertidal morphodynamics. *Geophysical Research Letters*, 39(14).

Feal-Pérez, A., & Blanco-Chao, R. (2013). Characterization of abrasion surfaces in rock shore environments of NW Spain. *Geo-Marine Letters,* 33(2-3): 173-181.

Fichaut, B., & Suanez, S. (2011). Quarrying, transport and deposition of clifftop storm deposits during extreme events: Banneg Island, Brittany. *Marine Geology,* 283(1): 36-55. DOI:org/10.1016/j.margeo.2010.11.003.

Finkl, C. W. (2004). Coastal classification: systematic approaches to consider in the development of a comprehensive scheme. *Journal of Coastal Research,* 201: 166-213.

Focke, J. W. (1978). Limestone cliff morphology and organism distribution on Curaçao (Netherlands Antilles). *Leidse Geologische Mededelingen*, 51(1): 131-150.

Ford, M. (2011). Shoreline changes on an urban atoll in the central Pacific Ocean: Majuro Atoll, Marshall Islands. *Journal of Coastal Research*, 28(1): 11-22.

Furlani, S., Biolchi, S., Devoto, S., Saliba, D., & Scicchitano, G. (2011a). Large Boulder Along the NE Maltese Coast: Tsunami or Storm Wave Deposits?. *Journal of Coastal Research*, 61: 470-470. DOI:org/10.2112/SI61-001.60

Furlani, S., Devoto, S., Biolchi, S., & Cucchi, F. (2011b). Factors triggering sea cliff instability along the Slovenian coasts. *Journal of Coastal Research*, 387-393.

Furlani, S., Devoto, S., Biolchi, S., & Cucchi, F. (2011c). Coastal cliff behaviour: The case study of Debeli rtič (SW Slovenia). In *Annales, series historia naturalis* (pp. 21-1).

Gale, A. S., Huggett, J. M., Palike, H., Laurie, E., Hailwood, E. A., & Hardenbol, J. (2006). Correlation of Eocene–Oligocene marine and continental records: orbital cyclicity, magnetostratigraphy and sequence stratigraphy of the Solent Group, Isle of Wight, UK. *Journal of the Geological Society*, 163(2): 401-415.

Gillespie, M. R., Barnes, R. P., & Milodowski, A. E. (2011). *British Geological Survey scheme for classifying discontinuities and fillings*. British Geological Survey.

Goktan, R. M., & Gunes, N. (2005). A comparative study of Schmidt hammer testing procedures with reference to rock cutting machine performance prediction. *International Journal of Rock Mechanics and Mining Sciences*, 3(42): 466-472.

Gómez-Pazo, A., Pérez-Alberti, A., & Trenhaile, A. (2019). Recording inter-annual changes on a boulder beach in Galicia, NW Spain using an unmanned aerial vehicle. *Earth Surface Processes and Landforms*, *44*(5): 1004-1014.

Gómez-Pujol, L., & Fornós, J. J. (2010). Coastal karren features in temperate microtidal settings: spatial organization and temporal evolution. Studia Universitatis Babeş-Bolyai, *Geologia*, 55: 37-44.

Gonçalves, J. A., & Henriques, R. (2015). UAV photogrammetry for topographic monitoring of coastal areas. *ISPRS Journal of Photogrammetry and Remote Sensing*, *104*: 101-111.

Goto, K., Chavanich, S. A., Imamura, F., Kunthasap, P., Matsui, T., Minoura, K., Sugawara, D., & Yanagisawa, H. (2007). Distribution, origin and transport process of boulders deposited by the 2004 Indian Ocean tsunami at Pakarang Cape, Thailand. *Sedimentary Geology*, 202(4): 821-837.

Goto, K., Okada, K., & Imamura, F. (2009). Characteristics and hydrodynamics of boulders transported by storm waves at Kudaka Island, Japan. *Marine Geology*, 262(1): 14-24. DOI: 10.1016/j.margeo.2009.03.001

Goto, K., Okada, K., & Imamura, F. (2010a). Numerical analysis of boulder transport by the 2004 Indian Ocean tsunami at Pakarang Cape, Thailand. *Marine Geology*, 268(1-4): 97-105.

Goto, K., Kawana, T., & Imamura, F. (2010b). Historical and geological evidence of boulders deposited by tsunamis, southern Ryukyu Islands, Japan. *Earth-Science Reviews*, 102(1-2): 77-99. DOI:org/10.1016/j.earscirev.2010.06.005

Goto K, Miyagi K, Kawamata H, Imamura F. 2010c. Discrimination of boulders deposited by tsunamis and storm waves at Ishigaki Island, Japan. *Marine Geology,* 269(1-2): 34-45. DOI:org/10.1016/j.margeo.2009.12.004

Goto, K., Miyagi, K., Kawana, T., Takahashi, J., & Imamura, F. (2011). Emplacement and movement of boulders by known storm waves-field evidence from the Okinawa Islands, Japan. *Marine Geology,* 283(1-4): 66-78. DOI.org/10.1016/j.margeo.2010.09.007.

Goto, K., Sugawara, D., Ikema, S., & Miyagi, T. (2012). Sedimentary processes associated with sand and boulder deposits formed by the 2011 Tohoku-oki tsunami at Sabusawa Island, Japan. *Sedimentary Geology*, 282: 188-198. DOI:10.1016/j.sedgeo.2012.03.017

Goudie, A. S. (2006). The Schmidt Hammer in geomorphological research. *Progress in Physical Geography*, 30(6): 703-718.

Gowell, M. R., Coombes, M. A., & Viles, H. A. (2015). Rock-protecting seaweed? Experimental evidence of bioprotection in the intertidal zone. *Earth Surface Processes and Landforms*, 40(10): 1364-1370.

Guilcher, A. (1953). Essai sur la zonation et la distribution des formes littorales de dissolution du calcaire. *Annales de Géographie*, 62: 161-179.

Guilcher, A. (1954). Morphologie littorale du calcaire en Méditerranée occidentale (Catalogne et environs d'Alger). *Bulletin de l'Association de Géographes Français*, 31(241): 50-58.

Guilcher, A. (1958). Coastal and submarine geomorphology; transl. from French. *London: Methuen & Co*.

Gunn, D. A., Pearson, S. G., Chambers, J. E., Nelder, L. M., Lee, J. R., Beamish, D., Busby, J.P., Tinsley, W. H. (2006). An evaluation of combined geophysical and geotechnical methods to characterize beach thickness. *Quarterly Journal of Engineering Geology and Hydrogeology*, 39(4): 339-355.

Hall, A. M. (2011). Storm wave currents, boulder movement and shore platform development: a case study from East Lothian, Scotland. *Marine Geology,* 283(1): 98-105. DOI: 10.1016/j.margeo.2010.10.024

Hall, A.M., Hansom, J.D., & Jarvis, J. (2008). Patterns and rates of erosion produced by high energy wave processes on hard rock headlands: The Grind of the Navir, Shetland, Scotland. *Marine Geology,* 248(1-2): 28-46. DOI:org/10.1016/j.margeo.2007.10.007

Hall, A. M., Hansom, J. D., Williams, D. M., & Jarvis, J. (2006). Distribution, geomorphology and lithofacies of cliff-top storm deposits: Examples from the high-energy coasts of Scotland and Ireland. *Marine Geology*, 232(3-4): 131-155. DOI: org/10.1016/j.margeo.2006.06.008

Hampson, G. J., Rodriguez, A. B., Storms, J. E., Johnson, H. D., Meyer, C. T., Steel, R. J., Burgess, P.M., Dalrymple, R. W. (2008). Geomorphology and high-resolution stratigraphy of progradational wave-dominated shoreline deposits: Impact on reservoir-scale facies architecture. *Recent advances in models of siliciclastic shallow-marine stratigraphy: SEPM Special Publication*, 90: 117-142.

Han, M., Yang, D.Y., Yu, J., & Kim, J.W. (2017). Typhoon impact on a pure gravel beach as assessed through gravel movement and topographic change at Yeocha beach, South Coast of Korea. *Journal of Coastal Research,* 33(4): 889-906. DOI:org/10.2112/JCOASTRES-D-16-00104.1.

Hansom, J.D., & Hall, A.M. (2009). Magnitude and frequency of extra-tropical North Atlantic cyclones: a chronology from cliff-top storm deposits. *Quaternary International,* 195(1-2): 42-52. DOI:org/10.1016/j.quaint.2007.11.010

Hansom, J. D., Barltrop, N. D. P., & Hall, A. M. (2008). Modelling the processes of cliff-top erosion and deposition under extreme storm waves. *Marine Geology*, 253(1-2): 36-50.

Hastewell, L.J., Schaefer, M., Bray, M., & Inkpen, R. (2019a). Intertidal boulder transport: A proposed methodology adopting Radio Frequency Identification (RFID) technology to quantify storm induced boulder mobility. *Earth Surface Processes and Landforms,* 44(3): 681-698. DOI:org/10.1002/esp.4523

Hastewell, L., Inkpen, R., & Bray, M. (2019b). Identification of plate-forme à vasques on a temperate shore platform? Quantitative analysis of morphology and relationships at Bembridge, Isle of Wight. *Zeitschrift für Geomorphologie,* 62(2): 145-162. DOI:org/10.1127/zfg/2019/0600

Hastewell, L.J., Inkpen, R., Bray, M., & Schaefer, M. (2020, *in review*). Quantification of contemporary storm-induced boulder production and transport on an intertidal shore platform using RFID technology.

Hénaff, A., Lageat, Y. & Costa, S. (2006). Geomorphology and shaping of Chalk shore platforms of the Channel coasts. *Zeitschrift für Geomorphologie*, 144: 61–91.

Héquette, A., & Cartier, A. (2016). Theoretical and observed breaking wave height on a barred macrotidal beach: implications for the estimation of breaker index on beaches with large tidal range. *Journal of Coastal Research,* 75(1): 861-866.

Herterich, J. G., Cox, R., & Dias, F. (2018). How does wave impact generate large boulders? Modelling hydraulic fracture of cliffs and shore platforms. *Marine Geology,* 399: 34-46. DOI:org/10.1016/j.margeo.2018.01.003

Hesp, P. A. (2013). A 34 year record of foredune evolution, Dark Point, NSW, Australia. *Journal of Coastal Research*, 65(sp2): 1295-1301.

Hills, E.S. (1972). Shore platforms and wave ramps. *Geological Magazine,* 109(2): 81-88. DOI:org/10.1017/S0016756800039479

Historic England (2016). Strategic Stone Study. A Building Stone Atlas of the Isle of Wight.

Hoek, E., & Bray, J. D. (1981). Rock Slope Engineering 3rd edition. The Institution of Mining and Metallurgy, CRC Press: London.

Holyoak, D. T., & Preece, R. C. (1983). Evidence of a high Middle Pleistocene sea-level from estuarine deposits at Bembridge, Isle of Wight, England. *Proceedings of the Geologists' Association*, 94(3): 231-244.

Hopson, P. (2011). The geological history of the Isle of Wight: an overview of the 'diamond in Britain's geological crown'. *Proceedings of the Geologists' Association*, 122(5): 745-763.

Imamura, F., Goto, K., & Ohkubo, S. (2008). A numerical model for the transport of a boulder by tsunami. *Journal of Geophysical Research, Oceans,* 113(C1). DOI:org/10.1029/2007JC004170.

Insole, A., & Daley, B. (1985). A revision of the lithostratigraphical nomenclature of the Late Eocene and Early Oligocene strata of the Hampshire Basin, Southern England. *Tertiary Research*, 7(3): 67-100.

Insole, A. N., Daley, B., & Gale, A. (1998). *The Isle of Wight* (No. 60). Geologists' Association guide. Geologists Association, London.

Isle of Wight Council & Royal Haskoning (2010). Isle of Wight Shoreline Management Plan 2: Main Report - Chapter 4; Policy Development Zone 3 - Bembridge and Sandown Bay (PDZ3). Accessed on 16th May 2017, from: http://www.coastalwight.gov.uk/smp/FINAL_SMP_for_web/pdf_MainDoc/Chapter4/Chapter4_PDZ3_Dec10_Final.pdf.

ISRM. (1978). Suggested methods for determining hardness and abrasiveness of rocks. In: Brown ET editor. Rock characterization, testing and monitoring: ISRM suggested Methods. Oxford: Pergamon. p. 95-6

Jeffery, Z., Penn, S., Giles, D. & Hastewell, L.J. (2019, in review): Quarterly Journal of Engineering Geology and Hydrogeology. Identification and classification of dissolution and anthropogenic features within the chalk of the Hampshire Basin using integrated LiDAR and ground based geophysical methods.

Jeong, E., Park, J. Y., & Hwang, C. S. (2018). Assessment of UAV Photogrammetric Mapping Accuracy in the Beach Environment. *Journal of Coastal Research*, 85(sp1): 176-180.

Jol, H. M., Smith, D. G., & Meyers, R. A. (1996). Digital ground penetrating radar (GPR): a new geophysical tool for coastal barrier research (examples from the Atlantic, Gulf and Pacific Coasts, USA). *Journal of Coastal Research*, 960-968.

Jolliffe, I. P. (1963). A study of sand movements on the Lowestoft sandbank using fluorescent tracers. *The Geographical Journal*, 129(4): 480-493.

Jolliffe, I.P. (1964). An experiment designed to compare the relative rates of movement of different sizes of beach pebble. *Proceedings of the Geologists' Association*, 75(1): 77-86. DOI: 10.1016/S0016-7878(64)80012-2

Kaplan, E., & Hegarty, C. (2005). Understanding GPS: principles and applications. Artech House.

Katz, O., Reches, Z., & Roegiers, J. C. (2000). Evaluation of mechanical rock properties using a Schmidt Hammer. *International Journal of rock mechanics and mining sciences*, 37(4): 723-728.

Kaye, C. A. (1959). Shoreline features and Quaternary shoreline changes, Puerto Rico. *US Geological Survey professional paper*, 317: 49-140.

Keen, A.M. (1961). A proposed reclassification of the gastropod family Vermetidae. *Bulletin of the British Museum* (Natural History) 7: 183–213.

Kennedy, A.B., Mori, N., Yasuda, T., Shimozono, T., Tomiczek, T., Donahue, A., Shimura, T., & Imai, Y. (2017). Extreme block and boulder transport along a cliffed coastline (Calicoan Island, Philippines) during Super Typhoon Haiyan. *Marine Geology,* 383: 65-77. DOI:org/10.1016/j.margeo.2016.11.004

Kennedy, D. M. (2010). Geological control on the morphology of estuarine shore platforms: Middle Harbour, Sydney, Australia. *Geomorphology,* 114(1-2): 71-77. DOI: org/10.1016/j.geomorph.2009.02.012

Kennedy, D. M. (2015). Where is the seaward edge? A review and definition of shore platform morphology. *Earth-Science Reviews*, 147: 99-108.

Kennedy, D. M., & Beban, J. G. (2005). Shore platform morphology on a rapidly uplifting coast, Wellington, New Zealand. *Earth Surface Processes and Landforms*, *30*(7): 823-832.

Kennedy, D. M., & Dickson, M. E. (2006). Lithological control on the elevation of shore platforms in a microtidal setting. *Earth Surface Processes and Landforms: The Journal of the British Geomorphological Research Group*, 31(12): 1575-1584.

Kennedy, D. M., Paulik, R., & Dickson, M. E. (2011). Subaerial weathering versus wave processes in shore platform development: reappraising the Old Hat Island evidence. *Earth Surface Processes and Landforms*, 36(5): 686-694.

Kennedy, D. M., Woods, J. L., Naylor, L. A., Hansom, J. D., & Rosser, N. J. (2019). Intertidal boulder-based wave hindcasting can underestimate wave size: Evidence from Yorkshire, UK. *Marine Geology,* 411: 98-106. DOI:org/10.1016/j.margeo.2019.02.002

Kidson, C., Carr, A.P., & Smith, D.B.(1958). Further experiments using radioactive methods to detect the movement of shingle over the sea bed and alongshore. *The Geographical Journal,* 124(2): 210-218. DOI:10.2307/1790248

Klemas, V. V. (2011). Remote sensing of wetlands: case studies comparing practical techniques. *Journal of Coastal Research*, 27(3): 418-427.

Klemas, V. V. (2015). Coastal and environmental remote sensing from unmanned aerial vehicles: An overview. *Journal of Coastal Research*, 31(5): 1260-1267.

Knight, J., & Burningham, H. (2011). Boulder dynamics on an Atlantic-facing rock coastline, northwest Ireland. *Marine Geology,* 283(1-4): 56-65. DOI:org/10.1016/j.margeo.2010.07.008

Knight, J., Burningham, H., & Barrett-Mold, C. (2009). The geomorphology and controls on development of a boulder-strewn rock platform, NW Ireland. *Journal of Coastal Research,* 56: 1646-1650.

Kogure, T., Aoki, H., Maekado, A., Hirose, T., & Matsukura, Y. (2006). Effect of the development of notches and tension cracks on instability of limestone coastal cliffs in the Ryukyus, Japan. *Geomorphology,* 80(3-4): 236-244. DOI:org/10.1016/j.geomorph.2006.02.012

Kroon, A., & Masselink, G. (2002). Morphodynamics of intertidal bar morphology on a macrotidal beach under low-energy wave conditions, North Lincolnshire, England. *Marine Geology*, 190(3-4): 591-608. DOI:10.1016/S0025-3227(02)00475-9

Kumar, V. S., Dhakate, R., Amarender, B., & Sankaran, S. (2016). Application of ERT and GPR for demarcating the saline water intrusion in coastal aquifers of Southern India. *Environmental Earth Sciences*, 75(5): 393.

Kumar, A., Narayana, A. C., & Jayappa, K. S. (2010). Shoreline changes and morphology of spits along southern Karnataka, west coast of India: A remote sensing and statistics-based approach. *Geomorphology*, 120(3-4): 133-152.

Lamarre, H., MacVicar, B., & Roy, A.G. (2005). Using passive integrated transponder (PIT) tags to investigate sediment transport in gravel-bed rivers. *Journal of Sedimentary Research*, 75(4): 736-741. DOI:10.2110/jsr.2005.059

Laporte-Fauret, Q., Marieu, V., Castelle, B., Michalet, R., Bujan, S., & Rosebery, D. (2019). Low-Cost UAV for high-resolution and large-scale coastal dune change monitoring using photogrammetry. *Journal of Marine Science and Engineering*, 7(3): 63.

Lau, A.A., Terry, J.P., Ziegler, A.D., Switzer, A.D., Lee, Y., & Etienne, S. (2016). Understanding the history of extreme wave events in the Tuamotu Archipelago of French Polynesia from large

carbonate boulders on Makemo Atoll, with implications for future threats in the central South Pacific. *Marine Geology,* 380: 174-90. DOI:org/10.1016/j.margeo.2016.04.018

Leckebusch, G.C., Koffi, B., Ulbrich, U., Pinto, J.G., Spangehl, T., & Zacharias, S. (2006). Analysis of frequency and intensity of European winter storm events from a multi-model perspective, at synoptic and regional scales. *Climate Research,* 31(1): 59-74. DOI:10.3354/cr031059

Lee, M.W., Bray, M., Workman, M., Collins, M.B., & Pope, D. (2000). Coastal shingle tracing: a case study using the 'Electronic Tracer System' (ETS). In *Tracers in Geomorphology*, Watson IDL (ed). Wiley: Chichester; 413-435.

Lee, M.W., Sear, D.A., Atkinson, P.M., Collins, M.B., & Oakey, R.J. (2007). Number of tracers required for the measurement of longshore transport distance on a shingle beach. *Marine Geology*, 240(1): 57-63. DOI:10.1016/j.margeo.2007.02.010

Liébault, F., Bellot, H., Chapuis, M., Klotz, S., Deschâtres, M. (2012). Bedload tracing in a high-sediment-load mountain stream. *Earth Surface Processes and Landforms,* 37(4): 385-99. DOI: 10.1002/esp.2245

Long, D. (2017). Cataloguing tsunami events in the UK. *Geological Society, London, Special Publications,* 456(1): 143-165. DOI:org/10.1144/SP456.10

Lorang, M. S. (2011). Predicting threshold entrainment mass for a boulder beach. *Journal of Coastal Research,* 16(2): 432-445.

Luo, Y., Weng, E., Wu, X., Gao, C., Zhou, Z., & Zhang, L. (2009). Parameter identifiability, constraint, and equifinality in data assimilation with ecosystem models. *Ecological Applications*, 19: 571-574.

Maiti, S., & Bhattacharya, A. K. (2009). Shoreline change analysis and its application to prediction: A remote sensing and statistics based approach. *Marine Geology*, 257(1-4): 11-23.

Mancini, F., Dubbini, M., Gattelli, M., Stecchi, F., Fabbri, S., & Gabbianelli, G. (2013). Using unmanned aerial vehicles (UAV) for high-resolution reconstruction of topography: The structure from motion approach on coastal environments. *Remote Sensing*, 5(12): 6880-6898.

Maouche, S., Morhange, C., & Meghraoui, M. (2009). Large boulder accumulation on the Algerian coast evidence tsunami events in the western Mediterranean. *Marine Geology*, 262(1-4): 96-104. DOI:org/10.1016/j.margeo.2009.03.013

Marine Licensing (Exempted Activities) Order 2011 (SI 2011/No. 409). Accessed on 2nd November 2017, from: http://www.legislation.gov.uk/uksi/2011/409/part/3/made

Masselink, G., Castelle, B., Scott, T., Dodet, G., Suanez, S., Jackson, D., Floc'h, F. (2016a). Extreme wave activity during 2013/2014 winter and morphological impacts along the Atlantic coast of Europe. *Geophysical Research Letters,* 43(5): 2135-43. DOI:10.1002/2015GL067492

Masselink, G., Scott, T., Poate, T., Russell, P., Davidson, M., & Conley, D. (2016b). The extreme 2013/2014 winter storms: hydrodynamic forcing and coastal response along the southwest coast of England. *Earth Surface Processes and Landforms,* 41(3): 378-391. DOI:10.1002/esp.3836

Mastronuzzi, G., & Sansò, P. (2000). Boulders transport by catastrophic waves along the Ionian coast of Apulia (southern Italy). *Marine Geology,* 170(1-2): 93-103. DOI:org/10.1016/S0025-3227(00)00068-2

Mastronuzzi, G., & Sansò, P. (2004). Large boulder accumulations by extreme waves along the Adriatic coast of southern Apulia (Italy). *Quaternary International,* 120(1): 173-184. DOI:org/10.1016/j.quaint.2004.01.016

Matthews, T., Murphy, C., Wilby, R. L., & Harrigan, S. (2014). Stormiest winter on record for Ireland and UK. *Nature Climate Change*, *4*(9), 738.

Mauz, B., Hijma, M. P., Amorosi, A., Porat, N., Galili, E., Bloemendal, J. (2013). Aeolian beach ridges and their significance for climate and sea level: Concept and insight from the Levant coast (East Mediterranean). *Earth-Science Reviews*, 121: 31-54.

McHenry, J. R., & McDowell, L. L. (1962). The use of radioactive tracers in sedimentation research. *Journal of Geophysical Research*, 67(4): 1465-1471.

McKenna, J. (2005). Boulder beaches. In *Encyclopaedia of Coastal Science* (pp. 206-208). Schwartz, M. (Ed.). Springer Science & Business Media, Kluwer, Dordrecht.

McKenna, J., Jackson, D. W., & Cooper, J. A. G. (2011). In situ exhumation from bedrock of large rounded boulders at the Giant's Causeway, Northern Ireland: An alternative genesis for large shore boulders (mega-clasts). *Marine Geology,* 283(1-4): 25-35. DOI:org/10.1016/j.margeo.2010.09.005

Met Office, (2018). UK Climate (Online). Accessed on 16th November 2018, from: https://www.metoffice.gov.uk/public/weather/climate/

Milazzo, M., Fine, M., La Marca, E. C., Alessi, C., & Chemello, R. (2015). Drawing the Line at Neglected Marine Ecosystems: Ecology of Vermetid Reefs in a Changing Ocean. Marine Animal Forests: *The Ecology of Benthic Biodiversity Hotspots*: 1-23. DOI.org/10.1007/978-3-319-17001-5_9-1

Miller, I.M., & Warrick, J.A. (2012). Measuring sediment transport and bed disturbance with tracers on a mixed beach. *Marine Geology*, 299: 1-7. DOI:10.1016/j.margeo.2012.01.002

Miller, I.M., Warrick, J.A., & Morgan, C. (2011). Observations of coarse sediment movements on the mixed beach of the Elwha Delta, Washington. *Marine Geology,* 282(3): 201-214. DOI:org/10.1016/j.margeo.2011.02.012.

Miller, W. R., & Mason, T. R. (1994). Erosional features of coastal beachrock and aeolianite outcrops in Natal and Zululand, South Africa. *Journal of Coastal Research*, 10(2): 374-394.

Morton, R. A., Richmond, B. M., Jaffe, B. E., & Gelfenbaum, G. (2008). Coarse-clast ridge complexes of the Caribbean: a preliminary basis for distinguishing tsunami and storm-wave origins. *Journal of Sedimentary Research*, 78(9): 624-637.

Moses, C.A. (2014). The rock coast of the British Isles: shore platforms. *Geological Society, London, Memoirs.* 40(1): 39-56. DOI:10.1144/M40.4

Moses, C., & Robinson, D. (2011). Chalk coast dynamics: implications for understanding rock coast evolution. *Earth-Science Reviews*, 109(3-4): 63-73.

Mottershead, D., Bray, M., Soar, P., & Farres, P. J. (2014). Extreme wave events in the central Mediterranean: geomorphic evidence of tsunami on the Maltese Islands. *Zeitschrift für Geomorphologie,* 58(3): 385-411. DOI:org/10.1127/0372-8854/2014/0129.

Mottershead, D. N., Bray, M. J., Soar, P. J., & Farres, P. J. (2015). Characterisation of erosional features associated with tsunami terrains on rocky coasts of the Maltese islands. *Earth Surface Processes and Landforms*, 40(15): 2093-2111.

Mottershead, D., Bray, M., Soar, P., & Hastewell, L.J. (2017). Storm or tsunami? Or Storm and tsunami? Boulder transport histories on the shoreline of Malta. International Tsunami Field Symposium. Lisbon, Portugal.

Mottershead, D., Bray, M., & Deguara, J. C. (2019). Tsunamigenic landscapes in the Maltese Islands: the comino channel coasts. In *Landscapes and Landforms of the Maltese Islands* (pp. 273-288). Springer, Cham.

Moura, D., Gabriel, S., Gamito, S., Santos, R., Zugasti, E., Naylor, L., Gomes, A., Tavares, A.M., & Martins, A. L. (2012). Integrated assessment of bioerosion, biocover and downwearing rates of carbonate rock shore platforms in southern Portugal. *Continental Shelf Research*, 38: 79-88. DOI.org/10.1016/j.csr.2012.03.003.

Müller, G., Wolters, G., & Cooker, M.J. (2003). Characteristics of pressure pulses propagating through water-filled cracks. *Coastal Engineering*, 1;49 (1-2): 83-98. DOI:10.1016/S0378-3839(03)00048-6

Munt, M. (2008). A history of geological conservation on the Isle of Wight. *Geological Society, London, Special Publications*, 300(1): 173-179.

Murfitt, S. L., Allan, B. M., Bellgrove, A., Rattray, A., Young, M. A., & Ierodiaconou, D. (2017). Applications of unmanned aerial vehicles in intertidal reef monitoring. *Scientific Reports*, 7(1): 10259.

Nagle-McNaughton, T., & Cox, R. (2020). Measuring Change Using Quantitative Differencing of Repeat Structure-From-Motion Photogrammetry: The Effect of Storms on Coastal Boulder Deposits. *Remote Sensing*, *12*(1): 42. DOI:org/10.3390/rs12010042

Nakata, T., & Kawana, T. (1995). Historical and prehistorical large tsunamis in the southern Ryukyus, Japan. In *Tsunami: Progress in prediction, disaster prevention and warning* (pp. 211-221). Springer, Dordrecht.

Nandasena, N.A., Paris, R., & Tanaka, N. (2011a). Numerical assessment of boulder transport by the 2004 Indian ocean tsunami in Lhok Nga, West Banda Aceh (Sumatra, Indonesia). *Computers & Geosciences*, 37(9): 1391-1399. DOI: 10.1016/j.cageo.2011.02.001

Nandasena, N.A., Paris, R., & Tanaka, N. (2011b). Reassessment of hydrodynamic equations: minimum flow velocity to initiate boulder transport by high energy events (storms, tsunamis). *Marine Geology*, 281(1): 70-84. DOI: 10.1016/j.margeo.2011.02.005

Nandasena, N.A., Tanaka, N., Sasaki, Y., & Osada, M. (2013). Boulder transport by the 2011 Great East Japan tsunami: Comprehensive field observations and whither model predictions? *Marine Geology*, 346: 292-309. DOI: 10.1016/j.margeo.2013.09.015

Nandasena, N.A., & Tanaka, N. (2013a). Boulder transport by high-energy (tsunamis): Model development for threshold entrainment and transport. *Research Report of Department of Civil and Environmental Engineering, Saitama Univ*, 39(1): 1-12.

Nandasena, N.A., & Tanaka, N. (2013b). Boulder transport by high energy: Numerical model-fitting experimental observations. *Ocean Engineering,* 57: 163-179. DOI: .org/10.1016/j.oceaneng.2012.09.012

Nathan Bradley, D., & Tucker, G.E. (2012). Measuring gravel transport and dispersion in a mountain river using passive radio tracers. *Earth Surface Processes and Landforms,* 37(10): 1034-1045. DOI:10.1002/esp.3223

Naylor, L. A., & Viles, H. A. (2002). A new technique for evaluating short-term rates of coastal bioerosion and bioprotection. *Geomorphology,* 47(1): 31-44. DOI.org/10.1016/S0169-555X(02)00139-3.

Naylor, L. A., & Stephenson, W. J. (2010). On the role of discontinuities in mediating shore platform erosion. *Geomorphology*, 114(1-2): 89-100.

Naylor, L. A., Coombes, M. A., & Viles, H. A. (2012). Reconceptualising the role of organisms in the erosion of rock coasts: a new model. *Geomorphology*, 157: 17-30. DOI.org/10.1016/j.geomorph. 2011.07.015.

Naylor, L.A., Rodrigues, B.A., Tancock, D., Brady, A. (2010). Boulder Dynamics: Research to understand boulder transport pathways and supply to Northam Pebble Ridge. Pilot Study Results and Recommendations. University of Exeter.

Naylor, L. A., Stephenson, W. J., Smith, H. C., Way, O., Mendelssohn, J., & Cowley, A. (2016). Geomorphological control on boulder transport and coastal erosion before, during and after an extreme extra-tropical cyclone. *Earth Surface Processes and Landforms,* 41(5): 685-700. DOI: 10.1002/esp.3900

Naylor, L.A., Stephenson, W.J., & Trenhaile, A.S. (2010). Rock coast geomorphology: recent advances and future research directions. *Geomorphology,* 114(1):3-11. DOI: 10.1016/j.geomorph.2009.02.004

Neumann, B., Vafeidis, A. T., Zimmermann, J., & Nicholls, R. J. (2015). Future coastal population growth and exposure to sea-level rise and coastal flooding-a global assessment. *PloS one*, *10*(3): e0118571. DOI:10.1371/journal.pone.0118571

Nicholas, A. P., & Quine, T. A. (2010). Quantitative assessment of landform equifinality and palaeoenvironmental reconstruction using geomorphic models. Geomorphology, 121: 167-183.

Nichols, M.H. (2004). A radio frequency identification system for monitoring coarse sediment particle displacement. *Applied Engineering in Agriculture,* 20(6): 783-787. DOI:org/10.13031/2013.17727.

Nordstrom, K.F., & Jackson, N.L. (1993). Distribution of surface pebbles with changes in wave energy on a sandy estuarine beach. *Journal of Sedimentary Research,* 63(6): 1152-1159.

Noormets, R., Crook, K.A., & Felton, E.A. (2004). Sedimentology of rocky shorelines: 3. Hydrodynamics of megaclast emplacement and transport on a shore platform, Oahu, Hawaii. *Sedimentary Geology*, 172(1-2): 41-65. DOI:org/10.1016/j.sedgeo.2004.07.006

Nott, J. (2003a). Waves, coastal boulder deposits and the importance of the pre-transport setting. *Earth and Planetary Science Letters*, 210(1-2): 269-276. DOI:10.1016/S0012-821X(03)00104-3

Nott, J. (2003b). Tsunami or storm waves?: Determining the origin of a spectacular field of wave emplaced boulders using numerical storm surge and wave models and hydrodynamic transport equations. *Journal of Coastal Research*, 19(2): 348-356.

Oak, H. L. (1984). The boulder beach: a fundamentally distinct sedimentary assemblage. *Annals of the Association of American Geographers*, *74*(1): 71-82.

Ogawa, H., Dickson, M.E., & Kench, P.S. (2011). Wave transformation on a sub-horizontal shore platform, Tatapouri, North Island, New Zealand. *Continental Shelf Research,* 31(14): 1409-1419. DOI:org/10.1016/j.csr.2011.05.006

Oliveira, S., Moura, D., Horta, J., Nascimento, A., Gomes, A., & Veiga-Pires, C. (2017). The morphosedimentary behaviour of a headland–beach system: Quantifying sediment transport using fluorescent tracers. *Marine Geology*, *388*: 62-73.

Ordnance Survey. (2017a). Accuracy [Online]. Accessed on 16th May 2017, from: https://www.ordnancesurvey.co.uk/business-and-government/help-and-support/navigation-technology/os-net/accuracy.html

Ordnance Survey. (2017b). OS-Net - Ordnance Survey [Online]. Accessed on 16th May 2017, from: https://www.ordnancesurvey.co.uk/gps/os-net-rinex-data/

Oregon RFID. (2017). HDX Long Range Readers [Online]. Accessed on 12th September 2017, from: https://www.oregonrfid.com/index.php?main_page=product_info&cPath=1&products_id=6&zenid=osn1jjl3mico7k8l9j0q5n3ho5

Osborne, P.D. (2005). Transport of gravel and cobble on a mixed-sediment inner bank shoreline of a large inlet, Grays Harbor, Washington. *Marine Geology,* 224(1): 145-56. DOI:10.1016/j.margeo.2005.08.004

Osborne, P.D., Macdonald, N., & Curtiss, G. (2011). Measurements and Modeling of Gravel Transport under Wind Waves, Vessel-Generated Waves, and Tidal Currents. Journal of Coastal Research. Special Issue 59: 165-172. DOI: 10.2112/SI59-017.1

Oxford Archaeology (2002). Bembridge Beach, Isle of Wight: IWCAC 3512. Archaeological Watching Brief Report. Accessed on 25th October 2017, from: https://library.thehumanjourney.net/761/1/IWCAC%203512-4891%20Isle%20of%20Wight%2C%20Bembridge%20Beach_A1b.pdf

Palchik, V., & Hatzor, Y. H. (2002). Crack damage stress as a composite function of porosity and elastic matrix stiffness in dolomites and limestones. *Engineering Geology*, 63(3-4): 233-245.

Pantin, H. M. (1961). Magnetic concrete as an artificial tracer mineral. *New Zealand Journal of Geology and Geophysics*, 4(4): 424-433.

Paris, R., Naylor, L.A., & Stephenson, W.J. (2011). Boulders as a signature of storms on rock coasts. *Marine Geology,* 283(1-4): 1-11. DOI:org/10.1016/j.margeo.2011.03.016.

Peres, J.M., & Picard, J. (1952). Les corniches calcaires d'origine biologique en Méditerranée occidentale. *Recueil des Travaux de la Station Marine d'Endoume*, 4: 2-33.

Pérez-Alberti, A., & Trenhaile, A. S. (2015a). An initial evaluation of drone-based monitoring of boulder beaches in Galicia, north-western Spain. *Earth Surface Processes and Landforms*, 40(1): 105-111. DOI:10.1002/esp.3654

Pérez-Alberti, A., & Trenhaile, A. S. (2015b). Clast mobility within boulder beaches over two winters in Galicia, northwestern Spain. *Geomorphology*, 248: 411-426. DOI:10.1016/j.geomorph.2015.08.001

Pignatelli, C., Sansò, P., & Mastronuzzi, G. (2009). Evaluation of tsunami flooding using geomorphologic evidence. *Marine Geology,* 260(1-4): 6-18. DOI:org/10.1016/j.margeo.2009.01.002

Pinsky, M. L., Guannel, G., & Arkema, K. K. (2013). Quantifying wave attenuation to inform coastal habitat conservation. *Ecosphere*, 4(8): 1-16. DOI.org/10.1890/ES13-00080.1.

Preece, R. C., & Scourse, J. D. (1987). Pleistocene sea-level history in the Bembridge area of the Isle of Wight. *Wessex and the Isle of Wight: Field Guide*, 136-155.

Preece, R. C., Scourse, J. D., Houghton, S. D., Knudsen, K. L., & Penney, D. N. (1990). The Pleistocene sea-level and neotectonic history of the eastern Solent, southern England. *Philosophical Transactions of the Royal Society of London. Biological Sciences*, 328(1249): 425-477.

Prisson, L. V. (1919). raphic Memoir of James Dwight Dana 1813-1895. National Academy of Sciences of the United States of America. raphic Memoirs, Part of Volume IX. Accessed on 1st June 2018, from: http://www.nasonline.org/publications/biographical-memoirs/memoir-pdfs/dana-james.pdf

Putman, J. L., & Smith, D. B. (1956). Radioactive tracer techniques for sand and silt movements under water. *The International Journal of Applied Radiation and Isotopes*, 1(1-2): 24-32.

Richardson, N. M. (1902). An experiment on the movements of a load of brickbats deposited on the Chesil Beach. In *Proceedings Dorset Natural History and Antiquarian Field Club* (Vol. 23, pp. 123-133).

Robinson, L. A. (1977). Erosive processes on the shore platform of northeast Yorkshire, England. *Marine Geology*, 23(4): 339-361.

Roig-Munar, F.X., Rodríguez-Perea, A., Vilaplana, J.M., Martín-Prieto, J.A., & Gelabert, B. (2019). Tsunami boulders in Majorca Island (Balearic Islands, Spain). *Geomorphology,* 334: 76-90. DOI:org/10.1016/j.geomorph.2019.02.012

Russell, R.C. (1960). The use of fluorescent tracers for the measurement of littoral drift. *Coastal Engineering Proceedings,* 1(7): 24. DOI:10.9753/icce.v7.24

Safriel, U. (1966). Regent vermetid formation on the Mediterranean shore of Israel. *Journal of Molluscan Studies*, 37: 27-34.

Salzmann, L., & Green, A. (2012). Boulder emplacement on a tectonically stable, wave-dominated coastline, Mission Rocks, northern KwaZulu-Natal, South Africa. *Marine Geology*, 323: 95-106. DOI:org/10.1016/j.margeo.2012.07.001

Sanders, N. K. (1968). *The development of Tasmanian shore platforms* (Doctoral dissertation, University of Tasmania).

Saptono, S., Kramadibrata, S., & Sulistianto, B. (2013). Using the Schmidt hammer on rock mass characteristic in sedimentary rock at tutupan coal mine. *Procedia Earth and Planetary Science*, 6: 390-395.

Schaefer, M., & Woodyer, T. (2015). Assessing absolute and relative accuracy of recreation-grade and mobile phone GNSS devices: a method for informing device choice. *Area*, 47(2): 185-196. DOI: 10.1111/area.12172

Scheffers, A. & Scheffers, S. (2006). Documentation of the impact of Hurricane Ivan on the coastline of Bonaire (Netherlands Antilles). *Journal of Coastal Research,* 22(6): 1437-1450. DOI:org/10.2112/05-0535.1

Scheffers, A., Scheffers, S., Kelletat, D., & Browne, T. (2009). Wave-emplaced coarse debris and megaclasts in Ireland and Scotland: boulder transport in a high-energy littoral environment. *The Journal of Geology*, 117(5): 553-573. DOI:10.1086/600865

Scicchitano, G., Monaco, C., & Tortorici, L. (2007). Large boulder deposits by tsunami waves along the Ionian coast of south-eastern Sicily (Italy). *Marine Geology*, 238(1-4): 75-91. DOI:org/10.1016/j.margeo.2006.12.005

Sear, D.A., Lee, M.W., Oakley, R.J., Carling, P.A., & Collins, M.B. (2000). Coarse sediment tracing technology in littoral and fluvial environments: a review. In *Tracers in Geomorphology*, Watson IDL (ed). Wiley: Chichester; 21-55.

Semedo, A., Weisse, R., Behrens, A., Sterl, A., Bengtsson, L., & Günther, H. (2012). Projection of global wave climate change toward the end of the twenty-first century. *Journal of Climate*, 26(21): 8269-8288.

Shah-hosseini, M., Morhange, C., Beni, A.N., Marriner, N., Lahijani, H., Hamzeh, M., & Sabatier, F. (2011). Coastal boulders as evidence for high-energy waves on the Iranian coast of Makran. *Marine Geology,* 290(1): 17-28. DOI:org/10.1016/j.margeo.2011.10.003.

Short, A.D. (1991). Macro-meso tidal beach morphodynamics: an overview. *Journal of Coastal Research*, 7(2): 417-436.

Small, C., & Nicholls, R. J. (2003). A global analysis of human settlement in coastal zones. *Journal of Coastal Research*, 19(3): 584-599.

Sousa, W.P. (1979). Disturbance in marine intertidal boulder fields: the nonequilibrium maintenance of species diversity. *Ecology*, 60(6): 1225-1239. DOI:org/10.2307/1936969

Spiske, M., & Bahlburg, H. (2011). A quasi-experimental setting of coarse clast transport by the 2010 Chile tsunami (Bucalemu, Central Chile). *Marine Geology,* 289(1-4): 72-85. DOI:org/10.1016/j.margeo.2011.09.007.

Spiske, M., Böröcz, Z., & Bahlburg, H. (2008). The role of porosity in discriminating between tsunami and hurricane emplacement of boulders - a case study from the Lesser Antilles, southern Caribbean. *Earth and Planetary Science Letters*, 268(3-4): 384-396.

Steers, J.A., & Smith, D.B. (1956). Detection of movement of pebbles on the sea floor by radioactive methods. *The Geographical Journal*, 122(3): 343-345.

Stephenson, W. J. (2000). Shore platforms: a neglected coastal feature?. *Progress in Physical Geography*, 24(3): 311-327.

Stephenson, W.J., & Abazović, A. (2016). Measuring Coastal Boulder Movement Under Waves Using Tri-Axial Accelerometers. *Journal of Coastal Research*, 75(sp1): 607-611. DOI:10.2112/SI75-122.1

Stephenson, W. J., Dickson, M. E. & Trenhaile, A. S. (2013). Rock coasts. In: Shroder, J. (Editor in Chief) & Sherman, D. J. (ed.) Treatise on Geomorphology. Academic Press, San Diego, vol. 10, *Coastal Geomorphology*, 289-307.

Stephenson, W. J., & Kirk, R. M. (2000). Development of shore platforms on Kaikoura Peninsula, South Island, New Zealand. Part one: the role of waves. *Geomorphology,* 32(1-2): 21-41. DOI:org/10.1016/S0169-555X(99)00061-6

Stephenson, W. J., & Naylor, L. A. (2011). Geological controls on boulder production in a rock coast setting: insights from South Wales, UK. *Marine Geology,* 283(1): 12-24. DOI:org/10.1016/j.margeo.2010.07.001.

Stevčić, Č., Pérez-Miguel, M., Drake, P., Tovar-Sánchez, A., & Cuesta, J. A. (2017). Macroinvertebrate communities on rocky shores: Impact due to human visitors. *Estuarine, Coastal and Shelf Science*, 211: 127-136. DOI.org/10.1016/j.ecss.2017.11.026.

Sumner, P., & Nel, W. (2002). The effect of rock moisture on Schmidt hammer rebound: tests on rock samples from Marion Island and South Africa. *Earth Surface Processes and Landforms*, 27(10): 1137-1142.

Sunamura, T. (1992). *Geomorphology of Rocky Coasts*, Vol. 3. John Wiley & Sons: Chichester.

Switzer, A. D., & Burston, J. M. (2010). Competing mechanisms for boulder deposition on the southeast Australian coast. *Geomorphology,* 114(1-2): 42-54. DOI:org/10.1016/j.geomorph.2009.02.009.

Taboroši, D., & Kázmér, M. (2013). Erosional and depositional textures and structures in coastal karst landscape. *In*: Lace M.J. & Mylroie J.E. (eds) Coastal Karst Landforms. *Coastal Research Library*, 5. Springer, Dordrecht, Netherlands. 15-57.

Tamura, T. (2012). Beach ridges and prograded beach deposits as palaeoenvironment records. *Earth-Science Reviews*, 114(3-4): 279-297.

Temme, A. J. A. M., Armitage, J., Attal, M., van Gorp, W., Coulthard, T. J., & Schoorl, J. M. (2017). Developing, choosing and using landscape evolution models to inform field-based landscape reconstruction studies. *Earth Surface Processes and Landforms*, 42(13): 2167-2183.

Terry, J.P., Dunne, K., & Jankaew, K. (2016). Prehistorical frequency of high-energy marine inundation events driven by typhoons in the Bay of Bangkok (Thailand), interpreted from coastal carbonate boulders. *Earth Surface Processes and Landforms,* 41(4): 553-562. DOI:org/10.1002/esp.3873

Terry, J.P, & Lau, A.A. (2018). Magnitudes of nearshore waves generated by tropical cyclone Winston, the strongest landfalling cyclone in South Pacific records. Unprecedented or unremarkable?. *Sedimentary Geology,* 364: 276-285. DOI:org/10.1016/j.sedgeo.2017.10.009

Thornton, L. E., & Stephenson, W. J. (2006). Rock strength: a control of shore platform elevation. *Journal of Coastal Research*, 22(1): 224-231.

Topcon. (2017). HiPer V - Topcon Positioning Systems, Inc. [Online]. Accessed on 16th May 2017, from: https://www.topconpositioning.com/gnss/integrated-gnss-receivers/hiper-v

Topcon. (2018). HiPer V - Topcon Positioning Systems, Inc. [Online]. Accessed on 14th December 2018, from: https://www.topconpositioning.com/sites/default/files/product_files/hiper_v_broch_7010_2121_reve_sm.pdf

Trenhaile, A. S. (1972). The shore platforms of the Vale of Glamorgan, Wales. *Transactions of the Institute of British Geographers*, 56: 127-144.

Trenhaile, A. S. (1980). Shore platforms: a neglected coastal feature. *Progress in Physical Geography*, 4(1): 1-23.

Trenhaile, A. S. (1983). The width of shore platforms; a theoretical approach. *Geografiska Annaler: Series A, Physical Geography*, 65(1-2): 147-158.

Trenhaile, A. S. (1987). *The Geomorphology of Rock Coasts*. Oxford University Press, USA.

Trenhaile, A. S. (1999). The width of shore platforms in Britain, Canada, and Japan. *Journal of Coastal Research*, 15(2):355-364.

Trenhaile, A.S. (2002). Rock coasts, with particular emphasis on shore platforms. *Geomorphology*, 48(1-3): 7-22. DOI:10.1016/S0169-555X(02)00173-3

Trenhaile, A.S. (2015). Coastal notches: their morphology, formation, and function. *Earth-Science Reviews,* 150: 285-304. DOI:org/10.1016/j.earscirev.2015.08.003

Trenhaile, A.S. (2016). Rocky coasts – their role as depositional environments. *Earth-Science Reviews,* 159: 1-13. DOI:org/10.1016/j.earscirev.2016.05.001.

Trenhaile, A.S. (2019). Hard-Rock Coastal Modelling: Past Practice and Future Prospects in a Changing World. *Journal of Marine Science and Engineering,* 7(2), 34. DOI:org/10.3390/jmse7020034

Trenhaile, A. S., & Kanyaya, J. I. (2007). The role of wave erosion on sloping and horizontal shore platforms in macro-and mesotidal environments. *Journal of Coastal Research,* 23(2): 298-309. DOI: org/10.2112/04-0282.1

Turner, I. L., Harley, M. D., & Drummond, C. D. (2016). UAVs for coastal surveying. *Coastal Engineering*, 114: 19-24.

Udden, J. A. (1914). Mechanical composition of clastic sediments. *Bulletin of the Geological Society of America*, 25(1): 655-744.

Vacchi, M., Rovere, A., Zouros, N., & Firpo, M. (2012). Assessing enigmatic boulder deposits in NE Aegean Sea: importance of historical sources as tool to support hydrodynamic equations. *Natural Hazards and Earth System Sciences*, 12(4): 1109-1118.

Van Sickle, J. (2008). GPS for land surveyors. CRC Press.

Viles, H., & Spencer, T. (2014). Coastal problems: geomorphology, ecology and society at the coast. Routledge.

Want, R. (2006). An introduction to RFID technology. *IEEE Pervasive Computing*, 5(1): 25-33. DOI: 10.1109/MPRV.2006.2

Watanabe, M., Goto, K., Imamura, F., Kennedy, A., Sugawara, D., Nakamura, N., & Tonosaki, T. (2019). Modeling boulder transport by coastal waves on cliff topography: Case study at Hachijo Island, Japan. *Earth Surface Processes and Landforms*. DOI:10.1002/esp.4684.

Weiss, R. (2012). The mystery of boulders moved by tsunamis and storms. *Marine Geology,* 295: 28-33. DOI:org/10.1016/j.margeo.2011.12.001

Wentworth, C. K. (1922). A scale of grade and class terms for clastic sediments. *The Journal of Geology*, 30(5): 377-392.

West, I.M. (2009). Kimmeridge Bay, Dorset. Geology of the Wessex Coast of Southern England. Accessed on 14th August 2019, from: http://www.southampton.ac.uk/~imw/Kimmeridge-Bay.htm

West, I.M. (2015). Whitecliff Bay, Isle of Wight. Geology of the Wessex Coast of Southern England. Accessed on 2nd May 2019, from: http://www.southampton.ac.uk/~imw/Whitecliff-Bay.htm

West, I.M. (2018). Lyme Regis to Charmouth: Geology of the Wessex Coast (Jurassic Coast, Dorset and East Devon World Heritage Site). Accessed on 1st September 2019, from: http://www.southampton.ac.uk/~imw/Lyme-Regis-to-Charmouth.htm

Wheatcroft, R. A., Jumars, P. A., Smith, C. R., & Nowell, A. R. M. (1990). A mechanistic view of the particulate biodiffusion coefficient: step lengths, rest periods and transport directions. *Journal of Marine Research*, *48*(1): 177-207.

Williams, D. M., & Hall, A. M. (2004). Cliff-top megaclast deposits of Ireland, a record of extreme waves in the North Atlantic-storms or tsunamis?. *Marine Geology,* 206(1-4): 101-117. DOI: org/10.1016/j.margeo.2004.02.002

Wolf, J., & Woolf, D.K. (2006). Waves and climate change in the north-east Atlantic. *Geophysical Research Letters*, 33: 1-4.

Woodroffe, C. D. (2014). The rock coasts of oceanic islands. In *Rock Coast Geomorphology*. Geological Society, London, Memoirs 40: (1), 247-261.

Wright, P., Cross, J.S., & Webber, N.B. (1978). Aluminium pebbles: A new type of tracer for flint and chert pebble beaches. *Marine Geology*, 27(1-2): 9-17. DOI:10.1016/0025-3227(78)90069-5

Xu, T., & Li, J. (2018). Assessing the spatial variability of the concrete by the rebound hammer test and compression test of drilled cores. *Construction and Building Materials*, 188: 820-832.

Yamada, M., Fujino, S., & Goto, K. (2014). Deposition of sediments of diverse sizes by the 2011 Tohoku-oki tsunami at Miyako City, Japan. *Marine Geology*, 358: 67-78.

Yasso, W. E. (1962). *Fluorescent coatings on coarse sediments: an integrated system* (No. CU-TR-1). COLUMBIA UNIV NEW YORK.

Yilmaz, I., & Sendir, H. (2002). Correlation of Schmidt hardness with unconfined compressive strength and Young's modulus in gypsum from Sivas (Turkey). *Engineering Geology*, 66(3-4): 211-219.

Young, I. R., Zieger, S., & Babanin, A. V. (2011). Global trends in wind speed and wave height. *Science*, 332(6028): 451-455.

Young, A. P., & Carilli, J. E. (2019). Global distribution of coastal cliffs. *Earth Surface Processes and Landforms*, 44(6): 1309-1316.

Zainali, A., & Weiss, R. (2015). Boulder dislodgement and transport by solitary waves: Insights from three-dimensional numerical simulations. *Geophysical Research Letters,* 42(11): 4490-4497. DOI:org/10.1002/2015GL063712

Zingg, T. (1935). Beitrag zur Schotteranalyse. *Schweizerische Mineralogische und Petrographische Mitteilungen,* 15: 39-140. DOI:org/10.3929/ethz-a-000103455.